

Fractional Modelling of Transport Problems in Fluid Mechanics and Heat-mass Transfer

Lead Guest Editor: Mustafa Inc

Guest Editors: Younes Menni and Sunil Kumar





Fractional Modelling of Transport Problems in Fluid Mechanics and Heat-mass Transfer

Advances in Mathematical Physics

Fractional Modelling of Transport Problems in Fluid Mechanics and Heat-mass Transfer

Lead Guest Editor: Mustafa Inc

Guest Editors: Younes Menni and Sunil Kumar



Copyright © 2022 Hindawi Limited. All rights reserved.

This is a special issue published in "Advances in Mathematical Physics." All articles are open access articles distributed under the Creative Commons Attribution License, which permits unrestricted use, distribution, and reproduction in any medium, provided the original work is properly cited.


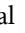
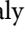











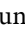
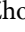









Chief Editor

Marta Chinnici, Italy

Associate Editors

Rossella Arcucci, United Kingdom
Marta Chinnici, Italy

Academic Editors

Stephen C. Anco , Canada
P. Areias , Portugal
Matteo Beccaria , Italy
Luigi C. Berselli , Italy
Carlo Bianca , France
Manuel Calixto , Spain
José F Cariñena , Spain
Mengxin Chen , China
Zengtao Chen , Canada
Alessandro Ciallella , Italy
John D. Clayton , USA
Giampaolo Cristadoro , Italy
Pietro D'Avenia , Italy
Claudio Dappiaggi , Italy
Manuel De León, Spain
Seyyed Ahmad Edalatpanah, Iran
Tarig Elzaki, Saudi Arabia
Zine El Abidine Fellah , France
Igor Leite Freire, Brazil
Maria L. Gandarias , Spain
Mergen H. Ghayesh, Australia
Ivan Giorgio , Italy
Leopoldo Greco , Italy
Sebastien Guenneau, France
ONUR ALP ILHAN , Turkey
Giorgio Kaniadakis, Italy
Boris G. Konopelchenko, Italy
Qiang Lai, China
Ping Li , China
Emmanuel Lorin, Canada
Guozhen Lu , USA
Jorge E. Macias-Diaz , Mexico
Ming Mei, Canada
Mohammad Mirzazadeh , Iran
Merced Montesinos , Mexico
André Nicolet , France
Bin Pang , China
Giuseppe Pellicane , South Africa
A. Plastino , Argentina




Eugen Radu, Portugal
Laurent Raymond , France
Marianna Ruggieri , Italy
Mahnoor Sarfraz , Pakistan
Mhamed Sayyouri , Morocco
Antonio Scarfone , Italy
Artur Sergyeyev, Czech Republic
Sergey Shmarev, Spain
Bianca Stroffolini , Italy
Lu Tang , China
Francesco Toppa , Brazil
Dimitrios Tsimpis, France
Emilio Turco , Italy
Mohammad W. Alomari, Jordan
Deng-Shan Wang, United Kingdom
Kang-Jia Wang , China
Renhai Wang , China
Ricardo Weder , Mexico
Jiahong Wu , USA
Agnieszka Wylomanska, Poland
Su Yan , USA
Shuo Yin , Ireland
Chunli Zhang , China
Yao-Zhong Zhang , Australia

Contents


Computational Simulations; Abundant Optical Wave Solutions Atangana Conformable Fractional Nonlinear Schrödinger Equation

Mostafa M. A. Khater , Mustafa Inc , Raghda A. M. Attia, and Dianchen Lu 
Research Article (13 pages), Article ID 2196913, Volume 2022 (2022)



Noninteger Derivative Order Analysis on Plane Wave Reflection from Electro-Magneto-Thermo-Microstretch Medium with a Gravity Field within the Three-Phase Lag Model

S. H. Elhag, Fatimah S. Bayones, A. A. Kilany , S. M. Abo-Dahab , Emad A.-B. Abdel-Salam, M. Elzagheer, and A. M. Abd-Alla 
Research Article (13 pages), Article ID 6559779, Volume 2022 (2022)





Statistical Study of the Entanglement for Qubit Interacting with an Electromagnetic Field

Neveen Sayed-Ahmed , M. M. Ameen, Taghreed M. Jawa, Tahani A. Aloafi, F. S. Bayones, Azhari A. Elhag, and J. Bouslimi
Research Article (9 pages), Article ID 5571796, Volume 2021 (2021)





On Fractional Diffusion Equation with Caputo-Fabrizio Derivative and Memory Term

Binh Duy Ho, Van Kim Ho Thi, Long Le Dinh , Nguyen Hoang Luc, and Phuong Nguyen 
Research Article (8 pages), Article ID 9259967, Volume 2021 (2021)



Numerical and Analytical Investigation for Darcy-Forchheimer Flow of a Williamson Fluid over a Riga Plate with Double Stratification and Cattaneo-Christov Dual Flux

S. Eswaramoorthi , Nazek Alessa , M. Sangeethavaanee , and Ngawang Namgyel 
Research Article (15 pages), Article ID 1867824, Volume 2021 (2021)




Natural Transform along with HPM Technique for Solving Fractional ADE

N. Pareek , A. Gupta , G. Agarwal , and D. L. Suthar 
Research Article (11 pages), Article ID 9915183, Volume 2021 (2021)

MHD Williamson Nanofluid Flow over a Stretching Sheet through a Porous Medium under Effects of Joule Heating, Nonlinear Thermal Radiation, Heat Generation/Absorption, and Chemical Reaction

J. Bouslimi , M. Omri, R. A. Mohamed, K. H. Mahmoud, S. M. Abo-Dahab , and M. S. Soliman
Research Article (16 pages), Article ID 9950993, Volume 2021 (2021)


Zero and Nonzero Mass Flux Effects of Bioconvective Viscoelastic Nanofluid over a 3D Riga Surface with the Swimming of Gyrotactic Microorganisms

T. S. Karthik, K. Loganathan , A. N. Shankar, M. Jemimah Carmichael, Anand Mohan, Mohammed K. A. Kaabar , and Safak Kayikci 
Research Article (13 pages), Article ID 9914134, Volume 2021 (2021)

Iterative Construction of Fixed Points for Operators Endowed with Condition (E) in Metric Spaces


Junaid Ahmad , Kifayat Ullah , Hüseyin Işık , Muhammad Arshad , and Manuel de la Sen 
Research Article (8 pages), Article ID 7930128, Volume 2021 (2021)

Remarks on the Systems of Semilinear Fractional Rayleigh-Stokes Equation

Le Dinh Long 

Research Article (9 pages), Article ID 6880435, Volume 2021 (2021)

Existence for Time-Fractional Semilinear Diffusion Equation on the Sphere

N. D. Phuong, Ho Duy Binh, Ho Thi Kim Van, and Le Dinh Long 



Research Article (8 pages), Article ID 6370636, Volume 2021 (2021)

A Numerical Algorithm Applied to Free Convection Flows of the Casson Fluid along with Heat and Mass Transfer Described by the Caputo Derivative

Ndolane Sene 



Research Article (11 pages), Article ID 5225019, Volume 2021 (2021)

Study of Magnetohydrodynamic Pulsatile Blood Flow through an Inclined Porous Cylindrical Tube with Generalized Time-Nonlocal Shear Stress

Nehad Ali Shah , A. Al-Zubaidi, and S. Saleem 

Research Article (11 pages), Article ID 5546701, Volume 2021 (2021)

Simultaneous Flow of n-Immiscible Fractional Maxwell Fluids with Generalized Thermal Flux and Robin Boundary Conditions

Abdul Rauf , Qammar Rubbab, Nehad Ali Shah , and Kaleem Razzaq Malik

Research Article (20 pages), Article ID 5572823, Volume 2021 (2021)

Research Article

Computational Simulations; Abundant Optical Wave Solutions Atangana Conformable Fractional Nonlinear Schrödinger Equation

Mostafa M. A. Khater ^{1,2}, Mustafa Inc ^{3,4,5}, Raghda A. M. Attia,^{6,7} and Dianchen Lu ¹

¹Department of Mathematics, Faculty of Science, Jiangsu University, Zhenjiang 212013, China

²Department of Basic Science, Obour High Institute for Engineering and Technology, Cairo 11828, Egypt

³Department of Computer Engineering, Biruni University, Istanbul, Turkey

⁴Science Faculty, Firat University, Elazig 23119, Turkey

⁵Department of Medical Research, China Medical University Hospital, China Medical University, Taichung, Taiwan

⁶Department of Basic Science, Higher Technological Institute 10th of Ramadan City, El Sharqia 44634, Egypt

⁷School of Management & Economics, Jiangsu University of Science and Technology, Zhenjiang 212003, China

Correspondence should be addressed to Mostafa M. A. Khater; mostafa.khater2024@yahoo.com and Mustafa Inc; minc@firat.edu.tr

Received 28 May 2021; Accepted 6 January 2022; Published 10 February 2022

Academic Editor: Jorge E. Macias-Diaz

Copyright © 2022 Mostafa M. A. Khater et al. This is an open access article distributed under the Creative Commons Attribution License, which permits unrestricted use, distribution, and reproduction in any medium, provided the original work is properly cited.

This research paper explores the Atangana conformable nonlinear fractional Schrödinger equation's optical soliton wave solutions through three recently introduced computational schemes. The simplest expanded equation, the generalized Kudryashov method, and the sech-tanh expansion approaches are used for describing the structure of optical solitons by nonlinear optical fibers with the modern fractional operator. Several formulas such as hyperbolic, trigonometric, logical, dim, light, moon-bright hybrid, singular, combined singular, and regular wave solutions have been created. The employed methods are effective and worthy of being tested. The features of the Hamiltonian process were used to analyze the stability properties of the solutions obtained.

1. Introduction

The nonlinear partial differential equation is one of the most exciting science types, as it can describe several nonlinear phenomena as nonlinear partial distinctiveness equations (NLPD) or a form of NLPD [1–3], including diffusion, heat, electrostatics, fluid dynamics, electrodynamic, elasticity, and quantum mechanics. Some equations include the uncertain functions of multivariable and partial byproducts, including integral and partial derivatives [4, 5]. Several investigators in various fields have been studying the fractional order in the NLPD equations [6]. This analysis is focused on the nonlocal properties that only occur in such a derivative, as they are not present in an integer derivative [7–9]. This property is generally used to describe a location, quantity, and nonlocal

Lagrangian behavior at a distance [10]. According to this property, various forms of concepts are employed to transform the NLPD equation into a standard differential equation with an integer order, including Riemann–Liouville, the two-scale fractal derivative, He fractional derivative, Caputo, and compliant fractional derivatives [11–13]. The compliant fractional derivative of Atangana is used here on the grounds of its supremacy over other concepts of fractional derivatives [14, 15]. This superiority is apparent in its capacity to extend all organizational characteristics, such as a chain law, quotient law, semigroup property, and element rule, to the traditional first derivative [16, 17].

Many analytical and semianalytical schemes are derived for the same purpose, such as Lie group method, (G'/G) -expansion method, tanh-expansion method,

extended tanh-expansion method, improved Bernoulli subequation function, Riccati–Bernoulli sub-ODE method, sinh-cosh method, simplest equation method, generalized Kudryashov method, Adomian decomposition method, homotopy perturbation method, general homotopy analysis method, and so on [18–25].

The rest of the paper's sections are ordered as follows: Section 2 studies the performance of the extended simplest equation [26, 27], the generalized Kudryashov [28, 29], and the sech-tanh expansion methods [30, 31] on the perturbed time-fractional nonlinear Schrödinger equation. Moreover, we study the stability property of obtained analytical wave solutions. Section 3 represents some of the obtained solutions in three & two-dimensional and contour plots. Section 4 gives the conclusion.

2. Application

In this section, we apply the Atangana conformable fractional operator to the perturbed time-fractional nonlinear Schrödinger equation that is given by [31–35].

$$i \frac{\partial^\vartheta \mathcal{F}}{\partial t^\vartheta} + \mathcal{F}_{xx} + \gamma \mathcal{F} |\mathcal{F}|^2 + i [\gamma_1 \mathcal{F}_{xxx} + \gamma_2 |\mathcal{F}|^2 \mathcal{F}_x + \gamma_3 (|\mathcal{F}|^2)_x \mathcal{F}] = 0, \quad (1)$$

where $t > 0, 0 < \vartheta < 1$, $i = \sqrt{-1}$, while α, γ are the arbitrary constants. Also, γ_1 represents the dispersion term, γ_2 is the nonlinear dispersion, γ_3 is the nonlinear dispersion term and $\mathcal{F} = \mathcal{F}(x, t)$ describes the propagation of optical solitons in optical fibers that exhibits a Kerr law nonlinearity. During the evolution age of communications, many fundamentals' applications are related to equation (1) such as plasma physics and optical fiber communications. This fiber is used to transmit light between the two ends of the fiber and the widespread use in fiber-optical links. They provide a broader and higher range of communication (data) than electrical cables. Typically crafted from drawing glass (silica) or plastic of a much thicker diameter than a human scalp.

Handling equation (1) via the Atangana conformable fractional in the next wave transformation $\mathcal{F}(x, t) = e^{i(hx - \Omega t)} \mathcal{Z}(\mathcal{Z})$, $\mathcal{Z} = x - c/\vartheta(t + (1/\Gamma(\vartheta)))^\vartheta$ where c is an arbitrary constant, yields

$$e^{i(hx - t\Omega)} (\mathcal{Z}(\mathcal{Z})(-h^2 + \Omega + h^3 \gamma_1) + \mathcal{Z}^3(\mathcal{Z})(\gamma - h\gamma_2) - i(c - 2h + 3h^2 \gamma_1) \mathcal{Z}'(\mathcal{Z}) + i\mathcal{Z}^2(\mathcal{Z})(\gamma_2 + 2\gamma_3) \mathcal{Z}'(\mathcal{Z}) + (1 - 3h\gamma_1) \mathcal{Z}''(\mathcal{Z}) + i\gamma_1 \mathcal{Z}'''(\mathcal{Z})) = 0. \quad (2)$$

Separating the real and imaginary part of equation (2) and integrating the imaginary part once with zero constant of integration lead to

$$(-h^2 + \Omega + h^3 \gamma_1) \mathcal{Z} + (\gamma - h\gamma_2) \mathcal{Z}^3 + (1 - 3h\gamma_1) \mathcal{Z}'' = 0, \quad (3)$$

$$-(c - 2h + 3h^2 \gamma_1) \mathcal{Z} + \frac{(\gamma_2 + 2\gamma_3)}{3} \mathcal{Z}^3 + \gamma_1 \mathcal{Z}'' = 0. \quad (4)$$

Comparing the coefficients of $\mathcal{Z}, \mathcal{Z}'', \mathcal{Z}^3$ in equations (3) and (4) explains the equivalence between both equations under the following constraint

$$\frac{-h^2 + \Omega + h^3 \gamma_1}{-(c - 2h + 3h^2 \gamma_1)} = \frac{3(\gamma - h\gamma_2)}{\gamma_2 + 2\gamma_3} = \frac{1 - 3h\gamma_1}{\gamma_1}. \quad (5)$$

This relation leads to $\Omega = -c + 2h + 3h\gamma_1 - 8h^2 \gamma_1 + 8h^3 \gamma_1^2/\gamma_1, \gamma_2 = 3\gamma\gamma_1 - 2\gamma_3 + 6h\gamma_1\gamma_3$. Applying the homogeneous balance rule to equation (4) for determining the balance between the nonlinear and highest order derivative terms.

2.1. Extended Simplest Equation Method. Applying this scheme to equation (4) leads to the following general solution

$$\mathcal{Z}(\mathcal{Z}) = \sum_{i=-n}^n a_i f(\mathcal{Z})^i = \frac{a_{-1}}{f(\mathcal{Z})} + a_0 + f(\mathcal{Z}) a_1, \quad (6)$$

where $a_i, (i = -1, 0, 1)$ are arbitrary constants. Also, $f(\mathcal{Z})$ satisfies the next auxiliary equation [26, 27]

$$f'(\mathcal{Z}) = \alpha + \lambda f(\mathcal{Z}) + \mu f(\mathcal{Z})^2, \quad (7)$$

where α, λ, μ are arbitrary constants. Substituting equations (6) along (7) into equation (4) and collecting all terms with the same power of $f(\mathcal{Z})^j, (j = -3, -2, \dots, 2, 3)$ lead to a system of algebraic equations. Solving this system yields the following families.

2.1.1. Family I

$$a_0 = \frac{\sqrt{3/2} \lambda \sqrt{\gamma_1}}{\sqrt{-\gamma_2 - 2\gamma_3}}, a_{-1} = 0, a_1 = \frac{\sqrt{6} \mu \sqrt{\gamma_1}}{\sqrt{-\gamma_2 - 2\gamma_3}}, c = \frac{1}{2} (4h - 6h^2 \gamma_1 - \lambda^2 \gamma_1 + 4\alpha \mu \gamma_1), \quad (8)$$

where $(-\gamma_2 - 2\gamma_3 > 0, \gamma_1 > 0)$.

2.1.2. Family II

$$a_0 = \frac{\sqrt{3/2} \lambda \sqrt{\gamma_1}}{\sqrt{-\gamma_2 - 2\gamma_3}}, a_{-1} = \frac{\sqrt{6} \alpha \sqrt{\gamma_1}}{\sqrt{-\gamma_2 - 2\gamma_3}}, a_1 = 0, c = \frac{1}{2} (4h - 6h^2 \gamma_1 - \lambda^2 \gamma_1 + 4\alpha \mu \gamma_1), \quad (9)$$

where $(-\gamma_2 - 2\gamma_3 > 0, \gamma_1 > 0)$.

Thus, the optical solitary wave solutions of the Atangana conformable fractional nonlinear Schrödinger equation are given based on family I as follows:

When $\lambda = 0$,
for $\alpha \mu > 0$,

$$\begin{aligned}\mathcal{F}_1(x, t) &= \frac{\sqrt{6}e^{ihx-it\Omega}\sqrt{\alpha\mu}\sqrt{\gamma_1}\text{Tan}\left[\sqrt{\alpha\mu}\left(x+\theta+(t+1/\Gamma(\vartheta))^{\vartheta}(-4h+(6h^2-4\alpha\mu)\gamma_1)/2\vartheta\right)\right]}{\sqrt{-\gamma_2-2\gamma_3}}, \\ \mathcal{F}_2(x, t) &= \frac{\sqrt{6}e^{ihx-it\Omega}\sqrt{\alpha\mu}\text{Cot}\left[\sqrt{\alpha\mu}\left(x+\theta+(t+1/\Gamma(\vartheta))^{\vartheta}(-4h+(6h^2-4\alpha\mu)\gamma_1)/2\vartheta\right)\right]\sqrt{\gamma_1}}{\sqrt{-\gamma_2-2\gamma_3}}.\end{aligned}\quad (10)$$

For $\alpha\mu < 0$,

$$\mathcal{F}_3(x, t) = \frac{\sqrt{6}e^{ihx-it\Omega}\sqrt{-\alpha\mu}\sqrt{\gamma_1}\text{Tanh}\left[\sqrt{-\alpha\mu}\left(x+(t+1/\Gamma(\vartheta))^{\vartheta}(-4h+(6h^2-4\alpha\mu)\gamma_1)/2\vartheta\right)\mp\text{Log}[\theta/2]\right]}{\sqrt{-\gamma_2-2\gamma_3}}, \quad (11)$$

$$\mathcal{F}_4(x, t) = \frac{\sqrt{6}e^{ihx-it\Omega}\sqrt{-\alpha\mu}\text{Coth}\left[\sqrt{-\alpha\mu}\left(x+(t+1/\Gamma(\vartheta))^{\vartheta}(-4h+(6h^2-4\alpha\mu)\gamma_1)/2\vartheta\right)\mp\text{Log}[\theta/2]\right]\sqrt{\gamma_1}}{\sqrt{-\gamma_2-2\gamma_3}}. \quad (12)$$

When $\alpha = 0$;

For $\lambda > 0$

$$\mathcal{F}_5(x, t) = -\frac{\sqrt{3/2}e^{ihx-it\Omega}\lambda\sqrt{\gamma_1}}{\left(-1+e^{\lambda\left(x+\theta+(t+1/\Gamma(\vartheta))^{\vartheta}(-4h+(6h^2+\lambda^2)\gamma_1)/2\vartheta}\right)\mu\right)\sqrt{-\gamma_2-2\gamma_3}} - \frac{\sqrt{3/2}e^{ihx-it\Omega+\lambda\left(x+\theta+(t+1/\Gamma(\vartheta))^{\vartheta}(-4h+(6h^2+\lambda^2)\gamma_1)/2\vartheta}\right)\lambda\mu\sqrt{\gamma_1}}{\left(-1+e^{\lambda\left(x+\theta+(t+1/\Gamma(\vartheta))^{\vartheta}(-4h+(6h^2+\lambda^2)\gamma_1)/2\vartheta}\right)\mu\right)\sqrt{-\gamma_2-2\gamma_3}}. \quad (13)$$

For $\lambda < 0$

$$\mathcal{F}_6(x, t) = \frac{\sqrt{3/2}e^{ihx-it\Omega}\lambda\sqrt{\gamma_1}}{\sqrt{-\gamma_2-2\gamma_3}} - \frac{\sqrt{6}e^{ihx-it\Omega}\mu\sqrt{\gamma_1}}{\sqrt{-\gamma_2-2\gamma_3}} + \frac{\sqrt{6}e^{ihx-it\Omega}\mu\sqrt{\gamma_1}}{\left(1+e^{\lambda\left(x+\theta+(t+1/\Gamma(\vartheta))^{\vartheta}(-4h+(6h^2+\lambda^2)\gamma_1)/2\vartheta}\right)\mu\right)\sqrt{-\gamma_2-2\gamma_3}}. \quad (14)$$

When $4\alpha\mu > \lambda^2$

$$\begin{aligned}\mathcal{F}_7(x, t) &= \frac{e^{ihx-it\Omega}\sqrt{-3\lambda^2/2+6\alpha\mu}\sqrt{\gamma_1}\text{Tan}\left[1/2\sqrt{-\lambda^2+4\alpha\mu}\left(x+\theta+(t+1/\Gamma(\vartheta))^{\vartheta}(-4h+(6h^2+\lambda^2-4\alpha\mu)\gamma_1)/2\vartheta\right)\right]}{\sqrt{-\gamma_2-2\gamma_3}}, \\ \mathcal{F}_8(x, t) &= \frac{e^{ihx-it\Omega}\sqrt{-3\lambda^2/2+6\alpha\mu}\text{Cot}\left[1/2\sqrt{-\lambda^2+4\alpha\mu}\left(x+\theta+(t+1/\Gamma(\vartheta))^{\vartheta}(-4h+(6h^2+\lambda^2-4\alpha\mu)\gamma_1)/2\vartheta\right)\right]\sqrt{\gamma_1}}{\sqrt{-\gamma_2-2\gamma_3}}.\end{aligned}\quad (15)$$

Additionally, the optical solitary wave solutions of the Atangana conformable fractional nonlinear Schrödinger equation are given based on family II by

When $\lambda = 0$,
for $\alpha\mu > 0$,

$$\begin{aligned}\mathcal{F}_9(x, t) &= \frac{\sqrt{6}e^{ihx-it\Omega}\sqrt{\alpha\mu}\text{Cot}\left[\sqrt{\alpha\mu}\left(x+\theta+(t+1/\Gamma(\vartheta))^{\vartheta}(-4h+(6h^2-4\alpha\mu)\gamma_1)/2\vartheta\right)\right]\sqrt{\gamma_1}}{\sqrt{-\gamma_2-2\gamma_3}}, \\ \mathcal{F}_{10}(x, t) &= \frac{\sqrt{6}e^{ihx-it\Omega}\sqrt{\alpha\mu}\sqrt{\gamma_1}\text{Tan}\left[\sqrt{\alpha\mu}\left(x+\theta+(t+1/\Gamma(\vartheta))^{\vartheta}(-4h+(6h^2-4\alpha\mu)\gamma_1)/2\vartheta\right)\right]}{\sqrt{-\gamma_2-2\gamma_3}}.\end{aligned}\quad (16)$$

For $\alpha\mu < 0$,

$$\mathcal{F}_{11}(x, t) = -\frac{\sqrt{6}e^{ihx-it\Omega}\sqrt{-\alpha\mu}\coth\left[\sqrt{-\alpha\mu}\left(x+(t+1/\Gamma(\vartheta))^{\vartheta}(-4h+(6h^2-4\alpha\mu)\gamma_1)/2\vartheta\right)\mp\text{Log}[\theta]/2\right]\sqrt{\gamma_1}}{\sqrt{-\gamma_2-2\gamma_3}}, \quad (17)$$

$$\mathcal{F}_{12}(x, t) = -\frac{\sqrt{6}e^{ihx-it\Omega}\sqrt{-\alpha\mu}\sqrt{\gamma_1}\tanh\left[\sqrt{-\alpha\mu}\left(x+(t+1/\Gamma(\vartheta))^{\vartheta}(-4h+(6h^2-4\alpha\mu)\gamma_1)/2\vartheta\right)\mp\text{Log}[\theta]/2\right]}{\sqrt{-\gamma_2-2\gamma_3}}. \quad (18)$$

When $4\alpha\mu > \lambda^2$,

$$\mathcal{F}_{13}(x, t) = \frac{\sqrt{3/2}e^{ihx-it\Omega}\lambda\sqrt{\gamma_1}}{\sqrt{-\gamma_2-2\gamma_3}} - \frac{2\sqrt{6}e^{ihx-it\Omega}\alpha\mu\sqrt{\gamma_1}}{\sqrt{-\gamma_2-2\gamma_3}\left(\lambda - \sqrt{-\lambda^2+4\alpha\mu}\tan\left[1/2\sqrt{-\lambda^2+4\alpha\mu}\left(x+\theta+(t+1/\Gamma(\vartheta))^{\vartheta}(-4h+(6h^2+\lambda^2-4\alpha\mu)\gamma_1)/2\vartheta\right)\right]\right)}, \quad (19)$$

$$\mathcal{F}_{14}(x, t) = \frac{\sqrt{3/2}e^{ihx-it\Omega}\lambda\sqrt{\gamma_1}}{\sqrt{-\gamma_2-2\gamma_3}} - \frac{2\sqrt{6}e^{ihx-it\Omega}\alpha\mu\sqrt{\gamma_1}}{\left(\lambda - \sqrt{-\lambda^2+4\alpha\mu}\cot\left[1/2\sqrt{-\lambda^2+4\alpha\mu}\left(x+\theta+(t+1/\Gamma(\vartheta))^{\vartheta}(-4h+(6h^2+\lambda^2-4\alpha\mu)\gamma_1)/2\vartheta\right)\right]\right)\sqrt{-\gamma_2-2\gamma_3}}.$$

2.2. Generalized Kudryashov Method. Applying this scheme to equation (4) leads to the following general solution

$$\mathcal{Q}(\mathfrak{Z}) = \frac{\sum_{i=0}^m a_i \mathcal{Q}(\mathfrak{Z})^i}{\sum_{j=0}^n b_j \mathcal{Q}(\mathfrak{Z})^j} = \frac{a_0 + \mathcal{Q}(\mathfrak{Z})a_1 + \mathcal{Q}(\mathfrak{Z})^2 a_2}{b_0 + \mathcal{Q}(\mathfrak{Z})b_1}, \quad (20)$$

where $a_i b_j$, ($i = 0, 1, 2, j = 0, 1$) are arbitrary constants. Also, $\mathcal{Q}(\mathfrak{Z})$ satisfies the next auxiliary equation [26, 27]:

$$\mathcal{Q}'(\mathfrak{Z}) = \mathcal{Q}(\mathfrak{Z})^2 - \mathcal{Q}(\mathfrak{Z}). \quad (21)$$

Substituting equation (21) along (22) into equation (4) and collecting all terms with the same power of $\mathcal{Q}(\mathfrak{Z})^j$, ($j = 0, 1, \dots, 5, 6$) lead to a system of algebraic equations. Solving this system yields the following families.

2.2.1. Family I

$$\begin{aligned} a_0 &= \frac{a_1 b_0}{-2b_0 + b_1}, a_2 = -\frac{2a_1 b_1}{-2b_0 + b_1}, c \\ &= \frac{1}{2}(4h - \gamma_1 - 6h^2 \gamma_1), \gamma_3 \\ &= \frac{-12b_0^2 \gamma_1 + 12b_0 b_1 \gamma_1 - 3b_1^2 \gamma_1 - 2a_1^2 \gamma_2}{4a_1^2}. \end{aligned} \quad (22)$$

2.2.2. Family II

$$\begin{aligned} a_0 &= -\frac{a_1}{2}, a_2 = -a_1, b_1 = -2b_0, c = 2h - 2\gamma_1 - 3h^2 \gamma_1, \gamma_3 \\ &= \frac{-24b_0^2 \gamma_1 - a_1^2 \gamma_2}{2a_1^2}. \end{aligned} \quad (23)$$

2.2.3. Family III

$$\begin{aligned} a_0 &= -\frac{a_1}{4}, a_2 = -a_1, b_1 = -2b_0, c = \frac{1}{2}(4h - \gamma_1 - 6h^2 \gamma_1), \gamma_3 \\ &= \frac{-24b_0^2 \gamma_1 - a_1^2 \gamma_2}{2a_1^2}. \end{aligned} \quad (24)$$

2.2.4. Family IV

$$\begin{aligned} a_1 &= 0, a_2 = -4a_0, b_1 = 2b_0, c = \frac{1}{2}(4h - \gamma_1 - 6h^2 \gamma_1), \gamma_3 \\ &= \frac{-3b_0^2 \gamma_1 - 2a_0^2 \gamma_2}{4a_0^2}. \end{aligned} \quad (25)$$

Consequently, the optical solitary wave solutions of the Atangana conformable fractional nonlinear Schrödinger equation are given based on the above families respectively by

$$\mathcal{F}_{15}(x, t) = \frac{e^{i(hx-t\Omega)}\left(-Ae^x + e^{(t+1/\Gamma(\vartheta))^{\vartheta}(4h-\gamma_1-6h^2\gamma_1)/2\vartheta}\right)a_1}{\left(Ae^x + e^{(t+1/\Gamma(\vartheta))^{\vartheta}(4h-\gamma_1-6h^2\gamma_1)/2\vartheta}\right)(2b_0-b_1)}, \quad (26)$$

$$\mathcal{F}_{16}(x, t) = \frac{e^{i(hx-t\Omega)}\left(A^2 e^{2x} + e^{2(t+1/\Gamma(\vartheta))^{\vartheta}(2h-2\gamma_1-3h^2\gamma_1)/\vartheta}\right)a_1}{2\left(-A^2 e^{2x} + e^{2(t+1/\Gamma(\vartheta))^{\vartheta}(2h-2\gamma_1-3h^2\gamma_1)/\vartheta}\right)b_0}, \quad (27)$$

$$\mathcal{F}_{17}(x, t) = \frac{e^{i(hx-t\Omega)} \left(-Ae^x + e^{(t+1/\Gamma(\vartheta))^{\vartheta} (4h-\gamma_1-6h^2\gamma_1)/2\vartheta} \right) a_1}{4 \left(Ae^x + e^{(t+1/\Gamma(\vartheta))^{\vartheta} (4h-\gamma_1-6h^2\gamma_1)/2\vartheta} \right) b_0}, \quad (28)$$

$$\mathcal{F}_{18}(x, t) = -\frac{e^{i(hx-t\Omega)} \left(-Ae^x + e^{(t+1/\Gamma(\vartheta))^{\vartheta} (4h-\gamma_1-6h^2\gamma_1)/2\vartheta} \right) a_0}{\left(Ae^x + e^{(t+1/\Gamma(\vartheta))^{\vartheta} (4h-\gamma_1-6h^2\gamma_1)/2\vartheta} \right) b_0}. \quad (29)$$

2.3. Sech-Tanh Expansion Method. Applying this scheme to equation (4) leads to the following general solution:

$$\begin{aligned} \mathcal{G}(\mathfrak{Z}) &= a_0 + \sum_{i=1}^n \text{Sech}(\mathfrak{Z})^{i-1} (a_i \text{Sech}(\mathfrak{Z}) + b_i \text{Tanh}(\mathfrak{Z})) \\ &= a_0 + \text{Sech}(\mathfrak{Z}) a_1 + b_1 \text{Tanh}(\mathfrak{Z}), \end{aligned} \quad (30)$$

where $a_i b_j$, ($i = 0, 1, j = 1$) are arbitrary constants. Substituting equation (30) into equation (4) and collecting all terms of $\text{Sech}(\mathfrak{Z})$, $\text{Sech}(\mathfrak{Z})^2$, $\text{Sech}(\mathfrak{Z})^3$, $\text{Tanh}(\mathfrak{Z})$, $\text{Sech}(\mathfrak{Z})^2 \text{Tanh}(\mathfrak{Z})$, $\text{Sech}(\mathfrak{Z}) \text{Tanh}(\mathfrak{Z})$ lead to a system of

algebraic equations. Solving this system yields the following families.

2.3.1. Family I

$$\left(a_0 = 0, a_1 = \frac{\sqrt{6} \sqrt{\gamma_1}}{\sqrt{\gamma_2 + 2\gamma_3}}, b_1 = 0, c = 2h + \gamma_1 - 3h^2\gamma_1 \right),$$

where $(\gamma_2 + 2\gamma_3 > 0, \gamma_1 > 0)$. (31)

2.3.2. Family II

$$\left(a_0 = 0, a_1 = 0, b_1 = \frac{\sqrt{6} \sqrt{\gamma_1}}{\sqrt{-\gamma_2 - 2\gamma_3}}, c = 2h - 2\gamma_1 - 3h^2\gamma_1 \right),$$

where $(\gamma_2 + 2\gamma_3 < 0, \gamma_1 > 0)$. (32)

Consequently, the optical solitary wave solutions of the Atangana conformable fractional nonlinear Schrödinger equation are given based on the above families respectively by

$$\begin{aligned} \mathcal{F}_{19}(x, t) &= \frac{\sqrt{6} e^{i(hx-t\Omega)} \text{Sech} \left[x - (t + 1/\Gamma(\vartheta))^{\vartheta} (2h + \gamma_1 - 3h^2\gamma_1)/\vartheta \right] \sqrt{\gamma_1}}{\sqrt{\gamma_2 + 2\gamma_3}}, \\ \mathcal{F}_{20}(x, t) &= \frac{\sqrt{6} e^{i(hx-t\Omega)} \sqrt{\gamma_1} \text{Tanh} \left[x - (t + 1/\Gamma(\vartheta))^{\vartheta} (2h - 2\gamma_1 - 3h^2\gamma_1)/\vartheta \right]}{\sqrt{-\gamma_2 - 2\gamma_3}}. \end{aligned} \quad (33)$$

3. Stability Property of Solutions

This part studies the stability property of each one of the obtained solutions by using the Hamiltonian system property since the momentum M in this system is given by [36, 37]

$$M = \frac{1}{2} \int_{-l}^l \mathcal{G}^2(\mathfrak{Z}) d\mathfrak{Z}, \quad (34)$$

where $\mathcal{G}(\mathfrak{Z})$ is the solution of the model. Consequently, the condition for stability of the solutions can be formulated as

$$\frac{\partial M}{\partial c} > 0, \quad (35)$$

where c is the wave velocity. The momentum in the Hamiltonian system for equation (11) is given by

$$\begin{aligned} M &= \frac{1}{2} \left(c \left((-1095.1320422182555 + 1337.3986588468201i) + (10799.999990891356 + 6.613092659621341 \times 10^{-14}i) c \right) \right. \\ &\quad + \left((-67.49999939305316 + 10.602875127368723i) - (63.68904259247388 - 1.479114197289397 \times 10^{-31}i) c \right) \\ &\quad \cdot \text{Log} \left[1 + (2.061153687919397 \times 10^{-9} - 2.524185266461253 \times 10^{-25}i) e^{-18.87082757451449c} \right] \\ &\quad \left. + \left((-67.49999939305316 + 10.602875127368723i) + (63.68904259247388 - 1.479114197289397 \times 10^{-31}i) c \right) \right) \end{aligned}$$

$$\begin{aligned}
& \cdot \text{Log}\left[1. + \left(4.851651799965657 \times 10^8 + 5.941559847405437 \times 10^{-8}i\right)e^{-18.87082757451449c}\right] \\
& + ((67.49999939305316 - 10.602875127368721i) + (3.482018748651115 \times 10^{-15} \\
& + ((67.49999939305316 - 10.602875127368721i) + (3.482018748651115 \times 10^{-15} - 2.524185266461253 \times 10^{-25}i) \\
& \cdot e^{(-1.031709266497698 \times 10^{-15} - 16.849090974083545i)c}] + (67.49999939305316 - 10.602875127368723i) \\
& \cdot \text{Log}\left[1. + \left(4.851651799965657 \times 10^8 + 5.941559847405437 \times 10^{-8}i\right)e^{(-1.031709266497698 \times 10^{-15} - 16.849090974083545i)c}\right] \\
& - (3.482018748651115 \times 10^{-15} + 56.8656816165352i)c \\
& \cdot \text{Log}\left[1. + \left(4.851651799965657 \times 10^8 + 5.941559847405437 \times 10^{-8}i\right)e^{(-1.031709266497698 \times 10^{-15} - 16.849090974083545i)c}\right] \\
& - (67.49999939305316 - 10.602875127368723i) \\
& \cdot \text{Log}\left[\text{Sin}\left[(1.5707963267948966 + 9.999999984115489i) - (8.424545487041772 - 5.158546332488493 \times 10^{-16}i)c\right]\right] \\
& + (67.49999939305316 - 10.602875127368723i) \\
& \cdot \text{Log}[-1. \text{Sin}[(1.5707963267948966 + 9.999999984115489i) - (0. + 9.435413787257245i)c]] \\
& + (67.49999939305316 - 10.602875127368723i) \\
& \cdot \text{Log}[\text{Sin}[(1.5707963267948966 + 9.999999984115489i) + (0. + 9.435413787257245i)c]] \\
& - (67.49999939305316 - 10.602875127368723i) \\
& \cdot \text{Log}[-1. \text{Sin}[(1.5707963267948966 + 9.999999984115489i) + (8.424545487041772 - 5.158546332488493 \times 10^{-16}i)c]] \\
& - (3.3749999750136808 - 3.081487911019577 \times 10^{-33}i) \\
& \cdot \text{PolyLog}\left[2., \left(-4.851651799965657 \times 10^8 - 5.941559847405437 \times 10^{-8}i\right)e^{-18.87082757451449c}\right] \\
& + (3.3749999750136808 - 3.081487911019577 \times 10^{-33}i) \\
& \cdot \text{PolyLog}\left[2., \left(-2.061153687919397 \times 10^{-9} + 2.524185266461253 \times 10^{-25}i\right)e^{-18.87082757451449c}\right] \\
& + (3.3749999750136808 - 3.081487911019577 \times 10^{-33}i) \\
& \cdot \text{PolyLog}\left[2., \left(-4.851651799965657 \times 10^8 - 5.941559847405437 \times 10^{-8}i\right)e^{(-1.031709266497698 \times 10^{-15} - 16.849090974083545i)c}\right] \\
& - (3.3749999750136808 - 3.081487911019577 \times 10^{-33}i) \\
& \cdot \text{PolyLog}\left[2., \left(-2.061153687919397 \times 10^{-9} + 2.524185266461253 \times 10^{-25}i\right)e^{(-1.031709266497698 \times 10^{-15} - 16.849090974083545i)c}\right] \\
& \quad \quad \quad (36)
\end{aligned}$$

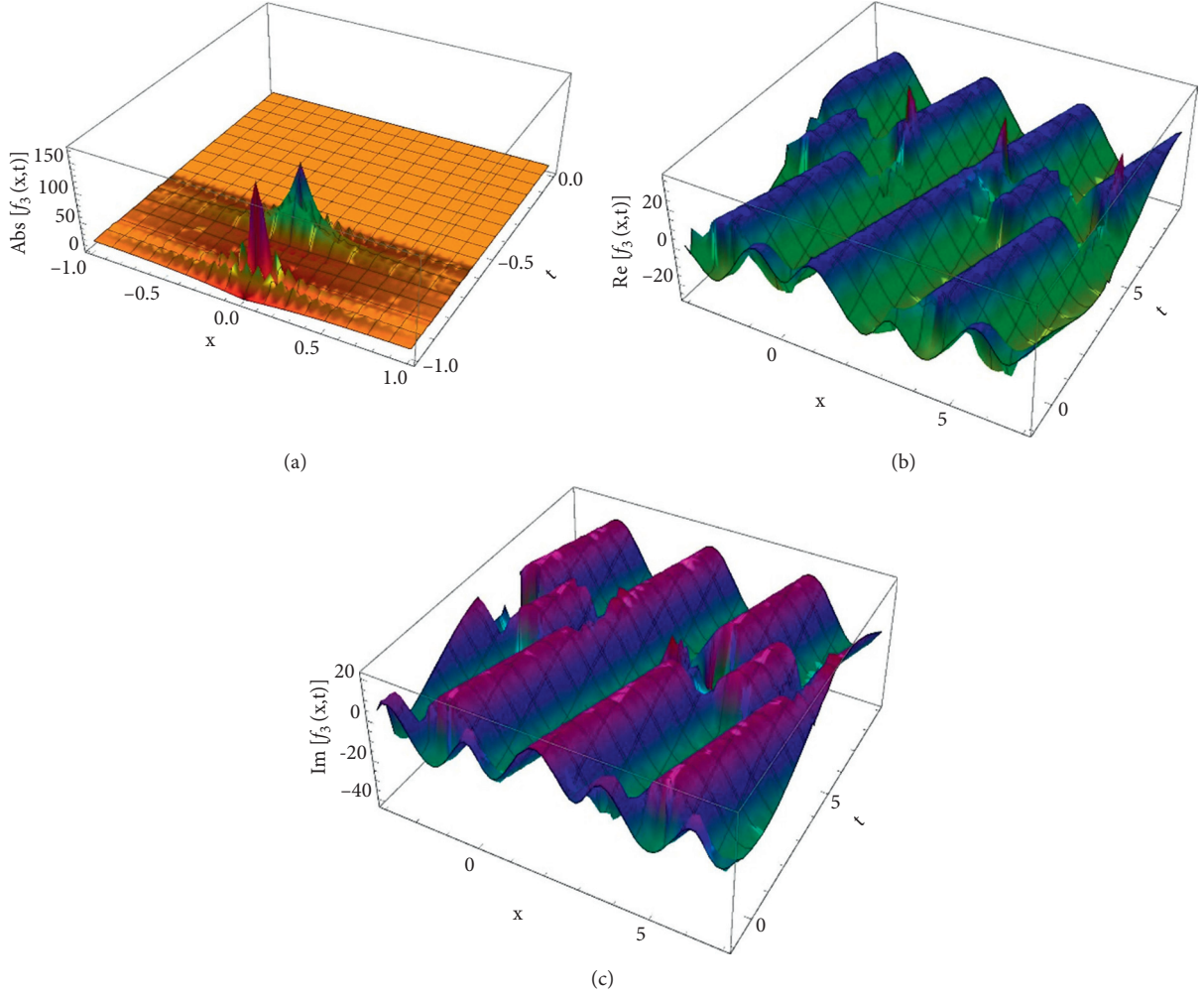


FIGURE 1: Optical soliton wave solutions of the absolute (a), real (b), and imaginary (c) value of equation (8) in three-dimensional view when $(\theta = 1, \alpha = -1, \mu = 4, \gamma_1 = 9, \vartheta = 0.5, \gamma_2 = -9, \gamma_3 = 4, \text{ and } h = 2)$.

and, thus

$$\frac{\partial M}{\partial c} \Big|_{c=-176} > 0. \quad (37)$$

We conclude that this solution is unstable on the interval $x \in [-5, 5], t \in [-5, 5]$ when $[\theta = 1, \alpha = -1, \mu = 4, \gamma_1 = 9, \vartheta = 0.5, \gamma_2 = -9, \gamma_3 = 4, h = 2, \lambda = 0]$. This result shows the ability of the solutions for their application. Applying the previous steps to other obtained solutions leads to studying the stability property of all solutions. This process makes choosing suitable stable solutions to use in model applications is very easy and interesting.

4. Representation of Obtained Solutions

This part studies the physical interpretation of obtained solutions under a suitable choice for the values of parameters. It represents each one of the selected solutions by three- and two-dimensional plots. For each kind, we mean

the shape of the solution in real and imaginary plots to show the similarities and differences between them in these cases. We have plotted each of $\mathcal{F}_3(x, t)$, $\mathcal{F}_{15}(x, t)$, and $\mathcal{F}_{20}(x, t)$, Figures 1–6 under the following conditions:

Figure 1 illustrates the optical periodic solitary wave solution of $\mathcal{F}_3(x, t)$ in three-dimensional view when $[\theta = 1, \alpha = -1, \mu = 4, \gamma_1 = 9, \vartheta = 0.5, \gamma_2 = -9, \gamma_3 = 4, h = 2]$ in the next interval $x \in [-5, 5], t \in [-5, 5]$ to explain the perspective view of the solution.

Figure 2 describes the optical periodic solitary wave solution of $\mathcal{F}_3(x, t)$ in two-dimensional view when $[\theta = 1, \alpha = -1, \mu = 4, \gamma_1 = 9, \vartheta = 0.5, \gamma_2 = -9, \gamma_3 = 4, h = 2]$ in the next interval $x \in [-5, 5], t \in [-5, 5]$ to represent the wave propagation pattern of the wave along the x -axis.

Figure 3 illustrates the optical periodic solitary wave solution of $\mathcal{F}_{15}(x, t)$ in three-dimensional view when $[A = 3, \gamma_1 = 1, A = -2, a_1 = 4, b_0 = 5, b_1 = -1, h = 2]$ in

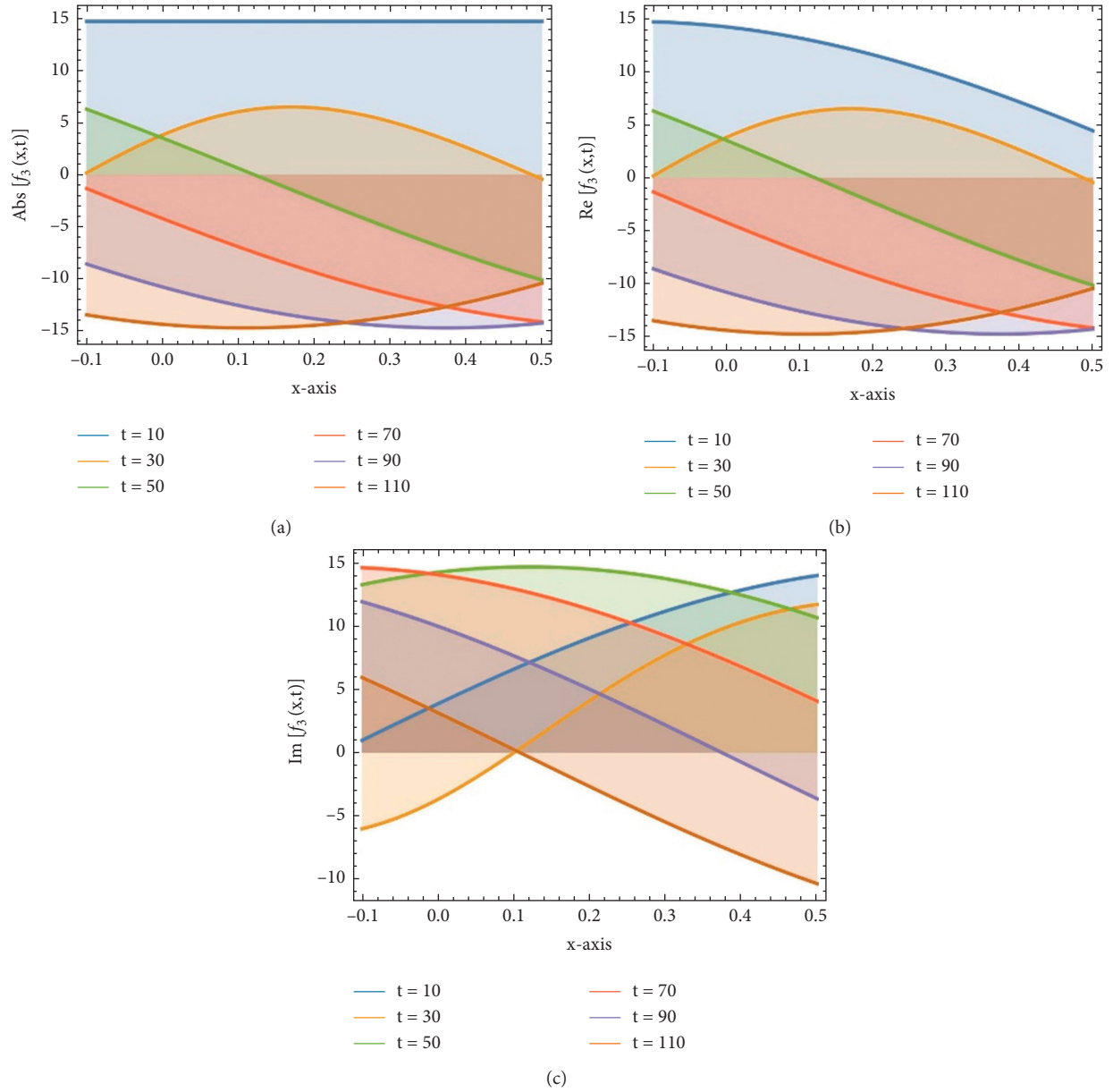


FIGURE 2: Optical soliton wave solutions of the absolute (a), real (b), and imaginary (c) value of equation (8) in two-dimensional view when $(\theta = 1, \alpha = -1, \mu = 4, \gamma_1 = 9, \vartheta = 0.5, \gamma_2 = -9, \gamma_3 = 4, \text{ and } h = 2)$.

the next interval $x \in [-5, 5], t \in [-5, 5]$ to explain the perspective view of the solution.

Figure 4 presents the optical periodic solitary wave solution of $\mathcal{F}_{15}(x, t)$ in two-dimensional view when $[A = 3, \gamma_1 = 1, A = -2, a_1 = 4, b_0 = 5, b_1 = -1, h = 2]$ in the next interval $x \in [-5, 5], t \in [-5, 5]$ to represent the wave propagation pattern of the wave along the x -axis.

Figure 5 illustrates the optical periodic solitary wave solution of $\mathcal{F}_{20}(x, t)$ in three-dimensional view when $[\gamma_1 = 4, \vartheta = 0.5, \gamma_2 = -1, \gamma_3 = -4, h = 2]$ in the next interval $x \in [-5, 5], t \in [-5, 5]$ to explain the perspective view of the solution.

Figure 6 illustrates the optical periodic solitary wave solution of $\mathcal{F}_{20}(x, t)$ in two-dimensional view when

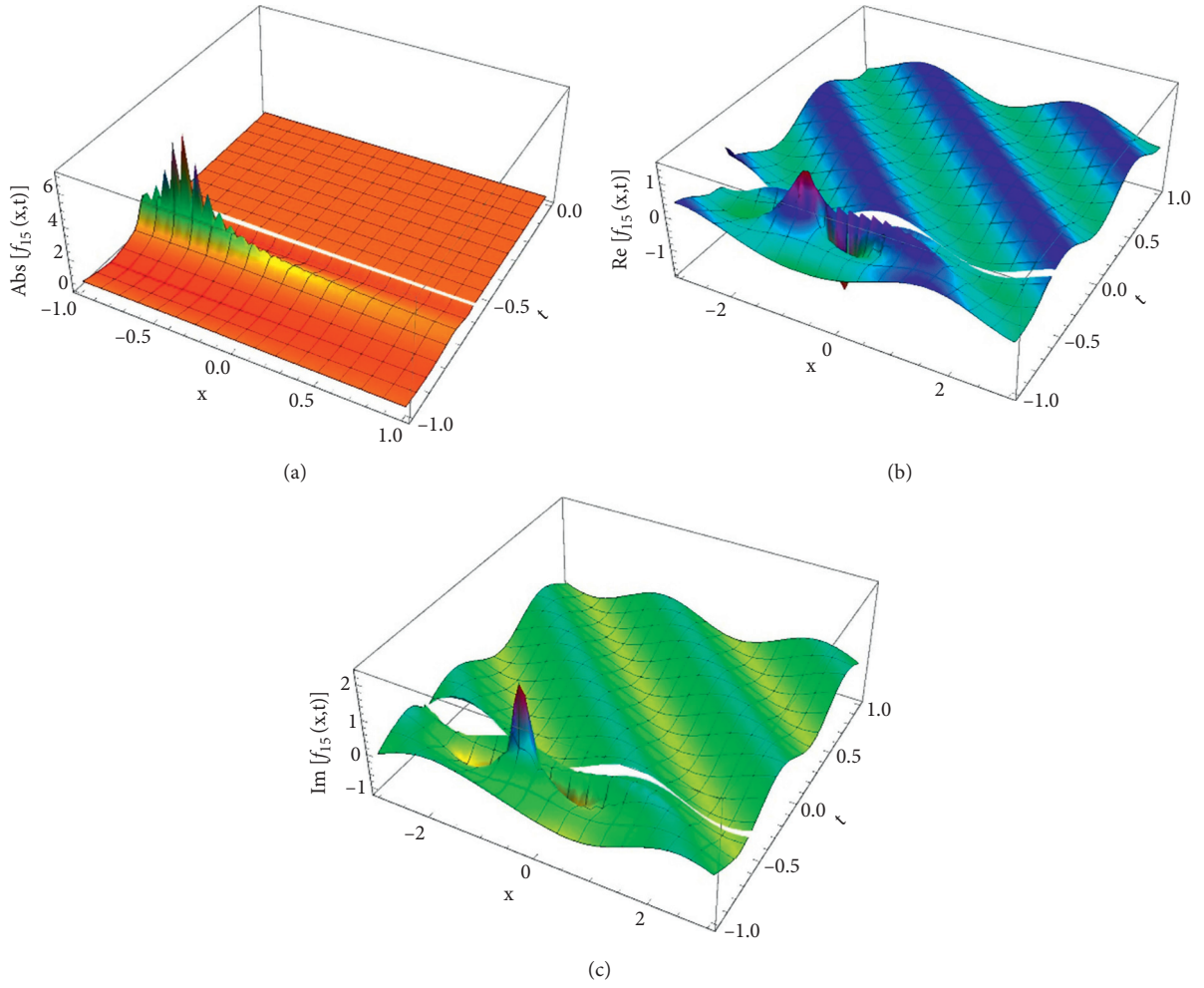


FIGURE 3: Optical soliton wave solutions of the absolute (a), real (b), and imaginary (c) value of equation (18) in three-dimensional view when $(A = 3, \gamma_1 = 1, A = -2, a_1 = 4, b_0 = 5, b_1 = -1, \text{ and } h = 2)$.

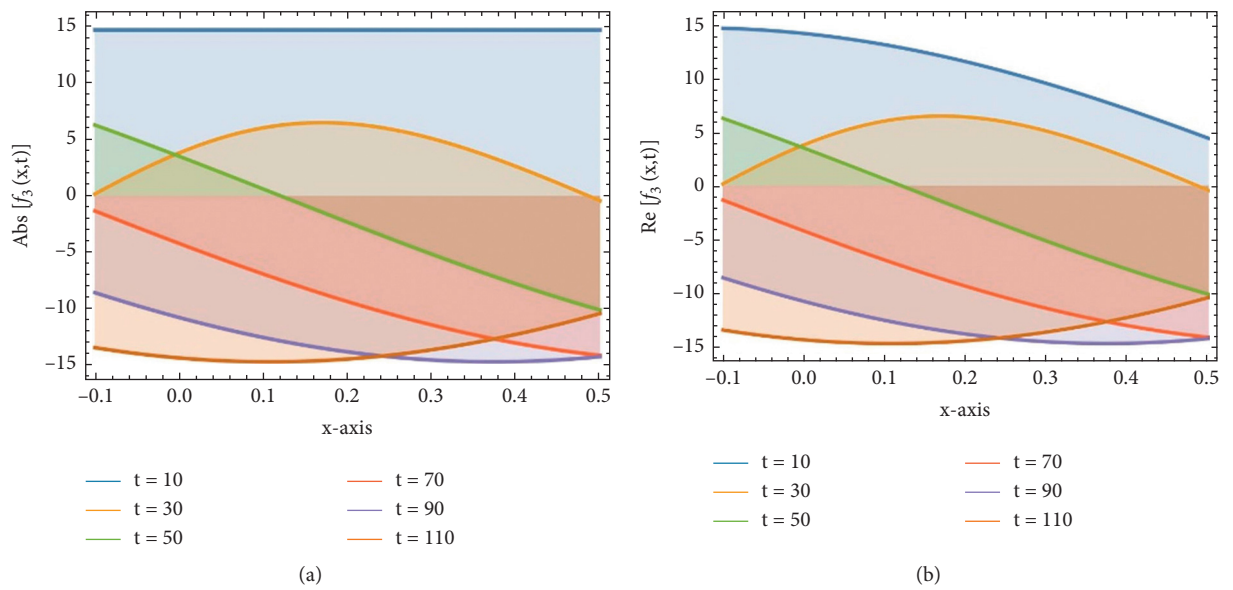


FIGURE 4: Continued.

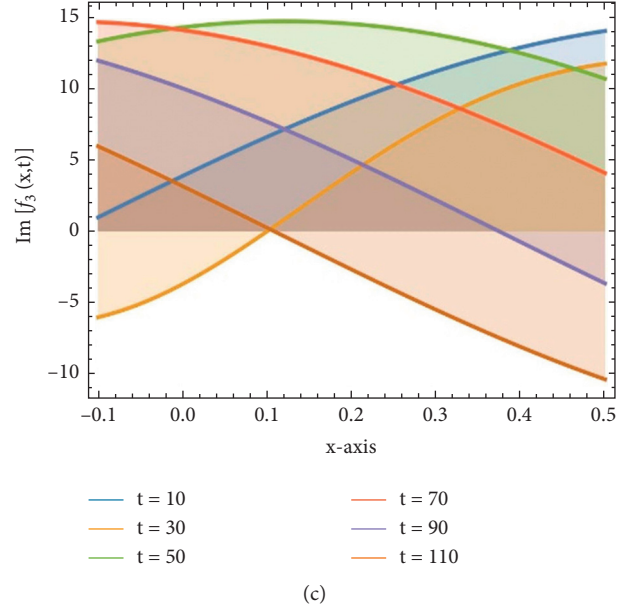


FIGURE 4: Optical soliton wave solutions of the absolute (a), real (b), and imaginary (c) value of equation (18) in two-dimensional view when ($A = 3$, $\gamma_1 = 1$, $A = -2$, $a_1 = 4$, $b_0 = 5$, $b_1 = -1$, and $h = 2$).

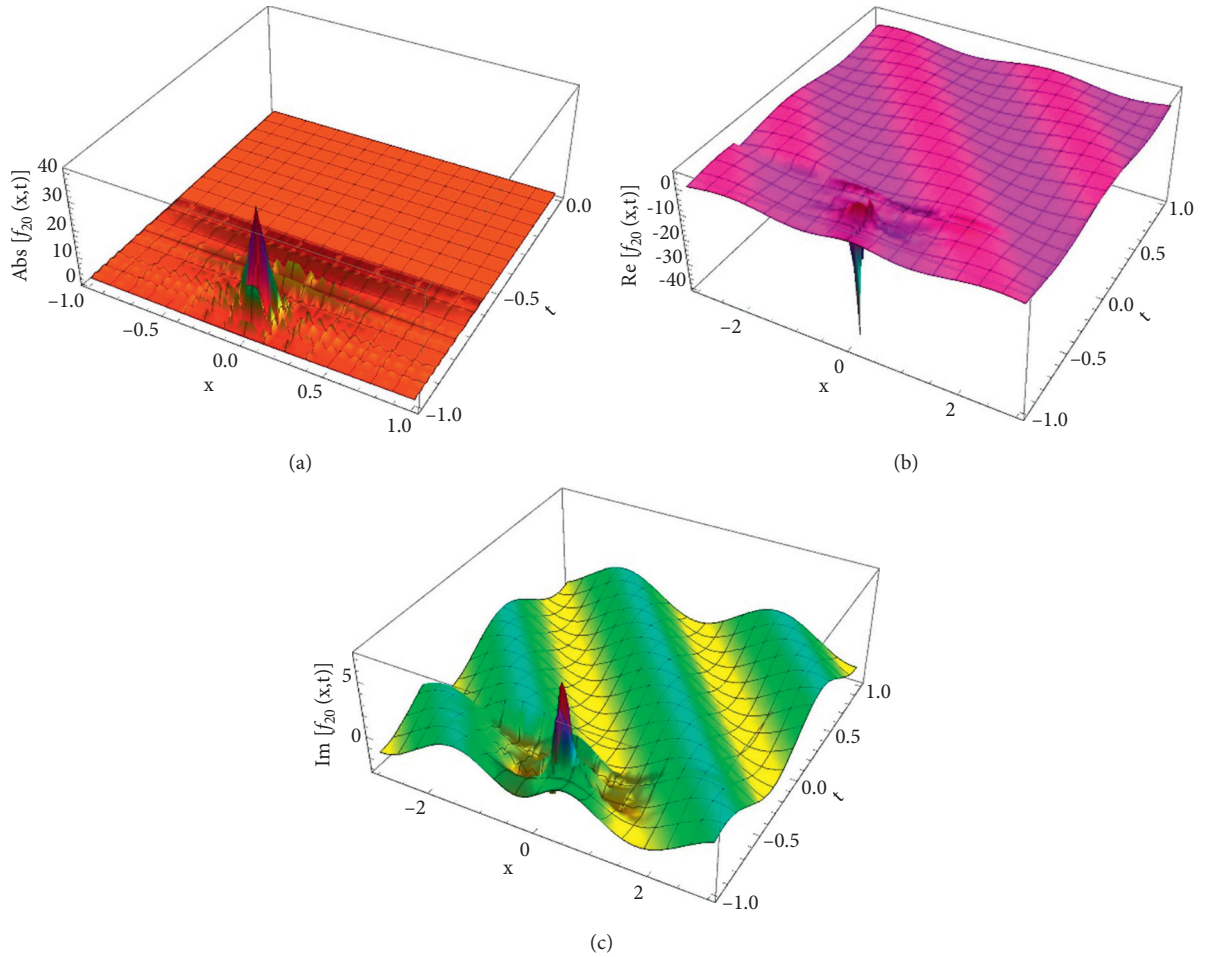


FIGURE 5: Optical soliton wave solutions of the absolute, real, and imaginary value of equation (26) in three-dimensional view ($\gamma_1 = 4$, $\vartheta = 0.5$, $\gamma_2 = -1$, $\gamma_3 = -4$, and $h = 2$).

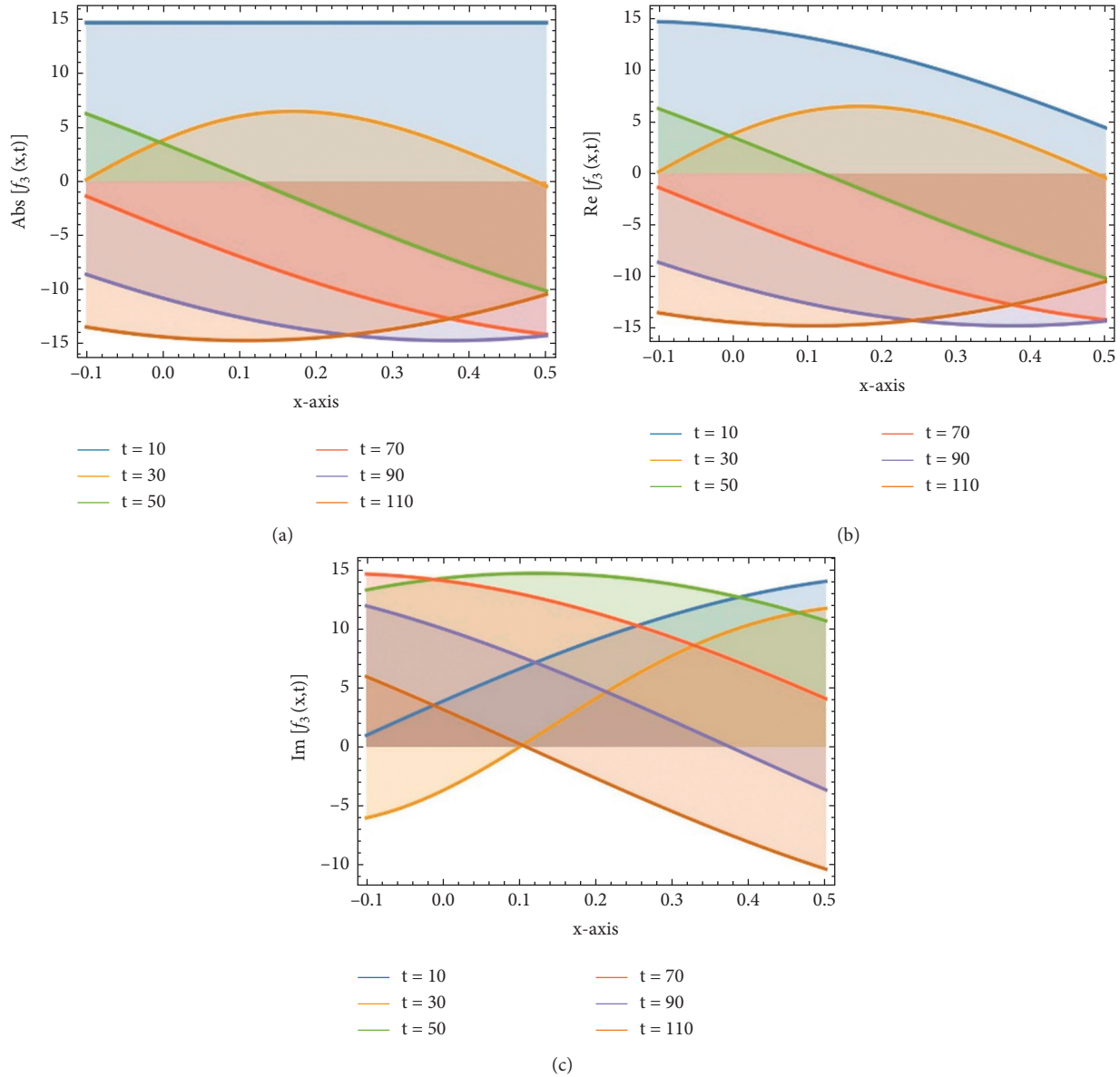


FIGURE 6: Optical soliton wave solutions of the absolute, real, and imaginary value of equation (26) in two-dimensional view when $(\gamma_1 = 4, \vartheta = 0.5, \gamma_2 = -1, \gamma_3 = -4, h = 2)$.

$[\gamma_1 = 4, \vartheta = 0.5, \gamma_2 = -1, \gamma_3 = -4, h = 2]$ in the next interval $x \in [-5, 5], t \in [-5, 5]$ to represent the wave propagation pattern of the wave along the x -axis.

5. Conclusion

The consistent fragmental derivative concept of Atangana successfully enables us to introduce three recent computational systems for the disturbed time-fractional nonlinear Schrödinger equation. This model has been given modern wave analytical solutions. We have researched the reliability of strategies to illustrate their potential to work in the sample implementations. The robust and efficient implementation of the computing schemes has been tested, demonstrating its capacity with an integer or fractional order to handle many nonlinear partial equations.

Data Availability

No data were used to support this study.

Conflicts of Interest

The authors declare that they have no conflicts of interest.

References




- [1] J. Manafian, O. A. Ilhan, O. Alp Ilhan, and S. Abid Mohammed, "Forming localized waves of the nonlinearity of the DNA dynamics arising in oscillator-chain of Peyrard-Bishop model," *AIMS Mathematics*, vol. 5, no. 3, pp. 2461–2483, 2020.
- [2] O. A. Ilhan, J. Manafian, A. A. Alizadeh, and H. M. Baskonus, "New exact solutions for nematicons in liquid crystals by the

- $\tan(\phi/2)$ -expansion method arising in fluid mechanics," *The European Physical Journal Plus*, vol. 135, no. 3, pp. 1–19, 2020.
- [3] J. Manafian, O. A. Ilhan, K. K. Ali, and S. Abid, "Cross-kink wave solutions and semi-inverse variational method for $(3+1)$ -dimensional potential-YTSE equation," *East Asian Journal on Applied Mathematics*, vol. 10, no. 3, pp. 549–565, 2020.
 - [4] Q. Lu, O. A. Ilhan, J. Manafian, and L. Avazpour, "Multiple rogue wave solutions for a variable-coefficient Kadomtsev–Petviashvili equation," *International Journal of Computer Mathematics*, vol. 98, no. 7, pp. 1457–1473, 2020.
 - [5] M. Dehghan, J. Manafian, and A. Saadatmandi, "Analytical treatment of some partial differential equations arising in mathematical physics by using threeexp-function method," *International Journal of Modern Physics B*, vol. 25, no. 22, pp. 2965–2981, 2011.
 - [6] P. Wan, J. Manafian, H. F. Ismael, and S. A. Mohammed, "Investigating one-, two-, and triple-wave solutions via multiple exp-function method arising in engineering sciences," *Advances in Mathematical Physics*, vol. 2020, Article ID 8018064, 18 pages, 2020.
 - [7] C. Yue, D. Lu, M. M. Khater, A. H. Abdel-Aty, W. Alharbi, and R. A. Attia, "On explicit wave solutions of the fractional nonlinear DSW system via the modified khater method," *Fractals*, vol. 28, no. 8, Article ID 2040034, 2020.
 - [8] T. A. Sulaiman, U. Younas, A. Yusuf, M. Younis, M. Bilal, and Shafqat-Ur-Rehman, "Extraction of new optical solitons and MI analysis to three coupled Gross-Pitaevskii system in the spinor Bose-Einstein condensate," *Modern Physics Letters B*, vol. 35, no. 6, Article ID 2150109, 2021.
 - [9] A. H. Abdel-Aty, M. M. Khater, R. A. Attia, M. Abdel-Aty, and H. Eleuch, "On the new explicit solutions of the fractional nonlinear space-time nuclear model," *Fractals*, vol. 28, no. 8, Article ID 2040035, 2020.
 - [10] M. Alquran, F. Yousef, F. Alquran, T. A. Sulaiman, and A. Yusuf, "Dual-wave solutions for the quadratic-cubic conformable-Caputo time-fractional Klein-Fock-Gordon equation," *Mathematics and Computers in Simulation*, vol. 185, pp. 62–76, 2021.
 - [11] M. Alquran, I. Jaradat, A. Yusuf, and T. A. Sulaiman, "Heart-cusp and bell-shaped-cusp optical solitons for an extended two-mode version of the complex Hirota model: application in optics," *Optical and Quantum Electronics*, vol. 53, no. 1, pp. 1–13, 2021.
 - [12] J. Dan, S. Sain, A. Ghose-Choudhury, and S. Garai, "Solitary wave solutions of nonlinear PDEs using Kudryashov's R function method," *Journal of Modern Optics*, vol. 67, no. 19, pp. 1499–1507, 2021.
 - [13] J. Li, R. A. M. Attia, M. M. A. Khater, and D. Lu, "The new structure of analytical and semi-analytical solutions of the longitudinal plasma wave equation in a magneto-electro-elastic circular rod," *Modern Physics Letters B*, vol. 34, no. 12, Article ID 2050123, 2020.
 - [14] H. Ahmad, T. A. Khan, P. S. Stanimirovic, and I. Ahmad, "Modified variational iteration technique for the numerical solution of fifth order KdV type equations," *Journal of Applied and Computational Mechanics*, vol. 6, pp. 1220–1227, 2020.
 - [15] K. S. Al-Ghafri and E. V. Krishnan, "Comment on: 'Exact analytic solitary wave solutions for the RKL model' [math. Comput. Simulation 80 (4)(2009) 849–854]," *Mathematics and Computers in Simulation*, vol. 181, pp. 113–116, 2021.
 - [16] M. H. Srivastava, H. Ahmad, I. Ahmad, P. Thounthong, and N. M. Khan, "Numerical simulation of three-dimensional fractional-order convection-diffusion PDEs by a local meshless method," *Thermal Science*, vol. 25, pp. 347–358, 2020.
 - [17] J.-H. He, N. Qie, and C.-H. He, "Solitary waves travelling along an unsmooth boundary," *Results in Physics*, vol. 24, Article ID 104104, 2021.
 - [18] R. M. Jena and S. Chakraverty, "Residual power series method for solving time-fractional model of vibration equation of large membranes," *Journal of Applied and Computational Mechanics*, vol. 5, no. 4, pp. 603–615, 2019.
 - [19] C. Yue, M. M. A. Khater, R. A. M. Attia, and D. Lu, "Computational simulations of the couple Boiti-Leon-Pempinelli (BLP) system and the $(3+1)$ -dimensional Kadomtsev-Petviashvili (KP) equation," *AIP Advances*, vol. 10, no. 4, Article ID 045216, 2020.
 - [20] V. S. Guliyev, A. Ali, S. . Çelik, and M. N. Omarova, "Higher Order Riesz Transforms Related to Schrodinger Type Operator on Local Generalized Morrey Spaces," *Journal of Pure and Applied Mathematics*, vol. 10, no. 1, pp. 58–75, 2019.
 - [21] D. Baleanu and J. Hassan Kamil, "A novel approach for korteweg-de vries equation of fractional order," *Journal of Applied and Computational Mechanics*, vol. 5, no. 2, pp. 192–198, 2019.
 - [22] M. M. A. Khater, R. A. M. Attia, and D. Lu, "Computational and numerical simulations for the nonlinear fractional Kolmogorov-Petrovskii-Piskunov (FKPP) equation," *Physica Scripta*, vol. 95, no. 5, Article ID 055213, 2020.
 - [23] C. Liu, H. Wang, and Z. Feng, "Global solution for a sixth-order nonlinear Schrödinger equation," *Journal of Mathematical Analysis and Applications*, vol. 490, no. 2, Article ID 124327, 2020.
 - [24] G. la Forgia, T. Tokyay, C. Adduce, and G. Constantinescu, "Bed shear stress and sediment entrainment potential for breaking of internal solitary waves," *Advances in Water Resources*, vol. 135, Article ID 103475, 2020.
 - [25] N. Faraz, M. Sadaf, G. Akram, I. Zainab, and Y. Khan, "Effects of fractional order time derivative on the solitary wave dynamics of the generalized ZK-Burgers equation," *Results in Physics*, vol. 25, Article ID 104217, 2021.
 - [26] S. El-Ganaini and E. M. E. Zayed, "Short comment on 'the extended simplest equation method and the $(G'/G-1/G)$ -expansion method'," *Optik*, vol. 206, Article ID 164258, 2020.
 - [27] O. A. Arqub and M. Al-Smadi, "Fuzzy conformable fractional differential equations: novel extended approach and new numerical solutions," *Soft Computing*, vol. 24, no. 16, pp. 12501–12522, 2020.
 - [28] A.-A. Hyder and M. A. Barakat, "General improved Kudryashov method for exact solutions of nonlinear evolution equations in mathematical physics," *Physica Scripta*, vol. 95, no. 4, Article ID 045212, 2020.
 - [29] S. F. Tian, X. F. Wang, T. T. Zhang, and W. H. Qiu, "Stability analysis, solitary wave and explicit power series solutions of a $(2+1)$ -dimensional nonlinear Schrödinger equation in a multicomponent plasma," *International Journal of Numerical Methods for Heat & Fluid Flow*, vol. 31, no. 5, pp. 1732–1748, 2021.
 - [30] D. D. Ganji and M. Abdollahzadeh, "Exact travelling solutions for the Lax's seventh-order KdV equation by sech method and rational exp-function method," *Applied Mathematics and Computation*, vol. 206, no. 1, pp. 438–444, 2008.
 - [31] M. Guo, H. Dong, J. Liu, and H. Yang, "The time-fractional mZK equation for gravity solitary waves and solutions using sech-tanh and radial basic function method," *Nonlinear Analysis: Modelling and Control*, vol. 24, no. 1, pp. 1–19, 2019.

- [32] A. Yildirim, "An algorithm for solving the fractional nonlinear schrödinger equation by means of the homotopy perturbation method," *International Journal of Nonlinear Sciences and Numerical Stimulation*, vol. 10, no. 4, pp. 445–450, 2009.
- [33] M. Ilie, J. Biazar, and Z. Ayati, "Resonant solitons to the nonlinear Schrödinger equation with different forms of nonlinearities," *Optik*, vol. 164, pp. 201–209, 2018.
- [34] M. Younis, H. ur Rehman, S. T. R. Rizvi, and S. A. Mahmood, "Dark and singular optical solitons perturbation with fractional temporal evolution," *Superlattices and Microstructures*, vol. 104, pp. 525–531, 2017.
- [35] S. Kumar, A. Kumar, and D. Baleanu, "Two analytical methods for time-fractional nonlinear coupled Boussinesq-Burger's equations arise in propagation of shallow water waves," *Nonlinear Dynamics*, vol. 85, no. 2, pp. 699–715, 2016.
- [36] Y. Z. Sun, Q. J. Liu, Y. H. Song, and T. L. Shen, "Hamiltonian modelling and nonlinear disturbance attenuation control of TCSC for improving power system stability," *IEE Proceedings-Control Theory and Applications*, vol. 149, no. 4, pp. 278–284, 2002.
- [37] M. Ramírez Barrios, J. Collado, and F. Dohnal, "Stability of coupled and damped Mathieu equations utilizing symplectic properties," in *Nonlinear Dynamics of Structures, Systems and Devices*, pp. 137–145, Springer, Cham, Switzerland, 2020.

Research Article

Noninteger Derivative Order Analysis on Plane Wave Reflection from Electro-Magneto-Thermo-Microstretch Medium with a Gravity Field within the Three-Phase Lag Model

S. H. Elhag,¹ Fatimah S. Bayones,¹ A. A. Kilany ,² S. M. Abo-Dahab ,³
Emad A.-B. Abdel-Salam,⁴ M. Elsagheer,² and A. M. Abd-Alla ²

¹Department of Mathematics and Statistics, College of Science, Taif University, PO. Box 11099, Taif 21944, Saudi Arabia

²Department of Mathematics Faculty of Science, Sohag University, Egypt

³Department of Computer Science, Faculty of Computers and Information, Luxor University, Egypt

⁴Department of Mathematics, Faculty of Science, New Valley University, Egypt

Correspondence should be addressed to A. A. Kilany; arabyatef@yahoo.com

Received 27 April 2021; Revised 28 June 2021; Accepted 18 November 2021; Published 6 January 2022

Academic Editor: Younes Menni

Copyright © 2022 S. H. Elhag et al. This is an open access article distributed under the Creative Commons Attribution License, which permits unrestricted use, distribution, and reproduction in any medium, provided the original work is properly cited.

The present research paper illustrates how noninteger derivative order analysis affects the reflection of partial thermal expansion waves under the generalized theory of plane harmonic wave reflection from a semivacuum elastic solid material with both gravity and magnetic field in the three-phase lag model (3PHL). The main goal for this study is investigating the fractional order impact and the applications related to the orders, especially in biology, medicine, and bioinformatics, besides the integer order considering an external effect, such as electromagnetic, gravity, and phase lags in a microstretch medium. The problem fractional form was formulated, and the boundary conditions were applied. The results were displayed graphically, considering the 3PHL model with magnetic field, gravity, and relaxation time. These findings were an explicit comparison of the effect of the plane wave reflection amplitude with integer derivative order analysis and noninteger derivative order analysis. The fractional order was compared to the correspondence integer order that indicated to the difference between them and agreement with the applications in biology, medicine, and other related topics. This phenomenon has more applications in relation to the biology and biomathematics problems.

1. Introduction

Recently, due attention has been made to study the interaction between electromagnetic field, thermal field, gravity, and the influence of microstretch due to its utilitarian features within different domains, such as physics, geophysics, geology, astronomy, and engineering. Choudhuri [1] proposed the problem of thermoelasticity theory with 3PHL. Kumar et al. [2] explored the plane strain problem within microstretch elastic solid. Kumar and Partap [3] examined the reflection of plane waves in a heat flux-dependent microstretch thermoelastic solid half space. Lord and Shulman [4] established generalized theories in which they replaced the Fourier law of thermal conductivity by Maxwell-Cattaneo law introducing a thermal relaxation time parameter within

Fourier's law. Green and Lindsay [5] illustrated binary relaxation parameters at the constitutive relationships regarding the entropy and stress tensor. After some years, Green and Naghdi [6–8] introduced new three models known as GN-I, GN-II, and GN-III. They argued that the linearized form of model-I agrees with the classical thermoelastic one. In model-II, the internal production rate of is typically zero, suggesting no dissipation of thermal energy. The model discloses undamped thermoelastic waves in a thermoelastic material. It is primarily indicated as the theory of thermoelasticity in the absence of the dissipation of energy. The former models are combined in model-III as special cases. The model discloses energy dissipation generally. Abbas and Kumar [9] discussed deformation because of the heat source in micropolar generalized thermoelastic

half-space using the finite element technique. The authors of [10] explored the stable solutions concerning the 3PHL thermal conductivity. Utilizing the theory, Kar and Kanoria [11] and Banik and Kanoria [12] resolved various issues.

The initial stresses in solids considerably affect the mechanical response of the material from a primarily stressed configuration. They are widely applied in soft biological tissues' performance, engineering structures, and geophysics. Elsaygher and Abo-Dahab [13] discussed the reflection of thermoelastic waves from insulated boundary fiber-reinforced half-space affected by the magnetic field and rotation. Abo-Dahab et al. [14] employed the Lord-Shulman and dual-phase lag models to explore how rotation and gravity affect an electro-magneto-thermoelastic medium in the presence of diffusion and voids. Using three thermoelastic theories, the authors of [15] discussed SV-waves occurrence at the interface between solid-liquid media under the initial stress and electromagnetic field. Abo-Dahab et al. [16] studied the impact of rotation and gravity on the reflection of P-waves from thermo-magneto-microstretch medium within the 3PHL model with initial stress.

Several definitions were introduced concerning fractional derivatives. For instance, Riemann–Liouville's definition is characterized by the fractional derivative of constant is not zero and applied for the non-differentiable functions. Caputo's definition can be applied to differentiable functions, and zero is the value of the fractional derivative of constant [17].

The fractional differential equations' theory and applications were studied by Kilbas et al. [18]. Hilfer [17] discussed the uses of fractional calculus in physics. Katugampola [19] used a novel method to a generalized fractional integral. The authors of [20] discussed analytically solving the space-time fractional nonlinear Schrödinger equation. Abdel-Salam and Hassan [21] studied solving the class of linear and nonlinear fractional differential equations. Abdel-Salam and Yousif [22] discussed solving the nonlinear space-time fractional differential equations by the fractional Riccati expansion approach. The approximate solution to the fractional Lane-Emden kind equations was studied by Nouh and Abdel-Salam [23]. Examining the fractional derivative for natural convection in a slanted cavity having porous media was discussed by Ahmed et al. [24]. The authors of [25] discussed the impacts of the rotation, voids, magnetic field, and initial stress on plane waves in generalized thermoelasticity. Marin et al. [26] explained extending the domain of the influence theory concerning the generalized thermoelasticity of anisotropic material in the presence of voids. Saeed et al. [27] discussed the GL model on the thermoelastic interaction in a poroelastic material by the finite element approach. Abo-Dahab et al. [28] discussed the impact of the electromagnetic field in the fiber-reinforced micropolar thermoelastic medium in the context of four models.

Many authors in [29–36] studied various applications of fractional calculus in mathematical modeling with a comparison to constant cases with physics properties. The analysis of the fractional derivative order and temperature-dependent characteristics on P- and SV-waves reflection influenced by initial stress and 3PHL model were considered

by Abo-Dahab et al. [37]. Alotaibi et al. [38] studied the fractional calculus of thermoelastic P-wave reflection influenced by the electromagnetic fields and gravity. Hobiny and Abbas [39] analytically solved the fractional order photo-thermoelasticity within a nonhomogenous semiconductor medium. Povstenko and Kyrylych [40] illustrated the fractional thermoelasticity issue concerning a plane with a line crack influenced by heat flux loading.

Many researchers in [41–47] investigated the effect of several variables in thermoelasticity with different models and archived all conditions to these models.

In this paper, the reflection of the plane waves from a semivacuum elastic solid material with the electromagnetic field and gravitational under the influence of relaxation times was studied. The necessary comparisons were made to simplify and explain the phenomenon at the fractional and non-fractional differentiations. The reflection appeared in the effect of the amplitude of the plane waves where the presence of the fractional differential was evident in each of the different results of the phenomenon. The fractional order was compared to the correspondence integer order that indicated the application and agreement with the applications in biology, bioinformatics, medicine, and related topics.

1.1. Formulation of the Problem. We utilized the generalized fractional thermo-microstretch's equations in a rectangular coordinate scheme (x, y, z) with z -axis directed into the media. We take the constant magnetic field intensity $H = (0, H_0, 0)$ to represent the y -axis direction. We consider with linearized equations of electrodynamics in the presence of displacement current due to motion as (Ezzat [48])

$$\begin{aligned}
 J &= \text{curl}_\alpha h - \varepsilon_0 D_t^\alpha E, \nabla_\alpha \\
 &= D_x^\alpha \underline{i} + D_y^\alpha \underline{j} + D_z^\alpha \underline{k}, \text{curl}_\alpha h \\
 &= \nabla_\alpha \times h = \begin{vmatrix} \underline{i} & \underline{j} & \underline{k} \\ D_x^\alpha & D_y^\alpha & D_z^\alpha \\ 0 & h_2 & 0 \end{vmatrix}, \\
 \text{curl}_\alpha E &= -\mu_0 D_t^\alpha h, \text{curl}_\alpha E \\
 &= \nabla_\alpha \times E = \begin{vmatrix} \underline{i} & \underline{j} & \underline{k} \\ D_x^\alpha & D_y^\alpha & D_z^\alpha \\ E_1 & 0 & E_3 \end{vmatrix}, \\
 E &= -\mu_0 (D_t^\alpha u \times H), D_t^\alpha u \times H = | \\
 &\underline{i} \underline{j} \underline{k} D_t^\alpha u_1 0 D_t^\alpha u_3 0 H_0 0 |, \nabla_\alpha \cdot h = 0, D_t^\alpha h_2 = 0. \quad (1)
 \end{aligned}$$

The fractional motion equation with gravitational and Lorentz's body forces as (Paria [49], Lord and Shulman [4])

$$D_t^\alpha \sigma_{ei} + F_i + G_i = \rho D_t^\alpha u_i, \quad (2)$$

where

$$F_i = \mu_0 (J \times H)_i, G_i = \rho g (D_x^\alpha u_3, 0, -D_z^\alpha u_1). \quad (3)$$

Using the previous equations, the following equations are obtained:

$$E = \mu_0 H_0 (D_t^\alpha u_3, 0, -D_t^\alpha u_1), \quad (4)$$

$$h = (0, h_2, 0) = (0, h, 0) = (0, -H_0 e, 0) e = D_x^\alpha u_1 + D_z^\alpha u_3, \quad (5)$$

$$\begin{aligned} J &= (-D_z^\alpha h - \varepsilon_0 \mu_0 H_0 D_t^{\alpha\alpha} u_3, 0, D_x^\alpha h + \varepsilon_0 \mu_0 H_0 D_t^{\alpha\alpha} u_1) \\ &= H_0 (-D_z^\alpha D_x^\alpha u_1 - D_z^{\alpha\alpha} u_3 - \varepsilon_0 \mu_0 D_t^{\alpha\alpha} u_3, 0, D_x^{\alpha\alpha} u_1 \\ &\quad + D_x^\alpha D_z^\alpha u_3 + \varepsilon_0 \mu_0 D_t^{\alpha\alpha} u_1). \end{aligned} \quad (6)$$

From equations (3) and (5), we obtain

$$\begin{aligned} F &= (F_1^\alpha, F_2^\alpha, F_3^\alpha) \\ &= (\mu_0 H_0^2 D_x^\alpha e - \varepsilon_0 \mu_0^2 H_0^2 D_t^{\alpha\alpha} u_1, 0, \mu_0 H_0^2 D_z^\alpha e - \varepsilon_0 \mu_0^2 H_0^2 D_t^{\alpha\alpha} u_3) \\ &= \mu_0 H_0^2 (D_x^{\alpha\alpha} u_1 + D_x^\alpha D_z^\alpha u_3 - \varepsilon_0 \mu_0 D_t^{\alpha\alpha} u_1, 0, D_z^{\alpha\alpha} u_1 \\ &\quad + D_z^\alpha D_x^\alpha u_3 - \varepsilon_0 \mu_0 D_t^{\alpha\alpha} u_3). \end{aligned} \quad (7)$$

So, the displacement vector $u = (u_1, u_2, u_3)$ has the components $u_1 = u_1(x, z, t)$, $u_2 = 0$, $u_3 = u_3(x, z, t)$.

The basic governing equations become

$$\begin{aligned} (\lambda + \mu)(D_x^{\alpha\alpha} u_1 + D_x^\alpha D_z^\alpha u_3) + (\mu + k)(D_x^{\alpha\alpha} u_1 + D_z^{\alpha\alpha} u_1) \\ - k D_z^\alpha \varphi_2 + \lambda_0 D_x^\alpha \varphi^* - \widehat{\gamma} D_x^\alpha T + F_1 + \rho g D_x^\alpha u_3 = \rho D_t^{\alpha\alpha} u_1, \end{aligned} \quad (8)$$

$$\begin{aligned} (\lambda + \mu)(D_x^{\alpha\alpha} u_3 + D_x^\alpha D_z^\alpha u_1) + (\mu + k)(D_x^{\alpha\alpha} u_3 + D_z^{\alpha\alpha} u_3) \\ + k D_x^\alpha \varphi_2 + \lambda_0 D_z^\alpha \varphi^* - \widehat{\gamma} D_z^\alpha T + F_3 - \rho g D_z^\alpha u_1 = \rho D_t^{\alpha\alpha} u_3, \end{aligned} \quad (9)$$

$$(a + b + c) \nabla_\alpha (\nabla_\alpha \cdot \varphi) - c \nabla_\alpha \times (\nabla_\alpha \times \varphi) + k (\nabla_\alpha \times u) - 2k \varphi = \rho j D_t^{\alpha\alpha} \varphi, \quad (10)$$

$$\alpha_0 \nabla_\alpha^2 \varphi^* - \frac{1}{3} b_1 \varphi^* - \frac{1}{3} b_0 (\nabla_\alpha \cdot u) + \frac{1}{3} \widehat{\gamma}_1 T = \frac{3}{2} \rho j D_t^{\alpha\alpha} \varphi^*, \quad (11)$$

$$\begin{aligned} (K^* + \tau_v^* D_t^\alpha + K \tau_T D_t^{\alpha\alpha}) \nabla_\alpha^2 T = \left(1 + \tau_q D_t^\alpha + \frac{\tau_q^2}{2} D_t^{\alpha\alpha} \right) \\ \cdot [\rho C_e D_t^{\alpha\alpha} T + \widehat{\gamma} T_0 D_t^{\alpha\alpha} e + \widehat{\gamma}_1 T_0 D_t^{\alpha\alpha} \varphi^*]. \end{aligned} \quad (12)$$

Such that $\tau_v^* = K + K^* \tau_v$, $\nabla_\alpha^2 = D_x^{\alpha\alpha} + D_z^{\alpha\alpha}$.

$$\begin{aligned} \sigma_{i\ell} &= (b_0 \varphi^* + \lambda D_r^\alpha u_r) \delta_{i\ell} + (\mu + k) D_i^\alpha u_\ell + \mu D_\ell^\alpha u_i \\ &\quad - k \varepsilon_{i\ell r} \varphi_r - \widehat{\gamma} T \delta_{i\ell}, \end{aligned}$$

$$m_{i\ell} = a D_r^\alpha \varphi_r \delta_{i\ell} + b D_\ell^\alpha \varphi_i + c D_i^\alpha \varphi_\ell,$$

$$\lambda_i = a_0 D_i^\alpha \varphi^*. \quad (13)$$

The constitutive relations take the following form:

$$\sigma_{xx} = (\lambda + 2\mu + k) D_x^\alpha u_1 + \lambda D_z^\alpha u_3 + b_0 \varphi^* - \widehat{\gamma} T,$$

$$\sigma_{zz} = (\lambda + 2\mu + k) D_z^\alpha u_3 + \lambda D_x^\alpha u_1 + b_0 \varphi^* - \widehat{\gamma} T,$$

$$\begin{aligned} \sigma_{xz} &= \mu D_z^\alpha u_1 + (\mu + k) D_x^\alpha u_3 + k \varphi_2, \sigma_{zx} \\ &= \mu D_x^\alpha u_3 + (\mu + k) D_z^\alpha u_1 - k \varphi_2, \end{aligned}$$

$$m_{xy} = c D_x^\alpha \varphi_2, m_{zy} = c D_z^\alpha \varphi_2,$$

$$\lambda_x = a_0 D_x^\alpha \varphi^*, \lambda_z = a_0 D_z^\alpha \varphi^*. \quad (14)$$

Moreover, we introduce these dimensionless quantities to make the solution easier

$$\begin{aligned} x_i' &= \frac{\omega^*}{c_0} x_i, u_i' = \frac{\rho c_0 \omega^*}{\widehat{\gamma} T_0} u_i, \Theta' \\ &= \frac{\widehat{\gamma}}{\rho c_0^2} (T - T_0), \{t', \tau_T', \tau_v', \tau_q'\} \\ &= \omega^* \{t, \tau_T, \tau_v, \tau_q\}, \sigma_{ij}' \\ &= \frac{\sigma_{ij}}{\widehat{\gamma} T_0}, m_{ij}' = \frac{\omega^*}{c_0 \widehat{\gamma} T_0} m_{ij}, \lambda_i' = \frac{\omega^*}{c_0 \widehat{\gamma} T_0} \lambda_i, \varphi'^* \\ &= \frac{\rho c_0^2}{\widehat{\gamma} T_0} \varphi^*, \varphi_2' = \frac{\rho c_0^2}{\widehat{\gamma} T_0} \varphi_2, g' = \frac{g}{c_0 \omega^*}, \omega^* \\ &= \frac{\rho C_e c_0^2}{k}, h' = \frac{h}{H_0}, \end{aligned} \quad (15)$$

$$c_0^2 = \frac{\lambda + 2\mu + k}{\rho}, i, j = 1, 2, 3. \quad (16)$$

Utilizing Equation (16), the governing Equations (8)–(12) recast in this form (after suppressing the primes)

$$\begin{aligned} \left(\frac{\mu + k}{\rho c_0^2} \right) \nabla_\alpha^2 u_1 + \left(\frac{\mu + \lambda}{\rho c_0^2} + R_H \right) D_x^\alpha e - \frac{k}{\rho c_0^2} D_z^\alpha \varphi_2 + \frac{\lambda_0}{\rho c_0^2} D_x^\alpha \varphi^* \\ - \frac{\rho c_0^2}{\widehat{\gamma} T_0} D_x^\alpha \Theta + g D_x^\alpha u_3 = \beta^2 D_t^{\alpha\alpha} u_1, \end{aligned} \quad (17)$$

$$\begin{aligned} \left(\frac{\mu + k}{\rho c_0^2} \right) \nabla_\alpha^2 u_3 + \left(\frac{\mu + \lambda}{\rho c_0^2} + R_H \right) D_z^\alpha e + \frac{k}{\rho c_0^2} D_x^\alpha \varphi_2 + \frac{\lambda_0}{\rho c_0^2} D_z^\alpha \varphi^* \\ - \frac{\rho c_0^2}{\widehat{\gamma} T_0} D_z^\alpha \Theta - g D_x^\alpha u_1 = \beta^2 D_t^{\alpha\alpha} u_3, \end{aligned} \quad (18)$$

$$\nabla_\alpha^2 \varphi_2 - \frac{2k c_0^2}{c_2 \omega^{*2}} \varphi_2 + \frac{k c_0^2}{c_2 \omega^{*2}} (D_z^\alpha u_1 - D_x^\alpha u_3) = \frac{\rho j c_0^2}{c_2} D_t^{\alpha\alpha} \varphi_2, \quad (19)$$

$$\left(\frac{C_1^2}{c_0^2} \nabla_\alpha^2 - \frac{C_2^2}{\omega^{*2}} - D_t^{\alpha\alpha} \right) \varphi^* - \frac{C_3^2}{\omega^{*2}} e + C_4 \Theta = 0, \quad (20)$$

$$(C_k + C_v D_t^\alpha + C_T D_t^{\alpha\alpha}) \nabla_\alpha^2 \Theta = \left(1 + \tau_q D_t^\alpha + \frac{\tau_q^2}{2} D_t^{\alpha\alpha} \right) \cdot [D_t^{\alpha\alpha} \Theta + \varepsilon_1 D_t^\alpha e + \varepsilon_2 D_t^{\alpha\alpha} \varphi^*], \quad (21)$$

$$\sigma_{xx} = a_1 \varphi^* + D_x^\alpha u_1 + a_2 D_z^\alpha u_3 - a_3 \Theta - 1, \quad (22)$$

$$\sigma_{zz} = a_1 \varphi^* + D_z^\alpha u_3 + a_2 D_x^\alpha u_1 - a_3 \Theta - 1, \quad (23)$$

$$\sigma_{xz} = a_4 D_z^\alpha u_1 + a_5 D_x^\alpha u_3 + a_6 \varphi_2, \quad (24)$$

$$\sigma_{zx} = a_4 D_z^\alpha u_3 + a_5 D_x^\alpha u_1 - a_6 \varphi_2, \quad (25)$$

$$m_{xy} = a_7 D_x^\alpha \varphi_2, \quad (26)$$

$$m_{zy} = a_7 D_z^\alpha \varphi_2, \quad (27)$$

$$\lambda_x = a_8 D_x^\alpha \varphi^*, \quad (28)$$

$$\lambda_z = a_8 D_z^\alpha \varphi^*, \quad (29)$$

where

$$\begin{aligned} R_H &= \frac{\mu_0 H_0^2}{\rho c_0^2}, b^2 = \left(1 + \frac{\varepsilon_0 \mu_0^2 H_0^2}{\rho} \right), (C_1^2, C_2^2, C_3^2) \\ &= \frac{2}{9\rho j} (3a_0, b_1, b_0), C_4 = \frac{2\rho c_0^4 \hat{\gamma}_1}{9j\gamma \Lambda^2 T_0 \omega^{*2}} \\ c_2 &= (2a + 2b + c), C = \frac{2c_0^2 \hat{\gamma}_1}{9j\hat{\gamma} \omega^{*2}}, (C_k, C_v, C_T) \\ &= \frac{1}{\rho c_0^2 C_e} (K^*, \tau_v^*, K\tau_T \omega^*), \varepsilon_1 = \frac{\gamma \Lambda^3 T_0}{\rho^3 c_0^4 C_e}, \\ \varepsilon_2 &= \frac{\hat{\gamma}_1 \gamma \Lambda^2 T_0^2}{\rho^3 c_0^4 C_e}, (a_1, a_2) = \frac{1}{\rho c_0^2} (b_0, \lambda), a_3 \\ &= \frac{\rho c_0^2}{\hat{\gamma} T}, (a_4, a_5, a_6) = \frac{1}{\rho c_0^2} (\mu, \mu + k, k), \\ (a_7, a_8) &= \frac{\omega^{*2}}{\rho c_0^4} (c, a_0). \end{aligned} \quad (30)$$

The components of the displacement $u_1(x, z, t)$ and $u_3(x, z, t)$ take the following form concerning the potential functions $\Phi(x, z, t)$ and $\Psi(x, z, t)$

$$u_1 = D_x^\alpha \Phi + D_z^\alpha \Psi, u_3 = D_z^\alpha \Phi - D_x^\alpha \Psi, \vec{\Psi} = (0, -\Psi, 0). \quad (31)$$

Using Equation (31) in Equations (17)–(21), we get

$$(\nabla_\alpha^2 - \zeta_0 D_t^{\alpha\alpha}) \Phi - \zeta_1 D_x^\alpha \Psi - \zeta_2 \Theta + \zeta_3 \varphi^* = 0, \quad (32)$$

$$\zeta_4 D_x^\alpha \Phi + (\nabla_\alpha^2 - \zeta_5 D_t^{\alpha\alpha}) \Psi - \zeta_6 \varphi_2 = 0, \quad (33)$$

$$\frac{kc_0^2}{c\omega^{*2}} \nabla_\alpha^2 \Psi + \left(\nabla_\alpha^2 - \frac{2kc_0^2}{c\omega^{*2}} - \frac{j\rho c_0^2}{c} D_t^{\alpha\alpha} \right) \varphi_2 = 0, \quad (34)$$

$$\left(\frac{C_1^2}{c_0^2} \nabla_\alpha^2 - \frac{C_2^2}{\omega^{*2}} - D_t^{\alpha\alpha} \right) \varphi^* - \frac{C_3^2}{\omega^{*2}} \nabla_\alpha^2 \Phi + a_0 \Theta = 0, \quad (35)$$

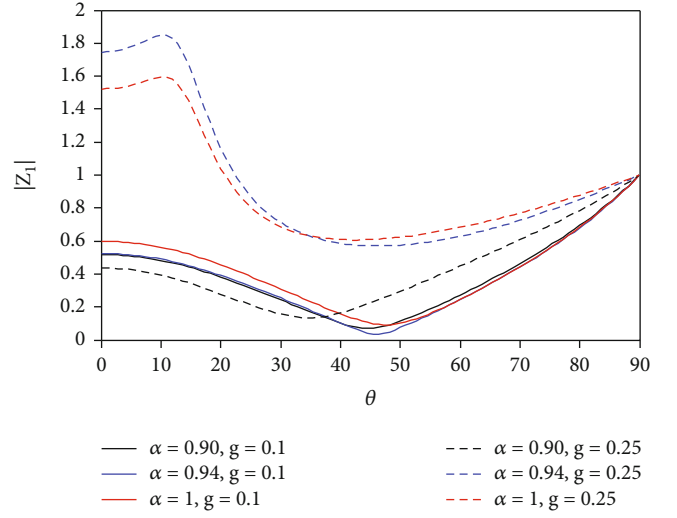


FIGURE 1: The various values of the amplitudes $|z_1|$ concerning the angle of incidence θ for various values of the fractional parameter of the diverse values of gravity g .

$$\begin{aligned} C_k \nabla_\alpha^2 \Theta + C_v \nabla_\alpha^2 (D_t^\alpha \Theta) + C_T \nabla_\alpha^2 (D_t^{\alpha\alpha} \Theta) &= \left(1 + \tau_q D_t^\alpha + \frac{\tau_q^2}{2} D_t^{\alpha\alpha} \right) \\ &\cdot [D_t^{\alpha\alpha} \Theta + \varepsilon_1 \nabla_\alpha^2 (D_t^{\alpha\alpha} \Phi) + \varepsilon_2 D_t^{\alpha\alpha} \varphi^*], \end{aligned} \quad (36)$$

where

$$\begin{aligned} (\zeta_0, \zeta_1, \zeta_2, \zeta_3) &= \frac{1}{1 + R_H} \left(b^2, g, \frac{\rho c_0^2}{\hat{\gamma} T_0}, \frac{b_0}{\rho c_0^2} \right), (\zeta_4, \zeta_5, \zeta_6) \\ &= \frac{\rho c_0^2}{\mu + k} \left(g, b^2, \frac{k}{\rho c_0^2} \right). \end{aligned} \quad (37)$$

1.2. Solution of the Problem. In this section, solving Equations (32)–(36) is assumed as

$$\begin{aligned} (\Phi, \Psi, \Theta, \varphi^*, \varphi_2) &= (\bar{\Phi}, \bar{\Psi}, \bar{\Theta}, \bar{\varphi}^*, \bar{\varphi}_2) \exp \\ &\cdot [i\xi(x^\alpha \sin \theta + z^\alpha \cos \theta) - i\omega t^\alpha]. \end{aligned} \quad (38)$$

Substituting from Equation (38) into Equations (32)–(36), the result is

$$\alpha^2 (-\xi^2 + \zeta_0 \omega^2) \bar{\Phi} - i\alpha \zeta_1 \xi \sin \theta \bar{\Psi} - \zeta_2 \bar{\Theta} + \zeta_3 \bar{\varphi}^* = 0, \quad (39)$$

$$i\alpha \zeta_4 \sin \theta \bar{\Phi} + \alpha^2 (-\xi^2 + \omega^2 \zeta_5) \bar{\Psi} - \zeta_6 \bar{\varphi}_2 = 0, \quad (40)$$

$$-\frac{k\alpha^2 \xi^2 c_0^2}{c\omega^{*2}} \bar{\Psi} + \left(-\alpha^2 \xi^2 + \frac{j\rho c_0^2 \omega^2 \alpha^2}{c} - \frac{2kc_0^2}{c\omega^{*2}} \right) \bar{\varphi}_2 = 0, \quad (41)$$

$$\frac{\alpha^2 \xi^2 C_3^2}{\omega^{*2}} \bar{\Phi} + a_0 \bar{\Theta} + \left(-\frac{\alpha^2 \xi^2 C_1^2}{c_0^2} - \frac{C_2^2}{\omega^{*2}} + \alpha^2 \omega^2 \right) \bar{\varphi}^* = 0, \quad (42)$$

$$-\varepsilon_1 \alpha^4 \xi^2 \omega^2 \tau_q^* \bar{\Phi} + \left[(-C_k + iC_v \alpha \omega + C_T \alpha^2 \omega^2) \alpha^2 \xi^2 + \alpha^2 \omega^2 \tau_q^* \right] \bar{\Theta} + \varepsilon_2 \alpha^2 \omega^2 \tau_q^* \bar{\varphi}^* = 0. \quad (43)$$

where $\tau_q^* = 1 - i\alpha\omega\tau_q - ((\alpha^2\omega^2\tau_q^2)/2)$.

To help identify the nontrivial solution, we change from Equation (39) into Equations (33)–(38) and get

$$\begin{vmatrix} \alpha^2(\zeta_0\omega^2 - \xi^2) & -i\alpha\xi_1 \sin \theta & -\zeta_2 & \zeta_3 & 0 \\ i\alpha\xi_4 \sin \theta & \alpha^2(-\xi^2 + \omega^2\zeta_5) & 0 & 0 & -\zeta_6 \\ 0 & -\frac{k\alpha^2\xi^2 c_0^2}{c\omega^{*2}} & 0 & 0 & \alpha^2\left(\frac{j\rho c_0^2\omega^2}{b} - \xi^2\right) - \frac{2kc_0^2}{b\omega^{*2}} \\ \frac{\alpha^2\xi^2 C_3^2}{\omega^{*2}} & 0 & a_0 & \alpha^2\left(\omega^2 - \frac{C_1^2\xi^2}{C_0^2}\right) - \frac{C_2^2}{\omega^{*2}} & 0 \\ -\varepsilon_1\alpha^4\xi^2\omega^2\tau_q^* & 0 & \alpha^2\xi^2(i\alpha\omega C_v + \alpha^2\omega^2 C_T - C_k) + \alpha^2\omega^2\tau_q^* & \varepsilon_2\alpha^2\omega^2\tau_q^* & 0 \end{vmatrix} = 0, \quad (44)$$

which tends to

$$L\alpha^{10}\xi^{10} + M\alpha^8\xi^8 + N\alpha^6\xi^6 + O\alpha^4\xi^4 + P\alpha^2\xi^2 + Q = 0. \quad (45)$$

where L, M, N, O, P , and Q are in the Appendix.

From Equation (45), we can identify five diverse velocities accompanying five waves.

After that, $\Phi, \Psi, \Theta, \varphi^*$, and φ_2 are written as

$$\begin{aligned} (\Phi, \Psi, \Theta, \varphi^*, \varphi_2) &= (1, \eta_0, \kappa_0, \chi_0, \vartheta_0) A_0 \exp \\ &\quad \cdot [i\xi(x^\alpha \sin \theta + z^\alpha \cos \theta) - i\omega t^\alpha] \\ &\quad \sum_{j=1}^5 \left(1, \eta_j, \kappa_j, \chi_j, \vartheta_j \right) A_j \exp [i\xi_j(x^\alpha \sin \theta_j - z^\alpha \cos \theta_j) - i\omega t^\alpha]. \end{aligned} \quad (46)$$

Based on Equations (40) and (41), the result is

$$\begin{aligned} \eta_j &= \frac{-i\xi_j \zeta_4 \sin \theta_j \left(\xi_j^2 - ((j\rho c_0^2 \alpha^2 \omega^2)/\hat{\gamma}) + (2kc_0^2/c\omega^{*2}) \right)}{\left(\xi_j^2 - \alpha^2 \omega^2 \zeta_5 \right) \left(\xi_j^2 - ((j\rho c_0^2 \alpha^2 \omega^2)/\hat{\gamma}) + (2kc_0^2/c\omega^{*2}) \right) - p^* \xi_j^2 \zeta_6}, \kappa_j \\ &= \frac{ip^* \xi_j^3 \zeta_4 \sin \theta_j}{\left(\xi_j^2 - \alpha^2 \omega^2 \zeta_5 \right) \left(\xi_j^2 - ((j\rho c_0^2 \alpha^2 \omega^2)/\hat{\gamma}) + (2kc_0^2/c\omega^{*2}) \right) - p^* \xi_j^2 \zeta_6}, \end{aligned} \quad (47)$$

where $p^* = kc_0^2/\gamma\omega^{*2}$.

Also, from Equations (42) and (43), we get

$$\chi_j = \frac{-\varepsilon_2 \alpha^2 \omega^2 \tau_q^* \xi_j^2 (C_3^2/\omega^{*2}) - \varepsilon_1 \alpha^2 \omega^2 \tau_q^* \xi_j^2 \left[-(C_1^2/c_0^2) \xi_j^2 - (C_2^2/\omega^{*2}) + \alpha^2 \omega^2 \right]}{a_0 \varepsilon_2 \alpha^2 \omega^2 \tau_q^* - \left[(-C_k - i\alpha\omega C_v + \alpha^2 \omega^2 C_T) \xi_j^2 + \alpha^2 \omega^2 \tau_q^* \right] \left[-(C_1^2/c_0^2) \xi_j^2 - (C_2^2/\omega^{*2}) + \alpha^2 \omega^2 \right]},$$

1.3. The Boundary Conditions. The problem's boundary conditions are written as follows:

$$\sigma_{zz} + \tau_{zz} = 0, \sigma_{xz} + \tau_{xz} = 0, D_z^\alpha T = 0, m_{yz} = 0, \lambda_x = 0, \text{at } z = 0, \quad (49)$$

$$\begin{aligned} \sum_{j=1}^5 \left[a_1 \vartheta_j - \mu_e H_0^2 \xi_j^2 - a_3 \xi_j^2 \left(\sin^2 \theta_j + \frac{\eta_j}{2} \sin 2\theta_j \right) - a_2 \xi_j^2 \left(\cos^2 \theta_j - \frac{\eta_j}{2} \sin 2\theta_j + \frac{k_j}{\xi_j^2} \right) \right] A_j \\ = \left[a_1 \vartheta_1 - \mu_e H_0^2 \xi_1^2 - a_3 \xi_1^2 \left(\sin^2 \theta_0 + \frac{\eta_1}{2} \sin 2\theta_0 \right) - a_2 \xi_1^2 \left(\cos^2 \theta_0 - \frac{\eta_1}{2} \sin 2\theta_0 + \frac{k_1}{\xi_1^2} \right) \right] A_0, \end{aligned} \quad (50)$$

$$\begin{aligned} \sum_{j=1}^5 \left[(a_4 + a_5) \frac{\xi_j^2}{2} \sin 2\theta_j + a_4 \xi_j^2 \eta_j \cos^2 \theta_j - a_5 \xi_j^2 \eta_j \sin^2 \theta_j + a_6 \xi_j \right] A_j \\ = \left[-(a_4 + a_5) \frac{\xi_1^2}{2} \sin 2\theta_0 + a_4 \xi_1^2 \eta_1 \cos^2 \theta_0 - a_5 \xi_1^2 \eta_1 \sin^2 \theta_0 + a_6 \xi_1 \right] A_0, \end{aligned} \quad (51)$$

$$\sum_{j=1}^5 k_j \xi_j \cos \theta_j A_j = k_1 \xi_1 \cos \theta_0 A_0, \quad (52)$$

$$\sum_{j=1}^5 \zeta_j \xi_j \cos \theta_j A_j = \zeta_1 \xi_1 \cos \theta_0 A_0. \quad (53)$$

Finally,

$$\sum_{j=1}^5 \vartheta_j \xi_j \cos \theta_j A_j = -\vartheta_1 \xi_1 \cos \theta_0 A_0. \quad (54)$$

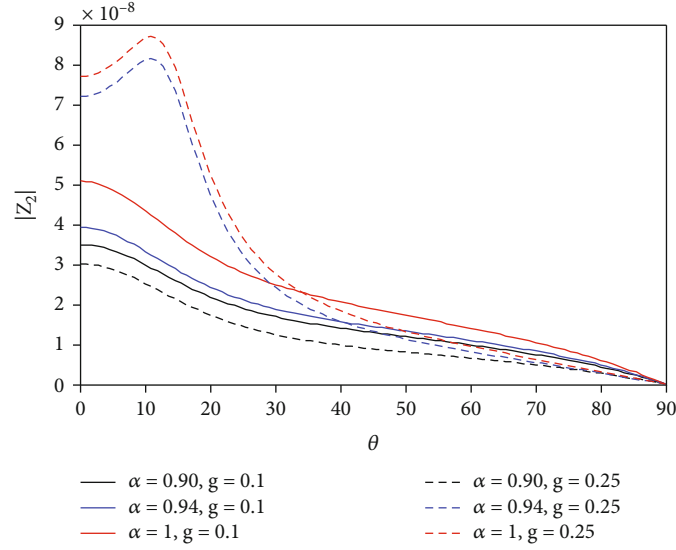


FIGURE 2: The various values of the amplitudes $|z_2|$ concerning the angle of incidence θ for various values of the fractional parameter of the diverse values of the values of gravity g .

Based on Equations (50)–(54), the result is

$$\begin{aligned}
 a_{ij}Z_j &= B_i, i, j = (1, 2, \dots, 5), Z_j = \frac{A_j}{A_0}, \\
 a_{1j} &= a_1\vartheta_j - \xi_j^2 \left[a_3 \left(\sin^2\theta_j + \frac{\eta_j}{2} \sin 2\theta_j \right) - a_2 \left(\cos^2\theta_j - \frac{\eta_j}{2} \sin 2\theta_j + \frac{k_j}{\xi_j^2} \right) + \mu_e H_0^2 \right], \\
 a_{2j} &= (a_4 + a_5) \frac{\xi_j^2}{2} \sin 2\theta_j + a_4 \xi_j^2 \eta_j \cos^2\theta_j - a_5 \xi_j^2 \eta_j \sin^2\theta_j + a_6 \xi_j, \\
 a_{3j} &= k_j \xi_j \cos \theta_j, a_{4j} = \zeta_j \xi_j \cos \theta_j A_j, a_{5j} = \vartheta_j \xi_j \cos \theta_j, \\
 B_1 &= -a_1\vartheta_1 + \xi_1^2 \left[a_3 \left(\sin^2\theta_0 + \frac{\eta_1}{2} \sin 2\theta_0 \right) - a_2 \left(\cos^2\theta_0 - \frac{\eta_1}{2} \sin 2\theta_0 + \frac{k_1}{\xi_1^2} \right) + \mu_e H_0^2 \right], \\
 B_2 &= -(a_4 + a_5) \frac{\xi_1^2}{2} \sin 2\theta_0 - a_4 \xi_1^2 \eta_1 \cos^2\theta_1 + a_5 \xi_1^2 \eta_1 \sin^2\theta_1 - a_6 \xi_1, \\
 B_3 &= k_1 \xi_1 \cos \theta_0, B_4 = \zeta_1 \xi_1 \cos \theta_0, B_5 = -\vartheta_1 \xi_1 \cos \theta_0.
 \end{aligned} \tag{55}$$

1.4. Numerical Results and Discussion. In this section, some numerical findings are discussed based on the illustration of the results obtained in the former sections and a comparison of such results in different cases.

Therefore, we chose these materials:

$$\begin{aligned}
 i &= \sqrt{-1}, a_0 = 0.779 \times 10^{-4}, b_0 = 0.5 \times 10^{11}, b_1 = 0.5 \times 10^{11}, j \\
 &= 0.2 \times 10^{-15}, \rho = 8954,
 \end{aligned}$$

$$\begin{aligned}
 C_e &= 383.1, k = 386, T_0 = 293, \lambda = 7.76 \times 10^{10}, \mu = 3.86 \times 10^{10}, c \\
 &= 0.779 \times 10^{-4},
 \end{aligned}$$

$$\begin{aligned}
 K^* &= 2.97 \times 10^{13}, \mu_0 = 0.1, \varepsilon_0 = 0.1, \omega = 0.034, \tau_T = 0.2, \tau_v \\
 &= 0.1, \tau_q = 0.5.
 \end{aligned} \tag{56}$$

Figure 1 highlights the various values of the amplitudes $|z_1|$ concerning the angle of incidence of the reflected waves θ for various values of the fractional parameter of two different values of gravity g . Clearly, the amplitudes of incidence waves $|z_1|$ decline when rising the gravity field. They decline then rise with the increase of θ to reach the unit at $\theta = 90^\circ$.

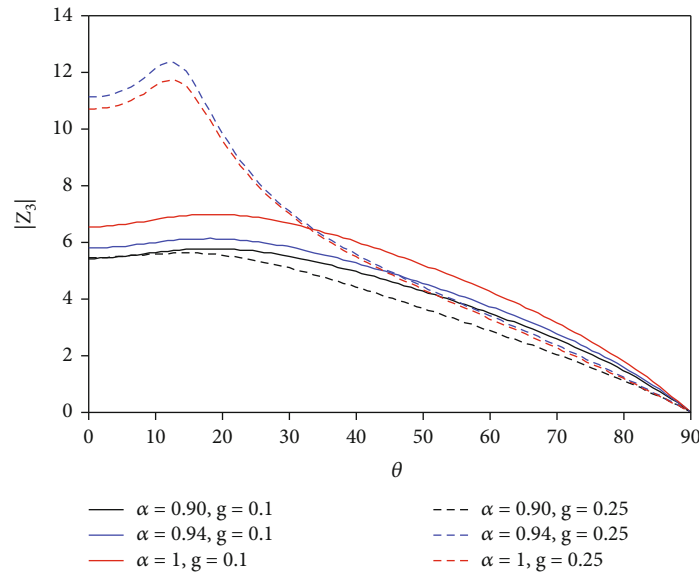


FIGURE 3: The various values of the amplitudes $|z_3|$ concerning the angle of incidence θ for various values of the fractional parameter of the diverse values of gravity g .

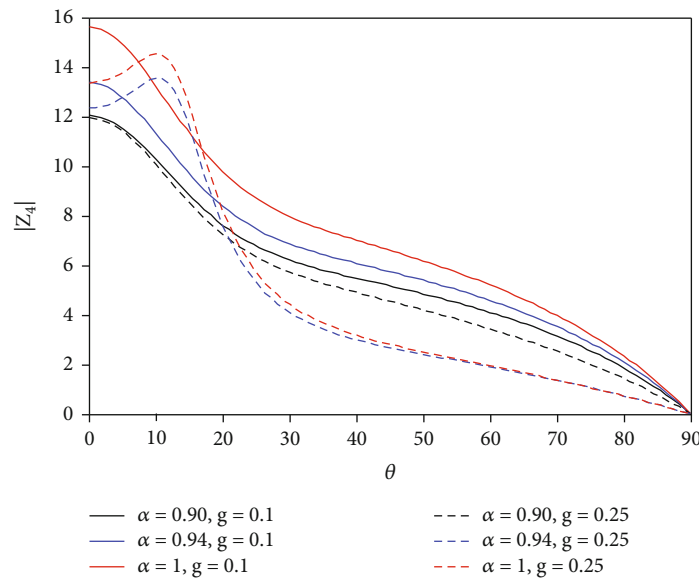


FIGURE 4: The various values of the amplitudes $|z_4|$ concerning the angle of incidence θ for various values of the fractional parameter of the diverse values of gravity g .

In the case of $g = 0.1$, the amplitude of the wave is less than in the case of $g = 0.25$, indicating that the greater the effect of gravity leads to an increase in the wave's amplitude.

Figure 2 displays the various values of amplitudes $|z_2|$ concerning the angle of incidence of the reflected waves θ for various values of the fractional parameter for the two diverse values of gravity g that shows the oscillatory performance in the entire range of angle θ . Clearly, the amplitudes of reflection waves $|z_2|$ rise when rising the gravity field, which rises then declines with increasing θ approaches zero at $\theta = 90^\circ$.

In the case of $|z_2|$, the wave amplitude started to increase significantly than $|z_1|$ at $g = 0.1$, and the effect of the fractional differential appears more clearly in the case of $\alpha = 0.90$ or $\alpha = 0.94$, both at $g = 0.1$ or $g = 0.25$.

Figure 3 highlights the various values of amplitudes $|z_3|$ concerning the angle of incidence of the reflected waves θ for various values of the fractional parameter for the two values of gravity g that shows the oscillatory performance in the entire range of angle θ . Clearly, the amplitudes of reflection waves $|z_3|$ rise when rising the gravity field and decline when rising θ until it equals zero at $\theta = 90^\circ$.

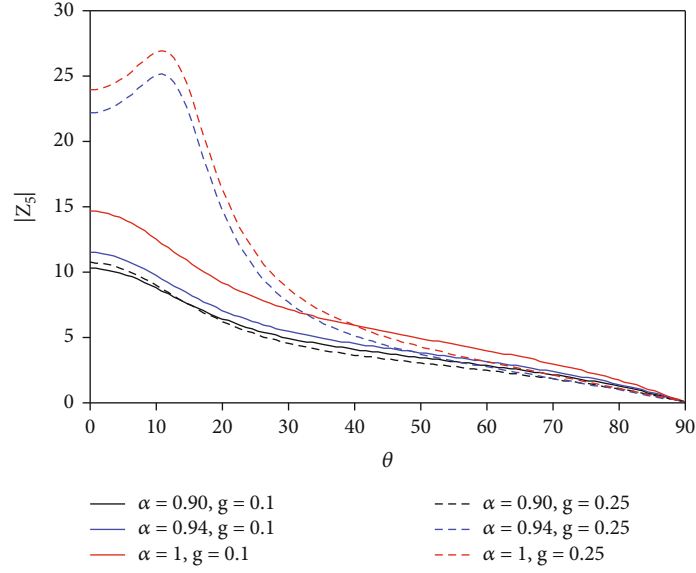


FIGURE 5: The various values of the amplitudes $|z_5|$ concerning the angle of incidence θ for various values of the fractional parameter of the diverse values of gravity g .

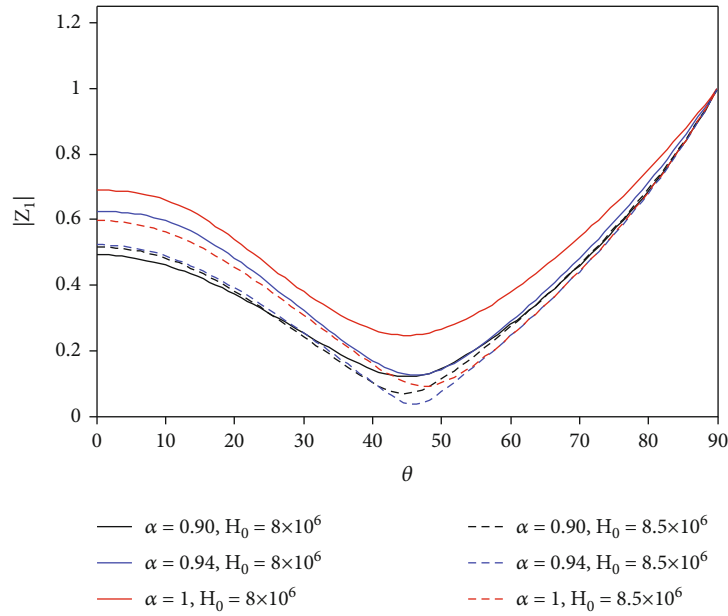


FIGURE 6: The various values of the amplitudes $|z_1|$ concerning the angle of incidence θ for various values of the fractional parameter of the diverse values of the magnetic field H_0 .

In the case of $|z_3|$, the effect of the wave amplitude shows a slight change in $0 \leq \theta \leq 10$, and it is not affected by the gravity at the lowest value of the fractional differential parameter at $\alpha = 0.90$, while the rest of the values for the fractional differential parameter are clear.

Figures 4 and 5 display the various values of amplitudes $|z_4|, |z_5|$ concerning the angle of incidence of the reflected waves θ regarding various values of the fractional parameter

for the two diverse values of gravity g that escalates in the whole entire of angle θ . Clearly, the amplitudes of the reflection waves $|z_4|, |z_5|$ increase with a higher gravity field. They rise then decline when rising θ until it equals zero at $\theta = 90^\circ$. In the wave amplitude $|z_4|$, the effect of the fractional differential parameter at $\alpha = 0.90$ takes the same behavior whether gravitational $g = 0.1$ or $g = 0.25$. In the case of $|z_5|$, the effect of the wave amplitude shows a slight change in $10 \leq \theta \leq 20$,

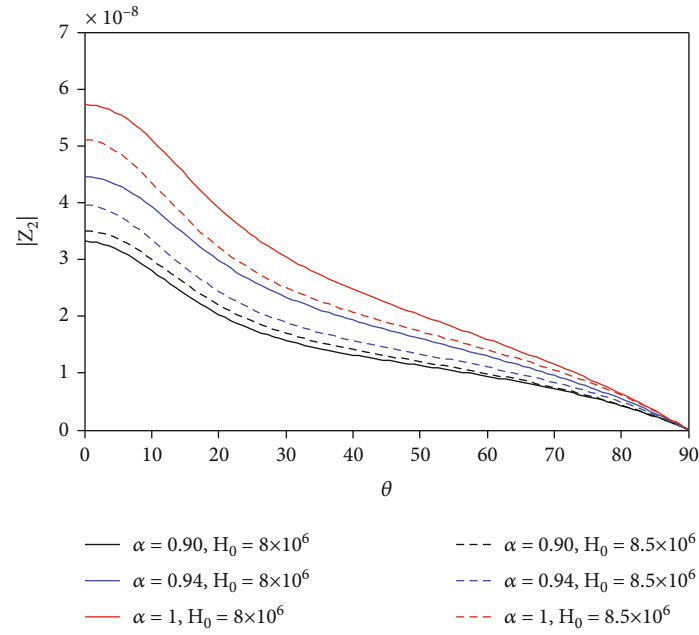


FIGURE 7: The various values of the amplitudes $|z_2|$ concerning the angle of incidence θ for various values of the fractional parameter of the diverse values of the magnetic field H_0 .

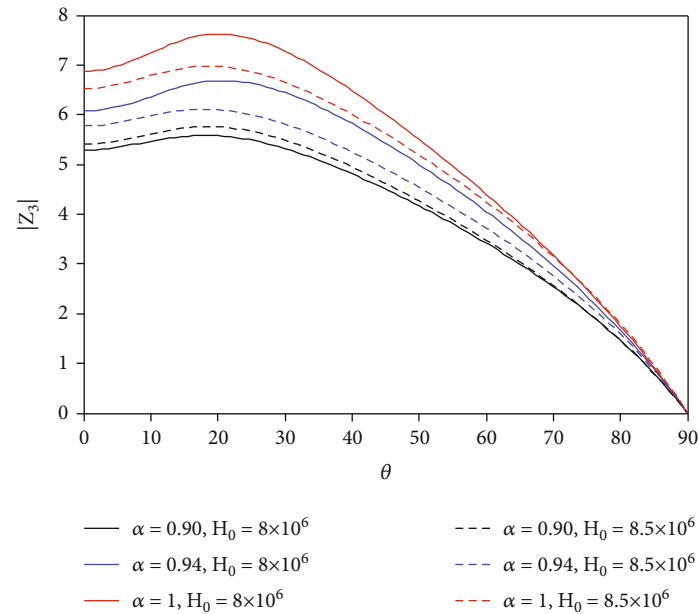


FIGURE 8: The various values of the amplitudes $|z_3|$ concerning the angle of incidence θ for various values of the fractional parameter of the diverse values of the magnetic field H_0 .

and it is not affected by the gravity at the lowest value of the fractional differential parameter at $\alpha = 0.90$, while the rest of the values for the fractional differential parameter are clear.

Figure 6 illustrates the magnitude of amplitude ratios $|z_1|$ concerning the angle of incidence of the reflected waves θ regarding various values of the fractional parameter α of two diverse values of the magnetic field H_0 . The amplitudes of incidence waves $|z_1|$ are lower when rising the magnetic

field H_0 that decline then grows with rising θ to reach the unit at $\theta = 90^\circ$. It appears that the amplitude of the wave is lower in the case of the fractional differential parameter at $\alpha = 0.90$ along $0 \leq \theta \leq 90$, while it increases with an increase of $\alpha = 0.94$ and is more amplitude in the case of $\alpha = 1$.

Figures 7–10 display the various values of amplitudes ($|z_2|$, $|z_3|$, $|z_4|$, $|z_5|$) concerning the angle of incidence of the reflected waves θ for various values of the fractional

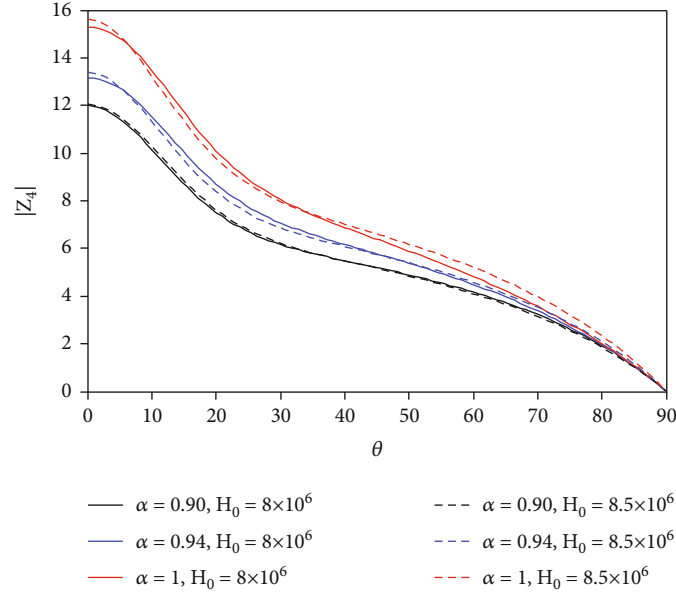


FIGURE 9: The various values of the amplitudes $|z_4|$ concerning the angle of incidence θ for various values of the fractional parameter of the diverse values of the magnetic field H_0 .

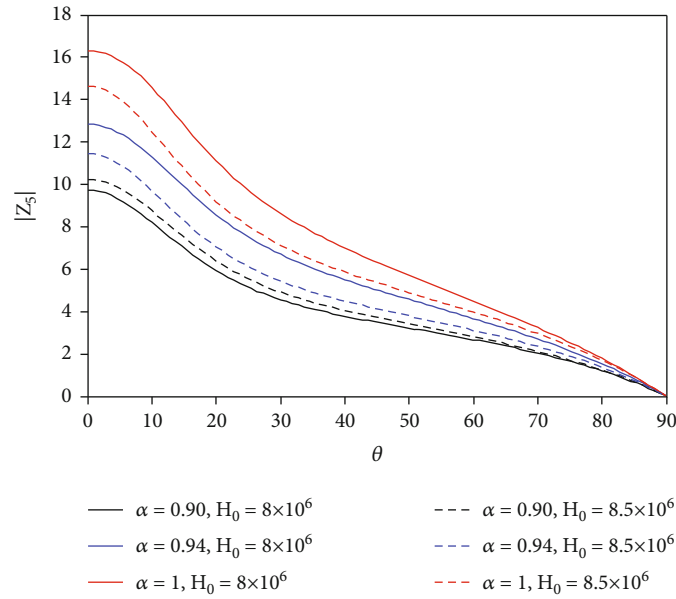


FIGURE 10: The various values of the amplitudes $|z_5|$ concerning the angle of incidence θ for various values of the fractional parameter of the diverse values of the magnetic field H_0 .

parameter α of the two different values of the magnetic field H_0 , which escalates in the entire range of angle θ . Obviously, the amplitude reflection waves ($|z_2|, |z_3|, |z_4|, |z_5|$) decrease with an increase of the magnetic field H_0 and decrease with an increase of θ until equal zero at $\theta = 90^\circ$. In the case of amplitudes ($|z_2|, |z_3|, |z_5|$), the behavior of the waves appears to be the same in all cases for different alpha values. At the same time, the effect of the fractal calculus parameter is less amplitude than the absence of fractional differential parameter. In the case of $|z_4|$, the impact of the magnetic field,

whether $H_0 = 8 \times 10^6$ or $H_0 = 8.5 \times 10^6$ is not affected by the wave amplitude, as we see the effect of fractional differentiation in all the fractional differential parameter values.

In sum, the method of the fractional derivative technique applies to other relevant issues in geology, geophysics, physics, astronomy, and engineering, agreeing with the integer derivative if $\alpha = 1$.

If the fractional order considers only an integer without an electric field, the results obtained are deduced to the results given in Othman et al. [46].

2. Conclusion

The plane harmonic waves' reflection from a semi-infinite elastic solid of thermo-microstretch was studied in this article under the thermoelasticity theory with three-phase lag. Expressing the reflection coefficients that represent the relationships of the amplitudes of the reflected waves to the amplitude of the incidence waves obtained the reflection coefficient ratio variations with the angle of incidence with changing the dielectric constant, magnetic field, and gravity field. The results were compared in the cases of the existence and negligence of the parameter fractional.

Due to their practical issues, we recommend utilizing the research findings in other fields, such as geophysics, engineering, geology, volcanoes, earthquakes, and structures. Future works will consider taking into account the effect of radiation, rotation, and other external parameters related to the phenomenon topics applicable in the environment.

Appendix

$$L = -\frac{C_1^2}{c_0^2}A, M = \alpha^2\omega^2\left(A + \left[(\zeta_5 + \zeta_0)A - \tau_q^*(1 + \varepsilon_1\zeta_2)\right]\frac{C_1^2}{c_0^2}\right) + \frac{A}{\omega^{*2}}\left(\zeta_6\frac{kC_1^2}{c} - C_2^2 + \zeta_3C_3^2\right) + AB\frac{C_1^2}{c_0^2},$$

$$N = \alpha^2\omega^2\left(\frac{A}{\omega^{*2}}\left[C_2^2(\zeta_0 + \zeta_5) - \frac{\zeta_6k}{c}(c_0^2 - \zeta_0C_1^2) - \zeta_3\zeta_5C_3^2\right] - AB\left(C_1^2\zeta_5 - 1 - \zeta_0\frac{C_1^2}{c_0^2}\right) + \tau_q^*B\frac{C_1^2}{c_0^2}(1 + \zeta_2\varepsilon_1) + \alpha^4\omega^4\left(\tau_q^*[1 + \zeta_2\varepsilon_1] - A[\zeta_6 + \zeta_0] + \tau_q^*\frac{C_1^2}{c_0^2}\left[\zeta_5 + \zeta_0 + \zeta_2\zeta_5\varepsilon_1 - \zeta_0\zeta_5\frac{A}{\tau_q^*}\right]\right) + \frac{A}{\omega^{*2}}(BC_2^2 - \zeta_3bC_3^2) + \zeta_6A\frac{kC_0^2}{c\omega^{*4}}(C_2^2 - \zeta_3C_3^2) - \zeta_1\zeta_4A\sin^2\theta\frac{C_1^2}{c_0^2},$$

$$Q = \zeta_0\zeta_5\alpha^6\omega^6\tau_q^*B\left(a_0\varepsilon_2 + \frac{C_2^2}{\omega^{*2}}\right) - \zeta_1\zeta_4\alpha^4\omega^4\tau_q^*B\sin^2\theta + \alpha^2\omega^2\zeta_1\zeta_4\tau_q^*B\sin^2\theta\left(a_0\varepsilon_2 + \frac{C_2^2}{\omega^{*2}}\right),$$

$$A = -C_k + i\alpha\omega C_\nu + \alpha^2\omega^2 C_T, B = \frac{j\rho c_0^2\alpha^2\omega^2}{c} - \frac{2kc_0^2}{c\omega^{*2}},$$

$$O = \alpha^6\omega^6\left(\zeta_0\zeta_5\left[A - \tau_q^*\frac{C_1^2}{c_0^2}\right] - \tau_q^*[\zeta_5 + \zeta_0] - \zeta_2\zeta_5\varepsilon_1\tau_q^*\right) + \alpha^4\omega^4\left(\tau_q^*a_0[\zeta_5\varepsilon_2 - \zeta_0\varepsilon_2 - \zeta_3\zeta_5\varepsilon_1] + \tau_q^*\frac{C_2^2}{\omega^{*2}}[\zeta_5 + \zeta_0] + \zeta_0\frac{A}{\omega^{*2}}\left[\zeta_6\frac{kC_0^2}{c} - \zeta_5C_2^2\right]\right)$$

$$+ AB\left[\zeta_5 + \zeta_0 + \zeta_0\zeta_5\frac{C_1^2}{c_0^2}\right] - \tau_q^*B\frac{C_1^2}{c_0^2}[\zeta_0 + \zeta_5 + \zeta_2\zeta_5\varepsilon_1] - \tau_q^*B[\zeta_2\varepsilon_1 + 1] - \zeta_6\tau_q^*\frac{kC_0^2}{c\omega^{*2}}[1 - \zeta_2\varepsilon_1] - \frac{\tau_q^*}{c\omega^{*2}}[\zeta_0\zeta_6kC_1^2 - \zeta_2\zeta_5\varepsilon_1cC_2^2] - \zeta_5\varepsilon_2\tau_q^*\frac{C_3^2}{\omega^{*2}}[\zeta_2\varepsilon_2 + \zeta_3] + \alpha^2\omega^2\left(\tau_q^*B\frac{C_2^2}{\omega^{*2}}[1 + \zeta_2\varepsilon_1] - \tau_q^*B\frac{C_3^2}{\omega^{*2}}[\zeta_3 + \zeta_2\varepsilon_2] + a_0\tau_q^*B[\varepsilon_2 - \zeta_3\varepsilon_1] - AB\frac{C_2^2}{\omega^{*2}}[\zeta_5 + \zeta_0] - \zeta_6\frac{kC_0^2}{c\omega^{*4}}\left[\zeta_0AC_2^2 - a_0\varepsilon_2\tau_q^*\omega^{*2} + \zeta_2\varepsilon_1\tau_q^*C_2^2 - \zeta_2\varepsilon_2\tau_q^*C_3^2\right] - \zeta_1\zeta_4\sin^2\theta\left[\tau_q^*\frac{C_1^2}{c_0^2} - A\right] + \zeta_3\zeta_5AB\frac{C_3^2}{\omega^{*2}} - \zeta_3\zeta_6a_0\varepsilon_1\tau_q^*\right) + \zeta_1\zeta_4A\sin^2\theta\left[B\frac{C_1^2}{c_0^2} - \frac{C_2^2}{\omega^{*2}}\right].$$

$$P = \zeta_0\zeta_5\alpha^8\omega^8\tau_q^* + \alpha^6\omega^6\left(\zeta_5\tau_q^*[\zeta_0a_0\varepsilon_2 + \zeta_2\varepsilon_1B] + \tau_q^*B[\zeta_5 + \zeta_0] + \zeta_0\zeta_5B\left[\tau_q^*\frac{C_1^2}{c_0^2} - A\right] - \zeta_0\frac{\tau_q^*}{\omega^{*2}}\left[\zeta_5C_2^2 - \zeta_6\frac{kC_0^2}{c}\right]\right) + \alpha^4\omega^4\left(\zeta_5\tau_q^*B\frac{C_3^2}{\omega^{*2}}[\zeta_2\varepsilon_2 + \zeta_3] - \tau_q^*B\frac{C_2^2}{\omega^{*2}}[\zeta_5 + \zeta_0 + \zeta_2\zeta_5\varepsilon_1] - a_0\tau_q^*B[\zeta_5\varepsilon_2 + \zeta_0\varepsilon_2 - \zeta_3\zeta_5\varepsilon_1] - \zeta_0\zeta_6\tau_q^*\frac{kC_0^2}{c\omega^{*2}}\left[a_0\varepsilon_2 + \frac{C_2^2}{\omega^{*2}}\right] + \zeta_0\zeta_5AB\frac{C_2^2}{\omega^{*2}} + \zeta_1\zeta_4\tau_q^*\sin^2\theta\right) + \alpha^2\omega^2\left(\zeta_1\zeta_4B\sin^2\theta\left[\tau_q^*\frac{C_1^2}{c_0^2} - A\right] - \zeta_1\zeta_4\tau_q^*\sin^2\theta\left[a_0\varepsilon_2 + \frac{C_2^2}{\omega^{*2}}\right] - \zeta_3\zeta_6\tau_q^*\frac{kC_0^2C_3^2}{c\omega^{*4}}\right) + \zeta_1\zeta_4AB\sin^2\theta\frac{C_2^2}{\omega^{*2}},$$

(A.1)

Nomenclature

\vec{B} :	Magnetic induction vector
C_e :	Specific heat per unit mass
\vec{E} :	Electrical density vector
e_{ij} :	Strain tensor
\vec{F}_i :	Body force vector of Lorentz
g :	Gravitational constant
\vec{H} :	Magnetic vector
\vec{h} :	Perturbed magnetic vector
\vec{H}_0 :	Elementary constant magnetic field vector
i :	$\sqrt{-1}$
j :	Microinertia moment
\vec{J} :	Electric current density vector
K, K^* :	Thermal conduction coefficients

m_{ij} :	Coupled stress tensor
t :	Time
T_0 :	The reference temperature
T :	The temperature distribution
u :	Displacement vector
a_0, b_0, b_1 :	Microstretch constants
$\alpha_{t_1}, \alpha_{t_2}$:	Coefficient of linear thermal expansion
δ_{ij} :	Kronecker delta
ε_0 :	Electric permeability
φ :	Rotation vector
φ^* :	Scalar microstretch
k, a, b, c :	Micropolar constants
λ, μ :	Lame' constants
μ_0 :	Magnetic permeability
$v = \omega/\xi$:	Velocity of the coupled waves
ρ :	Mass density
σ_{ij} :	Stress tensor
τ_{ij} :	Stress tensor of Maxwell
τ_q :	The phase-lag of the temperature influx
τ_T :	The phase-lag of the heat tendency
τ_v :	Thermal displacement phase lag
ω :	Complex frequency
ξ :	Wave number
$\hat{\gamma}$:	$(3\lambda + 2\mu + k)\alpha_{t_1}$
$\hat{\gamma}_1$:	$(3\lambda + 2\mu + k)\alpha_{t_2}$

Data Availability

The data supported from our published papers and all the results are new.

Conflicts of Interest

The authors declare no conflict of interests in publishing the present research paper.

Acknowledgments

The authors acknowledge the financial support of Taif University researchers, supporting project no. TURSP-2020/164, Taif University, Taif, Saudi Arabia.


References

- [1] S. K. R. Choudhuri, "On a thermoelastic three-phase-lag model," *Journal of Thermal Stresses*, vol. 30, no. 3, article 231238, 2007.
- [2] R. Kumar, R. Singh, and T. K. Chadha, "Plane strain problem in microstretch elastic solid," *Sadhana*, vol. 28, no. 6, pp. 975–990, 2003.
- [3] R. Kumar and G. Partap, "Reflection of plane waves in a heat flux dependent microstretch Thermoelastic solid half space," *International Journal of Applied Mechanics and Engineering*, vol. 10, pp. 253–266, 2005.
- [4] H. W. Lord and Y. Shulman, "A generalized dynamical theory of thermoelasticity," *Journal of the Mechanics and Physics of Solids*, vol. 15, no. 5, pp. 299–309, 1967.
- [5] A. E. Green and A. Lindsay, "Thermoelasticity," *Journal of Elasticity*, vol. 2, no. 1, pp. 1–7, 1972.
- [6] A. E. Green and P. M. Naghdi, "A re-examination of the basic postulates of thermomechanics," *Proceeding of the Royal Society London A*, vol. 432, no. 1885, pp. 171–194, 1991.
- [7] A. E. Green and P. M. Naghdi, "On undamped heat waves in an elastic solid," *Journal of Thermal Stresses*, vol. 15, no. 2, pp. 253–264, 1992.
- [8] A. E. Green and P. M. Naghdi, "Thermoelasticity without energy dissipation," *Journal of Elasticity*, vol. 31, no. 3, pp. 189–208, 1993.
- [9] I. A. Abbas and R. Kumar, "Deformation due to thermal source in micropolar generalized thermoelastic half-space by finite element method," *Journal of Computational and Theoretical Nanoscience*, vol. 11, no. 1, pp. 185–190, 2014.
- [10] R. Quintanilla and R. Racke, "A note on stability in three-phase-lag heat conduction," *International Journal of Heat and Mass Transfer*, vol. 51, no. 1-2, pp. 24–29, 2008.
- [11] A. Kar and M. Kanoria, "Generalized thermoelastic functionally graded orthotropic hollow sphere under thermal shock with three-phase-lag effect," *European Journal of Mechanics A-Solids*, vol. 28, no. 4, pp. 757–767, 2009.
- [12] S. Banik and M. Kanoria, "Generalized thermoelastic interaction in a functionally graded isotropic unbounded medium due to varying heat source with three-phase-lag effect," *Mathematics and Mechanics of Solids*, vol. 18, no. 3, pp. 231–245, 2013.
- [13] M. Elsagheer and S. M. Abo-Dahab, "Reflection of thermoelastic waves from insulated boundary fibre-reinforced half-space under influence of rotation and magnetic field," *Applied Mathematics & Information Sciences*, vol. 10, no. 3, pp. 1129–1140, 2016.
- [14] S. M. Abo-Dahab, A. M. Abd-Alla, and A. A. Kilany, "Effects of rotation and gravity on an electro-magneto-thermoelastic medium with diffusion and voids by using the Lord-Shulman and dual-phase-lag models," *Applied Mathematics and Mechanics (English Edition)*, vol. 40, no. 8, pp. 1135–1154, 2019.
- [15] A. M. Abd-Alla, S. M. Abo-Dahab, and A. A. Kilany, "SV-waves incidence at interface between solid-liquid media under electromagnetic field and initial stress in the context of three thermoelastic theories," *Journal of Thermal Stresses*, vol. 39, no. 8, pp. 960–976, 2016.
- [16] S. M. Abo-Dahab, A. M. Abd-Alla, A. A. Kilany, and M. Elsagheer, "Effect of rotation and gravity on the reflection of P-waves from thermo-magneto-microstretch medium in the context of three phase lag model with initial stress," *Journal of Microsystem Technologies*, vol. 24, no. 8, pp. 3357–3369, 2018.
- [17] R. Hilfer, *Applications of Fractional Calculus in Physics*, World Science, Singapore, 2000.
- [18] A. A. Kilbas, H. M. Srivastava, and J. J. Trujillo, *Theory and Applications of Fractional Differential Equations*, Elsevier B.V., Amsterdam, UK, 2006.
- [19] U. N. Katugampola, "New approach to a generalized fractional integral," *Applied Mathematics and Computation*, vol. 218, no. 3, pp. 860–865, 2011.
- [20] E.-A.-B. Abdel-Salam, E. A. Yousif, and M. A. El-Aasser, "Analytical solution of the space-time fractional nonlinear Schrödinger equation," *Reports on Mathematical Physics*, vol. 19, p. 77, 2016.
- [21] E.-A.-B. Abdel-Salam and G. F. Hassan, "Solutions to class of linear and nonlinear fractional differential equations,"

- Communications in Theoretical Physics*, vol. 65, no. 2, pp. 127–135, 2016.
- [22] E. A.-B. Abdel-Salam and E. A. Yousif, "Solution of nonlinear space-time fractional differential equations using the fractional Riccati expansion method," *Mathematical Problems in Engineering*, vol. 2013, Article ID 846283, 6 pages, 2013.
 - [23] M. I. Nouh and E.-A.-B. Abdel-Salam, "Approximate solution to the fractional Lane-Emden type equations," *Iranian Journal of Science and Technology Transaction a Science*, vol. 42, no. 4, pp. 2199–2206, 2018.
 - [24] S. E. Ahmed, M. A. Mansour, E.-A.-B. Abdel-Salam, and E. F. Mohamed, "Studying the fractional derivative for natural convection in slanted cavity containing porous media," *SN Applied Sciences*, vol. 1, no. 9, p. 1117, 2019.
 - [25] A. M. El-Naggar, Z. Kishka, A. M. Abd-Alla, I. A. Abbas, S. M. Abo-Dahab, and M. Elsagheer, "On the initial stress, magnetic field, voids and rotation effects on plane waves in generalized thermoelasticity," *Journal of Computational and Theoretical Nanoscience*, vol. 10, no. 6, pp. 1408–1417, 2013.
 - [26] M. Marin, M. I. A. Othman, and I. A. Abbas, "An extension of the domain of influence theorem for generalized thermoelasticity of anisotropic material with voids," *Journal of Computational and Theoretical Nanoscience*, vol. 12, no. 8, pp. 1594–1598, 2015.
 - [27] T. Saeed, I. Abbas, and M. Marin, "A GL model on thermoelastic interaction in a poroelastic material using finite element method," *Symmetry*, vol. 12, no. 3, p. 488, 2020.
 - [28] S. M. Abo-Dahab, A. M. Abd-Alla, and A. A. Kilany, "Electromagnetic field in fiber-reinforced micropolar thermoelastic medium using four models," *Journal of Ocean Engineering and Science*, vol. 5, no. 3, pp. 230–248, 2020.
 - [29] J. H. He, S. K. Elagan, and Z. B. Li, "Geometrical explanation of the fractional complex transform and derivative chain rule for fractional calculus," *Physics Letters A*, vol. 376, no. 4, pp. 257–259, 2012.
 - [30] K. M. Kolwankar and A. D. Gangal, "Fractional differentiability of nowhere differentiable functions and dimensions," *Chaos*, vol. 6, no. 4, pp. 505–513, 1996.
 - [31] K. M. Kolwankar and A. D. Gangal, "Local fractional Fokker-Planck equation," *Physical Review Letters*, vol. 80, no. 2, pp. 214–217, 1998.
 - [32] Y. Chen, Y. Yan, and K. Zhang, "On the local fractional derivative," *Journal of Mathematical Analysis and Applications*, vol. 362, no. 1, pp. 17–33, 2010.
 - [33] R. Khalil, M. al Horani, A. Yousef, and M. Sababheh, "A new definition of fractional derivative," *Journal of Computational and Applied Mathematics*, vol. 264, pp. 65–70, 2014.
 - [34] T. Abdeljawad, "On conformable fractional calculus," *Journal of Computational and Applied Mathematics*, vol. 279, pp. 57–66, 2015.
 - [35] F. Jarad, T. Abdeljawad, and Alzabut, "Generalized fractional derivatives generated by a class of local proportional derivatives," *The European Physical Journal Special Topics*, vol. 226, no. 16-18, pp. 3457–3471, 2017.
 - [36] T. Abdeljawad, F. Jarad, and Alzabut, "Fractional proportional differences with memory," *The European Physical Journal Special Topics*, vol. 226, no. 16-18, pp. 3333–3354, 2017.
 - [37] S. M. Abo-Dahab, A. A. Kilany, E. A.-B. Abdel-Salam, and A. Hatem, "Fractional derivative order analysis and temperature-dependent properties on p- and SV-waves reflection under initial stress and three-phase-lag model," *Results in Physics*, vol. 18, article 103270, 2020.
 - [38] H. Alotaibi, S. M. Abo-Dahab, H. R. Abdllrahim, and A. A. Kilany, "Fractional calculus of Thermoelastic p-waves reflection under influence of gravity and electromagnetic fields," *Fractals*, vol. 28, no. 8, article 2040037, 2020.
 - [39] A. Hobiny and I. Abbas, "Analytical solution of fractional order photo-thermoelasticity in a non-homogenous semiconductor medium," *Multidiscipline Modeling in Materials and Structures*, vol. 14, no. 5, pp. 1017–1030, 2018.
 - [40] Y. Povstenko and T. Kyrlych, "Fractional thermoelasticity problem for a plane with a line crack under heat flux loading," *Journal of Thermal Stresses*, vol. 41, no. 10-12, pp. 1313–1328, 2018.
 - [41] S. M. Abo-Dahab, S. Z. Rida, R. A. Mohamed, and A. A. Kilany, "Rotation, initial stress, gravity and electromagnetic field effect on P wave reflection from stress-free surface elastic half-space with voids under three thermoelastic models," *Mechanics and Mechanical Engineering*, vol. 22, no. 1, pp. 313–328, 2018.
 - [42] A. M. Abd-Alla, S. M. Abo-Dahab, and A. A. Kilany, "Effect of several fields on a generalized thermoelastic medium with voids in the context of Lord-Shulman or dual-phase-lag models," *Mechanics Based Design of Structures and Machines*, pp. 1–24, 2020.
 - [43] F. S. Bayones, S. M. Abo-Dahab, A. M. Abd-Alla, and A. A. Kilany, "Electromagnetic field and three-phase lag in a compressed rotating isotropic homogeneous micropolar thermo-viscoelastic half-space," *Mathematical Methods in the Applied Sciences*, vol. 44, no. 13, pp. 9944–9965, 2021.
 - [44] F. S. Bayones, S. M. Abo-Dahab, A. M. Abd-Alla, S. H. Elhag, A. A. Kilany, and M. Elsagheer, "Initial stress and gravity on P-wave reflection from electromagneto-Thermo- microstretch medium in the context of three-phase lag model," *Complexity*, vol. 2021, Article ID 5560900, 15 pages, 2021.
 - [45] F. S. Bayones, S. Mondal, S. M. Abo-Dahab, and A. A. Kilany, "Effect of moving heat source on a magneto-thermoelastic rod in the context of Eringen's nonlocal theory under three-phase lag with a memory dependent derivative," *Mechanics Based Design of Structures and Machines*, pp. 1–17, 2021.
 - [46] M. I. A. Othman, S. M. Abo-Dahab, and K. Lotfy, "Gravitational effect and initial stress on generalized magneto-thermo-microstretch elastic solid for different theories," *Applied Mathematics and Computation*, vol. 230, pp. 597–615, 2014.
 - [47] S. M. Abo-Dahab, A. A. Kilany, M. N. M. Allam, R. A. Mohamed, and S. Z. Rida, "Influence of several fields on Rayleigh waves propagation in a fiber-reinforced orthotropic half-space material under four thermoelastic models," *Waves in Random and Complex Media*, pp. 1–24, 2020.
 - [48] M. A. Ezzat, "State space approach to generalized magneto-thermoelasticity with two relaxation times in a medium of perfect conductivity," *International Journal of Engineering Science*, vol. 35, pp. 741–752, 1997.
 - [49] G. Paria, "Magneto-elasticity and magneto-thermoelasticity," *Advances in Applied Mechanics*, vol. 10, p. 73, 1967.

Research Article

Statistical Study of the Entanglement for Qubit Interacting with an Electromagnetic Field

Neveen Sayed-Ahmed ¹, M. M. Amein,¹ Taghreed M. Jawa,¹ Tahani A. Aloafi,¹
F. S. Bayones,¹ Azhari A. Elhag,¹ and J. Bouslimi²

¹Department of Mathematics, College of Science, Taif University, P.O. Box 11099 Taif 21944, Saudi Arabia

²Department of Physics, College of Science, Taif University, P.O. Box 11099, Taif 21944, Saudi Arabia

Correspondence should be addressed to Neveen Sayed-Ahmed; nevensayd@yahoo.com

Received 12 February 2021; Accepted 20 September 2021; Published 11 October 2021

Academic Editor: Mustafa Inc

Copyright © 2021 Neveen Sayed-Ahmed et al. This is an open access article distributed under the Creative Commons Attribution License, which permits unrestricted use, distribution, and reproduction in any medium, provided the original work is properly cited.

A statistical method is applied to predict the behaviour of a quantum model consisting of a qubit interacting with a single-mode cavity field. The qubit is prepared in excited state while the field starts from the binomial distribution state. The wave function of the proposed model is obtained. A von Neumann entropy is used to investigate the behaviour of the entanglement between the field and the qubits. Moreover, the atomic Q and Wigner functions are used to identify the behaviour of the distribution in a phase space. The simulation method is used to estimate the parameters of the proposed model to reach the best results. A numerical study is performed to estimate the specific dependency of the binomial distribution state. The results of entanglement were compared with the atomic Q and Wigner functions. The results showed that there are many maximum values of entanglement periodically. The results also confirmed a correlation between von Neumann entropy, the atomic Q , and Wigner functions.

1. Introduction

The problem of field interaction with an atom or atoms has gained the attention of many researchers in the field of optics and quantum information. Through the previous literature, it becomes clear that the interaction model of a qubit with two levels with a single-mode of the optical field is the most easiest model for estimating properties that have physical applications [1]. Therefore, researchers have been interested in studying this model on a large scale in the direction of information and quantum optics [2]. Moreover, many generalizations of this model were appeared, especially in field formulas; therefore, the combinations of the field modes such as bimode as either a converter or amplifier were discussed [3, 4]. Continuing the development of studies in the interaction of the field with the qubit, the effect of the interaction of two fields together on the interaction of the atom with the field was studied. The results showed nonclassical features in the phenomenon of collapse, revival, and

entropy of squeezing [3, 4]. On the other hand, a new type of generalization emerged from the Jaynes-Cummings model, which is the dependence of the coupling between the qubit and the field on time, which led to the results of increasing the correlation between the parts of the quantum system [5]. The theoretical efforts have been dealt with extensively by the experimental cavity of QED. Progress has been made in the quantum computation model, in which the quantum system is studied as a density operator or a matrix [6]. The study of the interaction of qubits with the single-mode field has received great interest from researchers. For example, the effect of stark displacement on the entanglement between quantum systems was investigated [7]. The analytical solution of the fractional Schrödinger equation was also used to describe the interaction between an atom with two levels and the placement of a single electromagnetic field inside a cavity [8]. Moreover, the effect of the interaction between the time-dependent field and a two-level atom with a single electromagnetic field

TABLE 1: ($M = 5$).

	Max	Min		Max	Min
S	0.693013	0.0000226021	ϕ	136.362	106.99
$\tau(S)$	7.02325	31.4164	W	0.00553529	-0.00140655
$\eta(S)$	0.0203785	0.620389	$\tau(W)$	2.87961	11.0223
Q	0.0027748	5.2415×10^{-6}	$\eta(W)$	0.985884	0.99747
$\tau(Q)$	0.0100093	31.3941	x	0.28476	-0.0930154
$\eta(Q)$	0.217574	0.00494274	y	0.79185	-0.738397
θ	113.035	128.731			

TABLE 2: ($M = 20$).

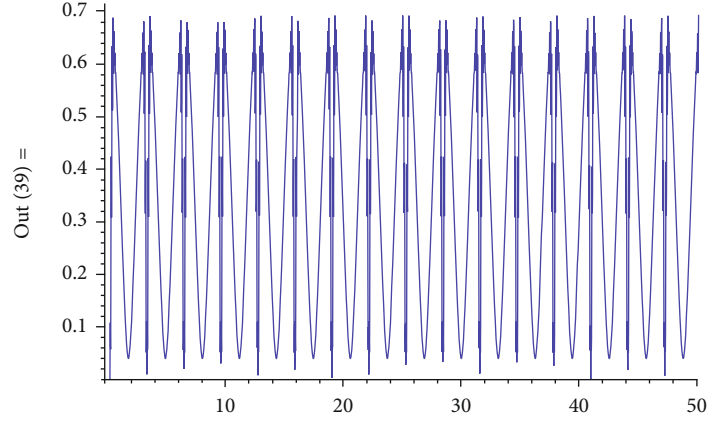
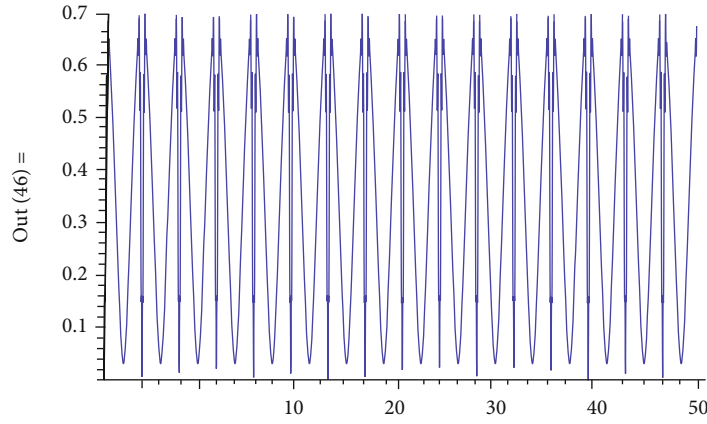
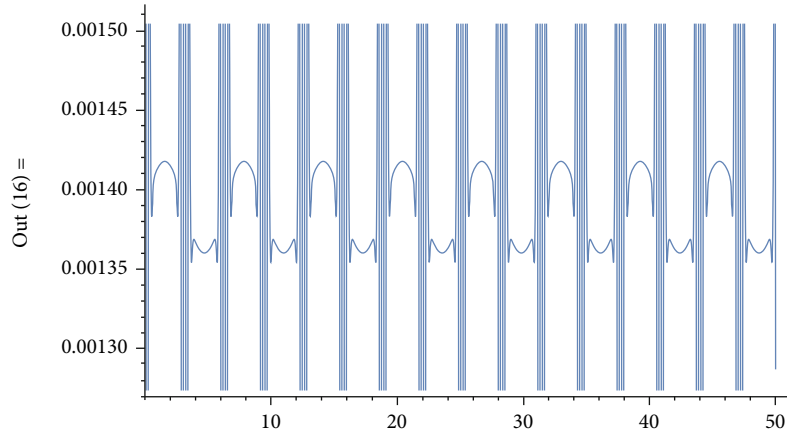
	Max	Min		Max	Min
S	0.692933	1.49224×10^{-7}	ϕ	349.464	40.5101
$\tau(S)$	9.02077	47.1239	W	0.00552633	-0.0006944
$\eta(S)$	0.811648	0.664846	$\tau(W)$	19.3756	32.0177
Q	0.0027569	5.47404×10^{-6}	$\eta(W)$	0.999427	0.996774
$\tau(Q)$	37.6882	34.555	x	-0.2998	-1.01915
$\eta(Q)$	0.352551	0.184801	y	0.853462	0.785669
θ	75.4497	65.8915			

TABLE 3: ($M = 50$).

	Max	Min		Max	Min
S	0.693125	0.0000714152	ϕ	197.615	64.7959
$\tau(S)$	37.9639	34.5578	W	0.00550693	2.45124×10^{-6}
$\eta(S)$	0.745945	0.548057	$\tau(W)$	24.0254	34.5578
Q	0.00276372	0.0000900447	$\eta(W)$	3.41675×10^{-6}	0.548057
$\tau(Q)$	47.1265	6.23383	x	0.104398	-1.05545
$\eta(Q)$	0.156082	0.0424479	y	0.105826	0.345778
θ	131.806	159.928			

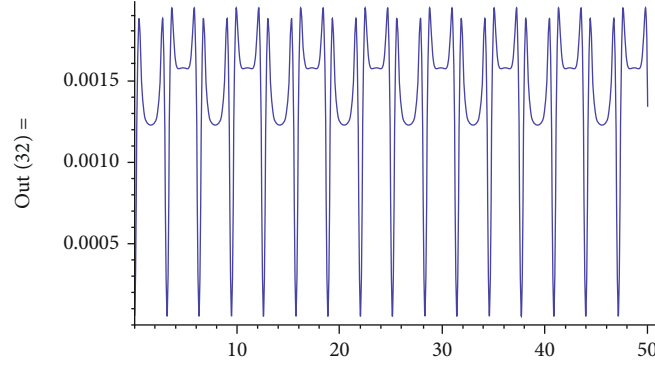
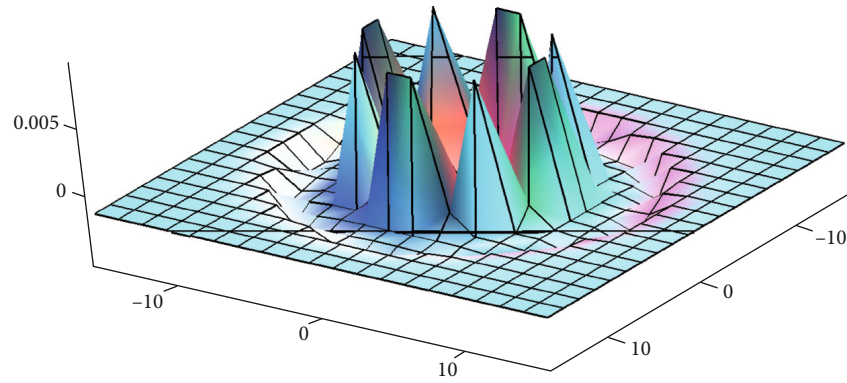
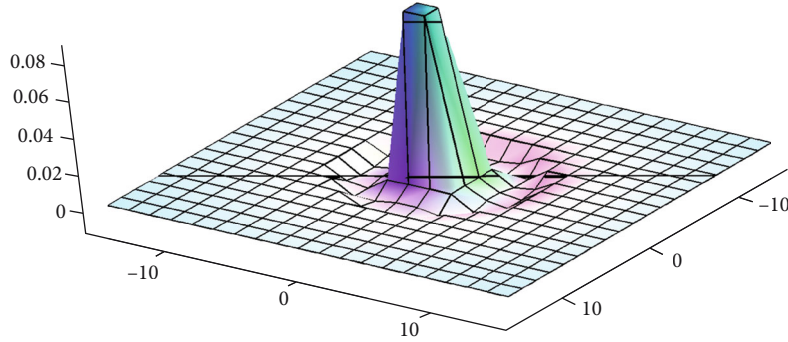
TABLE 4: ($M = 100$).

	Max	Min		Max	Min
S	0.693061	0.0000714152	ϕ	205.49	64.7959
$\tau(S)$	28.082	34.5578	W	0.0052686	-5.89211×10^{-8}
$\eta(S)$	0.360209	0.548057	$\tau(W)$	40.7896	9.4861
Q	0.00276632	0.0000900447	$\eta(W)$	0.295508	0.646471
$\tau(Q)$	12.6124	6.23383	x	0.113395	0.426285
$\eta(Q)$	0.00199163	0.0424479	y	-0.374566	0.37842
θ	113.02	159.928			

FIGURE 1: Maximum points for the S-function, $M = 50$, $0 \leq \tau \leq 50$.FIGURE 2: Minimum points for the S-function, $M = 50$, $0 \leq \tau \leq 50$.FIGURE 3: Maximum points for the Q-function, $M = 50$, $0 \leq \tau \leq 50$.

was studied [9]. The effect of the decay on the interaction of a three-level atom with a multiphoton field in the presence of Kerr like medium was also studied [10, 11]. In fact, the initial values of the parameters describing the quantum system are taken at random, while in this work, a statistical method is used to estimate the initial values that improve the entanglement between the parts of the system.

Undoubtedly, the entanglement of parts of quantum systems is an important measure for discovering the strength of the interaction between these systems. Therefore, attention has been given to many types of these measures to measure the degree of quantum entanglement between two systems. For example, the von Neumann entropy or linear entropy was used in the case of closed systems that start the

FIGURE 4: Minimum points for the Q -function, $M = 50$, $0 \leq \tau \leq 50$.FIGURE 5: Minimum points for the w -function, $M = 50$.FIGURE 6: Maximum points for the w -function, $M = 50$.

interaction from a separate state [12]. Moreover, the qubit and the electromagnetic field were prepared in a separate or superposition states. They were followed by a partially entangled state during the interaction of the quantum system. Therefore, von Neumann entropy or linear entropy is the two main measures that mean the local classical entanglement process.

The process of controlling the degree of entanglement between two atoms with two thermal fields through the amount of decomposition between the atomic transition and the gaps is one of the most important problems in quantum optics [13]. Open system correlation cannot be measured with a standard scale such as entropy or von

Neumann. Therefore, various attempts have been made to discover a new quantum estimator of correlation between parts of quantum systems [14, 15]. It is worth noting that the initial state is strongly influencing the amount of entanglement between parts of a quantum system. The effect of the nondeformed pair coherent states on a quantum system was investigated [16]. The effect of the nondeformed pair coherent state on the field cavity was studied, where strong entanglement was established in most of the interaction periods between quantum systems, while the deformed state generated weak entanglement [17].

The main goal of this work is to predict the degree of entanglement between quantum systems containing a qubit

interaction with a single-mode cavity field. Statistical simulation is used to obtain the regions of entanglement strength and to obtain nonclassical behaviour by studying the Q and Wigner functions.

The paper is arranged as follows: Section 2 contains the solution of the differential equations to obtain the general solution of the quantum system. Section 3 is devoted to discover the regions of entanglement between the parts of the system. Moreover, von Neumann entropy, the atomic Q-function, and W-function are examined. Some statistical characteristics are presented in Section 4. Finally, conclusion is drawn in Section 5.

2. Quantum System

Now, we assume that a two-level atom is injected into a cavity containing a medium described by Hamiltonian containing single-mode of cavity field and the two-level atom.

$$\frac{\hat{H}}{\hbar} = \Omega c\Lambda^\dagger \hat{c} + \frac{\omega_0}{2} \hat{\sigma}_z + \lambda (c\Lambda^\dagger \hat{\sigma}_- + \hat{c} \hat{\sigma}_+), \quad (1)$$

where $\hat{\sigma}_+$, $\hat{\sigma}_-$, and $\hat{\sigma}_z$ are su(2) representation, and \hat{c} and $c\Lambda^\dagger$ are the annihilation and creation operator, respectively. The frequency ω_0 is the energy difference between the upper and the lower levels of the atom. The $\hat{\sigma}_\pm$ is connected with the inversion operator $\hat{\sigma}_z$ by the commutation relations

$$[\hat{\sigma}_+, \hat{\sigma}_-] = \hat{\sigma}_z, [\hat{\sigma}_z, \hat{\sigma}_\pm] = \pm 2\hat{\sigma}_\pm. \quad (2)$$

The Heisenberg equation of motion is used to obtain the constants of motion. Through it, the general solution for the proposed quantum system is obtained. The equation of motion for any dynamical operator \hat{Y} is given by

$$\frac{d}{dt} \hat{Y} = \frac{1}{i\hbar} [\hat{Y}, \hat{H}] + \frac{\partial \hat{Y}}{\partial t}. \quad (3)$$

Hence, the equation of motion for $\hat{\sigma}_z$ and $c\Lambda^\dagger \hat{c}$ can be given as follows:

$$\frac{d\hat{\sigma}_z}{dT} = 2i\lambda (\hat{c}_1^\dagger \hat{\sigma}_- - \hat{c} \hat{\sigma}_+), \quad (4)$$

$$\frac{dc\Lambda^\dagger \hat{c}}{dT} = -i\lambda (c\Lambda^\dagger \hat{\sigma}_- - \hat{c} \hat{\sigma}_+), \quad (5)$$

Thus, we deduce that the operator $2\hat{N} = \hat{\sigma}_z + 2c\Lambda^\dagger \hat{c}$ is a constant of motion. Therefore, the Hamiltonian (1) becomes

$$\frac{\hat{H}}{\hbar} = \omega \hat{N} - \Delta \hat{\sigma}_z + \lambda_1 (\hat{c} \hat{\sigma}_+ + c\Lambda^\dagger \hat{\sigma}_-), \quad (6)$$

where $\Delta = 1/2(\omega - \omega_0)$.

The time evolution operator is given by

$$\hat{U}(t) = \exp(-i\hat{H}t) = \begin{bmatrix} \hat{F}_1(\hat{n}, t) \exp\{-i\omega \hat{n}t\} & -i \exp\{-i\omega \hat{n}t\} \lambda \hat{E}_1(\hat{n}, t) \hat{c} \\ -i \exp\{-i\omega(\hat{n}-1)t\} \lambda \hat{E}_2(\hat{n}, t) c\Lambda^\dagger & \exp\{-i\omega(\hat{n}-1)t\} \hat{F}_2(\hat{n}, t) \end{bmatrix}, \quad (7)$$

$$\hat{F}_j(\hat{n}, t) = \cos \hat{\mu}_j(\hat{n})t - \frac{i\Delta}{\hat{\mu}_j(\hat{n})} \sin \hat{\mu}_j(\hat{n})t, \hat{E}_j(\hat{n}, t) = \frac{\sin \hat{\mu}_j(\hat{n})t}{\hat{\mu}_j(\hat{n})}, j = 1, 2, \quad (8)$$

$$\mu_j^2(\hat{n}) = \Delta^2 + \nu_j(\hat{n}), j = 1, 2, \quad (9)$$

$$\hat{\nu}_1(\hat{n}) = \lambda^2(\hat{n} + 1), \hat{\nu}_2 = \hat{\nu}_1(\hat{n} - 1). \quad (10)$$

Assume that the atom is initially in the excited state $|+\rangle$, and the field in a Binomial state $|\eta, M\rangle$ [18], where

$$|\eta, M\rangle = \sum_{n=0}^M B(\eta, M, n) |n\rangle, \quad (11)$$

$$B(\eta, M, n) = \sqrt{\binom{M}{n} \eta^n (1-\eta)^{M-n}}, \quad (12)$$

where η is the characteristic probability of having each photon occurring, and M is the maximum photon number present in the field.

Therefore, the time-dependent wave function describing the proposed quantum system is given from the following relation,

$$|\psi_{AF}(t)\rangle = |a\rangle|+\rangle + |b\rangle|-\rangle, \quad (13)$$

where

$$|a\rangle = \sum_{n=0}^M B(\eta, M, n) F_1(n, t) |n\rangle, \quad (14)$$

$$|b\rangle = -i \sum_{n=0}^M B(\eta, M, n) \exp \{-i\omega n t\} \sqrt{v_1(n)} E_1(n, t) |n+1\rangle. \quad (15)$$

3. Nonclassical Properties

In this part, the values of the parameters of this system are estimated. This leads to the improvement of the values of the entanglement between the proposed system. There is no doubt that the use of a statistical method in estimating the parameters leads to better results than the use of random values for these parameters. In quantum information, systems of qubits that interact remarkably with photons (quantum electrodynamics) are a suitable environment for studying open quantum systems [19]. Aside from being a major candidate for quantum information manipulation, such quantum optical systems are of fundamental theoretical importance [20]. In particular, the experimental and theoretical study of quantum optical systems may yield insight into the links between mixedness and entanglement. The mixedness which is associated with the impurity of the quantum state is always measured by atomic entropy [21]. The reduced density operator is given by

$$\rho_A(t) = \text{Tr}_F(|\psi_{AF}(t)\rangle\langle\psi_{AF}(t)|) = \begin{bmatrix} \langle a|a\rangle & \langle b|a\rangle \\ \langle a|b\rangle & \langle b|b\rangle \end{bmatrix}, \quad (16)$$

Here, the von Neumann formula is used to measure the entanglement between parts of a quantum system. Therefore, the von Neumann entropy is given by the following relation,

$$S_A(T) = -\text{Tr}_A(\rho_A(t) \ln(\rho_A(t))) = -\sum_{j=1}^2 e_j \ln(e_j), \quad (17)$$

where e_1, e_2 are the eigenvalues of the atomic reduced density matrix, which are defined as follows,

$$e_1(t) = \frac{1 + \sqrt{1 - 4(\langle a|a\rangle\langle b|b\rangle - |\langle a|b\rangle|^2)}}{2}, \quad (18)$$

$$e_2(t) = \frac{1 - \sqrt{1 - 4(\langle a|a\rangle\langle b|b\rangle - |\langle a|b\rangle|^2)}}{2}. \quad (19)$$

Recently, some measures have emerged that lead to measuring the entanglement between parts of quantum systems. One of the most well-known of these measures is Wehrl entropy [22], which is formulated on atomic Q-function. Therefore, the atomic Q-function is defined as follows,

$$Q_A(t) = \frac{1}{2\pi} \langle \theta, \phi | \rho_A(t) | \theta, \phi \rangle, \quad (20)$$

where θ, ϕ are the atomic phase space parameters and $|\theta, \phi\rangle$

is the atomic coherent state, which is defined as

$$|\theta, \phi\rangle = \cos\left(\frac{\theta}{2}\right)|+\rangle + \sin\left(\frac{\theta}{2}\right)\exp(-i\phi)|-\rangle. \quad (21)$$

The expansion in terms of θ and ϕ can be deciphered as follows:

$$Q_A(t) = \frac{1}{2\pi} \left(\frac{1 + (\langle a|a\rangle - \langle b|b\rangle) \cos(\theta) + 2 \text{Re}(\langle a|b\rangle) \sin(\theta) \cos(\phi) + 2 \text{Im}(\langle a|b\rangle) \sin(\theta) \sin(\phi)}{2} \right), \quad (22)$$

$$0 \leq \theta \leq \pi, 0 \leq \phi \leq 2\pi. \quad (23)$$

Another measure of classical correlation for quantum systems in phase space is the Wigner function [23, 24], which is given by

$$W(x, y) = \frac{1}{\pi} \sum_{k=0}^{\infty} \sum_{n,m=0}^{\infty} (-1)^k (A_n(t) A_m^*(t) G_{k,n}(\Gamma) G_{m,k}(\Gamma) + B_n(t) B_m^*(t) G_{k,n+1}(\Gamma) G_{m+1,k}(\Gamma)), \quad (24)$$

$$A_n(t) = B(\eta, M, n) F(n, t), B_n(t) = -iB(\eta, M, n) \exp\{-i\omega n t\} \sqrt{v_1(n)} E_1(n, t), \quad (25)$$

$$G_{k,n}(\Gamma) = \exp\left(-\frac{|\Gamma|^2}{2}\right) \sum_{j=0}^{\min(k,n)} \frac{(-\Gamma)^{k-j} (\Gamma^*)^{n-j} \sqrt{k!n!}}{(k-j)!(n-j)!j!}, \quad (26)$$

$$\Gamma = x + iy. \quad (27)$$

4. Statistical Study

4.1. Statistical Study and Discussions. It is worth to investigate the relationship between S, Q , and W (i.e., when S is a maximum, is that would lead to Q to be maximum or minimum? Then what is the effect on the related parameters η, τ , and else). Some questions about the behaviour of equations (17), (23), and (24) and the related parameters in many cases have not a precise answer. Therefore, statistical studies are given in this subsection to give suitable answers in this point.

Statistical studies are used frequently to address and solve many of research questions. Simulation studies are creating data with numerical techniques like Monte-Carlo simulation by pseudorandom sampling based on computer packages for conducting experiments on the computer [25–30]. A Monte-Carlo simulation is defined as using random sampling from probability distributions in the computer experiments. Many researchers have used the simulation studies in their research, among them [16, 17]. The aim of simulation studies of this research is the ability to understand the behaviour of certain functions. This allows to consider some properties of the required equations (17), (23), and (24). The Monte-Carlo simulations are employed to investigate the behaviour of S, Q , and W functions and the related parameters by assuming that the parameters of

the S , Q , and W are random variables. Mathematica 10 program with 4 GB RAM and processor Core i7 is employed to generate samples for $\tau, \eta, \theta, \phi, x, y$, and M and then finding the corresponding dependent variables S, Q , and W . Depending on the interval of each variable, we assumed that

- (1) The parameter η of the binomial distribution is a random variable follows the standard uniform distribution in the form $f(\eta) = 1, 0 \leq \eta \leq 1$
- (2) The parameter τ is a random variable follows a uniform distribution in the form $f(\tau) = 1/50, 1 < \tau < 50, 0 \leq \tau \leq 50$
- (3) X has a standard normal distribution in the form $f(x) = 1/\sqrt{2\pi}e^{-0.5x^2}, -\infty < x < \infty$
- (4) Y has a standard normal distribution in the form $f(y) = 1/\sqrt{2\pi}e^{-0.5y^2}, -\infty < y < \infty$
- (5) The number of values which simulated was 5000 runs and $M = 5, 20, 50$ and 100. Then, finding the maximum and minimum for $S, Q, W, \tau(d), \eta(d), \theta, \phi, x$, and y for each value of M , where $d = S, Q$, and W . For instance, $\max \eta(S) = 0.0203785$ when $M = 5$ means that the value of $\eta = 0.0203785$ when S was maximum and similarly for Q and W . Some graphs are obtained to see the behaviour of S, Q , and W graphically at the maximum and minimum points which are given at Tables 1–4

Here, the results were obtained from the simulation method which are used to discuss the entanglement in the case of $M = 50$. For the data that estimated the maximum values of $S_A(T)$, the entanglement between the cavity field and the qubit returns between maximum and minimum values $(0, \ln(2))$; moreover, it repeats periodically. The function $S_A(T)$ reaches zero (pure state) only in two points, as evident from Figure 1. Whereas in the case of the minimum function $S_A(T)$, the entanglement between the field and the qubits reaches a state of separation periodically, as seen in Figure 2.

For the data that estimated the maximum values of $Q_A(t)$, in the case of $M = 50$, the atomic Q -function fluctuates chaotically, and the negative values are not shown of completely, see Figure 3. Moreover, the function $Q_A(t)$ is improved and oscillations appeared regularly as observed in Figure 3. For the data that estimated the minimum values of $Q_A(t)$, in the case of $M = 50$, the oscillations have the chaotic behaviour. The intensity of the oscillations increases when $M = 50$ is taken into account, as shown in Figure 4.

For the data that estimated the maximum values of $W(x, y)$, in the case $M = 50$, for the maximum data, the quasi-distribution $W(x, y)$ has one-peak centered in the center $(0, 0)$. The nonclassical behaviour appears around the peak. The maximum values of the function $W(x, y)$ which decrease after the minimum values data are included. The previous peak was divided into a crater with multiple peaks at the edges. In addition, the negative values appear significantly as shown in Figure 5.

4.2. Concluding Remarks. The aim of this study is to discover the behaviour of the three main functions S, Q , and W between each others and studying the impact of the related variables. A standard uniform distribution has used to generate values for η, τ, θ, ϕ , and the standard normal distribution has used to generate values for x and y . A random samples of $0 < \tau < 50, 0 < \eta \leq 1, 0 < \theta < \pi, 0 < \phi < 2\pi, -\infty < x < \infty$ and $-\infty < y < \infty$ are generated and then S, Q , and W are estimated by using Mathematica 10 program to make a numerical study. Depending on the statistical study presented on the previous Section 4, the values of S and Q are always positive but W may take negative values. There is no affection of $\tau, \eta, \theta, \phi, x, y$, and M on the behaviour of S, Q , and W functions. In addition, all cases of $M, W < Q < S$ as seen in Tables 1–4 and Figures 1–6, the remarks on the Tables can be written as follows.

4.3. Remarks

- (1) The S function always positive and less than $\ln 2$ and may take 0 by rounding, while the W function may take negative values
- (2) The behaviour of the functions S, Q , and W does not depend on the values of τ and η . A direct or an indirect relation between the specific functions and their parameters cannot be discovered
- (3) A similar behaviour of the S, Q , and W does not observe. There is no remark recorded that the three functions have a maximum or minimum at the same time and at the same values
- (4) The impact of increasing M is too low on S, Q , and W
- (5) The upper limit of Q function is $\ln 1.002779 \approx 0.0027748$ and does not less than 0
- (6) The upper limit of W function is $\ln 1.0055 \approx 0.00553$ and is not less than -0.00096
- (7) Depending on simulation study, there is no relation between θ and ϕ and the behaviour of Q
- (8) The signs of x and y may be the same or different in many cases, and there are no relation between x and y and the behaviour of W
- (9) In all cases of M , the relation $W < Q < S$ was verified

5. Conclusion

A statistical method is used to predict the behaviour of a quantum model consisting of a qubit interacting with a single-mode cavity field is addressed. The qubit is prepared in the excited state while the field is in the binomial distribution. The wave function of the proposed model is obtained and studied numerically. A von Neumann entropy is used to investigate the behaviour of the entanglement between the field and the qubits. Moreover, the atomic Q and Wigner functions are used to identify the behaviour of the distribution in a phase space. A numerical study is performed to

estimate the specific dependency of the binomial distribution state. The results of entanglement were compared with the atomic Q and Wigner functions (see Tables 1–4 and Figures 1–6). Finally, different values of the parameters $\tau, \eta, \theta, \phi, x$, and y are simulated and then the maximum and minimum values of S, Q , and W are obtained. In brief, depending on the statistical study which was presented on Section 4, the values of S and Q are always positive but W may take negative values. Furthermore, there is no affection of $\tau, \eta, \theta, \phi, x, y$, and M on the behaviour of S, Q , and W functions.

Data Availability

The data used are generated from the mathematical models in the article.

Conflicts of Interest

The authors have no conflicts of interest regarding the publication of the paper.

Acknowledgments

This research was funded by the Deanship of Scientific Research, Taif University, KSA (research group number 1-1441-100).

References

- [1] Saifullah et al., “Feedback control of probability amplitudes for two-level atom in optical field,” *Optics Communications*, vol. 281, no. 4, pp. 640–643, 2008.
- [2] S. V. Prants and V. Y. Sirotkin, “Effects of the Rabi oscillations on the atomic motion in a standing-wave cavity,” *Physical Review A*, vol. 64, no. 3, 2001.
- [3] M. S. Abdalla, E. M. Khalil, and A.-S. F. Obada, “Statistical properties of a two-photon cavity mode in the presence of degenerate parametric amplifier,” *Annals of Physics*, vol. 322, no. 11, pp. 2554–2568, 2007.
- [4] E. M. Khalil, M. S. Abdalla, and A.-S. F. Obada, “Entropy and variance squeezing of two coupled modes interacting with a two-level atom: frequency converter type,” *Annals of Physics*, vol. 321, no. 2, pp. 421–434, 2006.
- [5] S. Bougouffa, “Entanglement dynamics of two-bipartite system under the influence of dissipative environments,” *Optics Communication*, vol. 283, no. 14, pp. 2989–2996, 2010.
- [6] N. H. Abdel-Wahab and M. F. Mourad, “On the interaction between two two-level atoms and a two mode cavity field in the presence of detuning and cross-Kerr nonlinearity,” *Physica Scripta*, vol. 84, no. 1, article 015401, 2011.
- [7] A. Slaoui, A. Salah, and M. Daoud, “Influence of Stark-shift on quantum coherence and non-classical correlations for two two-level atoms interacting with a single-mode cavity field,” *Physica A: Statistical Mechanics and its Applications*, vol. 558, article 124946, 2020.
- [8] K. El Anouz, A. El Allati, A. Salah, and F. Saif, “Quantum fisher information: probe to measure fractional evolution,” *International Journal of Theoretical Physics*, vol. 59, no. 5, pp. 1460–1474, 2020.
- [9] N. H. Abdel-Wahab and A. Salah, “On the interaction between a time-dependent field and a two-level atom,” *Modern Physics Letters A*, vol. 34, no. 10, article 1950081, 2019.
- [10] A.-S. F. Obada, M. M. A. Ahmed, A. M. Farouk, and A. Salah, “A moving three-level Λ -type atom in a dissipative cavity,” *The European Physical Journal D*, vol. 71, no. 12, pp. 1–13, 2017.
- [11] N. H. Abd el-Wahab and A. Salah, “The influence of the classical homogenous gravitational field on interaction of a three-level atom with a single mode cavity field,” *Modern Physics Letters B*, vol. 29, no. 29, article 1550175, 2015.
- [12] J. K. Kalaga, A. Kowalewska-Kudlaszyk, W. Leoński, and A. Barasiński, “Quantum correlations and entanglement in a model comprised of a short chain of nonlinear oscillators,” *Physical Review A*, vol. 94, no. 3, 2016.
- [13] L.-T. Shen, Z.-B. Yang, H.-Z. Wu, X.-Y. Chen, and S.-B. Zheng, “Control of two-atom entanglement with two thermal fields in coupled cavities,” *Journal of the Optical Society of America B*, vol. 29, no. 9, article 2379, 2012.
- [14] J. K. Kalaga, W. Leonski, and R. Szczesniak, “Quantum steering and entanglement in three-mode triangle Bose-Hubbard system,” *Quantum Information Processing*, vol. 16, no. 11, p. 265, 2017.
- [15] S. L. Braunstein, *Quantum Computing: Where Do We Want to Go Tomorrow?*, Wiley-VCH, New York, 1999.
- [16] A.-S. F. Obada, M. M. A. Ahmed, and E. M. Khalil, “Generation of a nonlinear two-mode Stark shift through the adiabatic elimination method,” *Journal of Modern Optics*, vol. 53, no. 8, pp. 1149–1163, 2006.
- [17] E. M. Khalil, K. Berrada, S. Abdel-Khalek, A. Al-Barakaty, and J. Perina, “Entanglement and entropy squeezing in the system of two qubits interacting with a two-mode field in the context of power law potentials,” *Scientific Reports*, vol. 10, no. 1, article 76059, 2020.
- [18] R. Lo Franco, G. Compagno, A. Messina, and A. Napoli, “Generating and revealing a quantum superposition of electromagnetic-field binomial states in a cavity,” *Physical Review A*, vol. 76, no. 1, article 011804, 2007.
- [19] H. Mabuchi and A. C. Doherty, “Cavity quantum electrodynamics: coherence in context,” *Science*, vol. 298, no. 5597, pp. 1372–1377, 2002.
- [20] C. Monroe, “Quantum information processing with atoms and photons,” *Nature*, vol. 416, no. 6877, pp. 238–246, 2002.
- [21] G. Jaeger, A. V. Sergienko, B. E. A. Saleh, and M. C. Teich, “Entanglement, mixedness, and spin-flip symmetry in multiple-qubit systems,” *Physical Review A*, vol. 68, no. 2, article 022318, 2003.
- [22] A.-S. F. Obada, S. Abdel-Khalek, E. M. Khalil, and S. I. Ali, “Effects of Stark shift and decoherence terms on the dynamics of phase-space entropy of the multiphoton Jaynes Cummings model,” *Physica Scripta*, vol. 86, no. 5, article 055009, 2012.
- [23] E. Wigner, “On the quantum correction for thermodynamic equilibrium,” *Physics Review*, vol. 40, no. 5, pp. 749–759, 1932.
- [24] M. Y. Abd-Rabbou, E. M. Khalil, M. M. A. Ahmed, and A.-S. F. Obada, “External classical field and damping effects on a moving two level atom in a cavity field interaction with Kerr-like medium,” *International Journal of Theoretical Physics*, vol. 58, pp. 4012–4024, 2019.
- [25] T. Morris, I. White, and M. Crowther, “Using simulation studies to evaluate statistical methods,” *Statistics in Medicine*, vol. 38, no. 11, pp. 2074–2102, 2019.

- [26] A.-L. Boulesteix, R. H. H. Groenwold, M. Abrahamowicz et al., "Introduction to statistical simulations in health research," *Epidemiology Communication*, vol. 10, no. 12, article e039921, 2020.
- [27] M. M. Amein, "Estimation for unknown parameters of the Burr type-XII distribution based on an adaptive progressive type-II censoring scheme," *Journal of Mathematics and Statistics*, vol. 12, no. 2, pp. 119–126, 2016.
- [28] M. M. Mohie El-Din, M. M. Amein, A. R. Shafay, and S. Mohamed, "Bayesian prediction based on an adaptive type-II progressive censored data from the generalized exponential distribution," *International Journal of Computer Applications*, vol. 179, no. 46, pp. 1–6, 2018.
- [29] M. M. Amein and N. Sayed-Ahmed, "Estimation for unknown parameters of the extended Burr type-XII distribution based on type-I hybrid progressive censoring scheme," *International Journal of Applied Engineering Research*, vol. 13, no. 3, article 1761, 2018.
- [30] M. M. Amein, N. Sayed-Ahmed, and O. S. Bakri, "Interval estimation for Burr-X distribution under type-I hybrid progressive censoring scheme," *Journal of Statistics Applications & Probability*, vol. 7, no. 1, p. 1, 2020.

Research Article

On Fractional Diffusion Equation with Caputo-Fabrizio Derivative and Memory Term

Binh Duy Ho,¹ Van Kim Ho Thi,¹ Long Le Dinh ,¹ Nguyen Hoang Luc,¹ and Phuong Nguyen ²

¹Division of Applied Mathematics, Thu Dau Mot University, Binh Duong Province, Vietnam

²Faculty of Fundamental Science, Industrial University of Ho Chi Minh City, Vietnam

Correspondence should be addressed to Phuong Nguyen; nguyenducphuong@iuh.edu.vn

Received 6 May 2021; Revised 15 July 2021; Accepted 28 July 2021; Published 16 August 2021

Academic Editor: Mustafa Inc

Copyright © 2021 Binh Duy Ho et al. This is an open access article distributed under the Creative Commons Attribution License, which permits unrestricted use, distribution, and reproduction in any medium, provided the original work is properly cited.

In this paper, we examine a nonlinear fractional diffusion equation containing viscosity terms with derivative in the sense of Caputo-Fabrizio. First, we establish the local existence and uniqueness of lightweight solutions under some assumptions about the input data. Then, we get the global solution using some new techniques. Our main idea is to combine theories of Banach's fixed point theorem, Hilbert scale theory of space, and some Sobolev embedding.

1. Introduction

The fractional calculation has a long history and plays an important role in the simulation of physical phenomena or real life, for example, mechanics, electricity, chemistry, biology, economics, notably control theory, and images. It should be noted that the standard mathematical models of integer derivatives, including nonlinear models, do not work fully in many cases. Therefore, the advent of fractional calculus was significant in modeling physical and engineering processes, and it can be said that it is one of the best descriptors using fractional differential equations. In a series of research directions on fractional differential equations (FDE), the most prominent is the appearance of two derivatives: Caputo derivative and Riemann-Liouville derivative. Some works are attracting the attention of the community, like Debbouche and his group [1–3], Karapinar et al. [4–11], Inc and his group [12–16], Tuan and his group [17–20], and the references as follows: [21–23].

In this paper, we consider the fractional Sobolev equation:

$$\begin{cases} {}_{CF}D_t^\alpha u = \Delta u + G(u) + \int_0^t \psi(t-z)K(u(z))dz, & (x, t) \in \mathcal{M} \times (0, T), \\ u = 0, & (x, t) \in \partial\mathcal{M} \times (0, T), \\ u(x, 0) = u_0(x), \end{cases} \quad (1)$$

where ${}_{CF}D_t^\alpha$ is the Caputo-Fabrizio operator for fractional derivatives of order α which is defined as (see [24])

$${}_{CF}D_t^\alpha v(t) = \frac{H(\alpha)}{1-\alpha} \int_0^t \mathcal{D}_\alpha(t-v) \frac{\partial v(v)}{\partial v} dv, \quad \text{for } t \geq 0, \quad (2)$$

where we denote by the kernel $\mathcal{D}_\alpha(z) = \exp(-(\alpha/(1-\alpha))z)$ and $H(\alpha)$ satisfies $H(0) = H(1) = 1$ (see, e.g., [25, 26]).

The Caputo-Fabrizio fractional derivative was presented in 2015 [25] with the aim of avoiding singular kernels. It is also the convolution of the exponential function and the first-order derivative. The Caputo-Fabrizio fraction derivative is an operator that has been widely applied to several derivative modes in many fields, such as biology, physics, control systems, materials science, dynamics, and liquid learning [27–32].

Our main aim in this paper is to provide the local and global existence for problem (1) under some various assumptions on the input data. The difficulty in studying this problem is from the memory viscoelastic model appearing in the main equation. This term makes some of the assessments more complicated. Another difficulty is the study of the existence of global solutions. The topic of the existence of global solutions is still challenging for many mathematicians today. In the paper, we have to use a new norm in weighted space, thanks to the work of [33], to establish the global solution. The two main results in the paper are shown as follows:

- (i) The first result is related to the existence of local solutions. The main technique is to apply Banach's fixed point theorem
- (ii) The second result is very interesting, proving the existence of a global solution. To do this, we have to thank a lemma in [33], where we have chosen suitable assumptions for functions G and K , to obtain our purpose

The paper is organized as follows. In Section 2, we give preliminaries which are useful for the next results. Section 3 shows the local existence results. In Section 4, we provide global existence results.

2. Preliminaries

We recall the Hilbert scale space, which is given as follows:

$$H^r(\mathcal{M}) = \left\{ f \in L^2(\mathcal{M}), \sum_{n=1}^{\infty} \lambda_n^r \langle f, e_n \rangle_{L^2(\mathcal{M})}^2 < \infty \right\}, \quad (3)$$

for any $r \geq 0$. Here, the symbol $\langle \cdot, \cdot \rangle_{L^2(\mathcal{M})}$ denotes the inner product in $L^2(\mathcal{M})$. It is well known that $\mathcal{H}^r(\mathcal{M})$ is a Hilbert space corresponding to the following norm:

$$\|f\|_{H^r(\mathcal{M})} = \sqrt{\sum_{n=1}^{\infty} \lambda_n^r \langle f, e_n \rangle_{L^2(\mathcal{M})}^2}, \quad f \in \mathcal{H}^r(\mathcal{M}). \quad (4)$$

$H^v(\Omega) \equiv D((-\mathbb{L})^v)$ is a Hilbert space. Then, $D((-\mathbb{L})^{-v})$ is a Hilbert space with the norm:

$$\|v\|_{D((-\mathbb{L})^{-v})} = \left(\sum_{j=1}^{\infty} |\langle v, e_j \rangle|^2 \lambda_j^{-2v} \right)^{1/2}, \quad (5)$$

where $\langle \cdot, \cdot \rangle$ in the latter equality denotes the duality between $D((-\mathbb{L})^{-v})$ and $D((-\mathbb{L})^v)$.

Definition 1. The function v is called a mild solution of problem (1) if it satisfies that

$$\begin{aligned} \theta(t) &= \mathbf{P}_\alpha(t)u_0 + \int_0^t \mathbf{P}_\alpha(t-\tau)G(\theta(\tau))d\tau \\ &\quad + \int_0^t \mathbf{P}_\alpha(t-\tau) \int_0^\tau \psi(\tau-\xi)K(\theta(\xi))d\xi d\tau, \end{aligned} \quad (6)$$

where $\mathbf{P}_\alpha(t)$ is defined by

$$\begin{aligned} \mathbf{P}_\alpha(t)w &= (1 + \bar{\alpha}\lambda_n)^{-1} \exp\left(\frac{-\alpha\lambda_n}{1 + \bar{\alpha}\lambda_n}t\right) \langle w, e_n \rangle_{L^2(\mathcal{M})} e_n(x), \bar{\alpha} \\ &= 1 - \alpha, \end{aligned} \quad (7)$$

for any $w \in L^2(\mathcal{M})$.

Lemma 1. Let $\theta \in H^{r-2}(\mathcal{M}) \cap H^{r-2-2\beta}(\mathcal{M})$. Then,

$$\|\mathbf{P}_\alpha(t)\theta\|_{H^r(\mathcal{M})} \leq \bar{C}_{1,\alpha,\beta} t^{-\beta} \|\theta\|_{H^{r-2}(\mathcal{M})} + \bar{C}_{2,\alpha,\beta} t^{-\beta} \|\theta\|_{H^{r-2-2\beta}(\mathcal{M})}, \quad (8)$$

for any $0 < \beta < 1$.

Proof. By the definitions of the norm in $H^r(\mathcal{M})$ and using the inequality $e^{-y} \leq C - \beta y^{-\beta}$ for $\beta > 0$, we get the following confirmation:

$$\begin{aligned} \|\mathbf{P}_\alpha(t)\theta\|_{H^r(\mathcal{M})} &= \sqrt{\sum_{n=1}^{\infty} \lambda_n^r (1 + \bar{\alpha}\lambda_n)^{-2} \exp\left(\frac{-2\alpha\lambda_n}{1 + \bar{\alpha}\lambda_n}t\right) \langle \theta, e_n \rangle_{L^2(\mathcal{M})}^2} \\ &\leq C_\beta (1 - \alpha)^{-1} t^{-\beta} \sqrt{\sum_{n=1}^{\infty} \lambda_n^{r-2} \left(\frac{1 + (1 - \alpha)\lambda_n}{\alpha\lambda_n}\right)^{2\beta} \langle \theta, e_n \rangle_{L^2(\mathcal{M})}^2}. \end{aligned} \quad (9)$$

Since $0 < \beta < 1$, we know that

$$\left(\frac{1 + (1 - \alpha)\lambda_n}{\alpha\lambda_n}\right)^{2\beta} \leq \left(\frac{(1 - \alpha)^2}{\alpha^2} + \frac{1}{\alpha^2 \lambda_n^2}\right)^\beta \leq \left(\frac{(1 - \alpha)^{2\beta}}{\alpha^{2\beta}} + \alpha^{-2\beta} \lambda_n^{-2\beta}\right). \quad (10)$$

This follows from (9) that

$$\begin{aligned} \|\mathbf{P}_\alpha(t)\theta\|_{H^r(\mathcal{M})} &\leq C_\beta (1 - \alpha)^{-1} t^{-\beta} \frac{(1 - \alpha)^\beta}{\alpha^\beta} \sqrt{\sum_{n=1}^{\infty} \lambda_n^{r-2} \langle \theta, e_n \rangle_{L^2(\mathcal{M})}^2} \\ &\quad + C_\beta (1 - \alpha)^{-1} \alpha^{-\beta} t^{-\beta} \sqrt{\sum_{n=1}^{\infty} \lambda_n^{r-2-2\beta} \langle \theta, e_n \rangle_{L^2(\mathcal{M})}^2} \\ &\leq \bar{C}_{1,\alpha,\beta} t^{-\beta} \|\theta\|_{H^{r-2}(\mathcal{M})} + \bar{C}_{2,\alpha,\beta} t^{-\beta} \|\theta\|_{H^{r-2-2\beta}(\mathcal{M})}. \end{aligned} \quad (11)$$

□

3. Local Existence Results

In this section, we give the following theorem which shows the local existence result.

Theorem 1. *Let the two functions G and K be*

$$\begin{aligned} \|G(\theta_1) - G(\theta_2)\|_{L^2(M)} &\leq B_G \|\theta_1 - \theta_2\|_{L^2(M)}, \\ \|K(\theta_1) - K(\theta_2)\|_{L^2(M)} &\leq B_K \|\theta_1 - \theta_2\|_{L^2(M)}, \end{aligned} \quad (12)$$

for constants $B_G, B_K \geq 0$. Let us assume that there exists δ such that

$$|\psi(z)| \leq \mathcal{D}z^{-\delta}, \delta < 1. \quad (13)$$

Let $u_0 \in H^{p-2}(\mathcal{M}) \cap H^{p-2-2\beta}(\mathcal{M})$. Then, problem (1) has a local mild solution:

$$u \in L^\infty_\vartheta(0, T; H^p(\mathcal{M})), \quad (14)$$

where

$$0 < \beta \leq \vartheta < 1, 0 \leq p \leq 2. \quad (15)$$

Proof. Let the function \mathfrak{F} be as follows:

$$\begin{aligned} \mathfrak{F}\theta(t) &= \mathbf{P}_\alpha(t)u_0 + \int_0^t \mathbf{P}_\alpha(t-\tau)G(\theta(\tau))d\tau \\ &\quad + \int_0^t \mathbf{P}_\alpha(t-\tau) \int_0^\tau \psi(\tau-\xi)K(\theta(\xi))d\xi d\tau \\ &= \mathbf{P}_\alpha(t)u_0 + \mathfrak{F}_1\theta(t) + \mathfrak{F}_2\theta(t). \end{aligned} \quad (16)$$

Step 1. Estimate $\|\mathfrak{F}_1\theta_1 - \mathfrak{F}_1\theta_2\|_{H^p(\mathcal{M})}$ for any θ_1, θ_2 that belongs to the space $H^p(\mathcal{M})$.

From the definition of \mathfrak{F}_1 as in (16), we find that

$$\begin{aligned} \|\mathfrak{F}_1\theta_1 - \mathfrak{F}_1\theta_2\|_{H^p(\mathcal{M})} &= \left\| \int_0^t \mathbf{P}_\alpha(t-\tau)G(\theta_1(\tau))d\tau - \int_0^t \mathbf{P}_\alpha(t-\tau)G(\theta_2(\tau))d\tau \right\|_{H^p(\mathcal{M})} \\ &\leq \bar{C}_{1,\alpha,\beta} \int_0^t (t-\tau)^{-\beta} \|G(\theta_1(\tau)) - G(\theta_2(\tau))\|_{H^{p-2}(\mathcal{M})} d\tau \\ &\quad + \bar{C}_{2,\alpha,\beta} \int_0^t (t-\tau)^{-\beta} \|G(\theta_1(\tau)) - G(\theta_2(\tau))\|_{H^{p-2-2\beta}(\mathcal{M})} d\tau. \end{aligned} \quad (17)$$

Since $p \leq 2$, we know the Sobolev embedding $L^2(\mathcal{M})^\circ \hookrightarrow H^{p-2}(\mathcal{M})$, and so we get

$$\begin{aligned} \|G(\theta_1(\tau)) - G(\theta_2(\tau))\|_{H^{p-2}(\mathcal{M})} &\leq C_1 \|G(\theta_1(\tau)) - G(\theta_2(\tau))\|_{L^2(\mathcal{M})} \\ &\leq C_1 B_G \|\theta_1(\tau) - \theta_2(\tau)\|_{L^2(\mathcal{M})}, \\ \|G(\theta_1(\tau)) - G(\theta_2(\tau))\|_{H^{p-2-2\beta}(\mathcal{M})} &\leq C_{1,\beta} \|G(\theta_1(\tau)) - G(\theta_2(\tau))\|_{L^2(\mathcal{M})} \\ &\leq C_{1,\beta} B_K \|\theta_1(\tau) - \theta_2(\tau)\|_{L^2(\mathcal{M})}. \end{aligned} \quad (18)$$

From two above observations, we deduce that

$$\begin{aligned} t^\vartheta \|\mathfrak{F}_1\theta_1 - \mathfrak{F}_1\theta_2\|_{H^p(\mathcal{M})} &\leq (\bar{C}_{1,\alpha,\beta} C_1 B_G + \bar{C}_{2,\alpha,\beta} C_1 B_K) t^\vartheta \int_0^t (t-\tau)^{-\beta} \|\theta_1(\tau) \\ &\quad - \theta_2(\tau)\|_{L^2(\mathcal{M})} d\tau \\ &\leq \bar{C}_{3,p,\alpha,\beta} t^\vartheta \int_0^t (t-\tau)^{-\beta} \tau^{-\vartheta} \|\theta_1(\tau) - \theta_2(\tau)\|_{H^p(\mathcal{M})} d\tau \\ &\leq \bar{C}_{3,p,\alpha,\beta} t^\vartheta \left(\int_0^t (t-\tau)^{-\beta} \tau^{-\vartheta} d\tau \right) \|\theta_1 - \theta_2\|_{L^\infty_\vartheta(0,T;H^p(\mathcal{M}))} \\ &= \bar{C}_{3,p,\alpha,\beta} t^{1-\beta} \mathbf{B}(1-\beta, 1-\vartheta) \|\theta_1 - \theta_2\|_{L^\infty_\vartheta(0,T;H^p(\mathcal{M}))} \\ &\leq \bar{C}_{3,p,\alpha,\beta} T^{1-\beta} \mathbf{B}(1-\beta, 1-\vartheta) \|\theta_1 - \theta_2\|_{L^\infty_\vartheta(0,T;H^p(\mathcal{M}))}. \end{aligned} \quad (19)$$

Because the right side of the above expression does not depend on t , we have the following assertion:

$$\begin{aligned} \|\mathfrak{F}_1\theta_1 - \mathfrak{F}_1\theta_2\|_{L^\infty_\vartheta(0,T;H^p(\mathcal{M}))} \\ \leq \bar{C}_{3,p,\alpha,\beta} T^{1-\beta} \mathbf{B}(1-\beta, 1-\vartheta) \|\theta_1 - \theta_2\|_{L^\infty_\vartheta(0,T;H^p(\mathcal{M}))}. \end{aligned} \quad (20)$$

Step 2. Estimate $\|\mathfrak{F}_2\theta_1 - \mathfrak{F}_2\theta_2\|_{H^p(\mathcal{M})}$ for any θ_1, θ_2 that belongs to the space $H^p(\mathcal{M})$.

From the definition of \mathfrak{F}_2 as in (16), we find that

$$\begin{aligned} \|\mathfrak{F}_2\theta_1 - \mathfrak{F}_2\theta_2\|_{H^p(\mathcal{M})} &= \left\| \int_0^t \mathbf{P}_\alpha(t-\tau) \int_0^\tau \psi(\tau-\xi)K(\theta_1(\xi))d\xi d\tau \right. \\ &\quad \left. - \int_0^t \mathbf{P}_\alpha(t-\tau) \int_0^\tau \psi(\tau-\xi)K(\theta_2(\xi))d\xi d\tau \right\|_{H^p(\mathcal{M})} \\ &\leq \bar{C}_{1,\alpha,\beta} \int_0^t (t-\tau)^{-\beta} \left\| \int_0^\tau \psi(\tau-\xi)K(\theta_1(\xi))d\xi \right. \\ &\quad \left. - \int_0^\tau \psi(\tau-\xi)K(\theta_2(\xi))d\xi \right\|_{H^{p-2}(\mathcal{M})} d\tau \\ &\quad + \bar{C}_{2,\alpha,\beta} \int_0^t (t-\tau)^{-\beta} \left\| \int_0^\tau \psi(\tau-\xi)K(\theta_1(\xi))d\xi \right. \\ &\quad \left. - \int_0^\tau \psi(\tau-\xi)K(\theta_2(\xi))d\xi \right\|_{H^{p-2-2\beta}(\mathcal{M})} d\tau. \end{aligned} \quad (21)$$

It is easy to see that

$$\begin{aligned} \bar{C}_{1,\alpha,\beta} \left\| \int_0^\tau \psi(\tau-\xi)K(\theta_1(\xi))d\xi - \int_0^\tau \psi(\tau-\xi)K(\theta_2(\xi))d\xi \right\|_{H^{p-2}(\mathcal{M})} \\ \leq \bar{C}_{1,\alpha,\beta} C_1 B_G \mathcal{D} \int_0^\tau (\tau-\xi)^{-\delta} \|\theta_1(\xi) - \theta_2(\xi)\|_{L^2(\mathcal{M})} d\xi \\ \leq \bar{C}_{1,\alpha,\beta} C_1 B_G \mathcal{D} \int_0^\tau (\tau-\xi)^{-\delta} \xi^{-\vartheta} \xi^\vartheta \|\theta_1(\xi) - \theta_2(\xi)\|_{L^2(\mathcal{M})} d\xi \\ \leq \bar{C}_{1,\alpha,\beta} C_1 B_G \mathcal{D} \left(\int_0^\tau (\tau-\xi)^{-\delta} \xi^{-\vartheta} d\xi \right) \|\theta_1 - \theta_2\|_{L^\infty_\vartheta(0,T;H^p(\mathcal{M}))} \\ = \bar{C}_{1,\alpha,\beta} C_1 B_G \mathcal{D} \tau^{1-\delta-\vartheta} B(1-\delta, 1-\vartheta) \|\theta_1 - \theta_2\|_{L^\infty_\vartheta(0,T;H^p(\mathcal{M}))}. \end{aligned} \quad (22)$$

By a similar way as above, we also obtain that

$$\begin{aligned} & \bar{C}_{2,\alpha,\beta} \int_0^t (t-\tau)^{-\beta} \left\| \int_0^\tau \psi(\tau-\xi) K(\theta_1(\xi)) d\xi - \int_0^\tau \psi(\tau-\xi) K(\theta_2(\xi)) d\xi \right\|_{H^{p-2-2\beta}(\mathcal{M})} d\tau \\ & \leq \bar{C}_{2,\alpha,\beta} C_{1,\beta} B_K \mathcal{D} \tau^{1-\delta-\vartheta} B(1-\delta, 1-\vartheta) \|\theta_1 - \theta_2\|_{L^\infty_\vartheta(0,T;H^p(\mathcal{M}))}. \end{aligned} \quad (23)$$

From two recent observations and noting that $\beta + \delta < 2$, we find that

$$\begin{aligned} t^\vartheta \|\mathfrak{F}_2\theta_1 - \mathfrak{F}_2\theta_2\|_{H^p(\mathcal{M})} &= \bar{C}_3 B(1-\delta, 1-\vartheta) B(1-\beta, 2-\delta-\vartheta) t^{2-\beta-\delta} \|\theta_1 - \theta_2\|_{L^\infty_\vartheta(0,T;H^p(\mathcal{M}))} \\ &\leq \bar{C}_3 B(1-\delta, 1-\vartheta) B(1-\beta, 2-\delta-\vartheta) T^{2-\beta-\delta} \|\theta_1 - \theta_2\|_{L^\infty_\vartheta(0,T;H^p(\mathcal{M}))}, \end{aligned} \quad (24)$$

where

$$\bar{C}_3 = \bar{C}_{1,\alpha,\beta} C_1 B_G \mathcal{D} + \bar{C}_{2,\alpha,\beta} C_{1,\beta} B_K \mathcal{D}. \quad (25)$$

Due to the right hand side of (24) being independent of t , we can deduce that

$$\|\mathfrak{F}_2\theta_1 - \mathfrak{F}_2\theta_2\|_{L^\infty_\vartheta(0,T;H^p(\mathcal{M}))} \leq \bar{C}_3 \mathbf{B}(1-\delta, 1-\vartheta) \mathbf{B}(1-\beta, 2-\delta-\vartheta) T^{2-\beta-\delta} \|\theta_1 - \theta_2\|_{L^\infty_\vartheta(0,T;H^p(\mathcal{M}))}. \quad (26)$$

Combining (20) and (26), we derive that

$$\begin{aligned} \|\mathfrak{F}\theta_1 - \mathfrak{F}\theta_2\|_{L^\infty_\vartheta(0,T;H^p(\mathcal{M}))} &\leq \|\mathfrak{F}_1\theta_1 - \mathfrak{F}_1\theta_2\|_{L^\infty_\vartheta(0,T;H^p(\mathcal{M}))} \\ &\quad + \|\mathfrak{F}_2\theta_1 - \mathfrak{F}_2\theta_2\|_{L^\infty_\vartheta(0,T;H^p(\mathcal{M}))} \\ &\leq \bar{C}_{3,p,\alpha,\beta} T^{1-\beta} \mathbf{B}(1-\beta, 1-\vartheta) \|\theta_1 \\ &\quad - \theta_2\|_{L^\infty_\vartheta(0,T;H^p(\mathcal{M}))} \\ &\quad + \bar{C}_3 \mathbf{B}(1-\delta, 1-\vartheta) \mathbf{B}(1-\beta, 2-\delta \\ &\quad - \vartheta) T^{2-\beta-\delta} \|\theta_1 - \theta_2\|_{L^\infty_\vartheta(0,T;H^p(\mathcal{M}))}. \end{aligned} \quad (27)$$

Moreover, by applying Lemma 1 and noting that $\vartheta \geq \beta$, we can confirm the following results:

$$\begin{aligned} t^\vartheta \|\mathbf{P}_\alpha(t)u_0\|_{H^p(\mathcal{M})} &\leq t^\vartheta \left(\bar{C}_{1,\alpha,\beta} t^{-\beta} \|u_0\|_{H^{p-2}(\mathcal{M})} + \bar{C}_{2,\alpha,\beta} t^{-\beta} \|u_0\|_{H^{p-2-2\beta}(\mathcal{M})} \right) \\ &\leq \bar{C}_{1,\alpha,\beta} t^{\vartheta-\beta} \|u_0\|_{H^{p-2}(\mathcal{M})} + \bar{C}_{2,\alpha,\beta} t^{\vartheta-\beta} \|u_0\|_{H^{p-2-2\beta}(\mathcal{M})} \\ &\leq \bar{C}_{1,\alpha,\beta} T^{\vartheta-\beta} \|u_0\|_{H^{p-2}(\mathcal{M})} + \bar{C}_{2,\alpha,\beta} T^{\vartheta-\beta} \|u_0\|_{H^{p-2-2\beta}(\mathcal{M})}. \end{aligned} \quad (28)$$

□

4. Global Existence Results under a Global Lipschitz Case

In this section, we derive the global results under the assumption of the nonlinear source function F , a global Lipschitz.

Let F and g satisfy that

$$\|G(u) - F(v)\|_{H^s(\mathcal{M})} \leq L_g \|u - v\|_{H^q(\mathcal{M})}, \quad 1 \leq s \leq q, \quad (29)$$

$$\|K(u) - K(v)\|_{H^s(\mathcal{M})} \leq L_k \|u - v\|_{H^q(\mathcal{M})}, \quad 1 \leq s \leq q, \quad (30)$$

where K_f, K_g are postive constants. Our results in this section are to present the well-posedness of the problem. Let $\nu > 0$ and $q \geq 1$. In order to establish the existence of the mild solution, we need to define the following space:

$$\begin{aligned} \mathbf{X}_{d,m}((0, T]; H^q(\mathcal{M})) &= \left\{ f : \mathcal{M} \times [0, T] \longrightarrow \mathbb{R} : t^d e^{-mt} \|w(\cdot, t)\|_{H^q(\mathcal{M})} \right. \\ &\quad \left. < \infty, t \in [0, T] \right\}, \end{aligned} \quad (31)$$

associated with the following norm:

$$\|f\|_{\mathbf{X}_{d,m}((0,T];H^q(\mathcal{M}))} = \sup_{0 \leq t \leq T} t^d e^{-mt} \|w(\cdot, t)\|_{H^q(\mathcal{M})}. \quad (32)$$

Let us provide the following results that will be valuable in justifying our key results. We can find and view it in Lemma 8 of [33] (page 9).

Lemma 2. *Let $c > -1$, $d > -1$ such that $c + d \geq -1$, $h > 0$ and $t \in [0, T]$. For $\varepsilon > 0$, the following limit holds:*

$$\lim_{\varepsilon \rightarrow \infty} \left(\sup_{t \in [0, T]} t^h \int_0^1 \tau^c (1-\tau)^d e^{-\varepsilon t(1-\tau)} d\tau \right) = 0. \quad (33)$$

Now, we are in the position to introduce the main contributions of this work. Our main results address the global existence of the mild solution.

Theorem 2. Let $0 < \alpha < 1$. Let us assume that

$$|\theta(t)| \leq C_0 t^{-\delta}. \quad (34)$$

Let $u_0 \in H^{q-2-2\beta}(\mathcal{M}) \cap H^{q-2}(\mathcal{M})$. Then, there exists a positive number m_0 such that problem (1) has a unique solution in $\mathbf{X}_{d,m_0}((0, T]; H^q(\mathcal{M}))$. Here, β, d, δ satisfy that

$$0 < \beta \leq d < 1, \beta + d < 1, \beta + \delta < 2, \delta < 1. \quad (35)$$

Proof. Let the function $\mathfrak{F} : \mathbf{X}_{d,m}((0, T]; H^q(\mathcal{M})) \longrightarrow \mathbf{X}_{d,m}((0, T]; H^q(\mathcal{M}))$ be as follows:

$$\begin{aligned} \mathfrak{F}\theta(t) &= \mathbf{P}_\alpha(t)u_0 + \int_0^t \mathbf{P}_\alpha(t-\tau)G(\theta(\tau))d\tau \\ &\quad + \int_0^t \mathbf{P}_\alpha(t-\tau) \int_0^\tau \psi(\tau-\xi)K(\theta(\xi))d\xi d\tau \\ &= \mathbf{P}_\alpha(t)u_0 + \mathfrak{F}_1\theta(t) + \mathfrak{F}_2\theta(t). \end{aligned} \quad (36)$$

First, we have the following observation:

$$\|\mathbf{P}_\alpha(t)u_0\|_{H^q(\mathcal{M})} \leq \bar{C}_{1,\alpha,\beta} t^{-\beta} \|u_0\|_{H^{q-2}(\mathcal{M})} + \bar{C}_{2,\alpha,\beta} t^{-\beta} \|u_0\|_{H^{q-2-2\beta}(\mathcal{M})}. \quad (37)$$

By multiplying the two sides of the above inequality by $t^d e^{-mt}$ and noting that $e^{-mt} \leq 1$, one has

$$\begin{aligned} t^d e^{-mt} \|\mathbf{P}_\alpha(t)u_0\|_{H^q(\mathcal{M})} &\leq \bar{C}_{1,\alpha,\beta} t^{d-\beta} \|u_0\|_{H^{q-2}(\mathcal{M})} \\ &\quad + \bar{C}_{2,\alpha,\beta} t^{d-\beta} \|u_0\|_{H^{q-2-2\beta}(\mathcal{M})}. \end{aligned} \quad (38)$$

Noting that $d \geq \beta$, we deduce that if $u_0 \in H^{q-2-2\beta}(\mathcal{M}) \cap H^{q-2}(\mathcal{M})$, then the following holds:

$$\mathbf{P}_\alpha(t)u_0 \in X_{d,m}(\langle 0, T \rangle; H^q(\mathcal{M})). \quad (39)$$

Take two functions $\theta_1, \theta_2 \in \mathbf{X}_{d,m}((0, T]; H^q(\mathcal{M}))$. First, we need to derive the estimation for the term:

$$(I) = \left\| \int_0^t \mathbf{P}_\alpha(t-\tau)G(\theta_1(\tau))d\tau - \int_0^t \mathbf{P}_\alpha(t-\tau)G(\theta_2(\tau))d\tau \right\|_{H^q(\mathcal{M})}. \quad (40)$$

Using Lemma 1 and Sobolev embedding $H^s(\mathcal{M})^\circ \hookrightarrow H^{q-2}(\mathcal{M})$ and $H^s(\mathcal{M})^\circ \hookrightarrow H^{q-2-2\beta}(\mathcal{M})$ (since $s \geq q-2$), we arrive at

$$\begin{aligned} (I) &= \left\| \int_0^t \mathbf{P}_\alpha(t-\tau)G(\theta_1(\tau))d\tau - \int_0^t \mathbf{P}_\alpha(t-\tau)G(\theta_2(\tau))d\tau \right\|_{H^q(\mathcal{M})} \\ &\leq \bar{C}_{1,\alpha,\beta} \int_0^t (t-\tau)^{-\beta} \|G(\theta_1(\tau)) - G(\theta_2(\tau))\|_{H^{q-2}(\mathcal{M})} d\tau \\ &\quad + \bar{C}_{2,\alpha,\beta} \int_0^t (t-\tau)^{-\beta} \|G(\theta_1(\tau)) - G(\theta_2(\tau))\|_{H^{q-2-2\beta}(\mathcal{M})} d\tau \\ &\leq \left(\bar{C}_{1,\alpha,\beta} + \bar{C}_{2,\alpha,\beta} \right) \int_0^t (t-\tau)^{-\beta} \|G(\theta_1(\tau)) - G(\theta_2(\tau))\|_{H^s(\mathcal{M})} d\tau. \end{aligned} \quad (41)$$

Since the assumption (29), we know that

$$\begin{aligned} &\int_0^t (t-\tau)^{-\beta} \|G(\theta_1(\tau)) - G(\theta_2(\tau))\|_{H^s(\mathcal{M})} d\tau \\ &\leq L_g \int_0^t (t-\tau)^{-\beta} \|\theta_1(\tau) - \theta_2(\tau)\|_{H^q(\mathcal{M})} d\tau \\ &= L_g \left(\int_0^t (t-\tau)^{-\beta} \tau^{-d} e^{m\tau} \right) \|\theta_1 - \theta_2\|_{X_{d,m}((0,T];H^q(\mathcal{M}))}. \end{aligned} \quad (42)$$

Combining (40) and (41), we find that

$$\begin{aligned} &t^d e^{-mt} \left\| \int_0^t \mathbf{P}_\alpha(t-\tau)G(\theta_1(\tau))d\tau - \int_0^t \mathbf{P}_\alpha(t-\tau)G(\theta_2(\tau))d\tau \right\|_{H^q(\mathcal{M})} \\ &\leq \left(\bar{C}_{1,\alpha,\beta} + \bar{C}_{2,\alpha,\beta} \right) L_g t^d \\ &\quad \times \left(\int_0^t (t-\tau)^{-\beta} \tau^{-d} e^{-m(t-\tau)} d\tau \right) \|\theta_1 - \theta_2\|_{X_{d,m}((0,T];H^q(\mathcal{M}))} \\ &= \left(\bar{C}_{1,\alpha,\beta} + \bar{C}_{2,\alpha,\beta} \right) L_g t^{1-\beta} \\ &\quad \times \left(\int_0^1 (1-\xi)^{-\beta} \xi^{-d} e^{-mt(1-\xi)} d\xi \right) \|\theta_1 - \theta_2\|_{X_{d,m}((0,T];H^q(\mathcal{M}))}, \end{aligned} \quad (43)$$

where we have used the fact that

$$t^d \int_0^t (t-\tau)^{-\beta} \tau^{-d} e^{-m(t-\tau)} d\tau = t^{1-\beta} \int_0^1 (1-\xi)^{-\beta} \xi^{-d} e^{-mt(1-\xi)} d\xi. \quad (44)$$

Let us continue to treat the term. First, we need to derive the estimation for the term:

$$\begin{aligned} (II) &= \left\| \int_0^t \mathbf{P}_\alpha(t-\tau) \int_0^\tau \psi(\tau-\xi)K(\theta_1(\xi))d\xi d\tau \right. \\ &\quad \left. - \int_0^t \mathbf{P}_\alpha(t-\tau) \int_0^\tau \psi(\tau-\xi)K(\theta_2(\xi))d\xi d\tau \right\|_{H^q(\mathcal{M})}. \end{aligned} \quad (45)$$

Using Lemma 1 and Sobolev embedding $H^s(\mathcal{M})^\circ \hookrightarrow H^{q-2}(\mathcal{M})$ and $H^s(\mathcal{M})^\circ \hookrightarrow H^{q-2-2\beta}(\mathcal{M})$ (since $s \geq q-2$), we get the following bound:

$$\begin{aligned}
(II) &= \left\| \int_0^t \mathbf{P}_\alpha(t-\tau) \int_0^\tau \psi(\tau-\xi) K(\theta_1(\xi)) d\xi d\tau \right. \\
&\quad \left. - \int_0^t \mathbf{P}_\alpha(t-\tau) \int_0^\tau \psi(\tau-\xi) K(\theta_2(\xi)) d\xi d\tau \right\|_{H^q(\mathcal{M})} \\
&\leq \bar{C}_{1,\alpha,\beta} \int_0^t (t-\tau)^{-\beta} \left\| \int_0^\tau \psi(\tau-\xi) K(\theta_1(\xi)) d\xi \right. \\
&\quad \left. - \int_0^\tau \psi(\tau-\xi) K(\theta_2(\xi)) d\xi \right\|_{H^{q-2}(\mathcal{M})} d\tau \\
&\quad + \bar{C}_{2,\alpha,\beta} \int_0^t (t-\tau)^{-\beta} \left\| \int_0^\tau \psi(\tau-\xi) K(\theta_1(\xi)) d\xi \right. \\
&\quad \left. - \int_0^\tau \psi(\tau-\xi) K(\theta_2(\xi)) d\xi \right\|_{H^{q-2-2\beta}(\mathcal{M})} d\tau \\
&\leq (\bar{C}_{1,\alpha,\beta} + \bar{C}_{2,\alpha,\beta}) \int_0^t (t-\tau)^{-\beta} \left\| \int_0^\tau \psi(\tau-\xi) K(\theta_1(\xi)) d\xi \right. \\
&\quad \left. - \int_0^\tau \psi(\tau-\xi) K(\theta_2(\xi)) d\xi \right\|_{H^s(\mathcal{M})} d\tau.
\end{aligned} \tag{46}$$

Using the Lipschitz property of K , we know that

$$\begin{aligned}
&\left\| \int_0^\tau \psi(\tau-\xi) K(\theta_1(\xi)) d\xi - \int_0^\tau \psi(\tau-\xi) K(\theta_2(\xi)) d\xi \right\|_{H^q(\mathcal{M})} \\
&\leq C_\theta L_k \int_0^\tau (\tau-\xi)^{-\delta} \|\theta_1(\xi) - \theta_2(\xi)\|_{H^q(\mathcal{M})} d\xi \\
&= C_\theta L_k \int_0^\tau (\tau-\xi)^{-\delta} \xi^{-d} e^{m\xi} \xi^d e^{-m\xi} \|\theta_1(\xi) - \theta_2(\xi)\|_{H^q(\mathcal{M})} d\xi \\
&\leq C_\theta L_k \left(\int_0^\tau (\tau-\xi)^{-\delta} \xi^{-d} e^{m\xi} d\xi \right) \|\theta_1 - \theta_2\|_{X_{d,m}((0,T];H^q(\mathcal{M}))}.
\end{aligned} \tag{47}$$

It is obvious to see that

$$\begin{aligned}
&\int_0^\tau (\tau-\xi)^{-\delta} \xi^{-d} e^{m\xi} d\xi \leq e^{m\tau} \int_0^\tau (\tau-\xi)^{-\delta} \xi^{-d} d\xi \\
&= e^{m\tau} \tau^{1-\delta-d} \mathbf{B}(1-\delta, 1-d).
\end{aligned} \tag{48}$$

This implies that the following estimation is for the integral term on the right hand side of (45):

$$\begin{aligned}
&\int_0^t (t-\tau)^{-\beta} \left\| \int_0^\tau \psi(\tau-\xi) K(\theta_1(\xi)) d\xi - \int_0^\tau \psi(\tau-\xi) K(\theta_2(\xi)) d\xi \right\|_{H^q(\mathcal{M})} d\tau \\
&\leq C_\theta L_k B(1-\delta, 1-d) \\
&\quad \times \left(\int_0^t (t-\tau)^{-\beta} \tau^{1-\delta-d} e^{m\tau} d\tau \right) \|\theta_1 - \theta_2\|_{X_{d,m}((0,T];H^q(\mathcal{M}))}.
\end{aligned} \tag{49}$$

This implies that

$$\begin{aligned}
&t^d e^{-mt} \left\| \int_0^t \mathbf{P}_\alpha(t-\tau) \int_0^\tau \psi(\tau-\xi) K(\theta_1(\xi)) d\xi d\tau \right. \\
&\quad \left. - \int_0^t \mathbf{P}_\alpha(t-\tau) \int_0^\tau \psi(\tau-\xi) K(\theta_2(\xi)) d\xi d\tau \right\|_{H^q(\mathcal{M})} \\
&\leq C_3 t^d \left(\int_0^t (t-\tau)^{-\beta} \tau^{1-\delta-d} e^{-m(t-\tau)} d\tau \right) \|\theta_1 - \theta_2\|_{X_{d,m}((0,T];H^q(\mathcal{M}))} \\
&= C_3 t^{2-\beta-\delta} \int_0^1 (1-\xi)^{-\beta} \xi^{1-d-\delta} e^{-mt(1-\xi)} d\xi \|\theta_1 - \theta_2\|_{X_{d,m}((0,T];H^q(\mathcal{M}))},
\end{aligned} \tag{50}$$

where we note that

$$\begin{aligned}
C_3 &= (\bar{C}_{1,\alpha,\beta} + \bar{C}_{2,\alpha,\beta}) C_\theta L_k \mathbf{B}(1-\delta, 1-d), \\
t^d \int_0^t (t-\tau)^{-\beta} \tau^{1-\delta-d} e^{-m(t-\tau)} d\tau &= t^{2-\beta-\delta} \int_0^1 (1-\xi)^{-\beta} \xi^{1-d-\delta} e^{-mt(1-\xi)} d\xi.
\end{aligned} \tag{51}$$

Combining (42) and (49), we obtain the following bound:

$$\begin{aligned}
&t^d e^{-mt} \|\mathfrak{F}\theta_1(t) - \mathfrak{F}\theta_2(t)\|_{H^q(\mathcal{M})} \leq t^d e^{-mt} \left\| \int_0^t \mathbf{P}_\alpha(t-\tau) G(\theta_1(\tau)) d\tau \right. \\
&\quad \left. - \int_0^t \mathbf{P}_\alpha(t-\tau) G(\theta_2(\tau)) d\tau \right\|_{H^q(\mathcal{M})} \\
&\quad + t^d e^{-mt} \left\| \int_0^t \mathbf{P}_\alpha(t-\tau) \int_0^\tau \psi(\tau-\xi) K(\theta_1(\xi)) d\xi d\tau \right. \\
&\quad \left. - \int_0^t \mathbf{P}_\alpha(t-\tau) \int_0^\tau \psi(\tau-\xi) K(\theta_2(\xi)) d\xi d\tau \right\|_{H^q(\mathcal{M})} \\
&\leq (\bar{C}_{1,\alpha,\beta} + \bar{C}_{2,\alpha,\beta}) L_g t^{1-\beta} \\
&\quad \times \left(\int_0^1 (1-\xi)^{-\beta} \xi^{-d} e^{-mt(1-\xi)} d\xi \right) \|\theta_1 - \theta_2\|_{X_{d,m}((0,T];H^q(\mathcal{M}))} \\
&\quad + C_3 t^{2-\beta-\delta} \int_0^1 (1-\xi)^{-\beta} \xi^{1-d-\delta} e^{-mt(1-\xi)} d\xi \|\theta_1 - \theta_2\|_{X_{d,m}((0,T];H^q(\mathcal{M}))}.
\end{aligned} \tag{52}$$

From the condition (34), we can verify the following condition:

$$\begin{cases} 1-\beta > 0, \\ -\beta > -1, -d > -1, -\beta-d > -1, \\ \beta+\delta < 2, \\ 1-d-\delta > -1, -\beta+1-d-\delta > -1. \end{cases} \tag{53}$$

By using Lemma 2, we have two statements immediately:

$$\lim_{m \rightarrow \infty} \left(\sup_{t \in [0, T]} t^{1-\beta} \left(\int_0^1 (1-\xi)^{-\beta} \xi^{-d} e^{-mt(1-\xi)} d\xi \right) \right) = 0,$$

$$\lim_{m \rightarrow \infty} \left(\sup_{t \in [0, T]} t^{2-\beta-\delta} \int_0^1 (1-\xi)^{-\beta} \xi^{1-d-\delta} e^{-mt(1-\xi)} d\xi \right) = 0. \quad (54)$$

From the last two observations, we can find that the positive number m_0 such that

$$\begin{aligned} & (\tilde{C}_{1,\alpha,\beta} + \tilde{C}_{2,\alpha,\beta}) L_g t^{1-\beta} \left(\int_0^1 (1-\xi)^{-\beta} \xi^{-d} e^{-mt(1-\xi)} d\xi \right) \\ & + C_3 t^{2-\beta-\delta} \int_0^1 (1-\xi)^{-\beta} \xi^{1-d-\delta} e^{-mt(1-\xi)} d\xi \end{aligned} \quad (55)$$

is less than 1. By applying the Banach fixed point theorem, we know that problem (1) has a unique solution in $X_{d,m_0}((0, T]; H^q(\mathcal{M}))$. \square

5. Conclusion

The result of the paper is one of the first works on the topic of memory for equations with Caputo-Fabrizio derivatives. We obtain the following results: first, prove the existence of local solutions. The second is a survey of the global solution. The main technique is to use the Banach fixed point theorem in combination with Sobolev embeddings.

Data Availability

No data were used to support this study.

Conflicts of Interest

The authors declare that they have no competing interests.

Authors' Contributions

All authors contributed equally and significantly in writing this paper. Four authors read and approved the final manuscript.

Acknowledgments

This research is supported by the Industrial University of Ho Chi Minh City (IUH) under grant number 66/HD-DHCN.

References

- [1] J. Manimaran, L. Shangerganesh, and A. Debbouche, "Finite element error analysis of a time-fractional nonlocal diffusion equation with the Dirichlet energy," *Journal of Computational and Applied Mathematics*, vol. 382, article 113066, p. 11, 2021.
- [2] J. Manimaran, L. Shangerganesh, and A. Debbouche, "A time-fractional competition ecological model with cross-diffusion," *Mathematical Methods in the Applied Sciences*, vol. 43, no. 8, pp. 5197–5211, 2020.
- [3] N. H. Tuan, A. Debbouche, and T. B. Ngoc, "Existence and regularity of final value problems for time fractional wave equations," *Computers & Mathematics with Applications*, vol. 78, no. 5, pp. 1396–1414, 2019.
- [4] H. Afshari, S. Kalantari, and E. Karapinar, "Solution of fractional differential equations via coupled fixed point," *Electronic Journal of Differential Equations*, vol. 2015, no. 286, pp. 1–12, 2015.
- [5] S. D. Maharaj and M. Chaisi, "On the solution of a boundary value problem associated with a fractional differential equation," *Mathematical Methods in the Applied Sciences*, vol. 29, no. 1, pp. 12–83, 2020.
- [6] H. Afshari and E. Karapinar, "A discussion on the existence of positive solutions of the boundary value problems via ψ -Hilfer fractional derivative on b-metric spaces," *Advances in Difference Equations*, vol. 2020, no. 1, Article ID 616, 2020.
- [7] B. Alqahtani, H. Aydi, Karapinar, and Rakočević, "A solution for Volterra fractional integral equations by hybrid contractions," *Mathematics*, vol. 7, no. 8, p. 694, 2019.
- [8] E. Karapinar, A. Fulga, M. Rashid, L. Shahid, and H. Aydi, "Large contractions on quasi-metric spaces with an application to nonlinear fractional differential equations," *Mathematics*, vol. 7, no. 5, p. 444, 2019.
- [9] A. Salim, B. Benchohra, E. Karapinar, and J. E. Lazreg, "Existence and Ulam stability for impulsive generalized Hilfer-type fractional differential equations," *Advances in Difference Equations*, vol. 2020, no. 1, Article ID 601, 2020.
- [10] E. Karapinar, T. Abdeljawad, and F. Jarad, "Applying new fixed point theorems on fractional and ordinary differential equations," *Advances in Difference Equations*, vol. 2019, no. 1, Article ID 421, 2019.
- [11] A. Abdeljawad, R. P. Agarwal, E. Karapinar, and P. S. Kumari, "Solutions of the nonlinear integral equation and fractional differential equation using the technique of a fixed point with a numerical experiment in extended b-metric space," *Symmetry*, vol. 11, no. 5, p. 686, 2019.
- [12] A. Yusuf, B. Acay, U. T. Mustapha, M. Inc, and D. Baleanu, "Mathematical modeling of pine wilt disease with Caputo fractional operator," *Chaos, Solitons and Fractals*, vol. 143, article 110569, p. 13, 2021.
- [13] B. Acay and M. Inc, "Fractional modeling of temperature dynamics of a building with singular kernels," *Chaos Solitons and Fractals*, vol. 142, article 110482, p. 9, 2021.
- [14] Z. Korpinar, M. Inc, and M. Bayram, "Theory and application for the system of fractional Burger equations with Mittag-Leffler kernel," *Applied Mathematics and Computation*, vol. 367, article 124781, 2020.
- [15] X. J. Yang, Y. Y. Feng, C. Cattani, and M. Inc, "Fundamental solutions of anomalous diffusion equations with the decay exponential kernel," *Mathematical Methods in the Applied Sciences*, vol. 42, no. 11, pp. 4054–4060, 2019.
- [16] M. S. Hashemi, E. Darvishi, and M. Inc, "A geometric numerical integration method for solving the Volterra integro-differential equations," *International Journal of Computer Mathematics*, vol. 95, no. 8, pp. 1654–1665, 2018.
- [17] N. H. Tuan, Y. Zhou, T. N. Thach, and N. H. Can, "Initial inverse problem for the nonlinear fractional Rayleigh-Stokes equation with random discrete data," *Commun. Nonlinear Sci. Numer. Simul.*, vol. 78, article 104873, p. 18, 2019.
- [18] N. H. Tuan, L. N. Huynh, T. B. Ngoc, and Y. Zhou, "On a backward problem for nonlinear fractional diffusion equations," *Applied Mathematics Letters*, vol. 92, pp. 76–84, 2019.

- [19] T. B. Ngoc, Y. Zhou, D. O'Regan, and N. H. Tuan, "On a terminal value problem for pseudoparabolic equations involving Riemann-Liouville fractional derivatives," *Applied Mathematics Letters*, vol. 106, article 106373, p. 9, 2020.
- [20] H. T. Nguyen, H. C. Nguyen, R. Wang, and Y. Zhou, "Initial value problem for fractional Volterra integro-differential equations with Caputo derivative," *Discrete & Continuous Dynamical Systems-B*, 2021.
- [21] B. Nghia, N. Luc, H. Binh, and L. D. Long, "Regularization method for the problem of determining the source function using integral conditions," *Advances in the Theory of Nonlinear Analysis and its Application*, vol. 5, no. 3, pp. 351–362, 2021.
- [22] N. Hung, H. Binh, N. Luc, L. D. Long, and L. O. Le Dinh, "Stochastic sub-diffusion equation with conformable derivative driven by standard Brownian motion," *Advances in the Theory of Nonlinear Analysis and its Applications*, vol. 5, no. 3, pp. 287–299, 2021.
- [23] A. Ardjounia, "Asymptotic stability in Caputo-Hadamard fractional dynamic equations," *Results in Nonlinear Analysis*, vol. 4, no. 2, pp. 77–86, 2021.
- [24] J. Losada and J. J. Nieto, "Properties of a new fractional derivative without singular kernel," *Progress in Fractional Differentiation and Applications*, vol. 1, no. 2, pp. 87–92, 2015.
- [25] M. Caputo and M. Fabrizio, "A new definition of fractional derivative without singular kernel," *Progress in Fractional Differentiation and Applications*, vol. 1, no. 2, pp. 1–13, 2015.
- [26] M. Caputo and M. Fabrizio, "Applications of new time and spatial fractional derivatives with exponential kernels," *Progress in Fractional Differentiation and Applications*, vol. 2, no. 1, pp. 1–11, 2016.
- [27] T. M. Atanacković, S. Pilipović, and D. Zorica, "Properties of the Caputo-Fabrizio fractional derivative and its distributional settings," *Fractional Calculus and Applied Analysis*, vol. 21, pp. 29–44, 2018.
- [28] M. Enelund and P. Olsson, "Damping described by fading memory-analysis and application to fractional derivative models," *International Journal of Solids and Structures*, vol. 36, no. 7, pp. 939–970, 1999.
- [29] J. Singh, "Analysis of fractional blood alcohol model with composite fractional derivative," *Chaos, Solitons and Fractals*, vol. 140, article 110127, 2020.
- [30] J. Singh, D. Kumar, S. D. Purohit, A. M. Mishra, and M. Bohra, "An efficient numerical approach for fractional multidimensional diffusion equations with exponential memory," *Numerical Methods for Partial Differential Equations*, vol. 37, no. 2, pp. 1631–1651, 2021.
- [31] N. D. Phuong, L. V. C. Hoan, E. Karapinar, J. Singh, H. D. Binh, and N. H. Can, "Fractional order continuity of a time semi-linear fractional diffusion-wave system," *Alexandria Engineering Journal*, vol. 59, no. 6, pp. 4959–4968, 2020.
- [32] J. Singh, D. Kumar, and D. Baleanu, "A new analysis of fractional fish farm model associated with Mittag-Leffler-type kernel," *International Journal of Biomathematics*, vol. 13, no. 2, article 2050010, 2020.
- [33] Y. Chen, H. Gao, M. Garrido-Atienza, and B. Schmalfuss, "Pathwise solutions of SPDEs driven by Holder-continuous integrators with exponent larger than $1/2$ and random dynamical systems," *Discrete and Continuous Dynamical Systems; - Series A*, vol. 34, no. 1, pp. 79–98, 2014.

Research Article

Numerical and Analytical Investigation for Darcy-Forchheimer Flow of a Williamson Fluid over a Riga Plate with Double Stratification and Cattaneo-Christov Dual Flux

S. Eswaramoorthi ¹, Nazek Alessa ², M. Sangeethavaanee ¹, and Ngawang Namgyel ³

¹Department of Mathematics, Dr. N.G.P. Arts and Science College, Coimbatore, Tamil Nadu, India

²Department of Mathematical Sciences, Faculty of Science, Princess Nourah Bint Abdulrahman University, Riyadh, Saudi Arabia

³Department of Humanities and Management, Jigme Namgyel Engineering College, Royal University of Bhutan, Dewathang, Bhutan

Correspondence should be addressed to S. Eswaramoorthi; eswaran.bharathiar@gmail.com and Ngawang Namgyel; ngawangnamgyel@jnec.edu.bt

Received 26 May 2021; Revised 22 June 2021; Accepted 14 July 2021; Published 3 August 2021

Academic Editor: Mustafa Inc

Copyright © 2021 S. Eswaramoorthi et al. This is an open access article distributed under the Creative Commons Attribution License, which permits unrestricted use, distribution, and reproduction in any medium, provided the original work is properly cited.

The Darcy-Forchheimer flow of a Williamson fluid over a Riga plate was analyzed in this paper. Energy and mass equations are modeled with Cattaneo-Christov theory and double stratifications. The governing PDE models are altered into ODE models. These models are numerically solved by MATLAB bvp4c and analytically solved by the homotopy analysis method. The impact of governing flow parameters on fluid velocity, fluid temperature, fluid concentration, skin-friction coefficient, local Nusselt number, and local Sherwood number is scrutinized via graphs and tables. We acknowledged that the speed of the fluid becomes diminishes for more presence of porosity parameter. Also, we noted that the thermal and solutal boundary layer thicknesses are waning due to their corresponding stratification parameters. In addition, the maximum decreasing percentage of skin friction is obtained when the suction/injection parameter varies from 0.0 to 0.4 for Williamson and viscous fluids. The maximum increasing percentage of local Nusselt number occurs when the suction/injection parameter varies from 0.4 to 0.8 for Williamson and viscous fluids.

1. Introduction

Non-Newtonian fluids are extensively implemented in diverse industrial processes such as petroleum drilling, drawing of plastic films, fibre spinning, and food production. The Williamson fluid model is one of the simplest non-Newtonian models to replicate the viscoelastic shear-thinning attributes, see Williamson [1]. The flow of thermally radiative Williamson fluid on a stretching sheet with chemical reaction was disclosed by Krishnamurthy et al. [2]. They proved the fluid temperature falling off due to the presence of the Williamson parameter. Khan et al. [3] demonstrated the impact of slip flow of Williamson nanofluid in a porous medium. They exposed that the surface

drag force suppresses due to rising the Williamson fluid parameter. The 2D unsteady radiative Williamson fluid flow on a permeable stretching surface was deliberated by Hayat et al. [4]. They noticed that the fluid speed becomes slow when the Williamson parameter is high. Nadeem et al. [5] examined the Williamson fluid flow past a stretching sheet, and they found that the skin friction coefficient decreases with enhancing the Williamson parameter. Make use of the Keller box procedure to solve the problem of MHD flow of Williamson fluid over a stretching sheet by Salahuddin et al. [6]. Their outcome shows that the Williamson fluid parameter leads to suppress the fluid velocity. Few significant analysis for this area is seen in Refs. [7, 8].

Fluid flow over a porous medium is confronted in plentiful applications in industry. Few applications are wood drying, nuclear waste storage, food processing, oil purifying, drainage, and irrigation. Darcy's principle is applied to analyze the flow behavior under the condition of small velocity and low porosity. When the quantity of Reynolds number overcomes unity, the Darcy principle was not applicable. Forchheimer [9] defeated this limitation by inserting the square velocity term in the momentum equation. After that, this is known as the Forchheimer number, which is applicable for working higher Reynolds number. Numerical analysis for a Darcy-Forchheimer flow of viscous fluid over a plate was inspected by Mukhopadhyay et al. [10]. They noted that the permeability parameter leads to a decrease in the warmth of the fluid. Hayat et al. [11] demonstrate the 3D Williamson nanomaterial flow on a Darcy-Forchheimer porous medium. They concluded that the surface shear stress diminishes for growing the Forchheimer number. The Darcy-Forchheimer flow of a viscous fluid with heterogeneous-homogeneous chemical reactions was portrayed by Khan et al. [12]. Their results clearly show that the fluid speed becomes slowdown due to the availability of Darcy number. Haider et al. [13] scrutinize the Darcy-Forchheimer and slip flow of hybrid nanofluid on a rotating disk. They proved that the larger estimation of Forchheimer enhances the fluid temperature. Steady 3D Darcy-Forchheimer flow of carbon nanotubes on a rotating disk was revealed by Sadiq et al. [14]. Some important studies for these concepts are collected in Refs. [15–18].

The magnetic field plays a significant role in the development of fluid thermophysical traits. The demeanour of broadly used fluids like liquid metals, plasma, and electrolytes has a low conductor of electricity. Therefore, an external agent is required to boost up the heat transfer attributes through superior conductivity and thermophysical traits. A magnetic bar with permanently fixed magnets and alternate electronics, known as a Riga plate, can be acted as an external agent to improve fluid electricity. This plate was introduced by Gailitis and Lielausis [19]. Nanofluid flow over a Riga plate was deliberated by Ahmad et al. [20]. Nazeer et al. [21] inspected the chemically reacting Eyring-Powell nanofluid on a Riga plate. They proved that the fluid speed enhances when enhancing the modified Hartmann number. Chemically reacting Prandtl fluid on a Riga plate was addressed by Gireesha et al. [22]. Their results show that the velocity boundary layer thickens due to the more presence of the modified Hartmann number. Mehmood et al. [23] performed the impact of Soret and Dufour effects of a Casson fluid flow on a Riga plate with chemical reaction. Ayub et al. [24], Nayak et al. [25], and Rasool et al. [26] are few essential studies of fluid flow over a Riga plate.

Stratification is a natural process that combines two or more fluids with different densities, temperatures, and concentrations. The double stratification occurs due to both the heat and mass transfer differences. Cheng [27] examined the mass and heat transfer analysis of a power-law fluid in a stratified medium. He noticed that the heat transfer gradient declines for escalating the thermal stratification parameter. The radiative flow of a hyperbolic tangent fluid with chemical reaction and dual stratification's in a porous

medium was elucidated by Khan et al. [28]. They found that the fluid concentration downturns for the high magnitude of the stratified thermal parameter. Rehman et al. [29] evaluated the problem of a chemically reacting Williamson fluid with dual stratification, and they have seen that the rate of heat transfer rate is declined for the presence of thermal stratification parameter. The impact of solutal and thermal stratification of a Williamson nanofluid was deliberated by Khan et al. [30]. It is noticed that the horizontal velocity suppresses when the higher magnitude of the thermal stratification parameter. Mallawi et al. [31] derived the series solution of thermally radiative non-Newtonian fluid flow with double stratifications. They have seen that the fluid concentration depresses for enhancing the solutal stratification parameter. Time-dependent MHD nanofluid flow with dual stratifications was performed by Hayat et al. [32]. They proved that surface shear stress enriches for higher values of thermal and solutal stratification parameters.

The aforementioned inspection announces that most of the researchers are involved in revealing the nature of the Darcy-Forchheimer flow with Cattaneo-Christov theory through prescribed wall temperature but not analyzed dual stratifications on a Riga plate. Therefore, our key argument is to fulfill this gap. So, our study elucidates the outcome of the Darcy-Forchheimer flow of a Williamson fluid in the presence of double stratifications, thermal radiation, and chemical reaction on a Riga plate. These types of outcomes will be definitely helpful for a thermal engineer to modeling the thermal systems. Here, the heat and mass transfer phenomena are illustrated by the Cattaneo-Christov dual flux model and the Riga plate is used to control the fluid flow.

2. Mathematical Formulation

Let us consider the 2D Darcy-Forchheimer flow of a Williamson fluid on a Riga plate. Here, the surface temperature and the concentration are denoted by T_w and C_w which are always larger than the free stream temperature T_∞ and the free stream concentration C_∞ , respectively, see Figures 1(a) and 1(b). The thermal radiation and first-order chemical reaction are taking into account. Flow situation is manifested with double stratifications. The fluid phase is heat consumption/generation. In addition, the heat and mass transfer phenomenon is inspected through Cattaneo-Christov dual models. The governing equations are modeled as follows:

$$\frac{\partial u}{\partial x} + \frac{\partial v}{\partial y} = 0, \quad (1)$$

$$\begin{aligned} u \frac{\partial u}{\partial x} + v \frac{\partial u}{\partial y} = & \nu \frac{\partial^2 u}{\partial y^2} + \sqrt{2} \Gamma \nu \frac{\partial u}{\partial y} \frac{\partial^2 u}{\partial y^2} - \frac{\nu}{k_2} u - \frac{C_b}{x \sqrt{k_2}} u^2 \\ & + \frac{\pi J_0 M_0}{8\rho} \exp\left(-\frac{\pi}{a_1} y\right), \end{aligned} \quad (2)$$

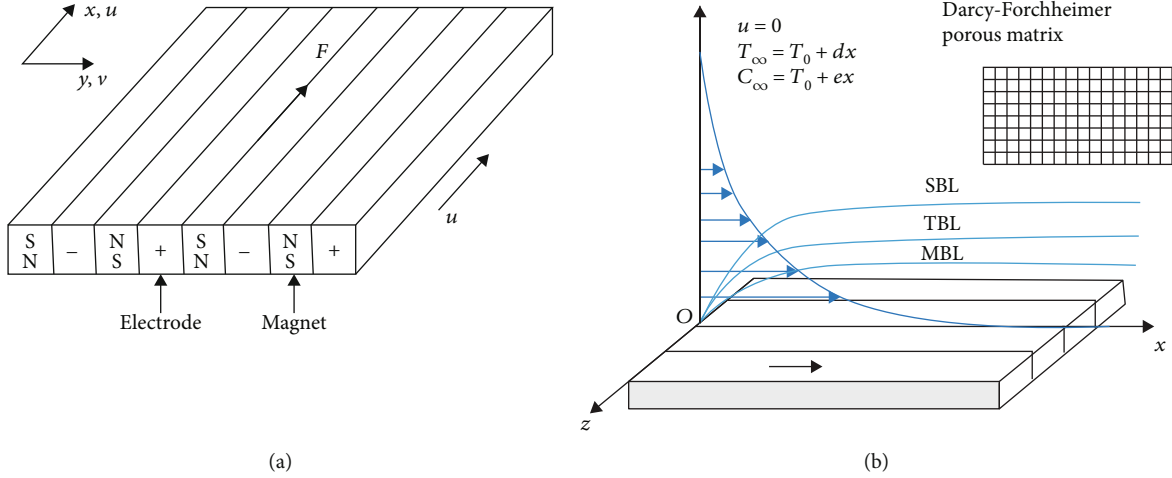


FIGURE 1: Sketch of Riga plate (a) and physical configuration of the problem (b).

$$u \frac{\partial T}{\partial x} + v \frac{\partial T}{\partial y} + \lambda_T \Omega_T = \alpha \frac{\partial^2 T}{\partial y^2} + \frac{1}{\rho C_p} \frac{16\sigma^* T_\infty^3}{3k^*} \frac{\partial^2 T}{\partial y^2} + \frac{Q}{\rho C_p} (T - T_\infty), \quad (3)$$

$$u \frac{\partial C}{\partial x} + v \frac{\partial C}{\partial y} + \lambda_C \Omega_C = D_B \frac{\partial^2 C}{\partial y^2} - k_1 (C - C_\infty), \quad (4)$$

where

$$\begin{aligned} \Omega_T &= u \frac{\partial u}{\partial x} \frac{\partial T}{\partial x} + v \frac{\partial v}{\partial y} \frac{\partial T}{\partial y} + u^2 \frac{\partial^2 T}{\partial x^2} + v^2 \frac{\partial^2 T}{\partial y^2} + 2uv \frac{\partial^2 T}{\partial x \partial y} \\ &\quad + u \frac{\partial v}{\partial x} \frac{\partial T}{\partial y} + v \frac{\partial u}{\partial y} \frac{\partial T}{\partial x}, \\ \Omega_C &= u \frac{\partial u}{\partial x} \frac{\partial C}{\partial x} + v \frac{\partial v}{\partial y} \frac{\partial C}{\partial y} + u^2 \frac{\partial^2 C}{\partial x^2} + v^2 \frac{\partial^2 C}{\partial y^2} + 2uv \frac{\partial^2 C}{\partial x \partial y} \\ &\quad + u \frac{\partial v}{\partial x} \frac{\partial C}{\partial y} + v \frac{\partial u}{\partial y} \frac{\partial C}{\partial x}, \end{aligned} \quad (5)$$

where u, v is the velocity in x and y directions, ν is the kinematic viscosity, Γ is the time constant, J_0 is the current density, ρ is the density of the fluid, M_0 is the magnetization of the magnet, a_1 is the width of the magnet and the electrodes, C_b is the drag coefficient, k_2 is the permeability of porous medium, T is the fluid temperature, λ_T is the relaxation time of heat flux, α is the thermal diffusivity, C_p is the specific heat, σ^* is the Stefan-Boltzmann constant, k^* is the mean absorption coefficient, Q is the heat generation/absorption coefficient, C is the fluid concentration, λ_C is the relaxation time of mass flux, D_B is the mass diffusivity, and k_1 is the chemical reaction parameter.

The boundary conditions are

$$\begin{aligned} u &= U_w(x), v = -V_w(x), T = T_w = T_0 + bx, C = C_w = C_0 + cx, \text{ at } y = 0, \\ u &\rightarrow 0, \frac{\partial u}{\partial y} \rightarrow 0, T \rightarrow T_\infty = T_0 + dx, C \rightarrow C_\infty = C_0 + ex \text{ at } y \rightarrow \infty. \end{aligned} \quad (6)$$

Now, we consider the following dimensionless variables:

$$\begin{aligned} \eta &= y \sqrt{\frac{a}{\nu}}, \\ u &= xaf', \\ v &= -\sqrt{a}vf, \\ \theta(\eta) &= \frac{T - T_\infty}{T_w - T_0}, \\ \phi(\eta) &= \frac{C - C_\infty}{C_w - C_0}. \end{aligned} \quad (7)$$

By using (7), we can modify equations (2)–(4) as follows:

$$f''' - f'^2 + ff'' + We f' f''' - \lambda f' - Fr f'^2 + Ha e^{-\beta \eta} = 0, \quad (8)$$

$$\begin{aligned} \frac{1}{Pr} \left(1 + \frac{4}{3} R \right) \theta'' + Hg \theta + f \theta' - f' \theta - S_1 f' - \Gamma_1 [f'^2 \theta \\ + S_1 f'^2 - f f' \theta' - f f' \theta - S_1 f f'' + f^2 \theta''] = 0, \end{aligned} \quad (9)$$

$$\begin{aligned} \frac{1}{Sc} \phi'' - f' \phi - S_2 f' + f \phi' - Cr \phi \\ - \Gamma_2 [f'^2 \phi + S_2 f'^2 - f f' \phi' - f f' \phi - S_2 f f'' + f^2 \phi''] = 0. \end{aligned} \quad (10)$$

$We = \Gamma x \sqrt{2a^3/\nu}$ is the Weissenberg number, $Ha = \pi J_0 M_0 / 8 \rho a^2 x$ is the modified Hartmann number, $\beta = \pi / (a_1 (a/\nu)^{1/2})$ is the dimensionless parameter, $\lambda = \nu / k_2 a$ is the local porosity parameter, $Fr = C_b / k_2^{1/2}$ is the Forchheimer number, $Pr = \nu / a$ is the Prandtl number, $R = 4\sigma^* T_\infty^3 / k k^*$ is

the radiation parameter, $S_1 = d/b$ is the thermal stratification parameter, $Hg = Q/\rho C_p a$ is the heat absorption/generation parameter, $\Gamma_1 = \lambda_T a$ is the heat relaxation time parameter, $Sc = \nu/D_B$ is the Schmidt number, $Cr = k_1/a$ is the chemical reaction parameter, $S_2 = e/c$ is the solutal stratification parameter, $\Gamma_2 = \lambda_C a$ is the mass relaxation time parameter, and $fw = -V_w/\sqrt{a\nu}$ is the suction/injection parameter.

The corresponding boundary conditions are

$$\begin{aligned} f(0) &= fw, \\ f'(0) &= 1, \\ \theta(0) &= 1 - S_1, \\ \phi(0) &= 1 - S_2, \end{aligned} \quad (11)$$

$$\begin{aligned} f'(\infty) &= 0, \\ \theta(\infty) &= 0, \\ \phi(\infty) &= 0. \end{aligned} \quad (12)$$

The skin friction coefficient, local Nusselt number, and local Sherwood number are expressed as

$$\begin{aligned} Cf &= \frac{2\tau_w}{\rho U_w^2}; \\ Nu &= \frac{xq_w}{k(T_w - T_\infty)}; \\ Sh &= \frac{xj_w}{D_B(C_w - C_\infty)}; \end{aligned} \quad (13)$$

here, the wall shear stress, heat, and mass flux are as follows:

$$\begin{aligned} \tau_w &= \mu \left(\frac{\partial u}{\partial y} \left[1 + \Gamma \sqrt{\frac{1}{2}} \frac{\partial u}{\partial y} \right] \right); \\ q_w &= -k \frac{\partial T}{\partial y} + q_r; \\ j_w &= -D_B \frac{\partial C}{\partial y}. \end{aligned} \quad (14)$$

The dimensionless form of the above parameters are expressed as

$$\begin{aligned} \frac{1}{2} Cf \sqrt{Re} &= f''(0) + \frac{We}{2} f'''(0)^2; \\ \frac{Nu}{\sqrt{Re}} &= -\left(1 + \frac{4}{3} R\right) \theta'(0); \\ \frac{Sh}{\sqrt{Re}} &= -\phi'(0). \end{aligned} \quad (15)$$

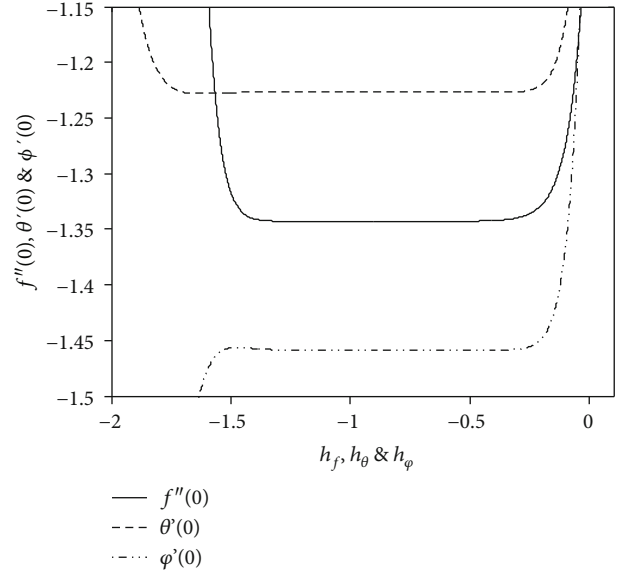


FIGURE 2: h - curve with 18th order of approximation.

TABLE 1: Order of order approximations and CPU timing.

Order	$-f''(0)$	$-\theta'(0)$	$-\phi'(0)$	CPU timings (sec.)
1	1.27000	1.21054	1.43054	0.58
5	1.34103	1.22687	1.45881	4.73
10	1.34290	1.22692	1.45860	33.06
13	1.34294	1.22692	1.45860	47.64
15	1.34294	1.22692	1.45860	139.76
20	1.34294	1.22692	1.45860	646.61
25	1.34294	1.22692	1.45860	2376.22
30	1.34294	1.22692	1.45860	7157.92

3. Solutions

3.1. Numerical Solution. In this section, the bvp4c solver has been used for gaining the solution. In order to solve the problem, equations (8)–(10) are commuted into a system of first-order differential equations with the boundary conditions also modified in the same manner. For this, let us take

$$\begin{aligned} f &= y_1, \\ f' &= y_2, \\ f'' &= y_3, \\ \theta &= y_4, \\ \theta' &= y_5, \\ \phi &= y_6, \\ \phi' &= y_7. \end{aligned} \quad (16)$$

TABLE 2: Numerical and analytical computation of local skin friction coefficient, local Nusselt number, and local Sherwood number for various values of We, λ , Fr, fw, and Ha.

We	λ	Fr	fw	Ha	Skin friction coefficient		Local Nusselt number		Local Sherwood number	
					Numerical	Analytical	Numerical	Analytical	Numerical	Analytical
0.0	0.2	0.4	0.3	0.3	-1.21627	-1.21624	2.06338	2.06344	1.46840	1.46841
0.1					-1.19072	-1.19070	2.05471	2.05477	1.46383	1.46385
0.2					-1.16263	-1.16259	2.04481	2.04487	1.45858	1.45860
0.3					-1.13089	-1.13083	2.03314	2.03319	1.45233	1.45235
0.4					-1.09319	-1.09164	2.01848	2.01859	1.44438	1.44442
0.5					-0.99995	-0.99998	1.99720	1.99782	1.43257	1.43294
0.2	0.0	0.4	0.3	0.3	-1.07827	-1.07818	2.07408	2.07422	1.47298	1.47303
	0.1				-1.12135	-1.12130	2.05904	2.05913	1.46558	1.46561
	0.2				-1.16263	-1.16259	2.04481	2.04487	1.45858	1.45860
	0.3				-1.20228	-1.20225	2.03132	2.03136	1.45194	1.45195
	0.4				-1.24046	-1.24042	2.01851	2.01853	1.44563	1.44564
	0.5				-1.27728	-1.27725	2.00630	2.00634	1.43961	1.43964
0.2	0.2	0.0	0.3	0.3	-1.05656	-1.05652	2.06805	2.06811	1.47074	1.47076
		0.3			-1.13706	-1.13702	2.05038	2.05043	1.46149	1.46151
		0.5			-1.18763	-1.18758	2.03940	2.03945	1.45575	1.45576
		0.8			-1.25946	-1.25942	2.02397	2.02406	1.44768	1.44773
		1.0			-1.30495	-1.30544	2.01430	2.01498	1.44262	1.44322
0.2	0.2	0.4	-1.0	0.3	-0.68939	-0.68936	1.22935	1.22940	0.91349	0.91350
			-0.5		-0.83580	-0.83579	1.47333	1.47339	1.07673	1.07675
			0.0		-1.02546	-1.02543	1.79633	1.79639	1.29221	1.29223
			0.5		-1.26411	-1.26408	2.24148	2.24153	1.59103	1.59105
			1.0		-1.55195	-1.55182	2.88826	2.88923	2.03343	2.03242
0.2	0.2	0.4	0.3	0.0	-1.29871	-1.29869	1.99254	1.99255	1.43332	1.43333
				0.5	-1.07378	-1.07374	2.07612	2.07619	1.47399	1.47401
				1.0	-0.85646	-0.85641	2.14556	2.14568	1.50882	1.50886
				1.5	-0.64420	-0.64411	2.20587	2.20586	1.53970	1.53989
				2.0	-0.43568	-0.43431	2.25965	2.26084	1.56771	1.57081

The system of equations are

$$\begin{aligned}
y'_1 &= y_2, \\
y'_2 &= y_3, \\
y'_3 &= \frac{y_2^2 - y_1 y_3 - \text{Hae}^{-\beta\eta} + \lambda y_2 + \text{Fry}_2^2}{1 + \text{Wey}_3}, \\
y'_4 &= y_5, \\
y'_5 &= \frac{-y_1 y_5 + y_2 y_4 + S_1 y_2 - \text{Hgy}_4 + \Gamma_1 [y_2^2 y_4 + S_1 y_2^2 - y_1 y_2 y_5 - y_1 y_3 y_4 - S_1 y_1 y_3]}{(1/\text{Pr})(1 + (4/3)R) - \Gamma_1 y_1^2}, \\
y'_6 &= y_7, \\
y'_7 &= \frac{-y_1 y_7 + y_2 y_6 + S_2 y_2 + \text{Cry}_6 + \Gamma_2 [y_2^2 y_6 + S_2 y_2^2 - y_1 y_2 y_7 - y_1 y_3 y_6 - S_2 y_1 y_3]}{(1/\text{Sc}) - \Gamma_2 y_1^2}.
\end{aligned} \tag{17}$$

With the boundary conditions

$$\begin{aligned}
 y_1(0) &= fw, \\
 y_2(0) &= 1, \\
 y_2(\infty) &= 0, \\
 y_4(0) &= 1 - S_1, \\
 y_4(\infty) &= 0, \\
 y_6(0) &= 1 - S_2, \\
 y_6(\infty) &= 0.
 \end{aligned} \tag{18}$$

The above set of equations are numerically solved by MATLAB built-in function `bvp4c`.

3.2. HAM Solution. The obtained ODE's (8)–(10) with conditions (11) are analytically solved by applying the HAM scheme. Because this method is powerful tool for solving nonlinear problems, see Sarwar and Rashidi [33]. Let the initial approximations are chosen as $f_0(\eta) = fw + 1 - 1/e^\eta$, $\theta_0(\eta) = (1 - S_1)/e^\eta$, and $\phi_0(\eta) = (1 - S_2)/e^\eta$, and linear operators are $L_f = D^3f - Df$, $L_\theta = D^2\theta - \theta$, and $L_\phi = D^2\phi - \phi$, where D is the differential operator and the linear property is $L_f[C_1 + C_2e^\eta + C_3(1/e^\eta)] = 0 = L_\theta[C_4e^\eta + C_5(1/e^\eta)] = L_\phi[C_6e^\eta + C_7(1/e^\eta)]$, where $C_k (k = 1 - 7)$ are constants.

After implementing the i^{th} order HAM technique, we found the following:

$$\begin{aligned}
 f_i(\eta) &= f_i^*(\eta) + C_1 + C_2e^\eta + C_3\frac{1}{e^\eta}, \\
 \theta_i(\eta) &= \theta_i^*(\eta) + C_4e^\eta + C_5\frac{1}{e^\eta}, \\
 \phi_i(\eta) &= \phi_i^*(\eta) + C_6e^\eta + C_7\frac{1}{e^\eta}.
 \end{aligned} \tag{19}$$

Here, $f_i^*(\eta)$, $\theta_i^*(\eta)$, and $\phi_i^*(\eta)$ are the particular solutions.

These HAM techniques have the parameters (h_f, h_θ , and h_ϕ), and these are responsible for the convergence of solutions, see Refs. [34–37]. Figure 2 portrays the range value of h_f, h_θ , and h_ϕ are $-1.3 \leq h_f \leq -0.4$, $-1.6 \leq h_\theta \leq -0.25$, and $-1.4 \leq h_\phi \leq -0.35$. We assign $h_f = h_\theta = h_\phi = -0.9$ for better convergency.

4. Results and Discussion

Here, we revealed the results by graphs and tables which describes the shift in velocity, temperature, concentration, skin friction coefficient, local Nusselt number, and local Sherwood number concerning the disparate values of the parameters, such as Weissenberg number (We), local porosity parameter (λ), Forchheimer number (Fr), modified Hartmann number (Ha), thermal radiation parameter (R), thermal stratification parameter (S_1), heat generation/absorption parameter (Hg), heat relaxation time parameter (Γ_1), chemical reaction parameter (Cr), solute stratification parameter (S_2), mass relaxation time parameter (Γ_2), and the suction/injection

TABLE 3: Numerical and analytical computation of local Nusselt number for various values of R , Hg , S_1 , and Γ_1 .

R	Hg	S_1	Γ_1	Local Nusselt number	
				Numerical	Analytical
0.0	-0.5	0.2	0.1	1.72351	1.72355
0.3				1.92821	1.92826
0.5				2.04481	2.04487
0.7				2.15002	2.15009
1.0				2.29156	2.29164
0.5	-0.5	0.2	0.1	2.04481	2.04487
	-0.2			1.88531	1.88544
	0.0			1.76494	1.94091
	0.2			1.62586	1.62695
	0.5			1.21530	1.27139
0.5	-0.5	0.0	0.1	2.33479	2.33481
		0.2		2.04481	2.04487
		0.4		1.75483	1.75492
		0.6		1.46484	1.46498
		0.8		1.17486	1.17503
		1.0		0.88488	0.88508
0.5	-0.5	0.2	0.0	1.90591	1.90597
			0.1	2.04481	2.04487
			0.2	2.18818	2.18824
			0.3	2.33609	2.33615
			0.4	2.48859	2.48865

TABLE 4: Numerical and analytical computation of local Sherwood number for various values of Cr , S_2 , and Γ_2 .

Cr	S_2	Γ_2	Local Sherwood number	
			Numerical	Analytical
-0.5	0.2	0.1	0.90317	0.89525
-0.2			1.06313	1.06391
0.0			1.14498	1.14517
1.5			1.31565	1.31568
1.0			1.45858	1.45860
1.0	0.0	0.1	1.69469	1.69469
	0.2		1.45858	1.45860
	0.4		1.22248	1.22250
	0.6		0.98637	0.98640
	0.8		0.75026	0.75030
	1.0		0.51416	0.51421
1.0	0.2	0.0	1.37297	1.37298
		0.1	1.45858	1.45860
		0.2	1.54716	1.54718
		0.3	1.63881	1.63884
		0.4	1.72399	1.73363

parameter (fw). The numerically obtained values are compared with the results fetched by the analytical approach by HAM.

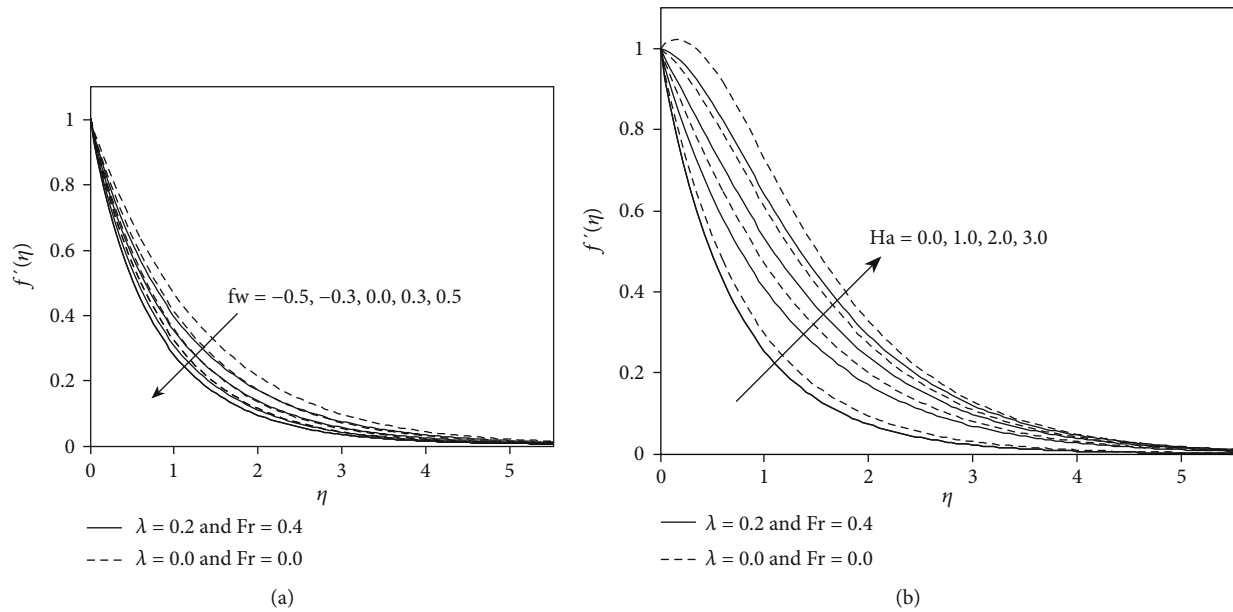
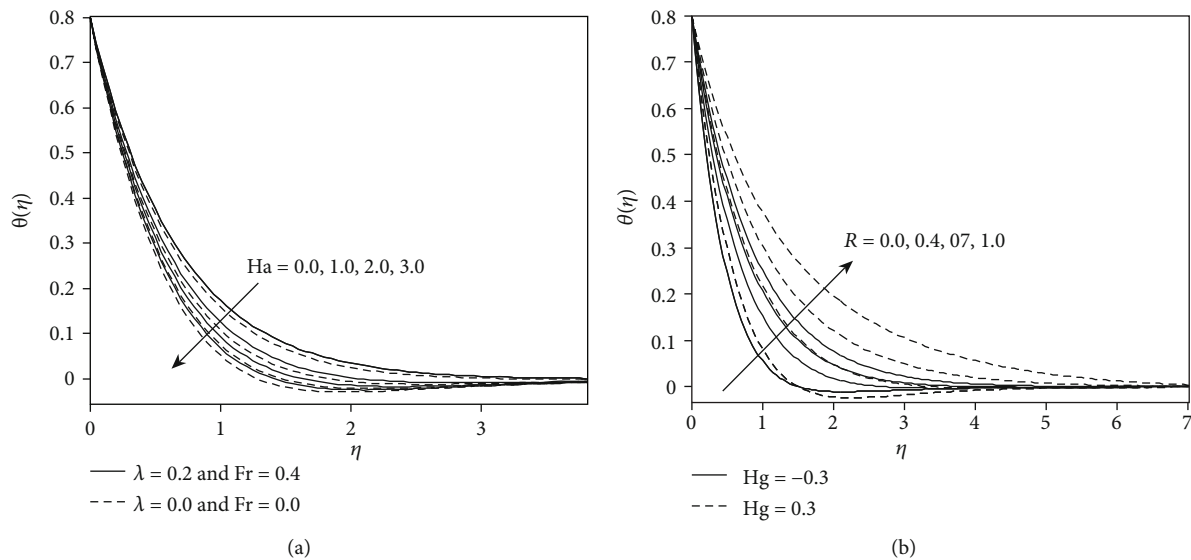
FIGURE 3: The velocity profile for disparate values of fw (a) and Ha (b).FIGURE 4: The temperature profile for disparate values of Ha (a) and R (b).

Table 1 provides the HAM order and CPU timings. From this table, we concluded that 13th order is sufficient for all profiles. Table 2 delineates the changes of skin friction coefficient, local Nusselt number, and local Sherwood number for the distinct values of We , λ , Fr , Ha , and fw . We noted that the surface shear stress upsurges when heightening the We and Ha values and it declines for enhancing the λ , Fr , and fw values. The local Nusselt and Sherwood numbers reduce for raising the We , λ , and Fr , and it rises for increasing the Ha and fw . Table 3 describes the influence of R , Hg , S_1 , and Γ_1 over the heat flux. The heat transfer gradient decimates when developing the Hg and S_1 values, and it grows when growing

the R and Γ_1 values. Table 4 helps to figure out the shift of mass flux for the various values of Cr , S_2 , and Γ_2 . The mass transfer rate escalates for the enriching values of Cr and Γ_2 , and it suppresses for increasing S_2 values. Also, we proved that our numerical and analytical results are almost same.

Figures 3(a) and 3(b) establish the impact of fw (a) and Ha (b) on velocity profile for DFRP and NDFRP. We uncovered that the fluid speed aggravates due to more presence of Hartmann number and quite the opposite behavior is obtained for the fw parameter. The MBLT is high in NDFRP compared to DFRP for both parameters. The outcomes for disparate values of Ha and R on temperature profile are

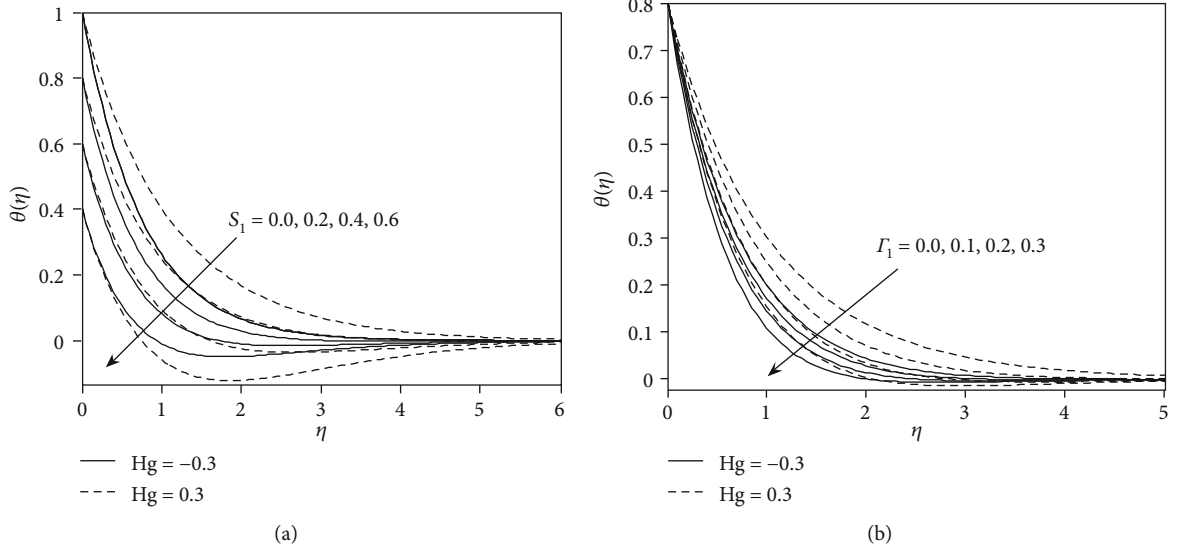


FIGURE 5: The temperature profile for disparate values of S_1 (a) and Γ_1 (b).

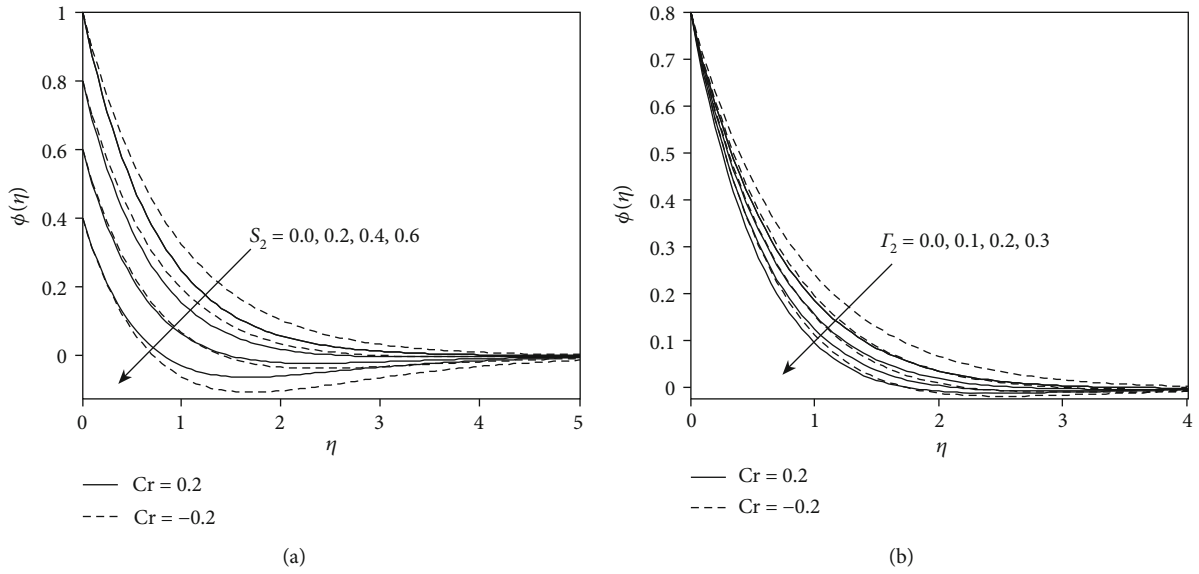
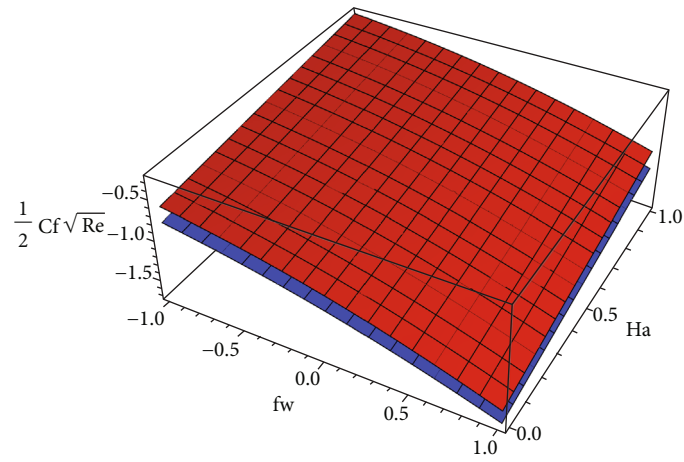


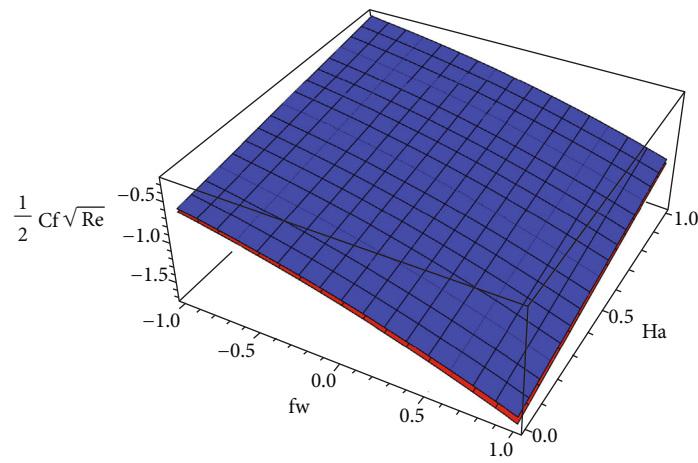
FIGURE 6: The concentration profile for disparate values of S_2 (a) and Γ_2 (b).

illustrated in Figures 4(a) and 4(b) for DFRP and NDFRP (a) and heat consumption/generation (b). We ascertained that the fluid temperature dwindles because of the high quantity of Hartmann number. However, it is enhanced for raising the radiation parameter. Figures 5(a) and 5(b) explains the changes of fluid temperature for distinct values of S_1 (a) and Γ_1 (b) for heat generation/consumption fluid. We revealed that the fluid warmth becomes subsides for hike values of S_1 and Γ_1 . In addition, the thermal boundary layer thickness is large in the heat generation case compared to the heat consumption case. The significance of S_2 and Γ_2 on concentration profile on destructive chemical reaction and the generative chemical reaction is plotted in Figures 6(a) and 6(b). We ascertained that the fluid concentration lessens for large values of S_2 and Γ_2 .

The variations of SFC for distinct combination of fw and Ha (a) for DF flow (lower plate) and NDF flow (upper plate) and (b) for DF flow of Williamson fluid (upper plate) and viscous fluid (lower plate) are portrayed in Figures 7(a) and 7(b). We found that the plate shear stress depresses for enhancing values of fw, and it raises for rising the values of Hartmann number. Figures 8(a) and 8(b) disclose the changes of LNN for disparate combination of fw and Ha (a) for DF flow (lower plate) and NDF flow (upper plate) and (b) for DF flow of Williamson fluid (lower plate) and viscous fluid (upper plate). We noted that heat transfer gradient escalates for increasing the values of fw and Ha. The alternations of LNN for various combination of (a) fw and Γ_1 with $Hg = -0.5$ (upper plate) and $Hg = 0.5$ (lower plate) and (b)

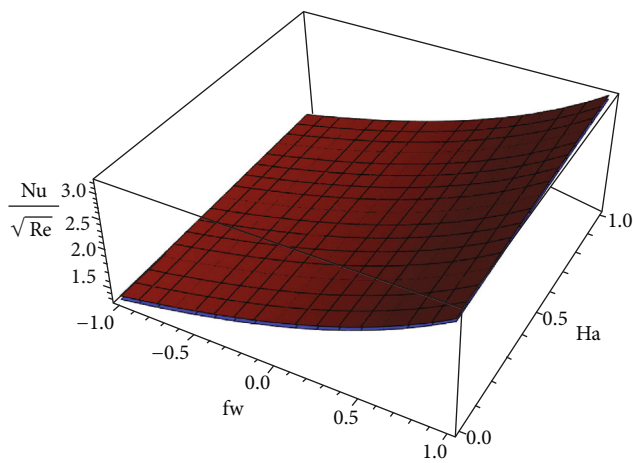


(a)

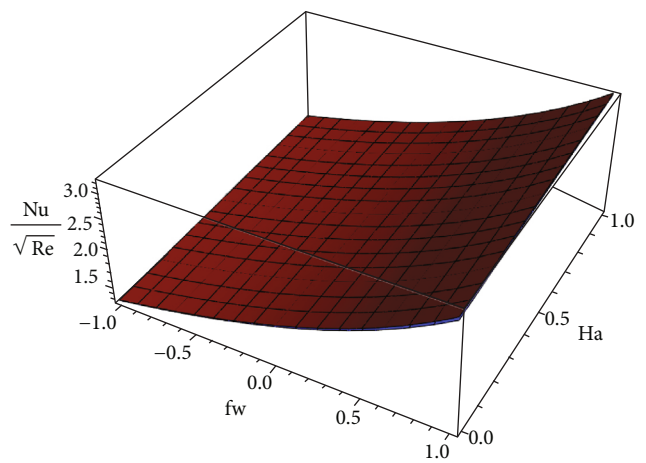


(b)

FIGURE 7: The variations of SFC for distinct combination of fw and Ha (a) for DF flow (lower plate) and NDF flow (upper plate) and (b) for DF flow of Williamson fluid (upper plate) and viscous fluid (lower plate).



(a)



(b)

FIGURE 8: The variations of LNN for distinct combination of fw and Ha (a) for DF flow (lower plate) and NDF flow (upper plate) and (b) for DF flow of Williamson fluid (lower plate) and viscous fluid (upper plate).

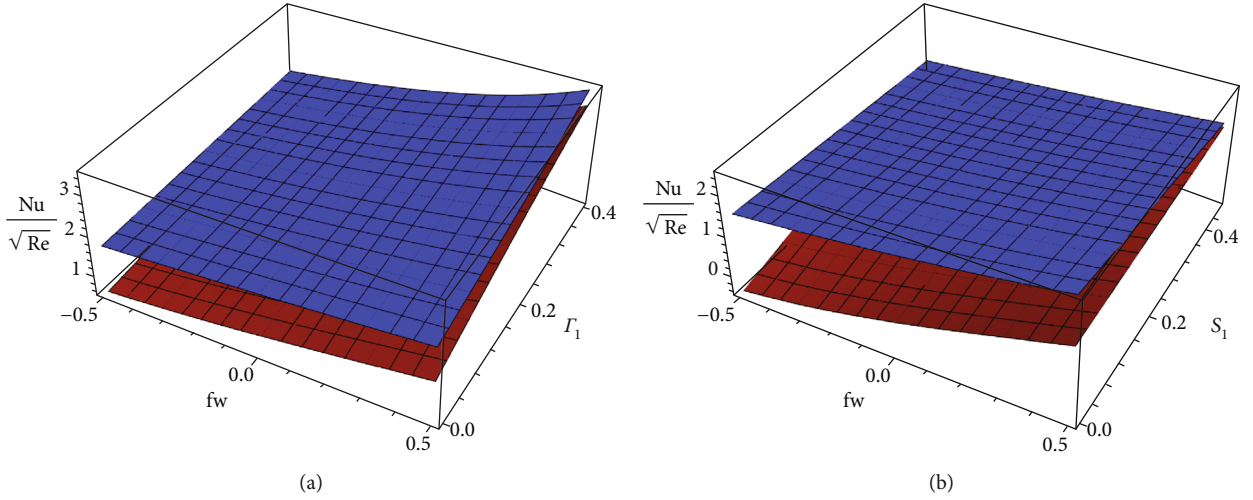


FIGURE 9: The variations of LNN for distinct combination of (a) fw and Γ_1 with Hg = -0.5 (upper plate) and Hg = 0.5 (lower plate) and (b) fw and S_1 with Hg = -0.5 (upper plate) and Hg = 0.5 (lower plate).

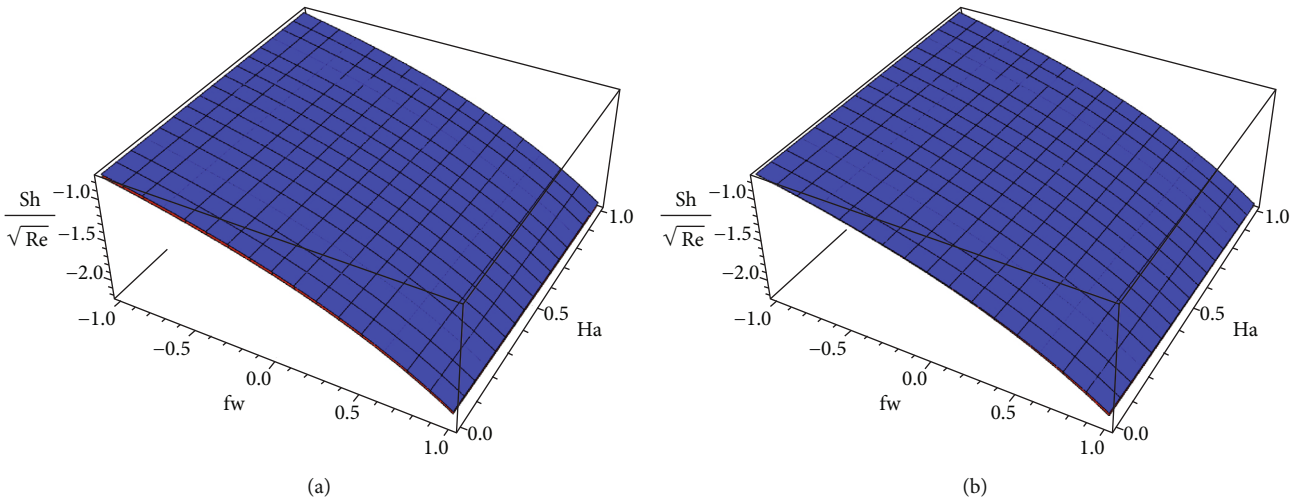


FIGURE 10: The variations of LSN for distinct combination of fw and Ha (a) for DF flow (upper plate) and NDF flow (lower plate) and (b) for DF flow of Williamson fluid (upper plate) and viscous fluid (lower plate).

fw and S_1 with Hg = -0.5 (upper plate) and Hg = 0.5 (lower plate) are plotted in Figures 9(a) and 9(b). We noticed that the heat transfer gradient upgrades for the available of fw, and it weakens for high quantity of S_1 and Γ_1 . In addition, the larger heat transfer gradient occurs in heat consumption case compared to heat generation case. Figures 10(a) and 10(b) express the LSN variation with respect to the distinct combination of fw and Ha (a) for DF flow (upper plate) and NDF flow (lower plate) and (b) for DF flow of Williamson fluid (upper plate) and viscous fluid (lower plate). We proved that the mass transfer gradient slashes due to larger values of fw and Ha. The deviation of LSN for different combination of (a) fw and Γ_2 with generative chemical reaction (upper plate) and destructive chemical reaction (lower plate) and (b) fw and S_2 with generative chemical reaction (upper plate) and destructive chemical reaction (lower plate) is

shown in Figures 11(a) and 11(b). We concluded that the LSN declines for upgrading the values of fw, Γ_2 , and S_2 .

The decrement percentage of SFC for various values of fw on Williamson fluid and viscous fluid is plotted in Figures 12(a) and 12(b) and observed that the maximum decreasing percentage of surface shear stress is obtained when fw varies from 0.0 to 0.4 for both fluids. Figures 13(a) and 13(b) give the increment percentage of LNN for various values of fw on Williamson fluid and viscous fluid. The maximum increment percentage has occurred when fw vary from 0.4 to 0.8 for both fluids. The decrement percentage of LSN for various values of fw on Williamson fluid and viscous fluid is illustrated in Figures 14(a) and 14(b), and we have seen that the maximum decrement percentage occurred when fw varies from 0.4 to 0.8 for both fluids. Figures 15(a) and 15(b) display the decrement/increment percentage of LNN

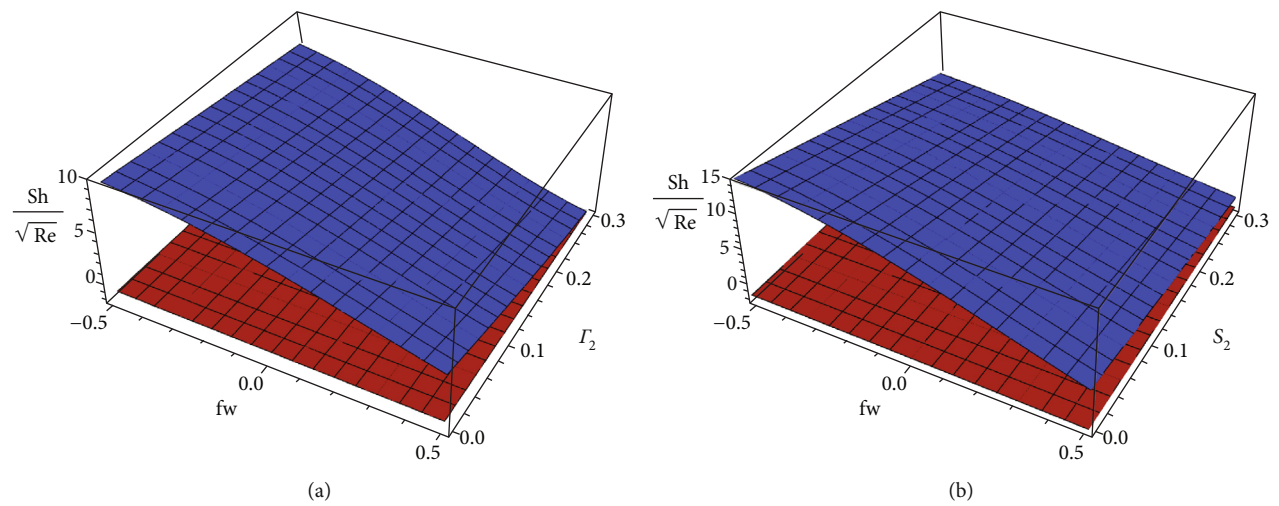


FIGURE 11: The variations of LSN for distinct combination of (a) fw and Γ_2 with generative chemical reaction (upper plate) and destructive chemical reaction (lower plate) and (b) fw and S_2 with generative chemical reaction (upper plate) and destructive chemical reaction (lower plate).

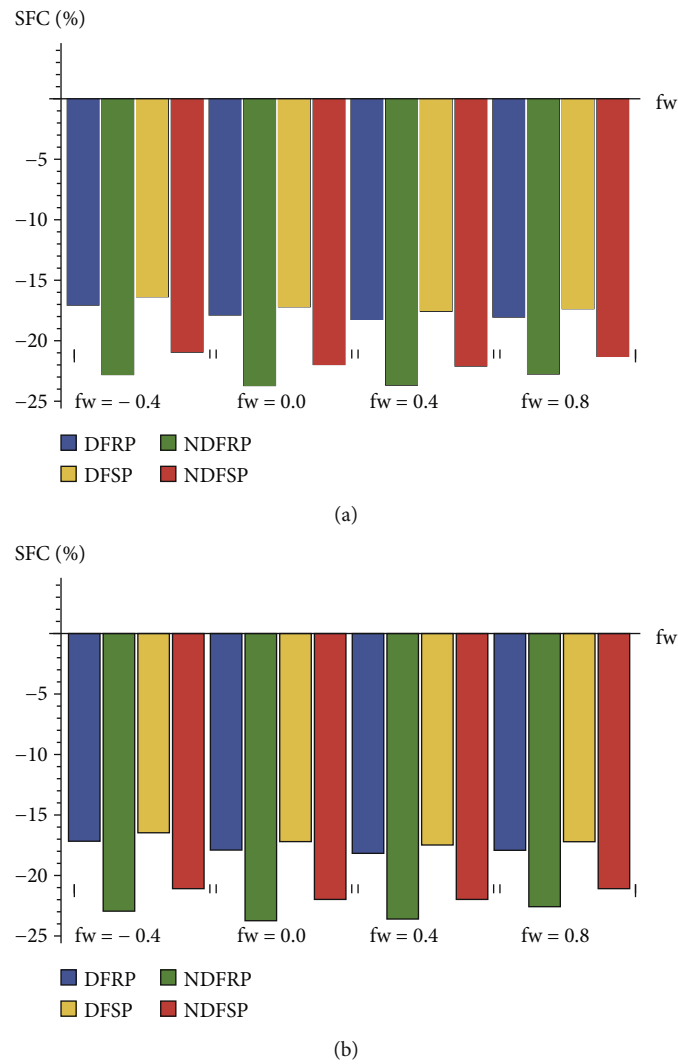


FIGURE 12: Decrement percentage of SFC for various values of fw on (a) Williamson fluid and (b) viscous fluid.

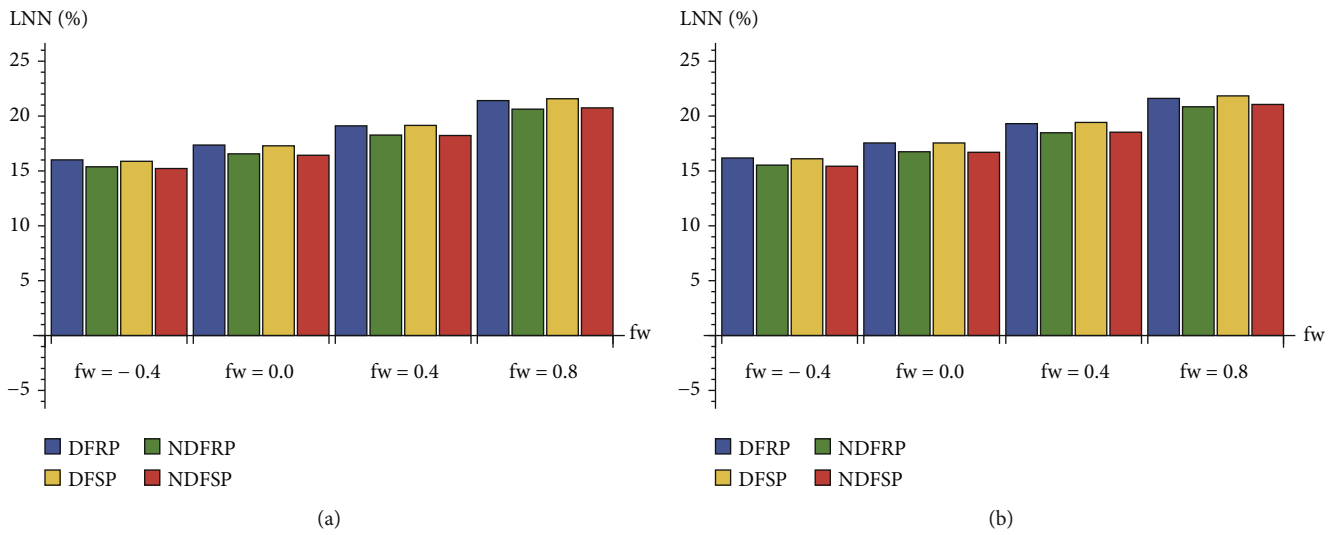


FIGURE 13: Increment percentage of LNN for various values of fw on (a) Williamson fluid and (b) viscous fluid.

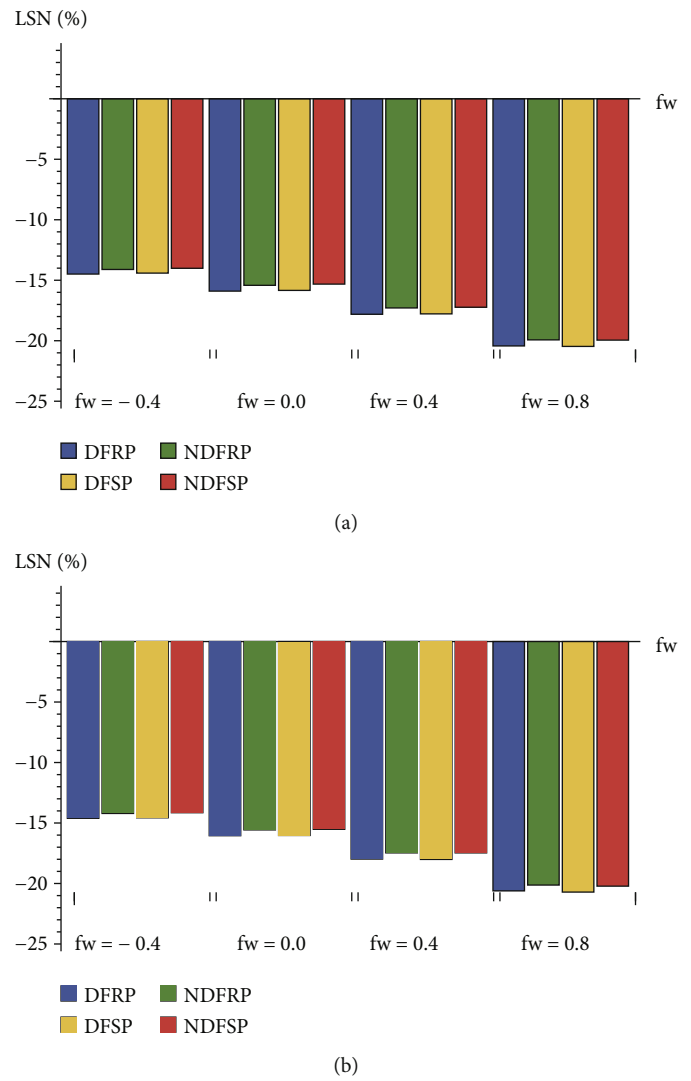


FIGURE 14: Decrement percentage of LSN for various values of fw on (a) Williamson fluid and (b) viscous fluid.

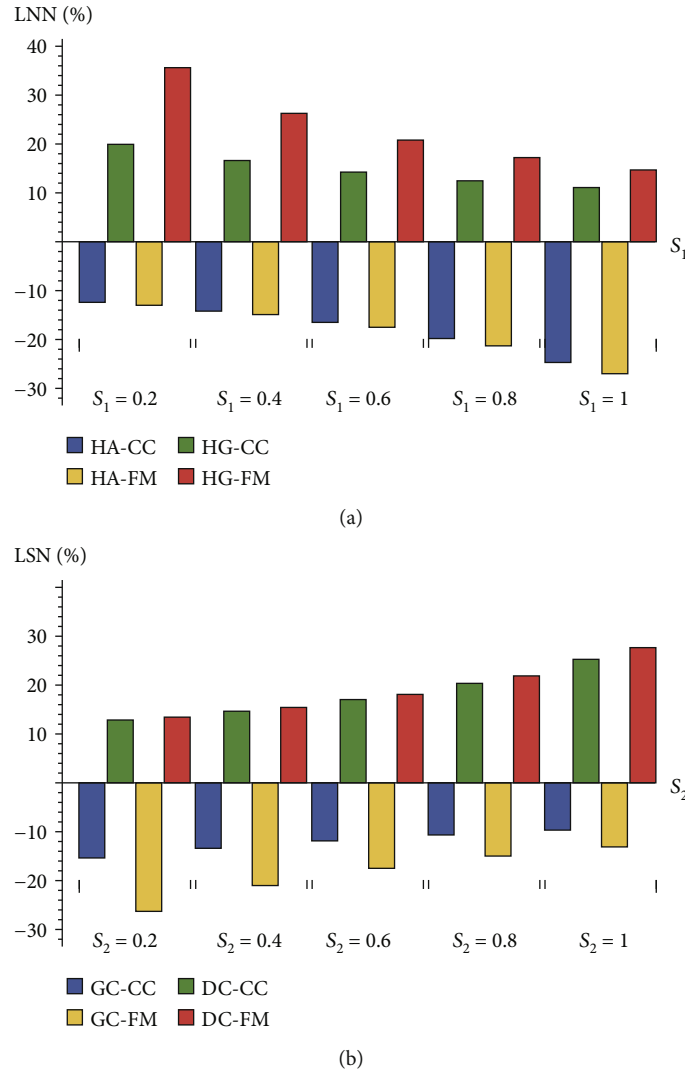


FIGURE 15: Decrement/increment percentage of (a) LNN for various values of S_1 and (b) LSN for various values of S_2 .

for various values of S_1 and LSN for various values of S_2 . We concluded that the heat transfer gradient enhances in heat generation case and maximum increment percentage is obtained when S_1 varies from 0 to 0.2 and it suppresses in heat consumption case and maximum decrement percentage is obtained when S_1 varies from 0.8 to 1. The mass transfer gradient enhances in destructive chemical reaction case and maximum increment percentage is obtained when S_2 varies from 0.8 to 1, and it suppresses in the generative case and maximum decrement percentage is obtained when S_2 varies from 0 to 0.2.

5. Conclusion

The current study figures out the Darcy-Forchheimer flow of the Williamson fluid over a Riga plate with Cattaneo-Christov double diffusion and double stratification. The solutions are fetched numerically by a bvp4c solver in MATLAB and analytically by HAM. The outcomes are employed as follows:

- (i) The fluid velocity drops when the suction/injection parameter enriches
- (ii) The larger values of the thermal radiation parameter boost up the temperature
- (iii) The high temperature is noticed in the heat generation case, and the low temperature is produced in the heat absorption case
- (iv) The generative chemical reaction case upturns the fluid concentration while the destructive chemical reaction case declines
- (v) The high wall shear stress is produced when enlarging the modified Hartmann number

Abbreviations

- CC: Cattaneo-Christov
 DC: Destructive chemical reaction
 DF: Darcy-Forchheimer

FM: Fourier model
 GC: Generative chemical reaction
 HA: Heat absorption
 HG: Heat generation
 LNN: Local Nusselt number
 LSN: Local Sherwood number
 MBLT: Momentum boundary layer thickness
 NDF: Non-Darcy-Forchheimer
 RP: Riga plate
 SFC: Skin friction coefficient
 SP: Stationary plate.

Data Availability

The raw data supporting the conclusions of this article will be made available by the authors without undue reservation.

Conflicts of Interest

The authors declare that they have no competing interests.

Authors' Contributions

All authors contributed equally to this work. And all the authors have read and approved the final version of the manuscript.

Acknowledgments

This research was funded by the Deanship of Scientific Research at Princess Nourah Bint Abdulrahman University through the Fast-track Research Funding Program.

References

- [1] R. V. Williamson, "The flow of pseudoplastic materials," *Industrial and Engineering Chemistry Research*, vol. 21, no. 11, pp. 1108–1111, 1929.
- [2] M. R. Krishnamurthy, B. C. Prasannakumara, B. J. Gireesha, and R. S. R. Gorla, "Effect of chemical reaction on MHD boundary layer flow and melting heat transfer of Williamson nanofluid in porous medium," *Engineering Science and Technology, An International Journal*, vol. 19, no. 1, pp. 53–61, 2016.
- [3] M. I. Khan, F. Alzahrani, A. Hobiny, and Z. Ali, "Modeling of Cattaneo-Christov double diffusions (CCDD) in Williamson nanomaterial slip flow subject to porous medium," *Journal of Materials Research and Technology*, vol. 9, no. 3, pp. 6172–6177, 2020.
- [4] T. Hayat, A. Shafiq, and A. Alsaedi, "Hydromagnetic boundary layer flow of Williamson fluid in the presence of thermal radiation and Ohmic dissipation," *Alexandria Engineering Journal*, vol. 55, no. 3, pp. 2229–2240, 2016.
- [5] S. Nadeem, S. T. Hussain, and C. Lee, "Flow of a Williamson fluid over a stretching sheet," *Brazilian Journal of Chemical Engineering*, vol. 30, no. 3, pp. 619–625, 2013.
- [6] T. Salahuddin, M. Y. Malik, H. Arif, S. Bilal, and M. Awais, "MHD flow of Cattaneo-Christov heat flux model for Williamson fluid over a stretching sheet with variable thickness: using numerical approach," *Journal of Magnetism and Magnetic Materials*, vol. 401, no. 1, pp. 991–997, 2016.
- [7] N. A. Khan and H. Khan, "A boundary layer flows of non-Newtonian Williamson fluid," *Nonlinear Engineering*, vol. 3, no. 2, pp. 107–115, 2014.
- [8] T. Kebede, E. Haile, G. Awgichew, and T. Walelign, "Heat and mass transfer in unsteady boundary layer flow of Williamson nanofluids," *Journal of Applied Mathematics*, vol. 2020, Article ID 1890972, 13 pages, 2020.
- [9] P. Forchheimer, "Wasserbewegung durch boden," *Zeitschrift des Vereines Deutscher Ingenieure*, vol. 45, pp. 1782–1788, 1901.
- [10] S. Mukhopadhyay, P. R. De, K. Bhattacharyya, and G. C. Layek, "Forced convective flow and heat transfer over a porous plate in a Darcy-Forchheimer porous medium in presence of radiation," *Meccanica*, vol. 47, no. 1, pp. 153–161, 2011.
- [11] T. Hayat, A. Aziz, T. Muhammad, and A. Alsaedi, "Darcy-Forchheimer three-dimensional flow of Williamson nanofluid over a convectively heated nonlinear stretching surface," *Communications in Theoretical Physics*, vol. 68, no. 3, pp. 387–394, 2017.
- [12] M. I. Khan, T. Hayat, and A. Alsaedi, "Numerical analysis for Darcy-Forchheimer flow in presence of homogeneous- heterogeneous reactions," *Results in Physics*, vol. 7, pp. 2644–2650, 2017.
- [13] F. Haider, T. Hayat, and A. Alsaedi, "Flow of hybrid nanofluid through Darcy-Forchheimer porous space with variable characteristics," *Alexandria Engineering Journal*, vol. 60, no. 3, pp. 3047–3056, 2021.
- [14] M. A. Sadiq, F. Haider, T. Hayat, and A. Alsaedi, "Partial slip in Darcy-Forchheimer carbon nanotubes flow by rotating disk," *International Communications in Heat and Mass Transfer*, vol. 116, p. 104641, 2020.
- [15] T. Muhammad, K. Rafique, M. Asma, and M. Alghamdi, "Darcy-Forchheimer flow over an exponentially stretching curved surface with Cattaneo-Christov double diffusion," *Physica A*, vol. 556, article 123968, 2020.
- [16] M. K. Nayak, S. Shaw, M. Ijaz Khan, V. S. Pandey, and M. Nazeer, "Flow and thermal analysis on Darcy-Forchheimer flow of copper-water nanofluid due to a rotating disk: a static and dynamic approach," *Journal of Materials Research and Technology*, vol. 9, no. 4, pp. 7387–7408, 2020.
- [17] K. Loganathan, N. Alessa, K. Tamilvanan, and F. S. Alshammari, "Significances of Darcy-Forchheimer porous medium in third-grade nanofluid flow with entropy features," *The European Physical Journal Special Topics*, vol. 230, no. 5, pp. 1293–1305, 2021.
- [18] J. C. Umavathi, O. Ojjela, and K. Vajravelu, "Numerical analysis of natural convective flow and heat transfer of nanofluids in a vertical rectangular duct using Darcy-Forchheimer-Brinkman model," *International Journal of Thermal Sciences*, vol. 111, pp. 511–524, 2017.
- [19] A. Gailitis and O. Lielausis, "On a possibility to reduce the hydrodynamic resistance of a plate in an electrolyte," *Applied Magnetohydrodynamics, Reports of the Physics Institute*, vol. 12, no. 1, pp. 143–146, 1961.
- [20] A. Ahmad, S. Asghar, and S. Afzal, "Flow of nanofluid past a Riga plate," *Journal of Magnetism and Magnetic Materials*, vol. 402, pp. 44–48, 2016.
- [21] M. Nazeer, M. I. Khan, M. U. Rafiq, and N. B. Khan, "Numerical and scale analysis of Eyring-Powell nanofluid towards a magnetized stretched Riga surface with entropy generation and internal resistance," *International Communications in Heat and Mass Transfer*, vol. 119, article 104968, 2020.

- [22] B. J. Gireesha, K. Ganesh Kumar, and B. C. Prasannakumar, "Scrutinization of chemical reaction effect on flow and mass transfer of Prandtl liquid over a Riga plate in the presence of solutal slip effect," *International Journal of Chemical Reactor Engineering*, vol. 16, no. 8, 2018.
- [23] R. Mehmood, M. K. Nayak, N. S. Akber, and O. D. Makinde, "Effects of thermal-diffusion and diffusion-thermo on oblique stagnation point flow of couple stress Casson fluid over a stretched horizontal Riga plate with higher-order chemical reaction," *Journal of Nanofluids*, vol. 8, no. 1, pp. 94–102, 2019.
- [24] M. Ayub, T. Abbas, and M. M. Bhatti, "Influence of slip effects on electromagnetic hydrodynamics (EMHD) nanoflow over a horizontal Riga plate," *European Physical Journal Plus*, vol. 131, no. 93, pp. 1–9, 2016.
- [25] N. K. Nayak, S. Shaw, O. D. Makinde, and A. J. Chamkha, "Investigation of partial slip and viscous dissipation effects on the radiative tangent hyperbolic nanoflow past a vertical permeable Riga plate with internal heating: Bungeni model," *Journal of Nanofluids*, vol. 8, pp. 1–12, 2019.
- [26] G. Rasool, T. Zhang, and A. Shafiq, "Second grade nanofluidic flow past a convectively heated vertical Riga plate," *Physica Scripta*, vol. 94, no. 12, p. 125212, 2019.
- [27] C. Y. Cheng, "Combined heat and mass transfer in natural convection flow from a vertical wavy surface in a power-law fluid saturated porous medium with thermal and mass stratification," *International Communications in Heat and Mass Transfer*, vol. 36, no. 4, pp. 351–356, 2009.
- [28] M. Khan, A. Rasheed, T. Salahuddin, and S. Ali, "Chemically reactive flow of hyperbolic tangent fluid flow having thermal radiation and double stratification embedded in porous medium," *Ain Shams Engineering Journal*, 2021.
- [29] K. U. Rehman, A. A. Khan, M. Y. Malik, U. Ali, and M. Naseer, "Numerical analysis subject to double stratification and chemically reactive species on Williamson dual convection fluid flow yield by an inclined stretching cylindrical surface," *Chinese Journal of Physics*, vol. 55, no. 4, pp. 1637–1652, 2017.
- [30] M. Khan, T. Salahuddin, M. Y. Malik, and F. O. Mallawi, "Change in viscosity of Williamson nanofluid flow due to thermal and solutal stratification," *International Journal of Heat and Mass Transfer*, vol. 126, pp. 941–948, 2018.
- [31] O. M. Mallawi, M. Bhuvaneswari, S. Sivasankaran, and S. Eswaramoorthi, "Impact of double-stratification on convective flow of a non-Newtonian liquid in a Riga plate with Cattaneo-Christov double-flux and thermal radiation," *Ain Shams Engineering Journal*, vol. 12, no. 1, pp. 969–981, 2021.
- [32] T. Hayat, M. Imtiaz, and A. Alsaedi, "Unsteady flow of nanofluid with double stratification and magnetohydrodynamics," *International Journal of Heat and Mass Transfer*, vol. 92, pp. 100–109, 2016.
- [33] S. Sarwar and M. M. Rashidi, "Approximate solution of two-term fractional-order diffusion, wave-diffusion, and telegraph models arising in mathematical physics using optimal homotopy asymptotic method," *Waves in Random and Complex Media*, vol. 26, no. 3, pp. 365–382, 2016.
- [34] S. Eswaramoorthi, M. Bhuvaneswari, S. Sivasankaran, and S. Rajan, "Soret and Dufour effects on viscoelastic boundary layer flow over a stretching surface with convective boundary condition with radiation and chemical reaction," *Scientia Iranica B*, vol. 23, no. 6, pp. 2575–2586, 2016.
- [35] H. Hassan and M. Mehdi Rashidi, "An analytic solution of micropolar flow in a porous channel with mass injection using homotopy analysis method," *International Journal of Numerical Methods for Heat & Fluid Flow*, vol. 24, no. 2, pp. 419–437, 2014.
- [36] K. Loganathan, N. Alessa, N. Namgyel, and T. S. Karthik, "MHD flow of thermally radiative Maxwell fluid past a heated stretching sheet with Cattaneo-Christov dual diffusion," *Journal of Mathematics*, vol. 2021, Article ID 5562667, 10 pages, 2021.
- [37] M. Bhuvaneswari, S. Eswaramoorthi, S. Sivasankaran, and A. S. Alshomrani, "Effect of viscous dissipation and convective heating on convection flow of a second grade fluid over a stretching surface: analytical and numerical study," *Scientia Iranica B*, vol. 26, no. 3, pp. 1350–1357, 2019.

Research Article

Natural Transform along with HPM Technique for Solving Fractional ADE

N. Pareek ¹, A. Gupta ², G. Agarwal ³, and D. L. Suthar ⁴

¹Department of Mathematics, Bhagat Singh Govt. P.G. College, Jaora, India

²Department of Mathematics, Govt. M.V.M, Bhopal, India

³Department of Mathematics and Statistics, Manipal University Jaipur, Rajasthan, India

⁴Department of Mathematics, Wollo University, P.O. Box: 1145, Dessie, Ethiopia

Correspondence should be addressed to D. L. Suthar; dlsuthar@gmail.com

Received 16 April 2021; Accepted 8 July 2021; Published 28 July 2021

Academic Editor: Younes Menni

Copyright © 2021 N. Pareek et al. This is an open access article distributed under the Creative Commons Attribution License, which permits unrestricted use, distribution, and reproduction in any medium, provided the original work is properly cited.

The authors of this paper solve the fractional space-time advection-dispersion equation (ADE). In the advection-dispersion process, the solute movement being nonlocal in nature and the velocity of fluid flow being nonuniform, it leads to form a heterogeneous system which approaches to model the same by means of a fractional ADE which generalizes the classical ADE, where the time derivative is substituted through the Caputo fractional derivative. For the study of such fractional models, various numerical techniques are used by the researchers but the nonlocality of the fractional derivative causes high computational expenses and complex calculations so the challenge is to use an efficient method which involves less computation and high accuracy in solving such models numerically. Here, in order to get the FADE solved in the form of convergent infinite series, a novel method NHPM (natural homotopy perturbation method) is applied which couples Natural transform along with the homotopy perturbation method. The homotopy perturbation method has been applied in mathematical physics to solve many initial value problems expressed in the form of PDEs. Also, the HPM has an advantage over the other methods that it does not require any discretization of the domains, is independent of any physical parameters, and only uses an embedding parameter $p \in [0, 1]$. The HPM combined with the Natural transform leads to rapidly convergent series solutions with less computation. The efficacy of the used method is shown by working out some examples for time-fractional ADE with various initial conditions using the NHPM. The Mittag-Leffler function is used to solve the fractional space-time advection-dispersion problem, and the impact of changing the fractional parameter α on the solute concentration is shown for all the cases.

1. Introduction and Preliminaries

Fractional calculus generalizes the integration and differentiation of integer order to arbitrary order that is being studied for the past 300 years. The growing interest of researchers in this field has led to solving the real-world issues in type of fractional differential equations due to their nonlocal behavior, and these equations are well suited to describe various phenomena in the field of engineering and science. Also, fractional derivatives are capable to model various processes mathematically which exhibit the memory and hereditary properties [1–5].

The ADE arises in the study of transport of solute or Brownian motion of particles in a fluid occurring due to the simultaneous occurrence of advection and particle dispersion. Fractional advection-dispersion equation describes the phenomena of anomalous diffusion of the particles in the transport process in a better way; as in anomalous diffusion, the solute transport is quicker or speedier than time's inferred square root given by Baeumer et al. [6]. The equation is used to study groundwater pollution, pollution of the atmosphere produced by smoke or dust, the spread of chemical solutes and contaminant discharges, etc. [7]. Hence, FADE has attracted the attention of many researchers.

Hence, the interest of the researchers lies in solving the FADE to find out the solute concentration at a particular instant of time and space. Analytical solution of one-dimensional ADE was found by Jaiswal et al. [8]. Huang et al. [9] solve the one-dimensional fractional flux ADE and found the finite element solutions. The intermediate fractional ADE was studied by El-Sayed et al. [10]. To solve the space-time fractional ADE, Momani and Odibat [7] utilized the ADM and variational iteration approach. In this continuation, Yildirim and Koçak [11] solve the space-time fractional ADE by applying homotopy perturbation technique in Caputo sense and Hikal and Abu Ibrahim [12] solved it by the Adomian decomposition method. Alliche and Chikh [13] studied the nonpremixed chaotic fire of the hydrogen-air downward injector system using the generalized finite rate chemistry model. Liu et al. [14] applied numerical methods to study various advection-dispersion models. Rocca et al. [15] developed a general solution to the fractional diffusion-advection equation for solar cosmic-ray transport. Ramani et al. [16] explored the fractional decreased differential transform approach for revisiting the analytical-approximate formulation of the time-fractional Rosenau-Hyman problem. The extended differential transform approach was used by Garg and Manohar [17] to solve the space-time fractional Fokker Planck (FFP) equation analytically. Also, Habenom et al. [18] studied the formulation of FFP equation using fractional power series technique. The N-transform was used by Khan and Khan [19] to study the unsteady fluid flow over a plane wall, and N-transform of some functions along with the properties was presented. Belgacem and Silambarasan [20] renamed it as Natural transform which they used to solve Bessel's differential equation with a polynomial coefficient and also Maxwell's equation.

In this article, first, we recall few concepts of fractional calculus, Natural transform, and HPM which have been used in our main findings, in Sections 2, 3, and 4, respectively. Then, we gave a solution to the space-time ADE by the NHPM in Section 5, and at the last, Section 6 contains some related examples, which show the efficiency of this method. In Section 7, a conclusion has been discussed.

2. Basic Definitions

The Riemann-Liouville and Caputo-type fractional integral operator and its properties are discussed in this section. These definitions and properties (see detail [1–3]) will be used to get the main results.

Definition 1. Let $f(x)$ with $x > 0$ be a real-valued function. If there is a real number $p > \mu$, it is said to be in the space \mathcal{C} in R . Such that $f(x) = x^p f_1(x)$, where $f_1(x) \in \mathcal{C}[0, \infty)$.

Definition 2. Let $f(x)$ with $x > 0$ be a real-valued function; then, it would seem to be in space \mathcal{C}_μ^n , $m \in N \cup \{0\}$, if $f^{(m)} \in \mathcal{C}_\mu$.

Definition 3. For a function $f \in C_\mu$, where $\mu = 1$, the R-L fractional integral operator of order $\vartheta = 0$ is described as

$$\begin{aligned} \mathbb{J}^\vartheta f(z) &= \frac{1}{\Gamma(\vartheta)} \int_0^z (z-t)^{\vartheta-1} f(t) dt; \vartheta > 0, z > 0, \\ \mathbb{J}^0 f(z) &= f(z), \\ \mathbb{J}^\vartheta \mathbb{J}^\vartheta f(z) &= \mathbb{J}^{\vartheta+\vartheta} f(z), \\ \mathbb{J}^\vartheta z^\vartheta &= \frac{\Gamma(\vartheta+1)}{\Gamma(\vartheta+\vartheta+1)} z^{\vartheta+\vartheta}. \end{aligned} \quad (1)$$

Definition 4. In Caputo's view, the fractional derivative of $f \in \mathcal{C}^{n-1}$ is expressed by

$$D^\vartheta f(z) = \begin{cases} \frac{1}{\Gamma(n-\vartheta)} \int_0^z (z-\tau)^{n-\vartheta-1} f^{(n)}(\tau) d\tau, & n-1 < \vartheta < n, n \in N^*, \\ \frac{d^n}{dt^n} f(z), & \vartheta = n. \end{cases} \quad (2)$$

Also,

$$\begin{aligned} D^\vartheta \mathcal{K} &= 0; \mathcal{K} \text{ being a constant,} \\ D^\vartheta z^\vartheta &= \begin{cases} \frac{\Gamma(\vartheta+1)}{\Gamma(\vartheta-\vartheta+1)} z^{\vartheta-\vartheta}, & \vartheta > \vartheta-1, \\ 0, & \vartheta = \vartheta-1. \end{cases} \end{aligned} \quad (3)$$

Definition 5. The two-parameter M-L function is described as follows:

$$E_{\vartheta, \vartheta}(z) = \sum_{k=0}^{\infty} \frac{z^k}{\Gamma(\vartheta k + \vartheta)}. \quad (4)$$

Consequently, the one-parameter M-L function is described as follows:

$$E_\vartheta(z) = E_{\vartheta,1}(z) = \sum_{k=0}^{\infty} \frac{z^k}{\Gamma(\vartheta k + 1)}. \quad (5)$$

3. Natural Transform

Over the set, Natural transform is specified:

$$A = \left\{ f(t): \exists M, \tau_1, \tau_2, |v(t)| < M e^{t/\tau_j}, \text{ if } t \in (-1)^j \times [0, \infty) \right\}, \quad (6)$$

$$\mathbb{N}[f(t)] = F(s, u) = \frac{1}{u} \int_0^\infty e^{-st/uv} f(t) dt; \quad u > 0, s > 0, t \in (0, \infty), \quad (7)$$

where s and u denote the Natural transform variables [21, 22].

Remark 6.

(i) If $u = 1$, (7) reduces to the Laplace transform

TABLE 1: Relation between \mathbb{N} -transforms, Sumudu transform, and Laplace transform.

$f(t)$	$\mathbb{N}[f(t)]$	$\mathbb{S}[f(t)]$	$\mathbb{L}[f(t)]$
1	$\frac{1}{s}$	1	$\frac{1}{s}$
t	$\frac{u}{s^2}$	u	$\frac{1}{s^2}$
e^{at}	$\frac{1}{s-au}$	$\frac{1}{1-au}$	$\frac{1}{s-a}$
$\frac{t^{n-1}}{(n-1)!}, n = 1, 2, \dots$	$\frac{u^{n-1}}{s^n}$	u^{n-1}	$\frac{1}{s^n}$
$\sin(t)$	$\frac{u}{s^2+u^2}$	$\frac{u}{1+u^2}$	$\frac{1}{1+s^2}$

TABLE 2: Properties of \mathbb{N} -transforms.

Function	Natural transform of the function
$f(t)$	$F(s, u)$
$f(at)$	$\frac{1}{a}F(s, u)$
$f'(t)$	$\frac{s}{u}F(s, u) - \frac{1}{u}f(0)$
$f''(t)$	$\frac{s^2}{u^2}F(s, u) - \frac{s}{u^2}f(0) - \frac{1}{u}f'(0)$
$af(t) \pm bg(t)$	$aF(s, u) \pm bG(s, u)$

(ii) If $s = 1$, (7) reduces to the Sumudu transform

\mathbb{N} -transforms of some elementary functions and the conversions to Sumudu and Laplace [19, 21–23] are given in Tables 1 and 2.

4. The Homotopy Perturbation Method

The general form of the time-dependent differential equation (see [24–26]) can be written as

$$\mathbb{A}(u(\zeta, t)) - f(\zeta, t) = 0, \quad (8)$$

where \mathbb{A} is the differential operator, $u(\zeta, t)$ is the unknown function, ζ is the independent variables for space, t is the independent variables for time, and $f(\zeta, t)$ is the analytic function.

In general, \mathbb{A} can be divided into \mathbb{L} (linear) and \mathbb{N} (non-linear) component s.t.:

$$\mathbb{A} = \mathbb{L} + \mathbb{N}. \quad (9)$$

By substituting the value of \mathbb{A} in (8),

$$\mathbb{L}(u(\zeta, t)) + \mathbb{N}(u(\zeta, t)) - f(\zeta, t) = 0. \quad (10)$$

Using the homotopy technique presented by Liao [27], a homotopy $\mathcal{O}(r, t : p)$ can be constructed which satisfies

$$\begin{aligned} \mathbb{H}(\mathcal{O}(\zeta, t : p), p) &= (1-p)\{\mathbb{L}(\mathcal{O}(\zeta, t : p)) - \mathbb{L}(u_0(\zeta, t))\} \\ &+ p\{\mathbb{A}(\mathcal{O}(\zeta, t : p)) - f(\zeta, t)\} = 0, \end{aligned} \quad (11)$$

where $p \in [0, 1]$ is an embedding parameter and $u_0(r, t)$ is an initial guess for $u(r, t)$ satisfying initial/boundary conditions. The homotopy equation (11) can be written in an equivalent form as

$$\begin{aligned} \mathbb{L}(\mathcal{O}(\zeta, t : p)) - \mathbb{L}(u_0(\zeta, t)) &+ p\{N(\mathcal{O}(\zeta, t : p)) \\ &+ \mathbb{L}(u_0(\zeta, t)) - f(\zeta, t)\} = 0. \end{aligned} \quad (12)$$

Hence, when $p = 0$, we obtain

$$\mathbb{H}(\mathcal{O}(\zeta, t : 0), 0) = \mathbb{L}(\mathcal{O}(\zeta, t : 0)) - \mathbb{L}(u_0(\zeta, t)) = 0, \quad (13)$$

and when $p = 1$, we get

$$\mathbb{H}(\mathcal{O}(\zeta, t : 1), 1) = \mathbb{A}(\mathcal{O}(\zeta, t : 1)) - f(\zeta, t) = 0. \quad (14)$$

We observe that $u(\zeta, t)$ is the solution of (14) as well as (8) and if \mathbb{L} is taken to be linear, $u_0(\zeta, t)$ is the only solution of (13). So, we have

$$\begin{aligned} \mathcal{O}(\zeta, t : 0) &= u_0(\zeta, t), \\ \mathcal{O}(\zeta, t : 1) &= u(\zeta, t). \end{aligned} \quad (15)$$

Change in p from 0 to 1 is followed by change in $\mathcal{O}(\zeta, t : p)$ from $u_0(\zeta, t)$ to $u(\zeta, t)$, termed as deformation. If the embedding parameter p ($1 \geq p \geq 0$) is thought to be tiny, according to the classic perturbation technique, the solution to the given equation may be assumed as a power series in p , so

$$\mathcal{O}(\zeta, t : p) = u_0(\zeta, t) + pu_1(\zeta, t) + p^2u_2(\zeta, t) + \dots, \quad (16)$$

for $p = 1$,

$$u(\zeta, t) = u_0(\zeta, t) + u_1(\zeta, t) + u_2(\zeta, t) + \dots, \quad (17)$$

which gives the approximate solution of (8). The series in (17) converges in most of the cases and leads to the exact solution.

5. Solution of the Space-Time ADE by the NHPM

The classical one-dimensional ADE with constant parameters is of the form (see [14])

$$\frac{\partial C}{\partial \tau} = D \frac{\partial^2 C}{\partial \xi^2} - V \frac{\partial C}{\partial \xi}, \quad (18)$$

where V is the drift velocity, ξ is the spatial coordinate, $D > 0$ is the constant diffusivity, and $C(\xi, \tau)$ is the solute concentration.

To write equation (18) in a simplified form by setting $t = \tau V$, $x = \xi$ and replacing $C(\xi, \tau)$ by $C(x, t)$, it reduced into

$$C_t = \mu C_{xx} - C_x, \quad (19)$$

where $\mu = D/V$.

We write the general form of the space-time fractional ADE as

$$D_t^\vartheta C = \mu D_x^{p\vartheta} C - D_x^{r\vartheta} C, \quad (20)$$

with $\vartheta = 1/m$, $0 < \vartheta \leq 1$, $1 < p\vartheta \leq 2$, $0 < r\vartheta \leq 1$, $m, p, r \in \mathbb{N}$, $0 < x < L$, $D_x^{p\vartheta} = D_x^\vartheta D_x^\vartheta \cdots D_x^\vartheta$ (p times), $D_x^{r\vartheta} = D_x^\vartheta D_x^\vartheta \cdots D_x^\vartheta$ (r times), D_t^α and D_x^ϑ are the Caputo fractional derivatives.

The initial condition is

$$C(x, 0) = f(x). \quad (21)$$

\mathbb{N} -transform of (20) is written as

$$\frac{s^\vartheta}{u^\vartheta} C(x, s, u) - \frac{s^{\vartheta-1}}{u^\vartheta} C(x, 0) = \mathbb{N}^+ \left[\mu D_x^{p\vartheta} C - D_x^{r\vartheta} C \right]. \quad (22)$$

Now, by substituting initial condition from (21) in the above equation, we obtain

$$C(x, s, u) = \frac{f(x)}{s} + \frac{u^\vartheta}{s^\vartheta} \mathbb{N}^+ \left[\mu D_x^{p\vartheta} C - D_x^{r\vartheta} C \right]. \quad (23)$$

Applying the inverse \mathbb{N} -transform on (23), we get

$$C(x, t) = f(x) + \mathbb{N}^{-1} \left[\frac{u^\vartheta}{s^\vartheta} \mathbb{N}^+ \left\{ \mu D_x^{p\vartheta} C - D_x^{r\vartheta} C \right\} \right]. \quad (24)$$

By using the homotopy perturbation method, we can write

$$C(x, t) = \sum_{n=0}^{\infty} p^n C_n(x, t). \quad (25)$$

Substituting (25) in (24),

$$\begin{aligned} \sum_{n=0}^{\infty} p^n C_n(x, t) &= f(x) \\ &+ p \left[\mathbb{N}^{-1} \left\{ \frac{u^\vartheta}{s^\vartheta} \mathbb{N}^+ \left(\sum_{n=0}^{\infty} \mu p^n D_x^{p\vartheta} C_n - \sum_{n=0}^{\infty} p^n D_x^{r\vartheta} C_n \right) \right\} \right]. \end{aligned} \quad (26)$$

Comparison of the coefficients of like powers of p on both sides yields to the corresponding assumptions:

$$p^0 : C_0(x, t) = f(x),$$

$$\begin{aligned} p^1 : C_1(x, t) &= \mathbb{N}^{-1} \left\{ \frac{u^\vartheta}{s^\vartheta} \mathbb{N}^+ \left(\mu D_x^{p\vartheta} C_0 - D_x^{r\vartheta} C_0 \right) \right\} \\ &= \mathbb{N}^{-1} \left\{ \frac{u^\vartheta}{s^\vartheta} \mathbb{N}^+ \left(\mu D_x^{p\vartheta} f(x) - D_x^{r\vartheta} f(x) \right) \right\} \\ &= \left(\mu D_x^{p\vartheta} f(x) - D_x^{r\vartheta} f(x) \right) \mathbb{N}^{-1} \left\{ \frac{u^\vartheta}{s^{\vartheta+1}} \right\} \\ &= \frac{t^\vartheta}{\Gamma(\vartheta+1)} \left(\mu D_x^{p\vartheta} - D_x^{r\vartheta} \right) f(x), \end{aligned}$$

$$\begin{aligned} p^2 : C_2(x, t) &= \mathbb{N}^{-1} \left\{ \frac{u^\vartheta}{s^\vartheta} \mathbb{N}^+ \left(\mu D_x^{p\vartheta} C_1 - D_x^{r\vartheta} C_1 \right) \right\} \\ &= \mathbb{N}^{-1} \left\{ \frac{u^\vartheta}{s^\vartheta} \mathbb{N}^+ \left(\mu D_x^{p\vartheta} \left(\mu D_x^{p\vartheta} f(x) - D_x^{r\vartheta} f(x) \right) \frac{t^\vartheta}{\Gamma(\vartheta+1)} \right. \right. \\ &\quad \left. \left. - D_x^{r\vartheta} \left(\mu D_x^{p\vartheta} f(x) - D_x^{r\vartheta} f(x) \right) \frac{t^\vartheta}{\Gamma(\vartheta+1)} \right) \right\} \\ &= \left(\mu^2 D_x^{2p\vartheta} f(x) - 2\mu D_x^{(p+r)\vartheta} f(x) + D_x^{2r\vartheta} f(x) \right) \\ &\quad \times \mathbb{N}^{-1} \left\{ \frac{u^\vartheta}{s^\vartheta} \mathbb{N}^+ \left(\frac{t^\vartheta}{\Gamma(\vartheta+1)} \right) \right\} \\ &= \left(\mu^2 D_x^{2p\vartheta} f(x) - 2\mu D_x^{(p+r)\vartheta} f(x) + D_x^{2r\vartheta} f(x) \right) \mathbb{N}^{-1} \left\{ \frac{u^{2\vartheta}}{s^{2\vartheta+1}} \right\} \\ &= \frac{t^{2\vartheta}}{\Gamma(2\vartheta+1)} \left(\mu D_x^{p\vartheta} - D_x^{r\vartheta} \right)^2 f(x). \end{aligned} \quad (27)$$

Similarly,

$$p^3 : C_3(x, t) = \frac{t^{3\vartheta}}{\Gamma(3\vartheta+1)} \left(\mu D_x^{p\vartheta} - D_x^{r\vartheta} \right)^3 f(x), \quad (28)$$

and so on.

The analytic series solution of (20) can be given as

$$C(x, t) = \lim_{N \rightarrow \infty} \sum_{n=0}^N C_n(x, t),$$

$$\begin{aligned} C(x, t) &= C_0(x, t) + C_1(x, t) + C_2(x, t) + C_3(x, t) + \cdots \\ &= f(x) + \frac{t^\alpha}{\Gamma(\vartheta+1)} \left(\mu D_x^{p\vartheta} - D_x^{r\vartheta} \right) f(x) + \frac{t^{2\alpha}}{\Gamma(2\vartheta+1)} \\ &\quad \cdot \left(\mu D_x^{p\vartheta} - D_x^{r\vartheta} \right)^2 f(x) + \frac{t^{3\alpha}}{\Gamma(3\vartheta+1)} \left(\mu D_x^{p\vartheta} - D_x^{r\vartheta} \right)^3 f(x) \cdots \\ &= \left\{ 1 + \frac{t^\alpha}{\Gamma(\vartheta+1)} \left(\mu D_x^{p\vartheta} - D_x^{r\vartheta} \right) + \frac{t^{2\alpha}}{\Gamma(2\vartheta+1)} \left(\mu D_x^{p\vartheta} - D_x^{r\vartheta} \right)^2 \right. \\ &\quad \left. + \frac{t^{3\alpha}}{\Gamma(3\vartheta+1)} \left(\mu D_x^{p\vartheta} - D_x^{r\vartheta} \right)^3 + \cdots \right\} f(x) \\ &= \sum_{n=0}^{\infty} \left\{ \frac{t^{n\alpha}}{\Gamma(n\vartheta+1)} \left(\mu D_x^{p\vartheta} - D_x^{r\vartheta} \right)^n \right\} f(x), \end{aligned} \quad (29)$$

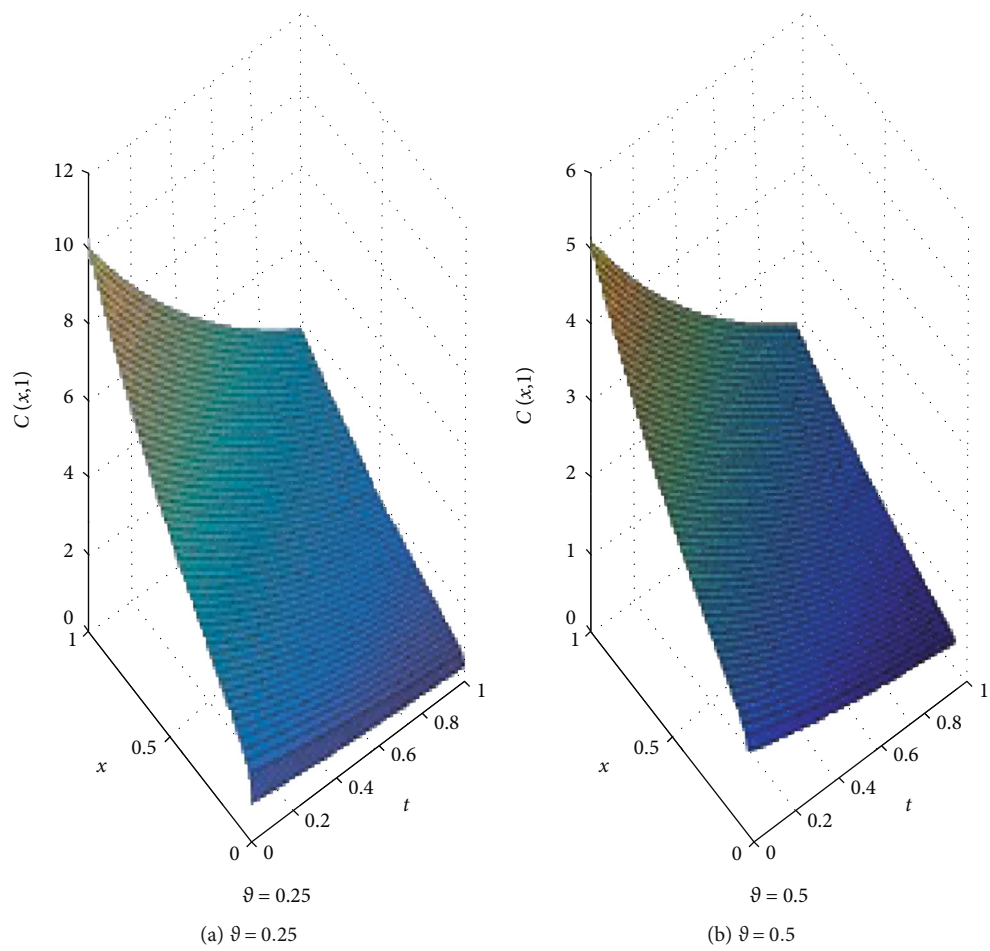


FIGURE 1: Continued.

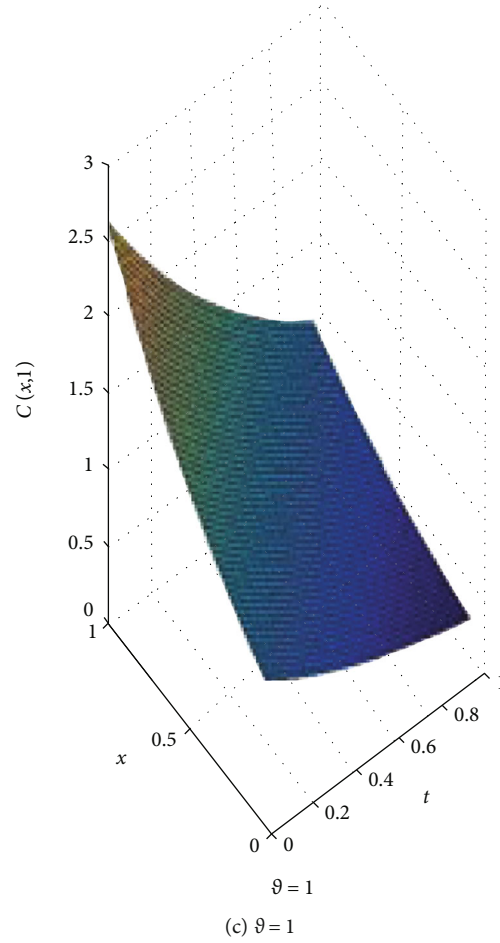


FIGURE 1: Variation of the concentration $C(x, t)$ with the fractional parameter α for $\mu = .01$.

which can also be written as

$$C(x, t) = \left[E_{\vartheta} \left\{ t^{\vartheta} \left(\mu D_x^{2\vartheta} - D_x^{\vartheta} \right) \right\} \right] f(x). \quad (30)$$

where $E_{\alpha}(x)$ is the one-parameter Mittag-Leffler function.

Remark 7. Setting $p = 2, r = 1$, (20) reduces to space-time fractional ADE of the form

$$D_t^{\vartheta} C = \mu D_x^{2\vartheta} C - D_x^{\vartheta} C, \quad (31)$$

and the solution is

$$C(x, t) = \left[E_{\vartheta} \left\{ t^{\vartheta} \left(\mu D_x^{2\vartheta} - D_x^{\vartheta} \right) \right\} \right] f(x), \quad (32)$$

if $f(x) = e^{-x}$, the solution is

$$C(x, t) = \left[E_{\vartheta} \left\{ t^{\vartheta} \left(\mu D_x^{2\vartheta} - D_x^{\vartheta} \right) \right\} \right] e^{-x} = \sum_{n=0}^{\infty} \frac{t^{n\vartheta}}{\Gamma(n\vartheta + 1)} \cdot \sum_{k=0}^n (-1)^k n_{c_k} \mu^{n-k} \sum_{s=\lfloor (2n-k)\vartheta \rfloor}^{\infty} \frac{(-1)^s x^{s-(2n-k)\vartheta}}{\Gamma(s - (2n-k)\vartheta + 1)}, \quad (33)$$

where $\lfloor \cdot \rfloor$ denotes the ceiling function.

This is the same as obtained by Hikal and Abu Ibrahim [12] using ADM.

6. Examples

Example 1. Consider the time-fractional ADE (setting $p = 2, r = 1, m = 1$ in (20)),

$$D_t^{\alpha} C = \mu D_x^2 C - D_x C, \quad (34)$$

the initial condition being

$$C(x, 0) = e^{-x}. \quad (35)$$

Solution: by applying the NHPM,

$$\begin{aligned} p^0 : C_0(x, t) &= e^{-x}, \\ p^1 : C_1(x, t) &= \mathbb{N}^{-1} \left\{ \frac{u^{\vartheta}}{s^{\vartheta}} \mathbb{N}^+ (\mu C_{0xx} - C_{0x}) \right\} = \frac{(\mu + 1)t^{\vartheta}}{\Gamma(\vartheta + 1)} e^{-x}, \\ p^2 : C_2(x, t) &= \mathbb{N}^{-1} \left\{ \frac{u^{\vartheta}}{s^{\vartheta}} \mathbb{N}^+ (\mu C_{1xx} - C_{1x}) \right\} = \frac{(\mu + 1)^2 t^{2\vartheta}}{\Gamma(2\vartheta + 1)} e^{-x}. \end{aligned} \quad (36)$$

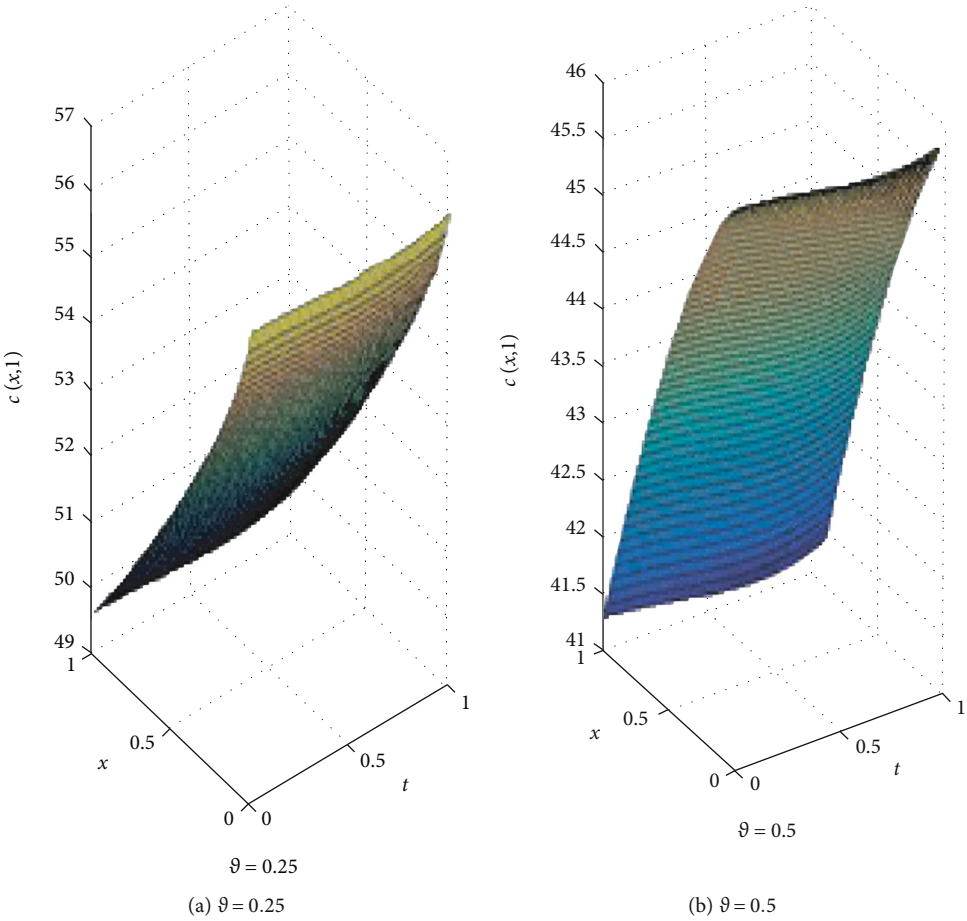


FIGURE 2: Continued.

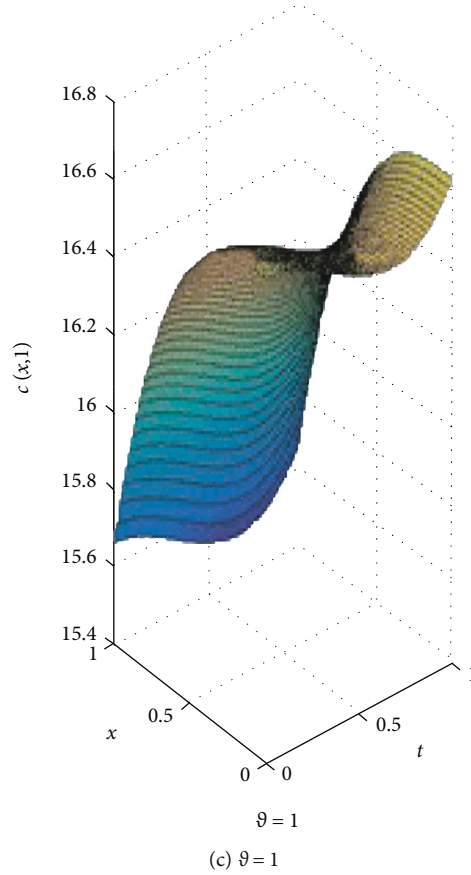


FIGURE 2: Variation of the concentration $C(x, t)$ with the fractional parameter α for $\mu = .01$.

Similarly,

$$p^3 : C_3(x, t) = \frac{(\mu + 1)^3 t^{3\vartheta}}{\Gamma(3\vartheta + 1)} e^{-x}, \quad (37)$$

and so on. Thus, the analytic series solution is given by

$$\begin{aligned} C(x, t) &= C_0(x, t) + C_1(x, t) + C_2(x, t) + C_3(x, t) + \dots \\ &= e^{-x} \left\{ 1 + \frac{(\mu + 1)t^\vartheta}{\Gamma(\vartheta + 1)} + \frac{(\mu + 1)^2 t^{2\vartheta}}{\Gamma(2\vartheta + 1)} + \frac{(\mu + 1)^3 t^{3\vartheta}}{\Gamma(3\vartheta + 1)} + \dots \right\} \\ &= e^{-x} E_\alpha((1 + \mu)t^\vartheta). \end{aligned} \quad (38)$$

The solution converges to the exact solution of the ADE for $\alpha = 1$ as obtained by El-Sayed et al. [10]:

$$C(x, t) = e^{(1+\mu)t-x}. \quad (39)$$

The result obtained for Example 1 is presented in Figure 1.

Example 2. Equation (34) with the initial condition $C(x, 0) = x^3 - x^2$.

Solution: by applying the NHPM, we obtain

$$\begin{aligned} p^0 : C_0(x, t) &= x^3 - x^2, \\ p^1 : C_1(x, t) &= \{-3x^2 + 2x(1 + 3\mu) - 2\mu\} \frac{t^\vartheta}{\Gamma(\vartheta + 1)}, \\ p^2 : C_2(x, t) &= (6x - 2 - 12\mu) \frac{t^{2\vartheta}}{\Gamma(2\vartheta + 1)}, \\ p^3 : C_3(x, t) &= -6 \frac{t^{3\vartheta}}{\Gamma(3\vartheta + 1)}, \\ p^4 : C_4(x, t) &= 0. \end{aligned} \quad (40)$$

Thus, the analytic series solution is given by

$$\begin{aligned} C(x, t) &= C_0(x, t) + C_1(x, t) + C_2(x, t) + C_3(x, t) + \dots C(x, t) \\ &= (x^3 - x^2) + \{-3x^2 + 2x(1 + 3\mu) - 2\mu\} \frac{t^\vartheta}{\Gamma(\vartheta + 1)} \\ &\quad + (6x - 2 - 12\mu) \frac{t^{2\vartheta}}{\Gamma(2\vartheta + 1)} - 6 \frac{t^{3\vartheta}}{\Gamma(3\vartheta + 1)}. \end{aligned} \quad (41)$$

The result obtained for Example 2 is presented in Figure 2.

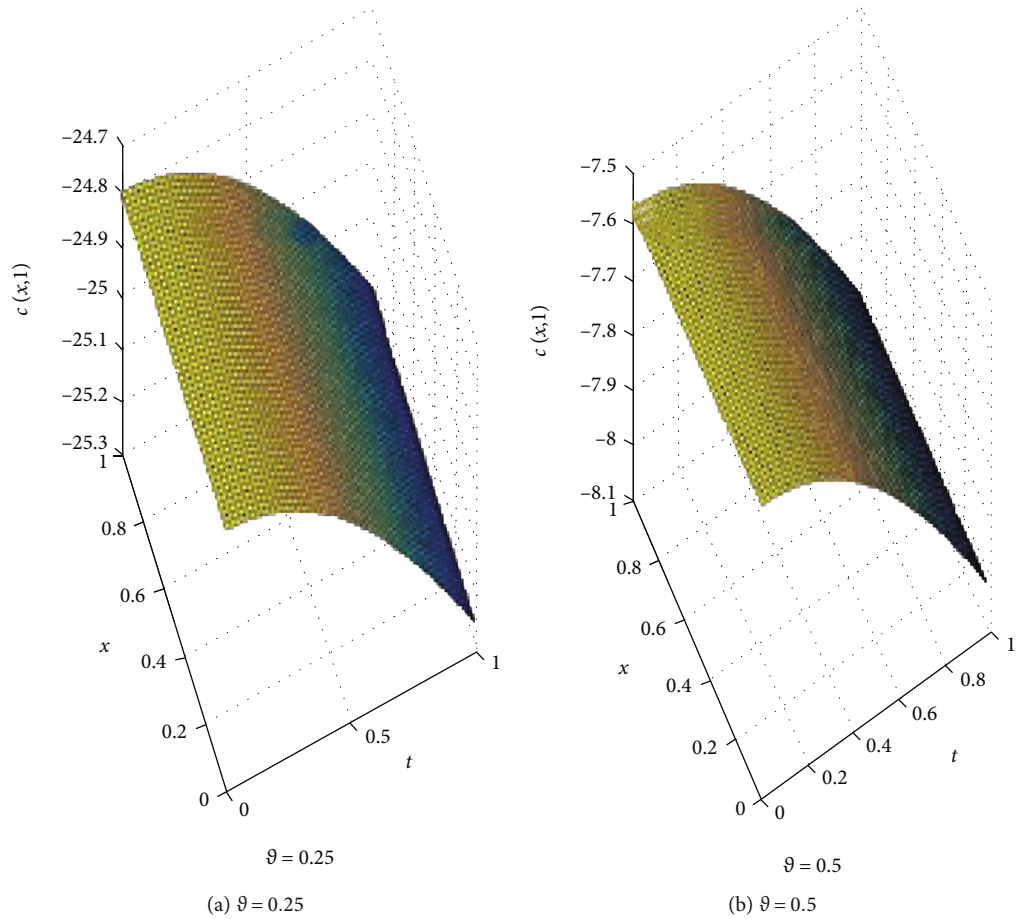


FIGURE 3: Continued.

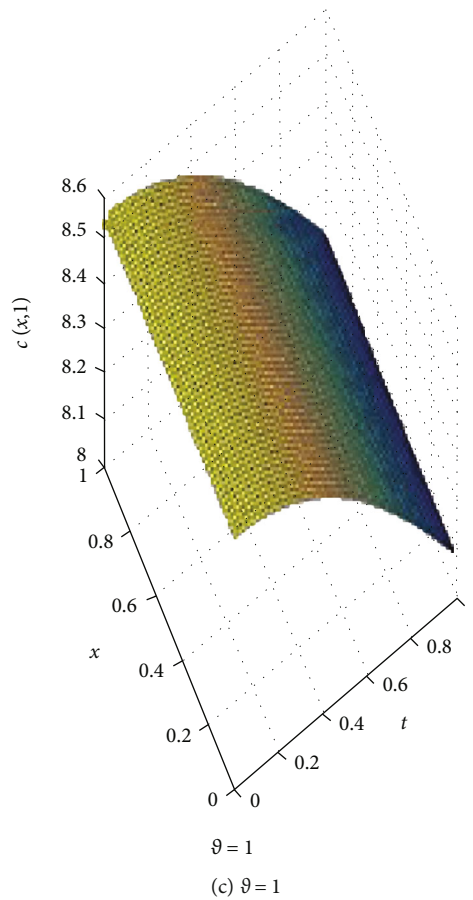


FIGURE 3: Variation of the concentration $C(x, t)$ with the fractional parameter α for $\mu = .01$.

Example 3. Equation (34) with the initial condition $C(x, 0) = \cos x$.

Solution: by applying the NHPM, we get

$$\begin{aligned}
 p^0 : C_0(x, t) &= \cos x, \\
 p^1 : C_1(x, t) &= (\sin x - \mu \cos x) \frac{t^\vartheta}{\Gamma(\vartheta + 1)}, \\
 p^2 : C_2(x, t) &= (-\cos x - 2\mu \sin x + \mu^2 \cos x) \frac{t^{2\vartheta}}{\Gamma(2\vartheta + 1)}, \\
 p^3 : C_3(x, t) &= (-\sin x + 3\mu \cos x + 3\mu^2 \sin x - \mu^3 \cos x) \frac{t^{3\vartheta}}{\Gamma(3\vartheta + 1)},
 \end{aligned} \tag{42}$$

and so on. Thus, the analytic series solution is given by

$$\begin{aligned}
 C(x, t) &= C_0(x, t) + C_1(x, t) + C_2(x, t) + C_3(x, t) + \dots C(x, t) \\
 &= \cos x + (\sin x - \mu \cos x) \frac{t^\vartheta}{\Gamma(\vartheta + 1)} \\
 &\quad + (-\cos x - 2\mu \sin x + \mu^2 \cos x) \frac{t^{2\vartheta}}{\Gamma(2\vartheta + 1)} \\
 &\quad + (-\sin x + 3\mu \cos x + 3\mu^2 \sin x - \mu^3 \cos x) \frac{t^{3\vartheta}}{\Gamma(3\vartheta + 1)} + \dots
 \end{aligned} \tag{43}$$

The result obtained for Example 3 is presented in Figure 3.

Remark 8. The convergence of the series solutions obtained for the above cases can be proved by means of a comparison test using the Mittag-Leffler function.

7. Conclusion

In the present article, the NHPM is successfully applied to find the solution for the general form of the space-time fractional ADE and the analytic solution is found in terms of M-L function for different cases. The results found show the dependence of solute concentration on the fractional order of the derivative along with the space and time variables. Solutions obtained for the three examples are plotted with spatial and time coordinate for different values of the fractional parameter α using MATLAB R2015a. Figure 1 exhibits a decrease in solute concentration corresponding to the increment in the fractional parameter α . For the second case, the solution is in exact form and is plotted in Figure 2 showing that as the fractional parameter α increases, the solute concentration decreases, whereas it increases with the corresponding increment in α for the third cases as is shown in Figure 3. Hence, the NHPM is a powerful technique to solve various models in the form of linear or nonlinear partial differential equations appearing in the field of science and

engineering. The approach should be expanded to solve the two or three dimensions of space-time fractional ADM.

Nomenclature

$C(\xi, \tau)$: Solute concentration (mol/kgw)
 $D > 0$: Constant diffusivity (m^2/sec)
 V : Drift velocity (m/sec)
 ξ : Spatial coordinate (m)
 τ : Time (sec).

Data Availability

No data were used to support this study.

Conflicts of Interest

There is no conflict of interest regarding the publication of this article.

References

- [1] I. Podlubny, *Fractional Differential Equations*, Academic Press, San Diego, 1999.
- [2] K. B. Oldham and J. Spanier, *The Fractional Calculus*, Academic Press, New York, 1974.
- [3] K. S. Miller and B. Ross, *An Introduction to the Fractional Calculus and Fractional Differential Equations*, John Wiley & Sons, New York, 1993.
- [4] L. Mistry, A. M. Khan, D. L. Suthar, and D. Kumar, "A new numerical method to solve non-linear fractional differential equations," *International Journal of Innovative Technology and Exploring Engineering*, vol. 8, no. 12, pp. 1–6, 2019.
- [5] P. Ramani, A. M. Khan, and D. L. Suthar, "Generalized differential transform method and its application to solve nonlinear partial differential equations with space and time fractional derivatives," *International Journal of Scientific Research and Review*, vol. 7, no. 2, pp. 1–9, 2019.
- [6] B. Baeumer, D. A. Benson, and M. M. Meerschaert, "Advection and dispersion in time and space," *Physica A*, vol. 350, no. 2–4, pp. 245–262, 2005.
- [7] S. Momani and Z. Odibat, "Numerical solutions of the space-time fractional advection-dispersion equation," *Numerical Methods for Partial Differential Equations*, vol. 25, no. 5, pp. 1238–1259, 2008.
- [8] D. K. Jaiswal, A. Kumar, and R. R. Yadav, "Analytical solution to the one-dimensional advection-diffusion equation with temporally dependent coefficients," *Journal of Water Resource and Protection*, vol. 3, no. 1, pp. 76–84, 2011.
- [9] Q. Huang, G. Huang, and H. Zhan, "A finite element solution for the fractional advection-dispersion equation," *Advances in Water Resources*, vol. 31, no. 12, pp. 1578–1589, 2008.
- [10] A. M. A. El-Sayed, S. H. Behiry, and W. E. Raslan, "Adomian's decomposition method for solving an intermediate fractional advection-dispersion equation," *Computer and Mathematics with Applications*, vol. 59, no. 5, pp. 1759–1765, 2010.
- [11] A. Yildirim and H. Kocak, "Homotopy perturbation method for solving the space-time fractional advection-dispersion equation," *Advances in Water Resources*, vol. 32, no. 12, pp. 1711–1716, 2009.
- [12] M. M. Hikal and M. A. Abu Ibrahim, "On Adomian's decomposition method for solving a fractional advection-dispersion equation," *International Journal of Pure and Applied mathematics*, vol. 104, no. 1, pp. 43–56, 2015.
- [13] M. Alliche and S. Chikh, "Study of non-premixed turbulent flame of hydrogen/air downstream co-current injector," *International Journal of Hydrogen Energy*, vol. 43, no. 6, pp. 3577–3585, 2018.
- [14] F. Liu, P. Zhuang, and K. Burrage, "Numerical methods and analysis for a class of fractional advection-dispersion models," *Computers & Mathematics with Applications*, vol. 64, no. 10, pp. 2990–3007, 2012.
- [15] M. C. Rocca, A. R. Plastino, A. Plastino, and A. L. De Paoli, "General solution of a fractional diffusion-advection equation for solar cosmic-ray transport," *Physica A*, vol. 447, pp. 402–410, 2016.
- [16] P. Ramani, A. M. Khan, and D. L. Suthar, "Revisiting analytical-approximate solution of time fractional Rosenau-Hyman equation via fractional reduced differential transform method," *International Journal on Emerging Technologies*, vol. 10, no. 2, pp. 403–409, 2019.
- [17] M. Garg and P. Manohar, "Analytical solution of space-time fractional Fokker Planck equations by generalized differential transform method," *Le Matematiche*, vol. 66, no. 2, pp. 91–101, 2011.
- [18] H. Habenom, D. L. Suthar, and M. Aychluh, "Solution of fractional Fokker Planck equation using fractional power series method," *Journal of Science and Arts*, vol. 48, no. 3, pp. 593–600, 2019.
- [19] Z. H. Khan and W. A. Khan, "N-transform properties and applications," *NUST journal of engineering sciences*, vol. 1, no. 1, pp. 127–133, 2008.
- [20] F. B. M. Belgacem and R. Silambarasan, "Maxwell's equations solutions through the natural transform," *Mathematics in Engineering, Science and Aerospace*, vol. 3, no. 3, pp. 313–323, 2012.
- [21] F. B. M. Belgacem and R. Silambarasan, "Theory of natural transform," *Mathematical Engineering, Science and Aerospace*, vol. 3, no. 1, pp. 100–124, 2012.
- [22] F. B. M. Belgacem and R. Silambarasan, "Advances in the natural transform," in *AIP Conference Proceedings; 1493 January 2012*, pp. 106–110, USA, 2012.
- [23] M. G. M. Hussain and F. B. M. Belgacem, "Transient solutions of Maxwell's equations based on Sumudu transform," *Progress in Electromagnetic Research*, vol. 74, pp. 273–289, 2007.
- [24] H. Ji-Huan, "Homotopy perturbation technique," *Computer Methods in Applied Mechanics and Engineering*, vol. 178, pp. 257–262, 1999.
- [25] H. Ji-Huan, "The homotopy perturbation method for nonlinear oscillators with discontinuities," *Applied Mathematical Computation*, vol. 151, pp. 287–292, 2004.
- [26] H. Ji-Huan, "Recent development of the homotopy perturbation method," *Topological Methods in Nonlinear Analysis*, vol. 31, pp. 205–209, 2008.
- [27] S. J. Liao, "On the homotopy analysis method for nonlinear problems," *Applied Mathematics and Computation*, vol. 147, pp. 499–513, 2007.

Research Article

MHD Williamson Nanofluid Flow over a Stretching Sheet through a Porous Medium under Effects of Joule Heating, Nonlinear Thermal Radiation, Heat Generation/Absorption, and Chemical Reaction

J. Bouslimi ¹, M. Omri,² R. A. Mohamed,³ K. H. Mahmoud,⁴ S. M. Abo-Dahab ^{3,5}
and M. S. Soliman³

¹Department of Physics, College of Science, Taif University, P. O. Box 11099, Taif 21944, Saudi Arabia

²Deanship of Scientific Research, King Abdulaziz University, Jeddah, Saudi Arabia

³Mathematics Department, Faculty of Science, South Valley University, Qena 83523, Egypt

⁴Department of Physics, College of Khurma University College, Taif University, P.O. Box 11099, Taif 21944, Saudi Arabia

⁵Computer Science Department, Faculty of Computers and Information, Luxor University, Luxor, Egypt

Correspondence should be addressed to J. Bouslimi; jamelabouiyes4@gmail.com

Received 1 April 2021; Accepted 25 May 2021; Published 21 July 2021

Academic Editor: Mustafa Inc

Copyright © 2021 J. Bouslimi et al. This is an open access article distributed under the Creative Commons Attribution License, which permits unrestricted use, distribution, and reproduction in any medium, provided the original work is properly cited.

In this article, the effect of electromagnetic force with the effect of thermal radiation on the Williamson nanofluid on a stretching surface through a porous medium was studied considering the effect of both heat generation/absorption and Joule heating. On the other hand, the effect of Brownian motion and thermophoresis coefficients was considered. The system of nonlinear partial differential equations governing the study of fluid flow has transformed into a system of ordinary differential equations using similarity transformations and nondimensional variables which were subsequently solved numerically by using the Runge-Kutta fourth-order method with shooting technique. Moreover, the effect of the resulting physical parameters on the distributions of velocity, temperature, and concentration of nanoparticles has been studied by using graphical forms with an interest in providing physical meanings to each parameter. Finally, special diagrams were made to explain the study of the effect of some physical parameters on the skin friction coefficient and the local Nusselt number; these results led to reinforcement in the values of the skin friction coefficient for the increased values of the magnetic field and the Darcy number while the effect on the local Nusselt number by thermal radiation as well as the heat generation/absorption coefficients became negative.

1. Introduction

In recent years, the study of non-Newtonian fluids has received the attention of researchers in the field of hydrodynamics around the world due to the enormous scientific developments in their applications. The Williamson fluid is one of the most important non-Newtonian fluids characterized by less viscosity with an increase in the rate of shear stress and very similar in its properties of polymeric solutions, for example. In another meaning, in the Williamson fluid model, the effective viscosity should lessen indefinitely

with the rising shear rate, which is nothing but infinite viscosity at stationary and nil viscosity as the shear rate tends to infinity. A model of Williamson has been discovered by Williamson [1] in 1929, while Subbarayudu et al. [2] investigated the assessment of time-dependent flow of Williamson fluid with radiative blood flow against a wedge. On the other hand, Lyubimova et al. [3] analyzed the stability of quasiequilibrium states and supercritical regimes of thermal vibrational convection of Williamson fluid in zero gravity conditions, but multiple solutions for MHD transient flow of Williamson nanofluids with convective heat transport

were studied by Hashim et al. [4]. Hamid et al. [5] discussed an investigation of thermal and solutal stratification effects on mixed convection flow and heat transfer of Williamson nanofluid.

Nanofluids are a modern class of fluids discovered by Choi [6]. Researchers in the field of studying fluids around the world have paid attention to this type of fluids, which plays an important role in many modern technological applications that serve life. On the other hand, nanofluids enter many industries, for example, the satellite industry. Nanofluids also have an important role in the medical fields, for example, also in the use of nanoparticles of gold in the treatment of cancerous tumors, as well as the manufacture of microscopic bombs that are used to eliminate cancerous tumors as well. Sajadifar et al. [7] examined fluid flow and heat transfer of non-Newtonian nanofluid in a microtube considering slip velocity and temperature jump boundary conditions, while Khan and Pop [8] investigated boundary-layer flow of a nanofluid past a stretching sheet, and at the same time, Farooq et al. [9] analyzed MHD stagnation point flow of viscoelastic nanofluid with nonlinear radiation effects. Very recently, Ahmed et al. [10] explained magnetohydrodynamic Maxwell nanofluid flow over a stretching surface through a porous medium: effects of nonlinear thermal radiation, convective boundary conditions, and heat generation/absorption. Alshomrani [11] studied generalized Fourier's and Fick's laws in bioconvection flow of magnetized Burgers nanofluid utilizing motile microorganisms. Alshomrani [12] investigated numerical investigation for bioconvection flow of viscoelastic nanofluid with magnetic dipole and motile microorganisms. Loganathan and Rajan [13] excogitated an entropy approach of Williamson nanofluid flow with Joule heating and zero nanoparticle mass flux. It was found from this study that the velocity distribution decreases with increasing the values of the magnetic field parameter while the temperature distribution increases with increasing the values of this parameter. Khan et al. [14] illustrated evaluating the characteristics of the magnetic dipole for shear-thinning Williamson nanofluid with thermal radiation. Khan et al. [15] represented changes in viscosity of Williamson nanofluid flow due to thermal and solutal stratification. Hayat et al. [16] explained mixed convective three-dimensional flow of Williamson nanofluid subject to chemical reaction. Ramzan et al. [17] analyzed Darcy-Forchheimer 3D Williamson nanofluid flow with generalized Fourier and Fick's laws in a stratified medium. It was observed from this study that the velocity distribution was decreased by the influence of the magnetic field parameter and also by the influence of the Williamson fluid parameter.

Electromagnetic fluid dynamics (magnetohydrodynamic fluid) is the study of fluids that have the characteristic of electromagnetic conductivity such as plasma fluids, metal fluids, and salt water, and the first to start studying this field is Alfven [18] in 1942. Mohamed et al. [19] studied MHD Jeffrey nanofluid flow over a stretching sheet through a porous medium in the presence of nonlinear thermal radiation and heat generation/absorption. Also, Chandrashekar et al. [20] examined a discontinuous Galerkin method for a two-dimensional reduced resistive MHD model. A numerical

study of MHD mixed convection under volumetric heat source in a vertical square duct with wall effects investigated by Liu et al. [21]. Tassone et al. [22] excogitated MHD mixed convection flow in the WCCL: heat transfer analysis and cooling system optimization. Motsa et al. [23] illuminated the spectral relaxation method and spectral quasilinearization. Khan et al. [24] studied peristaltic transport of a Jeffrey fluid with variable viscosity through a porous medium in an asymmetric channel. Ellahi [25] elucidated a study on the convergence of series solutions of non-Newtonian third-grade fluid with variable viscosity by means of the homotopy analysis method. Umar et al. [26] investigated numerical treatment for the three-dimensional Eyring-Powell fluid flow over a stretching sheet with velocity slip and activation energy. Ramesh et al. [27] explained heat transfer in MHD dusty boundary layer flow over an inclined stretching sheet with nonuniform heat source/sink.

Joule heating (also referred to as resistive or ohmic heating) describes the process where the energy of an electric current is converted into heat as it flows through a resistance. The explanation for this is that when electrical current flows through solid or liquid materials that conduct electricity, electrical energy is converted into heat energy through the occurrence of resistances inside the conductor. In this case, free electrons transfer energy by collisions. Ramzan et al. [28] studied radiative and Joule heating effects in the MHD flow of a micropolar fluid with partial slip and convective boundary condition. Mohamed et al. [29] discussed the thermal radiation and MHD effects on free convective flow of a polar fluid through a porous medium in the presence of internal heat generation and chemical reaction. Also, Tetbirt et al. [30] discussed a numerical study of magnetic effect on the velocity distribution field in a macro-/microscale of a micropolar and viscous fluid in a vertical channel. At some time, Ghadikolaei et al. [31] investigated numerical study on magnetohydrodynamic CNT-water nanofluids as a micropolar dusty fluid influenced by nonlinear thermal radiation and joule heating effect. It is worth noting that Gireesha et al. [32] investigated hall effects on dusty nanofluid two-phase transient flow past a stretching sheet using the KVL model. It was also reported that Aghanajafi et al. [33] explained numerical simulation of laminar forced convection of water-CuO nanofluid inside a triangular duct. But Hussain et al. [34] examined the effects of viscous dissipation and Joule heating on MHD Sisko nanofluid over a stretching cylinder. Moreover, free convective heat and mass transfer of MHD non-Newtonian nanofluids over a cone in the presence of a nonuniform heat source/sink was studied by Raju et al. [35]. Hayat et al. [36] excogitated radiative flow of Jeffrey fluid in a porous medium with power law heat flux and heat source. Meanwhile, Hartnett and Kostic [37] analyzed heat transfer to Newtonian and non-Newtonian fluids in rectangular ducts.

The main objective of the present work is to study the flow of a non-Newtonian Williamson fluid that contains nanoparticles on a stretching sheet through a porous medium under the influences of the magnetic field, nonlinear thermal radiation, and Joule heating in the presence of heat generation/absorption and chemical reaction on the distributions of

velocity, temperature, and concentration of nanoparticles taking into account studying effects of the Brownian motion coefficient and thermophoresis coefficient. On the other hand, the similarity transformations and nondimensional variables were used in converting the system of partial differential equations governing the movement of flow into a system of ordinary differential equations, which were solved by using the Runge-Kutta numerical method with a shooting technique. The graphs were used to study the effects of all physical parameters on the distributions of velocity, temperature, and concentration of nanoparticles.

2. Formulation of the Problem

In the beginning, the study of Williamson nanofluid flow can be shown in several steps: the first step is the fluid flow being steady and incompressible, the second step is that the flowing process is two-dimensional flow on a stretching surface through a porous medium, and the third step is the plate is stretched along the x -axis with a velocity $U_w(x) = Bx$, where B is the stretching rate. The basic equations for the balance of mass, momentum, energy, and nanoparticle volume fraction of the flow problem can be expressed in vector form as follows.

2.1. Continuity Equation. The continuity equation for conservation of mass becomes

$$\nabla \cdot \vec{q} = 0, \quad (1)$$

where ∇ is the differential operator and \vec{q} is the flow velocity vector.

2.2. Conservation of Momentum Equation. The Navier-Stokes equation for the balance of linear momentum is given by

$$\rho_f \left[\frac{\partial \vec{q}}{\partial t} + (\vec{q} \cdot \nabla) \vec{q} \right] = \nabla \cdot \bar{S} + \vec{F}_e - \frac{\mu}{K} \vec{q}, \quad (2)$$

where ρ_f is the density of the nanofluid, t is the time, \bar{S} is the Cauchy stress tensor, μ is the coefficient of dynamic viscosity, $\vec{F}_e = \vec{J} \times \vec{B}$ is the Lorentz force produced by the interaction of the applied magnetic field with velocity of fluid, $\vec{J} = \sigma(\vec{E} + \vec{q} \times \vec{B})$ is the current density, \vec{B} is the external magnetic field, σ is the electrical conductivity, and K is the permeability of the porous medium.

2.3. Conservation of Energy Equation. In the absence of viscous dissipation effects, the conservation of energy for heat transfer is given by the constitutive equation as

$$\begin{aligned} & (\rho c_p)_f \left[\frac{\partial T}{\partial t} + (\vec{q} \cdot \nabla) T \right] \\ &= \nabla \cdot (k \nabla T) + (\rho c_p)_p \left[D_B \nabla C \cdot \nabla T + \frac{D_T}{T_\infty} (\nabla T \cdot \nabla T) \right] \\ & \quad - \nabla q_r + J_h + Q(T - T_\infty), \end{aligned} \quad (3)$$

where c_p is the specific heat at constant pressure; $(\rho c_p)_f$ and $(\rho c_p)_p$ are the specific heat of the nanofluid and the nanoparticles, respectively; T is the temperature of the nanofluid; k is the thermal conductivity; D_B is the Brownian diffusion coefficient; D_T is the thermophoresis diffusion coefficient; T_∞ is the ambient temperature; q_r is the radiative heat flux; $J_h = \vec{F}_e \cdot \vec{q}$ is the Joule heating, and Q is the uniform volumetric heat generation/absorption.

2.4. Conservation of Nanoparticle Concentration Equation. For a homogeneous chemical reaction [38], the concentration equation of nanoparticle volume fraction becomes

$$\frac{\partial C}{\partial t} + (\vec{q} \cdot \nabla) C = D_B \nabla^2 C + \frac{D_T}{T_\infty} \nabla^2 T - R^*(C - C_\infty), \quad (4)$$

where C is the nanoparticle volume fraction and the rates $R^* > 0$ and $R^* < 0$ denote destructive and constructive reaction rates, respectively.

For the Williamson fluid model, Cauchy stress tensor \bar{S} is defined as [26]

$$\bar{S} = -P\bar{I} + \bar{\tau}, \quad (5)$$

$$\bar{\tau} = \left(\mu_\infty + \frac{\mu_0 - \mu_\infty}{1 - \Gamma \dot{\gamma}} \right) \bar{A}_1, \quad (6)$$

where P is pressure, \bar{I} is the unit tensor, $\bar{\tau}$ is the extra stress tensor, μ_0 is limiting viscosity at zero shear rate, μ_∞ is limiting viscosity at the infinite shear rate, $\Gamma > 0$ is a time constant, \bar{A}_1 is the first Rivlin-Erickson tensor, and $\dot{\gamma}$ is defined as follows:

$$\dot{\gamma} = \left(\frac{\pi}{2} \right)^{1/2}, \quad \pi = \text{trace}(\bar{A}_1)^2. \quad (7)$$

Here, it is considered the case for $\mu_\infty = 0$ and $\Gamma \dot{\gamma} < 1$; thus, Equation (6) can be written as follows:

$$\bar{\tau} = \left[\frac{\mu_0}{1 - \Gamma \dot{\gamma}} \right] \bar{A}_1 = \mu_0 (1 + \Gamma \dot{\gamma}) \bar{A}_1. \quad (8)$$

The right-hand side of Equation (8) is done by using binomial expansion. Making use of Equations (5) and (8) into Equations (1) to (4), the two-dimensional boundary layer equations governing the flow can be written as follows [39]:

$$\frac{\partial u}{\partial x} + \frac{\partial u}{\partial y} = 0, \quad (9)$$

$$u \frac{\partial u}{\partial x} + v \frac{\partial u}{\partial y} = v \frac{\partial^2 u}{\partial y^2} + \sqrt{2} \nu \Gamma \frac{\partial u}{\partial y} \frac{\partial^2 u}{\partial y^2} - \frac{\sigma B_0^2}{\rho} u - \frac{\nu}{K} u, \quad (10)$$

$$u \frac{\partial T}{\partial x} + v \frac{\partial T}{\partial y} = \alpha \frac{\partial^2 T}{\partial y^2} - \frac{1}{(\rho c_p)_f} \frac{\partial q_r}{\partial y} + \frac{(\rho c_p)_p}{(\rho c_p)_f} \cdot \left[D_B \left(\frac{\partial C}{\partial y} \frac{\partial T}{\partial y} \right) + \left(\frac{D_T}{T_\infty} \right) \left(\frac{\partial T}{\partial y} \right)^2 \right] + \frac{\sigma B_0^2}{(\rho c_p)_f} u^2 + \frac{Q}{(\rho c_p)_f} (T - T_\infty), \quad (11)$$

$$u \frac{\partial C}{\partial x} + v \frac{\partial C}{\partial y} = D_B \frac{\partial^2 C}{\partial y^2} + \frac{D_T}{T_\infty} \frac{\partial^2 T}{\partial y^2} - R^* (C - C_\infty), \quad (12)$$

where u is the velocity components in the direction of the x -axis and v is the velocity components in the direction of the y -axis; in addition, α represent the thermal diffusivity, ρ refer to density of the fluid, and ν is the kinematic viscosity of fluid; also, T and T_∞ , respectively, are fluid temperature and ambient fluid temperature. A uniform magnetic field of strength B_0 is applied in the transverse direction of the flow; due to the small magnetic Reynolds number, it is not necessary to introduce the effect of the induced magnetic field. It should be noted that D_B , D_T , σ , c_p , and R^* are, respectively, the Brownian diffusion coefficient, the thermophoresis diffusion coefficient, the electrical conductivity, the specific heat at constant pressure, and destructive and constructive reaction rates. Here, C and C_∞ are the concentration of nanoparticles and ambient nanoparticle concentration. It is worth noting that the effect of nonlinear thermal radiation, heat source/sink, and Joule heating is taken in the energy equation. The viscous dissipation is assumed to be negligibly small in the energy equation. The effects of the homogenous chemical reaction are taken in the concentration equation.

The boundary conditions for the present investigation problem can be written in the formula:

$$u = U_w(x), v = 0, T = T_w, D_B \frac{\partial C}{\partial y} + \frac{D_T}{T_\infty} \frac{\partial T}{\partial y} = 0, \quad \text{at } y = 0, \quad (13)$$

$$u \longrightarrow 0, v \longrightarrow 0, T \longrightarrow T_\infty, C \longrightarrow C_\infty, \quad \text{as } y \longrightarrow \infty, \quad (14)$$

where $U_w(x) = Bx$ represent the stretching surface velocity and $B > 0$ is the stretching rate, and the radiation heat flux q_r can be written as follows:

$$q_r = -\frac{4\sigma^*}{3k^*} \frac{\partial T^4}{\partial y} = -\frac{16\sigma^*}{3k^*} T^3 \frac{\partial T}{\partial y}, \quad (15)$$

$$\begin{aligned} \therefore \frac{1}{(\rho c_p)_f} \frac{\partial}{\partial y} (q_r) &= \frac{1}{(\rho c_p)_f} \frac{\partial}{\partial y} \left(-\frac{4\sigma^*}{3k^*} \frac{\partial T^4}{\partial y} \right) \\ &= -\frac{16\sigma^*}{3k^* (\rho c_p)_f} \frac{\partial}{\partial y} \left(T^3 \frac{\partial T}{\partial y} \right); \end{aligned} \quad (16)$$

when substituting by Equation (16) into Equation (11), the energy equation takes the following form:

$$\begin{aligned} u \frac{\partial T}{\partial x} + v \frac{\partial T}{\partial y} &= \alpha \frac{\partial^2 T}{\partial y^2} + \frac{16\sigma^*}{3k^* (\rho c_p)_f} \frac{\partial}{\partial y} \left(T^3 \frac{\partial T}{\partial y} \right) \\ &+ \frac{(\rho c_p)_p}{(\rho c_p)_f} \left[D_B \left(\frac{\partial C}{\partial y} \frac{\partial T}{\partial y} \right) + \left(\frac{D_T}{T_\infty} \right) \left(\frac{\partial T}{\partial y} \right)^2 \right] \\ &+ \frac{\sigma B_0^2}{(\rho c_p)_f} u^2 + \frac{Q}{(\rho c_p)_f} (T - T_\infty), \end{aligned} \quad (17)$$

where σ^* and k^* are the Stefan-Boltzmann constant and mean absorption coefficient; the similarity transformations and nondimensional variables can be written as follows:

$$\begin{aligned} \eta &= \sqrt{\frac{U_w(x)}{\nu x}} y, u = Bx f'(\eta), v = -\sqrt{B\nu} f(\eta), \theta(\eta) \\ &= \frac{T - T_\infty}{T_w - T_\infty}, \phi(\eta) = \frac{C - C_\infty}{C_\infty}, \end{aligned} \quad (18)$$

where η is the similarity variable and $f(\eta)$, $\theta(\eta)$, and $\phi(\eta)$, respectively, are the dimensionless stream function, temperature, and concentration of nanoparticles; the similarity transformations and the nondimensional variables (18) were used to convert the boundary layer governing partial differential Equations (10), (12), and (17) to a set of ordinary differential equations taking the mathematical formulas:

$$\begin{aligned} f'''(\eta) - \left(f'(\eta) \right)^2 + f(\eta) f''(\eta) \\ + \lambda f''(\eta) f'''(\eta) - M f'(\eta) - Da f'(\eta) = 0, \end{aligned} \quad (19)$$

$$\begin{aligned} \theta''(\eta) + Pr \left(R \left((1 + (\theta_w - 1)\theta(\eta))^3 \theta'(\eta) \right)' \right. \\ \left. + Nb \theta'(\eta) \phi'(\eta) + S \theta(\eta) + Nt \left(\theta'(\eta) \right)^2 \right. \\ \left. + MEc \left(f'(\eta) \right)^2 + \theta'(\eta) f(\eta) \right) = 0, \end{aligned} \quad (20)$$

$$\phi''(\eta) + Le \phi'(\eta) f(\eta) - Le \gamma \phi(\eta) + \left(\frac{Nt}{Nb} \right) \theta''(\eta) = 0, \quad (21)$$

where the boundary conditions (13) and (14) can be written after converting as new follows:

$$f(0) = 0, f'(0) = 1, \theta(\eta) = 1, Nb \phi'(0) + Nt \theta'(0) = 0, \quad (22)$$

$$f'(\infty) \longrightarrow 0, \theta(\infty) \longrightarrow 0, \phi(\infty) \longrightarrow 0, \quad (23)$$

with the knowledge that $M = \sigma B_0^2 / \rho B$ is the magnetic field parameter, $R = 16\sigma^* T_\infty^3 / 3k^*$ is the nonlinear thermal radiation parameter, $Pr = \nu / \alpha$ is the Prandtl number, $Nb = (\rho c_p)_p / D_B C_\infty / \nu (\rho c_p)_f$ is the Brownian motion parameter, $Nt =$

TABLE 1: A comparison between the numerical results of Khan and Pop [8] and the results of the current study through the values of $-\theta'(0)$ in the case of $Pr = Le = 10$ and in the absence of both M , Da , Ec , γ , S , and λ .

Nt	Nb = 0.1		Nb = 0.2		Nb = 0.3	
	$-\theta'(0)$	Present study	$-\theta'(0)$	Present study	$-\theta'(0)$	Present study
0.1	0.9524	0.9501	0.5056	0.5065	0.2522	0.2534
0.2	0.6932	0.6910	0.3654	0.3646	0.1816	0.1912
0.3	0.5201	0.5237	0.2731	0.2735	0.1355	0.1382
0.4	0.4026	0.4083	0.2110	0.2124	0.1046	0.1086
0.5	0.3211	0.3270	0.1681	0.1710	0.0833	0.0880

$(\rho c_p)_p D_T (T_w - T_\infty) / (\rho c_p)_f \nu T_\infty$ is the thermophoresis parameter, $Le = \nu / D_B$ is the Lewis number, $Da = \mu / \rho B K$ is the Darcy number, $S = Q / (\rho c_p)_f B$ is the heat generation ($S > 0$) or absorption ($S < 0$) parameter, $\gamma = R^* / B$ is the chemical reaction parameter, $Ec = U_w^2(x) / c_p (T_w - T_\infty)$ is the Eckert number, and finally $\lambda = \Gamma x \sqrt{2B^3 / \nu}$ is the non-Newtonian Williamson parameter.

Expression for the local Nusselt number Nu_x and the skin friction coefficient C_f are defined as

$$Nu_x = \frac{x q_w}{k} (T_w - T_\infty), \quad (24)$$

$$C_f = \frac{\tau_w}{\rho U_w^2(x)}. \quad (25)$$

And the reader will note that the dimensionless mass flux represented by a Sherwood number Sh_x is now identically zero and q_w and τ_w are the heat flux and the shear stress along the stretching surface, respectively, on the following mathematical formulas:

$$q_w = -\alpha \left(\frac{\partial T}{\partial y} \right)_{y=0} + (q_r)_{y=0}, \quad (26)$$

$$\tau_w = \mu \left[\frac{\partial u}{\partial y} + \frac{\Gamma}{\sqrt{2}} \left(\frac{\partial u}{\partial y} \right)^2 \right]_{y=0}. \quad (27)$$

When substituting Equations (26) and (27) into Equations (24) and (25), the mathematical nondimensional formulas of Equations (24) and (25) are

$$\frac{Nu_x}{\sqrt{Re_x}} = -(1 + R \theta_w^3) \theta'(0), \quad (28)$$

$$\sqrt{Re_x} C_f = f''(0) \left(1 + \frac{\lambda}{2} f''(0) \right), \quad (29)$$

where $Re_x = x U_w(x) / \nu$ is the local Reynolds number based on the stretching velocity $U_w(x)$. It should be noted that in the absence of a magnetic field, porous medium, nonlinear thermal radiation, heat generation/absorption, and finally the chemical reaction, the work is due to Nadeem and Husain [39].

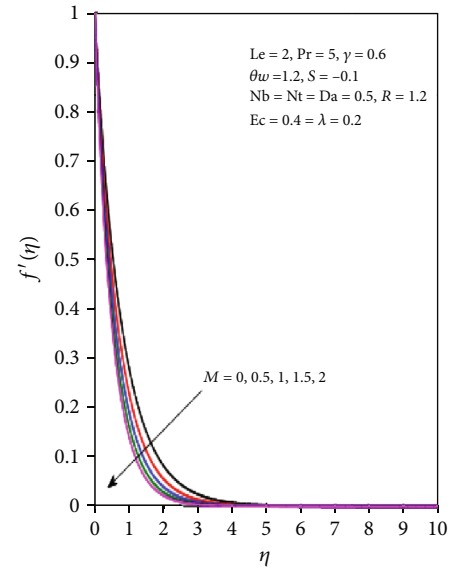


FIGURE 1: The velocity profile for different values of M .

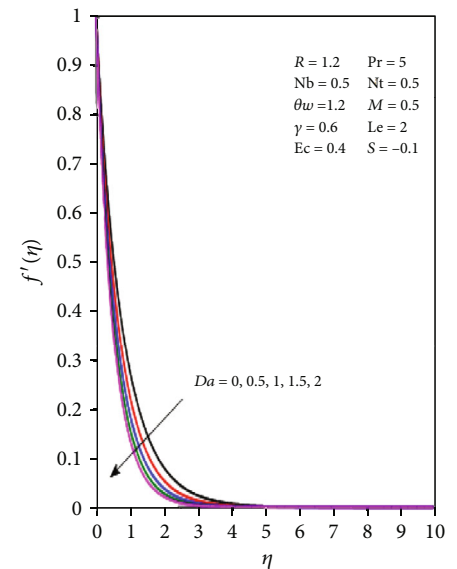


FIGURE 2: The velocity profile for different values of Da .

3. Numerical Solution

The Runge-Kutta numerical method is one of the most important numerical analysis methods that are used in solving a system of ordinary differential equations through which the differential equation is reduced degree to make it easier and simpler to solve. On the other hand, there are different formulas for the solution by the numerical method of Runge-Kutta method; for example, there is the Runge-Kutta method of the fourth order and also the Runge-Kutta method of the fifth order, and the most used method is the Runge-Kutta method of the fourth order because it gives accurate results and is easy to use, and its derivation depends on the Euler method. The numerical solutions of the current study are listed in several steps. In the first step, the system of partial differential Equations (10), (12), and

(17) for the current study has been converted into a system of ordinary differential Equations (19)–(21) using the similarity transformation and nondimensional variables (18); also, the boundary conditions (13) and (14) have been converted into the new forms (22) and (23). In the second step, the appropriate numerical method used in solving the new system of prior equations is the Runge-Kutta fourth-order with shooting technique, and by the way, this method was used to reduce the order of differential equations. In the third step, the program used to solve the system of ordinary differential equations is MATLAB, and the step size $\Delta\eta = 0.001$ is used to obtain the numerical solution with $\eta_{\max} = 10$; also, it used the bvp4c function in solving these equations. Differential Equations (19)–(21) can be rewritten in the simplest form as follows:

$$f'''(\eta) = \frac{\left((f'(\eta))^2 - f(\eta)f''(\eta) + Mf'(\eta) + Da f'(\eta) \right)}{(1 + \lambda f''(\eta))}, \quad (30)$$

$$\theta''(\eta) = - \frac{\text{Pr} \left(S\theta(\eta) + f(\eta)\theta'(\eta) + 3R(\theta_w - 1)(1 + (\theta_w - 1)\theta(\eta))^2 (\theta'(\eta))^2 + Nb\theta'(\eta)\phi'(\eta) + Nt(\theta'(\eta))^2 + MEc(f'(\eta))^2 \right)}{(1 + \text{Pr} R(1 + (\theta_w - 1)\theta(\eta))^3)}, \quad (31)$$

$$\phi''(\eta) = -Le\phi'(\eta)f(\eta) + Le\gamma\phi(\eta) - \left(\frac{Nt}{Nb} \right) \theta''(\eta). \quad (32)$$

In the last step, Equations (30)–(32) have been written inside the MATLAB program on the following formulas:

$$\begin{aligned} F(1) &= \xi(2), \\ F(2) &= \xi(3), \\ F(3) &= \frac{(\xi(2)^2 - \xi(1)\xi(3) + M\xi(2) + Da\xi(2))}{1 + \lambda\xi(3)}, \\ F(4) &= \xi(5), \\ F(5) &= - \frac{\text{Pr} \left(S\xi(4) + \xi(1)\xi(5) + Nb\xi(5)\xi(7) + Nt(\xi(5))^2 + MEc(\xi(2))^2 + 3R(\xi(5))^2(\theta_w - 1)(1 + (\theta_w - 1)\xi(4))^2 \right)}{(1 + \text{Pr} R(1 + (\theta_w - 1)\xi(4))^3)}, \\ F(6) &= \xi(7), \\ F(7) &= -Le\xi(7)\xi(1) + Le\gamma\xi(6) - \left(\frac{Nt}{Nb} \right) \xi(5). \end{aligned} \quad (33)$$

With the boundary conditions:

$$\begin{aligned}\xi_a(1) = 0, \xi_a(2) = 1, \xi_a(4) = 1, \text{Nb}\xi_a(7) + \text{Nt}\xi_a(5) = 0, \\ \xi_b(2) = 0, \xi_b(4) = 0, \xi_b(6) = 0.\end{aligned}\quad (34)$$

Taking into account both:

$$\begin{aligned}f(\eta) = \xi(1), f'(\eta) = \xi(2), f''(\eta) = \xi(3), f'''(\eta) \\ = F(3), \theta(\eta) = \xi(4), \theta'(\eta) = \xi(5), \\ \theta''(\eta) = F(5), \phi(\eta) = \xi(6), \phi'(\eta) = \xi(7), \phi''(\eta) \\ = F(7), f(0) = \xi_a(1), f'(0) = \xi_a(1), \\ \theta(0) = \xi_a(4), \theta'(0) = \xi_a(5), \phi'(0) = \xi_a(7), f'(\infty) \\ = \xi_b(2), \theta(\infty) = \xi_b(4), \phi(\infty) = \xi_b(6).\end{aligned}\quad (35)$$

To ensure the accuracy and correctness of the numerical solutions of the current study, a numerical comparison was made between the numerical values and results of the current study with the numerical values and results of the work published by Khan and Pop [8] in Table 1. The great convergence between the two studies was noted, which gives high credibility to the current study.

4. Results and Discussion

After converting the system of partial differential equations ruling to study the flow of fluid into a system of ordinary differential equations, it has a set of important parameters that we list in the following order M , Da , and λ which are the magnetic field, the Darcy number, and non-Newtonian Williamson parameters, respectively, while R , θ_w , and S represent the nonlinear thermal radiation, the ratio temperature, and the heat generation/absorption parameters, respectively; also, Pr is the Prandtl number and Nt is the thermophoresis parameter, while Ec , γ , Le , and Nb are the Eckert number, the chemical reaction, the Lewis number, and Brownian motion parameters, respectively. The effect of all the previous physical parameters on the velocity, temperature, and concentration of nanoparticle distributions has been studied by making graphical figures that clarify this and by showing the physical meanings of each parameter and its importance in this study, and we can list the results of this study in detail.

4.1. Velocity Distributions. It is known that the rate at which the fluid flows onto a specific surface is entirely determined by the distribution of velocity; therefore, velocity distributions play an important role in studying the changes that occur in the flow rate of the fluid. On the other hand, when affecting the flowing fluid with external forces, the behavior of the fluid's movement is changing, and one of these types of external forces is the magnetic field. Figure 1 shows the effect of the strength of the magnetic field parameter M on the fluid velocity distribution $f'(\eta)$. It is noticeable that the result of this effect is negative in the sense that the relationship between the magnetic field and the velocity distribution

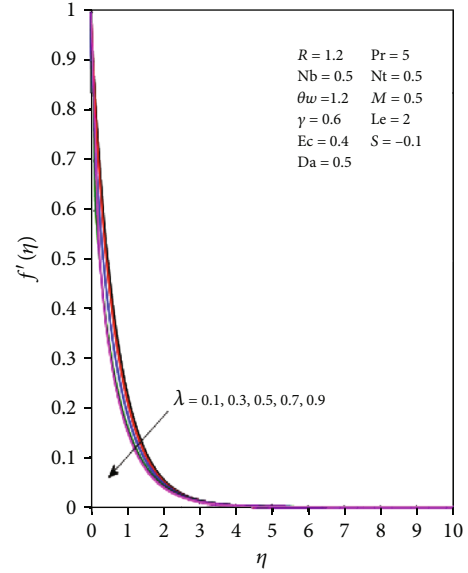
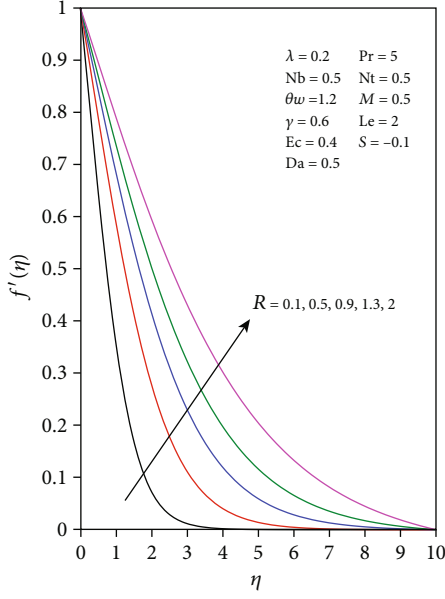
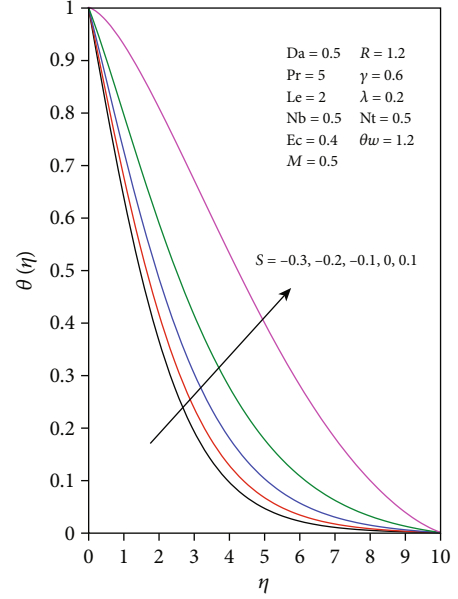
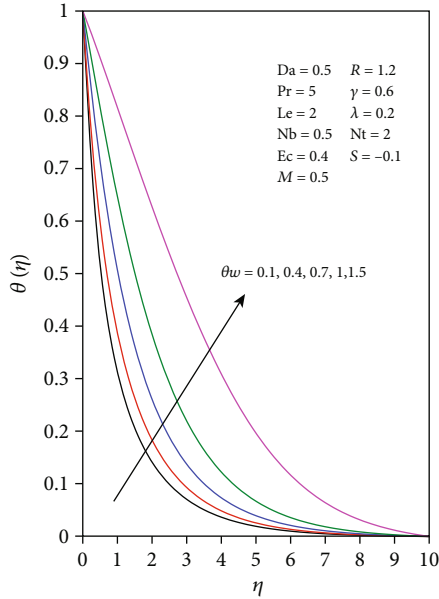


FIGURE 3: The velocity profile for different values of λ .

is inverse; the increase in the values of the magnetic field means a decrease in the velocity of the fluid. Physically, when influencing a moving fluid by the magnetic field, the fluid particles are stimulated, which creates a kind of counter force that slows and reduces the fluid's motion; moreover, this force is perpendicular to the velocity vector on the one hand and also perpendicular to the magnetic field vector on the other hand which is originally a resistance force called Lorentz force, while highlighting that the increase in the magnetic field reduces the thickness of the boundary layer. If you want to know the effect of the Darcy number Da on the velocity distribution, you should look at Figure 2. It becomes clear to you that the velocity distribution decreases under the influence of the large values that the Darcy number Da takes. Physically, the porous medium is the medium that contains a group of small voids called pores that are interrupted by the fluid when it moves on this medium. On the other hand, the permeability of the fluid through the porous medium is related to its porosity.

Also, the greater the values of the Darcy number Da , the greater the resistance of the porous medium to the movement of the fluid on it on the one hand, in addition to the fluid viscosity on the other hand, which leads to a decrease in the fluid velocity. Moving to Figure 3, it reviews the effect of the non-Newtonian Williamson coefficient λ on the velocity distribution, and it clears that this effect is negative in the sense that the increase in the values of this coefficient is followed by a decrease in velocity of the fluid, which makes its movement slow.

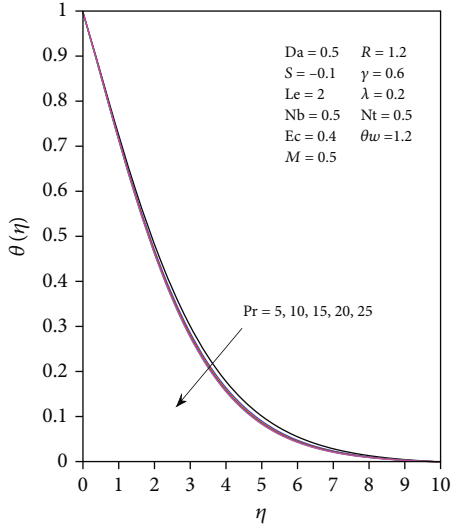
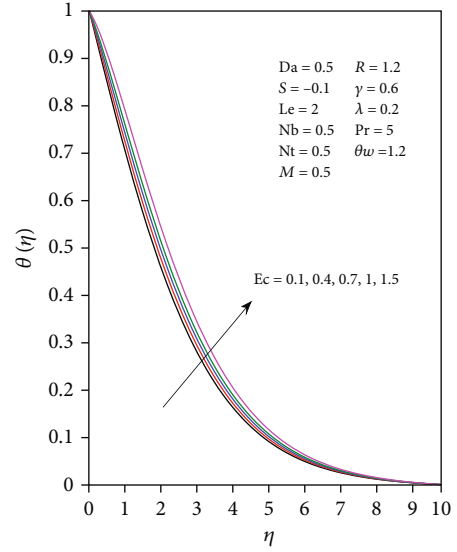
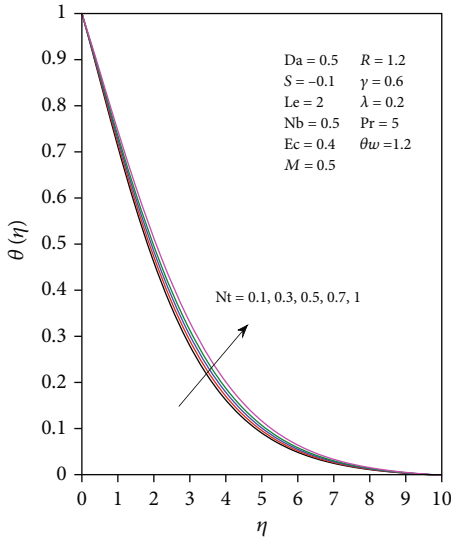
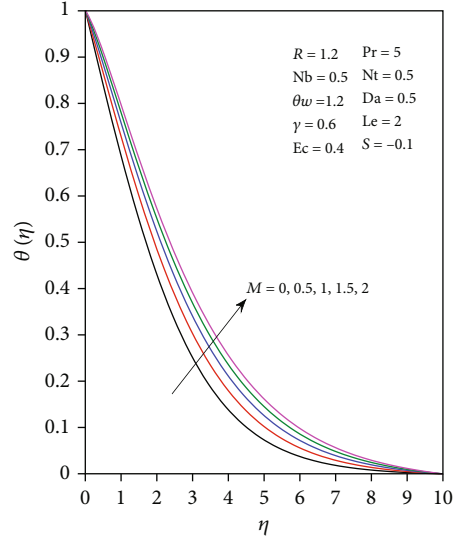
4.2. Temperature Distributions. The change in the fluid temperature plays an important role in the fluid's behavior in addition to its effect also on the particles inside the fluid. Now, we will study the effect of some physical parameters on the fluid temperature distribution $\theta(\eta)$ and note the changes taking place; for example, Figures 4 and 5 illustrate the effects of the nonlinear thermal radiation parameter R

FIGURE 4: Temperature profile for different values of R .FIGURE 6: Temperature profile for different values of S .FIGURE 5: Temperature profile for different values of θ_w .

and the ratio temperature parameter θ_w on the temperature distribution $\theta(\eta)$; it was noticed that the large values taken by the nonlinear thermal radiation parameter R and ratio temperature parameter θ_w work to enhance the heat transfer inside the fluid and work to stimulate it. Physically, the positive effect of the nonlinear thermal radiation parameter R on the temperature of the nanofluid leads to three things. Firstly, the heat transfer of all distances of the boundary layer is supported, or in other words, it raises the temperature of the boundary layer regularly. Secondly, it makes the nanoparticles inside the fluid gain thermal energy, which improves the transfer and thermal diffusion within the fluid due to the thermal conductivity of the nanoparticles.

Thirdly, it works to enhance the thermal transfer methods of the nanofluid, which is the thermal transfer method by conduction and the method of thermal transfer by load. On the other hand, the effect of the ratio temperature increases the boundary layer temperature and increases its thickness. When talking about the effect of the heat generation/absorption parameter S on the fluid temperature distribution $\theta(\eta)$, as shown in Figure 6, there is a significant enhancement in the distribution of the fluid temperature due to the enhancement in the values of parameter S .

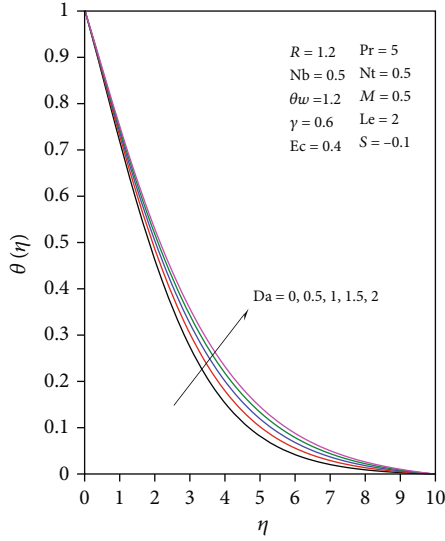
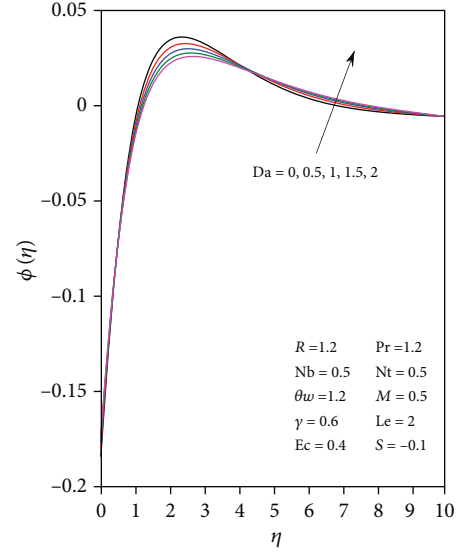
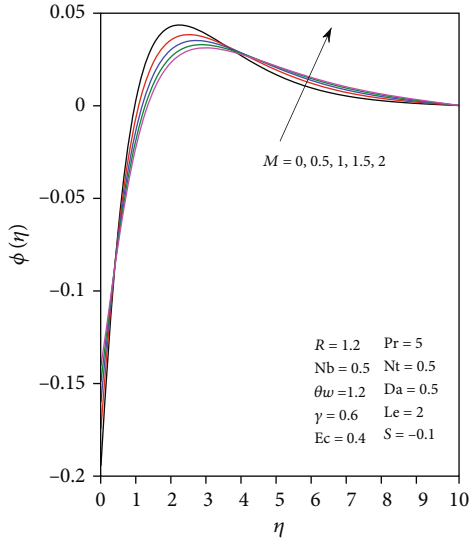
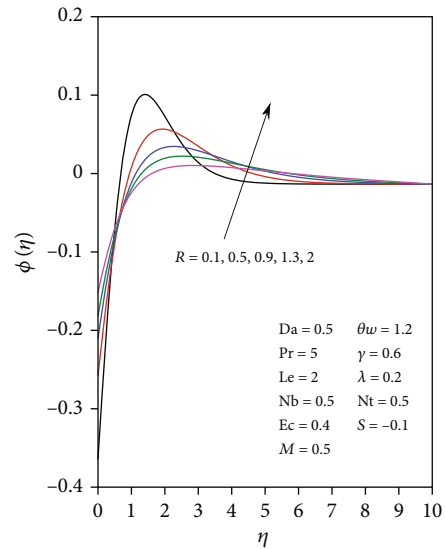
Physically, in the case of the phenomenon of heat generation, there is an enhancement in the transfer and thermal spread of the fluids, which raises temperature of fluid and also raises the temperature and thickness of the boundary layer with the increase in the values of the heat source type ($S > 0$), while the exact opposite occurs in the case of the heat absorption type ($S < 0$), but when moving upward from the state of heat absorption type to the state of heat generation type, there is an improvement in the rate of thermal diffusion and the thickness of the boundary layer. Figure 7 displays the impact of Prandtl number Pr on the temperature distribution $\theta(\eta)$; when this parameter takes a large value, the fluid temperature distribution is decreased. Physically, Prandtl number Pr is defined as the ratio of momentum diffusivity to thermal diffusivity; on the other hand, there are two types of Prandtl number Pr : the first type is $Pr > 1$; this means that the rate of momentum diffusion dominates the rate of thermal diffusion, and the second type is $Pr < 1$ which urges the opposite, and Figure 7 shows the case in which $Pr > 1$ such that the thermal diffusion within the fluid becomes small; thus, the fluid temperature and thickness of the boundary layer become decreasing. The distribution of the fluid temperature $\theta(\eta)$ changes with the effect of the thermophoresis parameter Nt values; as shown in Figure 8, the direct relationship between them refers to the enhancement in the values of the thermophoresis parameter Nt leading to an

FIGURE 7: Temperature profile for different values of Pr .FIGURE 9: Temperature profile for different values of Ec .FIGURE 8: Temperature profile for different values of Nt .FIGURE 10: Temperature profile for different values of M .

increase in the fluid temperature distribution $\theta(\eta)$. Physically, there are two different sources: the first is hot and the other is cold; the particles close to the hot medium absorb heat energy, which makes them move from the hot medium to the cold medium and raises its temperature by means of convection; this process is called the process of thermal potential difference; this is exactly what happens inside the fluid when it is exposed to a heat source. The fluid particles absorb heat energy that makes it spread throughout the fluid, raising its temperature as well as enhancing the thickness of the boundary layer of the fluid. Figure 9 studies the effect of the Eckert number Ec on the temperature distribution $\theta(\eta)$, so it was noted that the large values that take by this parameter affect the temperature distribution making this effect positive in the sense that it enhances the effect of temperature. Finally, the influence of the coefficient of the magnetic field M as well as the effect of the Darcy number Da on the

temperature distribution $\theta(\eta)$ is shown graphically in Figures 10 and 11, respectively; it is very clear from the study of the two figures that the fluid temperature and the boundary layer thickness increase with increasing values of these two parameters.

4.3. Concentration of Nanoparticle Distributions. The study of the concentration of nanoparticles within a fluid plays an important role in the properties and applications of this fluid from several sides; for example, the degree and efficiency of the thermal conductivity of a nanofluid are related to the concentration of nanoparticles inside it, and also, the degree and efficiency of its electrical conductivity are related to the concentration of nanoparticles. Figures 12 and 13 display the effect of both the magnetic field parameter M and the Darcy number Da on the distribution of the concentration of nanoparticles $\phi(\eta)$, and it is clear from the two figures that

FIGURE 11: Temperature profile for different values of Da .FIGURE 13: Concentration of nanoparticle profile for different values of Da .FIGURE 12: Concentration of nanoparticle profile for different values of Pr .FIGURE 14: Concentration of nanoparticle profile for different values of R .

the effect is very positive. Physically, firstly, the effect of the magnetic field M on the fluid works to reduce the movement of the fluid accompanied slowly in the movement of the nanofluid particles, which makes its concentration large. Secondly, the effect of the Darcy number Da on the fluid movement gives a great opportunity for collision of the nanoparticles with the pores of the porous medium, which causes it to accumulate inside the pores and the porous medium itself, and accordingly, the concentration of nanoparticles becomes increasing. On the other hand, Figures 14 and 15 show the effects of the nonlinear thermal radiation parameter R and the ratio temperature parameter θ_w on the concentration of nanoparticle distribution $\phi(\eta)$ within the fluid. It was noted that the reinforcement in the values of these two parameters works to strengthen the temperature of the nanoparticles and thickness of the boundary layer of the fluid, as it

works on a significant increase in the spread of the temperature in all parts of the fluid. Physically, nanoparticle fluid molecules are greatly affected by the radiation source that generates heat, which causes fluid particles to interact positively with this heat, which increases the mechanical energy of the nanoparticles, and this actually leads to their stimulation and increased concentration. The concentration of nanoparticles gives a good or positive impression in the event that it is affected by the heat generation/absorption parameter S because the mechanism of action of this parameter is very similar to the mechanism of nonlinear thermal radiation parameter R only in the case of heat generation; on the other side, the heat generation works to stimulate the temperature of nanoparticles and thus increases the concentration of nanoparticles $\phi(\eta)$ and adds to the positive effect on the

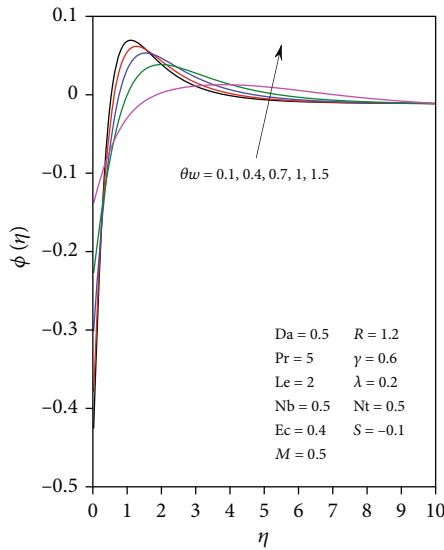


FIGURE 15: Concentration of nanoparticle profile for different values of θ_w .

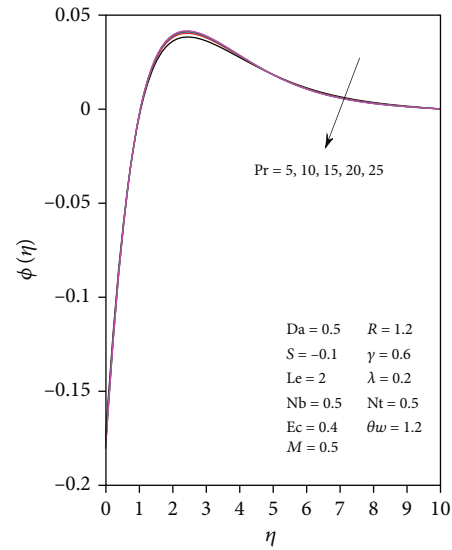


FIGURE 17: Concentration of nanoparticle profile for different values of Pr .

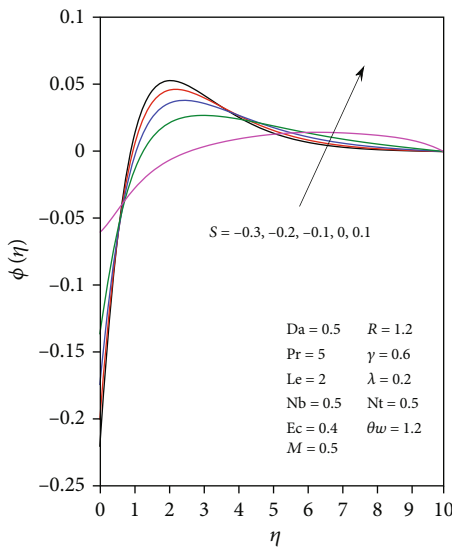


FIGURE 16: Concentration of nanoparticle profile for different values of S .

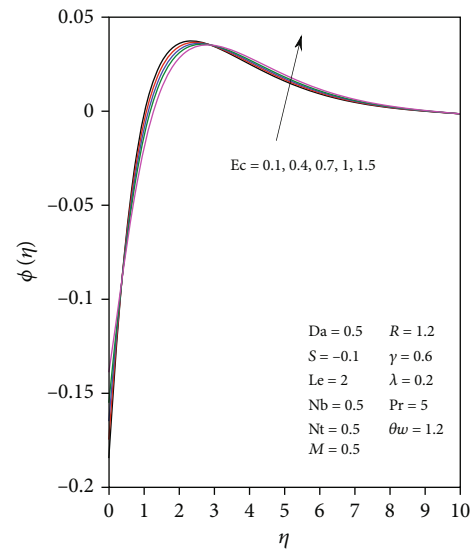


FIGURE 18: Concentration of nanoparticle profile for different values of Ec .

boundary layer in terms of thickness, while in the case of heat absorption, the opposite occurs, and this is shown in Figure 16. As for Figure 17, it shows the negative effect of Prandtl number Pr on the concentration of nanoparticle distribution $\phi(\eta)$ because in the case where $Pr > 1$, thermal diffusion equipment is very small compared to the momentum diffusion rate, and accordingly, the concentration of nanoparticles becomes small that is the physical meaning. Figures 18 and 19 show the effects of both the Eckert number Ec and the thermophoresis parameter Nt on the distribution of the concentration of nanoparticles $\phi(\eta)$ within the fluid; it was found that the increase in this parameters gives a large concentration of the nanofluid particles, at a time when the effects of both Lewis number Le and chemical reaction

parameter γ on the concentration of nanoparticles $\phi(\eta)$ inside the fluid were negative; this is illustrated in Figures 20 and 21. Finally, Figure 22 clears the effect of the Brownian motion parameter Nb on the distribution of the concentration of nanoparticles $\phi(\eta)$ within the fluid. It is noticeable that the distribution of the concentration of nanoparticles $\phi(\eta)$ decreases in the event that this parameter is enhanced. Physically, the Brownian motion of the nanofluid is a random motion of the nanoparticles present in this fluid in the absence of any external effects so that the movement of these particles is free in all directions, but in the case of a large thermal diffusion resulting from the effect of thermal radiation and the coefficient of thermophoresis, it becomes that the random movement of the nanoparticles is limited.

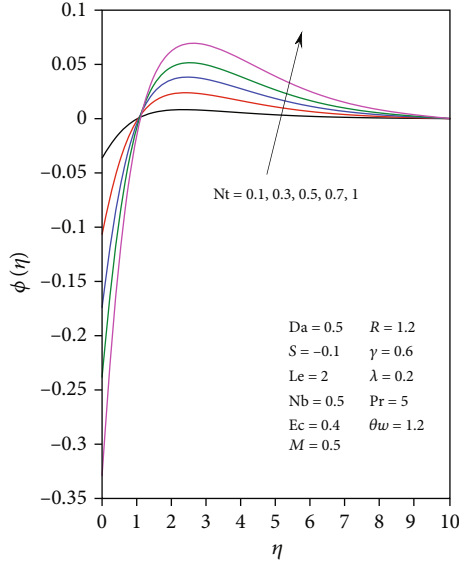


FIGURE 19: Concentration of nanoparticle profile for different values of Nt .

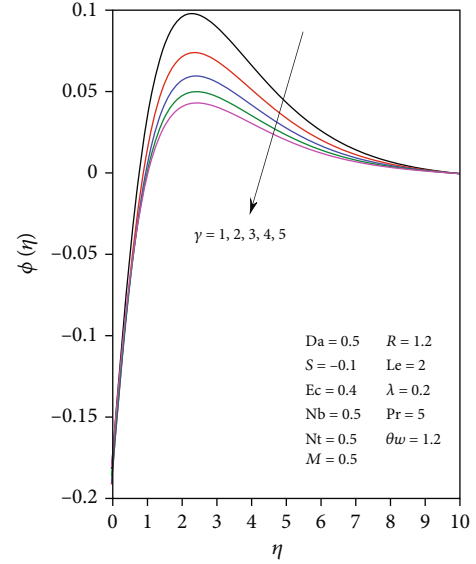


FIGURE 21: Concentration of nanoparticle profile for different values of γ .

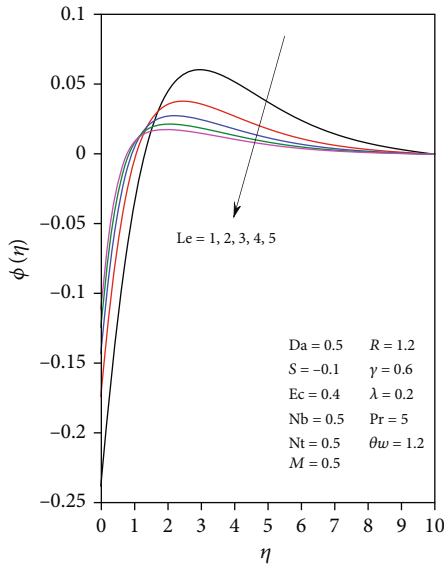


FIGURE 20: Concentration of nanoparticle profile for different values of S .

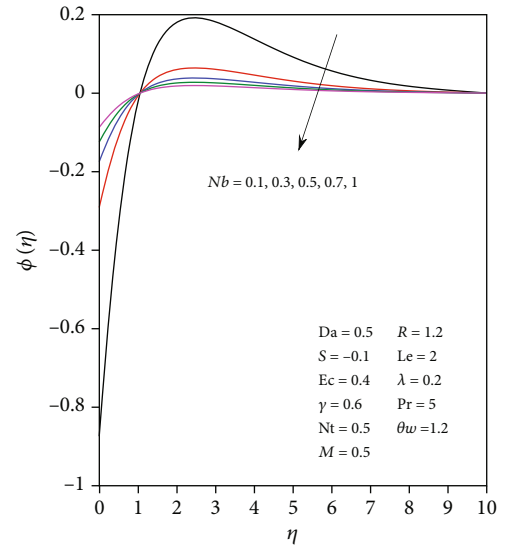
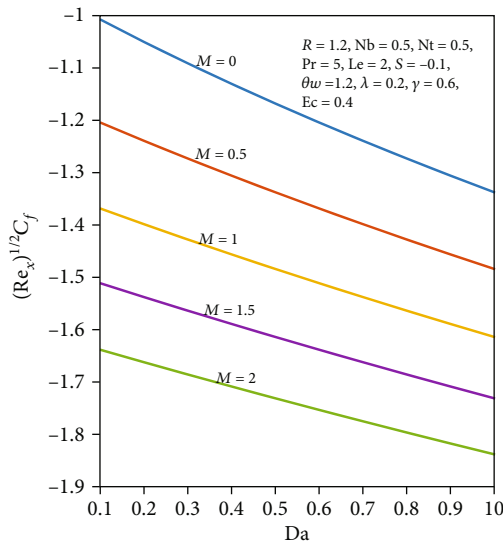
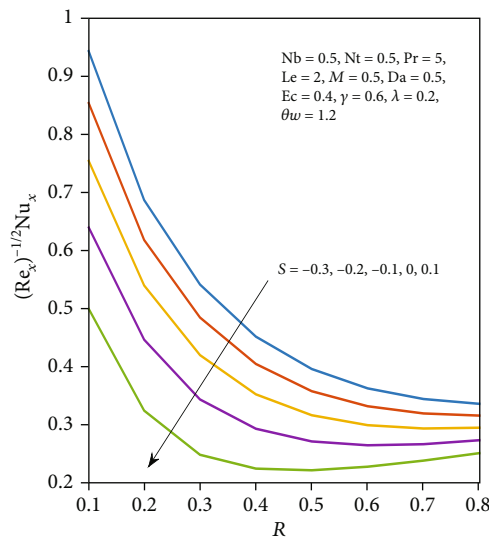


FIGURE 22: Concentration of nanoparticle profile for different values of Nb .

4.4. Skin Friction and Local Nusselt Number Profiles.

Figure 23 shows the change in the coefficient of skin friction when affecting it by the coefficient of the magnetic field M and the Darcy number Da . It is clear that the coefficient of skin friction decreases with increasing values of these parameters, meaning that the increase in both the values of the magnetic field and the Darcy number increases the rate of fluid velocity gradient regularly. On the other hand, Figures 24 and 25 show the effects of nonlinear thermal radiation parameter R , heat generation/absorption parameter S , and ratio temperature parameter θ_w on the local Nusselt number $Nu_x/\sqrt{Re_x}$; it is clear that this effect is negative in the sense of an increase in the values of previous parameters leading to a decrease in the local Nusselt number, and that

means that the ratio of convective to conductive heat transfer at a boundary in a fluid becomes small. Tables 2 and 3 show the numerical values of the local Nusselt number $Nu_x/\sqrt{Re_x}$ and skin friction coefficient $\sqrt{Re_x} C_f$ for all physical parameters resulting from the current numerical study of the Williamson fluid flow process that contains nanoparticles on an expanding surface in the presence of a porous medium. The following was observed that the skin friction coefficient $\sqrt{Re_x} C_f$ has become a constant value for all physical parameters with the exception of each of the magnetic field parameter M , Darcy number Da , and non-Newtonian Williamson parameter λ , whereas the values of the local Nusselt number $Nu_x/\sqrt{Re_x}$ decrease under the influence of all physical parameters.

FIGURE 23: Skin friction profile for different values of M , Da .FIGURE 24: Local Nusselt number profile for different values of S , R .

5. Conclusion

In this article, the two-dimensional electromagnetic flow of the Williamson nanofluid has been studied on a stretching sheet through a porous medium; on the other hand, the governing partial differential equations were converted into a system of ordinary differential equations using the similarity transformations and the nondimensional variable under the effects of nonlinear thermal radiation, heat generation/absorption, chemical reaction, Brownian motion parameter, thermophoresis parameter, magnetic field, Darcy number, Joule heating, Lewis number, Prandtl number, and Williamson non-Newtonian parameter on distribution of velocity, temperature, and concentration of nanoparticles; the most important points drawn from this study are the following:

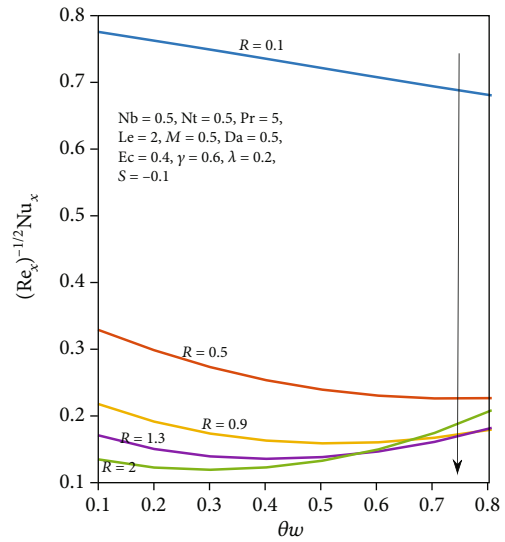
FIGURE 25: Local Nusselt number profile for different values of S , R .

TABLE 2: The numerical values of the skin friction coefficient $\sqrt{Re_x} C_f$ and the local Nusselt number $Nu_x/\sqrt{Re_x}$ for values of M , Da , and λ parameters when $R = 1.2$, $Nb = 0.5$, $Nt = 0.5$, $Pr = 5$, $Le = 2$, $S = -0.1$, $Ec = 0.4$, $\theta_w = 1.2$, and $\gamma = 0.6$.

M	Da	λ	$\sqrt{Re_x} C_f$	$\frac{Nu_x}{\sqrt{Re_x}}$
0	0.5	0.2	-1.16630705	0.32673441
0.5			-1.33621158	0.32351790
1			-1.48295534	0.32112657
1.5			-1.61309297	0.31923008
2			-1.73049604	0.31766292
0.5	0	0.2	-1.16630705	0.32463205
	0.5		-1.33621158	0.32351790
	1		-1.48295534	0.32272607
	1.5		-1.61309297	0.32212446
	2		-1.73049604	0.32164656
0.5	0.5	0.1	-1.37751997	0.32368673
		0.3	-1.28773536	0.32332326
		0.5	17.61631263	0.32263272
		0.7	0.36239912	0.32190223

- The velocity distribution $f'(\eta)$ of the fluid is negatively affected by the influence of the magnetic field parameter M , the Darcy number Da , and the non-Newtonian Williamson parameter λ at the time when their influence on the distributions of the temperature $\theta(\eta)$ and concentration of the nanoparticles $\phi(\eta)$ becomes positive
- The enhancement in the values of nonlinear thermal radiation R parameter and the ratio temperature θ_w resulted in the enhancement of both temperature $\theta(\eta)$ of the fluid and the concentration of the nanoparticles $\phi(\eta)$, while the opposite occurs when increasing the values of Prandtl number Pr

TABLE 3: The numerical values of the skin friction coefficient $\sqrt{\text{Re}_x} C_f$ and the local Nusselt number $\text{Nu}_x/\sqrt{\text{Re}_x}$ for all values of physical parameter when $M = \text{Da} = 0.5$ and $\lambda = 0.2$.

R	Nb	Nt	Pr	Le	S	Ec	θ_w	γ	$\sqrt{\text{Re}_x} C_f$	$\frac{\text{Nu}_x}{\sqrt{\text{Re}_x}}$
0.1	0.5	0.5	5	2	-0.1	0.4	1.2	0.6	-1.33621230	0.64166769
0.5									-1.33621158	0.27220459
0.9									-1.33621158	0.28419960
1.2	0.1	0.5	5	2	-0.1	0.4	1.2	0.6	-1.33621158	0.32351790
	0.3								-1.33621158	0.32351790
	0.5								-1.33621158	0.32351790
1.2	0.5	0.1	5	2	-0.1	0.4	1.2	0.6	-1.33621158	0.32410873
		0.3							-1.33621158	0.32381315
		0.5							-1.33621158	0.32351790
1.2	0.5	0.5	5	2	-0.1	0.4	1.2	0.6	-1.33621158	0.32351790
			10						-1.33621158	0.31230129
			15						-1.33621158	0.30971540
1.2	0.5	0.5	5	1	-0.1	0.4	1.2	0.6	-1.33621158	0.32356291
				2					-1.33621158	0.32351790
				3					-1.33621158	0.32349773
1.2	0.5	0.5	5	2	-0.3	0.4	1.2	0.6	-1.33621158	0.34389846
					-0.2				-1.33621158	0.33376466
					-0.1				-1.33621158	0.32351790
1.2	0.5	0.5	5	2	-0.1	0.1	1.2	0.6	-1.33621158	0.32487121
						0.4			-1.33621158	0.32351790
						0.7			-1.33621158	0.32216467
1.2	0.5	0.5	5	2	-0.1	0.4	0.1	0.6	-1.33621158	0.18104819
							0.4		-1.33621158	0.14127077
							0.7		-1.33621158	0.16205303
1.2	0.5	0.5	5	2	-0.1	0.4	1.2	1	-1.33621158	0.32350105
								2	-1.33621158	0.32347976
								3	-1.33621158	0.32346885

(iii) It was found that the distribution of the concentration of nanoparticles $\phi(\eta)$ decreased under the influences of the Lewis number Le , Brownian motion coefficient Nb , and chemical reaction parameter γ

(iv) The increase and enhancement in the effects of both heat generation/absorption S parameter and the Eckert number Ec resulted in an increase and enhancement in the distributions of both temperature $\theta(\eta)$ and concentration of nanoparticles $\phi(\eta)$

(v) Effects of heat generation/absorption parameter S , the nonlinear thermal radiation parameter R , and the ratio temperature parameter θ_w have a negative effect on the local Nusselt number $\text{Nu}_x/\sqrt{\text{Re}_x}$ so that the effects of the magnetic field M and Darcy number Da on the skin friction coefficient $\sqrt{\text{Re}_x} C_f$ were negative

\vec{B} : External magnetic field
 B_o : Uniform magnetic field
 B : Stretching parameter
 C : Nanoparticle volume fraction
 C_w : Nanoparticle fraction at wall
 c_p : Specific heat at constant pressure
 C_f : Skin friction coefficient
 D_B : Brownian diffusion coefficient
 D_T : Thermophoresis diffusion coefficient
 Da : Darcy number
 \vec{E} : Electric field intensity
 Ec : Eckert number
 \vec{F}_e : The Lorentz force
 I : Unit vector
 \vec{J} : The current density
 J_h : The Joule heating
 K : Permeability
 k : Thermal conductivity
 k^* : Mean absorption coefficient
 Le : Lewis number

Symbols

\bar{A}_1 : First Rivlin-Erickson tensor

M :	Magnetic field parameter
Nb :	Brownian motion parameter
Nt :	Thermophoresis parameter
Nu_x :	Nusselt number
P :	Pressure
Q :	Uniform volumetric heat source/sink
\vec{q} :	Velocity vector
q_w :	Heat flux
q_m :	Mass flux
q_r :	Nonlinear radiative heat flux
R :	Thermal radiation parameter
R^* :	Constructive reaction rates
Re_x :	Local Reynolds number
S :	Heat source/sink parameter
\bar{S} :	Cauchy stress tensor
Sh_x :	Local Sherwood number
T :	Fluid temperature
T_w :	Fluid temperature at wall
T_∞ :	Ambient fluid temperature
t :	Time
U_w :	Fluid velocity
u, v :	Velocity components
x, y :	Space coordinates
α :	Thermal diffusivity
ν :	Kinematic viscosity
ρ :	Density of the fluid
$\bar{\tau}$:	Extra stress tensor
τ_w :	Shear stress along stretching surface
σ^* :	Stefan-Boltzmann constant
λ :	Non-Newtonian Williamson parameter
η :	Similarity variable
ψ :	Dimensionless stream function
ϕ :	Dimensionless concentration function
θ :	Dimensionless temperature
Γ :	Time constant
θ_w :	Ratio temperature
$(\rho c_p)_p$:	Heat capacity of a nanoparticle
$(\rho c_p)_f$:	Heat capacity of the base fluid
μ_0 :	Limiting viscosity at zero shear rate
μ_∞ :	Limiting viscosity at infinite
γ :	Chemical reaction parameter.

Data Availability

No data were used to support the findings of this study.

Conflicts of Interest

The authors have no conflicts of interest regarding the publication of the paper.

Acknowledgments

The authors would like to acknowledge the financial support of Taif University researchers, supporting project no. TURSP-2020/162, Taif University, Saudi Arabia.

References

- [1] R. V. Williamson, "The flow of pseudoplastic materials," *Industrial and Engineering Chemistry*, vol. 21, no. 11, pp. 1108–1111, 1929.
- [2] K. Subbarayudu, S. Suneetha, and P. B. A. Reddy, "The assessment of time dependent flow of Williamson fluid with radiative blood flow against a wedge," *Propulsion and Power Research*, vol. 9, no. 1, pp. 87–99, 2020.
- [3] T. P. Lyubimova, A. V. Perminov, and M. G. Kazimardanov, "Stability of quasi-equilibrium states and supercritical regimes of thermal vibrational convection of a Williamson fluid in zero gravity conditions," *International Journal of Heat and Mass Transfer*, vol. 129, pp. 406–414, 2019.
- [4] Hashim, A. Hamid, and M. Khan, "Multiple solutions for MHD transient flow of Williamson nanofluids with convective heat transport," *Journal of the Taiwan Institute of Chemical Engineers*, vol. 103, pp. 126–137, 2019.
- [5] A. Hamid, M. A. Hashim, M. Khan, and A. S. Alshomrani, "An investigation of thermal and solutal stratification effects on mixed convection flow and heat transfer of Williamson nanofluid," *Journal of Molecular Liquids*, vol. 284, pp. 307–315, 2019.
- [6] S. U. S. Choi, *Enhancing Thermal Conductivity of Fluids with Nanoparticles*, Int. Mech. Eng. Cong. Exp. ASME, 1995.
- [7] S. A. Sajadifar, A. Karimipour, and D. Toghraie, "Fluid flow and heat transfer of non-Newtonian nanofluid in a microtube considering slip velocity and temperature jump boundary conditions," *European Journal of Mechanics - B/Fluids*, vol. 61, pp. 25–32, 2017.
- [8] W. A. Khan and I. Pop, "Boundary-layer flow of a nanofluid past a stretching sheet," *International Journal of Heat and Mass Transfer*, vol. 53, no. 11–12, pp. 2477–2483, 2010.
- [9] M. Farooq, M. I. Khan, M. Waqas, T. Hayat, A. Alsaedi, and M. I. Khand, "MHD stagnation point flow of viscoelastic nanofluid with non-linear radiation effects," *Journal of Molecular Liquids*, vol. 221, pp. 1097–1103, 2016.
- [10] S. E. Ahmed, R. A. Mohamed, A. M. Aly, and M. S. Soliman, "Magnetohydrodynamic Maxwell nanofluids flow over a stretching surface through a porous medium: effects of non-linear thermal radiation, convective boundary conditions and heat generation/absorption," *World Academy of Science, Engineering and Technology International Journal of Aerospace and Mechanical Engineering*, vol. 13, pp. 436–443, 2019.
- [11] A. S. Alshomrani, "On generalized Fourier's and Fick's laws in bio-convection flow of magnetized Burgers nanofluid utilizing motile microorganisms," *Mathematics*, vol. 8, no. 7, p. 1186, 2020.
- [12] A. S. Alshomrani, "Numerical investigation for bio-convection flow of viscoelastic nanofluid with magnetic dipole and motile microorganisms," *Arabian Journal for Science and Engineering*, vol. 46, no. 6, pp. 5945–5956, 2021.
- [13] K. Loganathan and S. Rajan, "An entropy approach of Williamson nanofluid flow with Joule heating and zero nanoparticle mass flux," *Journal of Thermal Analysis and Calorimetry*, vol. 141, no. 6, pp. 2599–2612, 2020.
- [14] W. A. Khan, M. Waqas, W. Chammam, Z. Asghar, U. A. Nisar, and S. Z. Abbas, "Evaluating the characteristics of magnetic dipole for shear-thinning Williamson nanofluid with thermal radiation," *Computer Methods and Programs in Biomedicine*, vol. 191, article 105396, 2020.

- [15] M. Khan, T. Salahuddin, M. Y. Malik, and F. O. Mallawi, "Change in viscosity of Williamson nanofluid flow due to thermal and solutal stratification," *International Journal of Heat and Mass Transfer*, vol. 126, pp. 941–948, 2018.
- [16] T. Hayat, M. Z. Kiyani, A. Alsaedi, M. I. Khan, and I. Ahmad, "Mixed convective three-dimensional flow of Williamson nanofluid subject to chemical reaction," *International Journal of Heat and Mass Transfer*, vol. 127, pp. 422–429, 2018.
- [17] M. Ramzan, H. Gul, and M. Zahri, "Darcy-Forchheimer 3D Williamson nanofluid flow with generalized Fourier and Fick's laws in a stratified medium," *Bulletin of the Polish Academy of Sciences, Technical Sciences*, vol. 68, pp. 327–335, 2020.
- [18] H. Alfvén, "Existence of electromagnetic-hydrodynamic waves," *Nature*, vol. 150, no. 3805, pp. 405–406, 1942.
- [19] R. A. Mohamed, A. M. Aly, S. E. Ahmed, and M. S. Soliman, "MHD Jeffrey nano fluids flow over a stretching sheet through a porous medium in presence of nonlinear thermal radiation and heat generation/absorption," *Transport Phenomena in Nano and Micro Scales*, vol. 8, pp. 9–22, 2020.
- [20] P. Chandrashekar, B. Nkonga, and A. Bhole, "A discontinuous Galerkin method for a two dimensional reduced resistive MHD model," *Computers & Fluids*, vol. 190, pp. 178–191, 2019.
- [21] Z.-H. Liu, M.-J. Ni, and N.-M. Zhang, "Numerical study of MHD mixed convection under volumetric heat source in vertical square duct with wall effects," *Theoretical and Applied Mechanics Letters*, vol. 9, no. 3, pp. 152–160, 2019.
- [22] A. Tassone, G. Caruso, F. Giannetti, and A. D. Nevo, "MHD mixed convection flow in the WCCL: heat transfer analysis and cooling system optimization," *Fusion Engineering and Design*, vol. 146, pp. 809–813, 2019.
- [23] S. S. Motsa, P. G. Dlamini, and M. Khumalo, "Spectral relaxation method and spectral quasilinearization method for solving unsteady boundary layer flow problems," *Advances in Mathematical Physics*, vol. 2014, Article ID 341964, 12 pages, 2014.
- [24] A. A. Khan, R. Ellahi, and K. Vafai, "Peristaltic transport of a Jeffrey fluid with variable viscosity through a porous medium in an asymmetric channel," *Advances in Mathematical Physics*, vol. 2012, Article ID 169642, 15 pages, 2012.
- [25] R. Ellahi, "A study on the convergence of series solution of non-Newtonian third grade fluid with variable viscosity by means of homotopy analysis method," *Advances in Mathematical Physics*, vol. 2012, Article ID 634925, 11 pages, 2012.
- [26] M. Umar, R. Akhtar, Z. Sabir et al., "Numerical treatment for the three-dimensional Eyring-Powell fluid flow over a stretching sheet with velocity slip and activation energy," *Advances in Mathematical Physics*, vol. 2019, Article ID 9860471, 12 pages, 2019.
- [27] G. K. Ramesh, B. J. Gireesha, and C. S. Bagewadi, "Heat transfer in MHD dusty boundary layer flow over an inclined stretching sheet with non-uniform heat source/sink," *Advances in Mathematical Physics*, vol. 2012, Article ID 657805, 13 pages, 2012.
- [28] M. Ramzan, M. Farooq, T. Hayat, and J. D. Chung, "Radiative and Joule heating effects in the MHD flow of a micropolar fluid with partial slip and convective boundary condition," *Journal of Molecular Liquids*, vol. 221, pp. 394–400, 2016.
- [29] R. A. Mohamed, S. M. Abo-Dahab, and T. A. Nofal, "Thermal radiation and MHD effects on free convective flow of a polar fluid through a porous medium in the presence of internal heat generation and chemical reaction," *Mathematical Problems in Engineering*, vol. 2010, pp. 1–27, 2010.
- [30] A. Tetbirt, M. N. Bouaziz, and M. T. Abbes, "Numerical study of magnetic effect on the velocity distribution field in a macro/micro-scale of a micropolar and viscous fluid in vertical channel," *Journal of Molecular Liquids*, vol. 216, pp. 103–110, 2016.
- [31] S. S. Ghadikolaei, K. Hosseinzadeh, and D. D. Ganjib, "Numerical study on magnetohydrodynamic CNTs-water nanofluids as a micropolar dusty fluid influenced by non-linear thermal radiation and Joule heating effect," *Powder Technology*, vol. 340, pp. 389–399, 2018.
- [32] J. Gireesha, B. Mahanthesh, G. T. Thammanna, and P. B. Sampathkumar, "Hall effects on dusty nanofluid two-phase transient flow past a stretching sheet using KVL model," *Journal of Molecular Liquids*, vol. 256, pp. 139–147, 2018.
- [33] A. Aghanajafi, D. Toghraie, and B. Mehmndoust, "Numerical simulation of laminar forced convection of water-CuO nanofluid inside a triangular duct," *Physica E: Low-dimensional Systems and Nanostructures*, vol. 85, pp. 103–108, 2017.
- [34] A. Hussain, M. Y. Malik, T. Salahuddin, S. Bilal, and M. Awais, "Combined effects of viscous dissipation and Joule heating on MHD Sisko nanofluid over a stretching cylinder," *Journal of Molecular Liquids*, vol. 231, pp. 341–352, 2017.
- [35] C. S. K. Raju, N. Sandeep, and A. Malvandi, "Free convective heat and mass transfer of MHD non-Newtonian nanofluids over a cone in the presence of non-uniform heat source/sink," *Journal of Molecular Liquids*, vol. 221, pp. 108–115, 2016.
- [36] T. Hayat, S. A. Shehzad, M. Qasim, and S. Obaidat, "Radiative flow of Jeffery fluid in a porous medium with power law heat flux and heat source," *Nuclear Engineering and Design*, vol. 243, pp. 15–19, 2012.
- [37] J. P. Hartnett and M. Kostic, "Heat transfer to Newtonian and non-Newtonian fluids in rectangular ducts," *Advances in Heat Transfer*, vol. 19, pp. 247–356, 1989.
- [38] I. Dapra and G. Scarpi, "Perturbation solution for pulsatile flow of a non-Newtonian Williamson fluid in a rock fracture," *International Journal of Rock Mechanics and Mining Sciences*, vol. 44, no. 2, pp. 271–278, 2007.
- [39] S. Nadeem and S. T. Hussain, "Flow and heat transfer analysis of Williamson nanofluid," *Applied Nanoscience*, vol. 4, no. 8, pp. 1005–1012, 2014.

Research Article

Zero and Nonzero Mass Flux Effects of Bioconvective Viscoelastic Nanofluid over a 3D Riga Surface with the Swimming of Gyrotactic Microorganisms

T. S. Karthik,¹ K. Loganathan ,² A. N. Shankar,³ M. Jemimah Carmichael,⁴ Anand Mohan,⁵ Mohammed K. A. Kaabar ,⁶ and Safak Kayikci ⁷

¹Department of Electronics and Communication Engineering, Aditya College of Engineering and Technology, Surampalem, 533 437 Andhra Pradesh, India

²Research and Development Wing, Live4Research, Tiruppur, 638 106 Tamilnadu, India

³Department of HSE Civil Engineering, University of Petroleum Energy Studies, Uttarakhand, India

⁴Department of Civil Engineering, Vignan's Lara Institute of Technology and Science, Guntur, Andhra Pradesh, India

⁵Department of Physics, LN Mithila University, Darbhanga, Bihar, India

⁶Jabalía Camp, UNWRA Palestinian Refugee Camp, Gaza Strip Jabalya, State of Palestine

⁷Department of Computer Engineering, Bolu Abant İzzet Baysal University, Bolu, Turkey

Correspondence should be addressed to K. Loganathan; loganathankaruppusamy304@gmail.com and Mohammed K. A. Kaabar; mohammed.kaabar@wsu.edu

Received 25 March 2021; Revised 15 May 2021; Accepted 11 June 2021; Published 16 July 2021

Academic Editor: Mustafa Inc

Copyright © 2021 T. S. Karthik et al. This is an open access article distributed under the Creative Commons Attribution License, which permits unrestricted use, distribution, and reproduction in any medium, provided the original work is properly cited.

This work addresses 3D bioconvective viscoelastic nanofluid flow across a heated Riga surface with nonlinear radiation, swimming microorganisms, and nanoparticles. The nanoparticles are tested with zero (passive) and nonzero (active) mass flux states along with the effect of thermophoresis and Brownian motion. The physical system is visualized via high linearity PDE systems and nondimensionalized to high linearity ordinary differential systems. The converted ordinary differential systems are solved with the aid of the homotopy analytic method (HAM). Several valuable and appropriate characteristics of related profiles are presented graphically and discussed in detail. Results of interest such as the modified Hartmann number, mixed convection parameter, bioconvection Rayleigh number, and Brownian motion parameter are discussed in terms of various profiles. The numerical coding is validated with earlier reports, and excellent agreement is observed. The microorganisms are utilized to improve the thermal conductivity of nanofluid, and this mechanism has more utilization in the oil refinery process.

1. Introduction

“Bioconvection” is known to be the convective movement within sight of swimming microorganisms. In this convective mode, the cells with bottom-heavy cells tend to swim at an angle to vertical, and this process is known as gyrotactic [1]. Therefore, the gyrotactic microorganisms are stable in the upper layer of the fluid, and consequently, stratification of the top-heavy fluid layer will become unbalanced. Thus, the system, which consists of a gyrotactic microorganism, induces one of the exciting characters in heat transfer that is “stability.” The reason is that nano-

fluids that have higher stability tend to improve the thermal efficiency of the heat exchanger (any energy systems). Hosseinzadeh et al. [2] examined the gyrotactic microorganism influence over a cylindrical surface with cross fluid flow. Mogharrebi et al. [3] present the MHD nanofluid flow towards a rotating cone with motile oxytactic microorganisms. Nowadays, the research on nanofluid through a Riga plate becomes an exciting area of research. For instance, mixed convective nanofluid flowed a Riga plate is studied numerically and analytically in [4]. It is shown that the desired size of the nanoparticle influences the skin friction coefficient. Ahmad et al. [5] studied the

role of nanofluid past a heated vertical Riga plate numerically. Influence on viscous dissipation and thermal radiation of nanofluid flow between the Riga plate is explored numerically [6]. They have used carbon nanotubes as the nanoparticle, and it is shown that by varying the radiation parameter, the local heat transfer rate elevates. The application of the Cattaneo-Christov approach heat generation and absorption for the second-grade fluid that passed through the Riga plate is presented numerically [7]. In line with the application of the Riga plate, the stagnation flow on the vacillating Riga plate is studied numerically [8]. The variable thicked Riga plate for melting heat transfer application is explored numerically, and it is reported that for higher values of modified Hartmann number, the velocity profile distribution increases [9]. Recently, several research papers have been devoted to the study of nanofluid and their applications in practical situations [10–13].

Further, the study on heat transfer characteristics of nanofluid is widely studied. For instance, viscoelastic fluid with Newtonian heating is numerically studied [14–17]. It is shown that $\text{Al}_2\text{O}_3/\text{water}$ nanofluid exhibits higher performance evaluation criteria. Besides, the study of viscoelastic nanofluid through the Riga plate is extensively studied. A nonuniform heat flux unsteady viscoelastic fluid that is unsteady is numerically investigated [18]. The viscoelastic nanofluid over an unsteady surface that is stretchable is evaluated numerically [19]. Also, the magnetic field effect on the Maxwell viscoelastic nanofluid over a plate that is moving at a uniform velocity is numerically assessed [20]. The temperature and velocity relaxation time influencing the heat transfer rate of the nanofluid are concluded by them. Besides that, the nonlinear effects on the MHD stagnation flow of viscoelastic nanofluid are explored numerically [21]. The Homotopy Analysis Method (HAM) is employed by Hayat et al. [22] to solve the 3D flow of a viscoelastic nanofluid over a stretching surface. The same research group extended their work towards the viscoelastic model for various applications [23–25]. A slew of researchers studies the gyrotactic microorganism impact. For example, mixed convection of nanofluid containing third-grade nanomaterial containing gyrotactic microorganisms is figured out numerically [26]. Walters B nanofluid with the incorporation of gyrotactic microorganisms is evaluated numerically [27]. Acharya et al. [28] reported the effects of solar radiation bioconvection nanofluid with gyrotactic microorganisms. The suspension of microorganisms induced with the effect of the magnetic field is reported [29, 30]. Also, numerous researches on gyrotactic microorganisms are studied and explored [30–35]. Analysis of active and passive controls with the chemical reaction of nanofluid is analyzed [36]. Using the homotopy perturbation method, unsteady nanofluid with active and passive controls is developed by Acharya et al. [37]. Over a bent surface, the active-passive control of dihydrogen monoxide nanofluid is explored numerically [38]. These controls are studied in various nanofluids with diverse applications [39–44].

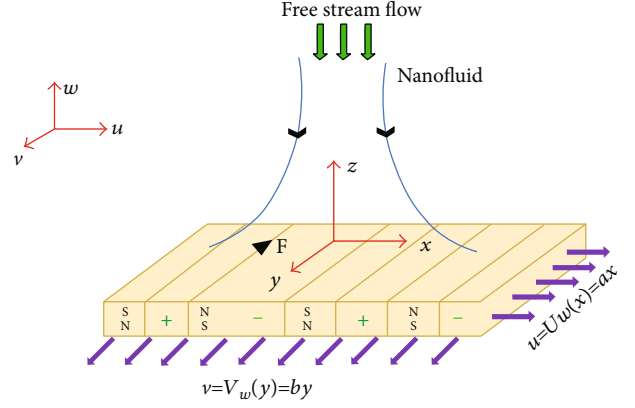


FIGURE 1: Geometry of flow problem.

By considering the earlier reports, it is concluded that no studies were found to analyze the bioconvection of viscoelastic nanofluid on a 3D Riga surface with a comparison of active and passive control. The present study explores the 3D viscoelastic nanofluid flow across the heated Riga surface with nonlinear radiation and heat generation/absorption effects. The effects of several parameters are compared with the active and passive control model of nanoparticles. The homotopy analytic method [45–51] is employed to study the present nonlinear ODE systems. The results are discussed in terms of various profiles. The numerical coding of the present study is validated with earlier reports. The relevant research is applied to multiple engineering streams like bioengineering, chemical, nuclear, thermal, and mechanical.

2. Problem Development

We have considered bioconvective viscoelastic nanofluid flow with $u_w = ax$ in the x direction $v_w = by$ in the y direction over a 3D Riga surface with gyrotactic microorganisms swimming. The surface is expanding in all three directions, namely, x , y , and z . It is assumed that nanoparticles do not influence the swimming microorganism; also, the nanoparticles are assumed to be stable in the fluid layer. Also, the nanoparticles have no effect on the velocity and temperature of the swimming microorganisms. The geometrical configuration is shown in Figure 1. By considering the above assumptions, the governing equations are described below [42]:

$$\begin{aligned} \frac{\partial u}{\partial x} + \frac{\partial v}{\partial y} + \frac{\partial w}{\partial z} &= 0, \\ u \frac{\partial u}{\partial x} + v \frac{\partial u}{\partial y} + w \frac{\partial u}{\partial z} &= v \frac{\partial^2 u}{\partial z^2} \\ &- \alpha \left[u \frac{\partial^3 u}{\partial x \partial z^2} + w \frac{\partial^3 u}{\partial z^3} - \frac{\partial u}{\partial x} \frac{\partial^2 u}{\partial z^2} - \frac{\partial u}{\partial z} \frac{\partial^2 w}{\partial z^2} - 2 \frac{\partial u}{\partial z} \frac{\partial^2 u}{\partial x \partial z} - 2 \frac{\partial w}{\partial z} \frac{\partial^2 u}{\partial z^2} \right] \\ &+ \frac{1}{\rho_f} \left[(1 - C_\infty) \rho_f \beta g (T - T_\infty) - (\rho_p - \rho_f) g (C - C_\infty) \right. \\ &\left. - (n - n_\infty) g \omega (\rho_m - \rho_f) \right] + \frac{\pi j_0 M_0 \exp(-(\pi/e)z)}{8\rho}, \end{aligned}$$

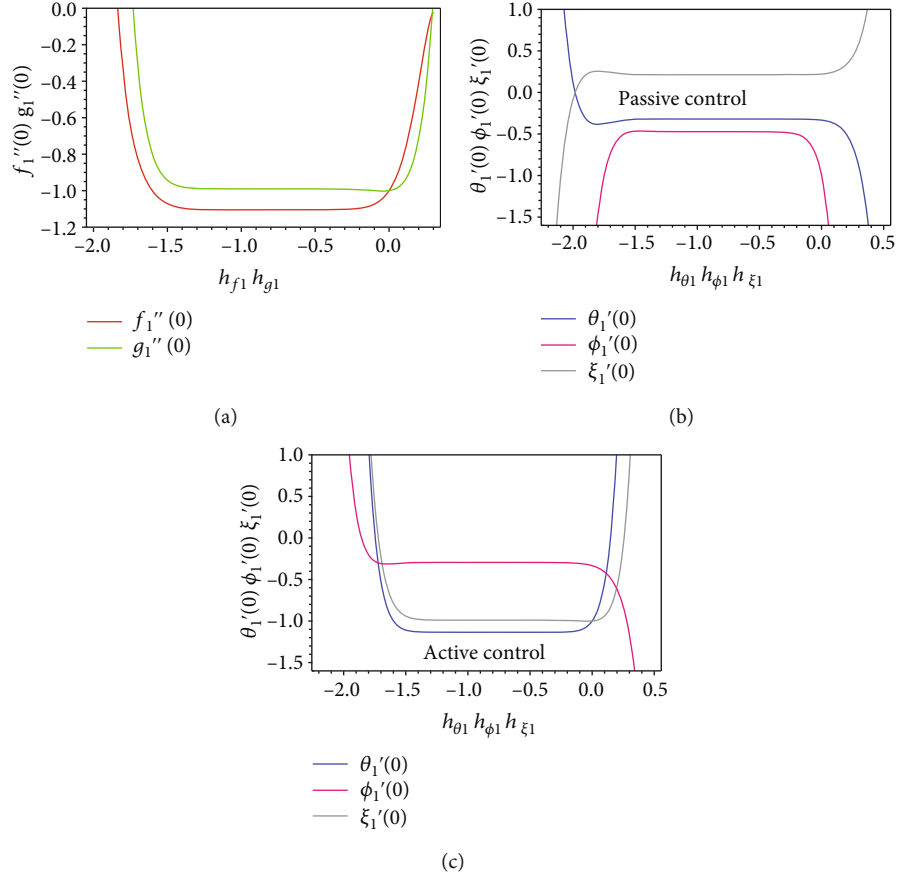


FIGURE 2: Convergence plots of the HAM solution.

$$u \frac{\partial v}{\partial x} + v \frac{\partial v}{\partial y} + w \frac{\partial v}{\partial z} = v \frac{\partial^2 v}{\partial z^2} - \alpha \left[v \frac{\partial^3 v}{\partial y \partial z^2} + w \frac{\partial^3 v}{\partial z^3} - \frac{\partial v}{\partial y} \frac{\partial^2 v}{\partial z^2} - \frac{\partial v}{\partial z} \frac{\partial^2 w}{\partial z^2} - 2 \frac{\partial v}{\partial z} \frac{\partial^2 v}{\partial y \partial z} - 2 \frac{\partial w}{\partial z} \frac{\partial^2 v}{\partial z^2} \right],$$

$$\rho c_p \left[u \frac{\partial T}{\partial x} + v \frac{\partial T}{\partial y} + w \frac{\partial T}{\partial z} \right] = k \frac{\partial^2 T}{\partial z^2} + \tau \left[D_B \frac{\partial C}{\partial z} \frac{\partial T}{\partial z} + \frac{D_T}{T_\infty} \left(\frac{\partial T}{\partial z} \right)^2 \right] - \frac{\partial q_r}{\partial z} + \frac{Q_0}{\rho c_p} (T - T_\infty),$$

$$u \frac{\partial C}{\partial x} + v \frac{\partial C}{\partial y} + w \frac{\partial C}{\partial z} = D_B \frac{\partial^2 C}{\partial z^2} + \frac{D_T}{T_\infty} \frac{\partial^2 T}{\partial z^2} - K_m (C - C_\infty),$$

$$u \frac{\partial N}{\partial x} + v \frac{\partial N}{\partial y} + w \frac{\partial N}{\partial z} - D_N \left(\frac{\partial^2 N}{\partial z^2} \right) = - \frac{dW_c}{(C_w - C_\infty)} \left[\frac{\partial}{\partial z} \left(N \frac{\partial C}{\partial z} \right) \right].$$

(1)

TABLE 1: Order of approximation for $-f_1''(0)$ and $-g_1''(0)$.

Order of approximation	$-f_1''(0)$		$-g_1''(0)$	
	Active	Passive	Active	Passive
1	1.1062	1.0642	1.0062	1.0437
5	1.1410	1.0997	0.9900	1.0467
10	1.1409	1.1019	0.9892	1.0456
15	1.1408	1.1023	0.9892	1.0455
20	1.1408	1.1025	0.9892	1.0455
25	1.1408	1.1025	0.9892	1.0454
30	1.1408	1.1025	0.9892	1.0454
35	1.1408	1.1025	0.9892	1.0454

With boundary conditions

$$\begin{aligned} u(x, y, 0) &= ax, v(x, y, 0) = by, w(x, y, 0) = 0, -k \frac{\partial T}{\partial z}(x, y, 0) \\ &= h_f [T_f(x, y, 0) - T(x, y, 0)], C(x, y, 0) \\ &= C_w(x), (\text{AC}), D_B \frac{\partial C}{\partial z}(x, y, 0) + \frac{D_T}{T_\infty} \frac{\partial T}{\partial z}(x, y, 0) \\ &= 0, (\text{PC}) N(x, y, 0) = N_w(x), \end{aligned}$$

(2)

$$\begin{aligned}
u(x, y, \infty) = 0, v(x, y, \infty) = 0, \frac{\partial u}{\partial z}(x, y, \infty) = 0, \frac{\partial v}{\partial z}(x, y, \infty) \\
= 0, T(x, y, \infty) = T_\infty, C(x, y, \infty) = C_\infty, N(x, y, \infty) \\
= N_\infty.
\end{aligned} \quad (3)$$

Now, we state the nondimensional similarity variables below:

$$\begin{aligned}
f_1'(\eta) &= \frac{u}{ax}, \eta = \left(\frac{a}{v}\right)^{0.5} z, g_1'(\eta) = \frac{v}{ay}, [f_1(\eta) + g_1(\eta)] \\
&= -\frac{w}{(av)^{0.5}}, \theta(\eta) = \frac{T - T_\infty}{T_f - T_\infty}, \phi(\eta) \\
&= \frac{C - C_\infty}{C_w - C_\infty} (\text{AC}), \phi(\eta) = \frac{C - C_\infty}{C_\infty} (\text{PC}), \xi(\eta) \\
&= \frac{N - N_\infty}{N_w - N_\infty}.
\end{aligned} \quad (4)$$

Using the transformations in Equation (1), we get

$$\begin{aligned}
&f_1''' - (f_1')^2 + (f_1 + g_1)f_1'' + \gamma \left[(f_1 + g_1)f_1^{iv} + (f_1'' - g_1'')f_1'' - 2(f_1' + g_1')f_1''' \right] \\
&+ (\lambda\theta_1 - \text{Nr}\phi_1 - \text{Rb}\xi_1) + Qe^{-d_1\eta} = 0, \\
&g_1''' - (g_1')^2 + (f_1 + g_1)g_1'' + \gamma \left[(f_1 + g_1)g_1^{iv} + (f_1'' - g_1'')g_1'' - 2(f_1' + g_1')g_1''' \right] = 0, \\
&\frac{1}{\text{Pr}}\theta_1'' + \frac{\text{Rd}}{\text{Pr}}((\theta_1(\theta_w - 1) + 1))^2(3\theta_1'^2(\theta_w - 1) + (\theta_1(\theta_w - 1) + 1)\theta_1'') \\
&+ (f_1 + g_1)\theta_1' + \text{Nb}\phi_1'\theta_1' + \text{Nt}(\theta_1')^2 + \text{Hg}\theta, \\
&\phi_1''' + \text{Le}(f_1 + g_1)\phi_1' + \frac{\text{Nt}}{\text{Nb}}\theta_1'' - \text{LeCr}\phi_1 = 0,
\end{aligned}$$

$$\xi_1'' + \text{Lb}(f_1 + g_1)\xi_1' - P_e \left[\phi_1''(\xi_1 + \Omega) + \phi_1'\xi_1' \right] = 0. \quad (5)$$

Boundary condition (2) and (3) in expressions of f_1 , g_1 , θ_1 , ϕ_1 , and ξ_1 is developed:

$$\begin{aligned}
f_1(0) = 0, g_1(0) = 0, f_1'(0) = 1, g_1'(0) = \epsilon, f_1'(\infty) = 0, g_1'(\infty) = 0, \\
f_1''(\infty) = 0, g_1''(\infty) = 0, \theta_1'(0) = -\text{Bi}(1 - \theta_1(0)), \theta_1(\infty) = 0, \\
\text{Nb}\phi_1' + \text{Nt}\theta_1' = 0, \phi_1(\infty) = 0 (\text{PC}), \\
\phi_1(0) = 1, \phi_1(\infty) = 0 (\text{AC}), \\
\xi_1(0) = 1, \xi_1(\infty) = 0.
\end{aligned} \quad (6)$$

TABLE 2: Order of approximation for $-\theta_1'(0)$, $-\phi_1'(0)$, and $-\xi_1'(0)$.

Order of approximation	$-\theta_1'(0)$		$-\phi_1'(0)$		$-\xi_1'(0)$	
	Active	Passive	Active	Passive	Active	Passive
1	0.3141	0.3241	0.975	— 0.2161	0.917	0.6363
5	0.3010	0.3196	0.9274	— 0.2131	0.8585	0.4737
10	0.3003	0.3193	0.9334	— 0.2129	0.8653	0.4657
15	0.3002	0.3193	0.9336	— 0.2129	0.8657	0.4645
20	0.3002	0.3193	0.9336	— 0.2129	0.8657	0.4641
25	0.3002	0.3193	0.9336	— 0.2129	0.8657	0.4641
30	0.3002	0.3193	0.9336	— 0.2129	0.8657	0.4641
35	0.3002	0.3193	0.9336	— 0.2129	0.8657	0.4641

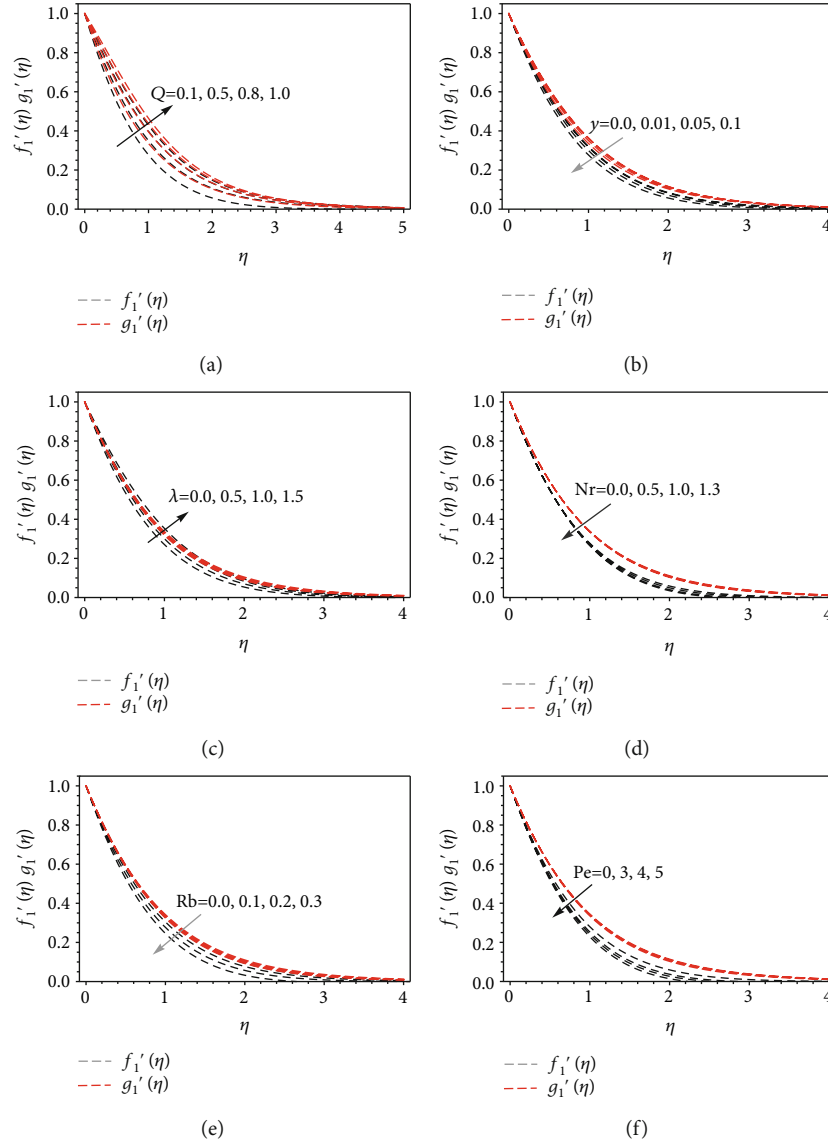
TABLE 3: Comparison of $-f_1''(0)$ and $-g_1''(0)$ for various values of ϵ with limiting conditions $Q = d_1 = \lambda = \text{Nr} = \text{Rb} = 0$.

ϵ	$-f_1''(0)$		$-g_1''(0)$	
	Qayyum et al. [14]	Present	Qayyum et al. [14]	Present
0.0	1.000000	1.00000	0.000000	0.00000
0.1	1.020259	1.02026	0.066947	0.06685
0.2	1.039495	1.03950	0.148736	0.14874
0.3	1.057954	1.05795	0.243359	0.24336
0.4	1.075788	1.07579	0.349208	0.34921
0.5	1.093095	1.09309	0.465204	0.46521
0.6	1.109946	1.10995	0.590528	0.59053
0.7	1.126397	1.12640	0.724531	0.72453
0.8	1.142488	1.14249	0.866682	0.86668
0.9	1.158253	1.15825	1.016538	1.01654
1.0	1.173720	1.17371	1.173720	1.17371

The dimensionless variables are

$$\begin{aligned}
\gamma &= \frac{\alpha a}{v}, \epsilon = \frac{b}{a}, \text{Pr} = \frac{\rho c_p}{k}, \text{Bi} = \frac{h_f}{k} \sqrt{\frac{v}{a}}, \text{Nb} = \frac{\tau D_B}{v} C_\infty, \text{Nt} \\
&= \frac{\tau D_T}{v} (T_f - T_\infty), \text{Cr} = \frac{K_m}{a}, \text{Hg} = \frac{Q_0}{\rho c_p a}, Q = \frac{\pi j_0 M_0}{8a^3 x \rho}, \theta_w \\
&= \frac{T_w}{T_\infty}, \text{Lb} = \frac{v}{D_m}, \text{Pe} = \frac{dW_c}{D_m}, \lambda = \frac{\beta \omega (1 - C_\infty)(T_w - T_\infty)}{au_w}, \text{Nr} \\
&= \frac{(\rho_p - \rho_f)(C_w - C_\infty)}{\beta \rho_f (T_f - T_\infty)}, \text{Rb} = \frac{\omega(N_w - N_\infty)(\rho_m - \rho_f)}{\beta \rho_f (1 - C_\infty)(T_f - T_\infty)}.
\end{aligned} \quad (7)$$

The nondimensional structure of surface drag force (C_{fx} & C_{fy}) and heat transfer rate (Nu), mass transfer rate (Sh),

FIGURE 3: Velocity profile on x and y directions for various values of Q , γ , λ , Nr , Rb , and Pe .

and microorganism (Nn) density number is stated as

$$C_{fx} \text{Re}^{0.5} = \left[f_1'' + \gamma \left\{ 2f_1' f_1'' - f_1''' (f_1 + g_1) + (f_1' + g_1') f_1'' \right\} \right]_{\eta=0},$$

$$C_{fy} \text{Re}^{0.5} = \left[g_1'' + \gamma \left\{ 2g_1' g_1'' - g_1''' (f_1 + g_1) + (f_1' + g_1') g_1'' \right\} \right]_{\eta=0},$$

$$\text{Nu} \text{Re}^{-0.5} = - \left[1 + \frac{4}{3} \text{Rd}(\theta_w)^3 \right]_{\eta=0},$$

$$\text{Sh} \text{Re}^{-0.5} = - \left[\phi_1' \right]_{\eta=0} \text{ (AC)},$$

$$\text{Sh} \text{Re}^{-0.5} = \left[\frac{\text{Nt}}{\text{Nb}} \theta_1' \right]_{\eta=0} \text{ (PC)},$$

$$\text{Nn} \text{Re}^{-0.5} = - \left[\xi_1' \right]_{\eta=0}.$$

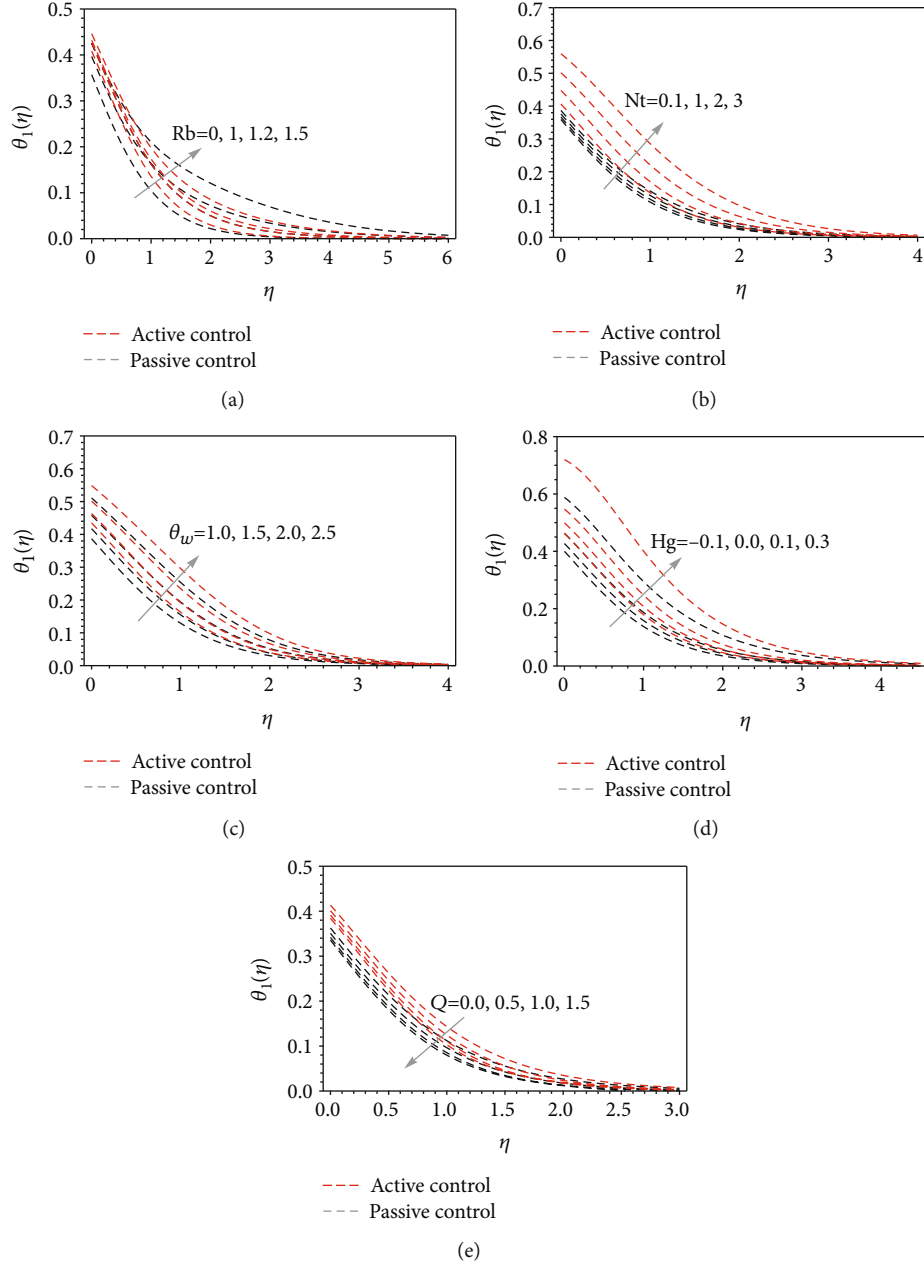
(8)

3. Solution Approach: Homotopy Analysis Method (HAM)

The primary assumptions of the homotopy analytic method are stated as follows:

$$\begin{aligned} f_{1(0)} &= 1 - \exp(-\eta), g_{1(0)} = \epsilon * 1 - \exp(-\eta), \theta_{1(0)} \\ &= \frac{\text{Bi} * \exp(-\eta)}{1 + \text{Bi}}, \phi_{1(0)} = \exp(-\eta) \text{ (AC)}, \phi_{1(0)} \\ &= - \left(\frac{\text{Nt}}{\text{Nb}} \right) * \frac{\text{Bi} * \exp(-\eta)}{1 + \text{Bi}} \text{ (PC)}, \xi_{1(0)} = \exp(-\eta). \end{aligned} \quad (9)$$

The auxiliary linear operators L_{f_1} , L_{g_1} , L_{θ_1} , L_{ϕ_1} , and L_{ξ_1}

FIGURE 4: Temperature profiles for various values of Rb, Nt, Hg, θ_w , and Q.

are derived as

$$\begin{aligned} L_{f_1} &= f_1'''(\eta) - f_1'(\eta), L_{g_1} = g_1'''(\eta) - g_1'(\eta), L_{\theta_1} \\ &= \theta_1''(\eta) - \theta_1(\eta), L_{\phi_1} = \phi_1''(\eta) - \phi_1(\eta), L_{\xi_1} \\ &= \xi_1''(\eta) - \xi_1(\eta). \end{aligned} \quad (10)$$

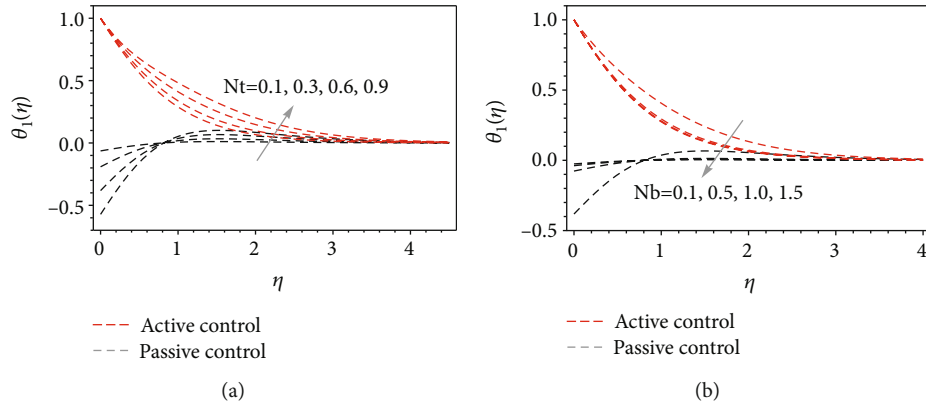
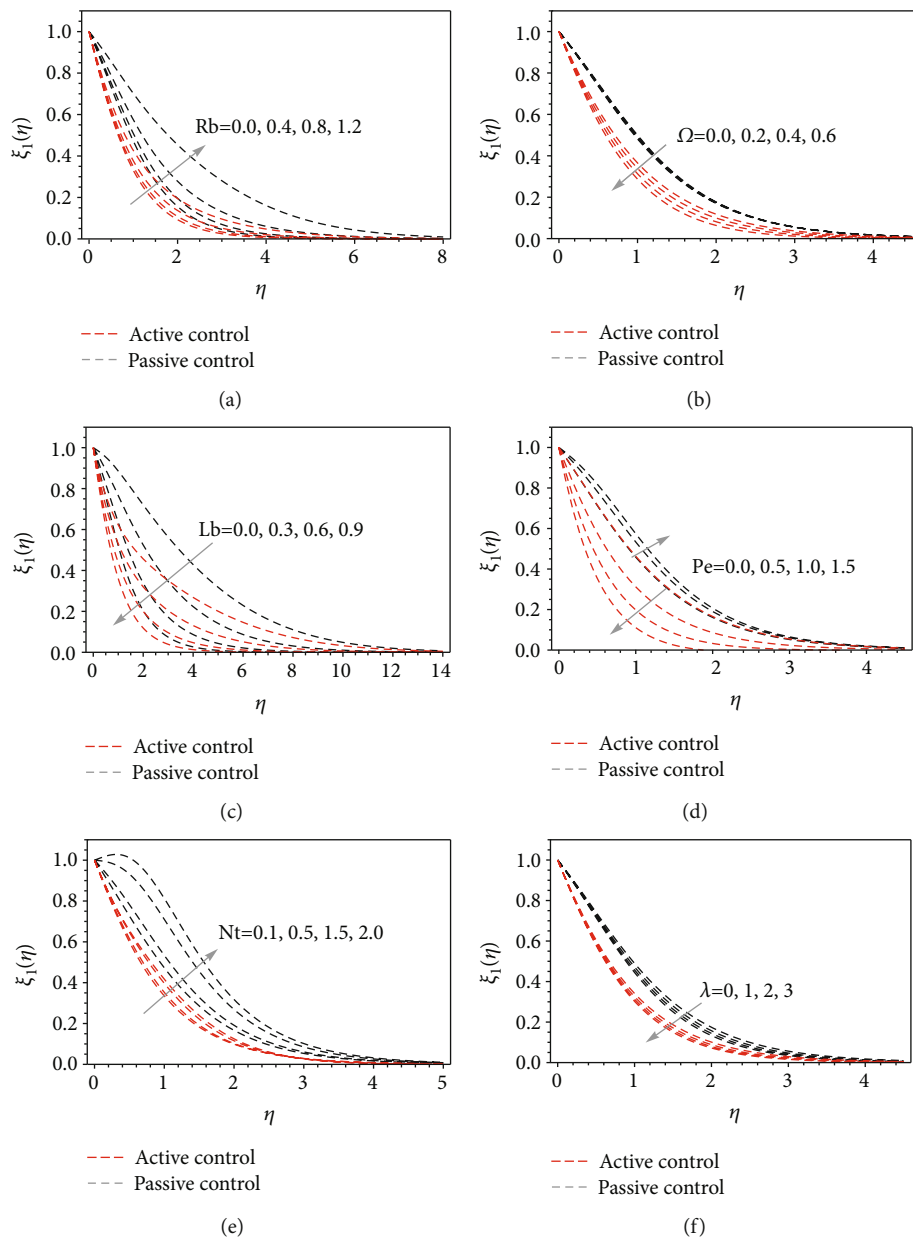
The above linear operators satisfying

$$\begin{aligned} L_{f_1} [S_1 + S_2 e^\eta + S_3 e^{-\eta}] &= 0, L_{g_1} [S_4 + S_5 e^\eta + S_6 e^{-\eta}] \\ &= 0, L_{\theta_1} [S_7 e^\eta + S_8 e^{-\eta}] = 0, L_{\phi_1} [S_9 e^\eta + S_{10} e^{-\eta}] \\ &= 0, L_{\xi_1} [S_{11} e^\eta + S_{12} e^{-\eta}] = 0. \end{aligned} \quad (11)$$

The appropriate solutions $[f_{1m}^*, g_{1m}^*, \theta_{1m}^*, \phi_{1m}^*, \xi_{1m}^*]$ are

$$\begin{aligned} f_{1m}(\eta) &= f_{1m}^*(\eta) + S_1 + S_2 e^\eta + S_3 e^{-\eta}, \\ g_{1m}(\eta) &= g_{1m}^*(\eta) + S_4 + S_5 e^\eta + S_6 e^{-\eta}, \\ \theta_{1m}(\eta) &= \theta_{1m}^*(\eta) + S_7 e^\eta + S_8 e^{-\eta}, \\ \phi_{1m}(\eta) &= \phi_{1m}^*(\eta) + S_9 e^\eta + S_{10} e^{-\eta}, \\ \xi_{1m}(\eta) &= \xi_{1m}^*(\eta) + S_{11} e^\eta + S_{12} e^{-\eta}, \end{aligned} \quad (12)$$

where $S_j (j = 1 - 12)$ denote the arbitrary conditions.

FIGURE 5: Nanoparticle concentration profile for various values of Nt and Nb .FIGURE 6: Motile density profile for various values of Rb , Ω , Lb , Pe , Nt , and λ .

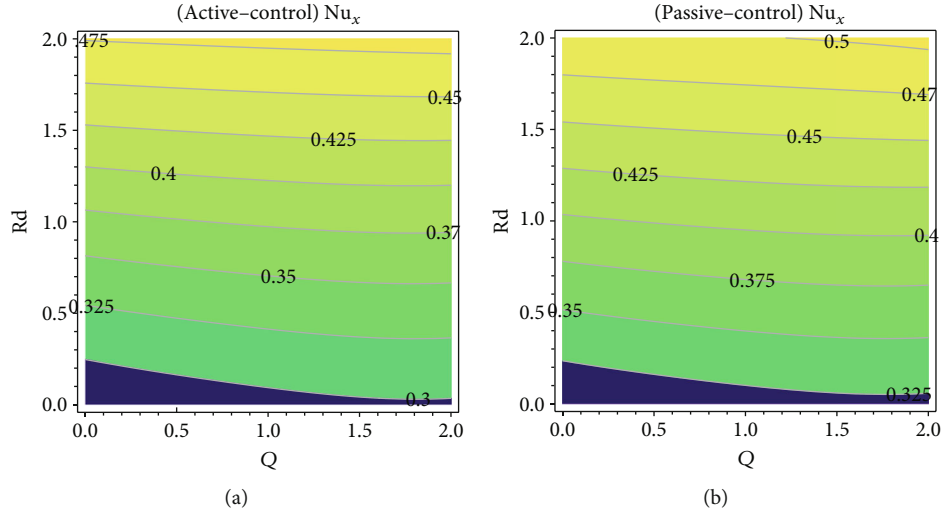


FIGURE 7: The effect of Nusselt number for combined parameters Rd and Q .

4. Convergence Analysis

To analyze the convergence of the numerical code, the convergence analysis is carried out for the value of \mathbf{h} . The variable \mathbf{h} has control over the convergence and divergence of the numerical code, and it is shown in Figure 2. In the case of active and passive control, the values of $\mathbf{h}_f, \mathbf{h}_g, \mathbf{h}_\phi, \mathbf{h}_\theta, \mathbf{h}_\xi$ in the range of $-2.0 \leq \mathbf{h}_f, \mathbf{h}_g, \mathbf{h}_\phi, \mathbf{h}_\theta, \mathbf{h}_\xi \leq 0.5$. For the convergence study in the direction of x and y axes, the value of $\mathbf{h}_f, \mathbf{h}_g$ is in the range of -2.0 to 0.5 , respectively. The order of approximation is shown in Tables 1 and 2. Table 3 reports that the value of $f'_1(0)$ and $g'_1(0)$ is compared with earlier results with Qayyum et al. [14].

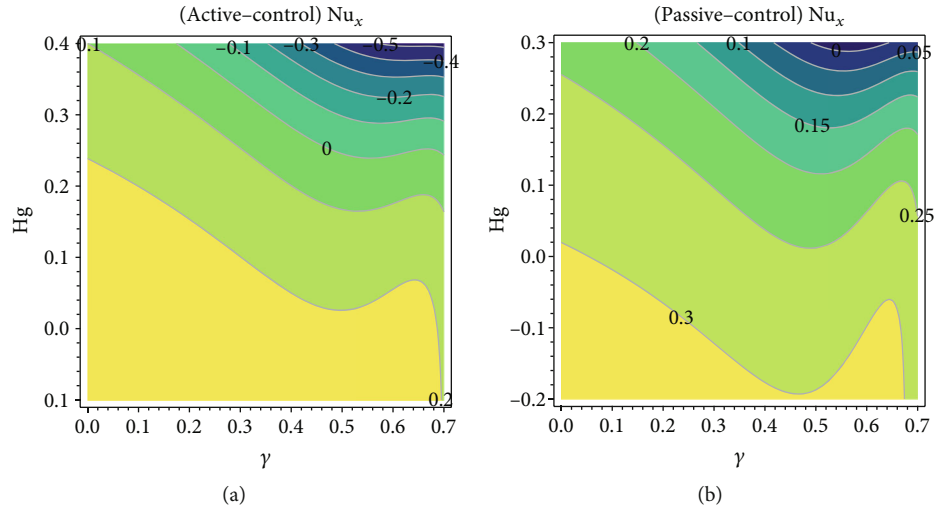
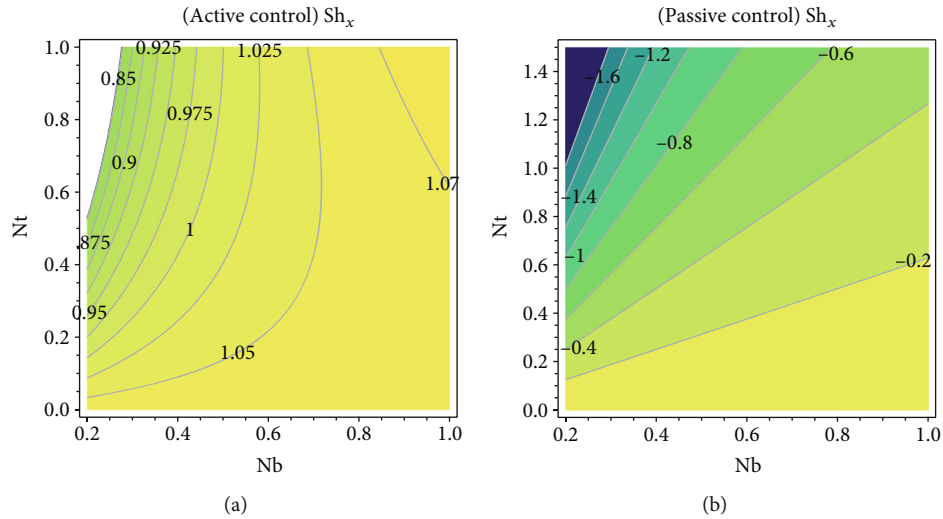
5. Results and Discussions

In this work, viscoelastic nanofluid past a stretching 3D Riga surface with gyrotactic microorganisms is explored numerically. The governing parameters such as velocity (f_1, g_1) parameters, temperature (θ_1) parameter, ξ , modified Hartmann number (Q), viscoelastic parameter (γ), mixed convection parameter (λ), buoyancy ratio parameter (Nr), bioconvection Rayleigh number (Rb), bioconvection Peclet number (Pe), heat generation/absorption parameter (Hg), thermophoresis parameter (Nt), and microorganism concentration difference parameter (Ω) are studied.

Figure 3(a) describes the impact of Q (modified Hartmann's number) on the velocity profile. It is observed that with an increase in Q , velocity profiles decrease in both directions (x, y). This is due to the increase in Q leading to an increase in Lorentz force and consequently velocity profile decreases. In Figure 3(b), it is noticed that as the viscoelastic parameter (γ) increases, the velocity profile decreases. In general, tensile stress is generated by viscoelasticity of the fluid. This stress opposes the fluid motion, and finally, the velocities of x and y directions are decays when the values of γ are improved. The increase in velocity profile is noted in

Figure 3(c) with an enhancement in the mixed convection parameter (λ). By definition, λ is the ratio between the buoyancy force and the viscous force. Figure 3(d) reveals that an increase in buoyancy ratio parameter velocity profile decreases. In this work, the thermal and concentration forces are considered, and those forces provide smaller resistance consequently due to this reason that the velocity profile decreases. Also, it is observed in Figure 3(e) that the extending values of bioconvection Rayleigh number have a tendency to diminish the velocity profile. In Figure 3(f), it is noted that an increase in the bioconvection Peclet number produces the diminishing performance in the swimming speed of microorganisms that cause a decreasing trend in the velocity profile.

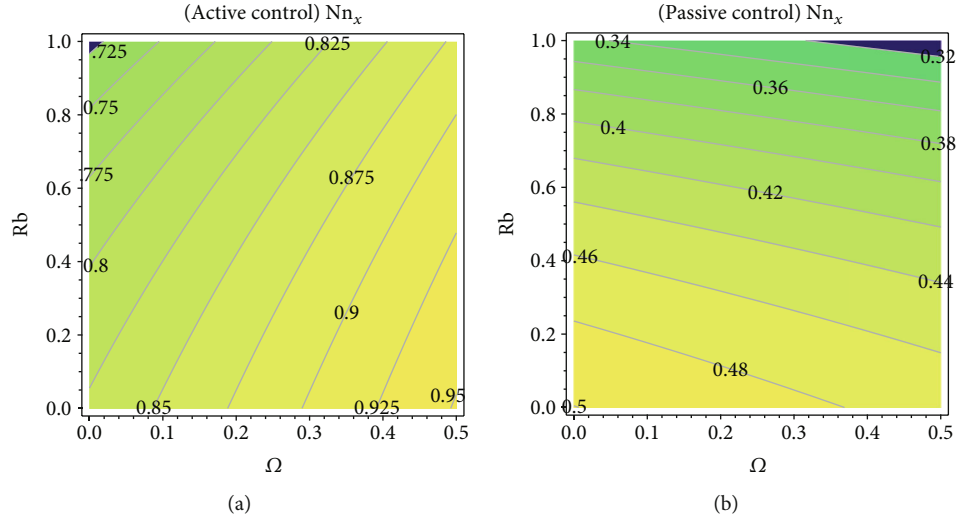
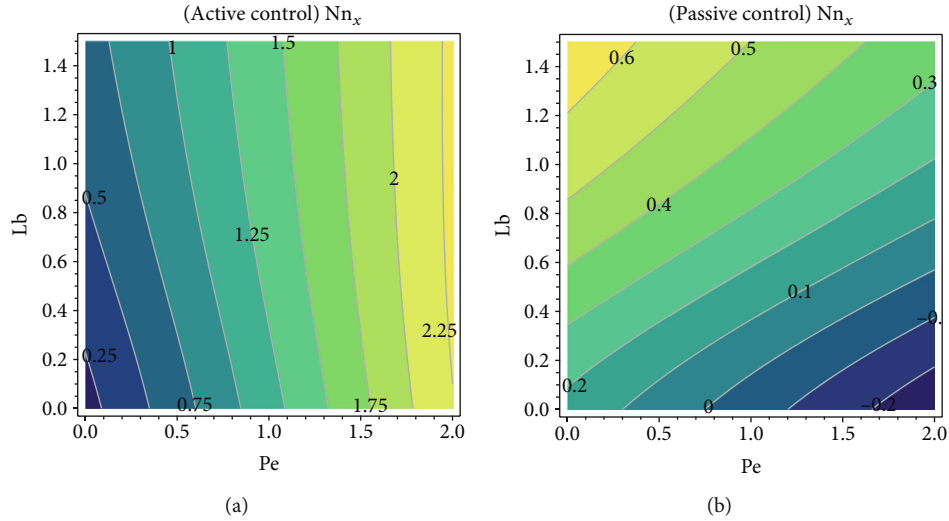
From Figure 4(a), it is evident that the increase in temperature profile increases with an increase in bioconvection Rayleigh number (Rb). In fact, for larger values of Rb , boundary layer thickness increases which increases the buoyancy forces; subsequently, temperature profile increases for both the cases of active and passive controls. The impact of temperature profile with regard to the thermophoresis parameter Nt is discussed in Figure 4(b). With an increase in the thermophoresis parameter, Nt temperature profile is increased. With an increase in Nt , more nanoparticles shifted to the colder place from the hotter one, so the temperature profile increases. An increase in temperature ratio parameter θ_w increases the temperature profile as observed in Figure 4(c). The ratio of temperature at the surface (T_w) to the temperature at free stream (T_∞) is mathematically defined as $\theta_w = T_w/T_\infty$. For nonlinear radiation, the value of θ_w must be higher than 1. Moreover, an increasing trend found in the temperature along the surface is noted for larger θ_w values. Consequently, thermal boundary and associated layer thickness improve. The effect of the heat generation/absorption parameter, Hg on the temperature profile, is proclaimed in Figure 4(d). As we increase Hg , more movement between the nanoparticles is reported; therefore, the temperature profile increases. The slowing moment of the liquid flow due to

FIGURE 8: The effect of Nusselt number for combined parameters Hg and γ .FIGURE 9: The effect of Sherwood number for combined parameters Nt and Nb .

the modified Hartmann number (Q) leads to producing a heat energy, and it is highly pronounced in the lesser value of modified Hartmann number Q , as seen in Figure 4(e).

Figure 5 illustrates the role of nanoparticle volume fraction on (a) thermophoresis parameter (Nt) and (b) Brownian motion parameter (Nb), for active and passive control cases. It is noted that for both behaviours of active and passive control, the Nb value increases. As we increase the Nb value, more resistive force is applied to the surface of the nanoparticle; thus, to increase the heat transfer, the nanoparticle volume fraction has to be increased. This increasing trend is reported in Figure 5(a) for both the cases of active and passive controls. As overturn to the above discussion, it is noted in Figure 5(b) that the volume fraction of nanoparticles decreases with an increase in the Brownian motion parameter, Nb . The fact is that the larger values of the Brownian motion parameter increase the length of the mean free path of the nanoparticle, which incredibly decreases the volume fraction of the nanoparticles.

The influence of the bioconvection Rayleigh number on the concentration of microorganisms is shown in Figure 6(a). With the increase in the Rayleigh number, the movement of microorganisms is increased; consequently, the concentration of microorganisms also increases. The role of the microorganism's concentration difference parameter Ω in concentration is explored in Figure 6(b). For both the cases of active and passive controls, the trend is reported to be the same. In Figure 6(c), it is seen that the concentration of microorganisms increases as the bioconvection Lewis number Lb decreases. It is due to the variation in the temperature difference between the nanoparticles. It is noted in Figure 6(d) that the trend of active and passive control is in an opposite direction for the variation in the bioconvection Peclet number, Pe . As we increase the value of Pe , the diffusivity of microorganisms is decreased. Therefore, the concentration of microorganisms is decreased for passive control. Whereas the scenario is in active control, the trend is increased. The thermophoresis parameter Nt effect on

FIGURE 10: The effect of motile microorganism's density number for combined parameters Rb and Ω .FIGURE 11: The effect of motile microorganism's density number for combined parameters Lb and Pe .

concentration of microorganisms is plotted in Figure 6(e). With the increase of Nt , the low heated nanoparticle is moved into the high heated surface which is induced by the increase in Nt . Hence, the concentration on microorganism is increased. In final, the variation in mixed convection parameter λ is analyzed in Figure 6(f). The increase in λ and the concentration on microorganisms is decreased. While for larger values of λ , temperature variation between the nanoparticles increases; therefore, this strongly affects the concentration of microorganisms.

Figures 7 and 8 depict the heat transfer rate (Nu_x) for different combinations of pertinent parameters. From Figure 7, the heat transfer rate enhances for higher values of modified Hartmann number (Q), and it decays for radiation parameter (Rd). Figure 8 elucidates that heat transfer rates reduce for larger values of γ and Hg . Figure 9 explores the combination of Nb and Nt in the mass transfer rate (Sh_x). It is noted from this figure that the mass transfer rate enhances for the Brownian motion parameter for active control while an opposite

behaviour is noticed for the thermophoresis parameter for both cases. Figures 10 and 11 portray the motile microorganism's density number rate (Nn_x) for different related parameters. From these figures, we found that the combined parameters Rb and Ω and Pe and Lb show the inverse effects on the microorganism's density number rate for active and passive controls.

6. Conclusion

In this work, the active and passive control of viscoelastic nanofluid flow over a 3D Riga plate is investigated analytically by the homotopy technique. Effects are studied with the influence of the gyrotactic microorganism in bioconvective heat transfer. The following outcomes are observed:

- (i) An increase in the modified Hartmann number produces the diminishing impact on velocity profile for both x and y directions

- (ii) Fluid velocity decays in both x and y directions for the augmentation in bioconvection Rayleigh number
- (iii) The microorganism profile is an increasing function of bioconvection Peclet number for active control, and it is decreasing for passive control
- (iv) Mass transfer rate enhances for Brownian motion parameter while an opposite behaviour is noticed for thermophoresis parameter for both cases
- (v) An increase in bioconvection Peclet number produces the inverse phenomena in microorganism profile for active and passive controls

Nomenclature

a, b :	Positive constants (-)
C :	Concentration (kgm^{-3})
C_{∞} :	Ambient concentration (kgm^{-3})
C_w :	Surface concentration of nanoparticles (kgm^{-3})
C_p :	Specific heat ($\text{J kg}^{-1} \text{K}^{-1}$)
C_{fx} :	Skin friction in x direction
C_{fy} :	Skin friction in y direction
d :	Chemotaxis constant (m)
D_B :	Brownian diffusion coefficient ($\text{m}^2 \text{s}^{-1}$)
D_T :	Thermophoretic diffusion coefficient ($\text{m}^2 \text{s}^{-1}$)
D_N :	Microorganism's diffusion coefficient ($\text{m}^2 \text{s}^{-1}$)
$f_1(\eta)$:	Velocity similarity function in x direction (-)
$g_1(\eta)$:	Velocity similarity function in y direction (-)
Hg:	Heat generation/absorption parameter (-)
k :	Thermal conductivity ($\text{m kgs}^{-3} \text{K}^{-1}$)
Le:	Lewis number (-)
L_b :	Bioconvection Lewis number (-)
Nb:	Brownian motion parameter (-)
Nt:	Thermophoresis parameter (-)
n_w :	Surface concentration of microorganisms (kgm^{-3})
n_{∞} :	Ambient concentration of microorganisms (kgm^{-3})
Nr:	Buoyancy ratio parameter (-)
Nu:	Nusselt number (-)
Nn:	Microorganisms' density number (-)
Pr:	Prandtl number (-)
P_e :	Bioconvection Peclet number (-)
Q :	Modified Hartmann number
Q_0 :	Dimensional heat generation/absorption coefficient
Rb:	Bioconvection Rayleigh number (-)
Rd:	Radiation parameter (-)
Sh:	Sherwood number (-)
T :	Temperature (K)
T_{∞} :	Ambient temperature (K)
u_w :	Velocity of the sheet (m s^{-1})
u, v, w :	Velocity components (m s^{-1})
W_c :	Maximum cell swimming speed (m s^{-1})
x, y, z :	Cartesian coordinates (m).

Greeks

α :	Material parameter of fluid
β :	Volume expansion coefficient (-)

γ :	Viscoelastic parameter (-)
$\phi_1(\eta)$:	Concentration similarity function (-)
ϵ :	Stretching ratio
η :	Similarity parameter (-)
$\xi_1(\eta)$:	Microorganisms' similarity function (-)
λ :	Mixed convection parameter (-)
ν :	Kinematic viscosity ($\text{m}^2 \text{s}^{-1}$)
τ :	Ratio of the effective heat capacity (-)
$\theta_1(\eta)$:	Temperature similarity function (-)
ρ :	Density (kgm^{-3})
ρ_f :	Density of nanofluid (kgm^{-3})
ρ_p :	Density of nanoparticles (kgm^{-3})
ρ_m :	Density of microorganism's particles (kgm^{-3})
σ :	Electrical conductivity ($\text{S}^3 \text{m}^2 \text{kg}^{-1}$)
ψ :	Stream function (ms^{-1})
Ω :	Microorganisms' concentration difference parameter (-).

Data Availability

The raw data supporting the conclusions of this article will be made available by the corresponding author without undue reservation.

Conflicts of Interest

The authors declare that they have no conflicts of interest.

Authors' Contributions

All authors listed have made a substantial, direct, and intellectual contribution to the work and approved it for publication.

References

- [1] T. J. Pedley and J. O. Kessler, "Hydrodynamic phenomena in suspensions of swimming microorganisms," *Annual Review of Fluid Mechanics*, vol. 24, no. 1, pp. 313–358, 1992.
- [2] K. Hosseinzadeh, S. Roghani, A. R. Mogharrebi, A. Asadi, M. Waqas, and D. D. Ganji, "Investigation of cross-fluid flow containing motile gyrotactic microorganisms and nanoparticles over a three-dimensional cylinder," *Alexandria Engineering Journal*, vol. 59, no. 5, pp. 3297–3307, 2020.
- [3] A. R. Mogharrebi, A. R. D. Ganji, K. Hosseinzadeh, S. Roghani, A. Asadi, and A. Fazlollahab, "Investigation of magnetohydrodynamic nanofluid flow contain motile oxytactic microorganisms over rotating cone," *International Journal of Numerical Methods for Heat & Fluid Flow*, 2021.
- [4] A. Ahmad, S. Asghar, and S. Afzal, "Flow of nanofluid past a Riga plate," *Journal of Magnetism and Magnetic Materials*, vol. 402, pp. 44–48, 2016.
- [5] R. Ahmad, M. Mustafa, and M. Turkyilmazoglu, "Buoyancy effects on nanofluid flow past a convectively heated vertical Riga- plate: a numerical study," *International Journal of Heat and Mass Transfer*, vol. 111, pp. 827–835, 2017.
- [6] N. Ahmed, Adnan, U. Khan, and S. T. Mohyud-Din, "Influence of thermal radiation and viscous dissipation on squeezed flow of water between Riga plates saturated with carbon

- nanotubes," *Colloids and Surfaces A: Physicochemical and Engineering Aspects*, vol. 522, pp. 389–398, 2017.
- [7] A. Anjum, N. A. Mir, M. Farooq et al., "Physical aspects of heat generation/absorption in the second grade fluid flow due to Riga plate: application of Cattaneo-Christov approach," *Results in Physics*, vol. 9, pp. 955–960, 2018.
 - [8] A. Anjum, N. A. Mir, M. Farooq, M. I. Khan, and T. Hayat, "Influence of thermal stratification and slip conditions on stagnation point flow towards variable thicked Riga plate," *Results in Physics*, vol. 9, pp. 1021–1030, 2018.
 - [9] M. Farooq, A. Anjum, T. Hayat, and A. Alsaedi, "Melting heat transfer in the flow over a variable thicked Riga plate with homogeneous-heterogeneous reactions," *Journal of Molecular Liquids*, vol. 224, pp. 1341–1347, 2016.
 - [10] Y. Menni, A. J. Chamkha, M. Ghazvini et al., "Enhancement of the turbulent convective heat transfer in channels through the baffling technique and oil/multiwalled carbon nanotube nanofluids," *Numerical Heat Transfer, Part A: Applications*, vol. 79, no. 4, pp. 311–351, 2021.
 - [11] K. Loganathan, N. Alessa, K. Tamilvanan, and F. S. Alshammari, "Significances of Darcy–Forchheimer porous medium in third-grade nanofluid flow with entropy features," *The European Physical Journal Special Topics*, 2021.
 - [12] K. Loganathan, K. Mohana, M. Mohanraj, P. Sakthivel, and S. Rajan, "Impact of third-grade nanofluid flow across a convective surface in the presence of inclined Lorentz force: an approach to entropy optimization," *Journal of Thermal Analysis and Calorimetry*, vol. 144, no. 5, pp. 1935–1947, 2021.
 - [13] R. Maouedj, Y. Menni, M. Inc, Y. M. Chu, H. Ameur, and G. Lorenzini, "Simulating the turbulent hydrothermal behavior of oil/MWCNT nanofluid in a solar channel heat exchanger equipped with vortex generators," *Computer Modeling in Engineering & Sciences*, vol. 126, no. 3, pp. 855–889, 2021.
 - [14] A. Qayyum, T. Hayat, M. S. Alhuthali, and H. M. Malaikah, "Newtonian heating effects in three-dimensional flow of viscoelastic fluid," *Chinese Physics B*, vol. 23, no. 5, p. 054703, 2014.
 - [15] M. Sheikholeslami, "New computational approach for exergy and entropy analysis of nanofluid under the impact of Lorentz force through a porous media," *Computer Methods in Applied Mechanics and Engineering*, vol. 344, pp. 319–333, 2019.
 - [16] M. Sheikholeslami, A. N. Keshteli, and H. Babazadeh, "Nanoparticles favorable effects on performance of thermal storage units," *Journal of Molecular Liquids*, vol. 300, p. 112329, 2020.
 - [17] M. Sheikholeslami, M. Jafaryar, A. Shafee, and H. Babazadeh, "Acceleration of discharge process of clean energy storage unit with insertion of porous foam considering nanoparticle enhanced paraffin," *Journal of Cleaner Production*, vol. 261, p. 121206, 2020.
 - [18] S. Khan, S. A. Shehzad, A. Rauf, and Z. Abbas, "Thermally developed unsteady viscoelastic micropolar nanofluid with modified heat/mass fluxes: a generalized model," *Physica A: Statistical Mechanics and its Applications*, vol. 550, p. 123986, 2020.
 - [19] M. Ahmad, T. Muhammad, I. Ahmad, and S. Aly, "Time-dependent 3D flow of viscoelastic nanofluid over an unsteady stretching surface," *Physica A: Statistical Mechanics and its Applications*, vol. 551, p. 124004, 2020.
 - [20] Z. Cao, J. Zhao, Z. Wang, F. Liu, and L. Zheng, "MHD flow and heat transfer of fractional Maxwell viscoelastic nanofluid over a moving plate," *Journal of Molecular Liquids*, vol. 222, pp. 1121–1127, 2016.
 - [21] M. Farooq, M. I. Khan, M. Waqas, T. Hayat, A. Alsaedi, and M. I. Khan, "MHD stagnation point flow of viscoelastic nanofluid with non-linear radiation effects," *Journal of Molecular Liquids*, vol. 221, pp. 1097–1103, 2016.
 - [22] T. Hayat, M. Sajid, and I. Pop, "Three-dimensional flow over a stretching surface in a viscoelastic fluid," *Nonlinear Analysis: Real World Applications*, vol. 9, no. 4, pp. 1811–1822, 2008.
 - [23] T. Hayat, T. Muhammad, A. Alsaedi, and M. S. Alhuthali, "Magnetohydrodynamic three-dimensional flow of viscoelastic nanofluid in the presence of nonlinear thermal radiation," *Journal of Magnetism and Magnetic Materials*, vol. 385, pp. 222–229, 2015.
 - [24] T. Hayat, F. Haider, T. Muhammad, and A. Alsaedi, "On Darcy–Forchheimer flow of viscoelastic nanofluids: a comparative study," *Journal of Molecular Liquids*, vol. 233, pp. 278–287, 2017.
 - [25] T. Hayat, S. Qayyum, S. A. Shehzad, and A. Alsaedi, "Cattaneo–Christov double-diffusion theory for three-dimensional flow of viscoelastic nanofluid with the effect of heat generation/absorption," *Results in Physics*, vol. 8, pp. 489–495, 2018.
 - [26] E. O. Alzahrani, Z. Shah, A. Dawar, and S. J. Malebary, "Hydromagnetic mixed convective third grade nanomaterial containing gyrotactic microorganisms toward a horizontal stretched surface," *Alexandria Engineering Journal*, vol. 58, no. 4, pp. 1421–1429, 2019.
 - [27] R. Naz, S. Tariq, and H. Alsulami, "Inquiry of entropy generation in stratified Walters' B nanofluid with swimming gyrotactic microorganisms," *Alexandria Engineering Journal*, vol. 59, no. 1, pp. 247–261, 2020.
 - [28] N. Acharya, K. Das, and P. K. Kundu, "Framing the effects of solar radiation on magneto-hydrodynamics bioconvection nanofluid flow in presence of gyrotactic microorganisms," *Journal of Molecular Liquids*, vol. 222, pp. 28–37, 2016.
 - [29] W. Khan and O. D. Makinde, "MHD nanofluid bioconvection due to gyrotactic microorganisms over a convectively heat stretching sheet," *International Journal of Thermal Sciences*, vol. 81, pp. 118–124, 2014.
 - [30] M. Ijaz Khan, M. Waqas, T. Hayat, M. Imran Khan, and A. Alsaedi, "Behavior of stratification phenomenon in flow of Maxwell nanomaterial with motile gyrotactic microorganisms in the presence of magnetic field," *International Journal of Mechanical Sciences*, vol. 131–132, pp. 426–434, 2017.
 - [31] H. Waqas, S. U. Khan, M. Hassan, M. M. Bhatti, and M. Imran, "Analysis on the bioconvection flow of modified second-grade nanofluid containing gyrotactic microorganisms and nanoparticles," *Journal of Molecular Liquids*, vol. 291, p. 111231, 2019.
 - [32] M. T. Sk, K. Das, and P. K. Kundu, "Multiple slip effects on bioconvection of nanofluid flow containing gyrotactic microorganisms and nanoparticles," *Journal of Molecular Liquids*, vol. 220, pp. 518–526, 2016.
 - [33] E. Elanchezhian, R. Nirmalkumar, M. Balamurugan, K. Mohana, K. M. Prabu, and A. Vilorio, "Heat and mass transmission of an Oldroyd-B nanofluid flow through a stratified medium with swimming of motile gyrotactic microorganisms and nanoparticles," *Journal of Thermal Analysis and Calorimetry*, vol. 141, no. 6, pp. 2613–2623, 2020.
 - [34] K. Hosseinzadeh, S. Roghani, A. R. Mogharrebi, A. Asadi, and D. D. Ganji, "Optimization of hybrid nanoparticles with mixture fluid flow in an octagonal porous medium by effect of radiation and magnetic field," *Journal of Thermal Analysis and Calorimetry*, vol. 143, no. 2, pp. 1413–1424, 2021.

- [35] M. Ijaz Khan, F. Haq, S. A. Khan, T. Hayat, and M. Imran Khan, "Development of thixotropic nanomaterial in fluid flow with gyrotactic microorganisms, activation energy, mixed convection," *Computer Methods and Programs in Biomedicine*, vol. 187, p. 105186, 2020.
- [36] G. K. Ramesh, "Analysis of active and passive control of nanoparticles in viscoelastic nanomaterial inspired by activation energy and chemical reaction," *Physica A: Statistical Mechanics and its Applications*, vol. 550, p. 123964, 2020.
- [37] N. Acharya, K. Das, and P. Kumar Kundu, "Fabrication of active and passive controls of nanoparticles of unsteady nanofluid flow from a spinning body using HPM," *The European Physical Journal Plus*, vol. 132, no. 7, p. 323, 2017.
- [38] N. Acharya, "Active-passive controls of liquid di-hydrogen mono-oxide based nanofluidic transport over a bended surface," *International Journal of Hydrogen Energy*, vol. 44, no. 50, pp. 27600–27614, 2019.
- [39] S. S. Giri, K. Das, and P. K. Kundu, "Stefan blowing effects on MHD bioconvection flow of a nanofluid in the presence of gyrotactic microorganisms with active and passive nanoparticles flux," *The European Physical Journal Plus*, vol. 132, no. 2, 2017.
- [40] T. Hayat, A. Aziz, T. Muhammad, and A. Alsaedi, "Active and passive controls of Jeffrey nanofluid flow over a nonlinear stretching surface," *Results in Physics*, vol. 7, pp. 4071–4078, 2017.
- [41] J. Jiang and X. Yu, "Fault-tolerant control systems: a comparative study between active and passive approaches," *Annual Reviews in Control*, vol. 36, no. 1, pp. 60–72, 2012.
- [42] S. Eswaramoorthi and M. Bhuvaneswari, "Passive and active control on 3D convective flow of viscoelastic nanofluid with heat generation and convective heating," *Frontiers of Mechanical Engineering*, vol. 5, 2019.
- [43] R. Tripathi, G. S. Seth, and M. K. Mishra, "Double diffusive flow of a hydromagnetic nanofluid in a rotating channel with Hall effect and viscous dissipation: active and passive control of nanoparticles," *Powder Technology*, vol. 28, no. 10, pp. 2630–2641, 2017.
- [44] N. Wang, A. Maleki, M. Alhuyi Nazari, I. Tlili, and M. Safdari Shadloo, "Thermal conductivity modeling of nanofluids contain MgO particles by employing different approaches," *Symmetry*, vol. 12, no. 2, p. 206, 2020.
- [45] S. Liao and Y. A. Tan, "A general approach to obtain series solutions of nonlinear differential equations," *Studies in Applied Mathematics*, vol. 119, no. 4, pp. 297–354, 2007.
- [46] K. Loganathan and S. Rajan, "An entropy approach of Williamson nanofluid flow with joule heating and zero nanoparticle mass flux," *Journal of Thermal Analysis and Calorimetry*, vol. 141, no. 6, pp. 2599–2612, 2020.
- [47] N. Freidoonimehr and A. B. Rahimi, "Brownian motion effect on heat transfer of a three-dimensional nanofluid flow over a stretched sheet with velocity slip," *Journal of Thermal Analysis and Calorimetry*, vol. 135, no. 1, pp. 207–222, 2019.
- [48] K. Loganathan, S. Sivasankaran, M. Bhuvaneswari, and S. Rajan, "Second-order slip, cross-diffusion and chemical reaction effects on magneto-convection of Oldroyd-B liquid using Cattaneo–Christov heat flux with convective heating," *Journal of Thermal Analysis and Calorimetry*, vol. 136, no. 1, pp. 401–409, 2019.
- [49] T. Hayat, M. Ijaz Khan, S. Qayyum, and A. Alsaedi, "Modern developments about statistical declaration and probable error for skin friction and Nusselt number with copper and silver nanoparticles," *Chinese Journal of Physics*, vol. 55, no. 6, pp. 2501–2513, 2017.
- [50] M. Farooq, M. Javed, M. Ijaz Khan, A. Anjum, and T. Hayat, "Melting heat transfer and double stratification in stagnation flow of viscous nanofluid," *Results in Physics*, vol. 7, pp. 2296–2301, 2017.
- [51] K. Loganathan, G. Muhiuddin, A. M. Alanazi, F. S. Alshammari, B. M. Alqurashi, and S. Rajan, "Entropy optimization of third-grade nanofluid slip flow embedded in a porous sheet with zero mass flux and a non-Fourier heat flux model," *Frontiers of Physics*, vol. 8, p. 250, 2020.

Research Article

Iterative Construction of Fixed Points for Operators Endowed with Condition (E) in Metric Spaces

Junaid Ahmad ¹, Kifayat Ullah ², Hüseyin Işık ³, Muhammad Arshad ¹,
and Manuel de la Sen ⁴

¹Department of Mathematics and Statistics, International Islamic University, H-10 Islamabad-44000, Pakistan

²Department of Mathematics, University of Lakki Marwat, Lakki Marwat, 28420 Khyber Pakhtunkhwa, Pakistan

³Department of Engineering Science, Bandırma Onyedi Eylül University, 10200 Bandırma, Balıkesir, Turkey

⁴Institute of Research and Development of Processes, University of the Basque Country, Campus of Leioa (Bizkaia), P.O. Box 644-Bilbao, Barrio Sarriena, 48940 Leioa, Spain

Correspondence should be addressed to Junaid Ahmad; ahmadjunaid436@gmail.com and Hüseyin Işık; isikhuseyin76@gmail.com

Received 22 April 2021; Accepted 14 June 2021; Published 9 July 2021

Academic Editor: Ming Mei

Copyright © 2021 Junaid Ahmad et al. This is an open access article distributed under the Creative Commons Attribution License, which permits unrestricted use, distribution, and reproduction in any medium, provided the original work is properly cited.

We consider the class of mappings endowed with the condition (E) in a nonlinear domain called 2-uniformly convex hyperbolic space. We provide some strong and Δ -convergence theorems for this class of mappings under the Agarwal iterative process. In order to support the main outcome, we procure an example of mappings endowed with the condition (E) and prove that its Agarwal iterative process is more effective than Mann and Ishikawa iterative processes. Simultaneously, our results hold in uniformly convex Banach, CAT(0), and some CAT(κ) spaces. This approach essentially provides a new setting for researchers who are working on the iterative procedures in fixed point theory and applications.

1. Introduction

Choose a metric space \mathcal{X} and $\emptyset \neq S \subseteq \mathcal{X}$. Then, a self-map $\mathcal{L} : S \rightarrow S$ is called nonexpansive if

$$q(\mathcal{L}s, \mathcal{L}s') \leq q(s, s'), \quad \text{for all } s, s' \in S. \quad (1)$$

As many know, Browder [1] (see also Kirk [2] and Gohde [3]) achieved an elementary fixed point theorem for nonexpansive map $\mathcal{L} : S \rightarrow S$ in the case when S is closed bounded convex in any given uniformly convex Banach space (UCBS). This remarkable theorem began the research of different results for nonexpansive maps. Among other things, Kirk [4] obtained this theorem in the nonlinear setting of CAT(0) metric spaces. The class of nonexpansive mappings is very important because of its useful applications in many fields of applied sciences. Thus, it is very natural and essential to study the extension of these maps. In 2008, Suzuki [5] considered an extension of nonexpansive maps by weakening the inequality of the nonexpansive maps in

the following way: a self-map $\mathcal{L} : S \rightarrow S$ is said to hold condition (C) if any given $s, s' \in S$,

$$\frac{1}{2} q(s, \mathcal{L}s) \leq q(s, s') \Rightarrow q(\mathcal{L}s, \mathcal{L}s') \leq q(s, s'). \quad (2)$$

Obviously, a nonexpansive map \mathcal{L} has condition (C), but an example in [5] shows the inverse is not valid in general. In [6], Nanjaras et al. improved the main outcome of Suzuki [5] to the nonlinear setting of CAT(0) spaces. In [7], Phuengratana used Ishikawa iteration [8] for reckoning of fixed points for the class of Suzuki mappings in a Banach space. Also, Basarir and Sahin [9] used Agarwal et al.'s [8] iteration for reckoning fixed points of Suzuki mappings in the nonlinear setting of CAT(0) spaces.

In [10], Garcia-Falset et al. suggested a new type of maps which is properly more general than Suzuki maps. A self-map \mathcal{L} of S is called Garcia-Falset nonexpansive or said to be endowed with the condition (E) if any given $s, s' \in S$, there

is a $\mu \geq 1$ such that

$$q(s, \mathcal{L}s') \leq \mu q(s, \mathcal{L}s) + q(s, s'). \quad (3)$$

Remark 1. If \mathcal{L} is nonexpansive, then it is easy to show $q(s, \mathcal{L}s') \leq q(s, \mathcal{L}s) + q(s, s')$ for each $s, s' \in S$. Hence, every nonexpansive map \mathcal{L} has condition (E) with $\mu = 1$. Similarly, if \mathcal{L} is Suzuki map, then, it satisfies $q(s, \mathcal{L}s') \leq 3q(s, \mathcal{L}s) + q(s, s')$ for every $s, s' \in S$. Hence, every Suzuki map \mathcal{L} has condition (E) with $\mu = 3$. Interestingly, the example constructed in this paper shows that there exists maps satisfying condition (E) but not the converse.

After establishing the existence of a fixed point result for an operator, a natural question arises on how to compute it by any appropriate numerical method. To work on such type of problems is not easy. The well-known Banach Contraction Theorem (BCT) essentially suggests the Picard iteration $y_{k+1} = \mathcal{L}y_k$ to compute the unique fixed point of a given contraction in a metric space. Bagherboum [11] used Ishikawa iteration [12] for computing fixed points of Garcia-Falset mappings in the nonlinear setting of Busemann spaces. We know that the Picard iteration fails for solving nonexpansive problems. Now, we discuss some other methods which are different from the Picard iteration process.

One of the elementary iterative processes is due to Mann [13] stated as follows:

$$\begin{cases} y_1 \in S, \\ y_{k+1} = (1 - \alpha_k)y_k \oplus \alpha_k \mathcal{L}y_k, \end{cases} \quad (4)$$

where $\alpha_k \in [0, 1]$.

The Mann iteration (4) was extended to the setting of two steps by Ishikawa [12] as follows:

$$\begin{cases} y_1 \in S, \\ y_{k+1} = (1 - \alpha_k)y_k \oplus \alpha_k \mathcal{L}w_k, \\ w_k = (1 - \beta_k)y_k \oplus \beta_k \mathcal{L}y_k, \end{cases} \quad (5)$$

where $\alpha_k, \beta_k \in [0, 1]$.

In 2007, Agarwal et al. [8] studied the following iteration for contractions and observed that it is better than the above iterative processes:

$$\begin{cases} y_1 \in S, \\ y_{k+1} = (1 - \alpha_k)\mathcal{L}y_k \oplus \alpha_k \mathcal{L}w_k, \\ w_k = (1 - \beta_k)y_k \oplus \beta_k \mathcal{L}y_k, \end{cases} \quad (6)$$

where $\alpha_k, \beta_k \in [0, 1]$.

In this research, we consider the Agarwal iterative process (6) for the larger class of maps due to Garcia-Falset et al. [10]. We use a very general ground space called 2-uniformly convex hyperbolic metric space for establishing the main outcome. To support our results, we provide an

example of maps with condition (E) and prove that its Agarwal iterative process (6) is more effective than Mann (4) and Ishikawa iterative (5) processes. Simultaneously, our results hold in uniformly convex Banach, CAT(0), and some CAT(κ) spaces. In this way, we extend the corresponding results of Bagherboum [11], Phuengrattana [7], Basarir and Sahin [9], and Nanjaras et al. [6] as we consider the general setting of domain, larger class of maps, and faster iteration process.

Now, we present some well-known definitions and results which will be either used in the main results or to understand the given concept herein.

Definition 2 (see [14]). A given metric space (\mathcal{X}, q) is called Kolenbach-hyperbolic space or simply hyperbolic space when there is a map $C : \mathcal{X} \times \mathcal{X} \times [0, 1] \rightarrow \mathcal{X}$ such that for all $s, s', u, p \in \mathcal{X}$ and $i, j \in [0, 1]$, we have

- (C1) $q(u, C(s, s', i)) \leq (1 - i)q(u, s) + iq(u, s')$;
- (C2) $q(C(s, s', i), C(s, s', j)) = |i - j|q(s, s')$;
- (C3) $C(s, s', i) = C(s', s, 1 - i)$;
- (C4) $q(C(s, u, i), C(s', p, i)) \leq (1 - i)q(s, s') + iq(u, p)$.

Notice that, for given $s, s' \in \mathcal{X}$ and $i \in [0, 1]$, we shall use $(1 - i)s \oplus is'$ for $C(s, s', i)$. Also, the property (C1) gives

$$\begin{aligned} q(s, (1 - i)s \oplus is') &= iq(s, s') \text{ and } q(s', (1 - i)s \oplus is') \\ &= (1 - i)q(s, s'). \end{aligned} \quad (7)$$

Keep in mind that $\emptyset \neq S \subseteq \mathcal{X}$ is said to be convex in \mathcal{X} if for every $s, s' \in S$, $[s, s'] = \{(1 - \sigma)s \oplus \sigma s' : \sigma \in [0, 1]\} \subseteq S$.

Definition 3. A given hyperbolic space (\mathcal{X}, q, C) is said to be a uniformly convex hyperbolic space (UCHS), if there exist $r > 0$, $\sigma \in (0, 1]$ and $\varepsilon \in (0, 2]$ such that for each $s, s', p \in \mathcal{X}$ satisfying $q(s, p) \leq r$, $q(s', p) \leq r$ and $q(s, s') \geq 2\varepsilon$ follows that:

$$q\left(\frac{1}{2}s \oplus \frac{1}{2}s', p\right) \leq (1 - \sigma)r. \quad (8)$$

Moreover, if $f : (0, \infty) \times (0, 2] \rightarrow (0, 1]$ is given such that $\sigma = f(r, \varepsilon)$ for all $r \in (0, \infty)$ and $\varepsilon \in (0, 2]$, then, f is called a modulus of uniform convexity (MUC). Also, f is called monotone modulus of uniform convexity (MMUC) iff non-increasing in the variable r for every chosen fixed ε .

Definition 4. Suppose a pair (\mathcal{X}, q) is a given hyperbolic space. For any $r \in (0, \infty)$ and $\varepsilon \in (0, 2]$, define:

$$\varphi(r, \varepsilon) = \inf \left\{ \frac{1}{2}q^2(s, p) + \frac{1}{2}q^2(s', p) - q^2\left(\frac{1}{2}s \oplus \frac{1}{2}s', p\right) \right\}, \quad (9)$$

and keeping in mind that infimum is taken over every $s, s', p \in \mathcal{X}$ satisfying $q(s, p) \leq r$, $q(s', p) \leq r$, and $q(s, s') \geq 2\varepsilon$. Then, (\mathcal{X}, q) is called 2-uniformly convex hyperbolic space

(2-UCHS) provided that

$$c_M = \inf \left\{ \frac{\varphi(r, \varepsilon)}{r^2 \varepsilon^2} : r \in (0, \infty), \varepsilon \in (0, 2] \right\} > 0. \quad (10)$$

The following remark suggests that 2-UCHS is a more general domain than many other linear and nonlinear spaces.

Remark 5. Any given UCBS, CAT(0) space, and CAT(κ) spaces having $\kappa > 0$ and $\text{diam}(\mathcal{X}) \leq (\pi/2 - \varepsilon/\kappa^{1/2})$, $\varepsilon \in (0, \pi/2)$ can be considered as a 2-UCHS (see [15–17]).

Definition 6. Choose a complete 2-UCHS \mathcal{X} such that $\{y_k\} \subseteq \mathcal{X}$ is bounded and $\emptyset \neq S \subseteq \mathcal{X}$ is closed as well as convex. The asymptotic radius of $\{y_k\}$ corresponding to S is $r(S, \{y_k\}) = \inf \{ \limsup_{k \rightarrow \infty} q(y_k, u) : u \in S \}$. Moreover, the asymptotic center of $\{y_k\}$ corresponding to S is the set $A(S, \{y_k\}) = \{u \in S : \limsup_{k \rightarrow \infty} q(y_k, u) = r(S, \{y_k\})\}$. In addition, if the underlying space has MMUC, then the set $A(S, y_k)$ is singleton (see, e.g., [18]).

Definition 7. Choose a complete 2-UCHS \mathcal{X} such that $\emptyset \neq S \subseteq \mathcal{X}$ is closed as well as convex. Fix an element $w \in S$. Assume that $\{y_k\}$ is a bounded sequence in \mathcal{X} . Then, $\{y_k\}$ is called Δ -convergent to w iff the asymptotic center $A(S, \{z_k\}) = \{w\}$ for all subsequence $\{z_k\}$ of $\{y_k\}$. When w is Δ -limit of $\{y_k\}$, then we shall write $\Delta - \lim_{k \rightarrow \infty} y_k = w$.

Lemma 8 (see [19]). Any bounded sequence in a given 2-UCHS having MMUC has a Δ -convergent subsequence.

Lemma 9 (see [20]). Choose a complete 2-UCHS \mathcal{X} endowed with MMUC such that $\emptyset \neq S \subseteq \mathcal{X}$ and $\{y_k\} \subseteq S$ is bounded. Then, the asymptotic center of $\{y_k\}$ is always in S .

Mappings endowed with condition (E) enjoy the following useful properties which we have combined in a proposition form. For details, we refer the reader to [10].

Proposition 10. Choose a complete 2-UCHS \mathcal{X} such that $\emptyset \neq S \subseteq \mathcal{X}$. Suppose $\mathcal{L} : S \rightarrow S$.

- (i) When the map \mathcal{L} has condition (E) with nonempty fixed point set, then for each $s \in S$ and $\omega \in F_{\mathcal{L}}$, we have $q(\mathcal{L}s, \mathcal{L}\omega) \leq q(s, \omega)$
- (ii) When the map \mathcal{L} has condition (E) then fixed point set of \mathcal{L} is always closed in S

We now state an important characterization of a 2-UCHS, which was proved in [15].

Lemma 11. Choose a 2-UCHS (\mathcal{X}, q) . Then, the following inequality holds

$$q^2((1-\xi)s \oplus \xi s', g) \leq (1-\xi)q^2(s, g) + \xi q^2(s', g) - 4c_M \xi(1-\xi)q^2(s, s'), \quad (11)$$

for each $\xi \in [0, 1]$ and $s, s', g \in \mathcal{X}$.

2. Approximation Results

We now want to show our desirable strong and Δ -convergence results by considering the Agarwal iteration (6). It should be noted that \mathcal{X} will be considered complete and endowed with the MMUC. The notation $F_{\mathcal{L}}$ will simply denote the set of all fixed points of \mathcal{L} .

We suggest the following useful lemma which will provide a key role in main outcome.

Lemma 12. Choose a 2-UCHS \mathcal{X} such that $\emptyset \neq S \subseteq \mathcal{X}$ is closed as well as convex. Furthermore, let $\mathcal{L} : S \rightarrow S$ be endowed with condition (E) having $F_{\mathcal{L}} \neq \emptyset$. If $\{y_k\}$ is the Agarwal iterates (6), then, $\lim_{k \rightarrow \infty} q(y_k, \omega)$ exists for all $\omega \in F_{\mathcal{L}}$.

Proof. Assume that $\omega \in F_{\mathcal{L}}$. By using Proposition 10 (i), one has

$$\begin{aligned} q(w_k, \omega) &= q((1-\beta_k)y_k \oplus \beta_k \mathcal{L}y_k, \omega) \leq (1-\beta_k)q(y_k, \omega) \\ &\quad + \beta_k q(\mathcal{L}y_k, \omega) \leq (1-\beta_k)q(y_k, \omega) + \beta_k q(y_k, \omega) \\ &\leq q(y_k, \omega). \end{aligned} \quad (12)$$

Hence,

$$\begin{aligned} q(y_{k+1}, \omega) &= q((1-\alpha_k)\mathcal{L}y_k \oplus \alpha_k \mathcal{L}w_k, \omega) \\ &\leq (1-\alpha_k)q(\mathcal{L}y_k, \omega) + \alpha_k q(\mathcal{L}w_k, \omega) \\ &\leq (1-\alpha_k)q(y_k, \omega) + \alpha_k q(w_k, \omega) \leq q(y_k, \omega). \end{aligned} \quad (13)$$

From the above observations, we have $q(y_{k+1}, \omega) \leq q(y_k, \omega)$. Hence, the real sequence $\{q(y_k, \omega)\}$ is bounded below by 0 and nonincreasing as well, so $\lim_{k \rightarrow \infty} q(y_k, \omega)$ exists for every $\omega \in F_{\mathcal{L}}$.

The existence of a fixed point for a self-map $\mathcal{L} : S \rightarrow S$ having condition (E) in the nonlinear domain 2-UCBS can be established by the following way. This result provides a fundamental key for establishing the main results in the sequel.

Theorem 13. Choose a 2-UCHS \mathcal{X} such that $\emptyset \neq S \subseteq \mathcal{X}$ is closed as well as convex. Furthermore, let $\mathcal{L} : S \rightarrow S$ be endowed with condition (E). If $\{y_k\}$ is the Agarwal iterates (6) with restriction $\alpha_k, \beta_k \in [a, b] \subset (0, 1)$. Then, $F_{\mathcal{L}} \neq \emptyset$ iff $\{y_k\}$ is bounded and $\lim_{k \rightarrow \infty} q(y_k, \mathcal{L}y_k) = 0$.

Proof. Suppose that the iterative sequence $\{y_k\}$ is bounded having $\lim_{k \rightarrow \infty} q(\mathcal{L}y_k, y_k) = 0$. We may fix an element, namely, $\omega \in A(S, \{y_k\})$. By using condition (E) of \mathcal{L} , we have

$$\begin{aligned} r(\mathcal{L}\omega, \{y_k\}) &= \limsup_{k \rightarrow \infty} q(y_k, \mathcal{L}\omega) \leq \mu \limsup_{k \rightarrow \infty} q(\mathcal{L}y_k, y_k) \\ &\quad + \limsup_{k \rightarrow \infty} q(y_k, \omega) = \limsup_{k \rightarrow \infty} q(y_k, \omega) \\ &= r(\omega, \{y_k\}). \end{aligned} \quad (14)$$

It follows that $\mathcal{L}\omega \in A(S, \{y_k\})$. Since $A(S, \{y_k\})$ is singleton set, one has $\mathcal{L}\omega = \omega$. Thus, $F_{\mathcal{L}} \neq \emptyset$. Conversely, we suppose that $F_{\mathcal{L}} \neq \emptyset$ and $\omega \in F_{\mathcal{L}}$. Then, by the proof of Lemma 12, $\{y_k\}$ is bounded. By Lemma 11, we have

$$\begin{aligned} q^2(w_k, \omega) &\leq (1 - \beta_k)q^2(y_k, \omega) + \beta_k q^2(\mathcal{L}y_k, \omega) \\ &\quad - 4c_M \beta_k (1 - \beta_k) q^2(y_k, \mathcal{L}y_k) \leq (1 - \beta_k)q^2(y_k, \omega) \\ &\quad + \beta_k q^2(y_k, \omega) - 4c_M \beta_k (1 - \beta_k) q^2(y_k, \mathcal{L}y_k) \\ &\leq q^2(y_k, \omega) - 4c_M \beta_k (1 - \beta_k) q^2(y_k, \mathcal{L}y_k). \end{aligned} \quad (15)$$

Thus,

$$\begin{aligned} q^2(y_{k+1}, \omega) &\leq (1 - \alpha_k)q^2(\mathcal{L}y_k, \omega) + \alpha_k q^2(\mathcal{L}w_k, \omega) \\ &\quad - 4c_M \alpha_k (1 - \alpha_k) q^2(\mathcal{L}y_k, \mathcal{L}w_k) \\ &\leq (1 - \alpha_k)q^2(y_k, \omega) + \alpha_k q^2(w_k, \omega) \\ &\quad - 4c_M \alpha_k (1 - \alpha_k) q^2(\mathcal{L}y_k, \mathcal{L}w_k) \\ &\leq (1 - \alpha_k)q^2(y_k, \omega) + \alpha_k q^2(w_k, \omega) \\ &\quad - 4c_M \alpha_k (1 - \alpha_k) q^2(\mathcal{L}y_k, \mathcal{L}w_k) \\ &\leq (1 - \alpha_k)q^2(y_k, \omega) + \alpha_k q^2(w_k, \omega) \\ &\leq q^2(y_k, \omega) - 4c_M \alpha_k \beta_k (1 - \beta_k) q^2(y_k, \mathcal{L}y_k). \end{aligned} \quad (16)$$

Since $c_M > 0$, it follows that

$$\sum_{k=1}^{\infty} a^2(1-b)q^2(y_k, \mathcal{L}y_k) \leq \sum_{k=1}^{\infty} \alpha_k \beta_k (1 - \beta_k) q^2(y_k, \mathcal{L}y_k) < \infty. \quad (17)$$

Thus, $\lim_{k \rightarrow \infty} q^2(y_k, \mathcal{L}y_k) = 0$ and hence

$$\lim_{k \rightarrow \infty} q(y_k, \mathcal{L}y_k) = 0. \quad (18)$$

In some sense, the notion of Δ -convergence in nonlinear domains provides the analog of the notion of weak convergence in linear setting. To obtain the Δ -convergence for operators having the condition (E) in a 2-UCHS by using the Agarwal iterative sequence (6), we shall propose the following techniques.

Theorem 14. Choose a 2-UCHS \mathcal{X} such that $\emptyset \neq S \subseteq \mathcal{X}$ is closed as well as convex. Furthermore, let $\mathcal{L} : S \rightarrow S$ be

endowed with condition (E) and $F_{\mathcal{L}} \neq \emptyset$. If $\{y_k\}$ is the Agarwal iterates (6) with restriction $\alpha_k, \beta_k \in [a, b] \subset (0, 1)$, then, $\{y_k\}$ Δ -converges to a fixed point of \mathcal{L} .

Proof. It has been observed in Theorem 13 that the iterative sequence $\{y_k\}$ is bounded having $\lim_{k \rightarrow \infty} q(\mathcal{L}y_k, y_k) = 0$. We may consider the $\omega_{\Delta}(y_k) = \bigcup A(\{u_k\})$ and notice that the union has been imposed on all possible subsequences $\{u_k\}$ of the iterative sequence $\{y_k\}$. We want to show that $\omega_{\Delta}(y_k) \subseteq F_{\mathcal{L}}$. Suppose $u \in \omega_{\Delta}(y_k)$. Then, one can find a subsequence $\{u_k\}$ of $\{y_k\}$ in such a way that $A(\{u_k\}) = \{u\}$. By Lemmas 8 and 9, one can find a subsequence $\{v_k\}$ of $\{u_k\}$ in such a way that $\Delta - \lim_{k \rightarrow \infty} v_k = v \in S$. Keeping $\lim_{k \rightarrow \infty} \rho(v_k, \mathcal{L}v_k) = 0$ in mind and applying condition (E) of \mathcal{L} , one has

$$q(v_k, \mathcal{L}v) \leq \mu q(v_k, \mathcal{L}v_k) + q(v_k, v). \quad (19)$$

If we apply \limsup on both of the sides of above, then, we have $v \in F_{\mathcal{L}}$. By Lemma 12, $\lim_{k \rightarrow \infty} q(y_k, v)$ exists. Next, we show that $u = v$. Assume on contrary that $u \neq v$. Then, using the property of uniqueness of asymptotic centers, we get

$$\begin{aligned} \limsup_{k \rightarrow \infty} q(v_k, v) &= \limsup_{k \rightarrow \infty} q(v_k, u) \leq \limsup_{k \rightarrow \infty} q(u_k, u) \\ &< \limsup_{k \rightarrow \infty} q(u_k, v) = \limsup_{k \rightarrow \infty} q(y_k, v) \\ &= \limsup_{k \rightarrow \infty} q(v_k, v). \end{aligned} \quad (20)$$

The above strict inequality suggests a contradiction. So we must have $u = v \in F_{\mathcal{L}}$ and $\omega_{\Delta}(y_k) \subseteq F_{\mathcal{L}}$.

Finally, we show that $\{y_k\}$ is Δ -convergent in $F_{\mathcal{L}}$, that is, we want to show $\omega_{\Delta}(y_k)$ is singleton. Assume that $\{u_k\}$ is a subsequence of the sequence $\{y_k\}$. In the view of Lemmas 8 and 9, one can find a subsequence $\{v_k\}$ of $\{u_k\}$ in such a way that $\Delta - \lim_{k \rightarrow \infty} v_k = v \in S$. Suppose $A(\{u_k\}) = \{u\}$ and $A(\{y_k\}) = \{x\}$. We have already established that $u = v$ and $v \in F_{\mathcal{L}}$. Now, we have to show that $x = v$. Suppose not, then since $\lim_{k \rightarrow \infty} q(y_k, v)$ exists and also the asymptotic centers are consist of exactly one point, so

$$\begin{aligned} \limsup_{k \rightarrow \infty} q(v_k, v) &= \limsup_{k \rightarrow \infty} q(v_k, x) \leq \limsup_{k \rightarrow \infty} q(y_k, x) \\ &< \limsup_{k \rightarrow \infty} q(y_k, v) = \limsup_{k \rightarrow \infty} q(v_k, v). \end{aligned} \quad (21)$$

which is obviously a contradiction and so $x = v \in F_{\mathcal{L}}$. Hence, $\omega_{\Delta}(y_k) = \{x\}$. \square

Normally, we are interested in a strong convergence. To obtain the strong convergence theorems, we essentially impose some other assumptions on the domain or the operator. We first take a compact domain and establish a strong convergence theorem as follows.

Theorem 15. Choose a 2-UCHS \mathcal{X} such that $\emptyset \neq S \subseteq \mathcal{X}$ is compact as well as convex. Furthermore, let $\mathcal{L} : S \rightarrow S$ be endowed with condition (E) and $F_{\mathcal{L}} \neq \emptyset$. If $\{y_k\}$ is the

Agarwal iterates (6) with restriction $\alpha_k, \beta_k \in [a, b] \subset (0, 1)$. Then, $\{y_k\}$ converges strongly to a fixed point of \mathcal{L} .

Proof. Since S is compact, we may select a subsequence $\{y_{k_i}\}$ of $\{y_k\}$ such that $y_{k_i} \rightarrow g \in S$. By using condition (E) of \mathcal{L} , we have

$$q(y_{k_i}, \mathcal{L}g) \leq \mu q(y_{k_i}, \mathcal{L}y_{k_i}) + q(y_{k_i}, g). \quad (22)$$

In the view of Theorem 13, $\lim_{k \rightarrow \infty} q(y_{k_i}, \mathcal{L}y_{k_i}) = 0$. Hence, if we apply $k \rightarrow \infty$ on both of the sides of the above inequality, we get $y_{k_i} \rightarrow \mathcal{L}g$ by uniqueness of limits in metric spaces, $g = \mathcal{L}g$. Hence, g is the fixed point of \mathcal{L} . Moreover, by Lemma 12, $\lim_{k \rightarrow \infty} q(y_k, g)$ exists. So $\{y_k\}$ is strongly convergent to g . This completes the proof. \square

The compactness of the domain in the above theorem provided us a significant help. Now, one thinks about how to replace the compactness of the domain by any other assumption. We replace it by the following condition, which was essentially defined by Senter and Dotson [21].

Definition 16. A self-map \mathcal{L} on a subset S of a 2-UCHS \mathcal{X} is said to satisfy condition (I), if there exists some nondecreasing function $\eta : [0, \infty) \rightarrow [0, \infty)$ satisfying $\eta(0) = 0$, $\eta(a) > 0$ for every $a > 0$ and $q(s, \mathcal{L}s) \geq \eta(\inf_{\omega \in F_{\mathcal{L}}} q(s, \omega))$ for each $s \in S$.

Theorem 17. Choose a 2-UCHS \mathcal{X} such that $\emptyset \neq S \subseteq \mathcal{X}$ is closed as well as convex. Furthermore, let $\mathcal{L} : S \rightarrow S$ be endowed with conditions (E) and (I), and $F_{\mathcal{L}} \neq \emptyset$. If $\{y_k\}$ is the Agarwal iterates (6) with restriction $\alpha_k, \beta_k \in [a, b] \subset (0, 1)$. Then, $\{y_k\}$ converges strongly to a fixed point of \mathcal{L} .

Proof. Theorem 13 gives $\lim_{k \rightarrow \infty} q(y_k, \mathcal{L}y_k) = 0$. By condition (I), one has

$$\lim_{k \rightarrow \infty} q(y_k, F_{\mathcal{L}}) = 0. \quad (23)$$

Thus, one can choose a subsequence $\{y_{k_j}\}$ of $\{y_k\}$ and $\{\omega_j\}$ in $F_{\mathcal{L}}$ such that $q(y_{k_j}, \omega_j) \leq 1/2^j$ for every natural number j . Proof of Lemma 12 suggests that $\{y_k\}$ is nonincreasing, and so

$$q(y_{k_{j+1}}, \omega_j) \leq q(y_{k_j}, \omega_j) \leq \frac{1}{2^j}. \quad (24)$$

Now,

$$\begin{aligned} q(\omega_{j+1}, \omega_j) &\leq q(\omega_{j+1}, y_{k_{j+1}}) + \rho(y_{k_{j+1}}, \omega_j) \leq \frac{1}{2^{j+1}} + \frac{1}{2^j} \\ &\leq \frac{1}{2^{j-1}} \rightarrow 0, \text{ as } j \rightarrow \infty. \end{aligned} \quad (25)$$

From the above, one can easily conclude that the

TABLE 1: Strong convergence of Agarwal, Ishikawa, and Mann iterative schemes.

	Agarwal (6)	Ishikawa (5)	Mann (4)
y_1	0.9	0.9	0.9
y_2	0.693125000000000	0.738125000000000	0.794999999999999
y_3	0.533802517361111	0.605365017361111	0.702249999999999
y_4	0.411102077606577	0.49648339271074	0.620320833333333
y_5	0.316605697267843	0.40718533804957	0.547950069444444
y_6	0.243830359909748	0.33394853071982	0.484020000000000
y_7	0.187783242458271	0.27388417693063	0.42755326251928
y_8	0	0.22462306455213	0.37767204855870
y_9	0	0.18422211058060	0.33361030956019
y_{10}	0	0.05526663317418	0.29468910677816

sequence $\{\omega_j\}$ form a Cauchy sequence in the closed subset $F_{\mathcal{L}}$ of S . Hence, $\omega_j \rightarrow g \in F_{\mathcal{L}}$ and so g is a fixed point of \mathcal{L} . But Lemma 12 suggests that $\lim_{k \rightarrow \infty} q(y_k, g)$ exists. Thus, the element g is the strong limit point of the sequence $\{y_k\}$. \square

3. Numerical Observations

This section is devoted to some numerical computations. We first suggest a nontrivial example of \mathcal{L} endowed with the condition (E), but not with (C). This example shows that the class of Garcia-Falset is properly more general than the class of Suzuki mappings.

Example 1. Suppose $S = [0, 1]$ and \mathcal{L} is a self-map defined as follows:

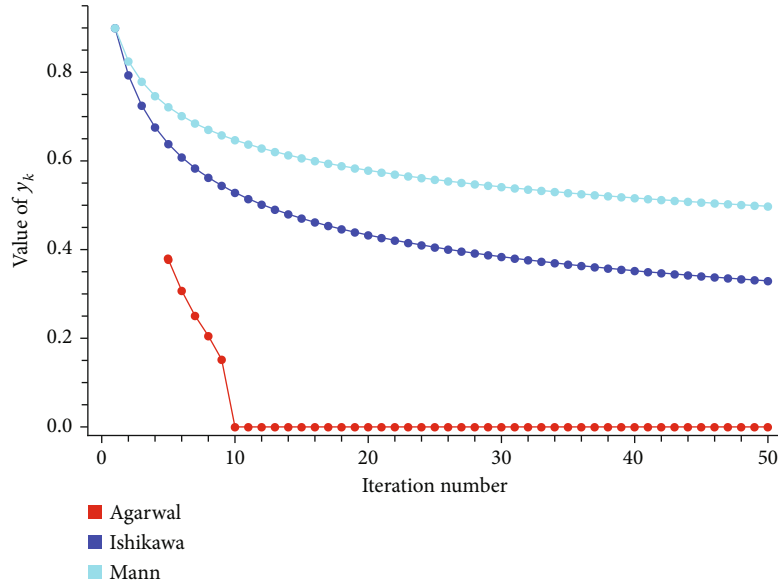
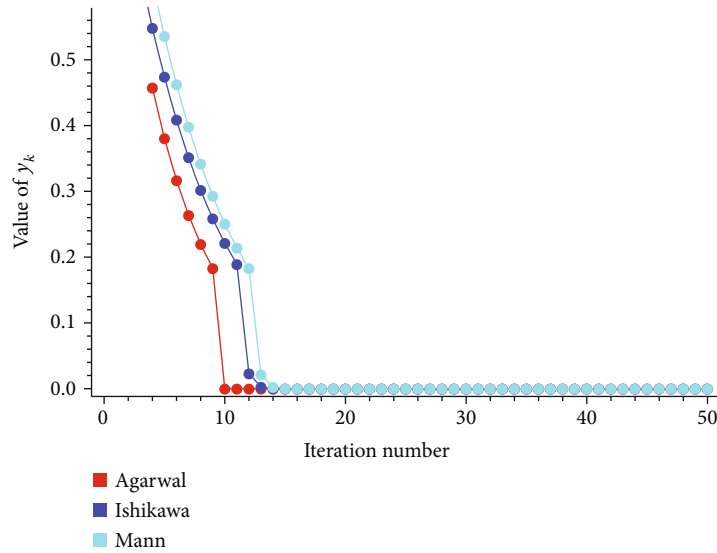
$$\mathcal{L}s = \begin{cases} 0, & \text{if } s \in S_1 = \left[0, \frac{1}{5}\right), \\ \frac{5s}{6}, & \text{if } s \in S_2 = \left[\frac{1}{5}, 1\right]. \end{cases} \quad (26)$$

We fix the value of $\mu = 6$. We shall prove that $q(s, \mathcal{L}s') \leq 6q(s, \mathcal{L}s) + q(s, s')$ for each $s, s' \in S$.

Case I. Assume that $s, s' \in S_1$. Then, $\mathcal{L}s = \mathcal{L}s' = 0$. Thus,

$$\begin{aligned} q(s, \mathcal{L}s') &= |s - \mathcal{L}s'| = |s| \leq 6|s| = 6|s - \mathcal{L}s| \leq 6|s - \mathcal{L}s| \\ &\quad + |s - s'| = 6q(s, \mathcal{L}s) + q(s, s'). \end{aligned} \quad (27)$$

Case II. Here, we choose $s, s' \in S_2$. Then $\mathcal{L}s = 5s/6$ and $\mathcal{L}s' = 5s'/6$.

FIGURE 1: $\alpha_k = 1/k + 1$, $\beta_k = k/k + 1$.FIGURE 2: $\alpha_k = 1 - 1/\sqrt{6k + 1}$, $\beta_k = 1/k^3$.

$= 5s'/6$. Thus,

So,

$$\begin{aligned}
 q(s, \mathcal{L}s') &\leq q(s, \mathcal{L}s) + q(\mathcal{L}s, \mathcal{L}s') = |s - \mathcal{L}s| + |\mathcal{L}s - \mathcal{L}s'| \\
 &= |s - \mathcal{L}s| + \left| \frac{5s}{6} - \frac{5s'}{6} \right| = |s - \mathcal{L}s| + \frac{5}{6}|s - s'| \\
 &\leq |s - \mathcal{L}s| + |s - s'| \leq 6|s - \mathcal{L}s| + |s - s'| \\
 &= 6q(s, \mathcal{L}s) + q(s, s').
 \end{aligned}$$

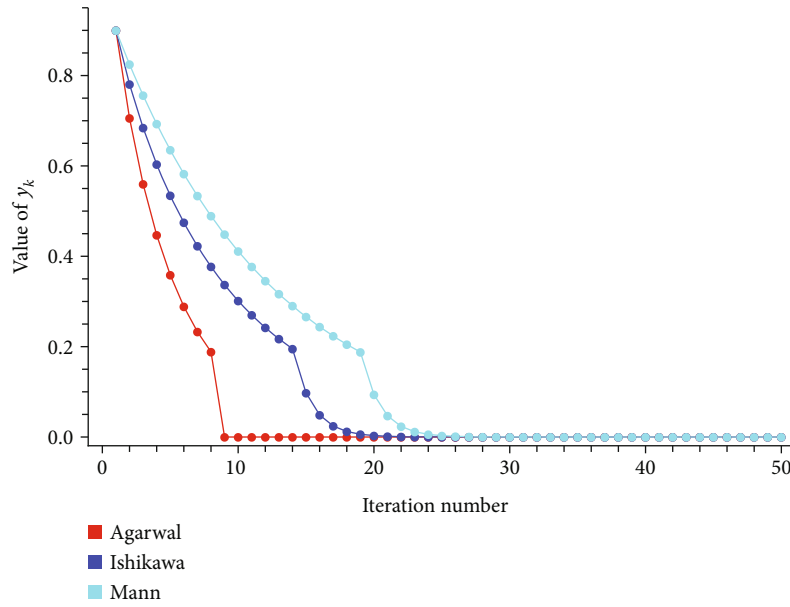
(28)

$$\begin{aligned}
 q(s, \mathcal{L}s') &= |s - \mathcal{L}s'| = \left| s - \left(\frac{5s'}{6} \right) \right| = \left| \frac{6s - 5s'}{6} \right| \\
 &= \left| \frac{s + 5s - 5s'}{6} \right| \leq \left| \frac{s}{6} \right| + \left| \frac{5s - 5s'}{6} \right| \leq |s| + |s - s'| \\
 &= |s - \mathcal{L}s| + |s - s'| \leq 6|s - \mathcal{L}s| + |s - s'| \\
 &= 6q(s, \mathcal{L}s) + q(s, s').
 \end{aligned}$$

(29)

Case III. If $s \in S_1$ and $s' \in S_2$. Then $\mathcal{L}s = 0$ and $\mathcal{L}s' = 5s'/6$.

Case IV. If $s \in S_2$ and $s' \in S_1$. Then $\mathcal{L}s = 5s/6$ and $\mathcal{L}s' = 0$ and

FIGURE 3: $\alpha_k = 1/2$, $\beta_k = 1/\sqrt{k+1}$.

so

$$\begin{aligned} q(s, \mathcal{L}s') &= |s - \mathcal{L}s'| = |s| = 6 \left| \frac{s}{6} \right| = 6|s - \mathcal{L}s| \leq 6|s - \mathcal{L}s| \\ &+ |s - s'| = 6q(s, \mathcal{L}s) + q(s, s'). \end{aligned} \quad (30)$$

Next, we provide the values for which \mathcal{L} does not satisfy condition (C). Choose $s = 1/8$ and $s' = 1/5$. It is easy to show $1/2d(s, \mathcal{L}s) < q(s, s')$, but $q(\mathcal{L}s, \mathcal{L}s') > q(s, s')$. For any choice of $k \in \mathbb{N}$, let $\alpha_k = 0.70$ and $\beta_k = 0.65$, then, the observations are given in Table 1.

Now, we study the behavior of Agarwal, Ishikawa, and Mann iterations under different cases. Notice that $q(y_k, \omega) < 10^{-10}$ is the stopping criteria, $y_1 = 0.9$, and we stop the iterates for $k = 50$. In this case, Figures 1, 2, and 3 show that the Agarwal iteration process converges faster to the fixed point $\omega = 0$ as compared to the other iterations.

4. Conclusions

In this paper, we have initiated the finding of fixed points for the generalized class of mappings due to Garcia-Falset et al. [10] in the general setting of 2-UCHS. We established several strong and Δ -convergence theorems under the Agarwal iterative process [8]. We have presented a new example of mapping having condition (E) but not (C) and proved that its Agarwal iterative process [8] is more effective than the corresponding Mann [13] and Ishikawa [12] iterative processes. In view of the above discussion, our results simultaneously hold in UCBS, CAT(0), and some CAT(κ) spaces. The present results can be extended and applied to many fields of applied sciences and differential equations. Thus, our results extend the corresponding results of Bagherboum [11], Phuengrat-

tana [7], Basarir and Sahin [9], and Nanjaras et al. [6] from the general setting of domains and faster iteration process.

Data Availability

The data used to support the findings of this study are included in the references within the article.

Conflicts of Interest

The authors declare no conflict of interest.

Authors' Contributions

All authors contributed equally and significantly in writing this article. All authors read and approved the final manuscript.

Acknowledgments

The authors are grateful to the Spanish Government for Grant RTI2018-094336-B-I00 (MCIU/AEI/FEDER, UE) and to the Basque Government for Grant IT1207-19.

References

- [1] F. E. Browder, "Nonexpansive nonlinear operators in a Banach space," *Proceedings of the National Academy of Sciences of the United States of America*, vol. 54, no. 4, pp. 1041–1044, 1965.
- [2] W. A. Kirk, "A fixed point theorem for mappings which do not increase distances," *The American Mathematical Monthly*, vol. 72, no. 9, pp. 1004–1006, 1965.
- [3] D. Gohde, "Zum Prinzip der Kontraktiven Abbildung," *Mathematische Nachrichten*, vol. 30, no. 3-4, pp. 251–258, 1965.
- [4] W. A. Kirk, "Geodesic geometry and fixed point theory," in *Seminar of Mathematical Analysis*, Colecc, Abierta: Malaga, Spain, 2003.

- [5] T. Suzuki, "Fixed point theorems and convergence theorems for some generalized nonexpansive mappings," *Journal of Mathematical Analysis and Applications*, vol. 340, no. 2, pp. 1088–1095, 2008.
- [6] B. Nanjaras, B. Panyanak, and W. Phuengrattana, "Fixed point theorems and convergence theorems for Suzuki-generalized nonexpansive mappings in $CAT(0)$ spaces," *Nonlinear Analysis: Hybrid Systems*, vol. 4, no. 1, pp. 25–31, 2010.
- [7] W. Phuengrattana, "Approximating fixed points of Suzuki-generalized nonexpansive mappings," *Nonlinear Analysis: Hybrid Systems*, vol. 5, no. 3, pp. 583–590, 2011.
- [8] R. P. Agarwal, D. O'Regon, and D. R. Sahu, "Iterative construction of fixed points of nearly asymptotically non-expansive mappings," *Journal of Nonlinear and convex Analysis*, vol. 8, pp. 61–79, 2007.
- [9] M. Basarir and A. Sahin, "On the strong and Δ -convergence of S-iteration process for generalized nonexpansive mappings on $CAT(0)$ spaces," *Thai Journal of Mathematics*, vol. 12, pp. 549–559, 2014.
- [10] J. Garcia-Falset, E. Llorens-Fuster, and T. Suzuki, "Fixed point theory for a class of generalized nonexpansive mappings," *Journal of Mathematical Analysis and Applications*, vol. 375, no. 1, pp. 185–195, 2011.
- [11] M. Bagherboum, "Approximating fixed points of mappings satisfying condition (E) in Busemann space," *Numerical Algorithms*, vol. 71, pp. 25–39, 2011.
- [12] S. Ishikawa, "Fixed points by a new iteration method," *Proceedings of American Mathematical Society*, vol. 44, no. 1, pp. 147–150, 1974.
- [13] W. R. Mann, "Mean value methods in iteration," *Proceedings of the American Mathematical Society*, vol. 4, no. 3, pp. 506–510, 1953.
- [14] L. Leustean, "A quadratic rate of asymptotic regularity for $CAT(0)$ -spaces," *Journal of Mathematical Analysis and Applications*, vol. 325, no. 1, pp. 386–399, 2007.
- [15] T. Laokul and B. Panyanak, "A generalization of the (CN) inequality and its applications," *Carpathian Journal of Mathematics*, vol. 36, no. 1, pp. 81–90, 2020.
- [16] M. A. Khamsi and A. R. Khan, "Inequalities in metric spaces with applications," *Nonlinear Analysis*, vol. 74, no. 12, pp. 4036–4045, 2011.
- [17] H. K. Xu, "Inequalities in Banach spaces with applications," *Nonlinear Analysis*, vol. 16, no. 12, pp. 1127–1138, 1991.
- [18] L. Leustean, "Nonexpansive iterations in uniformly convex W -hyperbolic spaces," in *Nonlinear Analysis and Optimization I. Nonlinear Analysis*, vol. 513 of Contemporary Mathematics, pp. 193–210, American Mathematical Society, Providence, RI, USA, 2010.
- [19] W. A. Kirk and B. Panyanak, "A concept of convergence in geodesic spaces," *Nonlinear Analysis: Theory, Methods & Applications*, vol. 68, no. 12, pp. 3689–3696, 2008.
- [20] S. Dhompongsa, W. A. Kirk, and B. Panyanak, "Nonexpansive set-valued mappings in metric and Banach spaces," *Journal of Nonlinear and Convex Analysis*, vol. 8, pp. 35–45, 2007.
- [21] H. F. Senter and W. G. Dotson, "Approximating fixed points of nonexpansive mappings," *Proceedings of American Mathematical Society*, vol. 44, no. 2, pp. 375–380, 1974.

Research Article

Remarks on the Systems of Semilinear Fractional Rayleigh-Stokes Equation

Le Dinh Long 

Division of Applied Mathematics, Thu Dau Mot University, Binh Duong Province, Vietnam

Correspondence should be addressed to Le Dinh Long; ledinhlong@tdmu.edu.vn

Received 25 April 2021; Accepted 7 June 2021; Published 28 June 2021

Academic Editor: Mustafa Inc

Copyright © 2021 Le Dinh Long. This is an open access article distributed under the Creative Commons Attribution License, which permits unrestricted use, distribution, and reproduction in any medium, provided the original work is properly cited.

In this paper, we study the Cauchy problem for a system of Rayleigh-Stokes equations. In this system of equations, we use derivatives in the classical Riemann-Liouville sense. This system has many applications in some non-Newtonian fluids. We obtained results for the existence, uniqueness, and frequency of the solution. We discuss the stability of the solutions and find the solution spaces. Our main technique is to use the Banach mapping theorem combined with some techniques in Fourier analysis.

1. Introduction

Let $\Omega \subset \mathbb{R}^N$ ($N \geq 1$) be a smooth domain with the boundary $\partial\Omega$, and $T > 0$ is a given time. In this paper, we study the initial value problem for systems of Rayleigh-Stokes problem as follows

$$\begin{cases} \partial_t u + (-\Delta)^\beta u - d\partial_t^\alpha \Delta u = \mathcal{G}(u, v), & (x, t) \in \Omega \times (0, T), \\ \partial_t v + (-\Delta)^\beta v - d\partial_t^\alpha \Delta v = \mathcal{H}(u, v), & (x, t) \in \Omega \times (0, T), \\ u(x, t) = 0, & x \in \partial\Omega, \\ u(x, 0) = \varphi(x), & x \in \Omega, \\ v(x, 0) = \theta(x), & x \in \Omega. \end{cases} \quad (1)$$

where (φ, θ) is Cauchy input data. Some functions \mathcal{G}, \mathcal{H} called the source data which are defined later. Here, $\partial_t = \partial/\partial t$, and ∂_t^α is the Riemann-Liouville fractional derivative of order $0 < \alpha < 1$ given by [1, 2]:

$$\partial_t^\alpha w(x, t) = \frac{1}{\Gamma(1-\alpha)} \frac{\partial}{\partial t} \left(\int_0^t (t-s)^{-\alpha} w(x, s) ds \right), \quad (2)$$

where $\Gamma(\cdot)$ is the Gamma function. As far as we know, there are currently several definitions for fraction derivatives and fraction integrals, such as Riemann-Liouville, Caputo, Hadamard, Riesz, and Grünwald-Letnikov. Some works are attracting the attention of the community, like Debbouche and his group [3–5], Karapinar et al. [6–13], Benchohra et al. [14–16], Inc et al. [17–20].

And some very interesting results about unchanged level derivatives are surveyed by.

In fluid dynamics, the Rayleigh problem is the first Stokes problem, which determines the flow generated by the sudden motion of an infinitely long plate from the resting state, named after Lord Rayleigh and Sir George Stokes. This problem is considered to be one of the simplest problems with the correct solution for the Navier-Stokes equation. In recent times, with the development of fractions, a number of authors such as Shen et al. [21] investigated Rayleigh-Stokes, which is a more general form than the classical model. The fractional Rayleigh-Stokes equation (1) has applications in non-Newtonian behavior of fluids [21], and other applications of this equation can be given in [21, 22]. We list some papers on fractional Rayleigh Stokes in the following.

(i) The initial and boundary values for the Rayleigh-Stokes problem in the case of homogeneity have been explored in a number of interesting papers; see for example [23–27] and its references

(ii) The authors in [21, 28, 29] used the Fourier transform and the fractional Laplace transform to obtain the exact solution

(iii) Numerical solutions for Problem (1) has been studied by many authors in [4, 23, 24, 30, 31]

(iv) In [32], the authors concerned with the following problem for a following stochastic Rayleigh-Stokes equation

$$\begin{cases} \partial_t X(t) + (1 + \alpha \partial_t^\beta) \mathcal{A}X(t) = f(t, X(t)) + \gamma(t) \dot{B}_Q^h(t), & t \in (0, T), \\ X(t)|_{\partial \mathcal{D}} = 0, X(0) = x_0, & t \in (0, T). \end{cases} \quad (3)$$

The existence and uniqueness of mild solution in each case are established separately by applying a standard method that is Banach fixed point theorem. In [22], Caraballo et al. investigated the following time-fractional Rayleigh-Stokes stochastic equation

$$\left(\frac{\partial}{\partial t} - \Delta - u \frac{\partial^\alpha}{\partial t^\alpha} \right) u = F(t, u) + \sigma(t, u) \dot{\mathcal{W}}(t), \text{ on } J \times \mathcal{X}, \quad (4)$$

where $\{\mathcal{W}(t, \cdot)\}_{t \in J}$ represents a standard Wiener process.

To the best of the author's knowledge, the problem of the system of equations for a fractional Rayleigh-Stokes with a nonlinear source, i.e., Problem (1), has yet to be studied. The goal of this paper is to develop a theory of the existence and regularity estimate for the mild solution to the Problem (1). Our main technique is to use the Banach mapping theorem combined with some techniques in Fourier analysis.

2. The Existence and Regularity of the Solution

In this section, we consider the existence and mild solution of Problem (1). Before going into the main theorem of this section, we briefly discuss spectral, eigenvalues, and related functional spaces on the Laplacian operator.

Let $\mathcal{A} = -\Delta$. The domain $D(\mathcal{A}^s)$ for $s \geq 0$ is a Banach space equipped with the norm

$$\|h\|_{D(\mathcal{A}^s)} := \left(\sum_{n=1}^{\infty} |\langle h, \varphi_n \rangle|^2 \lambda_n^{2s} \right)^{1/2}, \quad h \in D(\mathcal{A}^s). \quad (5)$$

The definition of the negative fractional power \mathcal{A}^{-s} can be found in [33]. Its domain $D(\mathcal{A}^{-s})$ is a Hilbert space endowed with the dual inner product $\langle \cdot, \cdot \rangle_{-s, s}$ taken between $D(\mathcal{A}^{-s})$ and $D(\mathcal{A}^s)$. This generates the norm

$$\|h\|_{D(\mathcal{A}^{-s})} = \left(\sum_{n=1}^{\infty} |\langle h, \varphi_n \rangle_{-s, s}|^2 \lambda_n^{-2s} \right)^{1/2}. \quad (6)$$

A couple (u, v) of functions $u(x, t), v(x, t): \bar{Q}_T \rightarrow \mathbb{R}$, $(\bar{Q}_T = \bar{\Omega} \times [0, T])$ are called a function of two variables x, t

$$\begin{aligned} (u, v): \bar{Q}_T &\rightarrow \mathbb{R}^2, \\ (u, v)(x, t) &= (u(x, t), v(x, t)). \end{aligned} \quad (7)$$

Here, the norm of $(u, v) \in \mathbb{X} \times \mathbb{X}$ (for any space \mathbb{X}) is defined

$$\|(u, v)\|_{(\mathbb{X})^2} = \|u\|_{\mathbb{X}} + \|v\|_{\mathbb{X}}. \quad (8)$$

Theorem 1. Let $(\varphi, \theta) \in H^m(\Omega) \times H^m(\Omega)$. Let \mathcal{G}, \mathcal{H} satisfies $\mathcal{G}(0, 0) = \mathcal{H}(0, 0) = 0$ and the globally Lipschitz function

$$\begin{aligned} \|\mathcal{G}(v_1, v_2) - \mathcal{G}(\bar{v}_1, \bar{v}_2)\| &\leq L_g \left(\|v_1 - \bar{v}_1\|_{L^2(\Omega)} + \|v_2 - \bar{v}_2\|_{L^2(\Omega)} \right), \\ \|\mathcal{H}(v_1, v_2) - \mathcal{H}(\bar{v}_1, \bar{v}_2)\| &\leq L_h \left(\|v_1 - \bar{v}_1\|_{L^2(\Omega)} + \|v_2 - \bar{v}_2\|_{L^2(\Omega)} \right), \end{aligned} \quad (9)$$

for any $v_1, \bar{v}_1, v_2, \bar{v}_2 \in L^2(\Omega)$. Then, problem (1) has a unique solution (u, v) belongs to $L^\infty(0, T; L^2(\Omega)) \times L^\infty(0, T; L^2(\Omega))$ and regularity estimates hold

$$\|(u, v)\|_{L^\infty(0, T; L^2(\Omega)) \times L^\infty(0, T; L^2(\Omega))} \leq \mathcal{D}_I \left(\|\varphi\|_{H^m(\Omega)} + \|\theta\|_{H^m(\Omega)} \right). \quad (10)$$

Proof. Assume that the mild solution u is described by a Fourier series

$$u(x, t) = \sum_j \langle u(x, t), e_j(x) \rangle e_j(x), \quad v(x, t) = \sum_j \langle v(x, t), e_j(x) \rangle e_j(x). \quad (11)$$

Thanks to the results of [24], we deduce that the solution of Problem (1) with the initial condition $u(x, 0) = \varphi(x)$ is given by

$$\begin{aligned} u_j(t) &= \left(\int_0^\infty e^{-\nu t} \mathcal{K}(j, \alpha, \beta, \nu) d\nu \right) \varphi_j \\ &\quad + \int_0^t \left(\int_0^\infty e^{-\nu(t-s)} \mathcal{K}(j, \alpha, \beta, \nu) d\nu \right) \\ &\quad \cdot \langle \mathcal{G}(u(x, s), v(x, s)), e_j(x) \rangle ds, \end{aligned} \quad (12)$$

where \mathcal{K} is represented as follows

$$\mathcal{K}(j, \alpha, \beta, \nu) = \frac{d}{\pi} \frac{\lambda_j^\beta \sin(\alpha\pi) \nu^\alpha}{\left(-\nu + \lambda_j^\beta d \nu^\alpha \cos \alpha\pi + \lambda_j^\beta \right)^2 + \left(\lambda_j^\beta d \nu^\alpha \sin \alpha\pi \right)^2}. \quad (13)$$

Hence, the mild solution of Problem (1) is given by

$$\begin{aligned} u(x, t) = & \sum_j \left(\int_0^\infty e^{-vt} \mathcal{K}(j, \alpha, \beta, v) dv \right) \varphi_j e_j(x) \\ & + \sum_j \left(\int_0^t \left(\int_0^\infty e^{-v(t-s)} \mathcal{K}(j, \alpha, \beta, v) dv \right) \right. \\ & \cdot \langle \mathcal{G}(u(x, s), v(x, s)), e_j(x) \rangle ds \Big) e_j(x), \end{aligned} \quad (14)$$

$$\begin{aligned} v(x, t) = & \sum_j \left(\int_0^\infty e^{-vt} \mathcal{K}(j, \alpha, \beta, v) dv \right) \theta_j e_j(x) \\ & + \sum_j \left(\int_0^t \left(\int_0^\infty e^{-v(t-s)} \mathcal{K}(j, \alpha, \beta, v) dv \right) \right. \\ & \cdot \langle \mathcal{H}(u(x, s), v(x, s)), e_j(x) \rangle ds \Big) e_j(x). \end{aligned} \quad (15)$$

We get the following estimate

$$\int_0^\infty e^{-vt} \mathcal{K}(j, \alpha, \beta, v) dv \leq \frac{\mathcal{C}(\alpha, \beta, d)}{1 + \lambda_j^\beta t^{1-\alpha}}. \quad (16)$$

Now, we continue to show that (1) has a unique mild solution.

For any $a \geq 0$, denote by $(L_a^\infty(0, T; H^m(\Omega)))^2$ the function space $(L^\infty(0, T; H^m(\Omega)))^2$ associated with the norm

$$\begin{aligned} \|(\chi_1, \chi_2)\|_{a,m} := & \sup_{0 \leq t \leq T} \|\exp(-at) \chi_1(\cdot, t)\|_{H^m(\Omega)} \\ & + \sup_{0 \leq t \leq T} \|\exp(-at) \chi_2(\cdot, t)\|_{H^m(\Omega)}, \end{aligned} \quad (17)$$

for any

$$(\chi_1, \chi_2) \in L^\infty(0, T; L^2(\Omega)) \times L^\infty(0, T; L^2(\Omega)). \quad (18)$$

Let us give the following operator

$$Q(\chi_1, \chi_2)(t) = (\mathcal{Q}_1(\chi_1, \chi_2)(t), \mathcal{Q}_2(\chi_1, \chi_2)(t)), \quad (19)$$

where \mathcal{Q}_1 and \mathcal{Q}_2 are defined by the following

$$\begin{aligned} \mathcal{Q}_1(\chi_1, \chi_2)(t) = & \sum_j \left(\int_0^\infty e^{-vt} \mathcal{K}(j, \alpha, \beta, v) dv \right) \varphi_j e_j(x) \\ & + \sum_j \left(\int_0^t \left(\int_0^\infty e^{-v(t-s)} \mathcal{K}(j, \alpha, \beta, v) dv \right) \right. \\ & \cdot \langle \mathcal{G}(\chi_1(x, s), \chi_2(x, s)), e_j(x) \rangle ds \Big) e_j(x), \end{aligned}$$

$$\begin{aligned} \mathcal{Q}_2(\chi_1, \chi_2)(t) = & \sum_j \left(\int_0^\infty e^{-vt} \mathcal{K}(j, \alpha, \beta, v) dv \right) \theta_j e_j(x) \\ & + \sum_j \left(\int_0^t \left(\int_0^\infty e^{-v(t-s)} \mathcal{K}(j, \alpha, \beta, v) dv \right) \right. \\ & \cdot \langle \mathcal{H}(\chi_1(x, s), \chi_2(x, s)), e_j(x) \rangle ds \Big) e_j(x). \end{aligned} \quad (20)$$

From two equality as above, if $(\chi_1, \chi_2) = (0, 0)$, we find that two following equality

$$\begin{aligned} \mathcal{Q}_1(\chi_1, \chi_2)(t) = & \sum_j \left(\int_0^\infty e^{-vt} \mathcal{K}(j, \alpha, \beta, v) dv \right) \varphi_j e_j(x), \\ \mathcal{Q}_2(\chi_1, \chi_2)(t) = & \sum_j \left(\int_0^\infty e^{-vt} \mathcal{K}(j, \alpha, \beta, v) dv \right) \theta_j e_j(x). \end{aligned} \quad (21)$$

Hence, we get that for any $a > 0$

$$\begin{aligned} & \|\exp(-at) \mathcal{Q}_1(\chi_1, \chi_2)(t)\|_{H^m(\Omega)} + \|\exp(-at) \mathcal{Q}_2(\chi_1, \chi_2)(t)\|_{H^m(\Omega)} \\ & = e^{-at} \sqrt{\sum_j \lambda_j^{2m} \left(\int_0^\infty e^{-vt} \mathcal{K}(j, \alpha, \beta, v) dv \right)^2 \varphi_j^2} \\ & \quad + e^{-at} \sqrt{\sum_j \lambda_j^{2m} \left(\int_0^\infty e^{-vt} \mathcal{K}(j, \alpha, \beta, v) dv \right)^2 \theta_j^2}. \end{aligned} \quad (22)$$

Since the fact that

$$\int_0^\infty e^{-vt} \mathcal{K}(j, \alpha, \beta, v) dv \leq \mathcal{C}(\alpha, \beta, d), \quad (23)$$

we know that

$$\sum_j \lambda_j^{2m} \left(\int_0^\infty e^{-vt} \mathcal{K}(j, \alpha, \beta, v) dv \right)^2 \varphi_j^2 \leq |\mathcal{C}(\alpha, \beta, d)|^2 \sum_j \lambda_j^{2m} \varphi_j^2, \quad (24)$$

$$\sum_j \lambda_j^{2m} \left(\int_0^\infty e^{-vt} \mathcal{K}(j, \alpha, \beta, v) dv \right)^2 \theta_j^2 \leq |\mathcal{C}(\alpha, \beta, d)|^2 \sum_j \lambda_j^{2m} \theta_j^2. \quad (25)$$

Combining (22), (24), and (25), we find that

$$\begin{aligned} & \|\exp(-at) \mathcal{Q}_1(\chi_1, \chi_2)(t)\|_{H^m(\Omega)} \\ & \quad + \|\exp(-at) \mathcal{Q}_2(\chi_1, \chi_2)(t)\|_{H^m(\Omega)} \\ & \leq \mathcal{C}(\alpha, \beta, d) \left(\|\varphi\|_{H^m(\Omega)} + \|\theta\|_{H^m(\Omega)} \right), \end{aligned} \quad (26)$$

which allows us to deduce that

$$Q(\chi_1, \chi_2) \in (L_a^\infty(0, T; L^2(\Omega)))^2, \text{ if } (\chi_1, \chi_2) = (0, 0). \quad (27)$$

Let two functions (χ_1, χ_2) and $(\bar{\chi}_1, \bar{\chi}_2)$ in the space $(L_a^\infty(0, T; L^2(\Omega)))^2$. Then, using Parseval's equality, we get

$$\begin{aligned} & \|\mathcal{Q}_1(\chi_1, \chi_2)(t) - \mathcal{Q}_1(\bar{\chi}_1, \bar{\chi}_2)(t)\|_{H^m(\Omega)} \\ & \leq \int_0^t \sqrt{\sum_j \lambda_j^{2m} \left(\int_0^\infty e^{-\nu(t-s)} \mathcal{K}(j, \alpha, \beta, \nu) d\nu \right) \langle \mathcal{G}(\chi_1(x, s), \chi_2(x, s)) - \mathcal{G}(\bar{\chi}_1(x, s), \bar{\chi}_2(x, s)), e_j(x) \rangle^2} ds. \end{aligned} \quad (28)$$

Noting that

$$\int_0^\infty e^{-\nu(t-s)} \mathcal{K}(j, \alpha, \beta, \nu) d\nu \leq \mathcal{C}(\alpha, \beta, d) \lambda_j^{-\beta} (t-s)^{\alpha-1}. \quad (29)$$

Hence, and noting that $\lambda_j^{m-\beta} \leq \lambda_1^{m-\beta}$, we find that

$$\begin{aligned} & e^{-at} \|\mathcal{Q}_1(\chi_1, \chi_2)(t) - \mathcal{Q}_1(\bar{\chi}_1, \bar{\chi}_2)(t)\|_{H^m(\Omega)} \\ & \leq \mathcal{C}(\alpha, \beta, d) \lambda_1^{m-\beta} e^{-at} \int_0^t (t-s)^{\alpha-1} \|\mathcal{G}(\chi_1(x, s), \chi_2(x, s)) \\ & \quad - \mathcal{G}(\bar{\chi}_1(x, s), \bar{\chi}_2(x, s))\|_{L^2(\Omega)} ds \\ & \leq \mathcal{C}(\alpha, \beta, d) \lambda_1^{m-\beta} L_g \int_0^t (t-s)^{\alpha-1} e^{-a(t-s)} e^{-as} \left(\|\chi_1(s) - \bar{\chi}_1(s)\|_{L^2(\Omega)} \right. \\ & \quad \left. + \|\chi_2(s) - \bar{\chi}_2(s)\|_{L^2(\Omega)} \right) ds. \end{aligned} \quad (30)$$

Let us emphasize that for $0 \leq s \leq T$ then

$$\begin{aligned} & e^{-as} \left(\|\chi_1(s) - \bar{\chi}_1(s)\|_{L^2(\Omega)} + \|\chi_2(s) - \bar{\chi}_2(s)\|_{L^2(\Omega)} \right) \\ & \leq C_{1,m} \sup_{0 \leq t \leq T} \|\exp(-at) \chi_1(\cdot, t)\|_{L^2(\Omega)} \\ & \quad + C_{1,m} \sup_{0 \leq t \leq T} \|\exp(-at) \chi_2(\cdot, t)\|_{L^2(\Omega)} \\ & = C_{1,m} \|(\chi_1, \chi_2)\|_{a,m}. \end{aligned} \quad (31)$$

Combining (30) and (31), we find that

$$\begin{aligned} & e^{-at} \|\mathcal{Q}_1(\chi_1, \chi_2)(t) - \mathcal{Q}_1(\bar{\chi}_1, \bar{\chi}_2)(t)\|_{H^m(\Omega)} \\ & \leq \mathcal{C}_1(\alpha, \beta, d, m) \left(\int_0^t (t-s)^{\alpha-1} e^{-a(t-s)} ds \right) \|(\chi_1, \chi_2)\|_{a,m}, \end{aligned} \quad (32)$$

where we denote

$$\mathcal{C}_1(\alpha, \beta, d, m) = \mathcal{C}(\alpha, \beta, d) C_{1,m} \lambda_1^{m-\beta} L_g. \quad (33)$$

Next, we need to deal with the integral quantity $\text{Int1} = \int_0^t (t-s)^{\alpha-1} e^{-a(t-s)} ds$. By change variable $s = t\gamma$, we find that

$$\begin{aligned} \text{Int1} &= \int_0^1 (t-t\gamma)^{\alpha-1} \exp(-at(1-\gamma)) t d\gamma \\ &= \int_0^1 t^\alpha (1-\gamma)^{\alpha-1} \exp(-at(1-\gamma)) d\gamma \\ &= (at(1-\gamma))^{\frac{\alpha}{2}} \exp(-at(1-\gamma)) \left(\frac{t}{a} \right)^{\alpha/2} \int_0^1 (1-\gamma)^{\alpha/2-1} d\gamma. \end{aligned} \quad (34)$$

Thank the inequality $y \leq e^y$ for $y \geq 0$, we know that

$$(at(1-\gamma))^{\alpha/2} \leq \exp(at(1-\gamma)). \quad (35)$$

Combining with the fact that $\int_0^1 (1-\gamma)^{\alpha/2-1} d\gamma = 2/\alpha$, we deduce that the following inequality

$$\int_0^t (t-s)^{\alpha-1} e^{-a(t-s)} ds \leq \frac{2}{\alpha} \left(\frac{T}{a} \right)^{\alpha/2}. \quad (36)$$

This inequality together with (32) leads to

$$\begin{aligned} & e^{-at} \|\mathcal{Q}_1(\chi_1, \chi_2)(t) - \mathcal{Q}_1(\bar{\chi}_1, \bar{\chi}_2)(t)\|_{H^m(\Omega)} \\ & \leq \frac{2\mathcal{C}_1(\alpha, \beta, d, m)}{\alpha} \left(\frac{T}{a} \right)^{\alpha/2} \|(\chi_1, \chi_2)\|_{a,m}. \end{aligned} \quad (37)$$

By a similar way, we also get that

$$\begin{aligned} & e^{-at} \|\mathcal{Q}_2(\chi_1, \chi_2)(t) - \mathcal{Q}_2(\bar{\chi}_1, \bar{\chi}_2)(t)\|_{H^m(\Omega)} \\ & \leq \frac{2\mathcal{C}_1(\alpha, \beta, d, m)}{\alpha} \left(\frac{T}{a} \right)^{\alpha/2} \|(\chi_1, \chi_2)\|_{a,m}. \end{aligned} \quad (38)$$

Therefore, we can deduce that

$$\|Q(\chi_1, \chi_2) - Q(\bar{\chi}_1, \bar{\chi}_2)\|_{a,m} \leq \frac{4\mathcal{C}_1(\alpha, \beta, d, m)}{\alpha} \left(\frac{T}{a} \right)^{\alpha/2} \|(\chi_1, \chi_2)\|_{a,m}. \quad (39)$$

Since the limitation

$$\lim_{a \rightarrow +\infty} \frac{4\mathcal{E}_1(\alpha, \beta, d, m)}{\alpha} \left(\frac{T}{a}\right)^{\alpha/2} = 0, \quad (40)$$

we know that there exists a positive a^* such that $4\mathcal{E}_1(\alpha, \beta, d, m)/\alpha(T/a^*)^{\alpha/2} < 1$. Thus, we can deduce that Q is contractive on $(L_a^\infty(0, T; H^m(\Omega)))^2$. Applying Banach fixed point theorem, we get that Q has a fixed point (u, v) , so, the function (u, v) is also the unique solution of (1). Since (14), we find that

$$\begin{aligned} \|u(\cdot, t)\|_{H^m(\Omega)} &\leq \left\| \sum_j \left(\int_0^\infty e^{-\nu t} \mathcal{K}(j, \alpha, \beta, \nu) d\nu \right) \varphi_j e_j(x) \right\|_{H^m(\Omega)} \\ &\quad + \left\| \sum_j \left(\int_0^t \left(\int_0^\infty e^{-\nu(t-s)} \mathcal{K}(j, \alpha, \beta, \nu) d\nu \right) \right. \right. \\ &\quad \cdot \left. \left. \langle \mathcal{G}(u(x, s), v(x, s)), e_j(x) \rangle ds \right) e_j(x) \right\|_{H^m(\Omega)} \\ &\leq \sqrt{\sum_j \lambda_j^{2m} \left(\int_0^\infty e^{-\nu t} \mathcal{K}(j, \alpha, \beta, \nu) d\nu \right)^2} \varphi_j^2 \\ &\quad + \int_0^t \sqrt{\sum_j \lambda_j^{2m} \left(\int_0^\infty e^{-\nu(t-s)} \mathcal{K}(j, \alpha, \beta, \nu) d\nu \right) \langle \mathcal{G}(u(x, s), v(x, s)), e_j(x) \rangle^2} ds. \end{aligned} \quad (41)$$

By looking at (24) and (29), we follow from (41) that

$$\begin{aligned} \|u(\cdot, t)\|_{H^m(\Omega)} &\leq \mathcal{E}(\alpha, \beta, d) \|\varphi\|_{H^m(\Omega)} \\ &\quad + \mathcal{E}(\alpha, \beta, d) \lambda_1^{m-\beta} \int_0^t (t-s)^{\alpha-1} \|\mathcal{G}(u(x, s), v(x, s))\|_{L^2(\Omega)} ds, \end{aligned} \quad (42)$$

where we have used that $\mathcal{G}(0, 0) = 0$ and

$$\|\mathcal{G}(u(x, s), v(x, s))\|_{L^2(\Omega)} \leq \mathcal{G}(0, 0) + L_g \left(\|u(\cdot, s)\|_{L^2(\Omega)} + \|v(\cdot, s)\|_{L^2(\Omega)} \right). \quad (43)$$

Hence, we derive that

$$\begin{aligned} \|u(\cdot, t)\|_{H^m(\Omega)} &\leq \mathcal{E}(\alpha, \beta, d) \|\varphi\|_{H^m(\Omega)} \\ &\quad + \mathcal{E}(\alpha, \beta, d) \lambda_1^{m-\beta} L_g \int_0^t (t-s)^{\alpha-1} \\ &\quad \cdot \left(\|u(\cdot, s)\|_{L^2(\Omega)} + \|v(\cdot, s)\|_{L^2(\Omega)} \right) ds. \end{aligned} \quad (44)$$

By a similar way, we also obtain that the following estimate

$$\begin{aligned} \|v(\cdot, t)\|_{H^m(\Omega)} &\leq \mathcal{E}(\alpha, \beta, d) \|\theta\|_{H^m(\Omega)} \\ &\quad + \mathcal{E}(\alpha, \beta, d) \lambda_1^{m-\beta} L_g \int_0^t (t-s)^{\alpha-1} \\ &\quad \cdot \left(\|u(\cdot, s)\|_{L^2(\Omega)} + \|v(\cdot, s)\|_{L^2(\Omega)} \right) ds. \end{aligned} \quad (45)$$

Combining (44) and (45), we get that

$$\begin{aligned} \|u(\cdot, t)\|_{H^m(\Omega)} + \|v(\cdot, t)\|_{H^m(\Omega)} &\leq \mathcal{E}(\alpha, \beta, d) \\ &\quad \cdot \left(\|\varphi\|_{H^m(\Omega)} + \|\theta\|_{H^m(\Omega)} \right) \\ &\quad + 2\mathcal{E}(\alpha, \beta, d) \lambda_1^{m-\beta} L_g \int_0^t (t-s)^{\alpha-1} \\ &\quad \cdot \left(\|u(\cdot, s)\|_{L^2(\Omega)} + \|v(\cdot, s)\|_{L^2(\Omega)} \right) ds. \end{aligned} \quad (46)$$

By applying Gronwall's inequality as in [34], we obtain that

$$\begin{aligned} \|u(\cdot, t)\|_{H^m(\Omega)} + \|v(\cdot, t)\|_{H^m(\Omega)} &\leq \mathcal{E}(\alpha, \beta, d) \\ &\quad \cdot \left(\|\varphi\|_{H^m(\Omega)} + \|\theta\|_{H^m(\Omega)} \right) E_{\alpha,1} \left(2\mathcal{E}(\alpha, \beta, d) \lambda_1^{m-\beta} L_g \right). \end{aligned} \quad (47)$$

Hence, we can deduce that (u, v) belongs to $L^\infty(0, T; L^2(\Omega)) \times L^\infty(0, T; L^2(\Omega))$, and furthermore, we also derive that

$$\|(u, v)\|_{L^\infty(0, T; L^2(\Omega)) \times L^\infty(0, T; L^2(\Omega))} \leq \mathcal{D}_1 \left(\|\varphi\|_{H^m(\Omega)} + \|\theta\|_{H^m(\Omega)} \right), \quad (48)$$

where we set

$$\mathcal{D}_1 = \mathcal{C}(\alpha, \beta, d) E_{\alpha,1} \left(2\mathcal{C}(\alpha, \beta, d) \lambda_1^{m-\beta} L_g \right). \quad (49)$$

□

Theorem 2. Let $(\varphi, \theta) \in H^{m+2}(\Omega) \times H^{m+2}(\Omega)$. Then, Problem (1) has a unique solution $(u, v) \in C^\alpha([0, T]; H^m(\Omega)) \times C^\alpha([0, T]; H^m(\Omega))$.

Proof. For $k > 0$, we set the following space

$$\begin{aligned} & C^k([0, T]; H^m(\Omega)) \times C^k([0, T]; H^m(\Omega)) \\ &= \left\{ (v_1, v_2) \in C([0, T]; H^m(\Omega)) \times C([0, T]; H^m(\Omega)) \mid \sup_{0 \leq t < s \leq T} \frac{\|v_1(\cdot, t) - v_1(\cdot, s)\|_{H^m(\Omega)}}{|t-s|^k} + \sup_{0 \leq t < s \leq T} \frac{\|v_2(\cdot, t) - v_2(\cdot, s)\|_{H^m(\Omega)}}{|t-s|^k} < \infty \right\}. \end{aligned} \quad (50)$$

It is easy to see that

$$\begin{aligned} u(x, t') - u(x, t) &= \sum_j \left[\int_0^\infty e^{-vt'} \mathcal{K}(j, \alpha, \beta, v) dv - \int_0^\infty e^{-vt} \mathcal{K}(j, \alpha, \beta, v) dv \right] \varphi_j e_j(x) \\ &\quad + \sum_j \left[\int_t^{t'} \left(\int_0^\infty e^{-vs} \mathcal{K}(j, \alpha, \beta, v) dv \right) \left\langle \mathcal{G}(u(x, t' - s), v(x, t' - s)), e_j(x) \right\rangle ds \right] e_j(x) \\ &\quad + \sum_j \left(\int_0^t \left(\int_0^\infty e^{-vs} \mathcal{K}(j, \alpha, \beta, v) dv \right) \left\langle \mathcal{G}(u(x, t' - s), v(x, t' - s)), e_j(x) \right\rangle ds - \mathcal{G}(u(x, t - s), v(x, t - s)), e_j(x) \right) e_j(x) \\ &= J_1(x, t' - t) + J_2(x, t' - t) + J_3(x, t' - t). \end{aligned} \quad (51)$$

First, we look at the second term $J_2(x, t' - t)$. Using the inequality, we find that

$$\begin{aligned} \|J_2(\cdot, t' - t)\|_{H^m(\Omega)} &\leq \int_t^{t'} \left\| \sum_j \left(\int_0^\infty e^{-vs} \mathcal{K}(j, \alpha, \beta, v) dv \right) \left\langle \mathcal{G}(u(x, t' - s), v(x, t' - s)), e_j(x) \right\rangle \right\|_{H^m(\Omega)} ds \\ &= \int_t^{t'} \sqrt{\sum_j \lambda_j^{2m} \left(\int_0^\infty e^{-vs} \mathcal{K}(j, \alpha, \beta, v) dv \right)^2 \left\langle \mathcal{G}(u(x, t' - s), v(x, t' - s)), e_j(x) \right\rangle^2} ds. \end{aligned} \quad (52)$$

Using (16), we obtain that

$$\begin{aligned} & \sqrt{\sum_j \lambda_j^{2m} \left(\int_0^\infty e^{-vs} \mathcal{K}(j, \alpha, \beta, v) dv \right)^2 \left\langle \mathcal{G}(u(x, t' - s), v(x, t' - s)), e_j(x) \right\rangle^2} \\ &\leq \mathcal{C}(\alpha, \beta, d) \lambda_1^{m-\beta} s^{\alpha-1} \left\| \mathcal{G}(u(x, t' - s), v(x, t' - s)) \right\|_{L^2(\Omega)} \\ &\leq \mathcal{C}(\alpha, \beta, d) \lambda_1^{m-\beta} L_g s^{\alpha-1} \left(\|u(\cdot, t' - s)\|_{L^2(\Omega)} + \|v(\cdot, t' - s)\|_{L^2(\Omega)} \right) \\ &\leq \mathcal{C}(\alpha, \beta, d) \lambda_1^{m-\beta} L_g s^{\alpha-1} \|(u, v)\|_{L^\infty(0, T; L^2(\Omega)) \times L^\infty(0, T; L^2(\Omega))} \leq \bar{\mathcal{D}}_1 s^{\alpha-1}. \end{aligned} \quad (53)$$

Combining (52) and (53) and using the inequality $(c + d)^\alpha \leq c^\alpha + d^\alpha$ for any $0 < \alpha < 1$, we get that

$$\|J_2(\cdot, t' - t)\|_{H^m(\Omega)} \leq \bar{\mathcal{D}}_1 \int_t^{t'} s^{\alpha-1} ds = \bar{\mathcal{D}}_1 \frac{(t')^\alpha - t^\alpha}{\alpha} \leq \bar{\mathcal{D}}_1 \frac{(t' - t)^\alpha}{\alpha}. \quad (54)$$

Next, we consider the second term $J_2(x, t' - t)$. It is easy to observe that

$$\begin{aligned} J_1(x, t' - t) &= \sum_j \left[\int_0^\infty e^{-vt'} \mathcal{K}(j, \alpha, \beta, v) dv - \int_0^\infty e^{-vt} \mathcal{K}(j, \alpha, \beta, v) dv \right] \varphi_j e_j(x) \\ &= \int_t^{t'} \left(\sum_j \bar{K}(s, j, \alpha, \beta, v) \varphi_j e_j(x) \right) ds. \end{aligned} \quad (55)$$

Here, we set the following function

$$\bar{K}(t, j, \alpha, \beta, \nu) = \frac{d}{dt} \left(\int_0^\infty e^{-\nu t} \mathcal{K}(j, \alpha, \beta, \nu) d\nu \right). \quad (56)$$

In order to give the further process, we use one result in Theorem 1 [24]. If $f \in H^2(\Omega)$, then, we get the following estimate

$$\sum_j \left| \bar{K}(s, j, \alpha, \beta, \nu) f_j \right|^2 \leq \mathcal{D}(\Omega, d, T, N)^2 s^{-2\alpha} \|f\|_{H^2(\Omega)}^2 \text{red} \cdot \quad (57)$$

Set the function $f^0(x) = \sum_j \lambda_j^m \varphi_j e_j(x)$. Since the fact that $\varphi \in H^{2+m}(\Omega)$, we know that f^0 belongs to the space $H^2(\Omega)$. Hence, using Parseval's equality, we get that

$$\begin{aligned} \|J_1(\cdot, t' - t)\|_{H^m(\Omega)} &\leq \int_t^{t'} \sqrt{\sum_j \lambda_j^{2m} |\bar{K}(s, j, \alpha, \beta, \nu)|^2 |\varphi_j|^2} ds \\ &\leq \int_t^{t'} \sqrt{\sum_j |\bar{K}(s, j, \alpha, \beta, \nu) f_j^0|^2} ds \\ &\leq \mathcal{D}(\Omega, d, T, N) \left(\int_t^{t'} s^{\alpha-1} ds \right) \|\varphi\|_{H^{2+m}(\Omega)} \\ &= \mathcal{D}(\Omega, d, T, N) \frac{(t')^\alpha - t^\alpha}{\alpha} \|\varphi\|_{H^{2+m}(\Omega)} \\ &\leq \mathcal{D}(\Omega, d, T, N) \frac{(t' - t)^\alpha}{\alpha} \|\varphi\|_{H^{2+m}(\Omega)}. \end{aligned} \quad (58)$$

Next, we treat the third term $J_3(x, t' - t)$. Using the inequality, we find that

$$\begin{aligned} \|J_3(\cdot, t' - t)\|_{H^m(\Omega)} &\leq \mathcal{C}(\alpha, \beta, d) \lambda_1^{m-\beta} \int_0^t s^{\alpha-1} \\ &\quad \cdot \left\| \mathcal{G}\left(u(x, t' - s), v(x, t' - s)\right) \right. \\ &\quad \left. - \mathcal{G}(u(x, t - s), v(x, t - s)) \right\|_{L^2(\Omega)} ds \\ &\leq \mathcal{C}(\alpha, \beta, d) \lambda_1^{m-\beta} \int_0^t (t - s)^{\alpha-1} \\ &\quad \cdot \left\| \mathcal{G}\left(u(x, s + t' - t), v(x, s + t' - t)\right) \right. \\ &\quad \left. - \mathcal{G}(u(x, s), v(x, s)) \right\|_{L^2(\Omega)} ds \\ &\leq \mathcal{C}(\alpha, \beta, d) \lambda_1^{m-\beta} L_g \int_0^t (t - s)^{\alpha-1} \\ &\quad \cdot \left(\left\| u(\cdot, s + t' - t) - u(\cdot, s) \right\|_{L^2(\Omega)} \right. \\ &\quad \left. - \left\| v(\cdot, s + t' - t) - v(\cdot, s) \right\|_{L^2(\Omega)} \right) ds. \end{aligned} \quad (59)$$

Combining (51), (52), (58), and (59), we obtain that

$$\begin{aligned} \|u(\cdot, t') - u(\cdot, t)\|_{H^m(\Omega)} &\leq \|J_1(\cdot, t' - t)\|_{H^m(\Omega)} \\ &\quad + \|J_2(\cdot, t' - t)\|_{H^m(\Omega)} + \|J_3(\cdot, t' - t)\|_{H^m(\Omega)} \\ &\leq \mathcal{D}(\Omega, d, T, N) \frac{(t' - t)^\alpha}{\alpha} \|\varphi\|_{H^{2+m}(\Omega)} \\ &\quad + \bar{\mathcal{D}}_1 \frac{(t' - t)^\alpha}{\alpha} + \mathcal{C}(\alpha, \beta, d) \lambda_1^{m-\beta} L_g \\ &\quad \cdot \int_0^t (t - s)^{\alpha-1} \left(\left\| u(\cdot, s + t' - t) - u(\cdot, s) \right\|_{L^2(\Omega)} \right. \\ &\quad \left. - \left\| v(\cdot, s + t' - t) - v(\cdot, s) \right\|_{L^2(\Omega)} \right) ds. \end{aligned} \quad (60)$$

By a similar way as above, we also obtain that

$$\begin{aligned} \|v(\cdot, t') - v(\cdot, t)\|_{H^m(\Omega)} &\leq \mathcal{D}(\Omega, d, T, N) \frac{(t' - t)^\alpha}{\alpha} \|\theta\|_{H^{2+m}(\Omega)} \\ &\quad + \bar{\mathcal{D}}_1 \frac{(t' - t)^\alpha}{\alpha} + \mathcal{C}(\alpha, \beta, d) \lambda_1^{m-\beta} L_h \\ &\quad \cdot \int_0^t (t - s)^{\alpha-1} \left(\left\| u(\cdot, s + t' - t) - u(\cdot, s) \right\|_{L^2(\Omega)} \right. \\ &\quad \left. - \left\| v(\cdot, s + t' - t) - v(\cdot, s) \right\|_{L^2(\Omega)} \right) ds. \end{aligned} \quad (61)$$

Combining (60) and (61), we derive that

$$\begin{aligned} \|u(\cdot, t') - u(\cdot, t)\|_{H^m(\Omega)} &+ \|v(\cdot, t') - v(\cdot, t)\|_{H^m(\Omega)} \\ &\leq \mathcal{D}(\Omega, d, T, N) \frac{(t' - t)^\alpha}{\alpha} \left(\|\varphi\|_{H^{2+m}(\Omega)} + \|\theta\|_{H^{2+m}(\Omega)} \right) \\ &\quad + 2\bar{\mathcal{D}}_1 \frac{(t' - t)^\alpha}{\alpha} + \bar{C} \int_0^t (t - s)^{\alpha-1} \left(\left\| u(\cdot, s + t' - t) - u(\cdot, s) \right\|_{H^m(\Omega)} \right. \\ &\quad \left. - \left\| v(\cdot, s + t' - t) - v(\cdot, s) \right\|_{H^m(\Omega)} \right) ds. \end{aligned} \quad (62)$$

Here, we set $\bar{C} = C_m 2\mathcal{C}(\alpha, \beta, d) \lambda_1^{m-\beta} (L_g + L_h)$. Let $h > 0$ fixed and let the following function

$$\begin{aligned} \mathcal{Y}_\rho(t) &= e^{-\rho t} \|u(\cdot, t + h) - u(\cdot, t)\|_{H^m(\Omega)} \\ &\quad + e^{-\rho t} \|v(\cdot, t + h) - v(\cdot, t)\|_{H^m(\Omega)}. \end{aligned} \quad (63)$$

From some above observations, we can deduce that

$$\begin{aligned}
 e^{\rho t} \mathcal{Y}_\rho(t) &\leq \mathcal{D}(\Omega, d, T, N) \frac{h^\alpha}{\alpha} \left(\|\varphi\|_{H^{2+m}(\Omega)} + \|\theta\|_{H^{2+m}(\Omega)} \right) \\
 &\quad + 2\bar{\mathcal{D}}_1 \frac{h^\alpha}{\alpha} + \bar{C} e^{\rho t} \int_0^t e^{-\rho(t-s)} (t-s)^{\alpha-1} e^{-\rho s} \\
 &\quad \cdot \left(\|u(\cdot, s+h) - u(\cdot, s)\|_{H^m(\Omega)} - \|v(\cdot, s+h) - v(\cdot, s)\|_{H^m(\Omega)} \right) ds \\
 &\leq \mathcal{D}(\Omega, d, T, N) \frac{h^\alpha}{\alpha} \left(\|\varphi\|_{H^{2+m}(\Omega)} + \|\theta\|_{H^{2+m}(\Omega)} \right) \\
 &\quad + 2\bar{\mathcal{D}}_1 \frac{h^\alpha}{\alpha} + \bar{C} e^{\rho t} \left(\int_0^t e^{-\rho(t-s)} (t-s)^{\alpha-1} ds \right) \max_{s \in [0, T]} \mathcal{Y}_\rho(s).
 \end{aligned} \tag{64}$$

From (36), we get that

$$\int_0^t (t-s)^{\alpha-1} e^{-\rho(t-s)} ds \leq \frac{2}{\alpha} \left(\frac{T}{\rho} \right)^{\alpha/2}. \tag{65}$$

This together with (64) that

$$\begin{aligned}
 \mathcal{Y}_\rho(t) &\leq \mathcal{D}(\Omega, d, T, N) \frac{h^\alpha}{\alpha} \left(\|\varphi\|_{H^{2+m}(\Omega)} + \|\theta\|_{H^{2+m}(\Omega)} \right) \\
 &\quad + 2\bar{\mathcal{D}}_1 \frac{h^\alpha}{\alpha} + \bar{C} \left(\frac{T}{\rho} \right)^{\alpha/2} \max_{s \in [0, T]} \mathcal{Y}_\rho(s) red.
 \end{aligned} \tag{66}$$

This implies that

$$\begin{aligned}
 \max_{t \in [0, T]} \mathcal{Y}_\rho(t) &\leq \mathcal{D}(\Omega, d, T, N) \frac{h^\alpha}{\alpha} \left(\|\varphi\|_{H^{2+m}(\Omega)} + \|\theta\|_{H^{2+m}(\Omega)} \right) \\
 &\quad + 2\bar{\mathcal{D}}_1 \frac{h^\alpha}{\alpha} + \bar{C} \left(\frac{T}{\rho} \right)^{\alpha/2} \max_{s \in [0, T]} \mathcal{Y}_\rho(s).
 \end{aligned} \tag{67}$$

Since $\bar{C}(T/\rho)^{\alpha/2} \rightarrow 0$ when $\rho \rightarrow +\infty$, we can choose $\rho^* > 0$ such that

$$\bar{C} \left(\frac{T}{\rho} \right)^{\alpha/2} < 1/2. \tag{68}$$

Hence, we follow from (67) and (64) that

$$\begin{aligned}
 \max_{t \in [0, T]} \mathcal{Y}_{\rho^*}(t) &\leq 2\mathcal{D}(\Omega, d, T, N) \frac{h^\alpha}{\alpha} \\
 &\quad \cdot \left(\|\varphi\|_{H^{2+m}(\Omega)} + \|\theta\|_{H^{2+m}(\Omega)} \right) + 4\bar{\mathcal{D}}_1 \frac{h^\alpha}{\alpha},
 \end{aligned} \tag{69}$$

which allows us to conclude that

$$\begin{aligned}
 &\|u(\cdot, t+h) - u(\cdot, t)\|_{H^m(\Omega)} + \|v(\cdot, t+h) - v(\cdot, t)\|_{H^m(\Omega)} \\
 &\leq 2e^{\rho^* t} \mathcal{D}(\Omega, d, T, N) \frac{h^\alpha}{\alpha} \left(\|\varphi\|_{H^{2+m}(\Omega)} + \|\theta\|_{H^{2+m}(\Omega)} \right) \\
 &\quad + e^{\rho^* t} 4\bar{\mathcal{D}}_1 \frac{h^\alpha}{\alpha} red.
 \end{aligned} \tag{70}$$

This inequality says that

$$(u, v) \in C^\alpha([0, T]; H^m(\Omega)) \times C^\alpha([0, T]; H^m(\Omega)). \tag{71}$$

□

Data Availability

No data were used to support this study.

Conflicts of Interest

The authors declare that they have no competing interests.

Authors' Contributions

Both authors contributed equally and significantly in writing this paper. Four authors read and approved the final manuscript.

References

- [1] A. A. Kilbas, H. M. Srivastava, and J. J. Trujillo, *Theory and Application of Fractional Differential Equations*, North-Holland Mathematics Studies, Elsevier Science B. V, Amsterdam, UK, 2006.
- [2] I. Podlubny, *Fractional Differential Equations*, Mathematics in Science and Engineering, Academic Press Inc, San Diego, CA, USA, 1990.
- [3] J. Manimaran, L. Shangerganesh, and A. Debbouche, "Finite element error analysis of a time-fractional nonlocal diffusion equation with the Dirichlet energy," *Journal of Computational and Applied Mathematics*, vol. 382, article 113066, 2021.
- [4] J. Manimaran, L. Shangerganesh, and A. Debbouche, "A time-fractional competition ecological model with cross-diffusion," *Mathematical Methods in the Applied Sciences*, vol. 43, no. 8, pp. 5197–5211, 2020.
- [5] M. Dehghan, "A computational study of the one-dimensional parabolic equation subject to nonclassical boundary specifications," *Numerical Methods for Partial Differential Equations*, vol. 22, no. 1, pp. 220–257, 2006.
- [6] S. D. Maharaj, M. Chaisi, and E. Karapinar, "New anisotropic models from isotropic solutions," *Mathematical Methods in the Applied Sciences*, vol. 29, no. 1, pp. 67–83, 2006.
- [7] H. Afshari and E. Karapinar, "A discussion on the existence of positive solutions of the boundary value problems via ψ -Hilfer fractional derivative on b-metric spaces," *Advances in Difference Equations*, vol. 2020, no. 1, 2020.
- [8] H. Afshari, S. Kalantari, and E. Karapinar, "Solution of fractional differential equations via coupled fixed point," *Electronic*

- Journal of Differential Equations*, vol. 2015, no. 286, pp. 1–12, 2015.
- [9] B. Alqahtani, H. Aydi, Karapinar, and Rakočević, “A solution for Volterra fractional integral equations by hybrid contractions,” *Mathematics*, vol. 7, no. 8, p. 694, 2019.
 - [10] E. Karapinar, A. Fulga, M. Rashid, L. Shahid, and H. Aydi, “Large contractions on quasi-metric spaces with an application to nonlinear fractional differential-equations,” *Mathematics*, vol. 7, no. 5, p. 444, 2019.
 - [11] A. Salim, B. Benchohra, E. Karapinar, and J. E. Lazreg, “Existence and Ulam stability for impulsive generalized Hilfer-type fractional differential equations,” *Advances in Difference Equations*, vol. 2020, no. 1, 2020.
 - [12] E. Karapinar, T. Abdeljawad, and F. Jarad, “Applying new fixed point theorems on fractional and ordinary differential equations,” *Advances in Difference Equations*, vol. 2019, no. 1, 2019.
 - [13] A. Abdeljawad, R. P. Agarwal, E. Karapinar, and P. S. Kumari, “Solutions of the nonlinear integral equation and fractional differential equation using the technique of a fixed point with a numerical experiment in extended b-metric space,” *Symmetry*, vol. 11, no. 5, p. 686, 2019.
 - [14] F. S. Bachir, S. Abbas, M. Benbachir, and M. Benchohra, “Hilfer-Hadamard fractional differential equations, existence and attractivity,” *Advances in the Theory of Nonlinear Analysis and its Application*, vol. 5, no. 1, pp. 49–57, 2021.
 - [15] A. Salim, M. Benchohra, J. E. Lazreg, and J. Henderson, “Nonlinear implicit generalized Hilfer-type fractional differential equations with non-instantaneous impulses in Banach spaces,” *Advances in the Theory of Nonlinear Analysis and its Application*, vol. 4, no. 4, pp. 332–348, 2020.
 - [16] Z. Baitichea, C. Derbazia, and M. Benchohrab, “ ψ -Caputo fractional differential equations with multi-point boundary conditions by topological degree theory,” *Results in Nonlinear Analysis*, vol. 3, no. 4, pp. 167–178, 2020.
 - [17] A. Yusuf, B. Acay, U. T. Mustapha, M. Inc, and D. Baleanu, “Mathematical modeling of pine wilt disease with Caputo fractional operator,” *Chaos Solitons and Fractals*, vol. 14, article 110569, 2021.
 - [18] B. Acay and M. Inc, “Fractional modeling of temperature dynamics of a building with singular kernels,” *Chaos Solitons Fractals*, vol. 142, article 110482, 2021.
 - [19] Z. Korpınar, M. Inc, and M. Bayram, “Theory and application for the system of fractional burger equations with Mittag leffler kernel,” *Applied Mathematics and Computation*, vol. 367, article 124781, 2020.
 - [20] X. J. Yang, Y. Y. Feng, C. Cattani, and M. Inc, “Fundamental solutions of anomalous diffusion equations with the decay exponential kernel,” *Mathematicsl Methods in the Applied Sciences*, vol. 42, no. 11, pp. 4054–4060, 2019.
 - [21] F. Shen, W. Tan, Y. Zhao, and T. Masuoka, “The Rayleigh-Stokes problem for a heated generalized second grade fluid with fractional derivative model,” *Nonlinear Analysis: Real World Applications*, vol. 7, no. 5, pp. 1072–1080, 2006.
 - [22] T. Caraballo, T. B. Ngoc, T. N. Thach, and N. H. Tuan, “On initial value and terminal value problems for subdiffusive stochastic Rayleigh-Stokes equation,” *Discrete & Continuous Dynamical Systems-B*, vol. 26, no. 8, article 4299, 2021.
 - [23] C. M. Chen, F. Liu, K. Burrage, and Y. Chen, “Numerical methods of the variable-order Rayleigh-Stokes problem for a heated generalized second grade fluid with fractional derivative,” *IMA Journal of Applied Mathematics*, vol. 78, no. 5, pp. 924–944, 2015.
 - [24] E. Bazhlekova, B. Jin, R. Lazarov, and Z. Zhou, “An analysis of the Rayleigh-Stokes problem for a generalized second-grade fluid,” *Numerische Mathematik*, vol. 131, no. 1, pp. 1–31, 2015.
 - [25] E. Bazhlekova and I. Bazhlevkov, “Viscoelastic flows with fractional derivative models: computational approach by convolutional calculus of Dimovski,” *Fractional Calculus and Applied Analysis*, vol. 17, no. 4, pp. 54–976, 2014.
 - [26] M. Khan, A. Anjum, C. Fetecau, and H. Qi, “Exact solutions for some oscillating motions of a fractional Burgers' fluid,” *Mathematical and Computer Modelling*, vol. 51, no. 5-6, pp. 682–692, 2010.
 - [27] M. A. Zaky, “An improved tau method for the multi-dimensional fractional Rayleigh-Stokes problem for a heated generalized second grade fluid,” *Computers & Mathematics with Applications*, vol. 75, no. 7, pp. 2243–2258, 2018.
 - [28] C. Xue and J. Nie, “Exact solutions of the Rayleigh-Stokes problem for a heated generalized second grade fluid in a porous half-space,” *Applied Mathematical Modelling*, vol. 33, no. 1, pp. 524–531, 2009.
 - [29] C. Zhao and C. Yang, “Exact solutions for electro-osmotic flow of viscoelastic fluids in rectangular micro-channels,” *Applied Mathematics and Computation*, vol. 211, no. 2, pp. 502–509, 2009.
 - [30] C. M. Chen, F. Liu, and V. Anh, “Numerical analysis of the Rayleigh-Stokes problem for a heated generalized second grade fluid with fractional derivatives,” *Applied Mathematics and Computation*, vol. 204, no. 1, pp. 340–351, 2008.
 - [31] C. M. Chen, F. Liu, and V. Anh, “A Fourier method and an extrapolation technique for Stokes' first problem for a heated generalized second grade fluid with fractional derivative,” *Journal of Computational and Applied Mathematics*, vol. 223, no. 2, pp. 777–789, 2009.
 - [32] N. H. Tuan, V. V. Tri, J. Singh, and T. N. Thach, “On a fractional Rayleigh–Stokes equation driven by fractional Brownian motion,” *Mathematical Methods in the Applied Sciences*, 2020.
 - [33] H. Brezis, *Functional Analysis*, Springer, New York, NY, USA, 2011.
 - [34] H. Ye, J. Gao, and Y. Ding, “A generalized Gronwall inequality and its application to a fractional differential equation,” *Journal of Mathematical Analysis and Applications*, vol. 328, no. 2, pp. 1075–1081, 2007.

Research Article

Existence for Time-Fractional Semilinear Diffusion Equation on the Sphere

N. D. Phuong,¹ Ho Duy Binh,² Ho Thi Kim Van,² and Le Dinh Long^{ID}²

¹Faculty of Fundamental Science, Industrial University of Ho Chi Minh City, Ho Chi Minh City 700000, Vietnam

²Division of Applied Mathematics, Thu Dau Mot University, Binh Duong Province, Vietnam

Correspondence should be addressed to Le Dinh Long; ledinhlong@tdmu.edu.vn

Received 1 May 2021; Accepted 28 May 2021; Published 24 June 2021

Academic Editor: Mustafa Inc

Copyright © 2021 N. D. Phuong et al. This is an open access article distributed under the Creative Commons Attribution License, which permits unrestricted use, distribution, and reproduction in any medium, provided the original work is properly cited.

Fractional diffusion on the sphere plays a large role in the study of physical phenomena customs and meteorology and geophysics. In this paper, we examine two types of the sphere problem: the initial value problem and the end value problem. We are interested in focus on the solution existence in a local or global form. In order to overcome difficult evaluations when evaluating, we need some new techniques. The main analytical tool is the use of the Banach fixed point theorem.

1. Introduction

When examining many physical and geophysical phenomena, one encounters problems directly or indirectly related to the sphere. To describe and explain quantitatively these models, they will be simulated with mathematical equations on the sphere. That is also the reason why the spherical equations have attracted many scientists interested and studied them. We can give some examples as follows. The weather forecasting models and the currents of groundwater in the ocean bed were simulated by equations on the sphere. For the readers' convenience, we have given a number of typical works that have had a great influence on the development of the analysis of PDEs on the sphere.

The qualitative and numerical methods have been considered by many authors, such as Thong et al. [1, 2]. Cauchy problems for elliptical queries on spheres have been studied in [3, 4]. The Navier-Stokes equation on the 2D unit sphere has been considered by the recent paper [5]. Recently, pseudo-parabolic equation on the sphere has been studied in [6]. Intuitively, we realize that the root structure of the differential equation on the sphere can be complex, so studying the types of partial derivative equations on the sphere requires mathematical tools with many new techniques.

According to the development of the mathematics disciplines, especially calculus, in the last few decades, fractional analysis has been one of the most influential disciplines in mathematics. Most of the problems related to it often have applications in modeling real-world problems. Fraction analysis has many applications in mechanics, physics, engineering science, etc. We would like to share many published works on these issues such as Karapinar et al. [7–14] and Inc and his group [15–19].

The main goal of this paper is to investigate the existence of the following equation

$$\frac{\partial}{\partial t} u(x, t) - \frac{\partial^{1-\alpha}}{\partial t} \Delta^* u(x, t) = \theta(t) F(u(x, t)), (x, t) \in S^2 \times [0, T], \quad (1)$$

with the initial Cauchy condition

$$u(x, 0) = f(x), \quad (2)$$

or the terminal value condition

$$u(x, T) = g(x), \quad (3)$$

where $\partial^\alpha/\partial t^\alpha$ called the Riemann-Liouville fractional derivative of order α , $0 < \alpha \leq 1$. Here, S^2 is a sphere on the R^3 . It is given by $\partial^{1-\alpha}/\partial t$ is the Riemann-Liouville fractional derivative of order $1 - \alpha$ given by

$$\frac{\partial^{1-\alpha}}{\partial t} v(t) := \frac{1}{\Gamma(\alpha)} \frac{d}{dt} \left(\int_0^t s^{\alpha-1} v(t-s) ds \right), \quad 0 < \alpha < 1, \quad (4)$$

and $D_{0^+}^{0.02cma} v(t) := (d/dt)v(t)$ if $\alpha = 1$. The functions ψ , F in (1) are defined later. The operator Δ^* is called Laplace-Beltrami which is introduced in more detail in Section 2. To the best of our knowledge, there are not any results on problem (1). Our main goal in this paper is to study two goals. Our first goal is to consider Cauchy initial problem (1)–(2). We get the global solution in a suitable space. Our second goal is to consider the Cauchy terminal problem (1)–(2). In this case, we get only local solutions in space L^∞ . For both of the above purposes, we use Banach fixed point theorem together with the evaluation of the sphere. In addition, to overcome the difficulties of proofing, we also cleverly make use of subtle evaluations of the Mittag-Leffler functions. The two main difficulties shown are as follows:

- (i) First, we deal with spherical harmonics on the sphere and require complex calculations
- (ii) Second, we must make sharp judgments for the Mittag-Leffler functions to achieve our goal

This paper is structured as follows. In Section 2, we introduce some preliminaries on Mittag-Leffler functions and their properties, Sobolev space on the sphere, and some other spaces. In Section 3, we focus on the initial value problem for problem (1)–(2). Section 4 provides the local well-posed result for terminal value problem (1)–(3).

2. Preliminaries

Mittag-Leffler is a function represented as the following form

$$E_{\alpha,\beta}(\xi) = \sum_{n=0}^{\infty} \frac{\xi^n}{\Gamma(n\alpha + \beta)}, \quad (5)$$

($\xi \in \mathbb{C}$), for $\alpha > 0$ and $\beta \in \mathbb{R}$. We call to mind the following lemmas (see for example [20]). We have the following lemma which is useful for next proof.

Lemma 1. *Let $0 < \alpha < 1$. Then, the function $E_{\alpha,1}(-z)$ satisfies the following property*

$$\frac{C_1}{1+z} \leq E_{\alpha,1}(-z) \leq \frac{C_2}{1+z}, \quad z > 0, \quad (6)$$

where C_1 and C_2 are the two positive constants.

Spherical harmonics are polynomials which satisfy $\Delta_x Y(x) = 0$ (where Δ_x is the Laplacian operator in R^3) and are restricted to the surface of the Euclidean sphere S^2 . The eigenvalues for $-\Delta^*$ in R^3 are

$$\lambda_j = j^2 + j, \quad j = 0, 1, 2, \dots, \quad (7)$$

and the eigenfunctions corresponding to λ_j are the spherical harmonics $\mathbf{W}_j(x)$ of order l , i.e.,

$$\Delta^* \mathbf{W}_j(x) = -\lambda_j \mathbf{W}_j(x). \quad (8)$$

The space of all spherical harmonics of degree j on S^2 , denoted by V_j , has an orthonormal basis $\{\mathbf{W}_{jk}(x) : k = 1, 2, 3, \dots, \mathcal{N}(2, j)\}$ where

$$\mathcal{N}(2, 0) = 1, \quad \mathcal{N}(2, j) = \frac{2j+1}{\Gamma(2)}, \quad j \geq 1. \quad (9)$$

Let any function $f \in L^2(S^2)$, so it is expressed by the expansion of spherical harmonics

$$f = \sum_{j=0}^{\infty} \sum_{k=1}^{(2j+1)/\Gamma(2)} \hat{f}_{jk} W_{jk}, \quad \hat{f}_{jk} = \int_{S^2} f \bar{\mathbf{W}}_{jk} dS, \quad (10)$$

where dS is the surface measure of the unit sphere. The Sobolev space $\mathbf{H}^v(S^2)$ is defined by

$$\mathbf{H}^v(S^2) = \left\{ g \in L^2(S^2) : \sum_{j=0}^{\infty} \sum_{k=1}^{(2j+1)/\Gamma(2)} (j^2 + j + 1)^v |g \wedge_{jk}|^2 < \infty \right\}, \quad (11)$$

with the following norm

$$\|g\|_{\mathbf{H}^v(S^2)} = \sqrt{\sum_{j=0}^{\infty} \sum_{k=1}^{(2j+1)/\Gamma(2)} (j^2 + j + 1)^v |g \wedge_{jk}|^2}. \quad (12)$$

The space $L_a^\infty(0, T; \mathbf{H}^v(S^2))$ is defined by

$$L_a^\infty(0, T; \mathbf{H}^v(S^2)) = \left\{ f \in L^\infty(0, T; \mathbf{H}^v(S^2)), e^{-at} \|f(\cdot, t)\|_{\mathbf{H}^v(S^2)} < \infty \right\}, \quad (13)$$

with corresponding norm as follows

$$\|f\|_{L_a^\infty(0, T; \mathbf{H}^v(S^2))} = \sup_{0 \leq t \leq T} e^{-at} \|f(\cdot, t)\|_{\mathbf{H}^v(S^2)}. \quad (14)$$

3. Global Existence for Mild Solution to Initial Value Problem

Theorem 2. Assume that $\theta : (0, T) \rightarrow \mathbb{R}$ such that

$$|\theta(z)| \leq C_\theta z^m, \quad -\frac{1}{2} < m. \quad (15)$$

Let F satisfies the condition

$$\|Fv_1 - Fv_2\|_{\mathbf{H}^v(S^2)} \leq K_f \|v_1 - v_2\|_{\mathbf{H}^v(S^2)}, \quad (16)$$

where K_f is a positive constant and v and v' satisfy that

$$0 < v - v' < \min \left(2, \frac{1}{\alpha} \right). \quad (17)$$

Then, problem (1)–(2) has a global existence in $L_a^\infty(0, T; \mathbf{H}^v(S^2))$ for a enough large.

Proof. As we know from [2] that Δ^* is the Laplace-Beltrami on the sphere S^2 . Any function $u \in L^2(S^2)$ can be described by the terms of spherical harmonics

$$\begin{aligned} u(x, t) &= \sum_{j=0}^{\infty} \sum_{k=1}^{(2j+1)/\Gamma(2)} \hat{u}_{jk}(t) \mathbf{W}_{jk}(x), \hat{u}_{jk}(t) \\ &= \int_{S^2} u(x, t) \bar{\mathbf{W}}_{jk}(x) dS, \end{aligned} \quad (18)$$

where dS is the surface measure of the unit sphere. Let us first give an expression of the mild solution.

$$\begin{aligned} \hat{u}_{jk}(t) &= E_{\alpha,1}(-(j^2 + j)t^\alpha) \hat{f}_{jk} \\ &+ \int_0^t E_{\alpha,1}(-(j^2 + j)(t-r)^\alpha) \theta(r) \hat{F}_{jk}(u)(r) dr. \end{aligned} \quad (19)$$

So, we get that the following equality

$$\begin{aligned} u(x, t) &= \sum_{j=0}^{\infty} \sum_{k=1}^{(2j+1)/\Gamma(2)} \left(E_{\alpha,1}(-(j^2 + j)t^\alpha) \hat{f}_{jk} \right) \mathbf{W}_{jk}(x) + \sum_{j=0}^{\infty} \sum_{k=1}^{(2j+1)/\Gamma(2)} \\ &\cdot \left(\int_0^t E_{\alpha,1}(-(j^2 + j)(t-r)^\alpha) \theta(r) \hat{F}_{jk}(u)(r) dr \right) \mathbf{W}_{jk}(x). \end{aligned} \quad (20)$$

Set the following function

$$\begin{aligned} \mathcal{J}w(t) &= \sum_{j=0}^{\infty} \sum_{k=1}^{(2j+1)/\Gamma(2)} \left(E_{\alpha,1}(-(j^2 + j)t^\alpha) \hat{f}_{jk} \right) \mathbf{W}_{jk}(x) + \sum_{j=0}^{\infty} \sum_{k=1}^{(2j+1)/\Gamma(2)} \\ &\cdot \left(\int_0^t E_{\alpha,1}(-(j^2 + j)(t-r)^\alpha) \theta(r) \hat{F}_{jk}(w)(r) dr \right) \mathbf{W}_{jk}. \end{aligned} \quad (21)$$

Setting the function

$$\mathcal{M}_1(x, t) = \sum_{j=0}^{\infty} \sum_{k=1}^{(2j+1)/\Gamma(2)} \left(E_{\alpha,1}(-(j^2 + j)t^\alpha) \hat{f}_{jk} \right) \mathbf{W}_{jk}(x). \quad (22)$$

Noting that $E_{\alpha,1}(-z) \leq C_2$ for any $z > 0$, and $f \in \mathbf{H}^v(S^2)$, the first term is bounded by

$$\begin{aligned} \|\mathcal{M}_1(\cdot, t)\|_{\mathbf{H}^v(S^2)}^2 &= \sum_{j=0}^{\infty} \sum_{k=1}^{(2j+1)/\Gamma(2)} (j^2 + j + 1)^v \left(E_{\alpha,1}(-(j^2 + j)t^\alpha) f \wedge_{jk} \right)^2 \\ &\leq |C_2|^2 \sum_{j=0}^{\infty} \sum_{k=1}^{(2j+1)/\Gamma(2)} (j^2 + j + 1)^v |f \wedge_{jk}|^2 \\ &= |C_2|^2 \|f\|_{\mathbf{H}^v(S^2)}^2, \end{aligned} \quad (23)$$

which allows us to get that

$$\|\mathcal{M}_1(\cdot, t)\|_{\mathbf{H}^v(S^2)} \leq C_2 \|f\|_{\mathbf{H}^v(S^2)}, \quad (24)$$

for any $0 \leq t \leq T$. This gives immediately that if $w = 0$ then $\mathcal{J}w$ belongs to the space $L^\infty(0, T; \mathbf{H}^v(S^2))$. Let us take two functions w and \bar{w} belong to the space $L^\infty(0, T; \mathbf{H}^v(S^2))$. Then, from (21), we have

$$\begin{aligned} \mathcal{J}w(t) - \mathcal{J}\bar{w}(t) &= \sum_{j=0}^{\infty} \sum_{k=1}^{(2j+1)/\Gamma(2)} \left(\int_0^t E_{\alpha,1}(-(j^2 + j)(t-r)^\alpha) \theta(r) \right. \\ &\cdot (F \wedge_{jk}(w)(r) - F \wedge_{jk}(\bar{w})(r)) dr \Big) \mathbf{W}_{jk}(x). \end{aligned} \quad (25)$$

Using Parseval's equality and Hölder inequality, one has

$$\begin{aligned} \|\mathcal{J}w(t) - \mathcal{J}\bar{w}(t)\|_{\mathbf{H}^v(S^2)}^2 &= \sum_{j=0}^{\infty} \sum_{k=1}^{(2j+1)/\Gamma(2)} (j^2 + j + 1)^v \\ &\cdot \left(\int_0^t E_{\alpha,1}(-(j^2 + j)(t-r)^\alpha) \theta(r) \right. \\ &\cdot (F \wedge_{jk}(w)(r) - F \wedge_{jk}(\bar{w})(r)) dr \Big)^2 \\ &\leq \sum_{j=0}^{\infty} \sum_{k=1}^{(2j+1)/\Gamma(2)} (j^2 + j + 1)^v \\ &\cdot \left(\int_0^t |E_{\alpha,1}(-(j^2 + j)(t-r)^\alpha) \theta(r)|^2 dr \right) \\ &\cdot \left(\int_0^t (F \wedge_{jk}(w)(r) - F \wedge_{jk}(\bar{w})(r))^2 dr \right). \end{aligned} \quad (26)$$

Let us review that $E_{\alpha,1}(-z) \leq (C_2/(1+z))$, we note that the following inequality

$$E_{\alpha,1}(-(j^2+j)t^\alpha) \leq \frac{C_2}{1+(j^2+j)t^\alpha} \leq C_2(j^2+j)^{-\beta} t^{-\alpha\beta}, \quad (27)$$

for $0 < \beta < 1$. Noting that $j^2 + j \geq ((j^2 + j + 1)/2)$ we get that the following inequality

$$\begin{aligned} (j^2 + j + 1)^\nu & \left(\int_0^t |E_{\alpha,1}(-(j^2+j)(t-r)^\alpha) \theta(r)|^2 dr \right) \\ & \leq |C_2|^2 |C_\theta|^2 4^{-\beta} (j^2 + j + 1)^{\nu-2\beta} \int_0^t (t-r)^{-2\alpha\beta} r^{2m} dr. \end{aligned} \quad (28)$$

Since the assumption $1 - 2\alpha\beta > 0$ and $1 + 2m > 0$, we can deduce that

$$\int_0^t (t-r)^{-2\alpha\beta} r^{2m} dr = t^{1-2\alpha\beta+2m} \mathbf{B}(1-2\alpha\beta, 1+2m). \quad (29)$$

Here, \mathbf{B} is beta function. Let us choose $\beta = 1/2(\nu - \nu')$; we see that β satisfies $1 - 2\alpha\beta > 0$. Combining (26) and (28), we provide that

$$\begin{aligned} \|\mathcal{F}w(t) - \mathcal{F}\bar{w}(t)\|_{\mathbf{H}^\nu(S^2)}^2 & \leq |\tilde{C}_1|^2 \sum_{j=0}^{\infty} \sum_{k=1}^{(2j+1)/T(2)} (j^2 + j + 1)^{\nu-2\beta} \\ & \quad \cdot \left(\int_0^t (F\wedge_{jk}(w)(r) - F\wedge_{jk}(\bar{w})(r))^2 dr \right) \\ & = |\tilde{C}_1|^2 \int_0^t \|F(w)(r) - F(\bar{w})(r)\|_{\mathbf{H}^{\nu-2\beta}(S^2)}^2 dr \\ & = |\tilde{C}_1|^2 \int_0^t \|F(w)(r) - F(\bar{w})(r)\|_{\mathbf{H}^{\nu'}(S^2)}^2 dr, \end{aligned} \quad (30)$$

where we set

$$|\tilde{C}_1|^2 = |C_2|^2 |C_\theta|^2 4^{-\beta} \mathbf{B}(1-2\alpha\beta, 1+2m). \quad (31)$$

Thanks to Lipschitz property of \mathcal{F} , we find that for any $a > 0$

$$\begin{aligned} e^{-2at} \|\mathcal{F}w(t) - \mathcal{F}\bar{w}(t)\|_{\mathbf{H}^\nu(S^2)}^2 & \leq |\tilde{C}_1|^2 K_f^2 T^{1-2\alpha\beta+2m} \int_0^t e^{-2a(t-r)} e^{-2ar} \|w(r) - \bar{w}(r)\|_{\mathbf{H}^\nu(S^2)}^2 dr \\ & \leq |\tilde{C}_1|^2 K_f^2 T^{1-2\alpha\beta+2m} \left(\int_0^t e^{-2a(t-r)} dr \right) \|w - \bar{w}\|_{L_a^\infty(0,T;\mathbf{H}^\nu(S^2))}^2. \end{aligned} \quad (32)$$

Due to the condition $\int_0^t e^{-2a(t-r)} dr \leq (1/2a)$, we know that the following estimate

$$\begin{aligned} e^{-2at} \|\mathcal{F}w(t) - \mathcal{F}\bar{w}(t)\|_{\mathbf{H}^\nu(S^2)}^2 & \leq \frac{|\tilde{C}_1|^2 K_f^2 T^{1-2\alpha\beta+2m}}{2a} \|w - \bar{w}\|_{L_a^\infty(0,T;\mathbf{H}^\nu(S^2))}^2. \end{aligned} \quad (33)$$

This implies immediately that

$$e^{-at} \|\mathcal{F}w(t) - \mathcal{F}\bar{w}(t)\|_{\mathbf{H}^\nu(S^2)} \leq \sqrt{\frac{|\tilde{C}_1|^2 K_f^2 T^{1-2\alpha\beta+2m}}{2a \|w - \bar{w}\|_{L_a^\infty(0,T;\mathbf{H}^\nu(S^2))}}}. \quad (34)$$

The right hand side of (34) is independent of t , so we can deduce that the following estimate

$$\|\mathcal{F}w - \mathcal{F}\bar{w}\|_{L_a^\infty(0,T;\mathbf{H}^\nu(S^2))} \leq \sqrt{\frac{|\tilde{C}_1|^2 K_f^2 T^{1-2\alpha\beta+2m}}{2a}} \|w - \bar{w}\|_{L_a^\infty(0,T;\mathbf{H}^\nu(S^2))}. \quad (35)$$

By choose a enough large such that $\sqrt{(|\tilde{C}_1|^2 K_f^2 T^{1-2\alpha\beta+2m}/2a)} < 1$, we find that \mathcal{F} is a contraction in $L_a^\infty(0, T; \mathbf{H}^\nu(S^2))$. Based on the Banach fixed point theorem, we have immediately concluded that problem (1)–(2) has a global existence in $L_a^\infty(0, T; \mathbf{H}^\nu(S^2))$. \square

4. Terminal Value Problem: Local Existence

In this section, we devoted the following problem with terminal condition

$$\begin{cases} \frac{\partial}{\partial t} w(x, t) - \frac{\partial^{1-\alpha}}{\partial t} \Delta^* w(x, t) = \theta(t) F(u(x, t)), & (x, t) \in S^2 \times (0, T), \\ w(x, T) = g(x), & x \in S^2, \end{cases} \quad (36)$$

where g is defined later. The purpose of this section is to study the existence and uniqueness of solution of problem (1)–(3).

Theorem 3. *Let us assume that $\psi : (0, T) \longrightarrow \mathbb{R}$ such that*

$$|\theta(z)| \leq C_\theta z^\delta, \delta > -1. \quad (37)$$

Let the function $g \in \mathbf{H}^2(S^2)$. Let F satisfies the condition

$$\|Fv_1 - Fv_2\|_{L^2(S^2)} \leq K_f \|v_1 - v_2\|_{L^2(S^2)}, \quad (38)$$

for any $K_f > 0$. Then, problem (1)–(3) has a local existence in $L^\infty(0, T; L^2(S^2))$.

Proof. Let us assume that $u(x, 0) = f(x)$. Then, we have

$$\begin{aligned}\hat{w}_{jk}(t) &= E_{\alpha,1}(-(j^2 + j)t^\alpha) \hat{f}_{jk} \\ &\quad + \int_0^t E_{\alpha,1}(-(j^2 + j)(t-r)^\alpha) \theta(r) \hat{F}_{jk}(w)(r) dr.\end{aligned}\quad (39)$$

Set $t = T$ into the above equation, we get that

$$\begin{aligned}\hat{w}_{jk}(T) &= E_{\alpha,1}(-(j^2 + j)T^\alpha) \hat{f}_{jk} \\ &\quad + \int_0^T E_{\alpha,1}(-(j^2 + j)(T-r)^\alpha) \theta(r) \hat{F}_{jk}(w)(r) dr.\end{aligned}\quad (40)$$

This implies that

$$\begin{aligned}\hat{f}_{jk} &= \frac{1}{E_{\alpha,1}(-(j^2 + j)T^\alpha)} \\ &\quad \cdot \left(\hat{g}_{jk} - \int_0^T E_{\alpha,1}(-(j^2 + j)(T-r)^\alpha) \theta(r) \hat{F}_{jk}(w)(r) dr \right).\end{aligned}\quad (41)$$

After some simple calculation, we have that

$$\begin{aligned}\hat{w}_{jk}(t) &= \frac{E_{\alpha,1}(-(j^2 + j)t^\alpha)}{E_{\alpha,1}(-(j^2 + j)T^\alpha)} \hat{f}_{jk} \\ &\quad + \int_0^t E_{\alpha,1}(-(j^2 + j)(t-r)^\alpha) \theta(r) \hat{F}_{jk}(w)(r) dr \\ &\quad - \frac{E_{\alpha,1}(-(j^2 + j)t^\alpha)}{E_{\alpha,1}(-(j^2 + j)T^\alpha)} \int_0^T E_{\alpha,1} \\ &\quad \cdot (-(j^2 + j)(T-r)^\alpha) \theta(r) \hat{F}_{jk}(w)(r) dr.\end{aligned}\quad (42)$$

So, we get that the following equality

$$\begin{aligned}w(x, t) &= \sum_{j=0}^{\infty} \sum_{k=1}^{(2j+1)/\Gamma(2)} \left(\frac{E_{\alpha,1}(-(j^2 + j)t^\alpha)}{E_{\alpha,1}(-(j^2 + j)T^\alpha)} \hat{g}_{jk} \right) \mathbf{w}_{jk}(x) \\ &\quad + \sum_{j=0}^{\infty} \sum_{k=1}^{(2j+1)/\Gamma(2)} \left(\int_0^t E_{\alpha,1}(-(j^2 + j) \right. \\ &\quad \cdot (t-r)^\alpha) \theta(r) \hat{F}_{jk}(w)(r) dr \Big) \mathbf{w}_{jk}(x) \\ &\quad - \sum_{j=0}^{\infty} \sum_{k=1}^{(2j+1)/\Gamma(2)} \left(\frac{E_{\alpha,1}(-(j^2 + j)t^\alpha)}{E_{\alpha,1}(-(j^2 + j)T^\alpha)} \int_0^T E_{\alpha,1} \right. \\ &\quad \cdot (-(j^2 + j)(T-r)^\alpha) \theta(r) \hat{F}_{jk}(w)(r) dr \Big) \mathbf{w}_{jk}(x).\end{aligned}\quad (43)$$

In order to apply Banach fixed point theorem, we need to set the following function

$$\begin{aligned}\mathcal{T}\theta(t) &= \underbrace{\sum_{j=0}^{\infty} \sum_{k=1}^{(2j+1)/\Gamma(2)} \left(\frac{E_{\alpha,1}(-(j^2 + j)t^\alpha)}{E_{\alpha,1}(-(j^2 + j)T^\alpha)} \hat{g}_{jk} \right) \mathbf{w}_{jk}}_{\mathcal{T}_0(t)} \\ &\quad + \underbrace{\sum_{j=0}^{\infty} \sum_{k=1}^{(2j+1)/\Gamma(2)} \left(\int_0^t E_{\alpha,1}(-(j^2 + j)(t-r)^\alpha) \theta(r) \hat{F}_{jk}(\theta)(r) dr \right) \mathbf{w}_{jk}}_{\mathcal{T}_1(t)} \\ &\quad - \underbrace{\sum_{j=0}^{\infty} \sum_{k=1}^{(2j+1)/\Gamma(2)} \left(\frac{E_{\alpha,1}(-(j^2 + j)t^\alpha)}{E_{\alpha,1}(-(j^2 + j)T^\alpha)} \int_0^T E_{\alpha,1}(-(j^2 + j)(T-r)^\alpha) \theta(r) \hat{F}_{jk}(\theta)(r) dr \right) \mathbf{w}_{jk}}_{\mathcal{T}_2(t)}.\end{aligned}\quad (44)$$

First, let us look at the expression as above and give an evaluation for $\|\mathcal{T}_2\theta_1(t) - \mathcal{T}_2\theta_2(t)\|$ for any $\theta_1, \theta_2 \in L^\infty(0, T; L^2(S^2))$. First, noting that

$$\begin{aligned}E_{\alpha,1}(-(j^2 + j)T^\alpha) &\geq \frac{C_1}{1 + (j^2 + j)T^\alpha}, \\ E_{\alpha,1}(-(j^2 + j)(T-r)^\alpha) &\leq \frac{C_2}{1 + (j^2 + j)(T-r)^\alpha},\end{aligned}\quad (45)$$

we get that

$$\begin{aligned} \frac{E_{\alpha,1}(-(j^2+j)(T-r)^\alpha)}{E_{\alpha,1}(-(j^2+j)T^\alpha)} &\leq \frac{C_2}{C_1} \frac{1+(j^2+j)T^\alpha}{1+(j^2+j)(T-r)^\alpha} \\ &\leq C_3 T^\alpha (T-r)^{-\alpha}. \end{aligned} \quad (46)$$

This implies immediately that

$$\begin{aligned} &\|\mathcal{T}_2\theta_1(t) - \mathcal{T}_2\theta_2(t)\|_{L^2(S^2)}^2 \\ &= \sum_{j=0}^{\infty} \sum_{k=1}^{(2j+1)I\Gamma(2)} \left(\frac{E_{\alpha,1}(-(j^2+j)t^\alpha)}{E_{\alpha,1}(-(j^2+j)T^\alpha)} \right. \\ &\quad \cdot \int_0^T E_{\alpha,1}(-(j^2+j)(T-r)^\alpha) \theta(r) \\ &\quad \cdot (F\wedge_{jk}(\theta_1)(r) - F\wedge_{jk}(\theta_2)(r)) dr \Big)^2 \\ &\leq \sum_{j=0}^{\infty} \sum_{k=1}^{(2j+1)I\Gamma(2)} \left(\int_0^T E_{\alpha,1}(-(j^2+j)(T-r)^\alpha) \right. \\ &\quad \cdot \frac{E_{\alpha,1}(-(j^2+j)t^\alpha)}{E_{\alpha,1}(-(j^2+j)T^\alpha)} \theta(r) dr \Big) \left(\int_0^T E_{\alpha,1}(-(j^2+j)(T-r)^\alpha) \right. \\ &\quad \cdot \frac{E_{\alpha,1}(-(j^2+j)t^\alpha)}{E_{\alpha,1}(-(j^2+j)T^\alpha)} \theta(r) (F\wedge_{jk}(\theta_1)(r) - F\wedge_{jk}(\theta_2)(r))^2 dr \Big), \end{aligned} \quad (47)$$

where we have used Hölder inequality. Using (46), we have that

$$\begin{aligned} &\int_0^T E_{\alpha,1}(-(j^2+j)(T-r)^\alpha) \frac{E_{\alpha,1}(-(j^2+j)t^\alpha)}{E_{\alpha,1}(-(j^2+j)T^\alpha)} \theta(r) dr \\ &\leq C_3 C_1 T^\alpha C_\theta \int_0^T (T-r)^{-\alpha} r^\delta dr \\ &= C_3 C_1 T^\alpha C_\theta T^{1-\alpha+\delta} \mathbf{B}(1-\alpha, 1+\delta) \\ &= C_3 C_1 C_\theta T^{1+\delta} \mathbf{B}(1-\alpha, 1+\delta), \\ &\int_0^T E_{\alpha,1}(-(j^2+j)(T-r)^\alpha) \frac{E_{\alpha,1}(-(j^2+j)t^\alpha)}{E_{\alpha,1}(-(j^2+j)T^\alpha)} \theta(r) (F\wedge_{jk}(\theta_1)(r) - F\wedge_{jk}(\theta_2)(r))^2 dr \\ &\leq C_3 C_1 T^\alpha C_\theta \int_0^T (T-r)^{-\alpha} r^\delta (F\wedge_{jk}(\theta_1)(r) - F\wedge_{jk}(\theta_2)(r))^2 dr. \end{aligned} \quad (48)$$

Hence, we can deduce that

$$\begin{aligned} &\|\mathcal{T}_2\theta_1(t) - \mathcal{T}_2\theta_2(t)\|_{L^2(S^2)}^2 \\ &\leq |C_3 C_1 C_\theta|^2 T^{1+\delta+\alpha} \mathbf{B}(1-\alpha, 1+\delta) \\ &\quad \cdot \int_0^T (T-r)^{-\alpha} r^\delta \|F(\theta_1)(r) - F(\theta_2)(r)\|_{L^2(S^2)}^2 dr. \end{aligned} \quad (49)$$

Lipschitz property of F as in (38) gives that

$$\begin{aligned} &\int_0^T (T-r)^{-\alpha} r^\delta \|F(\theta_1)(r) - F(\theta_2)(r)\|_{L^2(S^2)}^2 dr \\ &\leq K_f \int_0^T (T-r)^{-\alpha} r^\delta \|\theta_1(\cdot, r) - \theta_2(\cdot, r)\|_{L^2(S^2)}^2 dr \\ &\leq K_f \left(\int_0^T (T-r)^{-\alpha} r^\delta dr \right) \|\theta_1 - \theta_2\|_{L^\infty(0,T;L^2(S^2))}^2 \\ &= K_f T^{1-\alpha+\delta} \mathbf{B}(1-\alpha, 1+\delta) \|\theta_1 - \theta_2\|_{L^\infty(0,T;L^2(S^2))}^2. \end{aligned} \quad (50)$$

Combining (49) and (50), we find that

$$\begin{aligned} &\|\mathcal{T}_2\theta_1(t) - \mathcal{T}_2\theta_2(t)\|_{L^2(S^2)}^2 \\ &\leq |C_3 C_1 C_\theta|^2 T^{2+2\delta} |\mathbf{B}(1-\alpha, 1+\delta)|^2 \|\theta_1 - \theta_2\|_{L^\infty(0,T;L^2(S^2))}^2, \end{aligned} \quad (51)$$

which allows us to get that

$$\begin{aligned} &\|\mathcal{T}_2\theta_1(t) - \mathcal{T}_2\theta_2(t)\|_{L^2(S^2)} \\ &\leq C_3 C_1 C_\theta T^{1+\delta} \mathbf{B}(1-\alpha, 1+\delta) \|\theta_1 - \theta_2\|_{L^\infty(0,T;L^2(S^2))}. \end{aligned} \quad (52)$$

The term to the right of above expression is independent of t , so we get that

$$\begin{aligned} &\|\mathcal{T}_2\theta_1 - \mathcal{T}_2\theta_2\|_{L^\infty(0,T;L^2(S^2))} \\ &\leq C_3 C_1 C_\theta T^{1+\delta} \mathbf{B}(1-\alpha, 1+\delta) \|\theta_1 - \theta_2\|_{L^\infty(0,T;L^2(S^2))}. \end{aligned} \quad (53)$$

By a similar argument as above, we deduce that

$$\begin{aligned} &\|\mathcal{T}_1\theta_1(t) - \mathcal{T}_1\theta_2(t)\|_{L^2(S^2)}^2 \\ &= \sum_{j=0}^{\infty} \sum_{k=1}^{(2j+1)I\Gamma(2)} \left(\int_0^t E_{\alpha,1}(-(j^2+j)(t-r)^\alpha) \theta(r) \right. \\ &\quad \cdot (F\wedge_{jk}(\theta_1)(r) - F\wedge_{jk}(\theta_2)(r)) dr \Big)^2 \\ &\leq \sum_{j=0}^{\infty} \sum_{k=1}^{(2j+1)I\Gamma(2)} \left(\int_0^t E_{\alpha,1}(-(j^2+j)(t-r)^\alpha) \theta(r) dr \right) \\ &\quad \cdot \left(\int_0^t E_{\alpha,1}(-(j^2+j)(t-r)^\alpha) \theta(r) \right. \\ &\quad \cdot (F\wedge_{jk}(\theta_1)(r) - F\wedge_{jk}(\theta_2)(r))^2 dr \Big), \end{aligned} \quad (54)$$

where in the last inequality, we have used Hölder inequality. Let us repeat that $E_{\alpha,1}(-(j^2+j)(t-r)^\alpha) \leq C_2$, (14) and $\theta(r) \leq C_\theta r^\delta$, and thanks to that, we immediately have the following two estimations

$$\begin{aligned} & \int_0^t E_{\alpha,1}(-(j^2+j)(t-r)^\alpha)\theta(r)dr \\ & \leq C_2 C_\theta \int_0^t r^\delta dr = C_2 C_\theta \frac{t^{1+\delta}}{1+\delta} \leq \frac{C_2 C_\theta T^{1+\delta}}{1+\delta}. \end{aligned} \quad (55)$$

Combining (54) and (55), we arrive at

$$\begin{aligned} & \|\mathcal{T}_1\theta_1(t) - \mathcal{T}_1\theta_2(t)\|_{L^2(S^2)}^2 \\ & \leq \frac{C_2 C_\theta T^{1+\delta}}{1+\delta} C_2 C_\theta \int_0^t r^\delta \|F(\theta_1)(r) - F(\theta_2)(r)\|_{L^2(S^2)}^2 dr \\ & \leq \frac{K_f^2 C_2 C_\theta T^{1+\delta}}{1+\delta} C_2 C_\theta \int_0^t r^\delta \|\theta_1(\cdot, r) - \theta_2(\cdot, r)\|_{L^2(S^2)}^2 dr \\ & \leq \frac{K_f^2 C_2 C_\theta T^{1+\delta}}{1+\delta} C_2 C_\theta \left(\int_0^t r^\delta dr \right) \|\theta_1 - \theta_2\|_{L^\infty(0,T;L^2(S^2))}^2 \\ & \leq \left(\frac{K_f C_2 C_\theta T^{1+\delta}}{1+\delta} \right)^2 \mathbf{B}(1-\alpha, 1+\delta) \|\theta_1 - \theta_2\|_{L^\infty(0,T;L^2(S^2))}^2. \end{aligned} \quad (56)$$

The right hand side of (56) is independent of t ; we have the following conclusion immediately

$$\begin{aligned} & \|\mathcal{T}_1\theta_1 - \mathcal{T}_1\theta_2\|_{L^\infty(0,T;L^2(S^2))} \\ & \leq \frac{K_f C_2 C_\theta T^{1+\delta}}{1+\delta} \sqrt{\mathbf{B}(1-\alpha, 1+\delta)} \|\theta_1 - \theta_2\|_{L^\infty(0,T;L^2(S^2))}. \end{aligned} \quad (57)$$

From these two assertions (44), (53), and (57) and using the triangle inequality, we have the following affirmation

$$\begin{aligned} & \|\mathcal{T}\theta_1 - \mathcal{T}\theta_2\|_{L^\infty(0,T;L^2(S^2))} \\ & \leq \|\mathcal{T}_1\theta_1 - \mathcal{T}_1\theta_2\|_{L^\infty(0,T;L^2(S^2))} \\ & \quad + \|\mathcal{T}_2\theta_1 - \mathcal{T}_2\theta_2\|_{L^\infty(0,T;L^2(S^2))} \\ & \leq C_3 C_1 C_\theta T^{1+\delta} \mathbf{B}(1-\alpha, 1+\delta) \|\theta_1 - \theta_2\|_{L^\infty(0,T;L^2(S^2))} \\ & \quad + \frac{K_f C_2 C_\theta T^{1+\delta}}{1+\delta} \sqrt{\mathbf{B}(1-\alpha, 1+\delta)} \|\theta_1 \\ & \quad - \theta_2\|_{L^\infty(0,T;L^2(S^2))}. \end{aligned} \quad (58)$$

By choose T enough small, we can conclude that \mathcal{T} is a contraction. Next, we need to check that $\mathcal{T}_0(t)g \in L^\infty(0, T; L^2(S^2))$. Indeed, we get for any $0 \leq t \leq T$

$$\begin{aligned} \|\mathcal{T}_0(t)g\|_{L^2(S^2)}^2 & = \sum_{j=0}^{\infty} \sum_{k=1}^{(2j+1)/T(2)} \left(\frac{E_{\alpha,1}(-(j^2+j)t^\alpha)}{E_{\alpha,1}(-(j^2+j)T^\alpha)} \right)^2 |g^{\wedge_{jk}}|^2 \\ & \leq \sum_{j=0}^{\infty} \sum_{k=1}^{(2j+1)/T(2)} \left(\frac{1+(j^2+j)T^\alpha}{C_1} \right)^2 |f^{\wedge_{jk}}|^2 \\ & \leq \tilde{C} \|g\|_{\mathbf{H}^2(S^2)}^2. \end{aligned} \quad (59)$$

Using Banach fixed point theorem, we can conclude that \mathcal{T} has a fixed point w in $L^\infty(0, T; L^2(S^2))$. Hence, we get the desired result. \square

5. Conclusion

In this paper, this is one of our first results about fractional diffusion on the sphere. In this article, we are interested in the existing existence in local form and global format with the main tool is the Banach fixed point theorem. In the future, we study the ill-posedness of this problem and show the convergent rate between the sought solution and the regularized solution.

Data Availability

No data were used to support this study.

Conflicts of Interest

The authors declare that they have no competing interests.

Authors' Contributions

Both authors contributed equally and significantly in writing this paper. Four authors read and approved the final manuscript.

Acknowledgments

This research is supported by the Industrial University of Ho Chi Minh City (IUH) under grant number 66/HD-DHCN.

References

- [1] Q. T. L. Gia, N. H. Tuan, and T. Tran, "Solving the backward heat equation on the unit sphere," *ANZIAM Journal*, vol. 56, pp. C262–C278, 2016.
- [2] Q. T. Le Gia, "Approximation of parabolic PDEs on spheres using spherical basis functions," *Advances in Computational Mathematics*, vol. 22, no. 4, pp. 377–397, 2005.
- [3] Q. T. Le Gia, "Galerkin approximation for elliptic PDEs on spheres," *Journal of Approximation Theory*, vol. 130, no. 2, pp. 125–149, 2004.
- [4] Q. T. Le Gia, I. H. Sloan, and T. Tran, "Overlapping additive Schwarz preconditioners for elliptic PDEs on the unit sphere," *Mathematics of Computation*, vol. 78, no. 265, pp. 79–101, 2009.
- [5] Z. Brzeźniak, B. Goldys, and Q. T. Le Gia, "Random attractors for the stochastic Navier-Stokes equations on the 2D unit sphere," *Journal of Mathematical Fluid Mechanics*, vol. 20, no. 1, pp. 227–253, 2018.
- [6] N. D. Phuong and N. H. Luc, "Note on a nonlocal pseudo-parabolic equation on the unit sphere," *Dynamic Systems and Applications*, vol. 30, no. 2, pp. 295–304, 2019.
- [7] R. S. Adiguzel, U. Aksoy, and E. Karapinar, "New anisotropic models from isotropic solutions," *Mathematical Methods in the Applied Sciences*, vol. 29, no. 1, pp. 67–83, 2006.
- [8] H. Afshari and E. Karapinar, "A discussion on the existence of positive solutions of the boundary value problems via-Hilfer

- fractional derivative on b-metric spaces," *Advances in Difference Equations*, vol. 2020, no. 1, 11 pages, 2020.
- [9] H. Afshari, S. Kalantari, and E. Karapinar, "Solution of fractional differential equations via coupled fixed point," *Electronic Journal of Differential Equations*, vol. 2015, no. 1, pp. 1–12, 2015.
 - [10] B. Alqahtani, H. Aydi, E. Karapinar, and V. Rakocevic, "A solution for Volterra fractional integral equations by hybrid contractions," *Mathematics*, vol. 7, no. 8, p. 694, 2019.
 - [11] E. Karapinar, A. Fulga, M. Rashid, L. Shahid, and H. Aydi, "Large contractions on quasi-metric spaces with an application to nonlinear fractional differential-equations," *Mathematics*, vol. 7, no. 5, p. 444, 2019.
 - [12] A. Salim, B. Benchohra, E. Karapinar, and J. E. Lazreg, "Existence and Ulam stability for impulsive generalized Hilfer-type fractional differential equations," *Advances in Difference Equations*, vol. 2020, 21 pages, 2020.
 - [13] E. Karapinar, T. Abdeljawad, and F. Jarad, "Applying new fixed point theorems on fractional and ordinary differential equations," *Advances in Difference Equations*, vol. 2019, 25 pages, 2019.
 - [14] A. Abdeljawad, R. P. Agarwal, E. Karapinar, and P. S. Kumari, "Solutions of the nonlinear integral equation and fractional differential equation using the technique of a fixed point with a numerical experiment in extended b-metric space," *Symmetry*, vol. 11, no. 5, p. 686, 2019.
 - [15] A. Yusuf, B. Acay, U. T. Mustapha, M. Inc, and D. Baleanu, "Mathematical modeling of pine wilt disease with Caputo fractional operator," *Chaos, Solitons and Fractals*, vol. 143, p. 110569, 2021.
 - [16] B. Acay and M. Inc, "Fractional modeling of temperature dynamics of a building with singular kernels," *Chaos, Solitons and Fractals*, vol. 142, p. 110482, 2021.
 - [17] Z. Korpınar, M. Inc, and M. Bayram, "Theory and application for the system of fractional Burger equations with Mittag leffler kernel," *Applied Mathematics and Computation*, vol. 367, p. 124781, 2020.
 - [18] X. J. Yang, Y. Y. Feng, C. Cattani, and M. Inc, "Fundamental solutions of anomalous diffusion equations with the decay exponential kernel," *Mathematics Methods in the Applied Sciences*, vol. 42, no. 11, pp. 4054–4060, 2019.
 - [19] M. S. Hashemi, E. Darvishi, and M. Inc, "A geometric numerical integration method for solving the Volterra integro-differential equations," *International Journal of Computer Mathematics*, vol. 95, no. 8, pp. 1654–1665, 2018.
 - [20] I. Podlubny, *Fractional Differential Equations*, Academic Press, London, 1999.

Research Article

A Numerical Algorithm Applied to Free Convection Flows of the Casson Fluid along with Heat and Mass Transfer Described by the Caputo Derivative

Ndolane Sene 

Laboratoire Lmdan, Département de Mathématiques de la Décision, Université Cheikh Anta Diop de Dakar, Faculté des Sciences Economiques et Gestion, BP 5683, Fann, Dakar, Senegal

Correspondence should be addressed to Ndolane Sene; ndolanesene@yahoo.fr

Received 3 May 2021; Revised 3 June 2021; Accepted 12 June 2021; Published 23 June 2021

Academic Editor: Mustafa Inc

Copyright © 2021 Ndolane Sene. This is an open access article distributed under the Creative Commons Attribution License, which permits unrestricted use, distribution, and reproduction in any medium, provided the original work is properly cited.

In this paper, we present a class of numerical schemes and apply it to the diffusion equations. The objective is to obtain numerical solutions of the constructive equations of a type of Casson fluid model. We investigate the solutions of the free convection flow of the Casson fluid along with heat and mass transfer in the context of modeling with the fractional operators. The numerical scheme presented in this paper is called the fractional version of the Adams Basford numerical procedure. The advantage of this numerical technique is that it combines the Laplace transforms and the classical Adams Basford numerical procedure. Note that the usage of the Laplace transforms makes possible the applicability of the numerical approach to diffusion equations in general. The Caputo derivative will be used in the investigations. The influence of the considered Casson fluid model parameters as the Prandtl number Pr , the Schmidt number Sc , the material parameter of the Casson fluid β , and the order of the Caputo fractional derivative on the dynamics of the temperature, concentration, and velocity profiles has been presented analyzed. Graphical representations have supported the results of the paper.

1. Introduction

Fractional calculus has received much attraction over this last decade and grew many papers with many applications in sciences and engineering [1, 2], in mathematical physics [3, 4], in physics [3, 5], biology [6], and many other fields of sciences [7]. There exist, in our opinion, many interesting works on the application of fractional calculus in the literature; the authors of the following investigations [8, 9] can be considered references in fractional calculus. The importance of fractional calculus in real-world problems exists in many types of operators, those with singular kernels and those without singular kernels. For the operators with singular kernels, we can cite the Riemann-Liouville derivative [8, 9] and the Caputo derivative. The most used fractional operator with the singular kernel is the Caputo derivative [8, 9] because it has no problem in considering initial conditions and the fact that the derivative of the constant function gives a zero function, contrary to the Riemann-Liouville derivative,

which considers the unphysical initial conditions and the derivative of a constant function is not zero. We also have novel fractional operators called fractional operators with the exponential kernel as the Caputo-Fabrizio derivative [10] and the fractional derivative with Mittag-Leffler kernel as the Atangana-Baleanu fractional derivative [11]. One advantage of these two recent derivatives is that they remove the singularity existing in the definitions of the olds fractional operators. Many other fractional operators and generalizations of fractional operators exist in the literature (see in [12–14]). The advantages of the Caputo derivative, the Atangana-Baleanu derivative, and the Caputo-Fabrizio derivative in real-world modeling problems are that they consider the memory effect and generalize the integer-order derivative. New diffusion processes appear with the fractional operators as a subdiffusion process, superdiffusion process, and ballistic diffusion. For further applications of fractional derivatives and Laplace transforms in [15], Riaz et al. have presented the analytical solution of Oldroyd-B fluid in a circular duct that

applies a constant couple described by the fractional derivatives using the Laplace transform; in [16], Imran et al. have used the Caputo derivative to model natural convection flow subject to arbitrary velocity and Newtonian heating; the authors have proposed the exact solutions of the constructive equations of the considered model; in [17], Imran et al. have also used the Laplace transforms to get the exact solution of a class of Casson fluid models; in [18], Fetecau et al. study the Stokes problems for fluids of Brinkman type using Fourier sine transform. We can also draw recent investigations on fractional calculus; in [19], the authors have proposed the analytical solutions of the governing equations of gravity-driven thermal convection flow, which is based on a new method of derivations of the velocity field and temperature distribution. In [20], Abro has investigated the thermo-diffusion process on free convection flow in the context of modeling with the fractional operator. In [21], Qureshi et al. have focussed on the blood ethanol concentration system described by the fractional operator, and they have used real data application. In [22], the authors have used a fractional operator to propose a new iterative method for solving the fishery model. In [23], the authors have modeled the varicella-zoster virus using integer derivative, Caputo-Fabrizio derivative, and Atangana-Baleanu derivative. In [24], Jajarmi et al. have modeled the epidemic model with the nonsingular fractional operator and propose optimal control to control the disease.

Many papers in the literature address the analytical and semianalytical solutions of fluid and nanofluid models in general. In [25], Sheikh et al. propose a comparative study of the convective flow of a generalized Casson fluid described by the Atangana-Baleanu fractional derivative and the convective flow of a generalized Casson fluid described by the Caputo-Fabrizio fractional derivative. In [26], Hussanan et al. proposed an analytical solution via Laplace transform of the micropolar fluid flow model. In [27], the authors consider a generalized Casson fluid model with heat generation and chemical reaction and compare the model with Atangana-Baleanu derivative and the model with the derivative with the exponential kernel. In [28], Ali et al. propose applying a new fractional operator, namely, Caputo-Fabrizio derivative for MHD-free convection flow of the generalized Walters'-B fluid model. In [29], Khalid et al. address the unsteady MHD-free flow of a Casson fluid past an oscillating vertical plate with a constant wall temperature. For investigations of the nanofluids model, see the following investigations [30, 31]. In [32], the authors propose solutions to the Rayleigh-Stokes problem for a heated generalized second-grade fluid with Caputo fractional derivative model, the Laplace transforms, and the Fourier transform have been used for obtaining the analytical solutions. About works on Casson fluid model in fractional operators and integer-order derivative, in [33], Khan et al. propose fractional constitutive model of a generalized Casson fluid moving over an infinite, oscillating flat plate; they remarkably offer the exact solution using the exact solution using the Laplace transform method; in [34], Ali et al. investigate on a Casson fluid, along with magnetic particles in a horizontal cylinder; the exact solution is also proposed with the same Laplace transform, and the Caputo derivative has been used in the

modeling of the constructive equation; in [29], Khalid et al. studied the unsteady MHD free flow of a Casson fluid past an oscillating vertical plate with constant wall temperature; in [35], the author focused on the boundary layer flow of a non-Newtonian fluid accompanied by heat transfer toward an exponentially stretching surface in presence of suction or blowing at the surface and used Casson fluid to arrive at his objective.

Modeling fluid models using fractional-order derivative is also addressed in the literature (see in [25, 27]). Many papers in the literature use the homotopy procedure or the application of Fourier Laplace transforms. The Homotopy method application is limited due to the stability and convergence of the method. For example, with the homotopy method, the number of steps to consider making the scheme stable and convergent is the main inconvenience to the credibility of the obtained solution. The combination between the Laplace transforms and the Fourier-Laplace transform has many advantages, but the inconvenience is this method does not apply to some fluid models. Furthermore, we notice in the paper [25], the authors have studied the problem addressed in this paper by considering the Laplace transform. In many other investigations in the literature of Casson fluid models, analytical and semianalytical methods as in [29, 33–35] are proposed; the novelty of this paper in difference from the previous works is that we proposed a new numerical method to provide the solutions of the constructive equation of the model considered in this paper. The numerical scheme proposed in this paper combines the Adams Bashford numerical scheme and the Laplace transform. This paper novelty presents the solution of the free convection flow of the Casson fluid along with heat and mass transfer described by Caputo derivative using the previously cited fractional numerical procedure. The impact of the order of the Caputo derivative will be analyzed and illustrated as well. The effect on the dynamics of the free convection flow of the Casson fluid along with heat and mass transfer in the termal Grashof number, Prandtl number, mass Grashof number, Schmidt number, and material parameters of the Casson fluid will be analyzed.

2. Fractional Calculus Tool

We recall the fractional operators necessary for the rest of our investigations. We mean the Riemann-Liouville integral and the Caputo fractional derivative. These two operators are classical fractional calculus operators and are known to be with singularities. In the literature, there exist many other operators which can be used for the present investigations and are without singular kernels, like the derivative with Mittag-Leffler kernel and the derivative with the exponential kernel.

We describe the Riemann-Liouville fractional integral [8, 9] of the function $x : [0, +\infty[\rightarrow \mathbb{R}$ in the following form

$$(I^\alpha x)(t) = \frac{1}{\Gamma(\alpha)} \int_0^t (t-s)^{\alpha-1} x(s) ds, \quad (1)$$

where $\Gamma(\dots)$ is known as the Gamma function and with order α obeying the assumption that $\alpha > 0$.

Its associated derivative can also be represented; therefore, we describe the Riemann-Liouville fractional derivative [8, 9] of the function $x : [0, +\infty[\rightarrow \mathbb{R}$, of order α in the form

$$D^\alpha x(t) = \frac{1}{\Gamma(1-\alpha)} \frac{d}{dt} \int_0^t x(s)(t-s)^{-\alpha} ds, \quad (2)$$

where $t > 0$, the order of the operator obeys to the condition $\alpha \in (0, 1)$, and $\Gamma(\dots)$ denotes the Gamma Euler function.

The derivative which can be used in the modeling is called Caputo derivative [8, 9], and we represent it with the function $x : [0, +\infty[\rightarrow \mathbb{R}$, of order α as the following term:

$$D^\alpha x(t) = \frac{1}{\Gamma(1-\alpha)} \int_0^t \frac{dx}{ds} (t-s)^{-\alpha} ds, \quad (3)$$

where $t > 0$, the order of the fractional operator obeys to $\alpha \in (0, 1)$, and $\Gamma(\dots)$ is the so-called gamma Euler function.

The Laplace transform, which helps in general to solve the fractional differential equation, will also be used in this paper, and we try recalling it in this section. The Laplace transform of the Caputo derivative [8, 9] is represented as the following form:

$$\mathcal{L}\{(D_t^\alpha x)(t)\} = s^\alpha \mathcal{L}\{x(t)\} - s^{\alpha-1} x(0). \quad (4)$$

where the order α satisfies the relationship $\alpha \in (0, 1)$.

In the rest of this paper, the Laplace transform in Equation (4) will be combined with the numerical discretization of the Riemann-Liouville integral in Equation (1) to give a numerical approximation of the Caputo derivative represented in Equation (2).

3. Constructive Equations

In this section, we consider the fluid model described by fractional diffusion equations. The model investigated in this paper can be found in [25]. We particularly consider the governing equations of the Casson fluid's free convection flow along with the heat and mass transfer described by the Caputo fractional derivative. In this section, we set the fractional differential velocity equation described by the following form:

$$D_t^\alpha u = \left[1 + \frac{1}{\beta}\right] \frac{\partial^2 u}{\partial x^2} + Grw + Gmv, \quad (5)$$

combined with the fractional differential temperature equation

$$D_t^\alpha w = \frac{1}{Pr} \frac{\partial^2 w}{\partial x^2}, \quad (6)$$

and we add the fractional differential concentration equation

$$D_t^\alpha v = \frac{1}{Sc} \frac{\partial^2 v}{\partial x^2}, \quad (7)$$

with the initial conditions given by

$$u(x, 0) = v(x, 0) = w(x, 0) = 0, \quad (8)$$

and the functions u and v have as boundary conditions the following relation

$$u(0, t) = 1 \text{ and } v(0, t) = 1 \text{ and } w(0, t) = 1. \quad (9)$$

In the above equation, Gr represents the thermal Grashof number, Pr denotes the Prandtl number, Gm denotes the mass Grashof number, Sc denotes the Schmidt number, and β denotes the material parameter of the Casson fluid. Furthermore, u represents the velocity of the considered fluid, w represents the temperature, and v denotes the considered fluid concentration. As we notice, Equations (6) and (7) are fractional diffusion equations and represent the input of the fractional differential Equation (5). Equation (5) is specially called the fractional diffusion equation with a reaction term. Equation (5) describes the velocity of the model. Equation (7) represents the temperature distribution, and Equation (6) describes the fluid's concentration. Equations (5)–(7) can be solved using integral balance methods, double integral method and homotopy analysis method, and homotopy perturbation method. In this paper, Equations (5)–(7) will be subject to discretization. Note that it is important to mention that when the order $\alpha = 1$ in the Caputo derivative mentioned in Equation (2), we recover the classic fluid model described by the integer-order derivative. Then, the fractional context of the fluid model (5)–(7) is obtained when the order of the Caputo derivative is in $\alpha \in (0, 1)$. Furthermore, the behavior of the solution of model (5)–(7) in the interval $\alpha \in (1, 2)$ for example can be reported in the interval $(0, 1)$ by considering the change variable given as the form $\alpha = 1 + \beta$ where $\beta \in (0, 1)$. In conclusion, considering the study with the order of the Caputo derivative in $(0, 1)$ is sufficient in this investigation.

4. Numerical Procedure

In this section, the numerical scheme will be applied to obtain the solutions of the model presented in Equations (5)–(7). We adopt the Adams Bashford numerical scheme [36, 37] presented in the next paragraph. Let the fractional differential equations described by the following differential equation:

$$D_t^\alpha y = f(t, x), \quad (10)$$

where the function f is assumed to be Lipchitz continuous. This condition will guarantee the stability of the scheme described in this section. Here, we use the Caputo derivative, then the analytical solution of Equation (10) can be represented as the following form

$$x(t) = x(0) + I^\alpha f(t, x). \quad (11)$$

We now begin the discretization of the Equation (11) at the points t_n and t_{n+1} ; thus, we have the following representation

$$x(t_{n+1}) = x(0) + I^\alpha f(t_{n+1}, x_{n+1}), \quad (12)$$

$$x(t_n) = x(0) + I^\alpha f(t_n, x_n). \quad (13)$$

The difference between Equation (11) and Equation (12) gives the following relationship:

$$x(t_{n+1}) = x(t_n) + I^\alpha f(t_{n+1}, x_{n+1}) - I^\alpha f(t_n, x_n). \quad (14)$$

We now give the discretization of the fractional integral part of the previous equation; we have the following formula:

$$I^\alpha f(t_{n+1}, x_{n+1}) = A_{\alpha,1} = \frac{1}{\Gamma(\alpha)} \int_0^{t_{n+1}} (t_{n+1} - s)^{\alpha-1} f(s, x(s)) ds, \quad (15)$$

with the aid of the first-order interpolant polynomial of the function $f(\tau, x(\tau))$ described by the following representation:

$$p(\tau) = f(t_{j+1}, x_{j+1}) + \frac{\tau - t_{j+1}}{h} [f(t_{j+1}, x_{j+1}) - f(t_j, x_j)], \quad (16)$$

Using Equation (16) into Equation (15), we have the following relation:

$$A_{\alpha,1} = \frac{f(t_n, x_n)}{\Gamma(\alpha)h} \left[\frac{2ht_{n+1}^\alpha}{\alpha} - \frac{t_{n+1}^{\alpha+1}}{\alpha+1} \right] - \frac{f(t_{n-1}, x_{n-1})}{\Gamma(\alpha)h} \left[\frac{ht_{n+1}^\alpha}{\alpha} - \frac{t_{n+1}^{\alpha+1}}{\alpha+1} \right], \quad (17)$$

Similarly by the discretization of the integral form $A_{\alpha,2} = I^\alpha f(t_n, y_n)$, after calculation, we obtain the formula given by

$$A_{\alpha,2} = \frac{f(t_n, x_n)}{\Gamma(\alpha)h} \left[\frac{ht_n^\alpha}{\alpha} - \frac{t_n^{\alpha+1}}{\alpha+1} \right] - \frac{f(t_{n-1}, x_{n-1})t_n^{\alpha+1}}{\Gamma(\alpha)h}, \quad (18)$$

Combining Equation (17) and Equation (18) into Equation (14), we arrive at a numerical scheme with Adams Bashford procedure given as the following form:

$$x_{n+1} = x_n + A_{\alpha,1} - A_{\alpha,2}. \quad (19)$$

We set $t_n = nh$, and then, $t_{n+1} = (n+1)h$, replacing into Equation (17) the discretized form takes the form described by

$$A_{\alpha,1} = \frac{h^\alpha(n+1)^\alpha f(t_n, x_n)}{\Gamma(\alpha)} \left[\frac{1}{\alpha} - \frac{n+1}{\alpha+1} \right] - \frac{h^\alpha(n+1)^\alpha f(t_{n-1}, x_{n-1})}{\Gamma(\alpha)\alpha(\alpha+1)}, \quad (20)$$

Similarly, with the assumption $t_n = nh$, then $t_{n+1} = (n+1)h$, we replace in Equation (18) the discretized form takes the form described by

$$A_{\alpha,2} = \frac{h^\alpha(n)^\alpha f(t_n, x_n)}{\Gamma(\alpha)} \left[\frac{1}{\alpha} - \frac{n}{\alpha+1} \right] - \frac{h^\alpha(n)^{\alpha+1} f(t_{n-1}, x_{n-1})}{\Gamma(\alpha)}, \quad (21)$$

We can observe when the order α of the Caputo derivative converges to 1; we recover the original scheme

proposed by Adams Bashforth two-step method described as the form

$$x_{n+1} = x_n + \frac{3}{2}f(t_n, x_n) - \frac{1}{2}f(t_{n-1}, x_{n-1}). \quad (22)$$

Before closing this section, we focus on the stability of the proposed method. The necessary and sufficient condition will be to prove the function defined by $A_{\alpha,1} - A_{\alpha,2}$ is Lipchitz continuous. We can observe that the function $A_{\alpha,1} - A_{\alpha,2}$ depends on the function f . Thus, the Lipchitz continues of the function f implies the Lipchitz continuous of the function $A_{\alpha,1} - A_{\alpha,2}$.

This subsection will apply the numerical scheme previously described to obtain solutions of the diffusion equations presented in this section. The main idea of the application is for the first time to use the Laplace transforms. The obtained equation after applying the Laplace transform will be of one variable, and in this case, the numerical procedure can be used.

We begin the application of Equation (7). The first step will be to apply the Laplace transform to both sides of Equation (7). Then, we have the following relationship:

$$D_t^\alpha \tilde{v}(p, t) = \frac{1}{Sc} [p^2 \tilde{v}(p, t) - p v(0, t) - v(0, t)] - Sc \eta \tilde{v}(p, t). \quad (23)$$

For simplification in the style of writing, we suppose $\tilde{v} = \tilde{v}(p, t)$ and $f(t, \tilde{v}) = (1/Sc)[p^2 \tilde{v}(p, t) - p v(0, t) - v(0, t)] - Sc \eta \tilde{v}(p, t)$. Thus, Equation (23) can be rewritten as the following form:

$$D_t^\alpha \tilde{v} = f(t, \tilde{v}). \quad (24)$$

The numerical discretization of the previous Equation (24) is obtained from Equation (19) and is represented by the following form:

$$\tilde{v}_{n+1} = \tilde{v}_n + A_{\alpha,1} - A_{\alpha,2}, \quad (25)$$

where the intermediary discretizations are given by the forms

$$A_{\alpha,1} = \frac{h^\alpha(n+1)^\alpha f(t_n, \tilde{v}_n)}{\Gamma(\alpha)} \left[\frac{1}{\alpha} - \frac{n+1}{\alpha+1} \right] - \frac{h^\alpha(n+1)^\alpha f(t_{n-1}, \tilde{v}_{n-1})}{\Gamma(\alpha)\alpha(\alpha+1)}, \quad (26)$$

$$A_{\alpha,2} = \frac{h^\alpha(n)^\alpha f(t_n, \tilde{v}_n)}{\Gamma(\alpha)} \left[\frac{1}{\alpha} - \frac{n}{\alpha+1} \right] - \frac{h^\alpha(n)^{\alpha+1} f(t_{n-1}, \tilde{v}_{n-1})}{\Gamma(\alpha)}. \quad (27)$$

Applying the inverse of the Laplace transform to both sides of Equation (25), we obtain the following solution for our model:

$$v_{n+1} = v_n + A_{\alpha,1} - A_{\alpha,2}, \quad (28)$$

where the inverse of the Laplace transforms of the

transformations in Equations (26) and (27) are given by the following form:

$$A_{\alpha,1} = \frac{h^\alpha(n+1)^\alpha f(t_n, v_n)}{\Gamma(\alpha)} \left[\frac{1}{\alpha} - \frac{n+1}{\alpha+1} \right] - \frac{h^\alpha(n+1)^\alpha f(t_{n-1}, v_{n-1})}{\Gamma(\alpha)\alpha(\alpha+1)}, \quad (29)$$

$$A_{\alpha,2} = \frac{h^\alpha(n)^\alpha f(t_n, v_n)}{\Gamma(\alpha)} \left[\frac{1}{\alpha} - \frac{n}{\alpha+1} \right] - \frac{h^\alpha(n)^{\alpha+1} f(t_{n-1}, v_{n-1})}{\Gamma(\alpha)}, \quad (30)$$

and furthermore, the discretizations of the functions are given by the following forms:

$$f(t_n, v_n) = \frac{1}{\text{Sc}} \left[\frac{v_{i+1}^n - 2v_i^n + v_{i-1}^n}{\Delta^2 x} \right], \quad (31)$$

and that

$$f(t_{n-1}, v_{n-1}) = \frac{1}{\text{Sc}} \left[\frac{v_{i+1}^{n-1} - 2v_i^{n-1} + v_{i-1}^{n-1}}{\Delta^2 x} \right]. \quad (32)$$

We continue the application. We consider Equation (6). We repeat the same procedure by applying the Laplace transform to both sides of Equation (6); we have that

$$D_t^\alpha \tilde{w}(p, t) = \frac{1}{\text{Pr}} [p^2 \tilde{v}(p, t) - p w(0, t) - v(0, t)] + \kappa \tilde{w}(p, t). \quad (33)$$

We consider that the function $\tilde{w} = \tilde{w}(p, t)$ and furthermore the function $f(t, \tilde{w}) = (1/\text{Pr})[p^2 \tilde{w}(p, t) - p w(0, t) - w(0, t)] + \kappa \tilde{w}(p, t)$. Equation (33) becomes the following representation

$$D_t^\alpha \tilde{w} = f(t, \tilde{w}). \quad (34)$$

The numerical scheme of Equation (34) can be obtained from Equation (19) and is described by the following equation:

$$\tilde{w}_{n+1} = \tilde{w}_n + A_{\alpha,1} - A_{\alpha,2}, \quad (35)$$

where the intermediary schemes are given by the forms

$$A_{\alpha,1} = \frac{h^\alpha(n+1)^\alpha f(t_n, \tilde{w}_n)}{\Gamma(\alpha)} \left[\frac{1}{\alpha} - \frac{n+1}{\alpha+1} \right] - \frac{h^\alpha(n+1)^\alpha f(t_{n-1}, \tilde{w}_{n-1})}{\Gamma(\alpha)\alpha(\alpha+1)}, \quad (36)$$

$$A_{\alpha,2} = \frac{h^\alpha(n)^\alpha f(t_n, \tilde{w}_n)}{\Gamma(\alpha)} \left[\frac{1}{\alpha} - \frac{n}{\alpha+1} \right] - \frac{h^\alpha(n)^{\alpha+1} f(t_{n-1}, \tilde{w}_{n-1})}{\Gamma(\alpha)}. \quad (37)$$

Applying the inverse of the Laplace transform to both sides of Equation (35), we have the following solution for our fluid model:

$$w_{n+1} = w_n + A_{\alpha,1} - A_{\alpha,2}, \quad (38)$$

where the inverse of the Laplace transform of Equations (36) and (37) are represented in the following equations:

$$A_{\alpha,1} = \frac{h^\alpha(n+1)^\alpha f(t_n, w_n)}{\Gamma(\alpha)} \left[\frac{1}{\alpha} - \frac{n+1}{\alpha+1} \right] - \frac{h^\alpha(n+1)^\alpha f(t_{n-1}, w_{n-1})}{\Gamma(\alpha)\alpha(\alpha+1)}, \quad (39)$$

$$A_{\alpha,2} = \frac{h^\alpha(n)^\alpha f(t_n, w_n)}{\Gamma(\alpha)} \left[\frac{1}{\alpha} - \frac{n}{\alpha+1} \right] - \frac{h^\alpha(n)^{\alpha+1} f(t_{n-1}, w_{n-1})}{\Gamma(\alpha)}, \quad (40)$$

and Laplace transform furthermore; the numerical schemes of the functions coming from Equation (6) are given by the following equations:

$$f(t_n, w_n) = \frac{1}{\text{Pr}} \left[\frac{w_{i+1}^n - 2w_i^n + w_{i-1}^n}{\Delta^2 x} \right], \quad (41)$$

and that

$$f(t_{n-1}, w_{n-1}) = \frac{1}{\text{Pr}} \left[\frac{w_{i+1}^{n-1} - 2w_i^{n-1} + w_{i-1}^{n-1}}{\Delta^2 x} \right]. \quad (42)$$

We finish this section by giving the numerical scheme of the fluid model Equation (5). We apply the Laplace transform to Equation (5); we have the following:

$$D_t^\alpha \tilde{u} = \left[1 + \frac{1}{\beta} \right] [p^2 \tilde{u} - p u(0, t) - u(0, t)] + \text{Gr} \tilde{w} + \text{Gm} \tilde{v}. \quad (43)$$

We suppose the following functions which will help us in understanding the numerical scheme, $\tilde{u} = \tilde{u}(p, t)$ and $f(t, \tilde{u}) = [1 + (1/\beta)][p^2 \tilde{u} - p u(0, t) - u(0, t)] + \text{Gr} \tilde{w} + \text{Gm} \tilde{v}$. Thus, Equation (43) can be rewritten as the form

$$D_t^\alpha \tilde{u} = f(t, \tilde{u}). \quad (44)$$

The numerical procedure of the previous Equation (44) is obtained from Equation (19) and can be symbolized by the following representation

$$\tilde{u}_{n+1} = \tilde{u}_n + A_{\alpha,1} - A_{\alpha,2}, \quad (45)$$

with the intermediary discretization given by the equations

$$A_{\alpha,1} = \frac{h^\alpha(n+1)^\alpha f(t_n, \tilde{u}_n)}{\Gamma(\alpha)} \left[\frac{1}{\alpha} - \frac{n+1}{\alpha+1} \right] - \frac{h^\alpha(n+1)^\alpha f(t_{n-1}, \tilde{u}_{n-1})}{\Gamma(\alpha)\alpha(\alpha+1)}, \quad (46)$$

$$A_{\alpha,2} = \frac{h^\alpha(n)^\alpha f(t_n, \tilde{u}_n)}{\Gamma(\alpha)} \left[\frac{1}{\alpha} - \frac{n}{\alpha+1} \right] - \frac{h^\alpha(n)^{\alpha+1} f(t_{n-1}, \tilde{u}_{n-1})}{\Gamma(\alpha)}. \quad (47)$$

Utilizing the inverse of the Laplace transform on both sides of Equation (45), we obtain the following solution for our fluid model:

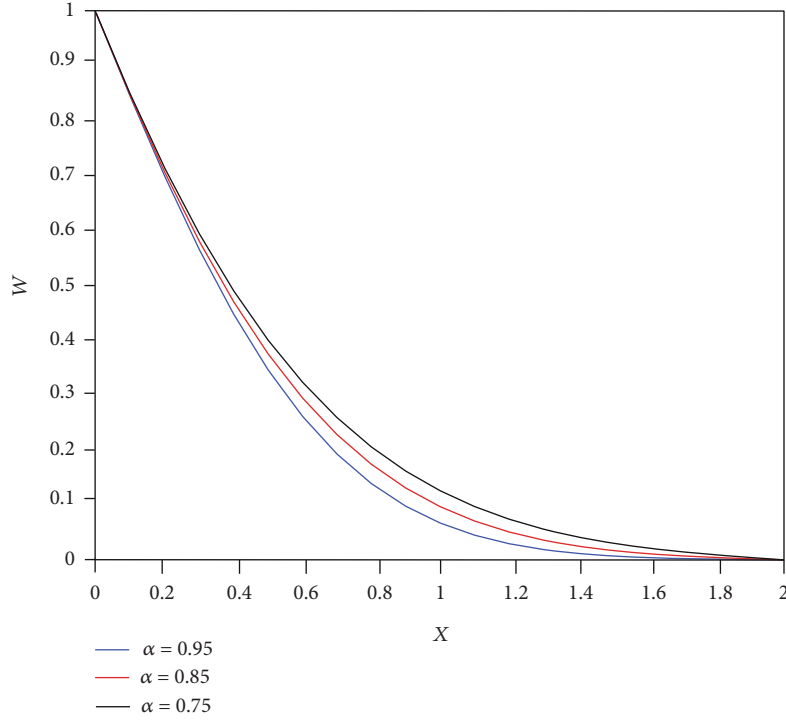


FIGURE 1: Dynamics of concentration in the fractional diffusion equation (Equation (6)).

$$u_{n+1} = u_n + A_{\alpha,1} - A_{\alpha,2}, \quad (48)$$

with the inverse of the Laplace transform of the transformations in Equations (49) and (50) are described by the following equations:

$$A_{\alpha,1} = \frac{h^\alpha(n+1)^\alpha f(t_n, u_n)}{\Gamma(\alpha)} \left[\frac{1}{\alpha} - \frac{n+1}{\alpha+1} \right] - \frac{h^\alpha(n+1)^\alpha f(t_{n-1}, u_{n-1})}{\Gamma(\alpha)\alpha(\alpha+1)}, \quad (49)$$

$$A_{\alpha,2} = \frac{h^\alpha(n)^\alpha f(t_n, u_n)}{\Gamma(\alpha)} \left[\frac{1}{\alpha} - \frac{n}{\alpha+1} \right] - \frac{h^\alpha(n)^\alpha f(t_{n-1}, u_{n-1})}{\Gamma(\alpha)}, \quad (50)$$

and in addition, the discretizations of the functions are given by the following equations:

$$f(t_n, u_n) = \left[1 + \frac{1}{\beta} \right] \left[\frac{u_{i+1}^{n-1} - 2u_i^{n-1} + u_{i-1}^{n-1}}{\Delta^2 x} \right] + Grw_i^n + Gmv_i^n, \quad (51)$$

and that

$$f(t_{n-1}, v_{n-1}) = \left[1 + \frac{1}{\beta} \right] \left[\frac{u_{i+1}^{n-1} - 2u_i^{n-1} + u_{i-1}^{n-1}}{\Delta^2 x} \right] + Grw_i^n + Gmv_i^n, \quad (52)$$

This section presents the numerical procedure to obtain the solutions of the fluid model shown in section 3. The main advantage is using the Laplace transform to make possible the

application of the numerical scheme presented in this section else; the applicability of the Adams Bashforth method is not trivial in many cases.

5. Discussion and Interpretation

In this section, we apply the Adams Bashford numerical scheme presented in the previous quarter. The numerical technique will be used to obtain the graphical representations. Additionally, the profile of the solution will be analyzed according to the variation of the model's parameters.

In our analysis, we begin with the constructive equation described in Equation (7). The first objective will be to analyze the impact of the Caputo derivative's order, the impact of the thermal Grashof number, the Prandtl number, the mass Grashof number, the Schmidt number, and the material parameter of the Casson fluid. We fix the time, and we depict the dynamics of the model according to the variation of the order of the Caputo derivative α . In Figures 1 and 2, we give the profile of the concentration and temperature with $Sc = 20$ and $Pr = 30$.

In Figures 1 and 2, we have considered the following orders $\alpha = 0.99$, $\alpha = 0.85$, and $\alpha = 0.75$. We notice from the statement that when the fractional operator's order increases, the temperature and concentration of the fluid decrease. This statement justifies the impact of the fractional-order derivative on the considered model. The main conclusion is the order of the Caputo derivative has an acceleration effect in the diffusion processes. The order of the fractional operator has the same influence on the temperature and the concentration distribution; it is normal because Equations (6) and (7) are diffusion equations, the small difference is, in Equation (6), we have

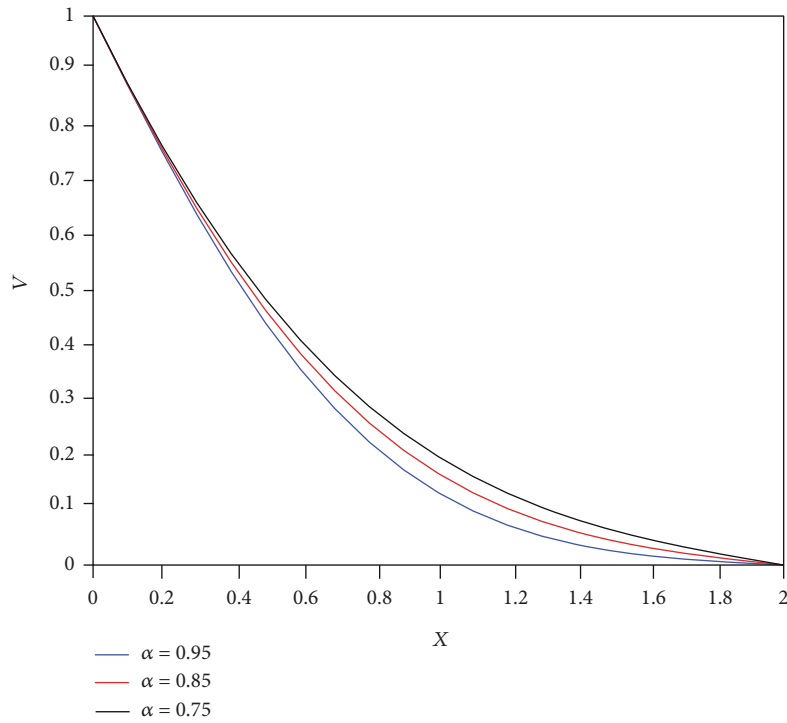


FIGURE 2: Dynamics of temperature in the fractional diffusion equation (Equation (7)).

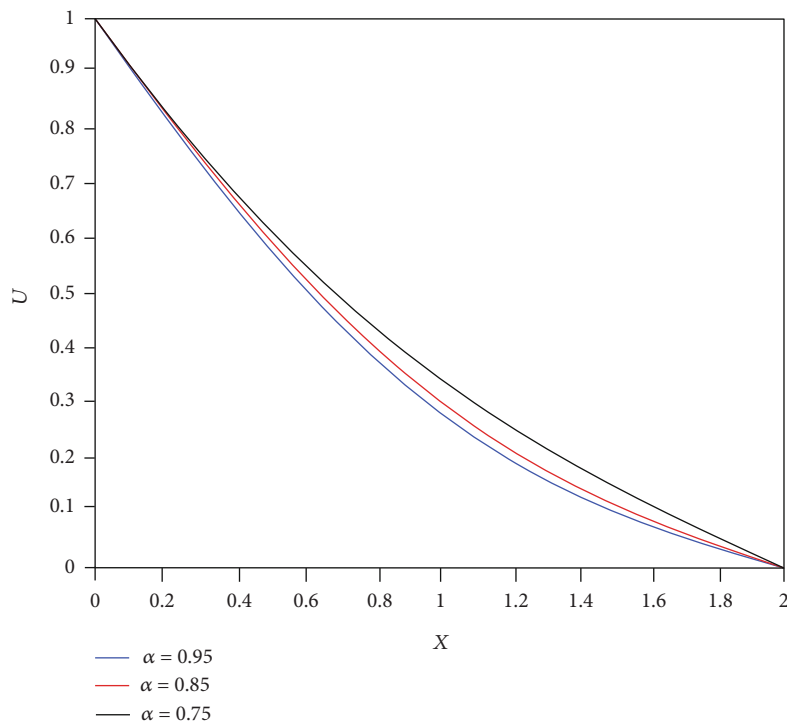


FIGURE 3: Dynamics of velocity using the fractional diffusion equation (Equation (5)).

$Pr = 30$, and in Equation (7), we have $Sc = 20$. In the studies in the paper [25], we can observe the behaviors of the profiles, the temperature, and the concentration distribution of the model (5)–(7) in [25] are the same as in Figures 1 and

2, which in particular validate our present investigations. In Figure 3, we consider the profile of the velocity with $\beta = 1$, $Gm = 15$, and $Gr = 15$. and $Pr = 30$, $Sc = 20$. The considered orders are $\alpha = 0.99$, $\alpha = 0.95$, and $\alpha = 0.90$.

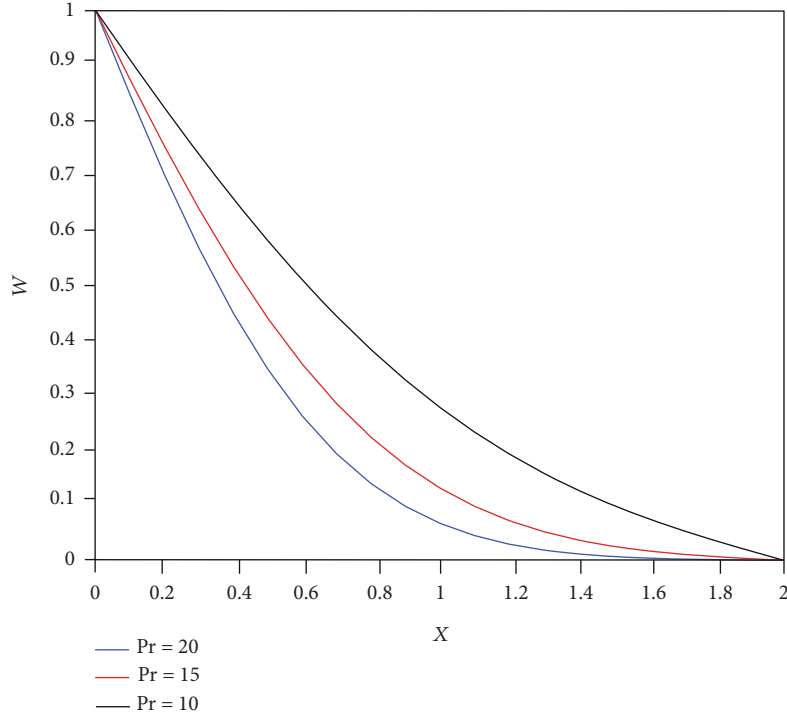


FIGURE 4: Dynamics of the temperature using the fractional diffusion equation (Equation (6)).

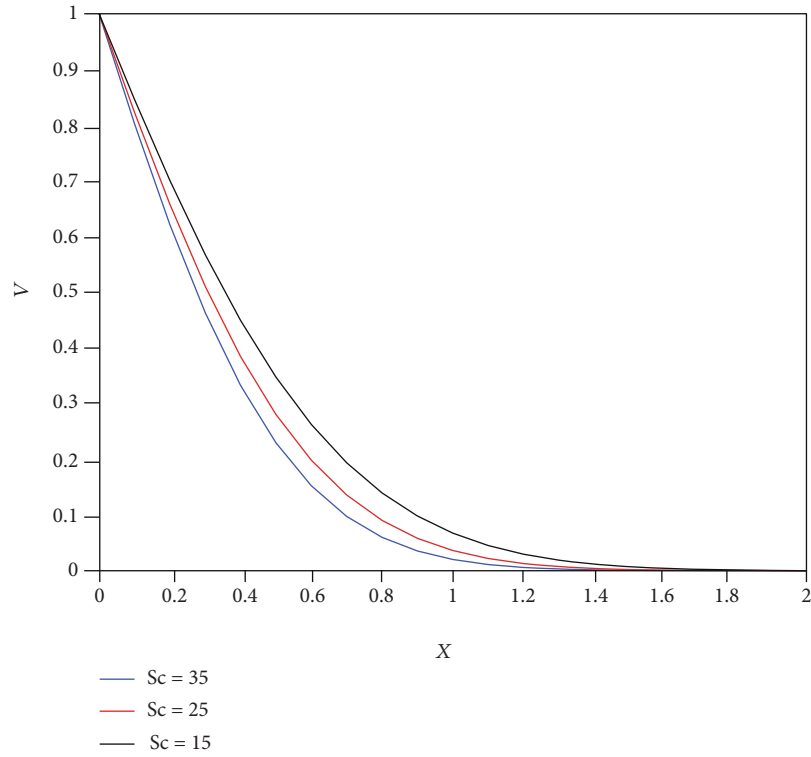


FIGURE 5: Dynamics of the concentration using the fractional diffusion equation (Equation (7)).

In Figure 3, we notice that the fractional-order derivative has an acceleration effect because when the order increases, the velocity of the temperature decreases as well. We now

analyze the impact of the Prandtl number on the temperature of the fluid model. Therefore, we fix into Equation (6) the order $\alpha = 0.95$. We consider the following values $Pr = 10$, Pr

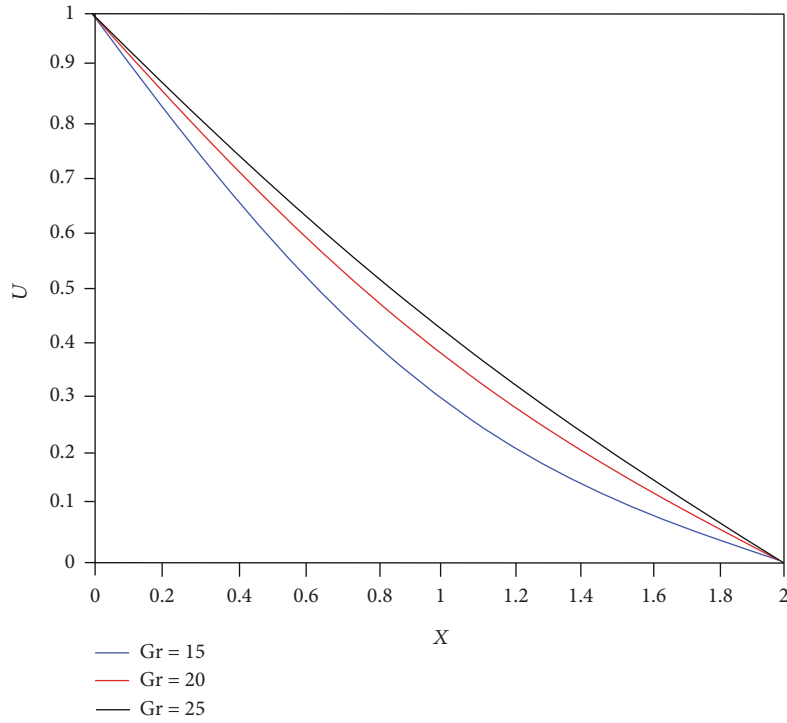


FIGURE 6: Dynamics of velocity of the fractional diffusion equation (Equation (5)).

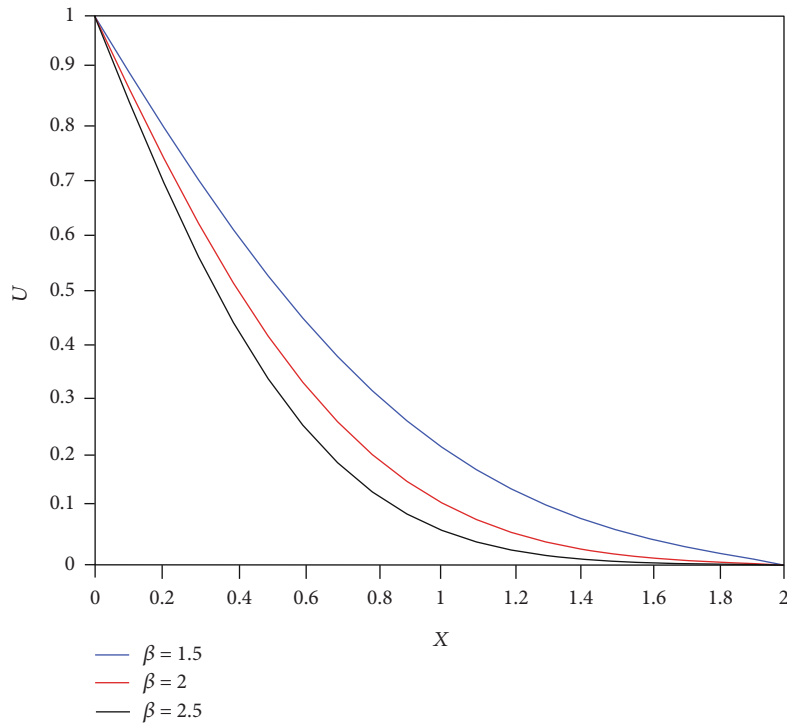


FIGURE 7: Dynamics of velocity using the fractional diffusion equation (Equation (5)).

$= 20$, and $Pr = 30$ in the following Figure 4. Our main observation in this figure is that when the Prandtl number increases, then the temperature of the fluid decreases considerably. Therefore, the Prandtl number plays a regulator role in the concentration model.

We now repeat the same analysis with the Schmidt number of the dynamics of the considered fluid concentration. We fix the order to $\alpha = 0.99$. In Figure 5, we set $Sc = 15$, $Sc = 25$, and $Sc = 35$, and we represent graphically the concentration profile.

We also notice that the Schmidt number has an acceleration effect in the diffusion process. We notice that when the order is fixed and when the Schmidt number increases, then the concentration profile decreases. Referring to Figures 4 and 5, we conclude that the Schmidt number and the Prandtl number have the same effects. We finish our analysis by analyzing the impact of the thermal Grashof number, mass Grashof number, and the material parameter of the Casson fluid on the dynamics of the velocity of the considered fluid. We begin by fixing $\beta = 0.5$, we set $Gm = 10$ and fix the order to $\alpha = 0.99$. We consider in this section the thermal Grashof number varies. In Figure 6 are represented the profiles of the velocities of the fluid at different values of the thermal Grashof number.

We remark that from Figure 6, we notice that when the thermal Grashof number increases, the velocity of the fluid increases with him. It is also not hard to see the mass Grashof number has the same influence on the velocity dynamics. We finish this section by analyzing the impact of the material parameters of the Casson fluid. We fix $Gm = 10$, $Pr = 10$, $Sc = 15$, and $Gr = 15$, and the order is considered as $\alpha = 0.99$. In Figure 7 are represented the velocity according to different values of the material parameters of the Casson fluid value.

In Figure 7, we notice that when the values of the Casson fluid's material parameter increase, then the velocity decreases as well.

The main findings of this section are summarized as follows. The increase in the mass Grashof number generates an increase in the dynamics of the Casson fluid's velocity. The increase in the Casson fluid's material parameters decreases the dynamics of the Casson fluid's velocity. The increase in the Prandtl number and Schmidt number generates a reduction in the temperature distribution and the concentration distribution.

6. Conclusion

We have proposed a numerical scheme to obtain the profile of the velocity, temperature, and concentration of the considered fluid. The method proposed in this paper is novel for this fluid model in the context of fractional-order derivative. We have found the Caputo derivative has an acceleration effect in the diffusion processes. Furthermore, the parameters used in our model play an important role in increasing or decreasing the Casson fluid dynamics considered in this paper. In this paper, we find that the Prandtl number Pr , the mass Grashof number Gr , the Schmidt number Sc , the material parameter of the Casson fluid β , and the order of the Caputo fractional derivative have an acceleration effect on the dynamics of the temperature, concentration, and velocity profiles of the considered Casson fluid model. In particular, the increase in the material parameter of the Casson fluid β generates the decrease of the velocity of the fluid. Contrary to the influence of the mass Grashof number Gr , which generates an increase in the velocity when his values increase. The Schmidt number Sc generates a decrease in the concentration when its values increase. The Prandtl number Pr also has the same influence; it generates a decrease in the temperature when its values increase. The method

applied in this paper can be experienced by the Stokes first problem described by the Caputo derivative and other second-grade fluids described by the fractional operators.

Data Availability

No data were used to support this study.

Conflicts of Interest

The authors declare that they have no conflict of interest.

References

- [1] V. F. Morales-Delgado, J. F. Gomez-Aguilar, M. A. Taneco-Hernandez, and R. F. Escobar-Jimenez, "Fractional operator without singular kernel: applications to linear electrical circuits," *International Journal of Circuit Theory and Applications*, vol. 46, no. 12, pp. 2394–2419, 2018.
- [2] D. Kumar, J. Singh, and D. Baleanu, "On the analysis of vibration equation involving a fractional derivative with Mittag-Leffler law," *Mathematical Methods in the Applied Sciences*, vol. 43, no. 1, pp. 443–457, 2019.
- [3] D. Avci, M. Yavuz, and N. Ozdemir, *Fundamental Solutions to the Cauchy and Dirichlet Problems for a Heat Conduction Equation Equipped with the Caputo-Fabrizio Differentiation*, Nova Science Publishers, 2019.
- [4] K. Saad, D. Baleanu, and A. Atangana, "New fractional derivatives applied to the Korteweg-de Vries and Korteweg-de Vries-Burger's equations," *Computational and Applied Mathematics*, vol. 37, no. 6, 2019.
- [5] D. Avci, N. Ozdemir, and M. Yavuz, *Fractional Optimal Control of Diffusive Transport Acting on a Spherical Region, Methods of Mathematical Modelling: Fractional Differential Equations*, CRC Press, 2019.
- [6] X. Wang and Z. Wang, "Dynamic analysis of a delayed fractional-order SIR model with saturated incidence and treatment functions," *International Journal of Bifurcation and Chaos*, vol. 28, no. 14, article 1850180, 2018.
- [7] A. Atangana and T. Mekkaoui, "Triniton the complex number with two imaginary parts: fractal, chaos and fractional calculus," *Chaos, Solitons & Fractals*, vol. 128, pp. 366–381, 2019.
- [8] A. A. Kilbas, H. M. Srivastava, and J. J. Trujillo, *Theory and Applications of Fractional Differential Equations*, North-Holland Mathematics Studies, Elsevier, Amsterdam, The Netherlands, 2006.
- [9] I. Podlubny, "Fractional differential equations," in *Mathematics in Science and Engineering*, p. 198, Academic Press, New York, NY, USA, 1999.
- [10] M. Caputo and M. Fabrizio, "A new definition of fractional derivative without singular kernel," *Progress in Fractional Differentiation and Applications*, vol. 1, no. 2, pp. 1–15, 2015.
- [11] A. Atangana and D. Baleanu, "New fractional derivatives with nonlocal and non-singular kernel: theory and application to heat transfer model," *Thermal Science*, vol. 20, no. 2, pp. 763–769, 2016.
- [12] J. Fahd, T. Abdeljawad, and D. Baleanu, "On the generalized fractional derivatives and their Caputo modification," *The Journal of Nonlinear Sciences and Applications*, vol. 10, pp. 2607–2619, 2017.

- [13] J. Fahd and T. Abdeljawad, "Generalized fractional derivatives and Laplace transform," *Discrete & Continuous Dynamical Systems-S*, vol. 13, no. 3, p. 709, 2020.
- [14] M. Roshdi Khalil, A. Y. Al Horani, and M. Sababheh, "A new definition of fractional derivative," *Journal of Computational and Applied Mathematics*, vol. 264, pp. 65–70, 2014.
- [15] M. B. Riaz, M. A. Imran, and K. Shabbir, "Analytic solutions of Oldroyd-B fluid with fractional derivatives in a circular duct that applies a constant couple," *Alexandria Engineering Journal*, vol. 55, no. 4, pp. 3267–3275, 2016.
- [16] M. A. Imran, "Applications of non-integer Caputo time fractional derivatives to natural convection flow subject to arbitrary velocity and Newtonian heating," *Neural Computing and Applications*, vol. 30, no. 5, pp. 1589–1599, 2018.
- [17] M. A. Imran, S. Sarwar, and M. Imran, "Effects of slip on free convection flow of Casson fluid over an oscillating vertical plate," *Boundary Value Problems*, vol. 30, 2016.
- [18] C. Fetecau, C. Fetecau, and M. A. Imran, "On stokes' problems for fluids of brinkman type," *Mathematical Reports*, vol. 13, no. 63, pp. 15–26, 2011.
- [19] B. Lohana, K. Ali Abro, and A. W. Shaikh, "Thermodynamical analysis of heat transfer of gravity-driven fluid flow via fractional treatment: an analytical study," *Journal of Thermal Analysis and Calorimetry*, vol. 144, no. 1, pp. 155–165, 2021.
- [20] K. A. Abro, "A fractional and analytic investigation of thermo-diffusion process on free convection flow: an application to surface modification technology," *The European Physical Journal Plus*, vol. 135, no. 1, pp. 31–45, 2019.
- [21] S. Qureshi, A. Yusuf, A. A. Shaikh, M. Inc, and D. Baleanu, "Fractional modeling of blood ethanol concentration system with real data application," *Chaos*, vol. 29, no. 1, article 013143, 2019.
- [22] M. M. Al Qurashi, Z. Korpınar, D. Baleanu, and M. Inc, "A new iterative algorithm on the time-fractional Fisher equation: residual power series method," *Advances in Mechanical Engineering*, vol. 9, no. 9, 2017.
- [23] S. Qureshi, A. Yusuf, A. A. Shaikh, and M. Inc, "Transmission dynamics of varicella zoster virus modeled by classical and novel fractional operators using real statistical data," *Physica A: Statistical Mechanics and its Applications*, vol. 534, p. 122149, 2019.
- [24] A. Jajarmi, A. Yusuf, D. Baleanu, and M. Inc, "A new fractional HRSV model and its optimal control: a non-singular operator approach," *Physica A: Statistical Mechanics and its Applications*, vol. 547, p. 123860, 2020.
- [25] N. A. Sheikh, F. Ali, M. Saqib, I. Khan, and S. A. A. Jan, "A comparative study of Atangana-Baleanu and Caputo-Fabrizio fractional derivatives to the convective flow of a generalized Casson fluid," *The European Physical Journal Plus*, vol. 132, no. 1, p. 54, 2017.
- [26] A. Hussanan, M. Z. Salleh, I. Khan, and S. Shafie, "Convection heat transfer in micropolar nanofluids with oxide nanoparticles in water, kerosene and engine oil," *Journal of Molecular Liquids*, vol. 229, pp. 482–488, 2017.
- [27] N. A. Sheikh, F. Ali, M. Saqib et al., "Comparison and analysis of the Atangana-Baleanu and Caputo-Fabrizio fractional derivatives for generalized Casson fluid model with heat generation and chemical reaction," *Results in Physics*, vol. 7, pp. 789–800, 2017.
- [28] F. Ali, M. Saqib, I. Khan, and N. A. Sheikh, "Application of Caputo-Fabrizio derivatives to MHD free convection flow of generalized Walters'-B fluid model," *The European Physical Journal Plus*, vol. 131, no. 10, p. 377, 2016.
- [29] A. Khalid, I. Khan, A. Khan, and S. Shafie, "Unsteady MHD free convection flow of Casson fluid past over an oscillating vertical plate embedded in a porous medium," *Engineering Science and Technology, an International Journal*, vol. 18, no. 3, pp. 309–317, 2015.
- [30] A. Wakif and R. Sehaqui, "Generalized differential quadrature scrutinization of an advanced MHD stability problem concerned water-based nanofluids with metal/metal oxide nanomaterials: a proper application of the revised two-phase nanofluid model with convective heating and through-flow boundary conditions," *Numerical Methods for Partial Differential Equations*, pp. 1–28, 2020.
- [31] A. Wakif, A. Chamkha, T. Thumma, I. L. Animasaun, and R. Sehaqui, "Thermal radiation and surface roughness effects on the thermo-magneto-hydrodynamic stability of alumina-copper oxide hybrid nanofluids utilizing the generalized Buongiorno's nanofluid model," *Journal of Thermal Analysis and Calorimetry*, vol. 143, pp. 1201–1220, 2021.
- [32] F. Shen, W. Tan, Y. Zhao, and T. Masuoka, "The Rayleigh-Stokes problem for a heated generalized second grade fluid with fractional derivative model," *Nonlinear Analysis: Real World Applications*, vol. 7, no. 5, pp. 1072–1080, 2006.
- [33] I. Khan, N. A. Shah, and D. Vieru, "Unsteady flow of generalized Casson fluid with fractional derivative due to an infinite plate," *The European Physical Journal Plus*, vol. 131, no. 6, p. 181, 2016.
- [34] F. Ali, N. A. Sheikh, I. Khan, and M. Saqib, "Magnetic field effect on blood flow of Casson fluid in axisymmetric cylindrical tube: a fractional model," *Journal of Magnetism and Magnetic Materials*, vol. 423, pp. 327–336, 2016.
- [35] S. Pramanik, "Casson fluid flow and heat transfer past an exponentially porous stretching surface in presence of thermal radiation," *Ain Shams Engineering Journal*, vol. 5, no. 1, pp. 205–212, 2014.
- [36] A. Atangana and S. I. Araz, "Extension of Atangana-Seda numerical method to partial differential equations with integer and non-integer order," *Alexandria Engineering Journal*, vol. 59, no. 4, pp. 2355–2370, 2020.
- [37] K. M. Owolabi and A. Atangana, "On the formulation of Adams-Bashforth scheme with Atangana-Baleanu-Caputo fractional derivative to model chaotic problems," *Chaos*, vol. 29, no. 2, article 023111, 2019.

Research Article

Study of Magnetohydrodynamic Pulsatile Blood Flow through an Inclined Porous Cylindrical Tube with Generalized Time-Nonlocal Shear Stress

Nehad Ali Shah ^{1,2}, A. Al-Zubaidi,³ and S. Saleem ³

¹*Informetrics Research Group, Ton Duc Thang University, Ho Chi Minh City, Vietnam*

²*Faculty of Mathematics & Statistics, Ton Duc Thang University, Ho Chi Minh City, Vietnam*

³*Department of Mathematics, College of Science, King Khalid University, Abha 61413, Saudi Arabia*

Correspondence should be addressed to Nehad Ali Shah; nehadali199@yahoo.com

Received 29 January 2021; Revised 23 April 2021; Accepted 6 May 2021; Published 18 May 2021

Academic Editor: Mustafa Inc

Copyright © 2021 Nehad Ali Shah et al. This is an open access article distributed under the Creative Commons Attribution License, which permits unrestricted use, distribution, and reproduction in any medium, provided the original work is properly cited.

The effects of pulsatile pressure gradient in the presence of a transverse magnetic field on unsteady blood flow through an inclined tapered cylindrical tube of porous medium are discussed in this article. The fractional calculus technique is used to provide a mathematical model of blood flow with fractional derivatives. The solution of the governing equations is found using integral transformations (Laplace and finite Hankel transforms). For the semianalytical solution, the inverse Laplace transform is found by means of Stehfest's and Tzou's algorithms. The numerical calculations were performed by using Mathcad software. The flow is significantly affected by Hartmann number, inclination angle, fractional parameter, permeability parameter, and pulsatile pressure gradient frequency, according to the findings. It is deduced that there exists a significant difference in the velocity of the flow at higher time when the magnitude of Reynolds number is small and large.

1. Introduction

The flow of blood into arteries is important in medical research. Computational blood flow simulation across vessels is one tool for integrating and interpreting clinical results. Specific hemodynamic flows may be predicted, which helps in disease detection. By deciding the form and design of blood vessels, it can also aid in the development of instruments that mimic or alter them. Blood movement in multi-stenosis arteries affected by pulsatile pressure gradient is one of the most difficult problems of fluid dynamics and biophysics. In the analysis that was carried out by Hatami et al. [1], blood was considered as a third grade non-Newtonian fluid conveying gold nanoparticles through a hollow porous vessel, and it was revealed that increase in the magnitude of the MHD (magnetohydrodynamics) parameter corresponds to a decrease in the velocity profile. The transient fluid dynamic equations of blood flow through stenosis geometry considering the non-Newtonian viscosity of blood and both magnetization and Lorentz forces was studied by

Amlimohamadi et al. [2]. They studied the real heart beating rate, the time-dependent inlet velocity alters, and the impact of the magnetic field on different heart cycles. In the presence of the external magnetic field, finite element simulation has been carried out by Alimohamadi and Imani [3] to investigate the pulsatile blood flow through stenosed artery.

A simple theory that models the flow of a magnetohydrodynamic blood through pump can be found in Roberts [4], Korchevskii, and Marochnik [5] while an explicit scientific report on the influence of a magnetic field on blood flow, flow of blood in branched arteries, blood flow with periodic body acceleration, flow of blood in the collapsed of veins, impact of slip velocity factor on the flow of blood in the microcirculation, combined effects of curved boundary on the temperature distribution, metabolic heat production, and blood flow has been deliberated upon by [6–11]. Tzirtzilakis [12] investigated the mathematical model for blood flow in the presence of the magnetic field. In consistent with the principles of magnetohydrodynamics, ferrohydrodynamics, and by involving the electrical conductivity, Mekheimer

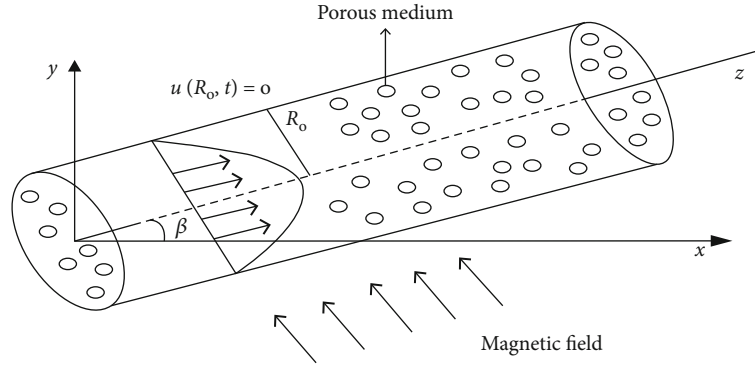


FIGURE 1: Schematic diagram of the flow geometry.

[13] discussed the influence of the uniform magnetic field on the peristaltic blood flow model. A mathematical governing model of blood flow in narrow and stenosis arteries under the influence of the magnetic field is presented by Jain et al. [14]. A numerical study of blood flow in stenosis tube due to the magnetic field is studied by Varshney and Gaurav [15]. Many other papers discussed blood flow models in stenosed arteries [16–19].

The effect of the magnetic field on parameters of blood in presence of magnetic particle through a circular tube is given by Sharma et al. [20]. The two-phase blood flow through a circular tube with magnetic properties has been studied by Zafar et al. [21]. He found the comparison of the analytical and semianalytical solutions of the classical model. The exact solutions of the blood flow model with fractional derivatives along with magnetic nanoparticles in the cylindrical domain have been found by Shah et al. [22].

Flow across a porous medium has a wide range of industrial applications. Blood flow through several stenosed porous arteries under the influence of a transverse magnetic field has been studied by Sinha et al. [23]. Magnetohydrodynamic MHD blood flow through porous vessel has been carried out by Ramamurthy and Shanker [24]. The peristaltic non-Newtonian Maxwell fluid flow through porous tube has been introduced by Eldesoky and Mousa [25].

In bioengineering, peristaltic blood flow in an inclined medium is a useful model. As a result, numerous studies of peristaltic blood flow models have been published. Through introducing a computational investigation of unsteady pulsatile blood flow through porous artery medium see [26]. Some important recent contributions to the mentioned topic are referenced in [27–30]. Generally, a fractional derivative model is obtained from the ordinary model by interchanging the derivatives of integer order with noninteger order.

Fractional dynamical systems demonstrate promise in the study of fluid flow models. In architecture and manufacturing, the fractional calculus approach has been used to obtain a useful generalization of physical concepts. Many students are interested in using fractional dynamics to solve problems in classical dynamics. However, Riemann–Liouville and Caputo fractional derivatives are commonly used, and this generalization can be done by using different other fractional approaches/definitions [31, 32].

Many models used fractional calculus to solve fluid flow problems [33, 34]. In the year 2016, Shah et al. [22] used Caputo-Fabrizio derivative to obtain the exact solutions of pulsatile blood flow in a circular cylinder. In the study, Laplace and Hankel transform was successfully used to further solve the momentum and energy equation. In that study, the influence of MHD, porous medium, and inclined surface was ignored. Motivating by Shah et al. [28], we have obtained the analytic and semianalytical solutions of unsteady MHD blood flow through an inclined porous tube that has been studied in the presence of peristaltic pressure gradient. The analysis is made by employing Laplace transformation method, and some valuable predictions have been carried out from the study. For the semianalytic solution, the inverse Laplace transform has been calculated by using numerical package though Mathcad because the velocity expressions of Laplace transform are in the complex form of modified Bessel functions. Therefore, it is almost impossible to find inverse Laplace analytically. To show the accuracy of our obtained results of inverse Laplace transform, these results are compared with two other inverse Laplace transform numerical algorithms, named as Stehfest's [35] and Tzou's [36] algorithms. Finally, the effect of pertinent physical parameters is discussed in detail.

2. Formulation of the Problem

Consider an inclined tapered axisymmetric cylindrical tube of radius R_0 with an unsteady pulsatile blood flow in a porous medium.

Figure 1 shows how a fluid subjected to a uniform transverse magnetic field behaves in a perpendicular direction to the tube. The induced magnetic field as well as the external electric field is not taken into account. The cylindrical coordinate system (r, θ, z) is introduced with the z -axis that lies along the center of the artery and r transverse to it. The unsteady magneto hydrodynamic incompressible flow of blood through an inclined tapered artery defined by following governing equations:

$$\begin{aligned} \nabla \cdot \vec{V} &= 0, \\ \rho \frac{D\vec{V}}{Dt} &= \nabla \cdot T - \frac{\mu \vec{V}}{k} + J \times B + \rho g \sin \beta, \end{aligned} \quad (1)$$

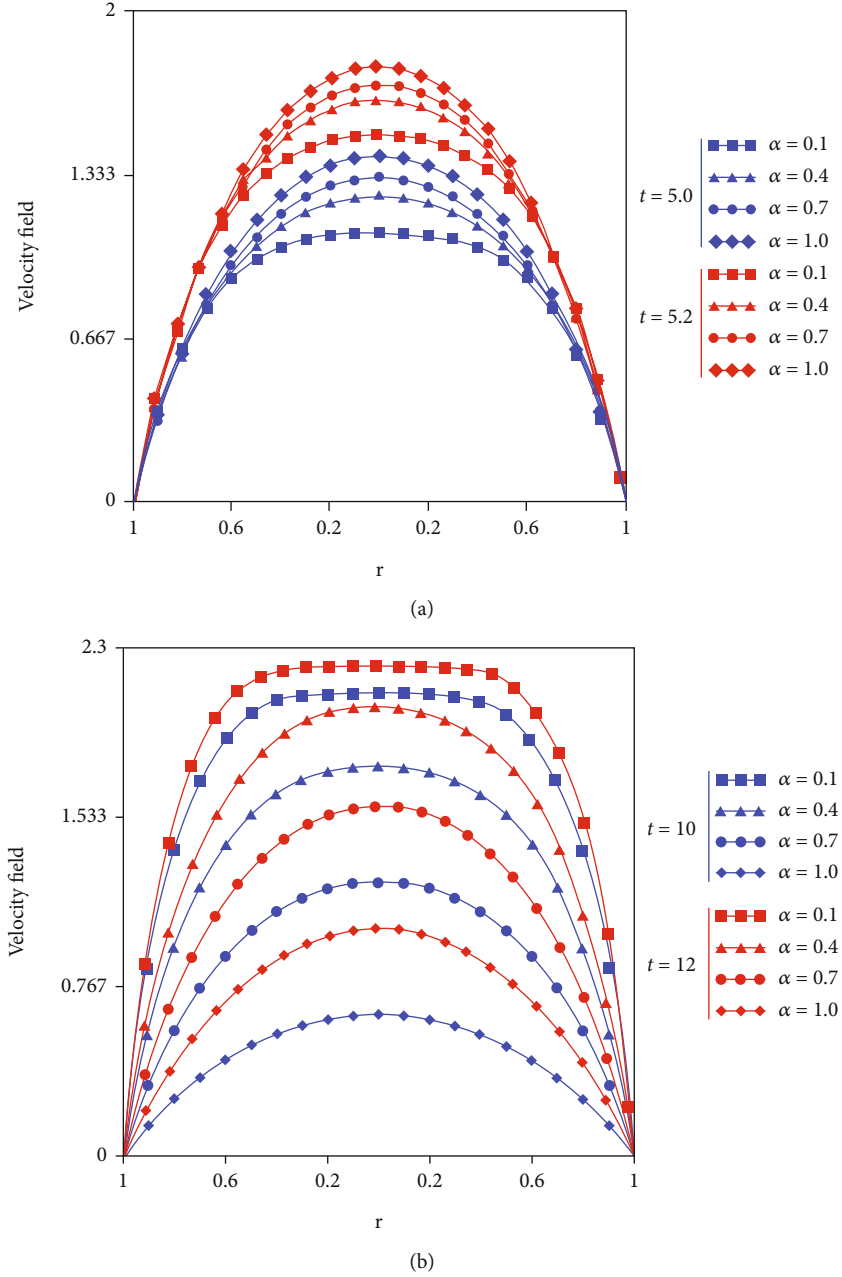


FIGURE 2: Profiles of dimensionless velocity for α versus r at $Re = 2.5$, $Ha = 0.5$, $K = 1$, $n = 0.8$, for small and large values of time t .

where \vec{V} is the velocity vector of the fluid, ρ is the fluid density, D/Dt is the material time derivative, and g is the external body force. Maxwell equations are written as

$$\nabla \cdot \vec{B} = 0, \nabla \times \vec{B} = \mu_0 \vec{J}, \nabla \times \vec{E} = -\frac{\partial \vec{B}}{\partial t}, \quad (2)$$

where μ_0 is the magnetic permeability, \vec{J} is the current density, \vec{B} is the magnetic field, and \vec{E} is the electric field. The electric current density can be written by Ohm's law as [37]

$$\vec{J} = \sigma (\vec{E} + \vec{V} \times \vec{B}), \quad (3)$$

where σ is the electric conductivity. The electromagnetic force F_{emag} can be expressed as

$$\vec{F}_{\text{emag}} = \vec{J} \times \vec{B} = \sigma (\vec{E} + \vec{V} \times \vec{B}) \times \vec{B} = -\sigma B_0^2 \omega(r, t) \vec{k}, \quad (4)$$

where \vec{k} is the unit vector in the z direction, and $\vec{V} = u(r, t) \vec{k}$ is the velocity of the blood along the axis of the cylindrical tube. The governing equation of the motion for flow in cylindrical polar coordinates [20–22, 38] is given by

$$\rho \frac{\partial u(r, t)}{\partial t} = -\frac{\partial p}{\partial z} + \frac{1}{r} \frac{\partial}{\partial r} (r \tau_{zr}(r, t)) - \frac{\mu}{k} u(r, t) - \sigma B_0^2 u(r, t) + \rho g \sin \beta, \quad (5)$$

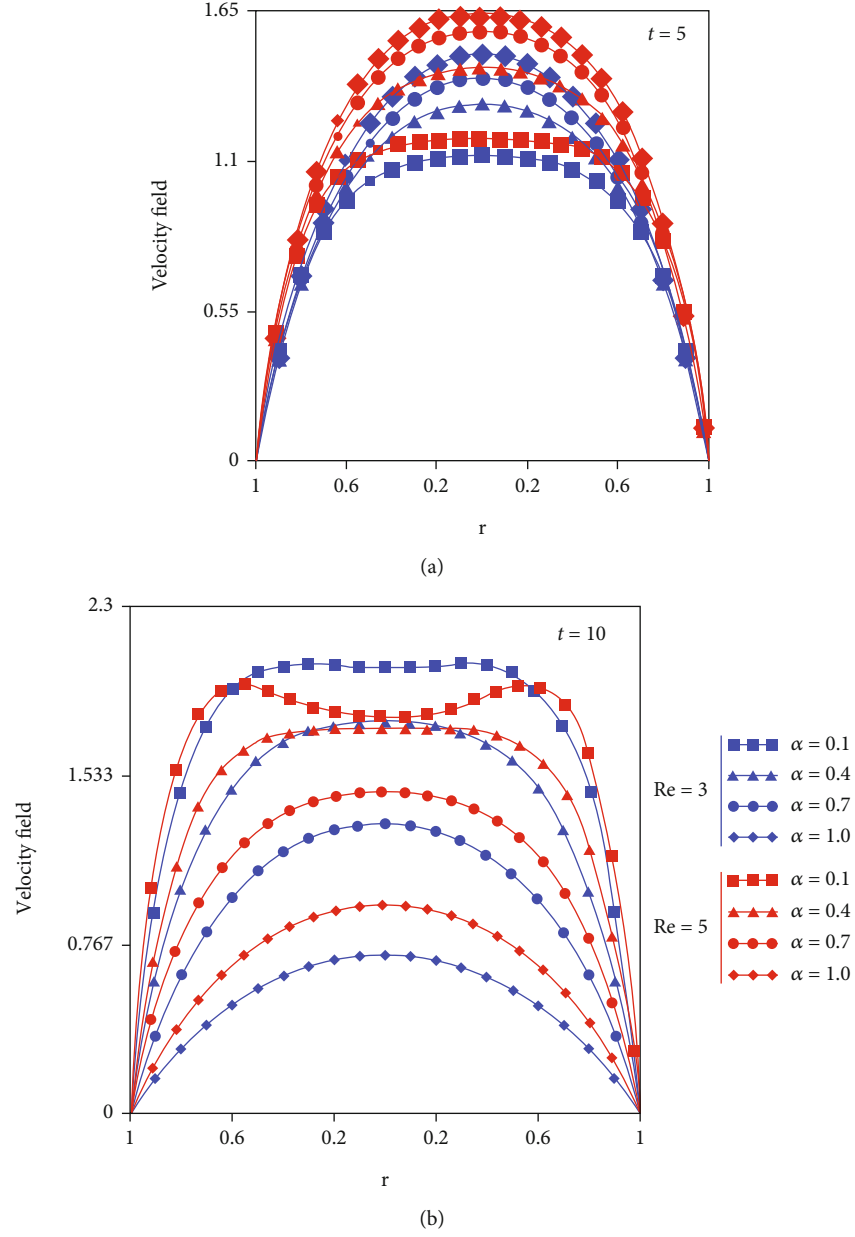


FIGURE 3: Profiles of dimensionless velocity for α versus r at $Re = 3, 5$, $Ha = 0.5$, $K = 1$, $n = 0.8$, for small and large values of time t .

$$\tau_{rz}(r, t) = \mu \frac{\partial u(r, t)}{\partial r}, \quad (6)$$

The boundary conditions that must be satisfied by the blood on the wall of artery are following

where the pressure gradient of the form as $-\partial p / \partial z = S_0 + S_1 \cos(\xi t)$, S_0 and S_1 are amplitudes of pulsatile systolic or diastolic pressure gradient, and ξ is the frequency of the pulse. The above model becomes also that we can write

$$u(r, 0) = 0, u(R_0, t) = 0, \left. \frac{\partial u(r, t)}{\partial r} \right|_{r=0} = 0. \quad (8)$$

Let us introduce the following dimensionless variables:

$$\rho \frac{\partial u(r, t)}{\partial t} = S_0 + S_1 \cos(\xi t) + \frac{1}{r} \frac{\partial r \tau_{rz}(r, t)}{\partial r} - \frac{\mu}{k} u(r, t) - \sigma B_0^2 u(r, t) + \rho g \sin \beta. \quad (7)$$

$$r^* = \frac{r}{R_0}, t^* = \frac{t}{t_0}, u^* = \frac{u}{u_0}, g^* = \frac{g t_0}{u_0}, S_0^* = \frac{t_0 S_0}{\rho u_0}, S_1^* = \frac{t_0 S_1}{\rho u_0}, \tau^* = \frac{R_0 \tau}{\mu u_0}, \quad (9)$$

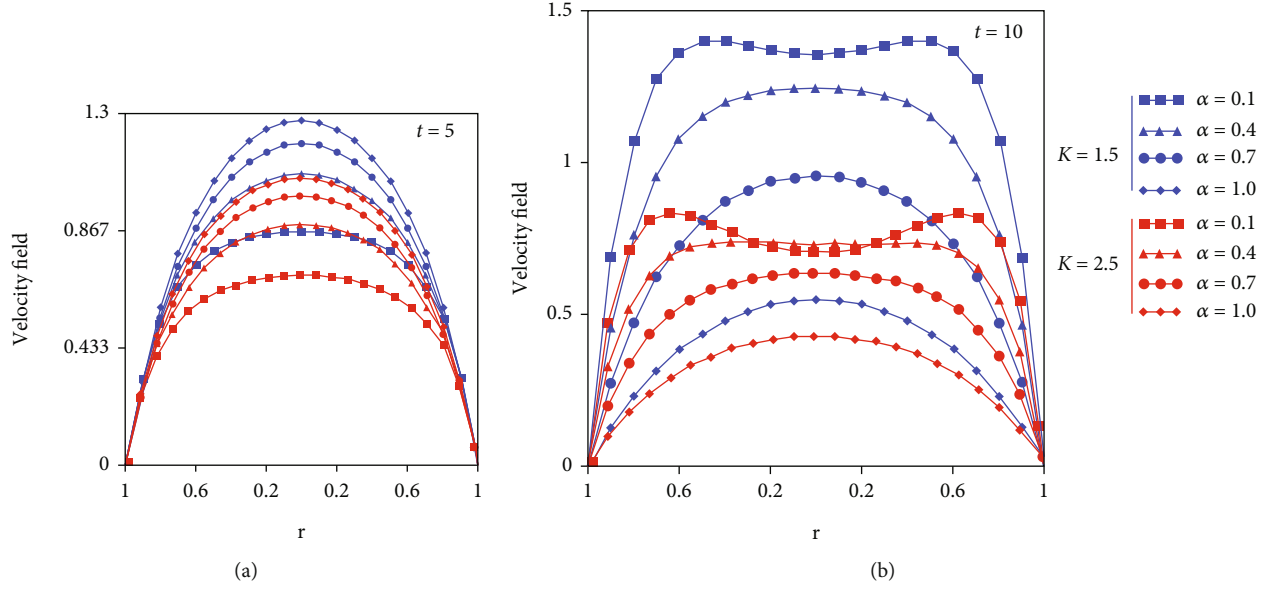


FIGURE 4: Profiles of dimensionless velocity for α versus r at $\text{Re} = 2.5$, $\text{Ha} = 0.5$, $K = 1.5, 2.5$, $n = 0.8$, for small and large values of time t .

where u_0 is the characteristic velocity, and t_0 is the characteristic time. Using the above dimensionless variables and parameters and after dropping out the $*$ notation in Eqs. (6), (7), and (8), we obtain

$$\frac{\partial u(r, t)}{\partial t} = S_0 + S_1 \cos(\xi t) + \frac{1}{\text{Re}} \frac{1}{r} \frac{\partial \tau_{rz}(r, t)}{\partial r} - Ku(r, t) - Ha^2 u(r, t) + m, \quad (10)$$

$$\tau_{rz}(r, t) = \frac{\partial u(r, t)}{\partial r}, \quad (11)$$

$$u(r, 0) = 0, u(1, t) = 0, \left. \frac{\partial u(r, t)}{\partial r} \right|_{r=0} = 0, \quad (12)$$

where $Ha = B_0 \sqrt{t_0 \nu \sigma / \mu}$ represents the Hartmann number, $\text{Re} = R_0^2 / \nu t_0$ describe the Reynolds number, and $m = t_0 g \sin \beta / \mu$ is the inclination parameter.

In the following, we develop a fractional model in which the classical constitutive Eqs. (9) and (11) are generalized by using the constitutive shear stress equation

$$\tau_{rz}(r, t) = {}^C D_t^{1-\alpha} \left(\frac{\partial u(r, t)}{\partial r} \right); 0 < \alpha \leq 1, \quad (13)$$

proposed by Scott-Blair [39]. The Caputo fractional derivative formula of order α is defined as [40]

$$D_t^\alpha u(y, t) = \begin{cases} \frac{1}{\Gamma(1-\alpha)} \int_0^t \frac{1}{(t-\tau)^\alpha} \frac{\partial u(y, \tau)}{\partial \tau} d\tau; & 0 < \alpha < 1, \\ \frac{\partial u(y, t)}{\partial t}; & \alpha = 1, \end{cases} \quad (14)$$

where Γ denotes the Gamma function.

Using Eq. (12) in Eq. (10), we obtain

$$\frac{\partial u(r, t)}{\partial t} = S_0 + S_1 \cos(\xi t) + \frac{1}{\text{Re}} {}^C D^{1-\alpha} \left(\frac{\partial^2 u(r, t)}{\partial r^2} + \frac{1}{r} \frac{\partial u(r, t)}{\partial r} \right) - Ku(r, t) - Ha^2 u(r, t) + m. \quad (15)$$

3. Analytical Solution

Taking Laplace transformation of Eq. (13), we obtain

$$q \bar{u}(r, q) = \frac{S_0}{q} + \frac{S_1 q}{q^2 + \xi^2} + \frac{1}{\text{Re}} q^{1-\alpha} \left(\frac{\partial^2 \bar{u}(r, q)}{\partial r^2} + \frac{1}{r} \frac{\partial \bar{u}(r, q)}{\partial r} \right) - K \bar{u}(r, q) - Ha^2 \bar{u}(r, q) + \frac{m}{q}. \quad (16)$$

Applying finite Hankel transform to Eq. (16) and using initial and boundary conditions in Eq. (12), we obtain

$$\bar{u}_H(r_n, q) = \frac{J_1(r_n)}{r_n} \left(\frac{S_0}{q} + \frac{S_1 q}{q^2 + \xi^2} + \frac{m}{q} \right) \cdot \frac{1}{q + (r_n^2 / \text{Re}) q^{1-\alpha} + K + Ha^2}, \quad (17)$$

where $\bar{u}_H(r_n, q) = \int_0^1 \bar{u}(r, q) r J_0(r r_n) dr$ is the finite Hankel transform of function $\bar{u}(r, q)$ and $r_n, n = 1, 2, \dots$ is the positive roots of the equation $J_0(x) = 0$, and J_0 being the Bessel function of the first kind and order zero.

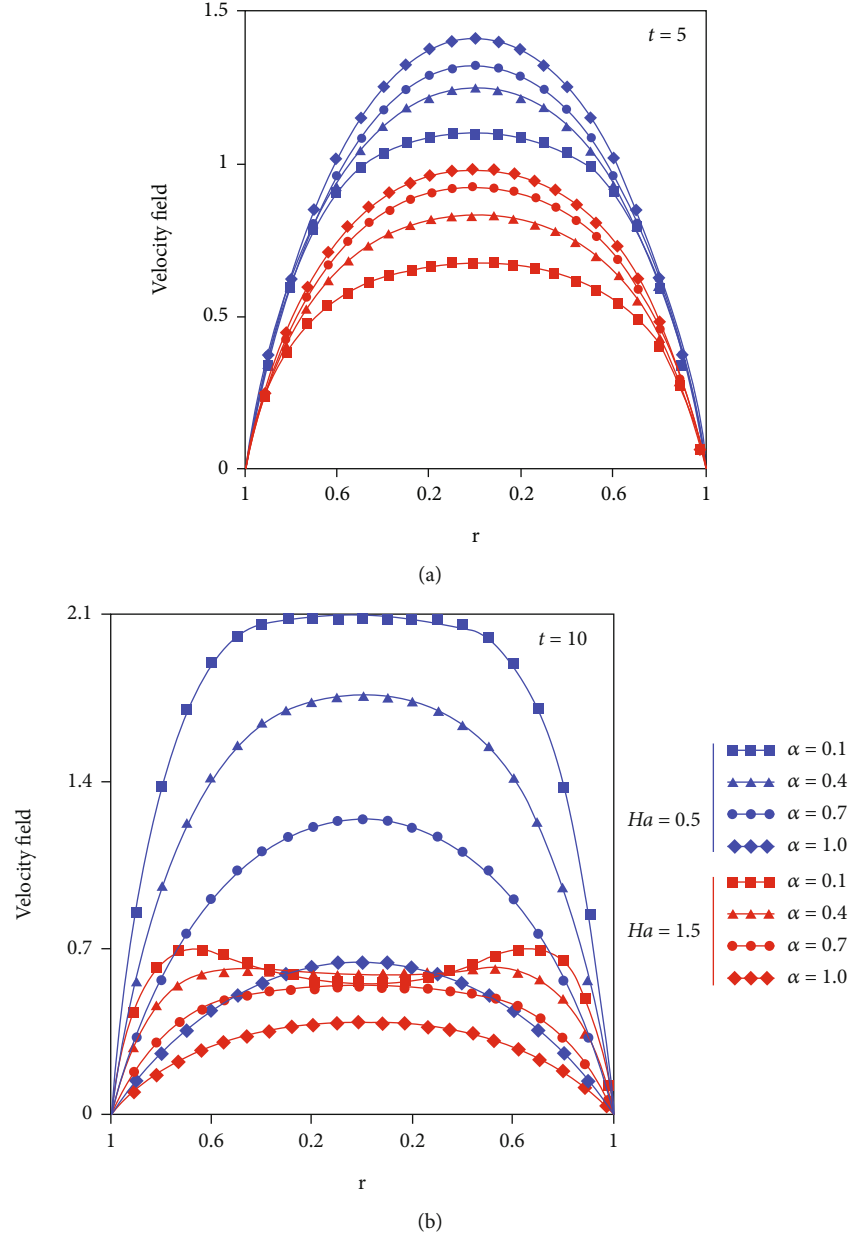


FIGURE 5: Profiles of dimensionless velocity for α versus r at $\text{Re} = 2.5$, $\text{Ha} = 0.5, 1.5$, $K = 1, n = 0.8$, for small and large values of time t .

Using the series formula $1/z + a = \sum_{k=0}^{\infty} (-1)^k z^k / a^{k+1}$; $|z/a| < 1$, Eq. (17) can be written as

$$\bar{u}_H(r_n, q) = \frac{J_1(r_n)}{r_n} \left(\frac{S_0}{q} + \frac{S_1 q}{q^2 + \xi^2} + \frac{m}{q} \right) \sum_{k=0}^{\infty} \frac{(-1)^k (r_n^2 / \text{Re})^k q^{k-ak}}{(q + K + \text{Ha}^2)^{k+1}}. \quad (18)$$

Applying inverse Laplace transform to Eq. (18), we obtain

$$u_H(r_n, t) = \frac{J_1(r_n)}{r_n} (S_0 + S_1 \cos(\xi t) + m) * \sum_{k=0}^{\infty} (-1)^k \left(\frac{r_n^2}{\text{Re}} \right)^k G_{1, k-ak, k+1}(K + \text{Ha}^2, t), \quad (19)$$

here $*$ represents the convolution product and

$$G_{a,b,c}(d, t) = L^{-1} \left\{ \frac{p^b}{(p^a - d)^c} \right\}, R(p) > 0, R(ac - b) > 0, \left| \frac{d}{p^a} \right| < 1, \quad (20)$$

is the generalized G-function of Lorenzo and Hartley [41]. Taking inverse Hankel transform of Eq. (19), we obtain

$$\begin{aligned} u(r, t) &= 2 \sum_{n=1}^{\infty} \frac{J_0(rr_n)}{J_1^2(r_n)} u_H(r_n, t) \\ &= 2 \sum_{n=1}^{\infty} \frac{J_0(rr_n)}{r_n J_1(r_n)} (S_0 + S_1 \cos(\xi t) + m) \\ &\quad * \sum_{k=0}^{\infty} (-1)^k \left(\frac{r_n^2}{\text{Re}} \right)^k G_{1, k-ak, k+1}(K + \text{Ha}^2, t). \end{aligned} \quad (21)$$

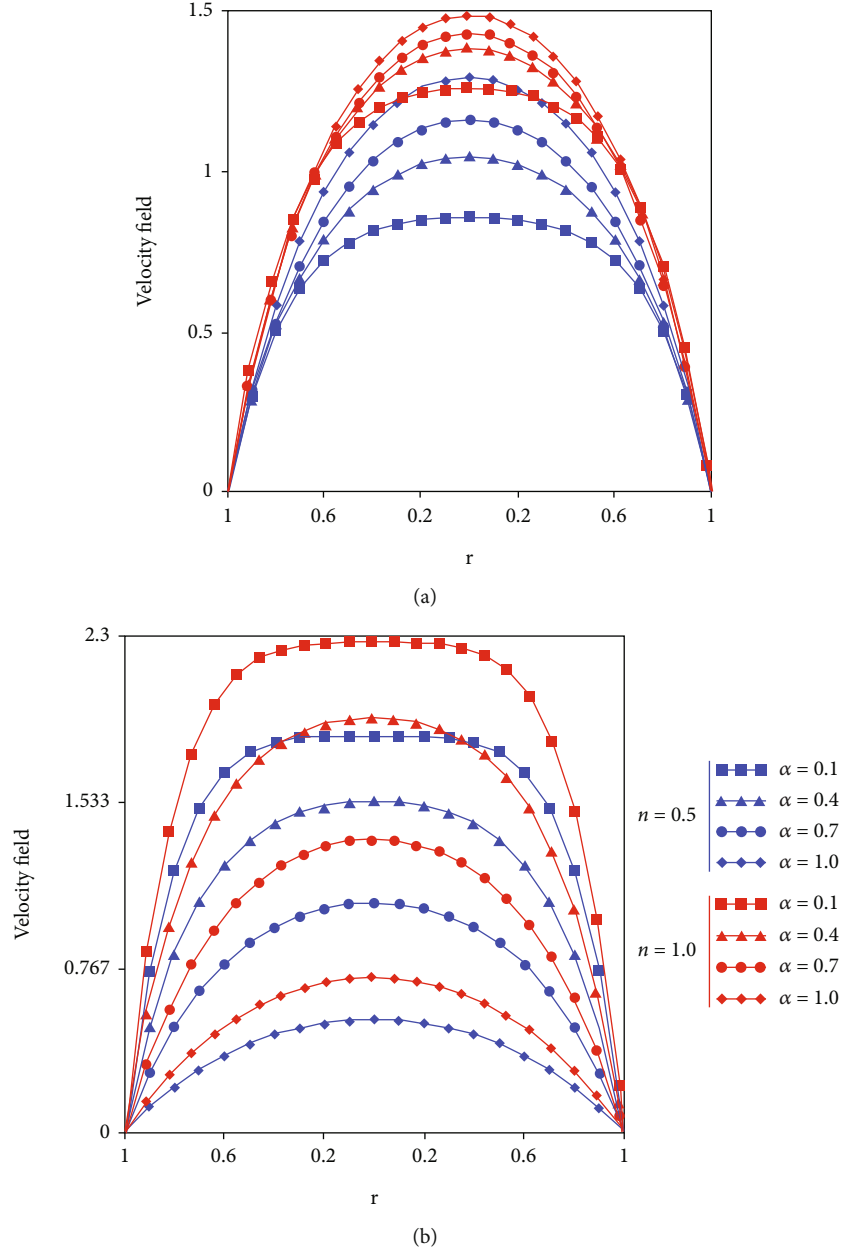


FIGURE 6: Profiles of dimensionless velocity for α versus r at $\text{Re} = 2.5$, $\text{Ha} = 0.5$, $K = 1$, $n = 0.5, 1$, for small and large values of time t .

4. Semianalytical Solution

Taking Laplace transformation of Eq. (13), we obtain

$$q\bar{u}(r, q) = \frac{S_0}{q} + \frac{S_1 q}{q^2 + \xi^2} + \frac{1}{\text{Re}} q^{1-\alpha} \left(\frac{\partial^2 \bar{u}(r, q)}{\partial r^2} + \frac{1}{r} \frac{\partial \bar{u}(r, q)}{\partial r} \right) - K\bar{u}(r, q) - \text{Ha}^2 \bar{u}(r, q) + \frac{m}{q}. \quad (22)$$

By rearranging Eq. (22), we have

$$\frac{\partial^2 \bar{u}(r, q)}{\partial r^2} + \frac{1}{r} \frac{\partial \bar{u}(r, q)}{\partial r} - A(q)\bar{u}(r, q) = B(q), \quad (23)$$

where $A(q) = \text{Re} (Kq^{\alpha-1} + \text{Ha}^2 q^{\alpha-1} + q^\alpha)$ and $B(q) = -\text{Re} ((mq^\alpha/q^2) + (S_0 q^\alpha/q^2) + (S_1 q^\alpha/q^2 + \xi^2))$.

The solution of above nonhomogeneous second order differential Eq. (23) by using the initial and boundary conditions (12) in the transform domain is written as

$$\bar{u}(r, q) = \frac{B(q)}{A(q)} \left[\frac{I_0(r\sqrt{A(q)})}{I_0(\sqrt{A(q)})} - 1 \right]. \quad (24)$$

By writing $\bar{u}(y, q)$ in suitable and simple form, we can determine its inverse Laplace transform traditionally but Eq. (24) is in a complex form of the modified Bessel function, and it is not easy to use for some practical applications.

TABLE 1: Comparison of two Laplace inverse numerical algorithms with analytical solution.

r	$u(r, t)$ [Eq. (21)]	$u_s(r, t)$ [Stehfest's]	$u_T(r, t)$ [Tzou's]	$ u(r, t) - u_s(r, t) $	$ u(r, t) - u_T(r, t) $
0	0.684151	1.099209	0.827544	0.415058	0.143394
0.1	0.802388	1.096127	0.82701	0.293739	0.024621
0.2	0.747556	1.086239	0.824787	0.338683	0.077232
0.3	0.791451	1.06753	0.818938	0.276079	0.027487
0.4	0.74445	1.036351	0.805933	0.291901	0.061483
0.5	0.787414	0.986957	0.780184	0.199542	7.230026e-3
0.6	0.734645	0.910795	0.733327	0.17615	1.318152e-3
0.7	0.790328	0.79549	0.653183	5.161311e-3	0.137146
0.8	0.706713	0.623425	0.522325	0.083288	0.184388
0.9	0.767713	0.3698	0.316108	0.397913	0.451604
1	0	1.479346×10^{-7}	0	1.479346e-7	0

Moreover, the numerical Laplace method is considered as an effective tool in computing the fractional differential equations. Sheng et al. [42] reported that the numerical inverse Laplace transform algorithms are efficacious and reliable for fractional-order differential equations. Stehfest's algorithm [31] successfully used by Tong et al. [43] and Jiang et al. [44]. Therefore, in this work, we apply the numerical algorithm of the inverse Laplace transform method to Eq. (24) and analyze the flow properties. Stehfest's formula is defined as

$$u(r, t) = \frac{\ln(2)}{t} \sum_{j=1}^{2m} d_j \bar{u}\left(r, j \frac{\ln(2)}{t}\right), \quad (25)$$

where m is a positive integer.

$$d_j = (-1)^{j+m} \sum_{i=\lceil \frac{j+1}{2} \rceil}^{\min(j, m)} \frac{i^m (2n)!}{(m-i)! (i-1)! (j-i)! (2i-j)!}, \quad (26)$$

and $[r]$ denotes the integer value function or bracket function.

Tzou's formula can be defined as

$$u(r, t) = \frac{e^{4.7}}{t} \left[u\left(r, \frac{4.7}{t}\right) + \operatorname{Re} \left[\sum_{j=1}^{\infty} (-1)^j u\left(r, \frac{4.7 + j\pi i}{t}\right) \right] \right]. \quad (27)$$

The numerical solutions of transformed Eq. (24) have been obtained by using algorithms (25) and (27), and results are presented in tables.

5. Numerical Results and Discussion

In this section, the analyses of physical parameters on the fluid flow are presented as Figures 2–6.

In Figure 2, we present the effect of the fractional parameter α for different small and large values of time t . From Figure 2(a), it is observed that for a small value of time, the ordinary fluid velocity is maximum than fractional fluid flow. While by increasing the value of time, the fluid flow velocity

decreases. In Figure 2(b), the influence is opposite than Figure 2(a), for a large value of time. A further attempt was made to quantify the effect on the velocity profile by using the slope of linear regression through the data points as presented by Animasaun and Pop [45]. In between the artery ($-0.2 \leq r \leq 0.2$), the optimal effect is seen when $t = 5.0$ the slope of regression line through the data in known velocity and the order of Caputo fractional derivatives is -0.3173000 . When $t = 5.2$, a decrease in the velocity field is also noticed, and the rate is estimated using the same approach as -0.2705067 . Due to the singular kernel of the fractional derivative for small values and large values of the time t , the flow has opposite influence. It is worthy to note that the effects of fractional parameter α as reported in this study complement that of ref. [46] in which heat transfer in the flow of a fractional viscous fluid over an infinite vertical plate with exponential heating using a fractional derivative with nonsingular kernel is deliberated upon. Consecutively, the effect of Reynolds number Re on the flow is presented in Figure 3, for small and large values of time. It is deduced that there exists a significant difference between the flow when $t = 5$, $Re = 3$ and $t = 5$, $Re = 5$. At the initial time ($t = 5$), it is seen that the velocity of the flow increases with the order of Caputo fractional derivative when $Re = 3$ and $Re = 5$, see Figure 3(a). It is worth pointing out that the maximum velocity field is obtained at larger values of Reynolds number. At larger values of time, it is interesting to reveal that a decrease in the velocity field is guaranteed, see Figure 3(b). When $Re = 3$, the slope of regression line through the data in known velocity and the order of Caputo fractional derivatives is -0.4527000 . However, when $Re = 5$, the rate of decrease in the velocity field is quantified using the slope of regression line as -0.7884667 .

The effect of the porous parameter K is presented in Figure 4, for small and large values of time. For a small time, it is seen that the velocity increases due to an increase in the magnitude of the porous parameter K . For large values of time, interesting results found that in the medium of the cylinder for fractional parameter less than 0.7 by increasing K , the velocity increases on the other hand, and for fractional parameter greater than 0.7 by increasing K , the velocity decreases. Figure 5 reveals the influence of Hartman number

TABLE 2: Effect of noninteger order of fractional parameter on the velocity field.

α	$u(r, t)$ [Eq. (21)]	$u_s(r, t)$ [Stehfest's]	$u_T(r, t)$ [Tzou's]	$ u(r, t) - u_s(r, t) $	$ u(r, t) - u_T(r, t) $
0	0.659024	0.986618	0.769764	0.327593	0.11074
0.1	0.74445	1.036351	0.805933	0.291901	0.061483
0.2	0.814984	1.074099	0.831608	0.259115	0.016623
0.3	0.872347	1.102689	0.849336	0.230342	0.023011
0.4	0.918044	1.124687	0.861515	0.206643	0.056529
0.5	0.953435	1.142488	0.870428	0.189053	0.083007
0.6	0.979774	1.158389	0.878262	0.178615	0.101513
0.7	0.998231	1.174669	0.887155	0.176438	0.111077
0.8	1.009872	1.19366	0.899271	0.183787	0.110601
0.9	1.01565	1.217833	0.916927	0.202184	0.098723
1	1.016406	1.249903	0.942799	0.233496	0.073608

Ha. It is observed that by increasing the value of Ha , the velocity of the fluid is found to be an increasing function when $t = 5$ and a decreasing function when $t = 10$. Physically, the negligible increasing effect in the velocity field can be traced to the fact that the effects of Lorentz force have not been fully materialized at initial time. The effect of the inclination parameter n is represented in Figure 6. It is clear from Figure 6(a) by increasing the value of n the velocity increases by considering the small value of time t . By increasing the value of time $t = 10$, the influence of n is much more.

In Tables 1 and 2, we make a comparison between analytical solution in Eq. (21) with numerical algorithms, named as Stehfest's [35] and Tzou's [36] algorithms. It is found that the analytical solution in Eq. (21) is in a good agreement with Tzou's algorithm.

6. Conclusion

The effect of a uniform magnetic field on unsteady blood flow through a peristaltic pressure gradient in an inclined porous tube has been investigated. The solution was discovered using the Laplace transformation technique, and the analysis yielded some useful predictions. For the semianalytical solution, the inverse Laplace transform has been calculated by using numerical package though Mathcad, since the velocity expressions of Laplace transform are in the complex form of modified Bessel functions. Therefore, it is very difficult to find inverse Laplace analytically. To show the accuracy of our obtained result, the result was compared with two other inverse Laplace transform numerical algorithms, named as Stehfest's [33] and Tzou's [34] algorithms. The effects of pertinent physical parameters are discussed in detail. These are some main results of the study:

- (1) For small values of time, the fractional parameter α is inversely proportional to the velocity field, and it shows an opposite behavior for greater values of time
- (2) There exists a significant difference in the velocity of the flow at a higher time when the magnitude of Reynolds number is small and large

- (3) The effect of porous permeability and inclination is opposite to the velocity field as compared to the magnetic field. By increasing these parameters, the higher velocity field is ascertained
- (4) Hartman number has dual effects on the velocity of the flow due to the fact that the impact of Lorentz force at the initial time is infinitesimal
- (5) By comparing the analytical solution in Eq. (21) with numerical algorithms, named as Stehfest's and Tzou's algorithms, it is found that the analytical solution in Eq. (21) is in a good agreement with Tzou's algorithm

Data Availability

The data used to support the findings of this study are available from the corresponding author upon request.

Conflicts of Interest

The authors declare that they have no conflicts of interest.

Acknowledgments

The authors extend their appreciation to the Deanship of Scientific Research at King Khalid University for funding this work through research group program under Grant No. RGP.1/324/42.

References

- [1] H. Hatami, J. Hatami, and D. D. Ganji, "Computer simulation of MHD blood conveying gold nanoparticles as a third grade non-Newtonian nanofluid in a hollow porous vessel," *Computer Methods and Programs in Biomedicine*, vol. 113, no. 2, pp. 632–641, 2014.
- [2] H. Amlimohamadi, M. Akram, and K. Sadeghy, "Flow of a Casson fluid through a locally-constricted porous channel: a numerical study," *Korea-Australia Rheology Journal*, vol. 28, no. 2, pp. 129–137, 2016.
- [3] H. Alimohamadi and M. Imani, "Finite element simulation of two-dimensional pulsatile blood flow through a stenosed

- artery in the presence of external magnetic field," *International Journal for Computational Methods in Engineering Science and Mechanics*, vol. 15, no. 4, pp. 390–400, 2014.
- [4] V. C. Roberts, "Magnetohydrodynamic pumping of blood," *Medical and Biological Engineering and Computing*, vol. 10, no. 1, pp. 57–59, 1972.
 - [5] M. Korchevskii and L. S. Marochnik, "Magnetohydrodynamic version of movement of blood," *Biophysics*, vol. 10, pp. 411–414, 1965.
 - [6] V. A. Vardanyan, "Effect of a magnetic field on blood flow," *Biophysics*, vol. 18, pp. 515–521, 1973.
 - [7] P. K. Suri and R. Suri Pushpa, "Blood flow in a branched-arteries," *Indian Journal of Pure and Applied Mathematics*, vol. 12, pp. 907–918, 1981.
 - [8] P. Chaturani and V. Palanisamy, "Pulsatile flow of blood with periodic body acceleration," *International Journal of Engineering Science*, vol. 29, no. 1, pp. 113–121, 1991.
 - [9] K. W. Chow and C. C. Mak, "A simple model for the two dimensional blood flow in the collapse of veins," *Journal of Mathematical Biology*, vol. 52, no. 6, pp. 733–744, 2006.
 - [10] D. Pal, N. Rudraiah, and R. Devanathan, "The effects of slip velocity at a membrane surface on blood flow in the microcirculation," *Journal of Mathematical Biology*, vol. 26, no. 6, pp. 705–712, 1988.
 - [11] D. F. Jamil, S. Saleem, R. Roslan et al., "Analysis of non-Newtonian magnetic Casson blood flow in an inclined Stenosed artery using Caputo-Fabrizio fractional derivatives," *Computer Methods and Programs in Biomedicine*, vol. 203, article 1106044, p. 106044, 2021.
 - [12] E. E. Tzirtzilakis, "A mathematical model for blood flow in magnetic field," *Physics of Fluids*, vol. 17, no. 7, article 077103, 2005.
 - [13] K. S. Mekheimer, "Peristaltic flow of blood under effect of a magnetic field in a non-uniform channels," *Applied Mathematics and Computation*, vol. 153, no. 3, pp. 763–777, 2004.
 - [14] M. Jain, G. C. Sharma, and A. Singh, "Mathematical analysis of MHD flow of blood in very narrow capillaries," *Inter. J. Eng. Transactions B*, vol. 22, pp. 307–315, 2009.
 - [15] V. K. G. Varshney, V. Katiyar, and S. Kumar, "Effect of magnetic field on the blood flow in artery having multiple stenosis: a numerical study," *International Journal of Engineering, Science and Technology*, vol. 2, no. 2, pp. 67–82, 2010.
 - [16] K. S. Mekheimer, T. Elnaqeeb, M. A. El Kot, and F. Alghamdi, "Simultaneous effect of magnetic field and metallic nanoparticles on a micropolar fluid through an overlapping stenotic artery: blood flow model," *Physics Essays*, vol. 29, no. 2, pp. 272–283, 2016.
 - [17] T. Elnaqeeb, K. S. Mekheimer, and F. Alghamdi, "Cu-blood flow model through a catheterized mild stenotic artery with a thrombosis," *Mathematical Biosciences*, vol. 282, pp. 135–146, 2016.
 - [18] T. Elnaqeeb, N. A. Shah, and K. S. Mekheimer, "Hemodynamic characteristics of gold nanoparticle blood flow through a tapered stenosed vessel with variable nanofluid viscosity," *BioNanoScience*, vol. 9, no. 2, pp. 245–255, 2019.
 - [19] T. Elnaqeeb, "Modeling of au (NPs)-blood flow through a catheterized multiple stenosed artery under radial magnetic field," *The European Physical Journal Special Topics*, vol. 228, no. 12, pp. 2695–2712, 2019.
 - [20] S. Sharma, U. Singh, and V. K. Katiyar, "Magnetic field effect on flow parameters of blood along with magnetic particles in a cylindrical tube," *Journal of Magnetism and Magnetic Materials*, vol. 377, pp. 395–401, 2015.
 - [21] A. A. Zafar, N. A. Shah, and I. Khan, "Two phase flow of blood through a circular tube with magnetic properties," *Journal of Magnetism and Magnetic Materials*, vol. 477, pp. 382–387, 2019.
 - [22] N. Ali Shah, D. Vieru, and C. Fetecau, "Effects of the fractional order and magnetic field on the blood flow in cylindrical domains," *Journal of Magnetism and Magnetic Materials*, vol. 409, pp. 10–19, 2016.
 - [23] J. C. Misra, A. Sinha, and G. C. Shit, "Mathematical modeling of blood flow in a porous vessel having double stenoses in the presence of an external magnetic field," *International Journal of Biomathematics*, vol. 4, no. 2, pp. 207–225, 2011.
 - [24] G. Ramamurthy and B. Shanker, "Magnetohydrodynamic effects on blood flow through a porous channel," *Medical & Biological Engineering & Computing*, vol. 32, no. 6, pp. 655–659, 1994.
 - [25] I. M. Eldesoky and A. A. Mousa, "Peristaltic flow of a compressible non-Newtonian Maxwellian fluid through porous medium in a tube," *International Journal of Biomathematics*, vol. 3, no. 2, pp. 255–275, 2010.
 - [26] I. M. Eldesoky, "Slip effects on the unsteady MHD pulsatile blood flow through porous medium in an artery under the effect of body acceleration," *International Journal of Mathematics and Mathematical Sciences*, vol. 2012, Article ID 860239, 26 pages, 2012.
 - [27] K. Hosseinzadeh, S. Salehi, M. R. Mardani, F. Y. Mahmoudi, M. Waqas, and D. D. Ganji, "Investigation of nano-Bioconvective fluid motile microorganism and nanoparticle flow by considering MHD and thermal radiation," *Informatics in Medicine Unlocked*, vol. 21, article 100462, 2020.
 - [28] K. Hosseinzadeh, S. Roghani, A. R. Mogharrebi, A. Asadi, and D. D. Ganji, "Optimization of hybrid nanoparticles with mixture fluid flow in an octagonal porous medium by effect of radiation and magnetic field," *Journal of Thermal Analysis and Calorimetry*, vol. 143, no. 2, pp. 1413–1424, 2021.
 - [29] M. Inc and A. Akgul, "Approximate solutions for MHD squeezing fluid flow by a novel method," *Boundary Value Problems*, vol. 2014, no. 1, Article ID 18, 2014.
 - [30] J. V. Ramana Reddy, D. Srikanth, and S. V. S. N. V. G. Krishna Murthy, "Mathematical modelling of pulsatile flow of blood through catheterized unsymmetric stenosed artery—Effects of tapering angle and slip velocity," *European Journal of Mechanics - B/Fluids*, vol. 48, pp. 236–244, 2014.
 - [31] A. Akgul, D. Baleanu, and M. Inc, "On the solutions of electrohydrodynamic flow with fractional differential equations by reproducing kernel method," *Open Physics*, vol. 128, pp. 218–223, 2017.
 - [32] R. Hilfer, *Threefold Introduction to Fractional Derivatives: In Anomalous Transport*, Wiley-VCH Verlag Germany, 2008.
 - [33] N. A. Shah, T. Elnaqeeb, and S. Wang, "Effects of Dufour and fractional derivative on unsteady natural convection flow over an infinite vertical plate with constant heat and mass fluxes," *Computational and Applied Mathematics*, vol. 37, no. 4, pp. 4931–4943, 2018.
 - [34] N. A. Shah, T. Elnaqeeb, I. L. Animasaun, and Y. Mahsud, "Insight into the natural convection flow through a vertical cylinder using Caputo time-fractional derivatives," *International Journal of Applied and Computational Mathematics*, vol. 4, no. 3, p. 80, 2018.

- [35] H. Stehfest, "Algorithm 368: numerical inversion of Laplace transforms [D5]," *Communications of the ACM*, vol. 13, no. 1, pp. 47–49, 1970.
- [36] D. Y. Tzou, *Macro to Micro Scale Heat Transfer: The Lagging Behavior*, Taylor and Francis, Washington, 1997.
- [37] S. S. Ardahaie, A. J. Amiri, A. Amouei, K. Hosseinzadeh, and D. D. Ganji, "Investigating the effect of adding nanoparticles to the blood flow in presence of magnetic field in a porous blood arterial," *Informatics in Medicine Unlocked*, vol. 10, pp. 71–81, 2018.
- [38] M. Gholinia, K. Hosseinzadeh, and D. D. Ganji, "Investigation of different base fluids suspend by CNTs hybrid nanoparticle over a vertical circular cylinder with sinusoidal radius," *Case Studies in Thermal Engineering*, vol. 21, p. 100666, 2020.
- [39] A. Jaishankar and G. H. McKinley, "Power-law rheology in the bulk and at the interface: quasi-properties and fractional constitutive equations," *Proceedings of the Royal Society A: Mathematical, Physical and Engineering Sciences*, vol. 469, no. 2149, article 20120284, 2012.
- [40] M. Partohaghghi, M. Inc, M. Bayram, and D. Baleanu, "On numerical solution of the time fractional advection-diffusion equation involving atangana-baleanu-caputo derivative," *Open Physics*, vol. 17, no. 1, pp. 816–822, 2019.
- [41] C. F. Lorenzo and T. Hartley, *Generalized Functions for the Fractional Calculus*, NASA/TP—1999-209424/REV1, 1999.
- [42] H. Sheng, Y. Li, and Y. Q. Chen, "Application of numerical inverse Laplace transform algorithms in fractional calculus," *Journal of the Franklin Institute*, vol. 348, no. 2, pp. 315–330, 2011.
- [43] D. K. Tong, X. Zhang, and X. Zhang, "Unsteady helical flows of a generalized Oldroyd-B fluid," *Journal of Non-Newtonian Fluid Mechanics*, vol. 156, no. 1-2, pp. 75–83, 2009.
- [44] Y. Jiang, H. Qi, H. Xu, and X. Jiang, "Transient electroosmotic slip flow of fractional Oldroyd-B fluids7," *Microfluidics and Nanofluidics*, vol. 21, no. 1, 2017.
- [45] I. L. Animasaun and I. Pop, "Numerical exploration of a non-Newtonian Carreau fluid flow driven by catalytic surface reactions on an upper horizontal surface of a paraboloid of revolution, buoyancy and stretching at the free stream," *Alexandria Engineering Journal*, vol. 56, no. 4, pp. 647–658, 2017.
- [46] N. A. Shah, A. A. Zafar, and C. Fetecau, "Free convection flows over a vertical plate that applies shear stress to a fractional viscous fluid," *Alexandria Engineering Journal*, vol. 57, no. 4, pp. 2529–2540, 2017.

Research Article

Simultaneous Flow of n-Immiscible Fractional Maxwell Fluids with Generalized Thermal Flux and Robin Boundary Conditions

Abdul Rauf¹,^{ID} Qammar Rubbab,² Nehad Ali Shah^{3,4},^{ID} and Kaleem Razaq Malik¹

¹Department of Computer Science, Air University Multan Campus, Multan 60000, Pakistan

²Department of Mathematics, The Woman University Multan, Multan, Pakistan

³Informetrics Research Group, Ton Duc Thang University, Ho Chi Minh, Vietnam

⁴Faculty of Mathematics & Statistics, Ton Duc Thang University, Ho Chi Minh, Vietnam

Correspondence should be addressed to Nehad Ali Shah; nehad.ali.shah@tdtu.edu.vn

Received 28 January 2021; Revised 24 February 2021; Accepted 14 March 2021; Published 14 April 2021

Academic Editor: Mustafa Inc

Copyright © 2021 Abdul Rauf et al. This is an open access article distributed under the Creative Commons Attribution License, which permits unrestricted use, distribution, and reproduction in any medium, provided the original work is properly cited.

In a rectangular region, the multilayered laminar unsteady flow and temperature distribution of the immiscible Maxwell fractional fluids by two parallel moving walls are studied. The flow of the fluid occurs in the presence of Robin's boundaries and linear fluid-fluid interface conditions due to the motion of the parallel walls on its planes and the time-dependent pressure gradient. The problem is defined as a mathematical model which focuses on the fluid memory, which is represented by a constituent equation with the Caputo time-fractional derivative. The integral transformations approach (the Laplace transform and the finite sine-Fourier transform) is used to determine analytical solutions for velocity, shear stress, and the temperature fields with fluid interface, initial, and boundary conditions. For semianalytical solutions, the algorithms of Talbot are used to calculate the Laplace inverse transformation. We used the Mathcad software for graphical illustration and numerical computation. It has been observed that the memory effect is significant on both fluid motion and temperature flow.

1. Introduction

In nature, there often exist flows of immiscible materials. Due to its broad application in research, medicine, geophysics, industry, petroleum engineering, and hydrogeology, the study of simultaneous flow of two or more immiscible fluids is significant [1–4]. The numerous applications include the recovery of petroleum oil, blood flow through the veins of a capillary vessel, the treatment of machinery, the processing of organic film and mucus in living cells, the removal of carbon dioxide from the environment, the control of groundwater, crude oil pipeline flows, and the formation of blisters in microfluid and bubble trains.

In some industrial problems, fluid flow is multicomponent, and therefore, there are layers of fluids having different densities and viscosities. The interface of these layers creates moving boundaries in between the walls of the channel in which fluid is flowing. This causes flow phenomenon to be

not only nonlinear but also very complex and its study challenging.

A long-wave technique was used for the first study of the linear stability of the viscoelastic two-layered simultaneous Poiseuille and Couette flow by Yih [5]. It has been seen that the Kelvin-Helmholtz instability can occur due to viscosity and density stratification. Several scientists subsequently researched the stability/instability of the immiscible fluid flow in two or multifaceted layers [6–8]. The existence and uniqueness of the simultaneous multilayered Couette/Poiseuille fluid motions in channel/pipes were investigated by Le Meur [9], and the approximated Oldroyd differential component and the viscosity proportions were found important to a unique result. The Couette-Poiseuille motion of the two-layer fluids was taken into account by Kalogirou and Blyth [10] to examine stability. The fluid in the bottom layer is surrounded by surfactants which adsorbed on the interface. The thickness ratio of the fluid viscosity is considerably

higher, and when the flow is relatively stable, the surfactant is soluble enough.

Immiscible fluid flows are frequently encountered in the design of industrial processes and equipment. Indeed, several flow patterns of interest exist for different flow conditions in liquid-liquid flows. In [11], the two-phase flow of immiscible fluids in porous media is described in continuous models as the momentum exchanges between the two steps by simply making generalizations of the Darcy law for single phases of development and adding saturation-dependent porosity and permeability. By extending the principle of Buckley-Leverett, authors examine the effect of the cross-cutting words on concentration profiles and pressure losses for various fluids. It has been shown that the outcomes on dual-phase flow might increase when the impact of the fluid-fluid interfaces appears close to that of the solid-fluid interfaces with the permeability of the porous medium. Hisham et al. [12] reported a two-layer analysis in the presence of time-dependent pressure gradient of the immiscible Maxwell fluids between two simultaneous moving plates. With the support of integral transformation, Laplace and finite Fourier Sine transformation, analytical solutions for velocity, and shear stress are retrieved. The increase in kinematic viscosity decreases the maximum speed value. In a rectangular channel with two parallel translating plates in the presence of a time-dependent pressure gradient, Rauf et al. [13] proposed analytical and semianalytical solutions for the velocity fields and temperature fields for the simultaneous flow of the n -immiscible Maxwell fractional fluid. It has been found that the heat transfer in ordinary fluids is higher than those of thermal memory fluids; however, the memory parameters affect the fluids' velocities as accelerating factors. Some other important multilayer flow problems are studied in [14–16]. The parallel flow of the fractional Maxwell fluid inside a cylindrical domain has been studied by Rauf et al. [17] in the presence of pressure gradient in the flow direction. The Laplace transformations, in combination with the finite Weber and Hankel transformation of zeroth order provide analytical solutions to flow velocities and shear stresses. The fluid velocity was shown to decrease as the values of the fractional parameters have been increased. The study of multilayer flow of generalized immiscible Maxwell fluids between two parallel plates with Robin boundary conditions is still lacking in the literature. The aim of this article is to fill this gap in the literature.

The fractional operators have been intensively incorporated in recent decades for mathematical modeling of the numerous topics in real life. Many dynamic memory processes can be investigated using time-fractional derivative operators. The fractional calculus thus became an essential component in biology, chemistry, physics, and many areas of engineering. Hristov [18, 19], Povstenko and Kyrylych [20, 21], Zheng et al. [22], Baleanu et al. [23, 24], and Hilfer [25] have a comprehensive description of the theory of fractional operators with their properties and applications. References [26–38] include mathematical observations and potential implementations and applications of the fractional differential Calculus.

In this paper, we have studied the multilayer flow between the two parallel plates of immiscible fractional

Maxwell fluids. In the vicinity of the fractional heat flux in fluid layers, we assumed an unsteady, incompressible, and fully established one-dimensional fluid motion induced by the motion of the boundary plates and by the applied pressure gradient as a function of time. Moreover, we took into account the Robin boundary conditions on the boundary plates and the linear interfacial fluid-fluid conditions between two consecutive layers. We have used finite Fourier sine-cosine transformation, which is ideal for the Robin-type boundary conditions, along with the Laplace transformation, to explore analytical solutions for velocities and shear stresses. Using the Laplace transform along with Tablot's techniques for the numerical inversion of Laplace, a semianalytical solution is recovered for thermal profile.

2. Mathematical Modeling

The flow region is

$$D' = \left\{ (x', y', z') \mid x', z' \in (-\infty, \infty), y' \in [0, h'] \right\}, \quad (1)$$

with the boundary plates positioned at $y' = 0$ and $y' = h' > 0$. To begin with at time $t' = 0$, the two walls and the fluids inside are at rest with the atmospheric temperature T_{20} . After this instance, the boundary plate positioned at $y' = 0$ move with velocity $u'_{10} = U_0 f'_1(t')$ along the x' -axis and the wall temperature $T_0 g'_1(t')$, while the channel plate $y' = h'$ moves with the wall velocity $u'_{20} = U_0 f'_2(t')$ analogous with the x' -axis and the wall temperature $T_0 g'_2(t')$ (Figure 1). It has been assumed that the functions $f'_1(t')$, $f'_2(t')$, $g'_1(t')$, and $g'_2(t')$ are piece-wise continuous functions, and $f'_1(0) = g'_1(0) = f'_2(0) = g'_2(0) = 0$. We consider that the velocity vector is of the form $\vec{V}' = (u'(y', t'), 0, 0)$. We assume the simultaneous n -immiscible Maxwell fluids between two parallel boundary planes. It divides the domain of flow $[0, h']$ into n subdomains $0 = h'_0 < h'_1 < h'_2 \dots < h'_n = h'$. In the region $y' \in [h'_{i-1}, h'_i]$, $h'_{i-1} < h'_i$, Maxwell fluid flow has the viscosity μ_i , relaxation time $\lambda'_i = \mu_i/G_i$, density ρ_i , G_i , the elastic modulus, temperature $T'_i(y', t')$, velocity $u'_i(y', t')$, the shear stress $\tau'_i(y', t')$, and the thermal flux $q'_i(y', t')$, where $i = 1, 2, \dots, n$.

The Maxwell fluids are supposed to be incompressible and immiscible, and the stream is linear, unsteady, and completely established. The fluid flow is produced by the applied pressure gradient as a function of time towards flow and by the motion of the boundary walls. In view of the assumptions on the velocity vectors, the continuity equation is indistinguishably fulfilled by all velocities $u'_i(y', t')$, $i \in I_n^1$, where $I_n^1 := \{1, 2, \dots, n\}$, and we assume that $I_{n-1}^1 := \{1, \dots, n-1\}$. The system of constitutive equations of motion and the initial, boundary, and the fluid-fluid interface conditions are given, respectively, as follows:

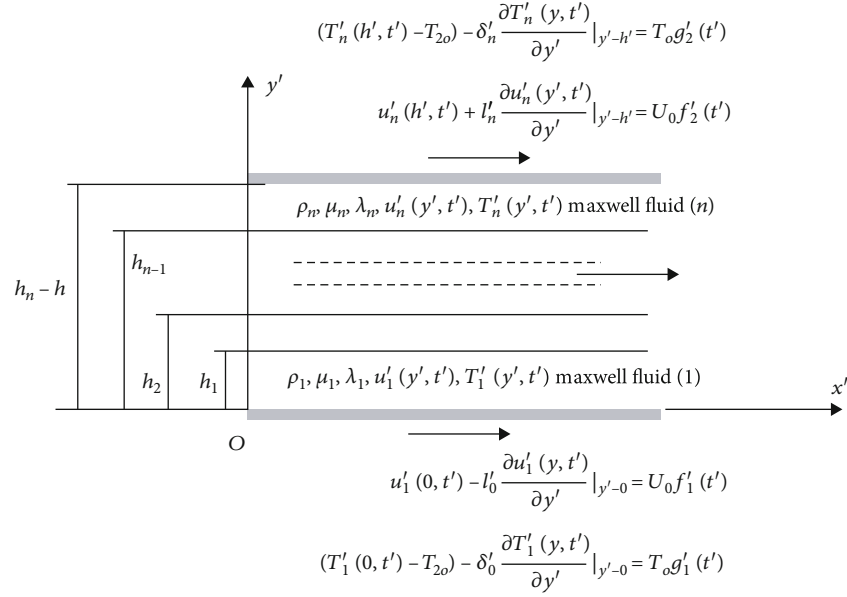


FIGURE 1: Geometry of the problem.

(i) The n-linear momentum equations:

$$\rho_i \frac{\partial u'_i}{\partial t'} = \frac{\partial \tau'_i}{\partial y'} - \frac{\partial p'_i}{\partial x'}, i \in I_n^1. \quad (2)$$

(iii) The corresponding n-initial conditions:

$$u'_i(y', 0) = 0, \tau'_i(y', 0) = 0, i \in I_n^1. \quad (4)$$

(ii) The n-constitutive equations:

$$\tau'_i + \lambda'_i \frac{\partial \tau'_i}{\partial t'} = \mu_i \frac{\partial u'_i}{\partial y'}, i \in I_n^1. \quad (3)$$

(iv) The boundary condition:

$$\begin{aligned} \text{at the lower wall } y' = 0, u'_1(0, t') - l'_0 \frac{\partial u'_1(y', t')}{\partial y'} \Big|_{y'=0} &= U_0 f'_1(t'), \\ \text{at the upper wall } y' = h'_n = h', u'_n(h', t') + l'_n \frac{\partial u'_n(y', t')}{\partial y'} \Big|_{y'=h'} &= U_0 f'_2(t'). \end{aligned} \quad (5)$$

(v) At the interface, we assume the continuity of Robin conditions:

$$\tau'_i(h'_i, t') = \tau'_{i+1}(h'_i, t'), i \in I_{n-1}^1. \quad (6)$$

$$\begin{aligned} u'_i(h'_i, t') + l'_i \frac{\partial u'_i(y', t')}{\partial y'} \Big|_{y'=h'_i} \\ = u'_{i+1}(h'_i, t') - l'_i \frac{\partial u'_{i+1}(y', t')}{\partial y'} \Big|_{y'=h'_i}, \end{aligned}$$

The system of constitutive relations for temperature and heat flux is given by the following:

(i) The n-thermal transport balance equations:

$$\rho_i c_{ip} \frac{\partial T'_i(y', t')}{\partial t'} = - \frac{\partial q'_i(y', t')}{\partial y'}, i \in I_n^1. \quad (7)$$

(ii) The n-thermal fluxes with Fourier's law:

$$q'_i(y', t') = -k_i \frac{\partial T'_i(y', t')}{\partial y'}, i \in I_n^1, \quad (8)$$

where k_i and c_{ip} are the thermal conductivity and the specific heat at constant pressure, respectively. We consider the following:

(i) n-Initial conditions:

$$T'_i(y', 0) = T_{2o}, q'_i(y', 0) = q_0, i \in I_n^1. \quad (9)$$

(ii) Boundary conditions:

$$\begin{aligned} \left(T'_1(0, t') - T_{2o} \right) - \delta'_0 \frac{\partial T'_1(y', t')}{\partial y'} \Big|_{y'=0} &= T_o g'_1(t'), \\ \left(T'_n(h', t') - T_{2o} \right) + \delta'_n \frac{\partial T'_n(y', t')}{\partial y'} \Big|_{y'=h'} &= T_o g'_2(t'). \end{aligned} \quad (10)$$

(iii) Interface conditions:

$$\begin{aligned} \left(T'_i(h'_i, t') - T_{2o} \right) + \delta'_i \frac{\partial T'_i(y', t')}{\partial y'} \Big|_{y'=h'_i} \\ = \left(T'_{i+1}(h'_i, t') - T_{2o} \right) - \delta'_{i+1} \frac{\partial T'_{i+1}(y', t')}{\partial y'} \Big|_{y'=h'_i}, q'_i(h'_i, t') \\ = q'_{i+1}(h'_i, t'), i = 1, 2, \dots, n-1. \end{aligned} \quad (11)$$

Consider the nondimensional variables

$$\begin{aligned} x = \frac{x'}{h'}, y = \frac{y'}{h'}, t = \frac{v_1 t'}{h'^2}, u_i = \frac{u'_i}{U_0}, \tau_i = \frac{h' \tau'_i}{\mu_1 U_0}, v_i = \frac{\mu_i}{\rho_i}, \\ p = \frac{h' p'}{\mu_1 U_0}, \lambda_i = \frac{\lambda'_i v_1}{h'^2}, a_i = \frac{\rho_i}{\rho_1}, b_i = \frac{\mu_i}{\mu_1}, f_1(t) = f'_1 \left(\frac{h'^2 t'}{v_1} \right), \\ g_1(t) = g'_1 \left(\frac{h'^2 t'}{v_1} \right), T_i = \frac{T'_i - T_{2o}}{T_o}, q_i = \frac{q'_i}{q_0}, \sigma_i = \frac{v_i}{v_1}, \\ Pr_i = \frac{\mu_i c_{ip}}{k_i}, f_2(t) = f'_2 \left(\frac{h'^2 t'}{v_1} \right), h_i = \frac{h'_i}{h'}, g_2(t) = g'_2 \left(\frac{h'^2 t'}{v_1} \right), \\ l_j = \frac{l'_j}{h'}, \delta_j = \frac{\delta'_j}{h'}, i \in I_n^1, j = 0, 1, 2, \dots, n. \end{aligned} \quad (12)$$

The dimensionless form of the governing Equations (2)–(11) are reduced into the following form:

$$a_i \frac{\partial u_i}{\partial t} = - \frac{\partial p}{\partial x} + \frac{\partial \tau_i}{\partial y}, i \in I_n^1, \quad (13)$$

$$\tau_i + \lambda_i \frac{\partial \tau_i}{\partial t} = b_i \frac{\partial u_i}{\partial y}, i \in I_n^1, \quad (14)$$

$$v_1 \gamma_0 \rho_i c_{ip} \frac{\partial T_i}{\partial t} = - \frac{\partial q_i}{\partial y}, i \in I_n^1, \quad (15)$$

$$q_i = -\gamma_0 k_i \frac{\partial T_i}{\partial y}, i \in I_n^1, \quad (16)$$

along with the following:

(i) The dimensionless n-initial conditions:

$$T_i(y, 0) = 0, q_i(y, 0) = 1, u_i(y, 0) = 0, \tau_i(y, 0) = 0, i \in I_n^1. \quad (17)$$

(ii) The dimensionless boundary condition:

$$\begin{aligned} u_1(0, t) - l_0 \frac{\partial u_1(y, t)}{\partial y} \Big|_{y=0} &= f_1(t), \\ \text{on the bottom plate } y = 0, \\ T_1(0, t) - \delta_0 \frac{\partial T_1(y, t)}{\partial y} \Big|_{y=0} &= g_1(t), \end{aligned} \quad (18)$$

$$\begin{aligned} u_n(1, t) + l_n \frac{\partial u_n(y, t)}{\partial y} \Big|_{y=1} &= f_2(t), \\ \text{on the upper plate } y' = h_n = 1, \\ T_n(1, t) + \delta_n \frac{\partial T_n(y, t)}{\partial y} \Big|_{y=1} &= g_2(t). \end{aligned} \quad (19)$$

(iii) The nondimensional interface conditions:

$$\begin{aligned} u_i(h_i, t) + l_i \frac{\partial u_i(y, t)}{\partial y} \Big|_{y=h_i} \\ = u_{i+1}(h_i, t) - l_i \frac{\partial u_{i+1}(y, t)}{\partial y} \Big|_{y=h_i}, \tau_i(h_i, t) \\ = \tau_{i+1}(h_i, t), \end{aligned} \quad (20)$$

$$\begin{aligned} T_i(h_i, t) + \delta_i \frac{\partial T_i(y, t)}{\partial y} \Big|_{y=h_i} \\ = T_{i+1}(h_i, t) - \delta_i \frac{\partial T_{i+1}(y, t)}{\partial y} \Big|_{y=h_i}, q_i(h_i, t) \\ = q_{i+1}(h_i, t), i \in I_{n-1}^1, \end{aligned} \quad (21)$$

where $\gamma_0 = T_o/q_0 h'$ and T_o is the characteristic scale.

2.1. Generalized Constitutive Mathematical Model. Consider the following generalized constitutive mathematical relations:

$$\tau_i + \lambda_i \mathfrak{D}_t^{\alpha_i} \tau_i = b_i \frac{\partial u_i}{\partial y}, \alpha_i \in (0, 1], i \in I_n^1, \quad (22)$$

$$q_i = -\gamma_0 k_i \mathfrak{D}_t^{1-\beta_i} \left(\frac{\partial T_i}{\partial y} \right), \beta_i \in (0, 1], i \in I_n^1, \quad (23)$$

where the Caputo derivative \mathfrak{D}_t^σ is defined as

$$\mathfrak{D}_t^\sigma \mathfrak{F}(y, t) = \frac{1}{\Gamma(1-\sigma)} \int_0^t (t-\rho)^{-\sigma} \frac{\partial \mathfrak{F}(y, \rho)}{\partial \rho} d\rho, 0 \leq \sigma < 1. \quad (24)$$

For the special case $\sigma = 1$, $\mathfrak{D}_t^1 F(y, t) = \partial F(y, t)/\partial t$. It is significant to note that the fractional models (22) and (23) have the following equivalent formulae as

$$\begin{aligned} \tau_i(y, t) &= \left[\frac{b_i}{\lambda_i} t^{\alpha_i-1} E_{\alpha_i, \alpha_i} \left(-\frac{t^{\alpha_i}}{\lambda_i} \right) \right] * \frac{\partial u_i(y, t)}{\partial y} \\ &= \int_0^t \frac{b_i}{\lambda_i} (t-\tau)^{\alpha_i-1} E_{\alpha_i, \alpha_i} \left(-\frac{(t-\tau)^{\alpha_i}}{\lambda_i} \right) \frac{\partial u_i(y, \tau)}{\partial y} d\tau, i \in I_n^1, \end{aligned} \quad (25)$$

$$\begin{aligned} q_i(y, t) &= \frac{t^{\beta_i-1}}{\Gamma(\beta_i)} * \frac{\partial^2 T_i(y, t)}{\partial t \partial y} \\ &= \int_0^t \frac{(t-\tau)^{\beta_i-1}}{\Gamma(\beta_i)} \frac{\partial^2 T_i(y, \tau)}{\partial \tau \partial y} d\tau, i \in I_n^1. \end{aligned} \quad (26)$$

The relations (25) and (26) depict that the histories of the thermal and the velocity gradients impact the time-variation of heat flux and the shear stress, separately. Moreover, it has been seen from the above relations that the nonlocality kernel of the heat flux observes the power-law $t^{\beta_i-1}/\Gamma(\beta_i)$, while the nonlocality kernel for the shear stress is the function $(b_i/\lambda_i) t^{\alpha_i-1} E_{\alpha_i, \alpha_i}(-t^{\alpha_i}/\lambda_i)$, $E_{\alpha_i, \alpha_i}(\cdot)$ being the Mittag-Leffler function. In this study, we consider the pressure gradient in the flow direction as a known function, namely

$$-\frac{\partial p}{\partial x} = P(t), \quad (27)$$

where $P(t)$ is a peice-wise continuous function on $[0, \infty)$.

3. Solution of the Problem

We have applied the finite sine-Fourier transform coupled with the Laplace transform, to obtain explicit solutions of Equations (13), (15), (22), and (23) with conditions (17)–(20). We apply the Laplace transform to Equations (13), (15), and (18)–(23) along with the initial condition (17); we have

$$a_i s \bar{u}_i(y, s) = \frac{\partial \bar{\tau}_i(y, s)}{\partial y} + \bar{P}(s), i \in I_n^1, \quad (28)$$

$$\bar{\tau}_i(y, s) = \frac{b_i}{1 + \lambda_i s^{\alpha_i}} \frac{\partial \bar{u}_i(y, s)}{\partial y}, i \in I_n^1, \quad (29)$$

$$\nu_1 \gamma_0 \rho_i c_{ip} s \bar{T}_i(y, s) = -\frac{\partial \bar{q}_i(y, s)}{\partial y}, i \in I_n^1, \quad (30)$$

$$\bar{q}_i = -\gamma_0 k_i s^{1-\beta_i} \frac{\partial \bar{T}_i(y, s)}{\partial y}, i \in I_n^1, \quad (31)$$

$$\bar{u}_1(0, s) - l_0 \frac{\partial \bar{u}_1(y, s)}{\partial y} \Big|_{y=0} = \bar{f}_1(s), \quad (32)$$

$$\bar{u}_n(1, s) + l_n \frac{\partial \bar{u}_n(y, s)}{\partial y} \Big|_{y=1} = \bar{f}_2(s),$$

$$\bar{T}_1(0, s) - \delta_0 \frac{\partial \bar{T}_1(y, s)}{\partial y} \Big|_{y=0} = \bar{g}_1(s), \quad (33)$$

$$\bar{T}_n(1, s) + \delta_n \frac{\partial \bar{T}_n(y, s)}{\partial y} \Big|_{y=1} = \bar{g}_2(s),$$

$$\bar{u}_i(h_i, s) + l_i \frac{\partial \bar{u}_i(y, s)}{\partial y} \Big|_{y=h_i} = \bar{u}_{i+1}(h_i, s) - l_i \frac{\partial \bar{u}_{i+1}(y, s)}{\partial y} \Big|_{y=h_i}, \quad (34)$$

$$\bar{\tau}_i(h_i, s) = \bar{\tau}_{i+1}(h_i, s), i = 1, 2, \dots, n-1, \quad (35)$$

$$\bar{T}_i(h_i, s) + \delta_i \frac{\partial \bar{T}_i(y, s)}{\partial y} \Big|_{y=h_i} = \bar{T}_{i+1}(h_i, s) - \delta_i \frac{\partial \bar{T}_{i+1}(y, s)}{\partial y} \Big|_{y=h_i}, \quad (36)$$

$$\bar{q}_i(h_i, s) = \bar{q}_{i+1}(h_i, s), i = 1, 2, \dots, n-1. \quad (37)$$

3.1. Analytical Solutions for Velocity and Shear Stress. Combining Equations (28) and (29), we can write

$$a_i s (1 + \lambda_i s^{\alpha_i}) \bar{u}_i(y, s) = (1 + \lambda_i s^{\alpha_i}) \bar{P}(s) + b_i \frac{\partial^2 \bar{u}_i(y, s)}{\partial y^2}, i \in I_n^1, \quad (38)$$

where $\bar{\varphi}(y, s) = \int_0^\infty \varphi(y, t) \exp(-st) dt$ represents the Laplace transform of the function $\varphi(y, t)$. In case of nonhomogeneous Robin boundary and fluid-fluid interface conditions (32) and (34), the finite Fourier sine-cosine transform of the function $\bar{u}_i(y, s)$, $i \in I_n^1$, can be defined with the help of the Fourier series theory and the Sturm-Liouville theory as [39, 40].

$$\widehat{\bar{u}}_i(\eta_m^{(i)}, s) = \frac{1}{h_i - h_{i-1}} \int_{h_{i-1}}^{h_i} \bar{u}_i(y, s) \Phi_m^{(i)}(y) dy, \quad (39)$$

where $\Phi_m^{(i)}(y) = \sin(\eta_m^{(i)}(y - h_{i-1}/h_i - h_{i-1})) + (l_{i-1}/h_i - h_{i-1}) \eta_m^{(i)} \cos(\eta_m^{(i)}(y - h_{i-1}/h_i - h_{i-1}))$ and $\eta_m^{(i)}$ are the positive roots of the transcendental equation $\tan \eta_m^{(i)} = (h_i - h_{i-1})(l_{i-1} + l_i) \eta_m^{(i)} / l_{i-1} l_i \eta_m^{(i)2} - (h_i - h_{i-1})^2$. The inverse Fourier sine-cosine transform of $\widehat{\bar{u}}_i(\eta_m^{(i)}, s)$ is defined by

$$\bar{u}_i(y, s) = \sum_{m=1}^{\infty} \frac{\widehat{\bar{u}}_i(\eta_m^{(i)}, s)}{J_{mi}} \Phi_m^{(i)}(y), \quad (40)$$

where

$$J_{mi} = \frac{1}{h_i - h_{i-1}} \int_{h_{i-1}}^{h_i} \Phi_m^{(i)2}(y) dy$$

$$= \frac{l_{i-1}^2 \eta_m^{(i)2} - (h_i - h_{i-1})^2}{4\eta_m^{(i)} (h_i - h_{i-1})^2} \sin(2\eta_m^{(i)})$$

$$+ \frac{(h_i - h_{i-1})^2 + l_{i-1}(h_i - h_{i-1}) + l_{i-1}^2 \eta_m^{(i)2} - l_{i-1}(h_i - h_{i-1}) \cos(2\eta_m^{(i)})}{2(h_i - h_{i-1})^2}. \quad (41)$$

By direct computations, using the robin boundary condition (32) and interface fluid-fluid condition (34), we can write

$$\frac{\partial^2 \hat{u}_i}{\partial y^2}(\eta_m^{(i)}, s) = \frac{\eta_m^{(i)}}{(h_i - h_{i-1})^2} \left(\cos(\eta_m^{(i)}) \right.$$

$$\cdot \frac{(h_i - h_{i-1})^2 + l_{i-1}^2 \eta_m^{(i)2}}{l_{i-1} l_i \eta_m^{(i)2} - (h_i - h_{i-1})^2} \bar{w}_i(h_i, l_i, s)$$

$$\left. + \bar{v}_i(h_{i-1}, l_{i-1}, s) \right)$$

$$- \frac{\eta_m^{(i)2}}{(h_i - h_{i-1})^2} \hat{u}_i(\eta_m^{(i)}, s), i \in I_n^1, \quad (42)$$

where we rename $\bar{v}_i(h_{i-1}, l_{i-1}, s) = \bar{u}_i(h_{i-1}, s) - l_{i-1}(\partial \bar{u}_i(h_{i-1}, s)/\partial y)$, $\bar{w}_i(h_i, l_i, s) = \bar{u}_i(h_i, s) + l_i(\partial \bar{u}_i(h_i, s)/\partial y)$, $i \in I_{n-1}^1$, $\bar{v}_0(h_0, l_0, s) = f_1(s)$, and $\bar{w}_n(h_n, l_n, s) = f_2(s)$. With the application of finite Fourier sine-cosine transform (39) to Equation (38) corresponding to the robin boundary conditions (32) and interface fluid-fluid conditions (34), and using Equation (42), the transformed velocities take the form

$$\hat{u}_i(\eta_m^{(i)}, s) = \frac{(h_i - h_{i-1})^2 (1 + \lambda_i s^{\alpha_i}) \bar{P}(s)}{a_i (h_i - h_{i-1})^2 s (1 + \lambda_i s^{\alpha_i}) + b_i \eta_m^{(i)2}}$$

$$+ \frac{b_i \eta_m^{(i)}}{a_i (h_i - h_{i-1})^2 s (1 + \lambda_i s^{\alpha_i}) + b_i \eta_m^{(i)2}}$$

$$\times \left(\cos(\eta_m^{(i)}) \frac{(h_i - h_{i-1})^2 + l_{i-1}^2 \eta_m^{(i)2}}{l_{i-1} l_i \eta_m^{(i)2} - (h_i - h_{i-1})^2} \bar{w}_i(h_i, l_i, s) \right.$$

$$\left. + \bar{v}_i(h_{i-1}, l_{i-1}, s) \right), i \in I_n^1. \quad (43)$$

To apply the inverse Fourier sine-cosine transform, we rewrite Equation (44) in the following suitable form:

$$\hat{u}_i(\eta_m^{(i)}, s) = \frac{l_{i-1} \eta_m^{(i)} \sin(\eta_m^{(i)}) + (h_i - h_{i-1}) (1 - \cos(\eta_m^{(i)}))}{\eta_m^{(i)} (h_i - h_{i-1})} \frac{(h_i - h_{i-1} + l_i) \bar{v}_i(h_{i-1}, l_{i-1}, s) + l_{i-1} \bar{w}_i(h_i, l_i, s)}{(h_i - h_{i-1}) + l_{i-1} + l_i}$$

$$+ \frac{-l_{i-1} \eta_m^{(i)} - (h_i - h_{i-1} - l_{i-1}) \eta_m^{(i)} \cos(\eta_m^{(i)}) + (h_i - h_{i-1} + l_{i-1} \eta_m^{(i)2}) \sin(\eta_m^{(i)})}{(h_i - h_{i-1}) \eta_m^{(i)2}} \frac{(\bar{w}_i(h_i, l_i, s) - \bar{v}_i(h_{i-1}, l_{i-1}, s)) (h_i - h_{i-1})}{(h_i - h_{i-1}) + l_{i-1} + l_i}$$

$$+ \left(\frac{b_i \eta_m^{(i)}}{a_i (h_i - h_{i-1})^2 s (1 + \lambda_i s^{\alpha_i}) + b_i \eta_m^{(i)2}} + C_{1m}^{(i)} \right) \bar{v}_i(h_{i-1}, l_{i-1}, s)$$

$$+ \left(\frac{b_i \eta_m^{(i)} \cos(\eta_m^{(i)})}{a_i (h_i - h_{i-1})^2 s (1 + \lambda_i s^{\alpha_i}) + b_i \eta_m^{(i)2}} \frac{(h_i - h_{i-1})^2 + l_{i-1}^2 \eta_m^{(i)2}}{l_{i-1} l_i \eta_m^{(i)2} - (h_i - h_{i-1})^2} + C_{2m}^{(i)} \right) \bar{w}_i(h_i, l_i, s)$$

$$+ \frac{(h_i - h_{i-1})^2 (1 + \lambda_i s^{\alpha_i}) \bar{P}(s)}{a_i (h_i - h_{i-1})^2 s (1 + \lambda_i s^{\alpha_i}) + b_i \eta_m^{(i)2}}, \quad i \in I_n^1, \quad (44)$$

where

$$C_{1m}^{(i)} = -\frac{1}{\eta_m^{(i)}} + \frac{(h_i - h_{i-1})(l_{i-1} + l_i) \eta_m^{(i)} \cos(\eta_m^{(i)}) + (h_i - h_{i-1})^2 \sin(\eta_m^{(i)}) - l_i l_{i-1} \eta_m^{(i)2} \sin(\eta_m^{(i)})}{(h_i - h_{i-1})(h_i - h_{i-1} + l_{i-1} + l_i) \eta_m^{(i)2}},$$

$$C_{2m}^{(i)} = \frac{(h_i - h_{i-1})^2 \eta_m^{(i)} \cos(\eta_m^{(i)}) - ((h_i - h_{i-1})^2 + l_{i-1}(h_i - h_{i-1} + l_{i-1}) \eta_m^{(i)2}) \sin(\eta_m^{(i)})}{(h_i - h_{i-1})(h_i - h_{i-1} + l_{i-1} + l_i) \eta_m^{(i)2}}. \quad (45)$$

Considering the auxiliary relations along with their Fourier sine-cosine transform

$$\varphi_{1i}(y) = 1, y \in [h_{i-1}, h_i], \quad \widehat{\varphi}_{1i}(\eta_m^{(i)}) = \frac{l_{i-1}\eta_m^{(i)} \sin(\eta_m^{(i)}) + (h_i - h_{i-1})(1 - \cos(\eta_m^{(i)}))}{\eta_m^{(i)}(h_i - h_{i-1})}, \quad (46)$$

$$\varphi_{2i}(y) = \frac{y - h_{i-1}}{h_i - h_{i-1}}, y \in [h_{i-1}, h_i], \quad (47)$$

$$\widehat{\varphi}_{2i}(\eta_m^{(i)}) = \frac{-l_{i-1}\eta_m^{(i)} - (h_i - h_{i-1} - l_{i-1})\eta_m^{(i)} \cos(\eta_m^{(i)}) + (h_i - h_{i-1} + l_{i-1}\eta_m^{(i)2}) \sin(\eta_m^{(i)})}{(h_i - h_{i-1})\eta_m^{(i)2}}, \quad (48)$$

$$m = 1, 2, \dots, i \in I_n^1, h_0 = 0, h_n = 1, \quad (49)$$

the inverse Fourier sine-cosine transform of Equation (46) takes the form

$$\begin{aligned} \bar{u}_i(y, s) = & \frac{(h_i - h_{i-1} + l_i)\bar{v}_i(h_{i-1}, l_{i-1}, s) + l_{i-1}\bar{w}_i(h_i, l_i, s)}{(h_i - h_{i-1}) + l_{i-1} + l_i} \\ & + \frac{(\bar{w}_i(h_i, l_i, s) - \bar{v}_i(h_{i-1}, l_{i-1}, s))}{(h_i - h_{i-1}) + l_{i-1} + l_i} (y - h_{i-1}) \\ & + \sum_{m=1}^{\infty} \left(\frac{b_i \eta_m^{(i)}}{a_i(h_i - h_{i-1})^2 s(1 + \lambda_i s^{\alpha_i}) + b_i \eta_m^{(i)2}} + C_{1m}^{(i)} \right) \\ & \cdot \frac{\Phi_m^{(i)}(y)\bar{v}_i(h_{i-1}, l_{i-1}, s)}{J_{mi}} + \sum_{m=1}^{\infty} \\ & \cdot \left(\frac{b_i \eta_m^{(i)} \cos(\eta_m^{(i)})}{a_i(h_i - h_{i-1})^2 s(1 + \lambda_i s^{\alpha_i}) + b_i \eta_m^{(i)2}} \right. \\ & \cdot \left. \frac{(h_i - h_{i-1})^2 + l_{i-1}^2 \eta_m^{(i)2}}{l_{i-1} l_i \eta_m^{(i)2} - (h_i - h_{i-1})^2} + C_{2m}^{(i)} \right) \frac{\Phi_m^{(i)}(y)\bar{w}_i(h_i, l_i, s)}{J_{mi}} \end{aligned}$$

$$+ \sum_{m=1}^{\infty} \left(\frac{(h_i - h_{i-1})^2 (1 + \lambda_i s^{\alpha_i})}{a_i(h_i - h_{i-1})^2 s(1 + \lambda_i s^{\alpha_i}) + b_i \eta_m^{(i)2}} \right) \frac{\Phi_m^{(i)}(y)\bar{P}(s)}{J_{mi}}, i \in I_n^1. \quad (50)$$

Now, from (29) and (50), we obtain

$$\bar{\tau}_i(y, s) = \bar{T}_{i,1}(y, s)\bar{w}_i(h_i, l_i, s) - \bar{T}_{i,2}(y, s)\bar{v}_i(h_{i-1}, l_{i-1}, s) + \bar{T}_{i,3}(y, s)\bar{P}(s), i \in I_n^1, \quad (51)$$

where

$$\begin{aligned} \bar{T}_{i,1}(y, s) = & \frac{b_i}{(1 + \lambda_i s^{\alpha_i})(h_i - h_{i-1} + l_{i-1} + l_i)} + \frac{b_i}{(h_i - h_{i-1})(1 + \lambda_i s^{\alpha_i})} \sum_{m=1}^{\infty} \eta_m^{(i)} \\ & \cdot \left(\frac{b_i \eta_m^{(i)} \cos(\eta_m^{(i)})}{a_i(h_i - h_{i-1})^2 s(1 + \lambda_i s^{\alpha_i}) + b_i \eta_m^{(i)2}} \frac{(h_i - h_{i-1})^2 + l_{i-1}^2 \eta_m^{(i)2}}{l_{i-1} l_i \eta_m^{(i)2} - (h_i - h_{i-1})^2} + C_{2m}^{(i)} \right) \\ & \times \frac{\cos(\eta_m^{(i)}(y - h_{i-1}/h_i - h_{i-1})) - (l_{i-1}/h_i - h_{i-1})\eta_m^{(i)} \sin(\eta_m^{(i)}(y - h_{i-1}/h_i - h_{i-1}))}{J_{mi}}, \bar{T}_{i,2}(y, s) \\ = & \frac{b_i}{(1 + \lambda_i s^{\alpha_i})(h_i - h_{i-1} + l_{i-1} + l_i)} - \frac{b_i}{(h_i - h_{i-1})(1 + \lambda_i s^{\alpha_i})} \sum_{m=1}^{\infty} \eta_m^{(i)} \left(\frac{b_i \eta_m^{(i)}}{a_i(h_i - h_{i-1})^2 s(1 + \lambda_i s^{\alpha_i}) + b_i \eta_m^{(i)2}} + C_{1m}^{(i)} \right) \\ & \times \frac{\cos(\eta_m^{(i)}(y - h_{i-1}/h_i - h_{i-1})) - (l_{i-1}/h_i - h_{i-1})\eta_m^{(i)} \sin(\eta_m^{(i)}(y - h_{i-1}/h_i - h_{i-1}))}{J_{mi}}, \bar{T}_{i,3}(y, s) \\ = & b_i(h_i - h_{i-1})\bar{P}(s) \sum_{m=1}^{\infty} \frac{\eta_m^{(i)} \left(\cos(\eta_m^{(i)}(y - h_{i-1}/h_i - h_{i-1})) - (l_{i-1}/h_i - h_{i-1})\eta_m^{(i)} \sin(\eta_m^{(i)}(y - h_{i-1}/h_i - h_{i-1})) \right)}{J_{mi} \left(a_i(h_i - h_{i-1})^2 s(1 + \lambda_i s^{\alpha_i}) + b_i \eta_m^{(i)2} \right)}. \end{aligned} \quad (52)$$

Using Equations (32) and (34) in Equation (51), we get the following linear system (for detail, see “Appendix”):

$$\bar{M}(s)\bar{W}(s) = \bar{N}(s), \quad (53)$$

where

$$\bar{M}(s) = \begin{bmatrix} \bar{Y}_{1,1} & -\bar{Y}_{1,2} & 0 & 0 & \cdots & 0 \\ \bar{Y}_{2,1} & \bar{Y}_{2,2} & -\bar{Y}_{2,3} & 0 & \cdots & 0 \\ 0 & \bar{Y}_{3,2} & \bar{Y}_{3,3} & -\bar{Y}_{3,4} & \cdots & 0 \\ \vdots & \vdots & \ddots & \ddots & \ddots & \vdots \\ 0 & 0 & \cdots & \bar{Y}_{n-3,n-4} & \bar{Y}_{n-3,n-3} & -\bar{Y}_{n-3,n-2} \\ 0 & 0 & \cdots & \bar{Y}_{n-2,n-3} & \bar{Y}_{n-2,n-2} & -\bar{Y}_{n-2,n-1} \\ 0 & 0 & \cdots & 0 & \bar{Y}_{n-1,n-2} & \bar{Y}_{n-1,n-1} \end{bmatrix},$$

$$\bar{W}(s) = \begin{bmatrix} \bar{w}_1(h_1, l_1, s) \\ \bar{w}_2(h_2, l_2, s) \\ \vdots \\ \bar{w}_{n-1}(h_{n-1}, l_{n-1}, s) \end{bmatrix},$$

$$\bar{N}(s) = \begin{bmatrix} \bar{b}_1 \\ \bar{b}_2 \\ \vdots \\ \bar{b}_{n-1} \end{bmatrix}. \quad (54)$$

Finally, we obtain

$$\bar{W}(s) = \bar{M}^{-1}(s)\bar{N}(s). \quad (55)$$

Now, $\bar{w}_i(h_i, l_i, s) = \bar{v}_{i+1}(h_i, l_i, s), i \in I_{n-1}^{(1)}$, are known functions; therefore, the velocities $\bar{u}_1(y, s), \dots, \bar{u}_n(y, s)$ are known. In order to obtain the inverse Laplace transforms of the functions $\bar{u}_i(y, s), i \in I_n^1$, we consider the following auxiliary functions:

$$\begin{aligned} \bar{H}_{i0}(m, s) &= \frac{1}{a_i(h_i - h_{i-1})^2 s(1 + \lambda_i s^{\alpha_i}) + \eta_m^{(i)2}} \\ &= \frac{s^{-1}}{a_i(h_i - h_{i-1})^2 \lambda_i (s^{\alpha_i} + \lambda_i^{-1})} \\ &\quad \cdot \frac{1}{1 + \left(\eta_m^{(i)2} s^{-1} / a_i(h_i - h_{i-1})^2 \lambda_i (s^{\alpha_i} + \lambda_i^{-1}) \right)} \\ &= \frac{1}{a_i \lambda_i (h_i - h_{i-1})^2} \sum_{k=0}^{\infty} (-1)^k \\ &\quad \cdot \left(\frac{\eta_m^{(i)2}}{a_i (h_i - h_{i-1})^2 \lambda_i} \right)^k \left[\frac{s^{-k-1}}{(s^{\alpha_i} + \lambda_i^{-1})^{k+1}} \right], \end{aligned}$$

$$\begin{aligned} \bar{H}_{i1}(m, s) &= \frac{(1 + \lambda_i s^{\alpha_i})}{(h_i - h_{i-1})^2 a_i s(1 + \lambda_i s^{\alpha_i}) + b_i \left(\eta_m^{(i)} \right)^2} \\ &= \frac{1}{a_i (h_i - h_{i-1})^2} \sum_{k=0}^{\infty} (-1)^k \left(\frac{\eta_m^{(i)2}}{(h_i - h_{i-1})^2 a_i \lambda_i} \right)^k \\ &\quad \cdot \left[\frac{s^{-k-1}}{(s^{\alpha_i} + \lambda_i^{-1})^k} \right], \\ \bar{H}_{i4}(m, s) &= \frac{1}{(1 + \lambda_i s^{\alpha_i}) \left(a_i (h_i - h_{i-1})^2 s(1 + \lambda_i s^{\alpha_i}) + b_i \left(\eta_m^{(i)} \right)^2 \right)} \\ &= \frac{1}{a_i \lambda_i^2 (h_i - h_{i-1})^2} \sum_{k=0}^{\infty} (-1)^k \\ &\quad \cdot \left(\frac{\eta_m^{(i)2}}{a_i (h_i - h_{i-1})^2 \lambda_i} \right)^k \left[\frac{s^{-k-1}}{(s^{\alpha_i} + \lambda_i^{-1})^{k+2}} \right]. \end{aligned} \quad (56)$$

Since the generalized G-Lorenzo-Hartley function is defined by [41]

$$\begin{aligned} G_{\sigma_1, \sigma_2, \sigma_3}(t, \sigma) &= \mathcal{L}^{-1} \left[\frac{s^{\sigma_2}}{(s^{\sigma_1} - \sigma)^{\sigma_3}} \right] \\ &= \sum_{k=0}^{\infty} \frac{\Gamma(k + \sigma_3) \sigma^k t^{(k + \sigma_3)\sigma_1 - \sigma_2 - 1}}{k! \Gamma((k + \sigma_3)\sigma_1 - \sigma_2) \Gamma(\sigma_3)}, \end{aligned}$$

$$\operatorname{Re}(s) > 0, \operatorname{Re}(\sigma_1 \sigma_3 - \sigma_2) > 0, \left| \frac{\sigma}{s^{\sigma_1}} \right| < 1, \quad (57)$$

and for $\alpha_i, \beta_i > 0$,

$$\mathcal{L}^{-1} \left[\frac{s^{\alpha_i - \beta_i}}{s^{\alpha_i} - d} \right] = t^{\beta_i - 1} E_{\alpha_i, \beta_i}(dt^{\alpha_i}), \quad (58)$$

where $E_{\alpha_i, \beta_i}(\cdot)$ is the Mittag-Leffler function [42]. The inverse Laplace transform of $\bar{H}_{i0}(m, s)$, $\bar{H}_{i1}(m, s)$, and $\bar{H}_{i4}(m, s)$ takes the form

$$\begin{aligned} H_{i0}(m, t) &= \frac{1}{a_i \lambda_i (h_i - h_{i-1})^2} \sum_{k=0}^{\infty} (-1)^k \\ &\quad \cdot \left(\frac{\eta_m^{(i)2}}{a_i (h_i - h_{i-1})^2 \lambda_i} \right)^k [G_{\alpha_i, -k-1, k+1}(t, -\lambda_i^{-1})], \end{aligned} \quad (59)$$

$$H_{i1}(m, t) = \frac{1}{(h_i - h_{i-1})^2 a_i} \sum_{k=0}^{\infty} (-1)^k \frac{(\eta_m^{(i)})^{2k}}{((h_i - h_{i-1})^2 a_i \lambda_i)^{k+1}} \cdot [G_{\alpha, -k-1, k}(t, -\lambda_i^{-1})], \quad (60)$$

$$H_{i4}(m, t) = \frac{1}{a_i \lambda_i^2 (h_i - h_{i-1})^2} \sum_{k=0}^{\infty} (-1)^k \cdot \left(\frac{\eta_m^{(i)2}}{(h_i - h_{i-1})^2 a_i \lambda_i} \right)^k [G_{\alpha, -k-1, k+2}(t, -\lambda_i^{-1})], \quad (61)$$

where $\delta(t)$ is the Dirac delta function. Using Equations (59), (60), and (50), we obtain for velocities $u_i(y, t), i \in I_n^1$, with the following expressions:

$$u_i(y, t) = \frac{(h_i - h_{i-1} + l_i) \bar{v}_i(h_{i-1}, l_{i-1}, t) + l_{i-1} \bar{w}_i(h_i, l_i, t)}{(h_i - h_{i-1}) + l_{i-1} + l_i} + \frac{(\bar{w}_i(h_i, l_i, t) - \bar{v}_i(h_{i-1}, l_{i-1}, t))}{(h_i - h_{i-1}) + l_{i-1} + l_i} (y - h_{i-1})$$

$$+ \sum_{m=1}^{\infty} \left(b_i \eta_m^{(i)} H_{i0}(m, t) * v_i(h_{i-1}, l_{i-1}, t) + C_{1m}^{(i)} v_i(h_{i-1}, l_{i-1}, t) \right) \cdot \frac{\Phi_m^{(i)}(y)}{J_{mi}} + \sum_{m=1}^{\infty} \left(\frac{((h_i - h_{i-1})^2 + l_{i-1}^2 \eta_m^{(i)2}) b_i \eta_m^{(i)} \cos(\eta_m^{(i)})}{l_{i-1} l_i \eta_m^{(i)2} - (h_i - h_{i-1})^2} H_{i0}(m, t) * w_i(h_i, l_i, t) + C_{2m}^{(i)} w_i(h_i, l_i, t) \right) \frac{\Phi_m^{(i)}(y)}{J_{mi}} + \sum_{m=1}^{\infty} ((h_i - h_{i-1})^2 H_{i1}(m, t) * P(t)) \frac{\Phi_m^{(i)}(y)}{J_{mi}}, i \in I_n^1, \quad (62)$$

where $h_1(t) * h_2(t) = \int_0^t h_1(t - \tau) h_2(\tau) d\tau$ is the convolution product of the functions $h_1(t)$ and $h_2(t)$. The system of shear stresses $\tau_i(y, t), i \in I_n^1$, can be determined by applying inverse Laplace transform to Equation (51) and using Equations (59) and (61).

$$\tau_i(y, t) = T_{i1}(y, t) * w_i(h_i, l_i, t) - T_{i2}(y, t) * v_i(h_{i-1}, l_{i-1}, t) + T_{i3}(y, t) * P(t), \quad (63)$$

where

$$\begin{aligned} T_{i1}(y, t) &= \frac{b_i \lambda_i^{-1} t^{\alpha_i-1} E_{\alpha_i, \alpha_i}(-\lambda_i^{-1} t^{\alpha_i})}{(h_i - h_{i-1} + l_{i-1} + l_i)} + \frac{b_i}{(h_i - h_{i-1})} \sum_{m=1}^{\infty} \eta_m^{(i)} \cdot \left(b_i \eta_m^{(i)} \cos(\eta_m^{(i)}) \frac{(h_i - h_{i-1})^2 + l_{i-1}^2 \eta_m^{(i)2}}{l_{i-1} l_i \eta_m^{(i)2} - (h_i - h_{i-1})^2} H_{i4}(m, t) + C_{2m}^{(i)} \lambda_i^{-1} t^{\alpha_i-1} E_{\alpha_i, \alpha_i}(-\lambda_i^{-1} t^{\alpha_i}) \right) \\ &\cdot \frac{\cos(\eta_m^{(i)}(y - h_{i-1}/h_i - h_{i-1})) - (l_{i-1}/h_i - h_{i-1}) \eta_m^{(i)} \sin(\eta_m^{(i)}(y - h_{i-1}/h_i - h_{i-1}))}{J_{mi}}, \bar{T}_{i2}(y, s) \\ &= \frac{b_i \lambda_i^{-1} t^{\alpha_i-1} E_{\alpha_i, \alpha_i}(-\lambda_i^{-1} t^{\alpha_i})}{(h_i - h_{i-1} + l_{i-1} + l_i)} - \frac{b_i}{(h_i - h_{i-1})} \sum_{m=1}^{\infty} \eta_m^{(i)} \left(b_i \eta_m^{(i)} H_{i4}(m, t) + C_{1m}^{(i)} \lambda_i^{-1} t^{\alpha_i-1} E_{\alpha_i, \alpha_i}(-\lambda_i^{-1} t^{\alpha_i}) \right) \\ &\cdot \frac{\cos(\eta_m^{(i)}(y - h_{i-1}/h_i - h_{i-1})) - (l_{i-1}/h_i - h_{i-1}) \eta_m^{(i)} \sin(\eta_m^{(i)}(y - h_{i-1}/h_i - h_{i-1}))}{J_{mi}}, \bar{T}_{i3}(y, s) \\ &= b_i \sum_{m=1}^{\infty} \eta_m^{(i)} ((h_i - h_{i-1}) H_{i0}(m, t)) \times \frac{\cos(\eta_m^{(i)}(y - h_{i-1}/h_i - h_{i-1})) - (l_{i-1}/h_i - h_{i-1}) \eta_m^{(i)} \sin(\eta_m^{(i)}(y - h_{i-1}/h_i - h_{i-1}))}{J_{mi}}. \end{aligned} \quad (64)$$

At the end of this section, we mention that, in the case of a single fluid, there are interesting studies in the literature on the flow of Maxwell fluids with slip on the channel walls. Thus, in the particular case $\alpha = 1, n = 1, P(t) = f_2(t) = 0$, our results are equivalent with those

obtained in ([43], Equations (34) and (55)). Moreover for the Newtonian case with $n = 1, P(t) = 0, \lambda_1 = 0$, the velocity profile given by Equation (62) is equivalent to the solution obtained in [44], Equation (65) with $\varphi = 0$ and $(\rho\beta)_f = 0$.

3.2. *Solution for the Thermal Transport.* Using Equations (30) and (31), we can write the system of n-equation describing the Laplace transformed temperature profile:

$$\frac{\partial^2 \bar{T}_i}{\partial y^2} = Q_i s^{\beta_i} \bar{T}_i, i \in I_n^1, \quad (65)$$

where $Q_i = (a_i/b_i)Pr_i$. The general solution of Equation (65) is

$$\bar{T}_i(y, s) = C_{i1}(s)e^{-y\sqrt{Q_i s^{\beta_i}}} + C_{i2}(s)e^{y\sqrt{Q_i s^{\beta_i}}}, i \in I_n^1, \quad (66)$$

where the unknown parameters $C_{11}, C_{21}, \dots, C_{n1}, C_{12}, C_{22}, \dots, C_{n2}$ are to be computed by using Equations (33) and (36) and are given by the following linear system:

$$\mathfrak{A}(s)\mathfrak{Y}(s) = \mathfrak{B}(s), \quad (67)$$

where the $\mathfrak{A}(s)$ matrix is

$$\mathfrak{A}(s) = \begin{bmatrix} \mathbf{a}_0 & 0 & 0 & \cdots & 0 & \mathbf{c}_0 & 0 & 0 & \cdots & 0 \\ \mathbf{a}_1 & -\mathbf{c}_1 & 0 & \cdots & 0 & \mathbf{c}_1 & -\mathbf{d}_1 & 0 & \cdots & 0 \\ 0 & \mathbf{a}_2 & -\mathbf{c}_2 & \cdots & 0 & 0 & \mathbf{c}_2 & -\mathbf{d}_2 & \cdots & 0 \\ \vdots & \vdots & \ddots & \ddots & \vdots & \vdots & \vdots & \ddots & \ddots & \vdots \\ 0 & 0 & \cdots & \mathbf{a}_{n-1} & -\mathbf{c}_{n-1} & 0 & 0 & \cdots & \mathbf{c}_{n-1} & -\mathbf{d}_{n-1} \\ -\mathbf{p}_1 & \mathbf{q}_1 & 0 & \cdots & 0 & \mathbf{r}_1 & -\mathbf{s}_1 & 0 & \cdots & 0 \\ 0 & -\mathbf{p}_2 & \mathbf{q}_2 & \cdots & 0 & 0 & \mathbf{r}_2 & -\mathbf{s}_2 & \cdots & 0 \\ \vdots & \vdots & \ddots & \ddots & \vdots & \vdots & \vdots & \ddots & \ddots & \vdots \\ 0 & 0 & \cdots & -\mathbf{p}_{n-1} & \mathbf{q}_{n-1} & 0 & 0 & \cdots & \mathbf{r}_{n-1} & -\mathbf{s}_{n-1} \\ 0 & 0 & \cdots & 0 & \mathbf{q}_n & 0 & 0 & \cdots & 0 & \mathbf{s}_n \end{bmatrix}, \quad (68)$$

and the vectors $\mathfrak{Y}(\mathfrak{s})$ and $\mathfrak{B}(\mathfrak{s})$ are

$$\mathfrak{Y}(\mathfrak{s}) = \begin{bmatrix} C_{11} \\ C_{21} \\ \vdots \\ C_{n1} \\ C_{12} \\ C_{22} \\ \vdots \\ C_{n2} \end{bmatrix}, \mathfrak{B}(\mathfrak{s}) = \begin{bmatrix} \bar{g}_1(s) \\ 0 \\ 0 \\ \vdots \\ 0 \\ \bar{g}_n(s) \end{bmatrix}_{1 \times 2n}. \quad (69)$$

Here

$$\begin{aligned} \mathbf{a}_0 &= \left(1 + \delta_0 \sqrt{Q_1 s^{\beta_1}}\right), \mathbf{a}_i = \left(1 - \delta_i \sqrt{Q_i s^{\beta_i}}\right) e^{-h_i \sqrt{Q_i s^{\beta_i}}}, \\ \mathbf{c}_0 &= \left(1 - \delta_0 \sqrt{Q_1 s^{\beta_1}}\right), \mathbf{c}_i = \left(1 + \delta_i \sqrt{Q_i s^{\beta_i}}\right) e^{h_i \sqrt{Q_i s^{\beta_i}}}, \\ \mathbf{c}_i &= \left(1 + \delta_i \sqrt{Q_{i+1} s^{\beta_{i+1}}}\right) e^{-h_i \sqrt{Q_{i+1} s^{\beta_{i+1}}}}, \mathbf{d}_i = \left(1 - \delta_i \sqrt{Q_{i+1} s^{\beta_{i+1}}}\right) e^{h_i \sqrt{Q_{i+1} s^{\beta_{i+1}}}}, \\ \mathbf{p}_i &= l_i \sqrt{Q_i s^{\beta_i}} e^{-h_i \sqrt{Q_i s^{\beta_i}}}, \mathbf{r}_i = l_i \sqrt{Q_i s^{\beta_i}} e^{h_i \sqrt{Q_i s^{\beta_i}}}, l_i = \frac{k_i}{k_{i+1}}, \end{aligned}$$

$$\begin{aligned} \mathbf{q}_i &= \sqrt{Q_{i+1} s^{\beta_{i+1}}} e^{-h_i \sqrt{Q_{i+1} s^{\beta_{i+1}}}}, \mathbf{s}_i = \sqrt{Q_{i+1} s^{\beta_{i+1}}} e^{h_i \sqrt{Q_{i+1} s^{\beta_{i+1}}}}, i \in I_{n-1}^1, \\ \mathbf{q}_n &= \left(1 - \delta_n \sqrt{Q_n s^{\beta_n}}\right) e^{-\sqrt{Q_n s^{\beta_n}}}, \mathbf{s}_n = \left(1 + \delta_n \sqrt{Q_n s^{\beta_n}}\right) e^{\sqrt{Q_n s^{\beta_n}}}. \end{aligned} \quad (70)$$

We incorporate the following notations to describe the linear system (67) in an appropriate format:

$$\begin{aligned} M &= \begin{pmatrix} \mathbf{a}_0 & 0 & 0 & \cdots & 0 \\ \mathbf{a}_1 & -\mathbf{c}_1 & 0 & \cdots & 0 \\ 0 & \mathbf{a}_2 & -\mathbf{c}_2 & \cdots & 0 \\ \vdots & \vdots & \ddots & \ddots & \vdots \\ 0 & 0 & \cdots & \mathbf{a}_{n-1} & -\mathbf{c}_{n-1} \end{pmatrix}_{n \times n} & M = (M_{ij})_{i,j \in I_{n-1}^0}, \\ & & M_{0j} = \mathbf{a}_0 \delta_{0,j}, j \in I_{n-1}^0, \\ & & M_{ij} = \mathbf{a}_i \delta_{i,j+1} - \mathbf{b}_i \delta_{i+1,j+1}, \\ & & i \in I_{n-1}^1, j \in I_{n-1}^0, \\ N &= \begin{pmatrix} \mathbf{c}_0 & 0 & 0 & \cdots & 0 \\ \mathbf{c}_1 & -\mathbf{d}_1 & 0 & \cdots & 0 \\ 0 & \mathbf{c}_2 & -\mathbf{d}_2 & \cdots & 0 \\ \vdots & \vdots & \ddots & \ddots & \vdots \\ 0 & 0 & \cdots & \mathbf{c}_{n-1} & -\mathbf{d}_{n-1} \end{pmatrix}_{n \times n} & N = (N_{ij})_{i,j \in I_{n-1}^0}, \\ & & N_{0j} = \mathbf{c}_0 \delta_{0,j}, j \in I_{n-1}^0, \\ & & N_{ij} = \mathbf{c}_i \delta_{i,j+1} - \mathbf{d}_i \delta_{i+1,j+1}, \\ & & i \in I_{n-1}^1, j \in I_{n-1}^0, \end{aligned}$$

$$Q = \begin{pmatrix} 0 & -\mathbf{p}_2 & \mathbf{q}_2 & \cdots & 0 \\ \vdots & \vdots & \ddots & \ddots & \vdots \\ 0 & 0 & \cdots & -\mathbf{p}_{n-1} & \mathbf{q}_{n-1} \\ 0 & 0 & \cdots & 0 & \mathbf{q}_n \end{pmatrix}_{n \times n} ; i.e. \quad \begin{aligned} Q &= (Q_{ij})_{i,j \in I_{n-1}^0}, \\ Q_{ij} &= -\mathbf{p}_{i+1} \delta_{i+1,j+1} + \mathbf{q}_{i+1} \delta_{i+2,j+1}, \\ i &\in I_{n-2}^0, j \in I_{n-1}^0, \\ Q_{(n-1)j} &= \mathbf{q}_n \delta_{n-1,j}, j \in I_{n-1}^0, \end{aligned}$$

$$R = \begin{pmatrix} \mathbf{r}_1 & -\mathbf{s}_1 & 0 & \cdots & 0 \\ 0 & \mathbf{r}_2 & -\mathbf{s}_2 & \cdots & 0 \\ \vdots & \vdots & \ddots & \ddots & \vdots \\ 0 & 0 & \cdots & \mathbf{r}_{n-1} & -\mathbf{s}_{n-1} \\ 0 & 0 & \cdots & 0 & \mathbf{s}_n \end{pmatrix}_{n \times n} ; i.e. \quad \begin{aligned} R &= (R_{ij})_{i,j \in I_{n-1}^0}, \\ R_{ij} &= \mathbf{r}_{i+1} \delta_{i+1,j+1} - \mathbf{s}_{i+1} \delta_{i+2,j+1}, \\ i &\in I_{n-2}^0, j \in I_{n-1}^0, \\ R_{(n-1)j} &= \mathbf{s}_n \delta_{n-1,j}, j \in I_{n-1}^0, \end{aligned}$$

$$C_1 = \begin{pmatrix} \bar{g}_1(s) \\ 0 \\ \vdots \\ 0 \end{pmatrix}_{n \times 1}, C_2 = \begin{pmatrix} 0 \\ 0 \\ \vdots \\ 0 \\ \bar{g}_2(s) \end{pmatrix}_{n \times 1}, A = \begin{pmatrix} C_{11} \\ C_{21} \\ \vdots \\ C_{n1} \end{pmatrix}_{n \times 1}, B = \begin{pmatrix} C_{12} \\ C_{22} \\ \vdots \\ C_{n2} \end{pmatrix}_{n \times 1}, \quad (71)$$

where δ_{ij} is the Kronecker tensor. The linear system (67) is equivalent to

$$\begin{cases} MA + NB = C_1, \\ QA + RB = C_2. \end{cases} \quad (72)$$

Matrices M, N, Q, R are invertible and triangular. We can rewrite Equation (72) as

$$\begin{aligned} A &= S^{-1} (N^{-1} C_1 - R^{-1} C_2), \\ B &= R^{-1} C_2 - R^{-1} Q S^{-1} (N^{-1} C_1 - R^{-1} C_2). \end{aligned} \quad (73)$$

where we suppose that $S = N^{-1} M - R^{-1} Q$ is invertible. An easy computation shows that

$$R_0 = R^{-1} C_2 = \begin{pmatrix} \frac{\bar{g}_2(s) \mathbf{s}_1 \mathbf{s}_2 \cdots \mathbf{s}_{n-1}}{\mathbf{r}_1 \mathbf{r}_2 \cdots \mathbf{r}_{n-1} \mathbf{s}_n} \\ \frac{\bar{g}_2(s) \mathbf{s}_2 \cdots \mathbf{s}_{n-1}}{\mathbf{r}_2 \cdots \mathbf{r}_{n-1} \mathbf{s}_n} \\ \vdots \\ \frac{\bar{g}_2(s) \mathbf{s}_{n-1}}{\mathbf{r}_{n-1} \mathbf{s}_n} \\ \frac{\bar{g}_2(s)}{\mathbf{s}_n} \end{pmatrix},$$

$$C_0 := N^{-1} C_1 - R^{-1} C_2 = \begin{pmatrix} \frac{\bar{g}_1(s)}{\mathbf{a}_0} - \frac{\bar{g}_2(s) \mathbf{s}_1 \mathbf{s}_2 \cdots \mathbf{s}_{n-1}}{\mathbf{r}_1 \mathbf{r}_2 \cdots \mathbf{r}_{n-1} \mathbf{s}_n} \\ \frac{\bar{g}_1(s) \mathbf{b}_1}{\mathbf{a}_0 \mathbf{a}_1} - \frac{\bar{g}_2(s) \mathbf{s}_2 \cdots \mathbf{s}_{n-1}}{\mathbf{r}_2 \cdots \mathbf{r}_{n-1} \mathbf{s}_n} \\ \vdots \\ \frac{\bar{g}_1(s) \mathbf{b}_1 \mathbf{b}_2 \cdots \mathbf{b}_{n-2}}{\mathbf{a}_0 \mathbf{a}_1 \mathbf{a}_2 \cdots \mathbf{a}_{n-2}} - \frac{\bar{g}_2(s) \mathbf{s}_{n-1}}{\mathbf{r}_{n-1} \mathbf{s}_n} \\ \frac{\bar{g}_1(s) \mathbf{b}_1 \mathbf{b}_2 \cdots \mathbf{b}_{n-1}}{\mathbf{a}_0 \mathbf{a}_1 \mathbf{a}_2 \cdots \mathbf{a}_{n-1}} - \frac{\bar{g}_2(s)}{\mathbf{s}_n} \end{pmatrix}, \quad (74)$$

where

$$N^{-1} = \begin{pmatrix} \frac{1}{\mathbf{a}_0} & 0 & 0 & \cdots & 0 \\ \frac{\mathbf{c}_1}{\mathbf{a}_0 \mathbf{a}_1} & -\mathbf{c}_1 & 0 & \cdots & 0 \\ \frac{\mathbf{c}_1 \mathbf{c}_2}{\mathbf{a}_0 \mathbf{a}_1 \mathbf{a}_2} & -\frac{\mathbf{c}_1 \mathbf{c}_2}{\mathbf{a}_2} & -\mathbf{c}_2 & \cdots & 0 \\ \vdots & \vdots & \ddots & \ddots & \vdots \\ \frac{\mathbf{c}_1 \mathbf{c}_2 \cdots \mathbf{c}_{n-1}}{\mathbf{a}_0 \mathbf{a}_1 \mathbf{a}_2 \cdots \mathbf{a}_{n-1}} & -\frac{\mathbf{c}_1 \mathbf{c}_2 \cdots \mathbf{c}_{n-1}}{\mathbf{a}_2 \cdots \mathbf{a}_{n-1}} & \cdots & -\frac{\mathbf{c}_{n-2} \mathbf{c}_{n-1}}{\mathbf{a}_{n-1}} & -\mathbf{c}_{n-1} \end{pmatrix}_{n \times n}, \quad (75)$$

that is

$$N^{-1} = (n_{ij})_{i,j \in I_{n-1}^0},$$

$$n_{0j} = \frac{1}{\mathbf{a}_0} \delta_{0,j}, j \in I_{n-1}^0, \quad n_{i0} = \prod_{\ell=1}^i \frac{\mathbf{c}_\ell}{\mathbf{a}_0 \mathbf{a}_\ell}, i \in I_{n-1}^1,$$

$$n_{ij} = - \prod_{m=1}^i \frac{\mathbf{c}_m}{\mathbf{a}_m} \prod_{\ell=0}^{j-1} \frac{\mathbf{a}_{\ell+1}}{\mathbf{c}_\ell} \sum_{k=0}^{n-1} \delta_{i,j+k}, \quad i, j \in I_{n-1}^1,$$

$$R^{-1} = \begin{pmatrix} \frac{1}{\mathbf{r}_1} & \frac{\mathbf{s}_1}{\mathbf{r}_1 \mathbf{r}_2} & \frac{\mathbf{s}_1 \mathbf{s}_2}{\mathbf{r}_1 \mathbf{r}_2 \mathbf{r}_3} & \cdots & \frac{\mathbf{s}_1 \mathbf{s}_2 \cdots \mathbf{s}_{n-2}}{\mathbf{r}_1 \mathbf{r}_2 \mathbf{r}_3 \cdots \mathbf{r}_{n-1}} & \frac{\mathbf{s}_1 \mathbf{s}_2 \cdots \mathbf{s}_{n-1}}{\mathbf{r}_1 \mathbf{r}_2 \mathbf{r}_3 \cdots \mathbf{r}_{n-1} \mathbf{s}_n} \\ 0 & \frac{1}{\mathbf{r}_2} & \frac{\mathbf{s}_2}{\mathbf{r}_2 \mathbf{r}_3} & \cdots & \frac{\mathbf{s}_2 \cdots \mathbf{s}_{n-2}}{\mathbf{r}_2 \mathbf{r}_3 \cdots \mathbf{r}_{n-1}} & \frac{\mathbf{s}_2 \cdots \mathbf{s}_{n-1}}{\mathbf{r}_2 \mathbf{r}_3 \cdots \mathbf{r}_{n-1} \mathbf{s}_n} \\ \vdots & \vdots & \vdots & \ddots & \vdots & \vdots \\ 0 & 0 & 0 & \cdots & 0 & \frac{1}{\mathbf{s}_n} \end{pmatrix}_{n \times n}, \quad (76)$$

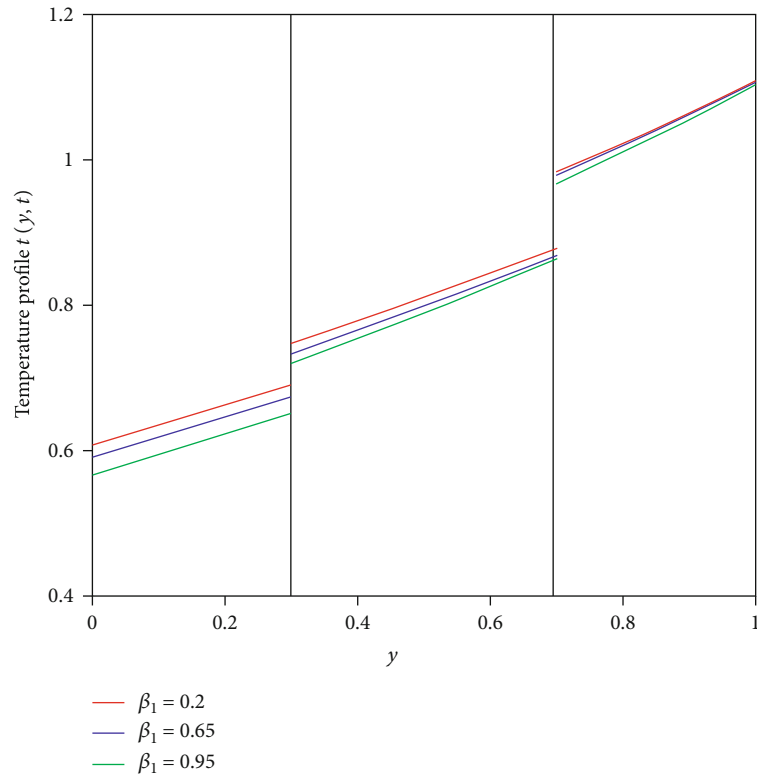


FIGURE 2: Temperature profiles $T_i(y, t)$, $i = 1, 2, 3$ versus y for fractional multilayer Maxwell fluid at $t = 0.002$, $\beta_2 = 0.6$, $\beta_3 = 0.8$, and different values of β_1 .

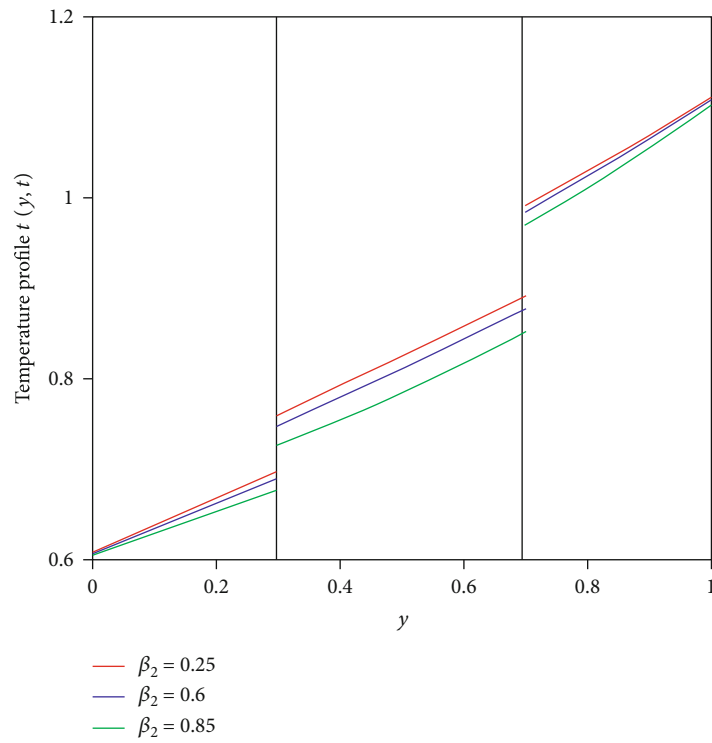


FIGURE 3: Temperature profiles $T_i(y, t)$, $i = 1, 2, 3$ versus y for fractional multilayer Maxwell fluid at $t = 0.002$, $\beta_1 = 0.2$, $\beta_3 = 0.8$, and different values of β_2 .

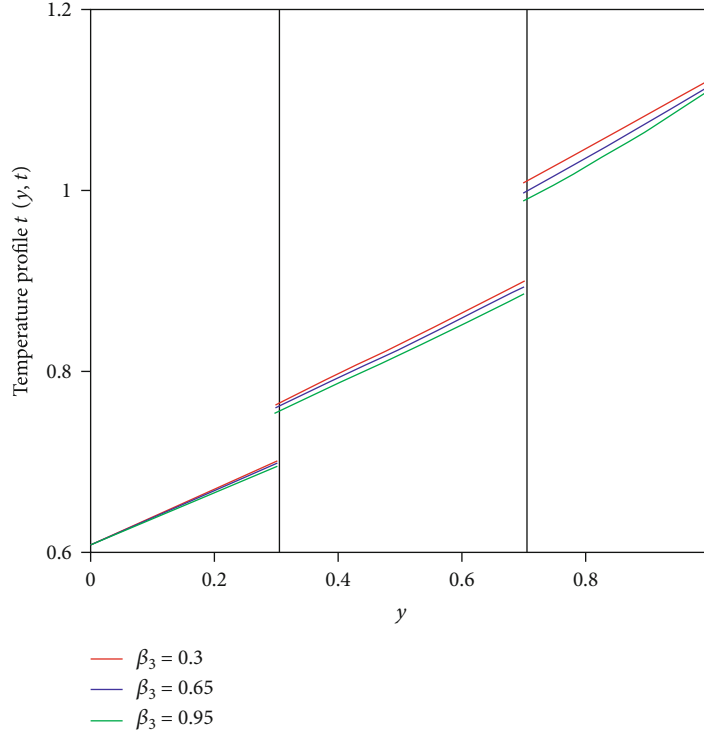


FIGURE 4: Temperature profiles $T_i(y, t)$, $i = 1, 2, 3$ versus y for fractional multilayer Maxwell fluid at $t = 0.002$, $\beta_1 = 0.2$, $\beta_2 = 0.4$, and different values of β_3 .

that is

$$R^{-1} = \left(\rho_{ij} \right)_{i,j \in I_{n-1}^0},$$

$$\begin{aligned} \rho_{ij} &= \sum_{k=0}^{n-1} \left(\prod_{m=0}^i \frac{\mathbf{r}_m}{\mathbf{s}_m} \prod_{\ell=0}^j \frac{\mathbf{s}_\ell}{\mathbf{r}_{\ell+1}} \right) \delta_{i=k,j}, \mathbf{r}_0 \\ &= \mathbf{s}_0 = \mathbf{r}_n = 1, i, j \in I_{n-1}^0. \end{aligned} \quad (77)$$

Now, the matrix $S = (S_{ij})_{i,j \in I_{n-1}^0}$ is defined by the elements

$$S_{ij} = \sum_{k=0}^{n-1} (n_{ik} M_{kj} - \rho_{ik} Q_{kj}). \quad (78)$$

This reduces the system (73) to

$$\begin{cases} A = S^{-1} C_0, \\ B = R_0 - R^{-1} Q S^{-1} C_0. \end{cases} \quad (79)$$

Now, we know the auxiliary functions C_{j1}, C_{j2} , $j \in I_n^1$; from the linear system (79), the analytical expressions for

the solution of temperature profiles $T_i(y, t)$ can be obtained from Equation (66), by using the inverse Laplace transform as

$$\begin{aligned} T_i(y, t) &= \frac{1}{2\pi i} \int_{\sigma-i\infty}^{\sigma+i\infty} e^{st} \left(C_{i1}(s) e^{-y\sqrt{Q_i s^{\beta_i}}} \right. \\ &\quad \left. + C_{i2}(s) e^{y\sqrt{Q_i s^{\beta_i}}} \right) ds, i \in I_n^1. \end{aligned} \quad (80)$$

Since the auxiliary functions C_{j1}, C_{j2} , $j \in I_n^1$, involved in Equation (79) are intricate, we therefore have used the following numerical Talbot's algorithms [45, 46] for the computation of the inverse Laplace transform.

Consider the function $g(y, t)$ has the Laplace transform $\bar{G}(y, s)$. The Talbot algorithm [45] approximates the function $g(y, t)$ as

$$\begin{aligned} g(y, t) &\cong \frac{r}{M} \left\{ \frac{\exp(rt)}{2} \bar{G}(y, r) \right. \\ &\quad \left. + \sum_{k=1}^{M-1} \operatorname{Re} [\exp(tz(\epsilon_k)) \bar{G}(y, z(\epsilon_k)) (1 + i\zeta(\epsilon_k))] \right\}, \end{aligned} \quad (81)$$

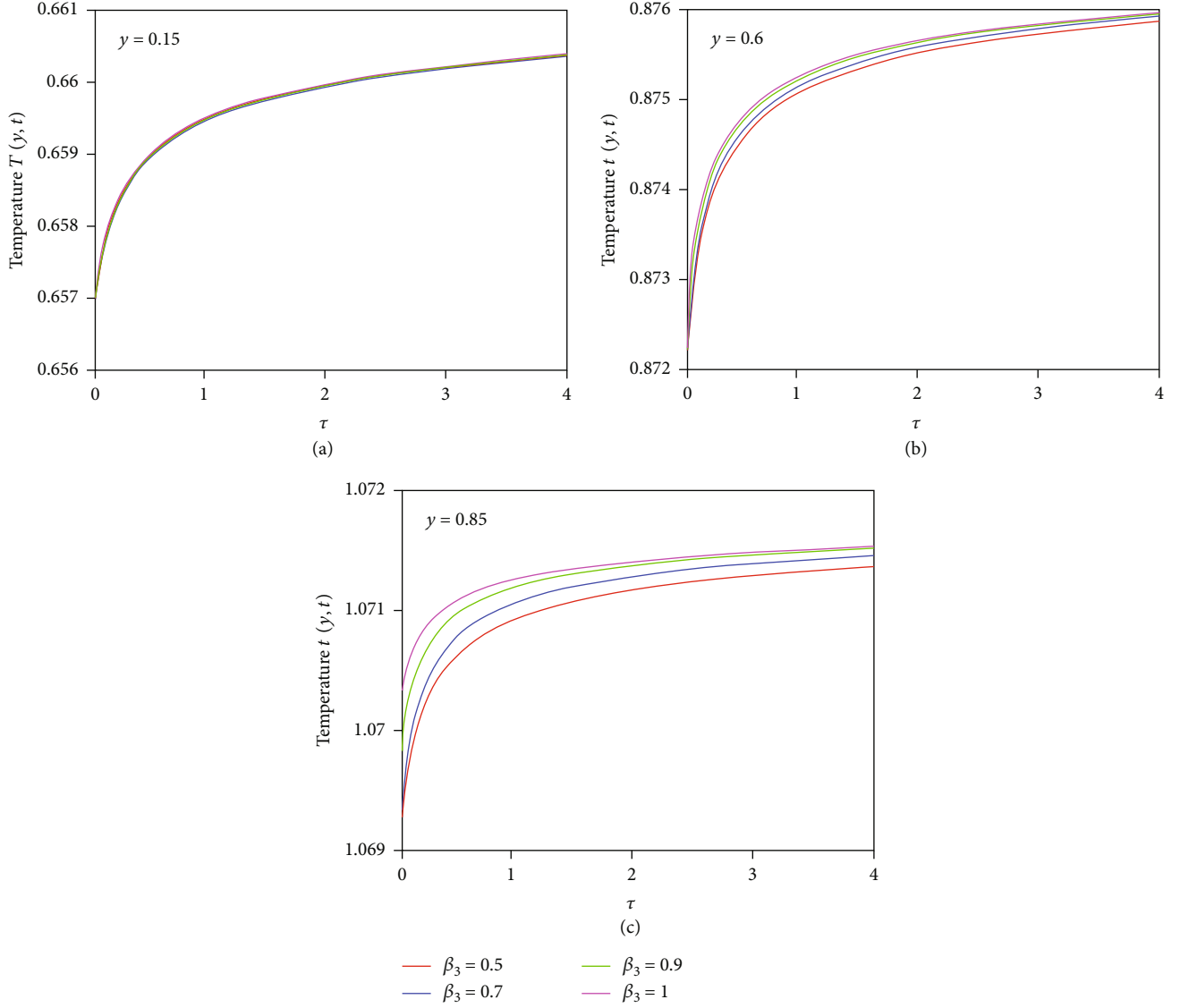


FIGURE 5: Temperature profiles $T_i(y, t)$, $i = 1, 2, 3$ versus t for fractional multilayer Maxwell fluid at $\beta_1 = 0.0.4$, $\beta_2 = 0.6$, and different values of y .

where

$$r = \frac{2M}{5t}, z(\varepsilon) = r\varepsilon(\cot \varepsilon + i), \varepsilon \in (-\pi, \pi), \quad (82)$$

$$\zeta(\varepsilon) = \varepsilon + (\varepsilon \cot \varepsilon - 1) \cot \varepsilon, \varepsilon_k = \frac{k\pi}{M}.$$

The function $g(y, t)$ can be approximated by another method, the improved Talbot algorithm [46].

$$g(y, t) \cong \frac{1}{t} \sum_{k=1}^M \exp(tz_1(\sigma_k)) \bar{G}(y, z_1(\sigma_k)) (\nu + i\zeta_1(\sigma_k)), \quad (83)$$

where

$$z_1(\varepsilon) = \frac{M}{t} [\nu\varepsilon + \mu\varepsilon \cot(\alpha\varepsilon) - \xi], \varepsilon \in [-\pi, \pi],$$

$$\zeta_1(\varepsilon) = \alpha\mu\varepsilon + \mu(\alpha\varepsilon \cot(\alpha\varepsilon) - 1) \cot(\alpha\varepsilon), \sigma_k = \frac{(2k-1)\pi}{M} - \pi. \quad (84)$$

Here, α, M, ν, μ, ξ are variables the user must define.

4. Numerical Results and Discussions

The unsteady, laminar flow with thermal conductivity of the simultaneous n -layer fractional immiscible Maxwell fluids in a rectangular channel has been examined. The motion of these fluids is produced by the time-based pressure gradient

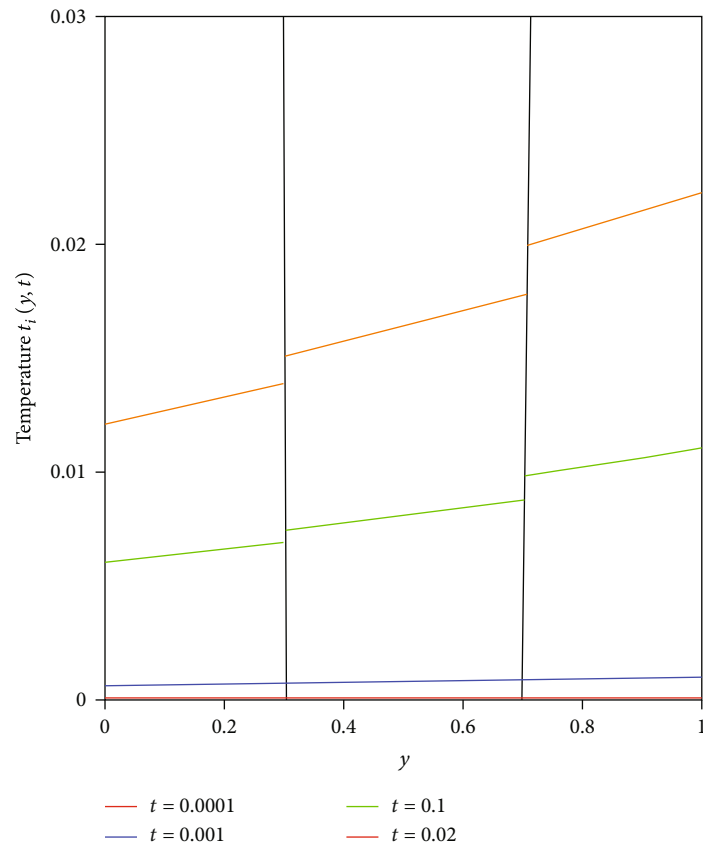


FIGURE 6: Temperature profiles $T_i(y, t)$, $i = 1, 2, 3$ for small values of the time t ($\beta_1 = 0.4$, $\beta_2 = 0.6$, and $\beta_3 = 0.8$).

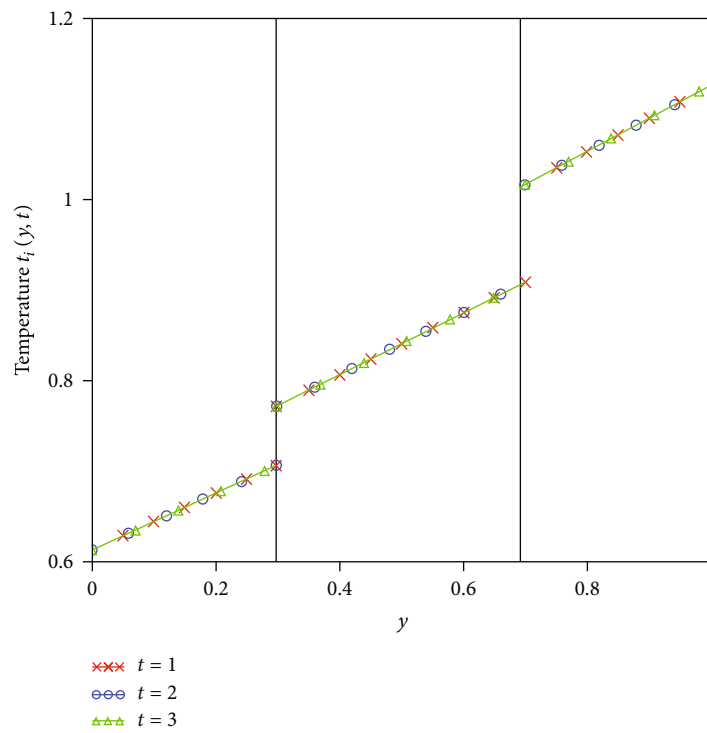


FIGURE 7: Temperature profiles $T_i(y, t)$, $i = 1, 2, 3$ for large values of the time t ($\beta_1 = 0.4$, $\beta_2 = 0.6$, and $\beta_3 = 0.8$).

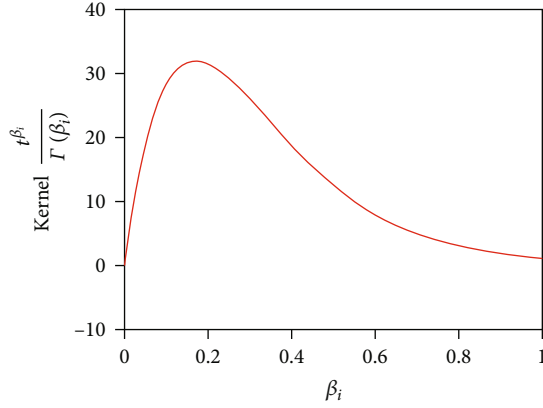


FIGURE 8: Variation of the kernels $t^{\beta_i}/\Gamma(\beta_i)$ with the fractional parameters β_i , $i = 1, 2, 3$.

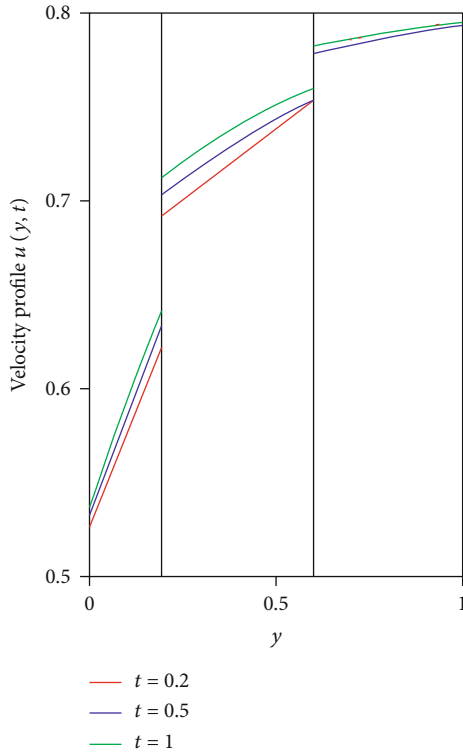


FIGURE 9: Velocity profiles $u_i(y, t)$, $i = 1, 2, 3$ versus y for fractional multilayer Maxwell fluid at $\alpha_1 = 0.2, \alpha_2 = 0.4, \alpha_3 = 0.8, \lambda_1 = 0.021, \lambda_2 = 0.042, \lambda_3 = 0.06$, and different values of time t .

in the flow direction and by the displacement of the channel boundaries with the time-based fluid-fluid interfacial conditions.

In this problem, the generalization puts into consideration the fractional constitutive equation of the Maxwell fluids based on the Caputo time-fractional derivative; therefore, the velocity gradient histories influence the fluid behavior. Such type of flow is so-called the flow with memory.

On the solid boundaries, the Robin boundary conditions are taken into account, whereas the velocity and shear stress are assumed continuous at the fluid-fluid interface $y = d_0$.

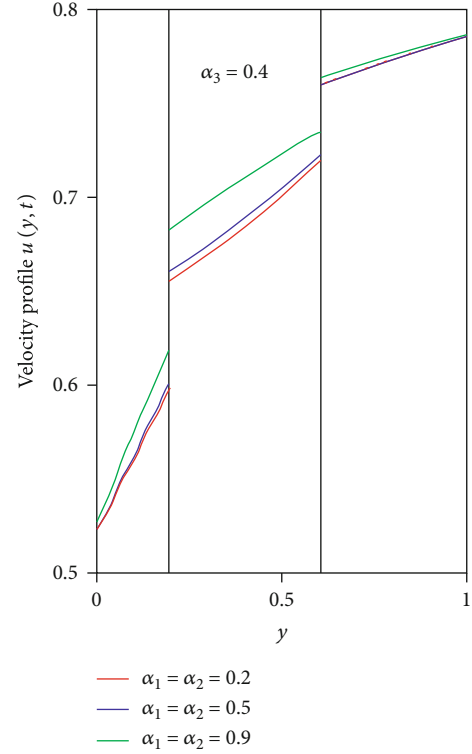


FIGURE 10: Velocity profiles $u_i(y, t)$, $i = 1, 2, 3$ versus y for fractional multilayer Maxwell fluid at $t = 0.19, \lambda_1 = 0.021, \lambda_2 = 0.042, \lambda_3 = 0.06$, and different values of fractional parameters $\alpha_1 = \alpha_2$.

Semianalytical results of the velocities, shear stresses, and temperature profiles are determined with the help of the Laplace transformation and the Talbot algorithms used for the numerical inverse Laplace transforms. Moreover, an analytical solution for the flow is recovered by using the Laplace transform in conjunction with the finite sine-Fourier transform.

The findings obtained are generic; therefore, several special cases can be considered. Multilayer flows of ordinary/-fractional Maxwell fluids can be analyzed as special cases by allowing certain fractional parameters to be equal to one.

With the help of the Mathcad software, numerical results have been illustrated for the obtained solutions of fluid velocities and temperatures. These results are shown in Figures 2–14. For graphical illustration of the fluid velocities, we have used the material parameters

$$\begin{aligned} \rho_1 &= 1000, \mu_1 = 0.05, G_1 = 1.2, cp_1 = 0.25, k_1 = 2.5, l_1 = 0.1, \sigma_0 = 0.05, \\ \rho_2 &= 1300, \mu_2 = 0.2, G_2 = 2.4, cp_2 = 0.27, k_2 = 2.7, l_2 = 0.15, \sigma_1 = 0.1, \\ \rho_3 &= 1500, \mu_3 = 0.6, G_3 = 5.0, cp_3 = 0.29, k_3 = 2.9, l_3 = 0.2, \sigma_2 = 0.15, \sigma_3 = 0.2. \end{aligned} \quad (85)$$

To analyze the temperature profiles of the three-layer fluids with $h_0 = 0, h_1 = 0.3, h_2 = 0.7, h_3 = 1$, we take the special instance when the functions $g_1(t), g_2(t)$ appearing in the Robin boundary conditions are constant, i.e., $g_1(t) = 0.6 H(t), g_2(t) = 1.2 H(t)$, where $H(t)$ is the Heaviside function. It is shown in Figure 2 that the variance of the fractional

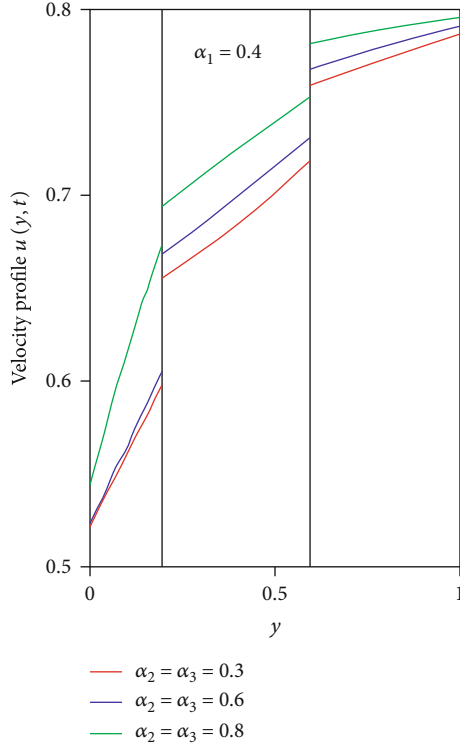


FIGURE 11: Velocity profiles $u_i(y, t)$, $i = 1, 2, 3$ versus y for fractional multilayer Maxwell fluid at $t = 0.19, \lambda_1 = 0.021, \lambda_2 = 0.042, \lambda_3 = 0.06$, and different values of fractional parameters $\alpha_2 = \alpha_3$.

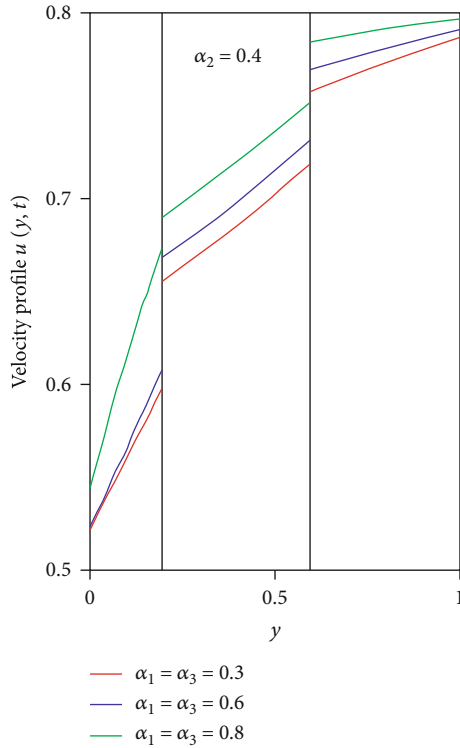


FIGURE 12: Velocity profiles $u_i(y, t)$, $i = 1, 2, 3$ versus y for fractional multilayer Maxwell fluid at $t = 0.19, \lambda_1 = 0.021, \lambda_2 = 0.042, \lambda_3 = 0.06$, and different values of fractional parameters $\alpha_1 = \alpha_3$.

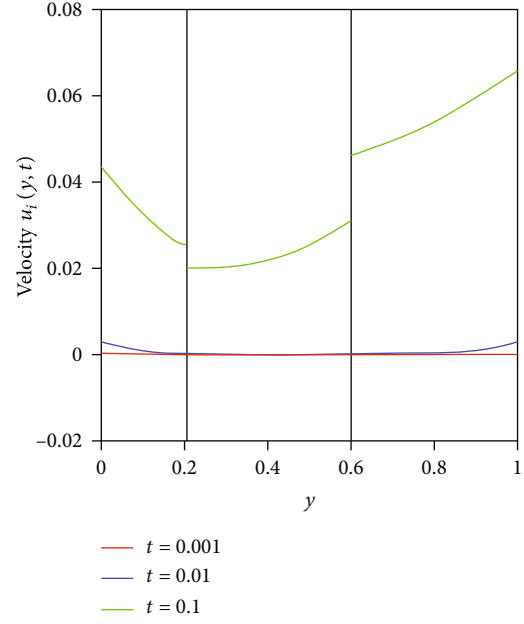


FIGURE 13: The profiles of velocity $u_i(y, t)$, $i = 1, 2, 3$, for small values of the time t ($\alpha_1 = 0.4, \alpha_2 = 0.6, \alpha_3 = 0.8, a_1 = 1, a_2 = 1.3, a_3 = 1.5, b_1 = 1, b_2 = 4, b_3 = 12, h_1 = 0.2, h_2 = 0.6$, and $\lambda_1 = 0.021, \lambda_2 = 0.042, \lambda_3 = 0.060$).

temperature variable β_1 of the fluid located in the first layer has a noticeable effect on the thermal profile in the first two layers; however, the effect on the temperature from the top-most layer is minor. This has been caused by the decrease in thermal profile in the first two layers with the increase in fractional variable β_1 . It is revealed in Figure 2 that the variance of the fractional temperature variable β_2 of the fluid located in the second layer has a noticeable effect on the thermal profile in the last two layers; however, the effect on the temperature from the first layer is negligible. This has been caused by the decrease in thermal profile in the last two layers with the increase in fractional variable β_1 . It is exposed in Figure 4 that the variance of the fractional temperature variable β_3 of the fluid located in the third layer has a noticeable effect on the thermal profile in the first and the last layers; however, the effect on the temperature from the middle layer is minor. This has been caused by the decrease in thermal profile in the first and the last layers with the increase in fractional variable β_3 .

It is recognized by Equation (26) that the heat flux memory kernel is the relation $h_{\beta_i}(t) = t^{\beta_i-1}/\Gamma(\beta_i)$ whose plot is shown in Figure 8. It is described in Figure 8 that, for $\beta_i \geq 0.2$ and $t = 0.002$, the kernel $h_{\beta_i}(t)$, $i = 1, 2, 3$, declines with β_i ; therefore, the temperature gradient distribution relation declines (memory impacts are softer). Time-evolution of the thermal layers, in various channel locations and for differing values of the temperature fractional variables, is shown in Figure 5. As shown in Figure 5, the thermal profile as a function of the fractional variables 5 has different characteristics for low, versus high, time values. This attitude reflects prior studies shown in Figures 2–4 and also with the progression of the heat memory kernel, $h_{\beta_i}(t)$, $i = 1, 2, 3$. We have to

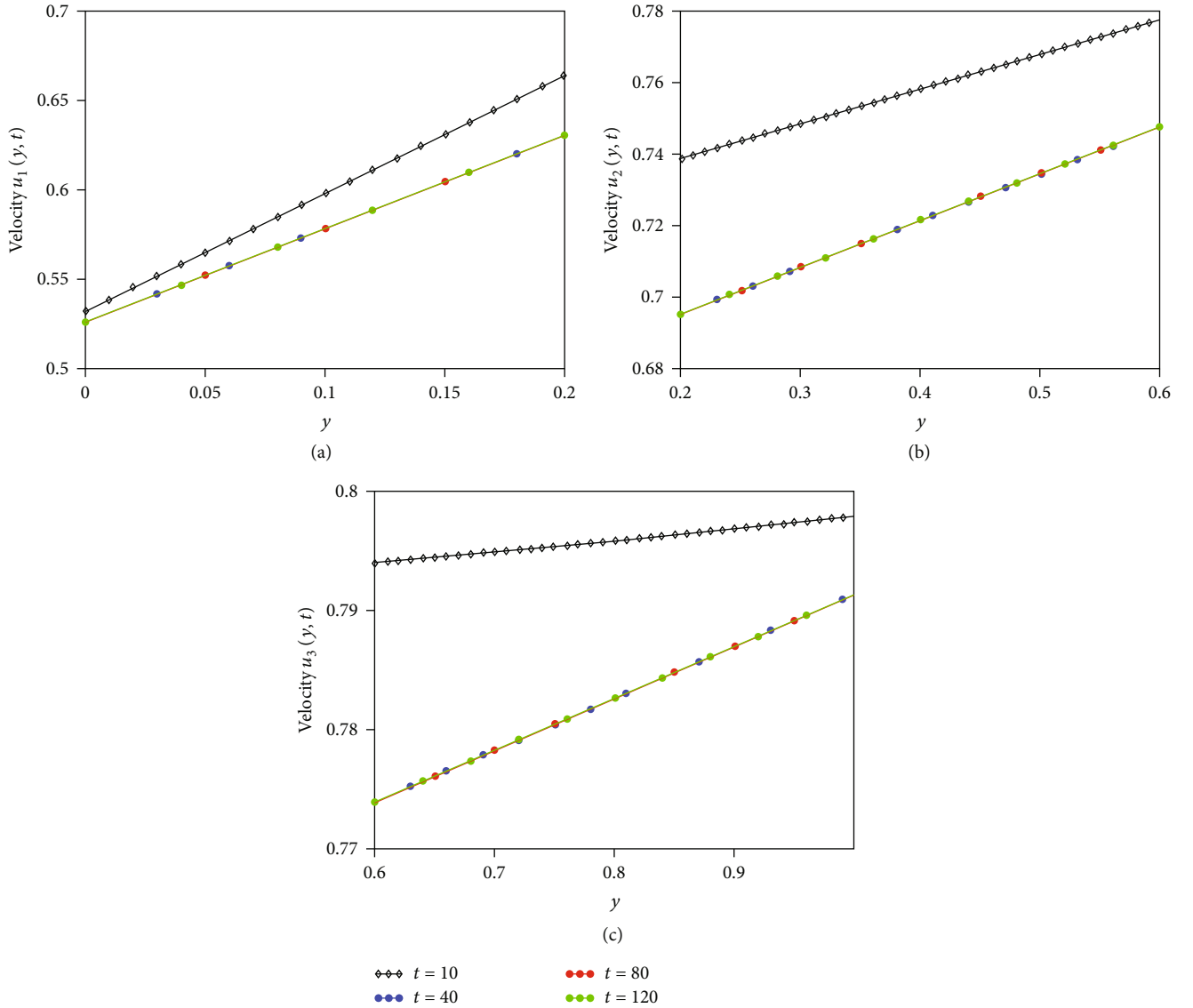


FIGURE 14: The profiles of velocity $u_i(y, t)$, $i=1, 2, 3$ for large values of the time t ($\alpha_1=0.4$, $\alpha_2=0.6$, $\alpha_3=0.8$ $a_1=1$, $a_2=1.3$, $a_3=1.5$, $b_1=1$, $b_2=4$, $b_3=12$, $h_1=0.2$, $h_2=0.6$, and $\lambda_1=0.021$, $\lambda_2=0.042$, $\lambda_3=0.060$).

mention that the temperatures of all layers vary for small time fluctuations, but after a low time valuation for t ($t=1$ in examined scenarios), the temperatures are just about unchanged (see Figures 6 and 7).

In order to examine the three layers, fluid velocities with $h_0=0$, $h_1=0.2$, $h_2=0.6$, $h_3=1$, we considered the particular case when the functions in the slip boundary conditions are constant, i.e., $f_1(t)=0.5H(t)$, $f_2(t)=0.8H(t)$, where $H(t)$ is the Heaviside function and the considered pressure gradient is $P(t)=\sin(t)$. Figure 9 illustrates the time effect on the velocity profile $u_i(y, t)$, $i=1, 2, 3$. The velocity profile is observed to increase with the increase in time. Figures 10–12 are plotted to study the influence of the velocity fractional parameters α_i on the velocity fields. It is observed that the velocity profile is increasing with the increase in the fractional parameters $\alpha_{i_1}=\alpha_{i_2}$ and for fixed $\alpha_{i_3}, i_1, i_2, i_3=1, 2, 3$. The fractional variables have braking impacts. The first two

layers' flows are accelerated; however, the last layer's fluid is slowed down.

In Figures 13 and 14, the profiles of velocity $u_i(y, t)$, $i=1, 2, 3$, for different values of the time t , are presented. It is observed that, for $t \geq 40$, the profiles of velocity are unchanged; therefore, the velocity is given by the permanent solution. It can be observed from Figures 6 and 13 that at a very short time, the profiles for velocities and temperatures are similar to the initial conditions, that is, zero everywhere.

5. Conclusions

Time-dependent simultaneous n-layer fluid flow in a rectangular channel was examined through heat exchange of Maxwell immiscible fluids with generic constitutive equations for the shear stress and heat flux.

The Caputo time-fractional derivative defines the generic constitutive relations; thus, the behavior of the fluid is determined by the histories of the temperature and velocity gradient.

We have used the finite Fourier and Laplace transform coupled with numerical Laplace inversions for the analytical and semianalytical results for the velocity, temperature, and shear stress profiles with the assumption that for the adjacent layers, the interfacial heat fluxes and shear stresses are equal and in the presence of the interface Robin-type interfacial conditions.

The results of this study attained are of a general nature; however, many specific situations can be produced. Multi-layer flows of ordinary/fractional Maxwell fluids can be analyzed as special cases by allowing certain fractional parameters to be equal to one.

With the help of the Mathcad software, numerical results have been illustrated for the obtained solutions of fluid velocities and temperatures.

For small and, respectively, large values of time t , the fluid flow and the heat transfer differ. Such specific characteristics are due to the differences in time and fractional parameters of the thermal/velocity kernels, so the memory influences have a tremendous impact on the fluids.

Appendix

Using the boundary conditions (32) and the interface conditions (34) in Equation. (63), we obtained the following algebraic system:

$$\bar{Y}_{1,1}\bar{w}_1(h_1, l_1, s) - \bar{Y}_{1,2}\bar{w}_2(h_2, l_2, s) = \bar{b}_1, \quad (\text{A.1})$$

$$\begin{aligned} \bar{Y}_{i,i-1}\bar{w}_{i-1}(h_{i-1}, l_{i-1}, s) + \bar{Y}_{i,i}\bar{w}_i(h_i, l_i, s) \\ - \bar{Y}_{i,i+1}\bar{w}_{i+1}(h_{i+1}, l_{i+1}, s) = \bar{b}_i, \quad i \in I_{n-2}^{(2)}, \end{aligned} \quad (\text{A.2})$$

$$\bar{Y}_{n-1,n-2}\bar{w}_{n-2}(h_{n-2}, l_{n-2}, s) + \bar{Y}_{n-1,n-1}\bar{w}_{n-1}(h_{n-1}, l_{n-1}, s) = \bar{b}_{n-1}, \quad (\text{A.3})$$

where

$$\begin{aligned} \bar{Y}_{1,1} &= \bar{T}_{1,1}(h_1, s) + \bar{T}_{2,2}(h_1, s), \quad \bar{Y}_{1,2} \\ &= \bar{T}_{2,1}(h_1, s), \quad \bar{Y}_{i,i-1} = -\bar{T}_{i,2}(h_i, s), \end{aligned}$$

$$\begin{aligned} \bar{Y}_{i,i} &= \bar{T}_{i,1}(h_i, s) + \bar{T}_{i+1,2}(h_i, s), \quad \bar{Y}_{i,i+1} \\ &= -\bar{T}_{i+1,1}(h_i, s), \quad i \in I_{n-1}^{(2)}, \end{aligned}$$

$$\bar{Y}_{n-1,n} = \bar{T}_{n,1}(h_{n-1}, s)\bar{f}_2(s),$$

$$\begin{aligned} \bar{b}_j &= (\bar{T}_{j+1,3}(h_j, s) - \bar{T}_{j,3}(h_j, s))\bar{P}(s) \\ &+ \delta_{j,n-1}\bar{Y}_{n-1,n} + \delta_{j,1}\bar{T}_{1,2}(h_1, s)\bar{f}_1(s), \quad j \in I_{n-1}^{(1)}. \end{aligned} \quad (\text{A.4})$$

$\delta_{j,n-1}$ is the Kronecker delta. The system (A.1) can be written in the following equivalent form:

$$\bar{M}(s)\bar{W}(s) = \bar{N}(s). \quad (\text{A.5})$$

Data Availability

The data used to support the findings of this study are available from the corresponding author upon request.

Conflicts of Interest

The authors declare that they have no conflicts of interest.

References

- [1] J. Bear, *Dynamics of Fluids in Porous Media*, Courier Corporation, 2013.
- [2] F. A. Dullien, *Porous Media: Fluid Transport and Pore Structure*, Academic press, 2012.
- [3] L. W. Lake, *Enhanced Oil Recovery*, Prentice Hall, Englewood Cliffs, 1989.
- [4] D. K. Satpathi, B. R. Kumar, and P. Chandra, "Unsteady-state laminar flow of viscoelastic gel and air in a channel: application to mucus transport in a cough machine simulating trachea," *Mathematical and Computer Modelling*, vol. 38, no. 1-2, pp. 63–75, 2003.
- [5] C. S. Yih, "Instability due to viscosity stratification," *Journal of Fluid Mechanics*, vol. 27, no. 2, pp. 337–352, 1967.
- [6] C. Gin and P. Daripa, "Stability results for multi-layer radial Hele-Shaw and porous media flows," *Physics of Fluids*, vol. 27, no. 1, article 012101, 2015.
- [7] K. Ward, F. Zoueshtiagh, and R. Narayanan, "Faraday instability in double-interface fluid layers," *Physical Review Fluids*, vol. 4, no. 4, article 043903, 2019.
- [8] E. S. Papaefthymiou and D. T. Papageorgiou, "Nonlinear stability in three-layer channel flows," *Journal of Fluid Mechanics*, vol. 829, 2017.
- [9] H. Le Meur, "Non-uniqueness and linear stability of the one-dimensional flow of multiple viscoelastic fluids," *ESAIM: Mathematical Modelling and Numerical Analysis*, vol. 31, no. 2, pp. 185–211, 1997.
- [10] A. Kalogirou and M. G. Blyth, "The role of soluble surfactants in the linear stability of two-layer flow in a channel," *Journal of Fluid Mechanics*, vol. 873, pp. 18–48, 2019.
- [11] S. Pasquier, M. Quintard, and Y. Davit, "Modeling two-phase flow of immiscible fluids in porous media: Buckley-Leverett theory with explicit coupling terms," *Physical Review Fluids*, vol. 2, no. 10, article 104101, 2017.
- [12] M. D. Hisham, A. Rauf, D. Vieru, and A. U. Awan, "Analytical and semi-analytical solutions to flows of two immiscible Maxwell fluids between moving plates," *Chinese Journal of Physics*, vol. 56, no. 6, pp. 3020–3032, 2018.
- [13] A. Rauf, Y. Mahsud, I. A. Mirza, and Q. Rubbab, "Multi-layer flows of immiscible fractional Maxwell fluids with generalized thermal flux," *Chinese Journal of Physics*, vol. 62, pp. 313–334, 2019.
- [14] A. Rauf and A. Muhammad, "Multi-layer flows of immiscible fractional second grade fluids in a rectangular channel," *SN Applied Sciences*, vol. 2, no. 10, pp. 1–17, 2020.

- [15] L. Luo, N. A. Shah, I. M. Alarifi, and D. Vieru, "Two-layer flows of generalized immiscible second grade fluids in a rectangular channel," *Mathematical Methods in the Applied Sciences*, vol. 43, no. 3, pp. 1337–1348, 2019.
- [16] A. Rauf and M. Naz, "Simultaneous flow of three immiscible fractional Maxwell fluids with the clear and homogeneous porous cylindrical domain," *Journal of Applied and Computational Mechanics*, vol. 6, pp. 1324–1334, 2020.
- [17] A. Rauf, Y. Mahsud, and I. Siddique, "Multi-layer flows of immiscible fractional Maxwell fluids in a cylindrical domain," *Chinese Journal of Physics*, vol. 67, pp. 265–282, 2020.
- [18] J. Hristov, "Chapter 10: Derivatives with non-singular kernels from the Caputo-Fabrizio definition and beyond: appraising analysis with emphasis on diffusion models," in *Frontiers in Fractional Calculus*, S. Bhalekar, Ed., vol. 1, pp. 270–342, Bentham Science Publishers, Sharjah, 2017.
- [19] J. Hristov, "Response functions in linear viscoelastic constitutive equations and related fractional operators," *Mathematical Modelling of Natural Phenomena*, vol. 14, no. 3, p. 305, 2019.
- [20] Y. Povstenko and T. Kyrlych, "Time-fractional heat conduction in a plane with two external half-infinite line slits under heat flux loading," *Symmetry*, vol. 11, no. 5, p. 689, 2019.
- [21] Y. Povstenko, "Fractional Cattaneo-type equations and generalized thermoelasticity," *Journal of Thermal Stresses*, vol. 34, no. 2, pp. 97–114, 2011.
- [22] Z. Zheng, W. Zhao, and H. Dai, "A new definition of fractional derivative," *International Journal of Non-Linear Mechanics*, vol. 108, pp. 1–6, 2019.
- [23] D. Baleanu, D. Kai, and E. S. Fractional Calculus, *Models and Numerical Methods*, World Scientific, Singapore, 2012.
- [24] D. Baleanu, A. Mousalou, and S. Rezapour, "The extended fractional Caputo-Fabrizio derivative of order $0 \leq \sigma < 1$ on $C R[0, 1]$ and the existence of solutions for two higher-order series-type differential equations," *Advances in Difference Equations*, vol. 2018, 2018.
- [25] R. Hilfer, "Chapter 3: mathematical and physical interpretations of fractional derivatives and integrals," in *Handbook of Fractional Calculus: Basic Theory*, vol. 1, pp. 47–96, de Gruyter, Berlin, 2019.
- [26] M. Caputo and M. Fabrizio, "A new definition of fractional derivative without singular kernel," *Progress in Fractional Differentiation and Applications*, vol. 1, no. 2, pp. 1–13, 2015.
- [27] B. Acay and M. Inc, "Electrical circuits RC, LC, and RLC under generalized type non-local singular fractional operator," *Fractal and Fractional*, vol. 5, no. 1, p. 9, 2021.
- [28] B. Acay and M. Inc, "Fractional modeling of temperature dynamics of a building with singular kernels," *Chaos, Solitons & Fractals*, vol. 142, p. 110482, 2021.
- [29] N. Ahmed, N. A. Shah, and D. Vieru, "Two-dimensional advection-diffusion process with memory and concentrated source," *Symmetry*, vol. 11, no. 7, p. 879, 2019.
- [30] Y. Mahsud, N. A. Shah, and D. Vieru, "Influence of time-fractional derivatives on the boundary layer flow of Maxwell fluids," *Chinese Journal of Physics*, vol. 55, no. 4, pp. 1340–1351, 2017.
- [31] Y. Jiang, H. Qi, H. Xu, and X. Jiang, "Transient electroosmotic slip flow of fractional Oldroyd-B fluids," *Microfluidics and Nanofluidics*, vol. 21, no. 1, p. 7, 2017.
- [32] A. Yusuf, B. Acay, U. T. Mustapha, M. Inc, and D. Baleanu, "Mathematical modeling of pine wilt disease with Caputo fractional operator," *Chaos, Solitons & Fractals*, vol. 143, p. 110569, 2021.
- [33] Y. Liu and B. Guo, "Effects of second-order slip on the flow of a fractional Maxwell MHD fluid," *Journal of the Association of Arab Universities for Basic and Applied Sciences*, vol. 24, pp. 232–241, 2018.
- [34] M. Inc, Z. Korpinar, B. Almohsen, and Y. M. Chu, "Some numerical solutions of local fractional tricom equation in fractal transonic flow," *Alexandria Engineering Journal*, vol. 60, no. 1, pp. 1147–1153, 2021.
- [35] I. Ahmad, H. Ahmad, M. Inc, S. W. Yao, and B. Almohsen, "Application of local meshless method for the solution of two term time fractional-order multi-dimensional PDE arising in heat and mass transfer," *Thermal Science*, vol. 24, Supplement 1, pp. 95–105, 2020.
- [36] J. Hristov, "Integral balance approach to 1-d space-fractional diffusion models," in *Mathematical Methods in Engineering*, pp. 111–131, Springer, Cham, 2019.
- [37] J. Hristov, "Integral-balance solution to nonlinear subdiffusion equation," *Frontier in Fractional Calculus*, vol. 1, pp. 71–106, 2018.
- [38] J. Hristov, "A transient flow of a non-Newtonian fluid modelled by a mixed time-space derivative: an improved integral-balance approach," in *Mathematical Methods in Engineering*, pp. 153–174, Springer, Cham, 2019.
- [39] X. Wang, H. Qi, B. Yu, Z. Xiong, and H. Xu, "Analytical and numerical study of electroosmotic slip flows of fractional second grade fluids," *Communications in Nonlinear Science and Numerical Simulation*, vol. 50, pp. 77–87, 2017.
- [40] D. Hilbert, *Methods of Mathematical Physics*, CUP Archive, 1955.
- [41] C. F. Lorenzo and T. T. Hartley, "Generalized functions for the fractional calculus," *Critical Reviews in Biomedical Engineering*, vol. 36, no. 1, pp. 39–55, 2008.
- [42] M. Arshad, J. Choi, S. Mubeen, and G. Rahman, "A new extension of the Mittag-Leffler function," *Korean Mathematical Society*, vol. 33, no. 2, pp. 549–560, 2018.
- [43] D. Vieru and A. A. Zafar, "Some Couette flows of a Maxwell fluid with wall slip condition," *Applied Mathematics & Information Sciences*, vol. 7, no. 1, pp. 209–219, 2013.
- [44] N. Ahmed, D. Vieru, C. Fetecau, and N. A. Shah, "Convective flows of generalized time-nonlocal nanofluids through a vertical rectangular channel," *Physics of Fluids*, vol. 30, no. 5, p. 052002, 2018.
- [45] J. Abate and P. P. Valkó, "Multi-precision Laplace transform inversion," *International Journal for Numerical Methods in Engineering*, vol. 60, no. 5, pp. 979–993, 2004.
- [46] B. Dingfelder and J. A. C. Weideman, "An improved Talbot method for numerical Laplace transform inversion," *Numerical Algorithms*, vol. 68, no. 1, pp. 167–183, 2015.